# THE PETROLOGY AND GEOCHEMISTRY OF CALEDONIAN BASIC BODIES OF NE SCOTLAND AND CONNEMARA

by

**Robert Patrick Mullen**

A thesis submitted to
The University of Birmingham
for the degree of
Doctor of Philosophy

School of Earth Sciences
University of Birmingham

June, 2002

## Abstract

The petrography, mineralogy and whole rock chemistry of a suite of Grampian-age, syn-orogenic basic plutons in Scotland and Connemara are examined. These bodies display mineralogical and chemical features consistent with having evolved by fractionation combined with melting and assimilation of their pelitic country rocks. Olivine compositions range from $Fo_{91.4}$ to $Fo_{1.2}$, with pyroxenes and other ferromagnesian phases showing concomitant extreme iron enrichment. Plagioclase feldspar ranges from $An_{96.6}$ to $An_{28.5}$ in composition, while apatite, zircon and quartz are present as late crystallising phases. Trends seen in the main silicate phases, and in whole rock chemistry, suggest a tholeiitic fractionation path, while evidence is seen in the central bodies for the presence of more than one phase of intrusive activity.

Modelling of the evolution of selected trends is consistent with the levels of fractionation and contamination predicted from the chemistry and petrography, with the shape of 'spider' and REE plots largely controlled by this contamination, and by the presence of cumulus accessory phases. Modelled levels of contamination vary from ~14 to 17% during the fractionation of the Middle Zones of the northeastern and central intrusions, and decreases to as little as ~3.5% with increasing evolution in the central intrusions.

A set of granular gabbros occurring within the Insch intrusion has been identified as resembling the probable parental magmas to the 'Younger' Basics. These samples are mineralogically and chemically distinct from the main cumulate sequence, and exhibit chemical properties (high $Al_2O_3$ content; low $^{87}Sr/^{86}Sr$ ratios; flat 'spider' and REE plots) consistent with the likely parental magmas responsible for this main cumulate sequence. It is suggested that they represent a partial mantle melt, with an added slab component indicating derivation in an arc-type setting.

## Acknowledgements

Firstly, I would like to express thanks to my supervisors, Drs. Morrison and Henney for their invaluable help and assistance over the past few years. I would also like to thank the many members of staff at Birmingham who have helped me, especially Rae Mackay, Andy Chambers, John Ashworth, Graham Hendry, Rob Ixer and Bill Owens. A special debt of gratitude also to Ivan Sansom for going well beyond the line of duty in assisting me with my work. Thanks also to Jane Harris for not banning me from the lab on a few occasions, to Paul Hands for providing me with innumerable thin sections, and to Aruna Mistry and Jon Clatworthy for their practical help and assistance.

Beyond Birmingham, thanks to Malcolm Hole and Jeremy Preston at Aberdeen, John Wadsworth at Manchester and the staff at Cambridge for their friendly help and assistance in raiding their sample collections, and to Drs. Mike Styles and Gus Gunn at the BGS for their help with use of the probe at Keyworth. I am also very grateful to Godfrey Fitton at Edinburgh and Nick Walsh and Nikki Paige at Royal Holloway for their assistance with my XRF and REE work. Thanks also to Bob Thompson and John Mendum for their helpful advice and support.

Many thanks to all the C-Dome diaspora including Hari, Clarke, Trev and Puppy for making the experience all the more bearable, and also the new C-Dome breed of Nordine and Hussein, even if they don't drink as much. Thanks also to many of the other post-grads past and present, including Canning, Kettle, Bryan, Simon, Dave, Hodge, Gareth, Graham, Liam, Dirk, and everyone else whom I've forgotten, for ensuring that I passed my non-academic time in a non-constructive fashion. Special thanks also to the Gimp for helping me in ways too numerous to mention, but especially for keeping me (semi-) sane over the last 12 months.

Finally and most importantly, my eternal gratitude to my Mum, Dad and Jenny for their help and support in every way imaginable throughout my time in Brum.

## Contents

## List of Figures

## List of Tables

## List of Plates

# Chapter 1 Introduction

## 1.1 Introduction

This thesis is based upon research into a set of basic intrusive bodies emplaced within the Caledonides of the British Isles. These early to mid Ordovician peridotitic, gabbroic and noritic complexes, located in northeast Scotland and Connemara, represent material intruded at several kilometres depth within the Caledonian orogenic belt (Figure 1.1), during a phase known as the Grampian Orogeny. They are well known for having developed igneous layering on a variety of scales, and for having locally melted and incorporated their country rocks (high-grade metasediments) on a large scale. In addition, their emplacement appears to be closely related to a series of major, crustal scale shear zones, which may or may not be synchronous with the magmatism.

Arc complexes within the region in early to mid Ordovician times have frequently been postulated, but evidence for their existence remains controversial. The Grampian Highland and Connemara regions provide a mid-crustal section through continental crust that was affected by tectonism, metamorphism and generation and emplacement of basic and granitic magma during the Caledonian orogeny, and may represent a cross-section through such an arc complex. Using a combination of detailed petrographic and petrologic work, whole rock major, trace, and REE geochemistry, and silicate mineral chemistry, various aspects of the origin and evolution of these rocks have been examined, and models for the fractionation and assimilation processes involved in their evolution investigated. Although the petrology and structural framework of these intrusions have been studied in some detail in the past, little or no modern work on their mineralogy, fractionation or geochemistry has been undertaken.

## 1.2 Purpose of the research

This study will attempt to:

i Describe the mineralogy, petrography and petrology of the individual intrusions, and of the suite as a whole, identifying mineral assemblages and associated fractionation trends.

ii Examine the geochemical evolution of the bodies, both individually (where possible) and as a whole, and to identify any significant variations within the trend.

iii Assess the role of contamination within the intrusions, and attempt to model the evolution of these intrusions using a combination of petrographic evidence, mineral compositions and major element chemistry.

iv Characterize the parental magma to the bodies and assess the possible arc-related nature to these bodies. Although contamination and fractionation of the bodies may obscure many of the chemical properties of the parental magma, it may still be possible to identify and assess possible source components.

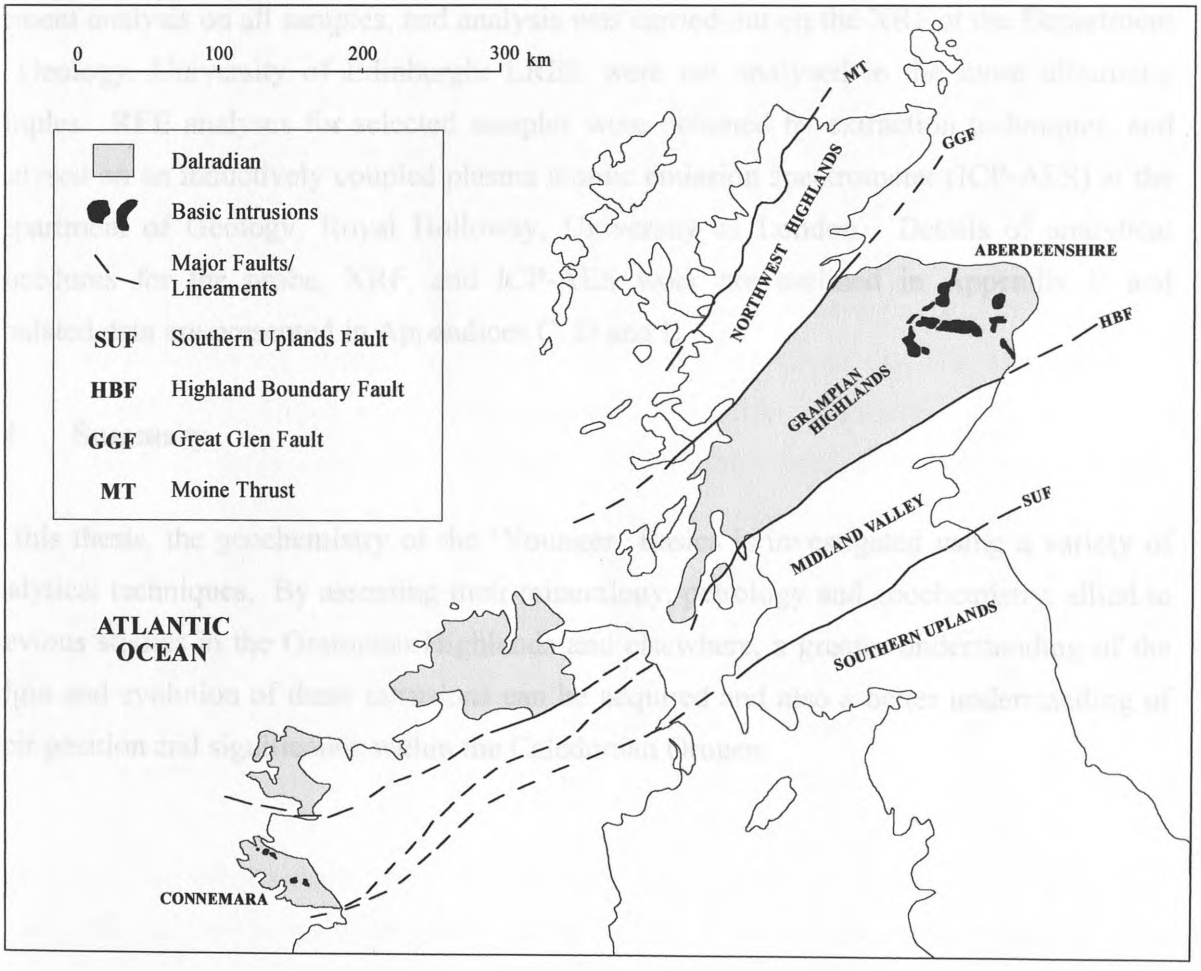


**Figure 1.1 Location of the study area within the British Isles**

## 1.3 Techniques used in the research

Over 150 samples from the intrusions and their country rocks were collected from various sources for geochemical analysis. Details of sample location and descriptions are found in Appendix A. Due to the poorly exposed nature of many of the intrusions, and the already detailed field relations mapped in the past, it was felt that field mapping and sample collection was beyond the scope of this project. Thin sections were prepared in the School of Earth Sciences, The University of Birmingham for conventional petrographic studies and polished thin sections were also prepared in the School of Earth Sciences for reflected light microscopy and selected mineral probe work. This probe work was carried out using a wavelength dispersive electron microprobe at the BGS, Keyworth, Nottingham.

All samples were powdered, and fused discs prepared for major element analysis on the School's X-ray Fluorescence spectrometer (XRF). Powder pellets were prepared for trace element analysis on all samples, and analysis was carried out on the XRF at the Department of Geology, University of Edinburgh; LREE were not analysed in the more ultramafic samples. REE analyses for selected samples were obtained by extraction techniques, and analysed on an inductively coupled plasma atomic emission spectrometer (ICP-AES) at the Department of Geology, Royal Holloway, University of London. Details of analytical procedures for the probe, XRF, and ICP-AES work are outlined in Appendix B and tabulated data are presented in Appendices C, D and E.

## 1.4 Summary

In this thesis, the geochemistry of the 'Younger' Basics is investigated using a variety of analytical techniques. By assessing their mineralogy, petrology and geochemistry, allied to previous studies in the Grampian Highlands and elsewhere, a greater understanding of the origin and evolution of these intrusions can be acquired and also a better understanding of their position and significance within the Caledonian Orogen.

# Chapter 2 Geological Setting

## 2.1 Introduction

The intrusions that form the basis of this study were emplaced in mid Ordovician times during the early to mid stages of the Caledonian Orogeny. They are situated within the Grampian Highlands in northeast Scotland and the Connemara region of western Ireland. Despite being spread over a wide geographical range (Figure 1.1), they are, in most cases, found intruded into a similar stratigraphic position within the Dalradian succession, and in a similar tectonic position within the orogeny; there are also strong petrographic, petrological and geochemical similarities between the various intrusions. The chief purpose of this chapter is to place the intrusions within a Caledonian context, in terms of space, time and orogenic evolution.

The 'Younger' Basic intrusions of NE Scotland are found spread over an area of ~ 400 $km^2$ within the northeast Grampian Highlands (Figure 2.1). They are confined to the south by the Highland Boundary Fault, to the north and east by the North Sea, and to the west by a major shear zone, the Portsoy-Duchray Hill Lineament, also known as the Portsoy Lineament. They consist of seven main intrusions with numerous smaller associated bodies, all of which are strongly linked to a series of shear zones that run throughout the area (Ashcroft *et al.*, 1984), such as this Portsoy Lineament. The terms 'Younger' Basics and 'Younger' Gabbros were coined by Read (1919) to differentiate between two texturally distinct suites of gabbros in the Grampian region. The other set of gabbroic bodies, the 'Older' Gabbros, tended to be smaller in volume, displaying more deformation and alteration than the 'Younger' Gabbros, and were consequently believed to be older in age. Since Read's original definition, many of the 'Older' Gabbros have been shown to be 'Younger' in age, in particular the Blackwater and Morven Cabrach intrusions. In spite of this, the terms have persisted in the literature and will be used here.

The Connemara Gabbros are found in two complexes in the north and south of the region, on the limbs of the Connemara Antiform (Figure 2.2). They are substantially smaller than the Grampian bodies; the northern suite, the Dawros-Currywongaun-Doughruagh Complex covers an area of ~ 4 $km^2$, while the southern group, the Cashel-Lough Wheelaun Complex spans an area of ~ 3 $km^2$. Again, they are strongly associated with shear zones running

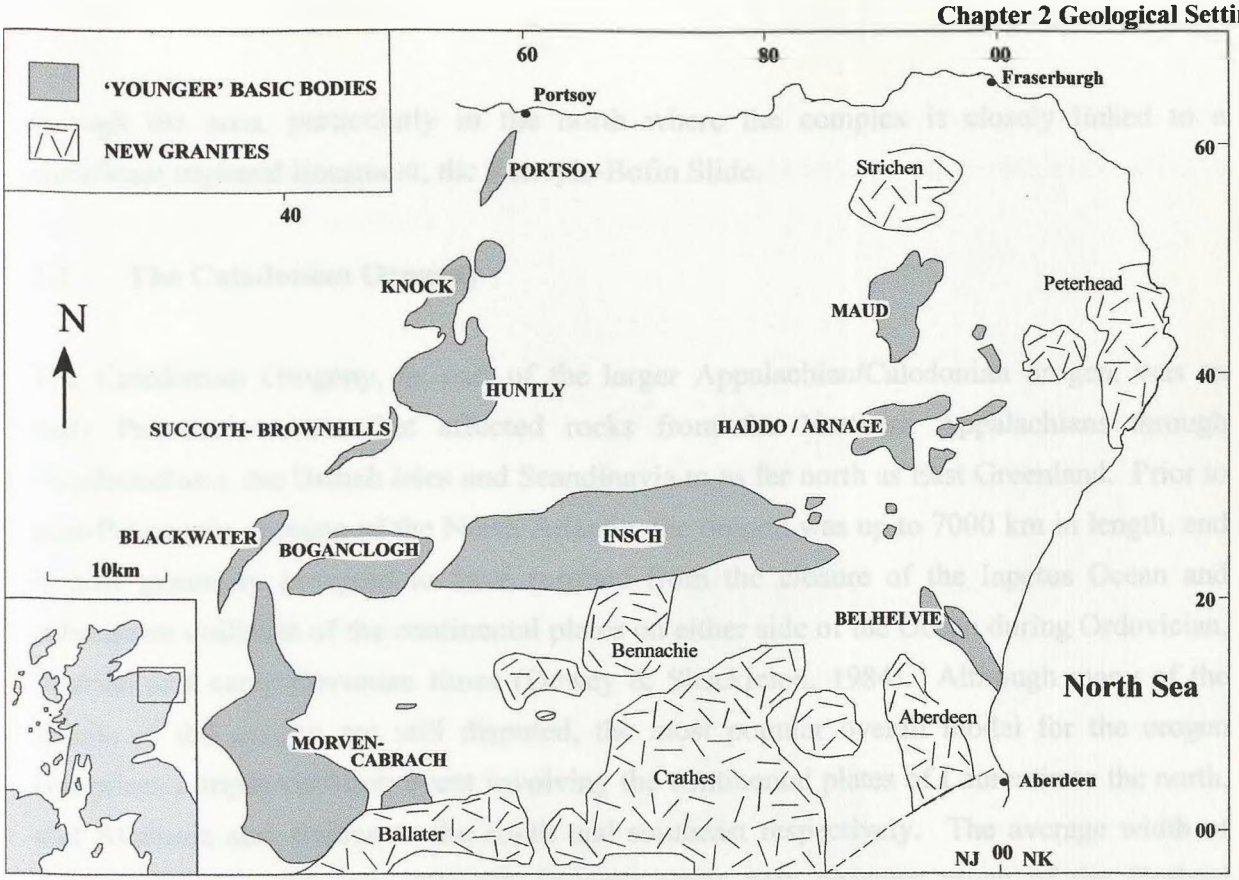


**Figure 2.1 Location of the 'Younger' Basics of the Grampian Highlands**

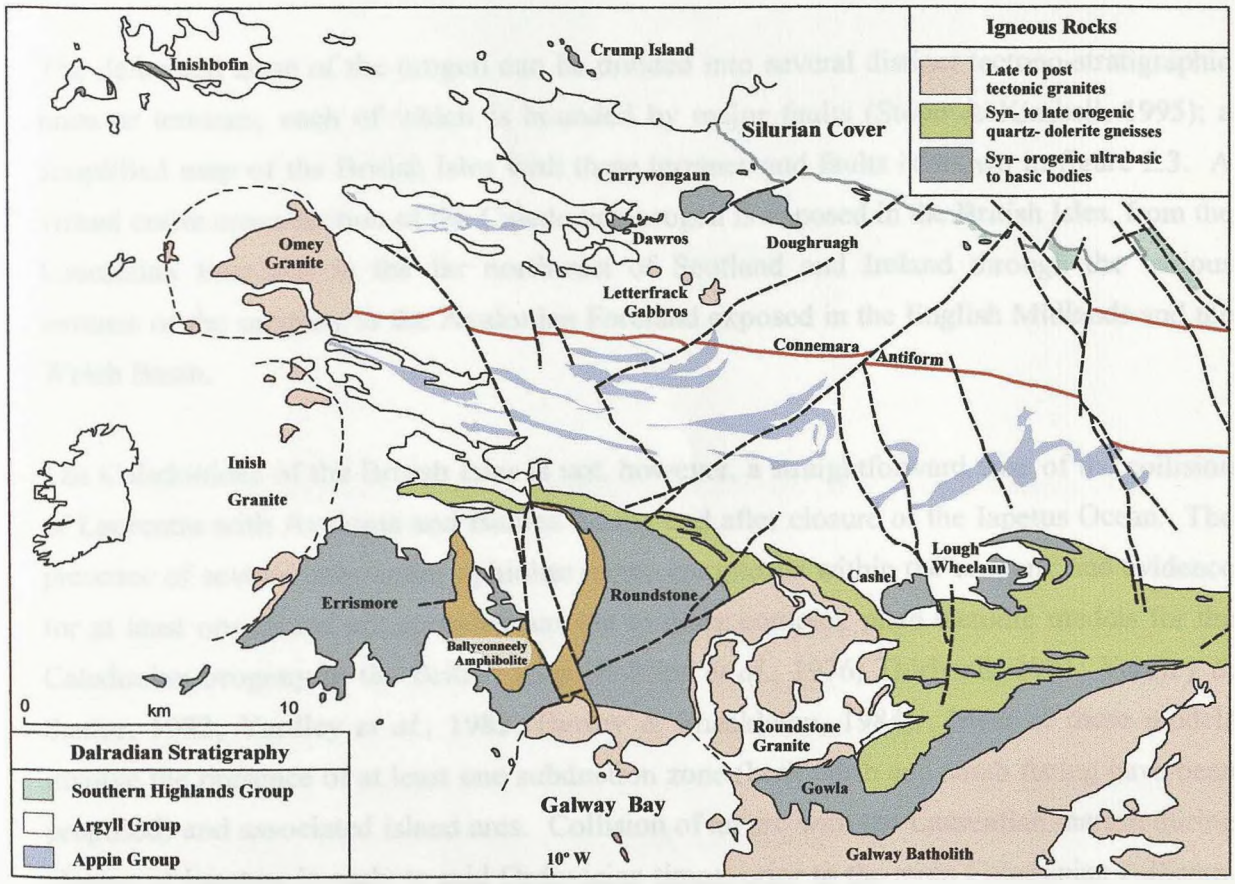


**Figure 2.2 Distribution of the Connemara Gabbros and other Caledonian igneous rocks within the Connemara region. Dalradian stratigraphy is also shown (after Leake & Tanner, 1994)**

through the area, particularly in the north where the complex is closely linked to a significant regional lineament, the Renvyle-Bofin Slide.

## 2.2 The Caledonian Orogeny

The Caledonian Orogeny, as part of the larger Appalachian/Caledonian orogen, was an early Palæozoic event that affected rocks from the Northern Appalachians through Newfoundland, the British Isles and Scandinavia to as far north as East Greenland. Prior to post-Palæozoic opening of the North Atlantic, the orogen was up to 7000 km in length, and is now generally accepted to have resulted from the closure of the Iapetus Ocean and subsequent collision of the continental plates on either side of the Ocean during Ordovician, Silurian and early Devonian times (Dewey & Shackleton, 1984). Although many of the details of the orogen are still disputed, the most popular overall model for the orogen comprises a triple collision event involving the continental plates of Laurentia to the north, and Avalonia and Baltica to the south and southeast respectively. The average width of the orogen is ~ 700 km, although younger cover now obscures much of the foreland regions.

The deformed zone of the orogen can be divided into several distinct tectono-stratigraphic units or terranes, each of which is bounded by major faults (Stone & Kimbell, 1995); a simplified map of the British Isles with these terranes and faults is shown in figure 2.3. A virtual entire cross-section of the Caledonian orogen is exposed in the British Isles, from the Laurentian Foreland in the far northwest of Scotland and Ireland through the various terranes of the orogeny to the Avalonian Foreland exposed in the English Midlands and the Welsh Basin.

The Caledonides of the British Isles is not, however, a straightforward case of the collision of Laurentia with Avalonia and Baltica during and after closure of the Iapetus Ocean. The presence of several substantial ophiolite nappe complexes within the orogeny and evidence for at least one island arc complex has led to more complex plate tectonic models for the Caledonian orogeny in the British Isles (Phillips *et al.*, 1976; Thirlwall, 1981; Yardley & Senior, 1982; Yardley *et al.*, 1982; Dewey & Shackleton, 1984). Most of these models involve the presence of at least one subduction zone (both north and south facing have been proposed) and associated island arcs. Collision of an arc with the Laurentian margin during closure of Iapetus, in early to mid Ordovician times, prior to the main Caledonian collision, is thought to have led to the accretion of this arc onto the Laurentian margin. The exact

nature of this event, known as the Grampian Orogeny (Dewey & Shackleton, 1984), has been somewhat complicated by the subsequent main Caledonian event, continental collision in Silurian and Devonian times.

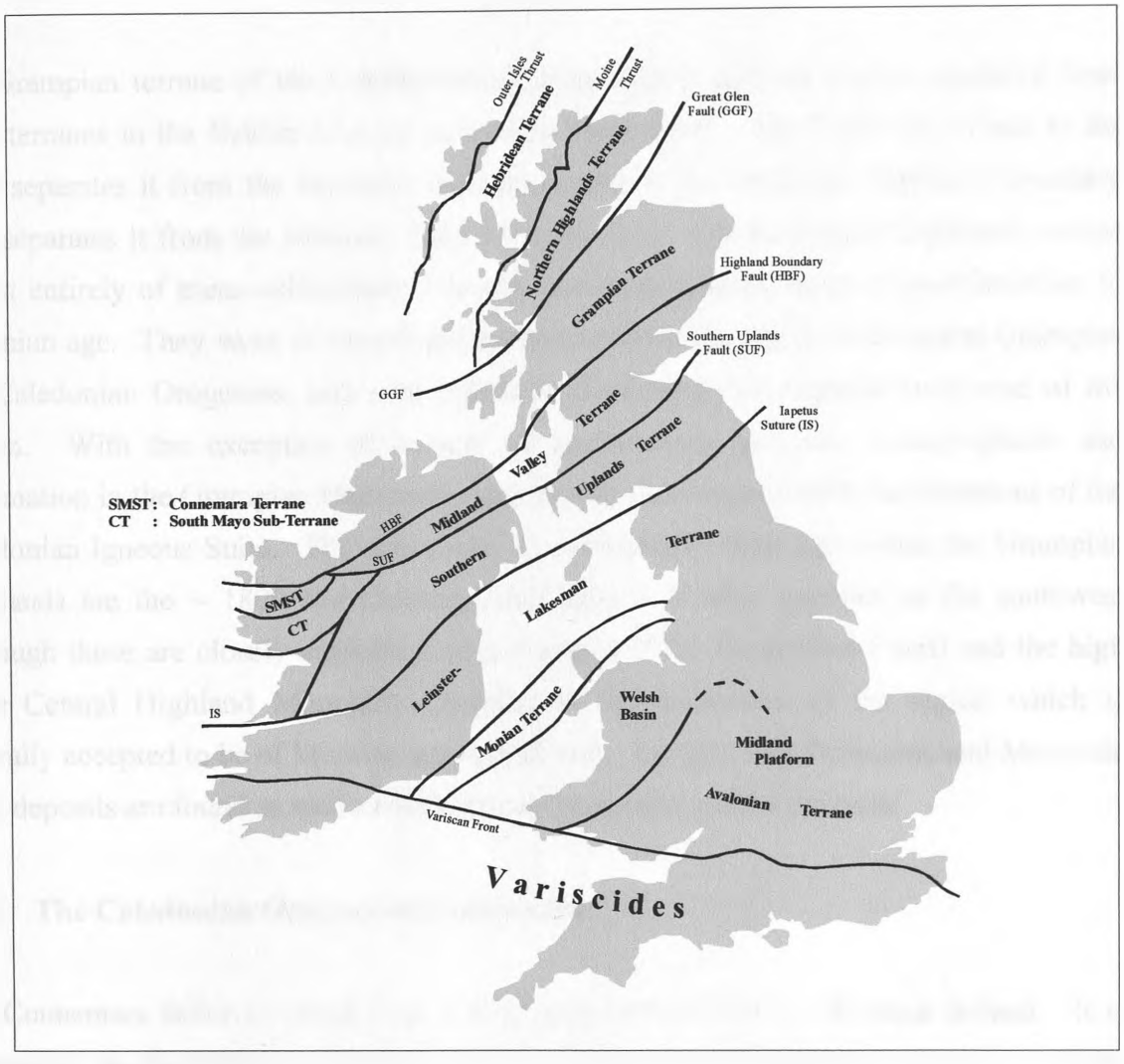


**Fig 2.3 Simplified map of terranes within the British Isles (after Stone & Kimbell, 1995)**

Stone & Kimbell (1995) have defined the Caledonian Orogen as being represented by a sequence of accreted terranes between the continental massifs of Laurentia and Avalonia/Gondwana/Baltica, while McKerrow *et al.* (2000) have suggested that the term 'Caledonian Orogeny' should be restricted to 'tectonic events within, and on the borders of, the Iapetus Ocean', and that the use of the term 'Caledonian' as a general time indicator is unwise, given that deformation events ranging from 540-400 Ma have been described as Caledonian. The Grampian Orogeny has been redefined (Soper *et al.*, 1999; based on

Lambert & McKerrow, 1976) as the orogeny resulting from the collision of an arc with the Laurentian continental margin. The Grampian Orogeny is generally accepted to be a mid Ordovician event and, as such, represents an early phase of the Caledonian Orogeny.

### 2.2.1 The Caledonian Orogeny in the Grampian Highlands

The Grampian terrane of the Caledonides is quite clearly defined, and is separated from other terranes in the British Isles by two major fault zones. The Great Glen Fault to the north separates it from the Northern Highlands, and to the south the Highland Boundary fault separates it from the Midland Valley (Figure 2.3). The Grampian Highlands consist almost entirely of meta-sedimentary, igneous and meta-igneous rocks of pre-Cambrian to Devonian age. They were deformed and metamorphosed during the subsequent Grampian and Caledonian Orogenies, and now represent the eroded and exposed root zone of the orogen. With the exception of a suite of post-tectonic granites, metamorphism and deformation in the Grampian Highlands were largely synchronous with the intrusions of the Caledonian Igneous Suite. The only rocks of substantially older age within the Grampian Highlands are the ~ 1800 Ma Colonsay and Rhinns of Islay gneisses in the southwest (although these are closely associated with a splay off the Great Glen Fault) and the high grade Central Highland Migmatite Complex in the north-west of the region which is generally accepted to be of Moinian age and affinity. Locally, late Palæozoic and Mesozoic basin deposits are found as well as widespread Quaternary glacial deposits.

### 2.2.2 The Caledonian Orogeny in Connemara

The Connemara Inlier is found over a wide area of Co. Galway, Western Ireland. It is confined to the South by the Galway Granite and its related migmatization, to the west by the Atlantic Ocean, and to the East and North by Silurian cover, which obscures a major terrane boundary, the underlying Doon Rock Fault. No rocks of certain pre-Caledonian age are known from Connemara; some units of uncertain affinity such as the Delaney Dome have been described as pre-Caledonian, although recent geochemical work (Draut & Clift, 2002) suggests they may be related to Grampian age volcanics. Older successions are known from north of Connemara, at Clare Island, the Ox Mountains and Annagh and, although some uncertainty exists, these are generally accepted to be pre-Caledonian in age. As is the case in the Grampian Highlands, the Connemara Inlier consists chiefly of metasediments and igneous and meta-igneous rocks, with little subsequent deposition

having taken place, except for the Silurian deposits to the north and east, and substantial Quaternary glacial cover.

### 2.2.3 Stratigraphy

In spite of their highly metamorphosed and deformed nature, a detailed stratigraphy of the Dalradian in the Grampian Highlands and Connemara is well established and simplified maps displaying the broad subdivisions of the Dalradian of the two regions into four main groups are displayed in Figures 2.4 and 2.5. Correlations of the Dalradian Supergroup from the Grampian Highlands through northwestern Ireland to Connemara have been well established over the past century or more. Although lateral variations are common, distinctive and often contemporaneous marker horizons have enabled overall correlations to be established. The Supergroup sequence was deposited within the confines of the Iapetus Ocean, mainly along the southeastern margin of the Laurentian continent, in late Proterozoic and early Palaeozoic times (Anderton, 1976), and consequently youngs as a whole to the southeast. Towards the top of the sequence the presence of several units that are difficult to trace laterally, combined with faulting and shearing, mean that precise correlations between the two regions are more difficult to determine.

The oldest of these groups, *the Grampian Group*, is a thick sequence of massive psammites and semi-pelites found in a broad SW trending zone adjacent to the Great Glen Fault. Its base is not seen due to a complex set of shear zones known as the Grampian Slide Zone. Grampian Group rocks are not exposed in Connemara. Above the Grampian Group, and conformable with it (although in places the contact is tectonic), is *the Appin Group*, a succession of shelf deposits comprising several sequences of pelites, quartzites, calc-silicates, and carbonates. Several marker horizon units enable accurate correlation within the Grampian Highlands and as far as Connemara where the lowermost units seen in the region are pelites and semi-pelites from the upper levels of the Appin Group. Allowing for subsequent faulting and deformation, the Appin Group tends to occur as a narrow band just to the SE of the Grampian group and in Connemara in the cores of early folds within the region (see figure 2.4). Although no major unconformities are seen in the Appin Group, several disconformities and slides mean that in most areas the group is only partially exposed.

Above the Appin Group, and again thought to be broadly conformable with it, is *the Argyll Group*, a sequence of continental shelf deposits including deltaic quartzites, carbonates, and

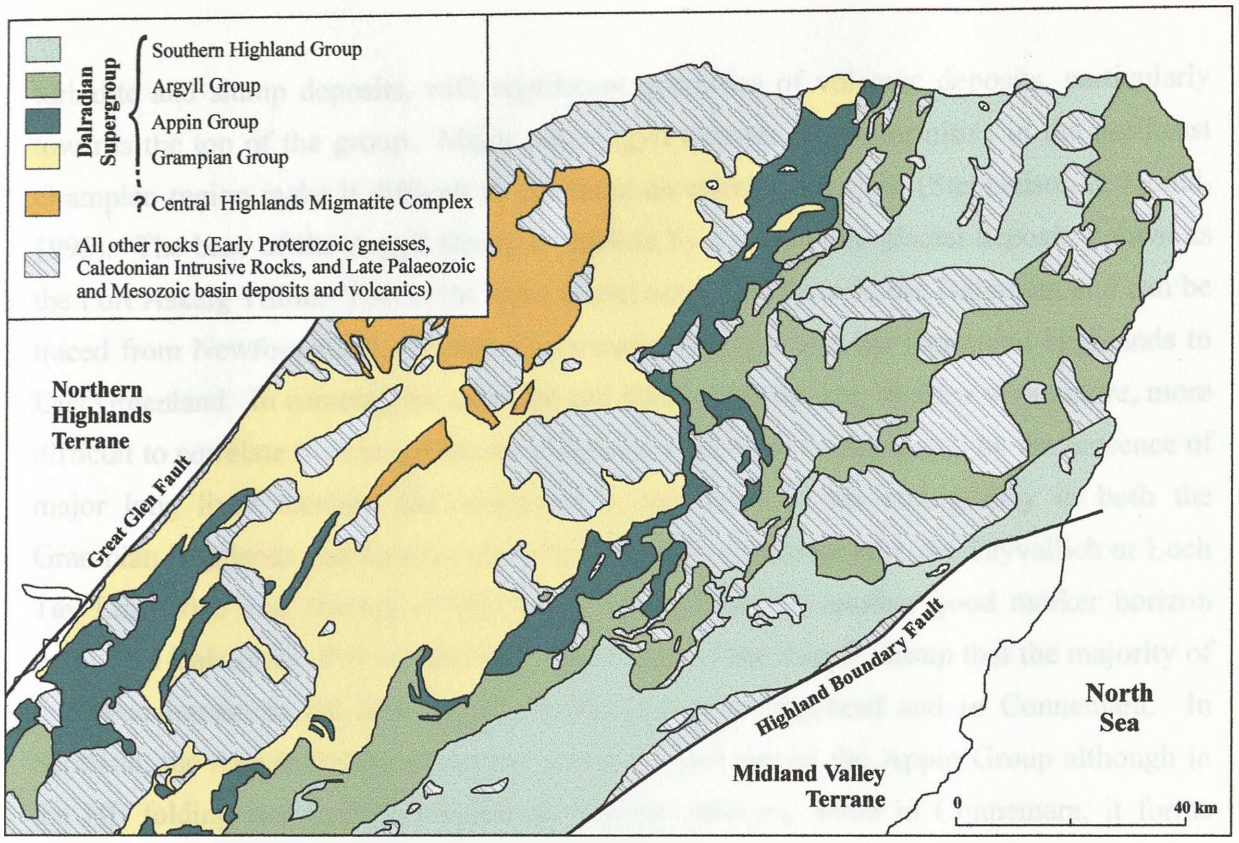


**Figure 2.4 Simplified Dalradian stratigraphy in the Grampian Highlands (after Stephenson & Gould, 1995)**

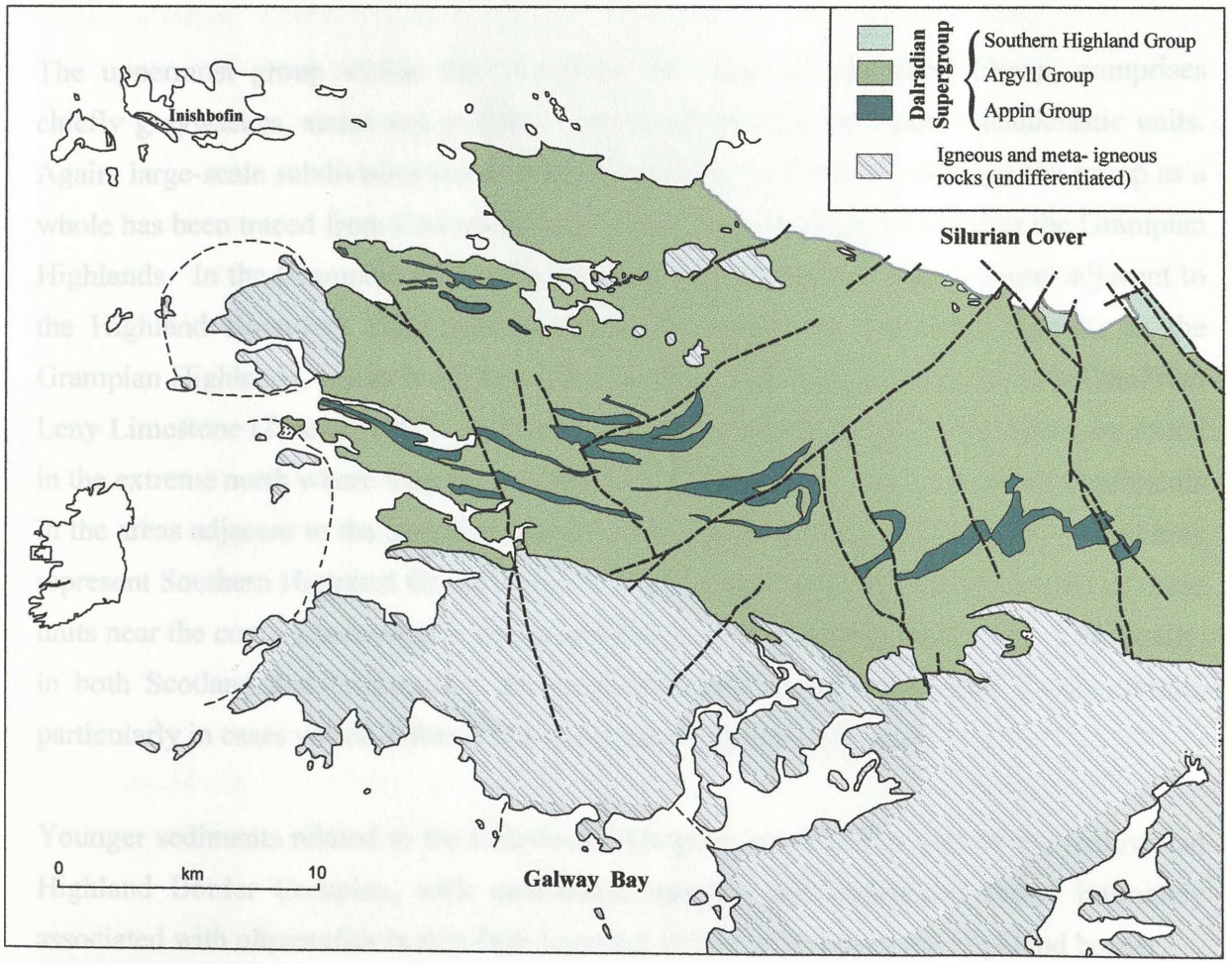


**Figure 2.5 Distribution of the Dalradian stratigraphy within the Connemara region. (after Leake & Tanner, 1994)**

turbidite and slump deposits, with significant quantities of volcanic deposits, particularly towards the top of the group. Major mid-Argyll tectonic disconformities in the northeast Grampian region make it difficult to construct an entire succession (Stephenson & Gould, 1995). The base of the Argyll Group is marked by a distinctive glacial deposit, known as the Port Askaig Tillite. This is the most useful marker horizon in the Dalradian and can be traced from Newfoundland, through Connemara, Donegal and the Grampian Highlands to East Greenland. In contrast, the turbidite and slump deposits are, by their very nature, more difficult to correlate over larger lateral distances, a problem compounded by the presence of major long lived tectonic discontinuities at this level in the stratigraphy in both the Grampian Highlands and Connemara; nevertheless, a carbonate unit, the Tayvallich or Loch Tay Limestone near the top of the Argyll Group provides another good marker horizon within the Dalradian. It is within these upper units of the Argyll Group that the majority of the basic intrusions are found, both in the Grampian Highland and in Connemara. In Scotland, the Argyll Group is found to the south and east of the Appin Group although in the NE folding and faulting complicate outcrop patterns, while in Connemara, it forms much of the Dalradian exposure throughout the region due to it presence on the limbs of a major late Caledonian structure, the Connemara Antiform.

The uppermost group within the Dalradian, *the Southern Highland Group*, comprises chiefly greywackes, slates and phyllites with localized limestone and volcaniclastic units. Again, large-scale subdivision and internal correlations are difficult although the group as a whole has been traced from Connemara and South Mayo, through Donegal to the Grampian Highlands. In the Grampian Highlands, the Southern Highland Group is found adjacent to the Highland Boundary Fault and represents the uppermost Dalradian deposits in the Grampian Highlands, where it can be shown locally to pass conformably into the Cambrian Leny Limestone (Tanner, 1995). In Connemara, Southern Highland Group rocks are found in the extreme north where they are overlain by Silurian Cover. Many of the metasediments in the areas adjacent to the intrusive complexes are of uncertain affinity, however, and may represent Southern Highland Group deposits. The poorly correlated nature of many of these units near the contact between the Appin and Southern Highland Groups means that locally, in both Scotland and Connemara, the exact affinities of individual units is not certain, particularly in cases where deformation and metamorphism are intense.

Younger sediments related to the Caledonian Orogeny are found as part of the Ordovician Highland Border Complex, with mudstones, arenites and carbonates found intimately associated with ultramafics in thin fault bounded slivers, adjacent to the Highland border.

### 2.2.4 Structure

The structure of the Grampian Highlands is quite complex in nature, and for over a century, workers have attempted to decipher the structural relations within the region. A simplified map of structural features in the northeast region is shown in figure 2.6. Although many key aspects of the structure of the Highlands remain controversial, the overall framework is generally accepted. Initial high-pressure medium temperature metamorphism associated with the onset of orogenic deformation was accompanied by early ($D_1$) deformation. This was followed by moderate pressure and higher temperature metamorphic conditions, leading to pervasive metamorphism and deformation. This metamorphic peak is associated with, and perhaps slightly postdates, $D_2$ and $D_3$ events. Late, more brittle structures have been assigned to $D_3$ and $D_4$ events. The main structures in the Grampian Highlands tend to form a mushroom-like shape, with folds and nappes facing away from a steep belt running up the centre of the Highlands. Along the Great Glen Fault, folds face to the northwest, while adjacent to the Highland Boundary Fault, the southeastward facing Tay Nappe dominates the structure.

In the northeast, several folding events are recognised, such the Boyndie Syncline, just east of Portsoy, while later structures are believed to be associated with the 'Younger' Gabbros. These structures, which are likely to have played an important role in the emplacement of the bodies, are a series of deep, steeply dipping, shear zones running adjacent to and through the intrusions. The best known of these shear zones, the Portsoy Lineament runs along the margins of, and through, the Huntly-Knock-Portsoy, Succoth-Brownhills and Morven Cabrach masses, while other shear zones dissect and bound the other bodies, most notably Insch and the northeastern bodies of Arnage and Haddo. Ashcroft *et al.* (1984) and Goodman (1994) have suggested that these shear zones are long-lived lineaments, which may represent reactivated rifted fault systems from the late-Proterozoic opening of the Iapetus Ocean. It is believed that the 'Younger' Basics subsequently exploited these shear zones as a conduit for emplacement, with shearing commencing before emplacement and continuing for some time afterwards. This will be discussed in more detail in Chapter 6. The northeastern extension of the Tay Nappe into the area adjacent to the intrusions has resulted in overturning of much of the Upper Dalradian stratigraphy. The principal late structures in the region are open folded structures such as the Turriff Syncline and the Buchan Anticline with pervasive fabrics only locally developed.

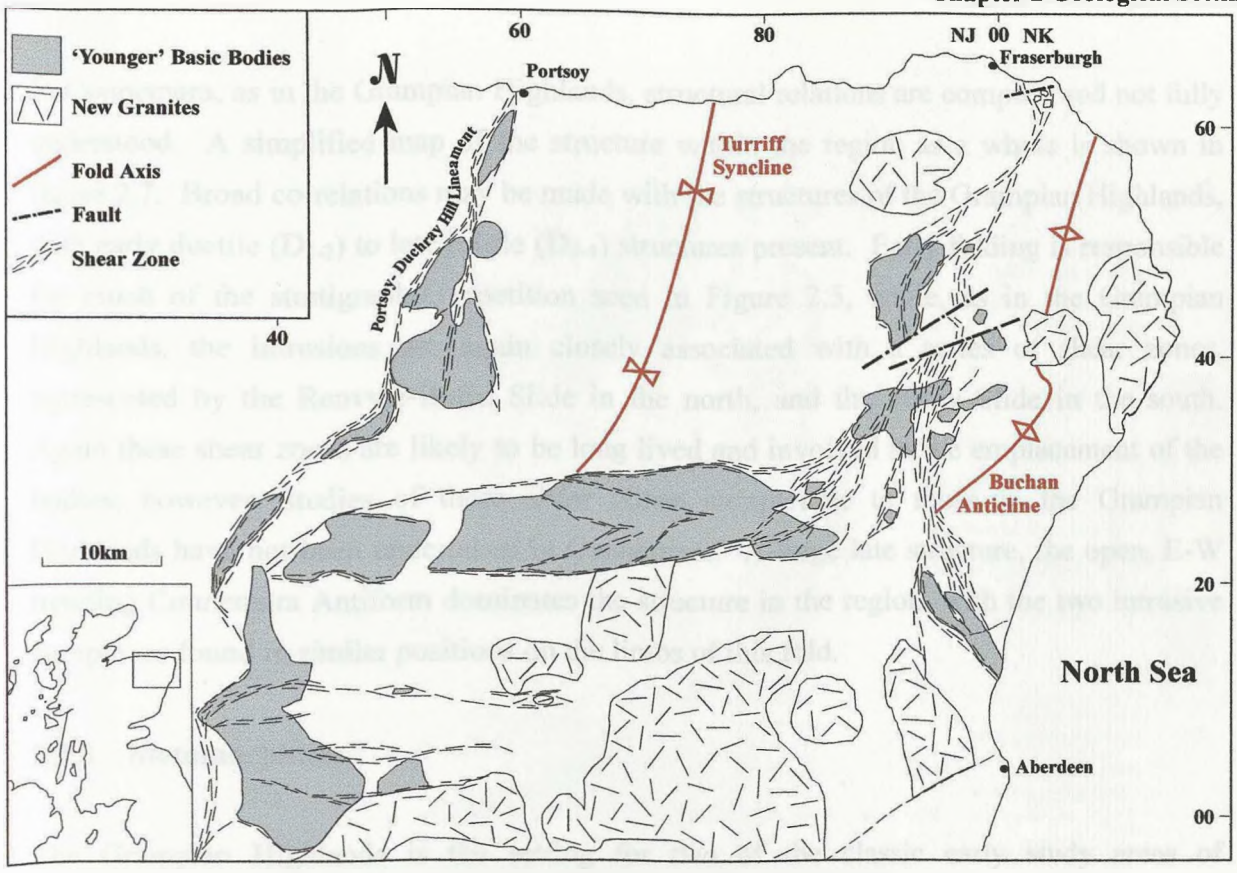


**Figure 2.6 Main structural features of the north- eastern Grampian Highlands (after Ashcroft et al., 1984, and Stephenson & Gould, 1995)**

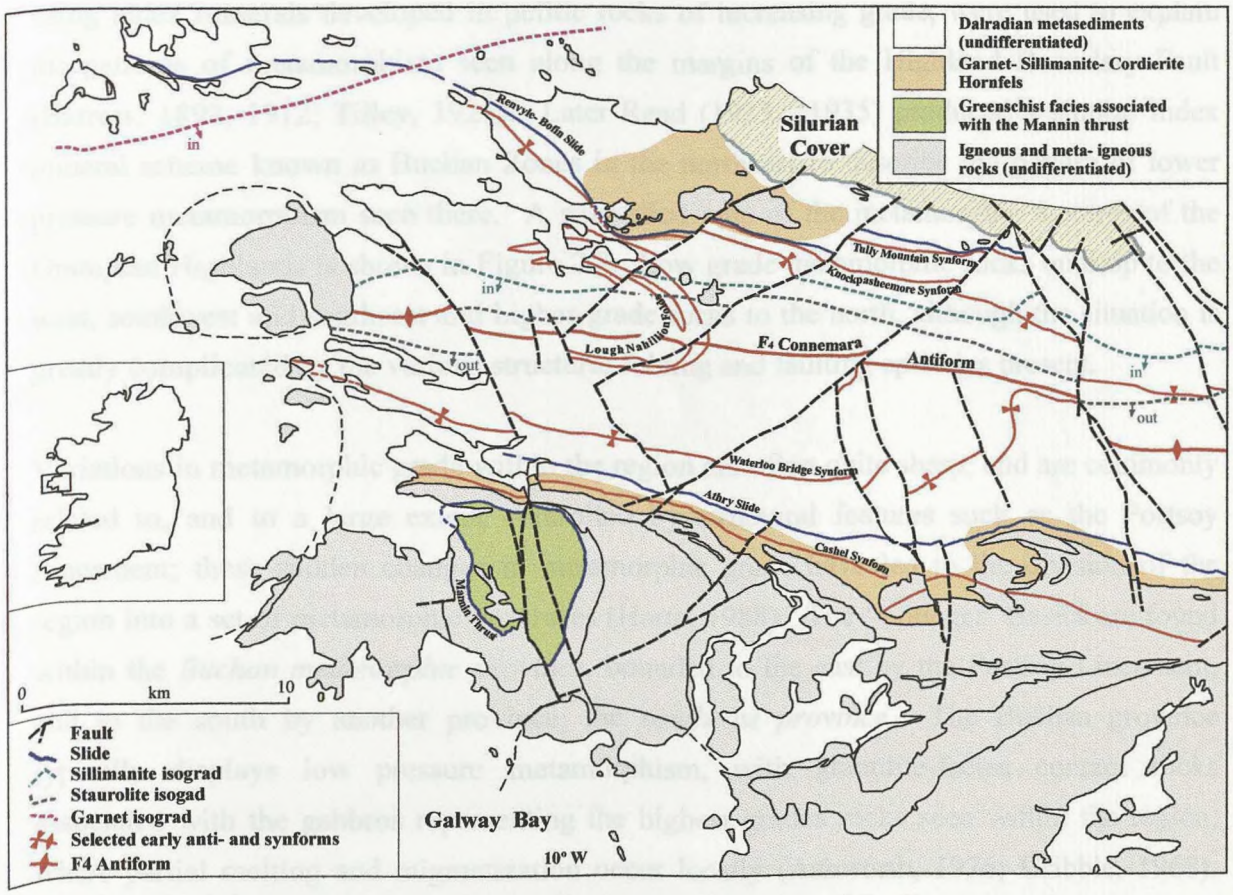


**Figure 2.7 Simplified structural and metamorphic features of the Connemara region (after Leake & Tanner, (1994).**

In Connemara, as in the Grampian Highlands, structural relations are complex and not fully understood. A simplified map of the structure within the region as a whole is shown in figure 2.7. Broad correlations may be made with the structures of the Grampian Highlands, with early ductile ($D_{1-2}$) to late brittle ($D_{3-4}$) structures present. Early folding is responsible for much of the stratigraphic repetition seen in Figure 2.5, while, as in the Grampian Highlands, the intrusions are again closely associated with a series of shear zones, represented by the Renvyle-Bofin Slide in the north, and the Athry Slide in the south. Again these shear zones are likely to be long lived and involved in the emplacement of the bodies; however, studies of these shear zones comparable to those in the Grampian Highlands have not been undertaken in Connemara. A large late structure, the open, E-W trending Connemara Antiform dominates the structure in the region, with the two intrusive complexes found in similar positions on the limbs of this fold.

### 2.2.5 Metamorphism

The Grampian Highlands is the setting for two of the classic early study areas of metamorphism and metamorphic grade, where many of the theories and understanding of the processes associated with metamorphism were formulated. Barrovian zones, identified using index minerals developed in pelitic rocks of increasing grade, were used to explain the patterns of metamorphism seen along the margins of the Highland Boundary Fault (Barrow, 1893, 1912; Tilley, 1925). Later Read (1923a, 1935) produced a similar index mineral scheme known as Buchan Zones in the northeast to describe the pattern of lower pressure metamorphism seen there. A simplified map of the metamorphic features of the Grampian Highlands is shown in Figure 2.8. Low grade metamorphic rocks outcrop to the west, southwest and southeast and higher-grade rocks to the north, although the situation is greatly complicated by the various structural folding and faulting episodes present.

Variations in metamorphic grade within the region are often quite sharp, and are commonly related to, and to a large extent controlled by structural features such as the Portsoy Lineament; these sudden changes in metamorphic grade have led to the division of the region into a set of metamorphic provinces (Harte, 1988). The 'Younger' Basics are found within the *Buchan metamorphic province*, bounded to the east by the Portsoy Lineament, and to the south by another province, the *southeast province*. The Buchan province typically displays low pressure metamorphism, with granulite-facies contact rocks associated with the gabbros representing the highest grades rocks seen within the region, where partial melting and migmatization occur locally (Ashworth, 1976; Gribble, 1968).

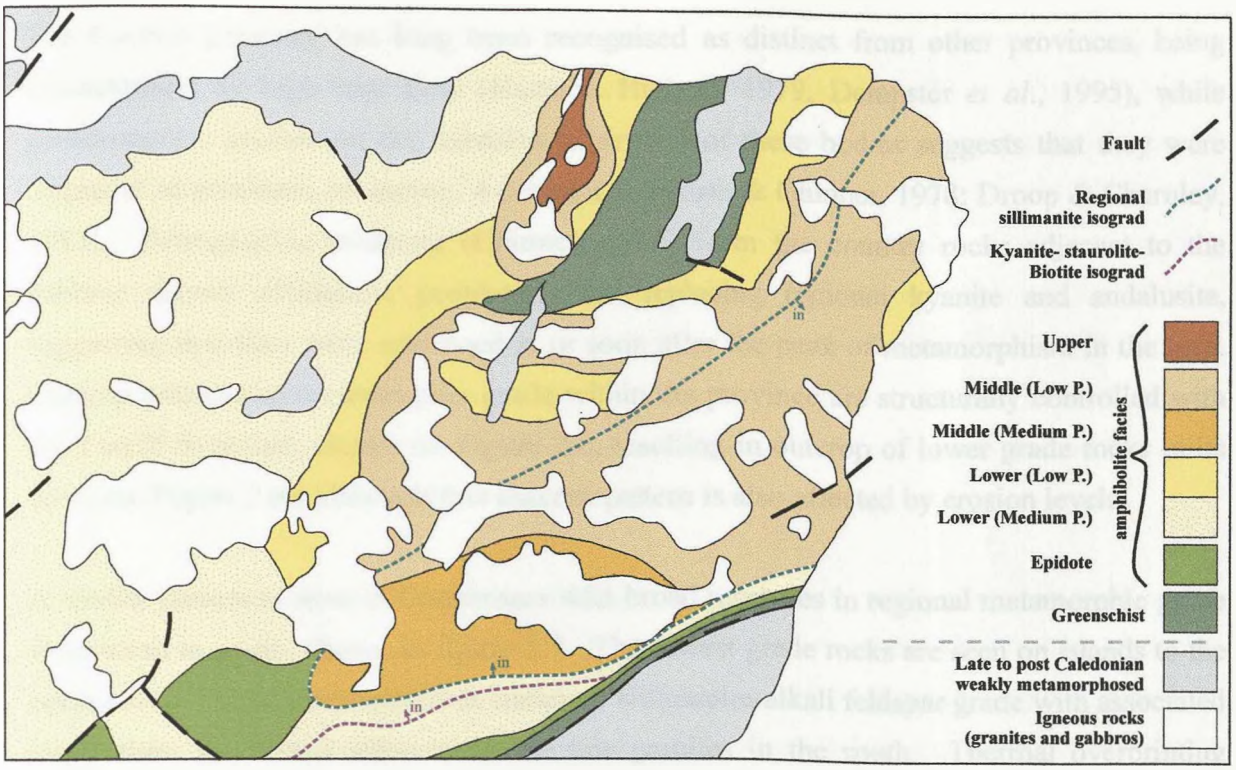


**Figure 2.8 Metamorphic grade and isograds from the northeastern Grampian Highlands (simplified from Fettes *et al.*, 1985).**

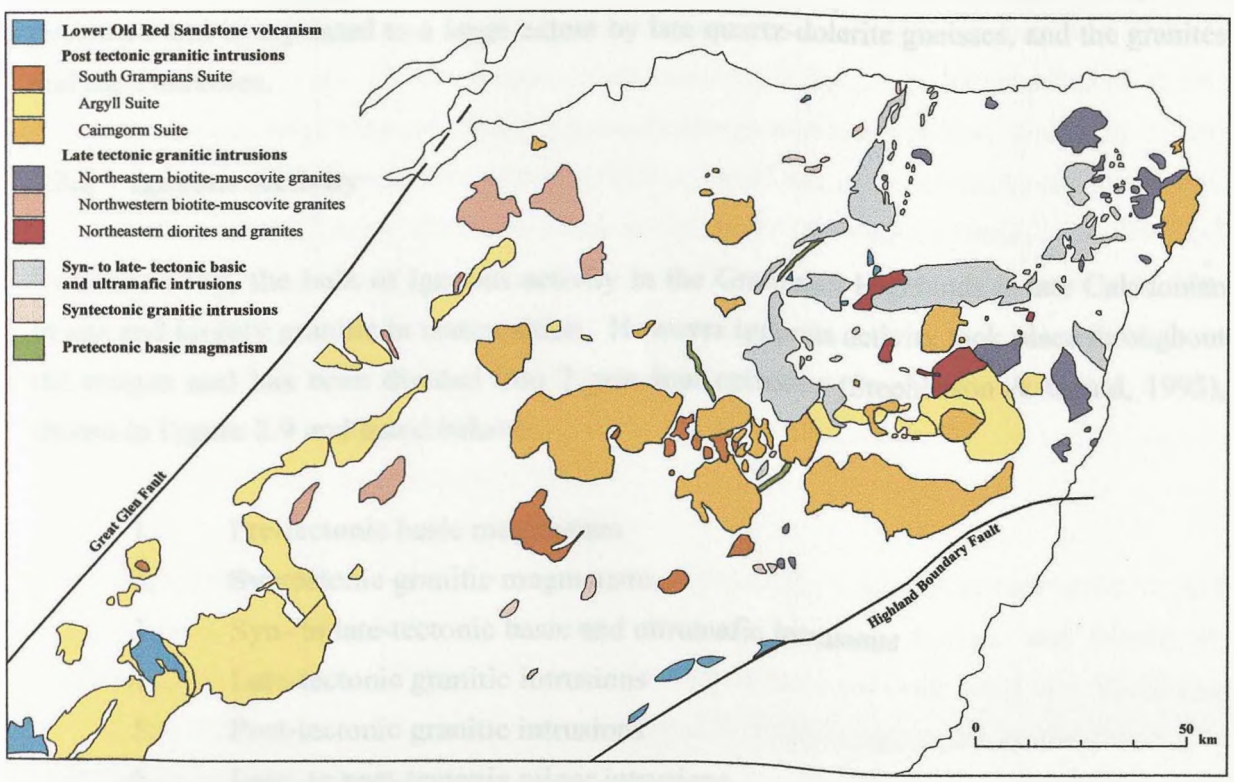


**Figure 2.9 Simplified map showing the distribution of igneous rocks in the Grampian Highlands (after Stephenson & Gould, 1995)**

The Buchan province has long been recognised as distinct from other provinces, being characterised by high heat flow (Harte & Hudson, 1979; Dempster *et al.*, 1995), while geobarometric studies on the aureoles of several of these bodies suggests that they were emplaced at pressures of approx. 4-5 kbar (Ashworth & Chinner, 1978; Droop & Charnley, 1985). Petrographic evidence (Chinner, 1960) from the country rocks adjacent to the gabbros shows sillimanite postdating and replacing regional kyanite and andalusite, suggesting that they were emplaced at or soon after the peak of metamorphism in the area. Outcrop patterns of metamorphic grade within the province are structurally controlled with the Turriff Syncline, shown on Figure 2.6, resulting in outcrop of lower grade rocks in its core (see Figure 2.8), although this outcrop pattern is also affected by erosion levels.

A similar pattern is seen in Connemara with broad increases in regional metamorphic grade from north to south, shown in figure 2.7. The lowest grade rocks are seen on islands to the northwest, while the highest-grade rocks, of sillimanite-alkali feldspar grade with associated migmatites, are found adjacent to the late granites in the south. Thermal overprinting associated with the assorted igneous suites is present through much of the region, with, locally, both the Dawros-Currywongaun-Doughruagh Complex and the Cashel-Lough Wheelaun Complex generating thermal aureoles; the Dawros-Currywongaun-Doughruagh aureole is more clearly defined as the aureole associated with the southern complex is deformed and overprinted to a large extent by late quartz-dolerite gneisses, and the granites and their aureoles.

### 2.2.6 Igneous Activity

Volumetrically, the bulk of igneous activity in the Grampian Highlands is late Caledonian in age and largely granitic in composition. However igneous activity took place throughout the orogen and has been divided into 7 principal episodes (Stephenson & Gould, 1995), shown in Figure 2.9 and listed below:

1. Pre-tectonic basic magmatism
2. Syntectonic granitic magmatism
3. Syn- to late-tectonic basic and ultramafic intrusions
4. Late-tectonic granitic intrusions
5. Post-tectonic granitic intrusions
6. Late- to post-tectonic minor intrusions
7. Lower Old Red Sandstone volcanism

Much of the *pre-tectonic basic magmatism* was contemporaneous with Dalradian sedimentation and, as mentioned before, resulted from high level rifting during deposition of the Argyll Group and later deposits. Minor volcanic deposits are widespread through the area, with the main extrusive activity in the Tayvallich-Loch Awe area; some of these lavas have been dated at 595±4 Ma (Halliday *et al.*, 1989). The *syntectonic granitic magmatism* is minor volumetrically and is concentrated in two regions, just west of the Portsoy Lineament and north of Tayside. One of the latter intrusions, the Ben Vuirich Granite, has yielded a U/Pb zircon age of 590±2 Ma (Rogers *et al.*, 1989). The *syn- to late-tectonic basic and ultramafic intrusions* are the subject of this study and will be discussed in greater detail in Chapters 4 and 5.

The *late-tectonic granitic intrusions* of the region have been subdivided into three suites, two S-type suites in the northeast (475-470 Ma) and the northwest (445-435 Ma), and an I-type diorite-tonalite suite (c. 453±3) in the northeast. One of these I-type diorites, the Kennethmont Complex, is emplaced within one of the syn- to late-tectonic basic intrusions, the Insch-Boganclogh basic mass (Stephenson & Gould, 1995). The main phase of igneous activity in the Grampian Highlands is represented by the *post-tectonic granitic intrusions*, which have been divided into three groups, the South Grampians Suite, the Argyll Suite and the Cairngorm Suite, all of which are I-type intrusions. The South Grampians Suite are a series of small dioritic to granitic plutons, linked to a series of northeast-trending faults in the southwest and southern Grampians, while the Argyll Suite are characterised by multi-phase or zoned complexes of tonalite-granodiorite-granite composition, found in central Aberdeenshire and in a northeast trending belt up to 50 km south of the Great Glen Fault. Some of these Argyll Suite intrusions, such as the Moor of Rannoch Granite and the Etive Complex, are among the largest in the Grampian Highlands. The Cairngorm Suite biotite-granites are located mainly in the central to northern Grampians; again, some of these granites, such as the Cairngorm and Mount Battock granites are quite substantial in size. These post-tectonic granitic intrusions are all thought to be of similar ages, emplaced at 420-395 Ma (Stephenson & Gould, 1995).

The *late- to post-tectonic minor intrusions* of the Grampian Highlands include appinites and lamprophyres in the eastern Grampians, and microdiorites, felsites and porphyries throughout the Grampian Highlands; some of the appinites have been dated at 429-422 Ma. This group of intrusions is not shown on Figure 2.9. Finally, *volcanism in the Lower Old Red Sandstone* is chiefly found in the SW Grampians at Glencoe and the Lorn Plateau lavas

(400±5 Ma), with minor extrusives in the northeast, the Highland Border region, and Kintyre.

Igneous activity within the Connemara Caledonides is more limited than in Scotland, and is shown in figure 2.2. Again, the bulk of the activity is in the form of late- to post-tectonic granitic intrusions mainly found bordering the Dalradian to the south. Four main phases of activity have been established in the region (Leake & Tanner, 1994):

1. Pre- to early volcanicity within the Dalradian
2. Syn-orogenic ultrabasic to basic bodies
3. Syn- to late orogenic quartz-dolerite gneisses
4. Late to post tectonic granites

The *pre- to early volcanicity* is present as regular, laterally impersistant, fine-grained amphibolites within the Appin and particularly Argyll groups of the Dalradian. The earliest intrusions in the region are the *syn-orogenic ultrabasic to basic bodies* represented by the Connemara Gabbros in both north and south Connemara. The main bodies are the two complexes which form the basis of this study, the Dawros-Currywongaun-Doughruagh and Cashel-Lough Wheelaun Complexes, but also the Errismore-Roundstone-Gowla intrusion and associated Ballyconneely Amphibolite in the southwest and numerous smaller associated bodies found adjacent to the main intrusions. The Errismore-Roundstone-Gowla body, the largest of these bodies is chiefly gabbroic in composition with faulting and shearing common. The adjacent Ballyconneely Amphibolite possibly represents a deformed later differentiate of the Errismore-Roundstone-Gowla body (Leake, 1989).

Recent dating suggests that a single probable *syn-tectonic granite*, the Oughterard Granite, is present within the Connemara region. Although its exact age is uncertain (radiometric dates vary from 473±7 Ma to 405±23 Ma), its actual age is probably around 462 Ma (Leake & Tanner, 1994, Friedrich *et al.*, 1999a). It is a multiply intruded pluton emplaced as three larger and numerous smaller bodies in southeast Connemara; it is not shown on figure 2.2, and has not been listed above.

Subsequent to these intrusions are the *syn- to late orogenic quartz-dolerite gneisses*, found mainly in southern Connemara. Although uncertainty exists as to a possible genetic relationship with the Connemara Gabbros (Leake, 1970a), it is clear that they postdate and inject the Gabbros and related country rocks, with the situation further complicated by the

late granites and their related migmatization, which appears to have been responsible for the gneissose nature of these quartz-diorites. A zircon U-Pb age from these quartz-diorite gneisses of $454 \pm {}^{6}_{14}$ Ma have been obtained from central southern Connemara, a time gap which implies a separate history from the Gabbros, a proposal also suggested geochemically by Leake (1989).

The final and largest intrusive phase of igneous activity in Connemara is the *late to post tectonic granites*. The majority of these intrusions were emplaced at c. 400 Ma and include the Omey and Inish Granites along the west coast, and the Roundstone Granite and the Galway Batholith along the southern Connemara margin. The Galway batholith is a complex intrusion, with numerous intrusive phases and a variety of rock types including granite, granodiorite, and adamellite, and is the largest intrusion in Connemara. Several smaller undated bodies south of Letterfrack in northern Connemara are assumed to be of similar age to the Galway batholith and thus part of the main post-tectonic suite of intrusions, despite being petrologically different to this suite.

Due to the limited nature of igneous activity in the Connemara region, each of the separate groups of igneous rocks cannot be satisfactorily correlated with the igneous phases in the Grampian Highlands. Pre-tectonic volcanism, syn-tectonic basic magmatism and voluminous late granitic magmatism are present in both regions, however, and a broad correlation can be drawn.

### 2.2.7 Summary

In general, the structural and metamorphic histories of orogenic belts are generally considered to be strongly linked and tend to follow a broad established pattern. However, in the Caledonides, specific correlations between structural and metamorphic events, and correlating these events to specific igneous episodes or suites has proved quite problematic. Broad correlations have been made for the orogenic history between the Grampian and Connemara Terranes, and their structural, metamorphic and igneous histories display many similarities. Two main phases of pervasive deformation ($D_1$ and $D_2$) and accompanying metamorphism are recognised in both regions. In the Grampian Highlands east of the Portsoy Lineament, the metamorphic mineral assemblages are characteristic of low-pressure conditions. Although there is some uncertainty, the 'Younger' Gabbros of the Grampian Highlands and the two complexes in Connemara are believed to have been emplaced around $D_2 - D_3$ times, while late-tectonic granites are thought to have been intruded around $D_3$ or

soon after. Late open folding accompanies decreasing pressures and temperatures ($D_4$) and denotes the end of orogenic activity, while brittle structures and retrogressive metamorphism related to post orogenic collapse and/or uplift are associated with post-tectonic granites. Despite uncertainty over some of the precise correlations, there is general acceptance that the 'Younger' Gabbros are related, and were emplaced into similar positions within the orogeny. However, correlations of igneous suites are complicated by many of the problems encountered in correlation of structure and metamorphism such as conflicting field evidence and radiometric ages, as will be discussed next.

## 2.3 The age of the bodies

For quite a few years, there have been significant inconsistencies in the correlations between stratigraphical, palæontological and radiometric ages for events within the Caledonides. To a large extent, the problem lies in the linking of radiometric evidence for whole rock ages, and for mineral cooling and blocking temperatures with a variety of other data sources. Many of the minerals and rocks chosen for radiometric dating contain varying proportions of inherited components from previous events; samples containing these inherited components yielded ages that now appear to be significantly older than the actual event. In the past ten years or so, radiometric dating techniques and their associated accuracy have advanced considerably. However, the vast bulk of radiometric ages for the Caledonides present in the literature, including many of the ages mentioned in this chapter, are more than 10 years old; as a result, the accuracy of many of these dates must be considered suspect.

Recent, more accurate, re-dating of several of these bodies highlights this problem: intrusions with ages that were previously assumed reliable are now being found to be significantly younger. One of the most striking examples of this is the age of the Grampian Orogeny itself. As recently as the last five years, authors have attempted to fit complex structural and metamorphic histories around radiometric dates from the associated igneous rocks. Ages from these bodies varied from 510 Ma to 490±1Ma (Jagger *et al.*, 1988) in Connemara and 491±6 to 476±5 Ma in the Grampian Highlands (Brown *et al.*, 1965), with the majority of the data around 490 Ma. Diachroneity in magmatic, metamorphic and structural evolution was invoked to explain this apparent spread in ages, particularly in Connemara, and some stratigraphic and palæontologic evidence was ignored or discounted. However, in the recent years, revised radiometric ages have shown both the Grampian and Connemara bodies to be around 470-472 Ma in age (see Table 2.1). These ages imply the

gabbroic suites in both terranes are largely contemporaneous and agree with structural and metamorphic dating evidence from the Scottish Highlands (Oliver, 2001), as well as a wealth of stratigraphical and palæontological evidence in both regions, and also with some of the discounted evidence (Downie, 1971; Molyneux, 1998). Consequently, the Grampian Orogeny is now believed to be a brief (15 - 10 Ma or less) event that took place around the Arenig-Llanvirn boundary (Friedrich *et al.*, 1999a, 1999b; Oliver *et al.*, 2000; Oliver, 2001).

As mentioned, the radiometric ages of many of the igneous phases in the Caledonides must be treated with extreme caution, with some of the *late-tectonic granitic intrusions*, which clearly postdate the 'Younger' Basics in the field displaying older radiometric ages. For example, the minor Ardlethen biotite-granite related to the Strichen biotite-muscovite-granite (476±5; Pidgeon & Aftalion, 1978) crosscuts the 'Younger' Arnage mass (Stephenson & Gould, 1995), which is likely to have an age close to 470 – 472 Ma, similar to the other 'Younger' Basics.

| Intrusion | Age (Ma) | Reference |
|---|---|---|
| Insch | 468 ± 8 | Rogers *et al.* (1994) |
| Insch | 470 ± 9 | Dempster *et al.* (2002) |
| Morven Cabrach | 472 | Rogers *et al.* (1994) |
| Morven Cabrach | c. 470 | Dempster *et al.* (2002) |
| Currywongaun | 474.5 ± 1.0 | Friedrich *et al.* (1999a) |
| Cashel-Lough Wheelaun | 470.1 ± 1.4 | Friedrich *et al.* (1999a) |

**Table 2.1 Recent ages for 'Younger' Basics bodies in northeast Scotland and Connemara. All of these dates have been acquired using high precision U-Pb zircon techniques.**

The precise age of the Dalradian rocks of the Grampian Highlands has also long been a source of uncertainty and confusion. Rare microfossils from the Argyll group yield an Upper Riphean to Vendian age (Downie *et al.*, 1971) but other palæontological evidence is at best controversial and has failed to become widely accepted, although this may be due in no small part, to the inconsistencies in the igneous dates. Radiometric dating has also been used on certain units within the Dalradian Supergroup; the oldest generally accepted dates coming from a pegmatitic fault zone near the base of the Grampian Group which, it is believed, formed during early shearing. These syntectonic pegmatites and quartz-muscovite

veins have been dated at 750 Ma using Rb/Sr mineral ages (Piasecki & van Breemen, 1979). The Port Askaig Tillite at the base of the Argyll is strongly believed to be synchronous with the Scandinavian Varanger Tillite, which has been dated, also using Rb/Sr methods at 653 Ma (Pringle, 1972), although recent chemo-stratigraphic correlations (Brasier & Shields, 2000) suggest the tillite may in fact be Sturtian (c. 723 Ma). Lavas at the top of the Argyll have been dated using U-Pb zircon dating at 595 Ma (Halliday *et al.*, 1989). For many years it was thought possible that, given rapid accumulation of the Southern Highland Group, the entire Dalradian Supergroup was Precambrian, although it is now generally accepted that there is stratigraphic continuity between the uppermost Dalradian units and the Lower Cambrian Leny Limestone (Pringle, 1940; Tanner, 1995), and indeed an Ordovician age has been proposed for an acritarch from a Southern Highland Group slate (Molyneux, 1998). In more recent years, efforts have concentrated on establishing the time span of the Supergroup as a whole and ascertaining if it is a continuous sequence of deposits or if there are any major unconformities within the succession (Prave, 1999; Tanner & Bluck, 1999; Dempster *et al.*, 2002).

## 2.4 Summary

The 'Younger' Gabbros have been placed within a stratigraphic, structural and metamorphic context within the Caledonian Orogeny as a whole. They are found within broadly similar positions within the Dalradian stratigraphy of the Laurentian margin and display similar structural and metamorphic relationships and histories in both the Grampian Highlands and in Connemara. Despite the complex evolutionary history of the Caledonian Orogeny, the intrusions can be seen to have many features in common; they are of quite similar age and are closely associated with the relatively brief Grampian Orogeny, an arc accretion event that occurred during Arenig to Llanvirn times.

# Chapter 3 Country Rocks

## 3.1 Introduction

It has long been accepted that assimilation and melting of country rocks, particularly those of a pelitic and semi-pelitic nature, are an important process involved in the evolution of the 'Younger' Gabbros of the Grampian Highlands and Connemara (Read, 1923b; Gribble 1967, 1968). In general, the main factors controlling the amount of partial melting and assimilation that takes place in a magma chamber are the temperature of the magma, and the temperature and composition of the country rock material. Magmas of basaltic composition, such as the magmas that are likely to have formed these intrusions, are generally intruded at quite high temperatures; evidently, magmas with higher temperatures possess greater thermal energy to enable partial melting to take place. The temperature of the country rock material is also an important factor, with cold wall rocks less susceptible to partial melting processes, while assimilation and contamination of country rock material is greatly enhanced if the country rock has a low fusion temperature.

If partial melting does take place, the melted fraction of pelitic material will normally be close to granitic in composition (Tuttle & Bowen, 1958), thus adding $SiO_2$, $Al_2O_3$ and alkalis to the magma, while leaving a depleted country rock residuum in the form of a hornfels or xenolith; this melting process can also be enhanced by the presence of water in the country rocks. If the level of melting is sufficiently advanced, reaction between the magma and country rock may be complete or close to complete, resulting in complete assimilation of the country rock, and the presence of a complete spectrum of country rock material, from unaltered country rock, through partially assimilated xenoliths, to fully assimilated country rock in the form of contaminated igneous rocks. Assimilation by mechanical breakdown of the country rock material is also possible. In such a scenario, melting does not occur and the individual crystals from the country rock are incorporated into the magma and resultant rocks. While this process may occur locally, the highly fusible nature of pelites, and the increase in contamination with evolution of the suite suggest that country rock melting is the dominant process responsible for the contamination.

The 'Younger' Basic bodies and their envelope rocks exhibit evidence for all of the conditions for melting described above. Although the actual temperature of emplacement

of these bodies has not been estimated, the temperature range of typical basaltic magmas at the time of emplacement at mid-crustal levels is likely to be in the region of 950 to 1100°C; such temperatures are considered sufficiently high to partially melt the country rocks of a body, particularly if they are pelitic or semi-pelitic in composition (Huppert & Sparks, 1985). The intrusions were emplaced at mid-crustal levels, within upper Dalradian sequences in which, as outlined in Chapter 2, rocks of a pelitic and semi-pelitic nature predominate. Extensive metamorphism and deformation of the Dalradian has been described from the northeast of Scotland (Fettes, 1970; Ashworth, 1975; Fettes *et al.*, 1985; Dempster *et al.*, 1995), with estimated pressure and temperature histories of the immediate country rocks (Ashworth & Chinner, 1978; Droop & Charnley, 1985; Wellings, 1998) suggesting a prolonged period of cooling, while emplacement of the bodies is largely believed to be close to synchronous with the peak of these metamorphic conditions. Consequently, the ambient temperature of the country rocks at the time of emplacement is likely to have been quite high. In addition, pelitic material is generally considered to possess quite low fusion temperatures and, as a result, tends to be quite easily melted under such conditions, particularly in the presence of water; the average LOI value in unhornfelsed pelitic schist samples is close to 2%. Field evidence for varying degrees of assimilation of these pelitic country rocks by the 'Younger' Basics is widespread, while existing geochemical evidence also points to significant levels of contamination; this evidence will be outlined in the next section.

This chapter will present the geochemistry of these country rocks in an attempt to assess their potential influence on the evolution of the intrusions, specifically the role of country rock contamination in the evolution of the bodies, which will be discussed in greater detail in later chapters. The details of the country rocks are not the main focus of this thesis and they have not been studied in detail. Consequently, much of the overall descriptions of the country rocks, and their relationship to the intrusions in the field, are based on published material, while mineralogical descriptions are based on a combination of published work and this study.

## 3.2 Previous research

There have been numerous studies of the 'Younger' Basics that demonstrate the contaminated nature of the bodies, both in northeast Scotland and in Connemara, using primarily field and thin section evidence. The northeastern bodies of Maud, Kinnadie, Arnage and Haddo in particular are regarded as classic examples of intrusions that have

assimilated large quantities of pelitic country rock during their evolution (Read, 1923b, 1935; Read & Farquhar, 1952; Gribble, 1966, 1967, 1968, 1970; Gribble & O'Hara, 1967). Several of these studies have also noted evidence for partial melting of the country rocks adjacent to the intrusions. Evidence for contamination is also present in the Central Intrusions (Read *et al.*, 1965; Clarke & Wadsworth, 1970; Busrewil *et al.*, 1973; Leslie 1984; Munro, 1986a) and the northwestern bodies (Weedon, 1970; Munro, 1970, 1984; Munro & Gallagher, 1984; Fletcher, 1989; Gunn *et al.*, 1996). Although the Morven Cabrach body is less well studied, field evidence for contamination has nevertheless been identified (Allan, 1970), while in Connemara, several field studies (Rothstein, 1957, 1958; Leake, 1958a, 1970b; Kanaris-Sotiriou & Angus, 1976) have shown evidence for significant degrees of contamination in both the northern and southern intrusive complexes. The regional studies of Read (1923a, 1935) and Stephenson & Gould (1995) in the Grampian Highlands, and Leake & Tanner (1994) in Connemara, have also identified contamination as a significant feature common to the bodies as a whole.

Geochemical approaches have also been taken to show that contamination is a significant process operating during the evolution of these bodies. The most significant of these studies (Gribble & O'Hara, 1967; Gribble, 1968, 1970) has shown that the pelitic country rocks of the Haddo and Arnage bodies have undergone partial melting at the time of intrusion of the igneous bodies. These investigations, in the CMAS phase system, have shown that these partially melted country rocks, which commonly contain cordierite, plot as a separate group to the original igneous rocks, which themselves are also considerably contaminated. Xenoliths in the cordierite-bearing rocks were considered to represent an infusible or restite-type material from the original country rock. These partially melted, cordierite-bearing rocks were also identified locally in the aureoles of the Insch and Huntly masses.

However assessing contamination using major element chemistry is more difficult, as while rocks with higher $SiO_2$, $Na_2O$ and $K_2O$ content can occur as a result of contamination, they can also result from simple igneous fractionation, or a combination of these two processes. Nevertheless, Gribble (1967) interpreted increased silica and alkali abundances in the Arnage and Haddo masses (in conjunction with field and thin section evidence) to represent contamination, resulting in a quartz-normative trend. Leake & Skirrow (1960), Gribble, (1967) and Evans (1964) have also attempted to show the effects, geochemically, of partial or complete assimilation, on the composition of the resultant rocks. The $^{87}Sr/^{86}Sr$ isotope studies of Pankhurst (1969, 1970) and Busrewil *et al.* (1973) have also shown that

contamination is likely to have played an important role in the evolution of at least the Insch-Boganclogh and Haddo/Arnage bodies. These bodies show strong increases in $^{87}Sr/^{86}Sr$ ratios with increasing evolution. Two theories have been proposed to explain these high isotopic ratios, with Busrewil *et al.* (1973) suggesting that they can be attributed to circulating fluids causing isotopic exchange with high $^{87}Sr/^{86}Sr$ country rocks during the cooling and crystallization of the body. There is, however, little evidence for hydrothermal systems in these bodies (Hall, 1996) and, in addition, it is difficult to account for the progressive rise in $^{87}Sr/^{86}Sr$ ratios with evolution of the bodies without invoking contamination. Wholescale melting and/or assimilation of the high $^{87}Sr/^{86}Sr$ ratio pelitic schist aureole has also been proposed (Gribble & O'Hara, 1967), and is considered to be a more likely explanation (Hall, 1996). This will be discussed in more detail in Chapter 6.

As discussed in Section 2.2.5, the northeast Grampian metamorphic province typically displays high heat flow conditions resulting in low-pressure, high-temperature metamorphism (Dempster *et al.*, 1995; Harte & Hudson, 1979), with granulite-facies contact rocks associated with the gabbros representing the highest grade rocks seen within the region, while partial melting and migmatization occurs locally (Ashworth, 1976; Gribble, 1968). Pressure and temperature estimates (Ashworth & Chinner, 1978; Droop & Charnley, 1985) based on mineral assemblages and compositions in the aureole rocks suggest that the Scottish intrusions were emplaced at mid-crustal levels of 4-5 kbar, with both the intrusions and their country rocks undergoing a slow and complex cooling history (Chinner, 1966; Dempster et al., 1995; Wellings, 1998), thus allowing considerable time for potential assimilation of country rock material.

## 3.3 Sample description and location

The country rock samples analysed as part of this study have been separated into three main groups, which are outlined in Table 3.1. The first group are pelitic schists which are largely unaffected by the thermal metamorphism associated with the intrusions; these have been classed as Type A country rocks and also contain some more psammitic samples. The second group, Type B country rocks, are hornfelses and xenoliths which display little or no evidence for mineralogical or chemical change, while the third group represents those hornfelsed and xenolithic samples displaying evidence for partial melting or whole rock chemical change; these are Type C country rocks. Leucosomes and desilicated hornfelses or xenoliths are included within this group. To a large extent, the division between the groups is somewhat arbitrary with the range of samples and their thermal effects are

gradational in nature; for example, several samples classed as Type B could also have been classed as Type C. The main purpose of these subdivisions is to highlight the increasing overall effects of country rock assimilation on the country rocks and, in later chapters, on the igneous rocks themselves. The locations of these country rock samples are shown in Chapter 4 in figures 4.3 to 4.9. Broadly speaking, much of the envelope to the bodies consists of upper Argyll and Southern Highland Group turbidites, slates and phyllites, with minor associated basic rocks. As mentioned in Chapter 2, inherent difficulties in the correlation of pelitic and semi-pelitic rocks, combined with poor exposure and high degrees of shearing in the region, mean that the precise Dalradian stratigraphical relations are unclear in the immediate vicinity of many of the intrusions. Consequently, attempts to assign individual samples to precise stratigraphical units are considered to be both unnecessary and beyond the scope of this project.

| Rock Type | Total samples |
|---|---|
| **Type A : Unaffected country rocks** | |
| Pelitic Schists: | 11 |
| Psammites | 3 |
| **Other lithologies** | |
| Basalts + Amphibolites | 1 + 1 |
| **Type B : Samples with little evidence for partial melting** | |
| Hornfelses | 19 |
| Xenoliths | 6 |
| **Type C : Samples with evidence for partial melting** | |
| Hornfelses | 9 |
| Xenoliths | 6 |
| Leucosomes | 3 |
| **Total** | **59** |

**Table 3.1 Summary of country rock lithologies sampled**

### 3.2.1 Type A unaffected country rocks (pelitic schists)

Numerous structural and metamorphic studies of regional metamorphism of the Dalradian have been undertaken and were discussed briefly in Chapter 2. It is well established that

those Dalradian country rocks not strongly affected by metamorphism and deformation associated with the igneous bodies have nevertheless undergone several phases of metamorphism of a regional nature, resulting in high levels of deformation and metamorphic mineral growth. Shearing related to the 'Younger' Basics is found locally within the unaffected schists. Although pelitic material tends to predominate lithologically, the nature of many of the original sediments means that in many areas, these pelites may be found interleaved, on quite a fine scale, with semi-pelitic and psammitic material.

Type A pelitic schists are mainly composed of varying proportions of quartz, plagioclase feldspar (usually oligoclase to andesine in composition), microcline, an iron oxide phase, and biotite, with the presence or absence of phases such as almandine garnet (see Plate 3.1), staurolite, and sillimanite dependant on the regional grade to which the sample has been metamorphosed. Atherton & Brotherton (1982) have noted that there is no systematic chemical difference between the chemistry of Dalradian pelites on the basis of their metamorphic grade, and that any variations evident between rocks in different metamorphic zones is likely to be as a result of original compositional variations. In thin section (see Plate 3.1), the schists are quite fine grained; quartz is typically a mosaic of strained or recrystallised crystals, and often it is difficult to distinguish between recrystallised vein quartz which is abundant, and quartz of sedimentary origin.

Biotite tends to define the schistosity of the rock and can comprise 30-40% of the rock, while feldspar is often also present as porphyroblastic growths, which are predominantly oligoclase in composition. Locally, many of the schists grade into what might be termed pelitic gneisses, with oligoclase augen common, but, for simplification, these more gneissic samples have been classified with the pelitic schists. White mica is commonly present in lower grade schists, while iron ore is also present in minor quantities. Where present, phases such as garnet, staurolite, andalusite and kyanite are usually found as typical porphyroblastic overgrowths (see Plate 3.1), and define the regional grade of metamorphism. Quartz veining is common within Dalradian schists, while late stage hydration and alteration is frequently found, with retrograde chlorite after biotite and sericite after feldspar common. Eleven samples classed as pelitic schists (Type A) have been analysed; five of these have also been analysed for REE.

Pelitic schists form the main country rock found adjacent to the 'Younger' Basics intrusions, although, as mentioned above, local semi-pelitic and psammitic horizons are present within these pelites. Three samples of a more psammitic composition have been

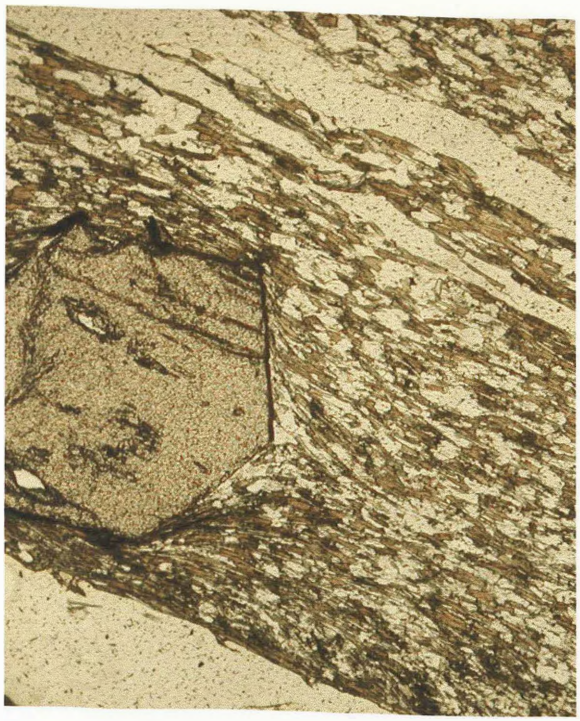

Plate 3.1 (a) PPL

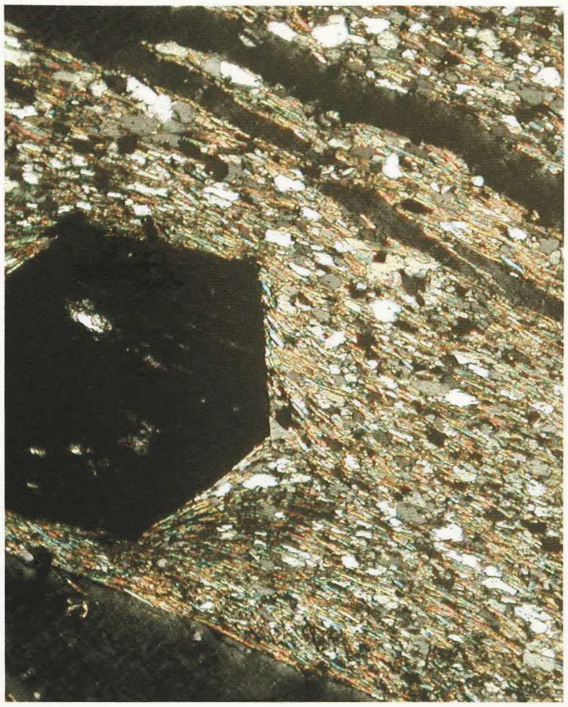

Plate 3.1 (b) XPL

**Plate 3.1 Sample MS1504, a typical Dalradian schist from near the Succoth-Brownhills mass. Consists mainly of biotite, showing well developed foliation, quartz and feldspar. Fine quartz veining and late porphyroblastic garnet are also present. Vertical scale = 1.6 mm.**

Plate 3.2 (a) PPL

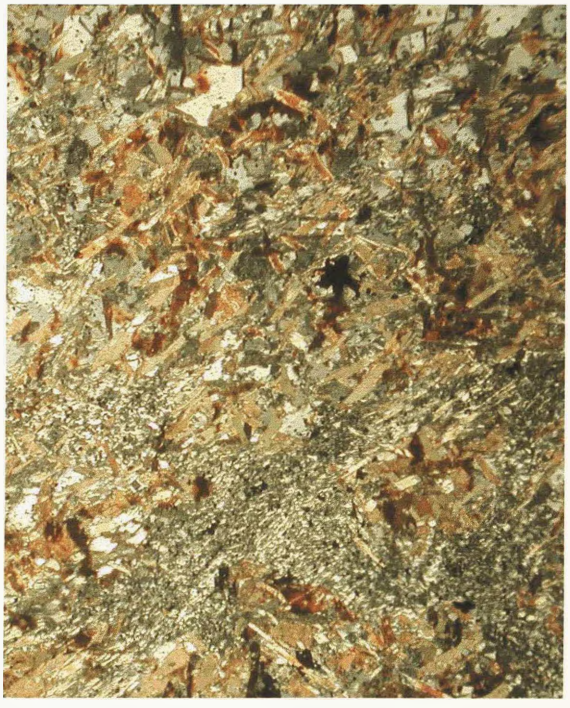

Plate 3.2 (b) XPL

**Plate 3.2 Sample Ab121, a cordierite-biotite hornfels from the aureole of the Belhelvie mass. A slight increase in grain size and biotite content is accompanied by a loss of foliation and decrease in quartz content. Vertical scale = 1.6 mm.**

analysed; in many respects, these are simply more silica-rich equivalents of the pelites, and display many characteristics in common with them. Consequently they will be classed as a part of the overall Type A group.

### 3.2.2 Other country rocks

Although shearing has substantially disrupted the intrusive margins, it is evident that pelitic and semi-pelitic material is the main country rock into which the intrusions have been emplaced. Local quartzites and limestones are occasionally found within these pelitic sequences, but not in any great abundance and have not been sampled. Experimental and field studies suggest that wholescale melting of quartzite is unlikely to occur under such conditions. The only other lithologies present in any significant quantity within the country rocks are local amphibolitic and basaltic material. The amphibolites are generally found as minor elongate intrusive pods or lenses, usually concordant with the bedding and foliation in the Dalradian. Although they may be quite abundant locally, they are a relatively minor component of the Upper Dalradian overall. The basaltic units in the Grampian Highlands are mainly present as lavas and tuffs, and are quite substantial in the Tayvallich-Loch Awe area to the southwest; however these units thin considerably away from this area and are present only as minor deposits in the northeast. One sample of each of these basic country rocks has been analysed; the amphibolite sample is quite coarse grained and garnet bearing, while the basalt is medium to fine grained, although extensive alteration makes it difficult to identify the mineralogy precisely.

### 3.2.3 Type B country rocks, with little or no evidence for partial melting

#### Hornfelses

The effects of the thermal metamorphism on the country rocks adjacent to the 'Younger' Basics is quite pronounced. Schistosity gives way to hornfelsed textures (Plate 3.2) as the contact is approached, usually accompanied by a slight increase in grainsize, and higher grade metamorphic assemblages tend to accompany this thermal metamorphism, with sillimanite overprinting of regional phases such as kyanite and andalusite common in both Connemara (Rothstein, 1957; Leake & Skirrow, 1960) and Scotland (Chinner, 1966; Ashworth, 1975). The shearing which is found locally within the unaffected schists, and believed to be connected with the emplacement of the masses, tends to increase as the contacts are reached, often resulting in sheared and mylonitized contact zones. In some

cases this shearing is quite extreme and hornfelsed material can be found several kilometres from the nearest intrusion (Stephenson & Gould, 1995), while conversely, unaffected pelitic schists can be found juxtaposed with country rocks such as in the margins of the Currywongaun body. The composition of these hornfelsed rocks is largely dependant on the original lithology, and generally tends to be pelitic in nature, although several quartz-rich hornfelses have also been sampled. Again, quartz, feldspar and biotite tend to predominate, with minor quantities of cordierite (see Plate 3.2), spinel, sillimanite, corundum, garnet and orthopyroxene (Read, 1935; Leake, 1958; Gribble 1968) often present. Nineteen Type B hornfelses in which evidence for desilication or partial melting is minimal have been analysed.

**Xenoliths**

In the field the most common evidence for contamination is the presence of xenolithic material within the bodies. Although generally most abundant adjacent to the margins of the bodies, xenoliths of varying size and composition may be found throughout the bodies (Gribble, 1967; Fletcher, 1989; this study). In many respects, this xenolithic material is similar to the hornfelses, with features such as internal shearing and hornfelsed textures common. Abundances of xenoliths are variable, with some of the bodies (e.g. the northeastern bodies) commonly containing xenoliths and others (e.g. Insch, Dawros) only containing minor amounts, although in many instances, poor exposure makes this difficult to establish with any degree of certainty. Interestingly, the high $^{87}Sr/^{86}Sr$ ratios indicative of contamination (Pankhurst, 1969) are not restricted to xenolith rich facies from the northeastern bodies of Arnage and Haddo, but are also found in the relatively xenolith free Insch and Boganclogh masses. The majority of xenoliths are pelitic or semi-pelitic in origin, reflecting the predominant envelope rock type, although Gribble (1968) has commented that 'the conspicuous appearance of the argillaceous types' may be responsible for this apparent predominance in the field. Occasional quartz-rich xenoliths are also found; many of these are unmelted Dalradian quartzite xenoliths or vein quartz that has separated from pelitic xenoliths, and several have been included in the database. Xenolith sizes are variable, generally from ~5cm (Read, 1923a, 1935; Gribble, 1968; this study) down to thin section scale, although larger xenoliths are occasionally found, such as in Huntly (Fletcher, 1989) and Connemara. Pelitic and semi-pelitic xenoliths are generally similar to hornfelsed material, with varying combinations and quantities of the minerals quartz, biotite, both feldspars, iron ore and regional metamorphic phases, while minor quantities of cordierite, spinel, sillimanite, corundum, and orthopyroxene may also be present (Read, 1935; Leake,

1958; Gribble 1968). Six Type B xenoliths that do not appear to have been significantly affected by partial melting or desilication have been analysed.

### 3.2.3 Type C country rocks, with evidence for partial melting

As mentioned, one of the most striking features of the contact zone is the level of shearing and accompanying mylonitization in the vicinity of the bodies. Locally these hornfelses show evidence in the field and thin section for desilication and/or partial melting, most notably in the aureole rocks of the northeastern bodies of Belhelvie, Arnage and Haddo (Gribble, 1967, 1968, 1970), but also locally adjacent to the Insch, Haddo, Arnage and Portsoy bodies (Read, 1923a; Gribble, 1970; Ashworth, 1976).

Desilication and/or partial melting tends to be gradational in nature and mineralogically, is shown by decreases in quartz, feldspar and biotite which are generally accompanied by increases in the abundance of iron oxides, and the development of phases such as sillimanite, orthopyroxene, spinel and, notably, cordierite (see Plate 3.2) and corundum. The loss of $SiO_2$ in the country rocks is likely to represent the initial fusion of the country rock, with melting probably occurring at quartz–feldspar interfaces, in accordance with the theories of Tuttle & Bowen (1958). Cordierite is increasingly abundant as the contact is approached in these areas, and is considered to be indicative of partially melted country rock (Gribble & O'Hara, 1967), while in samples in which partial melting has progressed further, corundum and spinel tend to develop; again, the presence of corundum is regarded as being indicative of partial melting (Tindle & Pearce, 1983). Hornfelsed and xenolith material in this group share most of the above features, with the xenoliths generally displaying more extreme degrees of melting than the hornfels, as is to be expected. The number of samples from this group are summarised in Table 3.1. Fifteen samples displaying evidence for desilication or partial melting have been sampled, including migmatitic and hornfelsed material and xenoliths, in addition to three partially melted leucosome samples. All have been classified as Type C country rocks.

The natural end members of this sequence from unaffected country rock pelitic schists, through hornfelses and xenoliths exhibiting various partial melted features, are contaminated gabbros. Again the boundary between partially melted metasediments and actual contaminated gabbros is somewhat obscure, but any samples in which there is no direct evidence of contamination (e.g. cordierite, restitic material etc.) have been classed as igneous, and will be discussed in subsequent chapters. As will be seen, many of these

igneous samples display mineralogical and whole rock geochemical evidence for contamination by country rock material. Assimilation of partial or complete melts of pelitic material usually has an effect on abundances of the constituent minerals in the resultant contaminated rock. The addition of silica results in the formation of orthopyroxene at the expense of olivine both in norm and modal abundances, while the addition of $Al_2SiO_5$ causes plagioclase to crystallize at the expense of clinopyroxene. Also, addition of $Na_2O$ and $K_2O$ should lead to the formation of additional biotite and/or amphibole in the rock. As a consequence, examination of the modal and norm compositions of contaminated gabbros or norites, and in particular comparison with comparable gabbroic rocks in which contamination is believed to have played less of a role in their formation, should reveal systematic differences in mineral abundances, specifically in the relative abundances of these main silicate phases. This will be examined in more detail in Chapters 4 & 6.

## 3.3 Chemistry

### 3.3.1 Introduction

Previous chemical work on Dalradian metasediments has concentrated largely on major element analysis, with limited published trace element analyses available. The main relevant published data are those of Atherton (1977), Atherton & Brotherton (1982), and Lambert *et al*, (1981, 1982) in the Grampian Highlands, and Evans (1964) and Ferguson & Al Ameen (1986) in Connemara, although analyses are present in numerous other publications. In addition, Pankhurst (1969) and Dempster *et al.*, (1995) have carried out isotopic studies of northeastern Dalradian pelites. The study of Atherton & Brotherton (1982), in particular, has examined the major element compositions of Dalradian in detail and concluded that, while there is substantial deviation within the data from the Dalradian in the northeast Grampian Highlands, no systematic differences were present in the data in terms of stratigraphy, location or metamorphic grade. Fifty-nine samples have been analysed for major and trace elements, with a limited number of REE analyses also carried out on the samples, and the data are presented in Appendix C.

### 3.3.2 Major Elements

Country rock major element data are shown plotted on a TAS plot in figure 3.1. Although it is not appropriate to represent country rocks on this plot, it is useful for examining the chemistry of these rocks, the differences between the various rock types, and also their

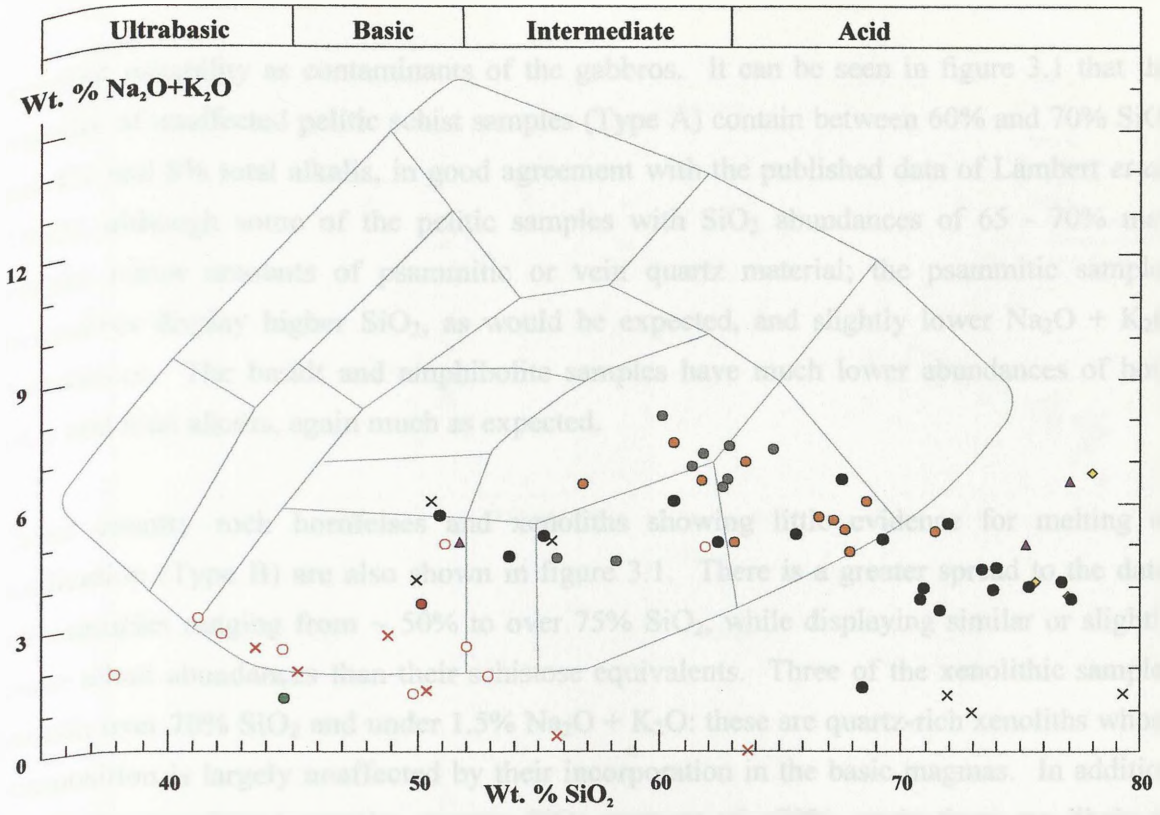


**Figure 3.1 TAS plot of country rocks from the Upper Dalradian of northeast Scotland and Connemara. Published schist values from Lambert *et al.* (1982).**

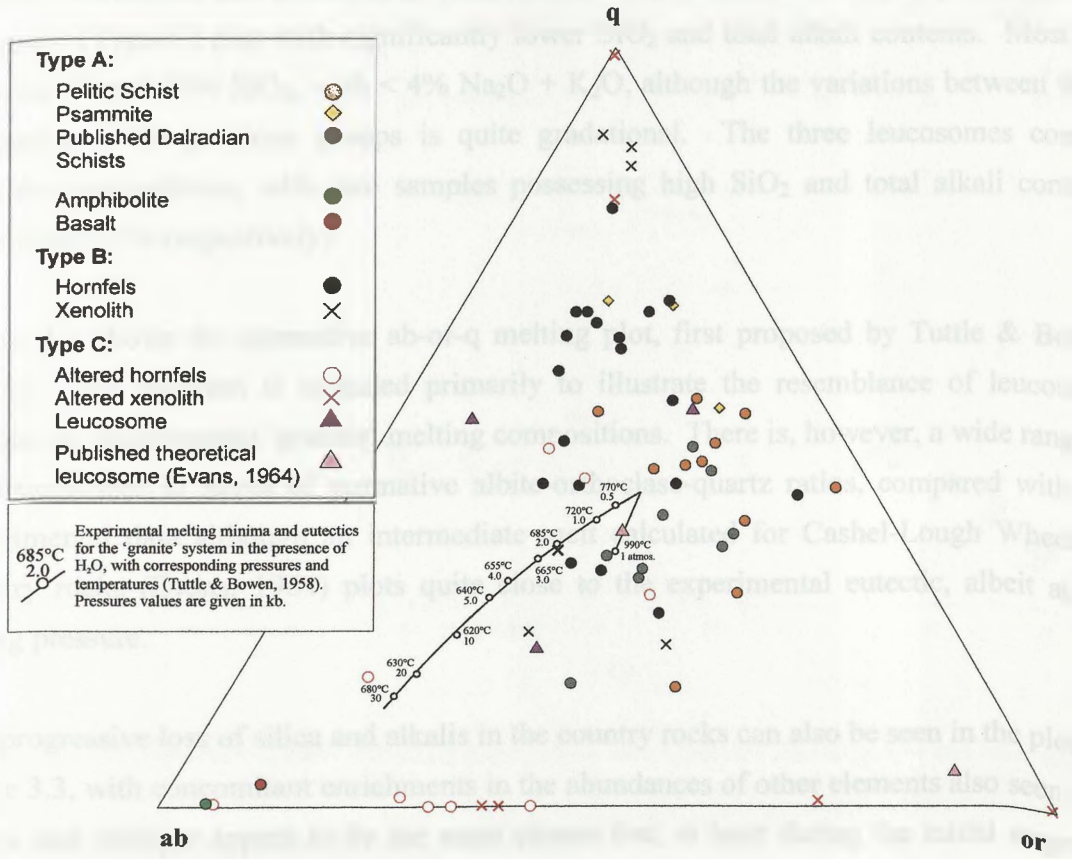


**Figure 3.2 Albite-quartz-orthoclase plot of country rocks from the Upper Dalradian of northeast Scotland and Connemara.**

potential suitability as contaminants of the gabbros. It can be seen in figure 3.1 that the majority of unaffected pelitic schist samples (Type A) contain between 60% and 70% $SiO_2$ and 4% and 8% total alkalis, in good agreement with the published data of Lambert *et al.* (1982), although some of the pelitic samples with $SiO_2$ abundances of 65 - 70% may contain minor amounts of psammitic or vein quartz material; the psammitic samples themselves display higher $SiO_2$, as would be expected, and slightly lower $Na_2O + K_2O$ abundances. The basalt and amphibolite samples have much lower abundances of both $SiO_2$ and total alkalis, again much as expected.

Those country rock hornfelses and xenoliths showing little evidence for melting or desilication (Type B) are also shown in figure 3.1. There is a greater spread to the data, with samples ranging from ~ 50% to over 75% $SiO_2$, while displaying similar or slightly lower alkali abundances than their schistose equivalents. Three of the xenolithic samples contain over 70% $SiO_2$ and under 1.5% $Na_2O + K_2O$: these are quartz-rich xenoliths whose composition is largely unaffected by their incorporation in the basic magmas. In addition ten of the hornfelsed samples contain $SiO_2$ contents of >70%; again these are likely to represent hornfelsed psammitic material or pelitic material in which fine vein quartz was present. Hornfelses and xenoliths in which evidence for desilication and/or partial melting is present (Type C) plot with significantly lower $SiO_2$ and total alkali contents. Most fall between 40 and 55% $SiO_2$, with < 4% $Na_2O + K_2O$, although the variations between these samples and the previous groups is quite gradational. The three leucosomes contain variable compositions, with two samples possessing high $SiO_2$ and total alkali contents (>75% and >5% respectively).

Figure 3.2 shows the normative ab-or-q melting plot, first proposed by Tuttle & Bowen (1958). This diagram is included primarily to illustrate the resemblance of leucosome samples to experimental 'granite' melting compositions. There is, however, a wide range to the leucosomes in terms of normative albite-orthoclase-quartz ratios, compared with the experimental data although an intermediate melt calculated for Cashel-Lough Wheelaun country rocks (Evans, 1964) plots quite close to the experimental eutectic, albeit at the wrong pressure.

The progressive loss of silica and alkalis in the country rocks can also be seen in the plots in figure 3.3, with concomitant enrichments in the abundances of other elements also seen. As quartz and feldspar appear to be the main phases lost, at least during the initial stages of partial melting, total normative quartz and feldspar $(q+ab+or)_N$ has been plotted against

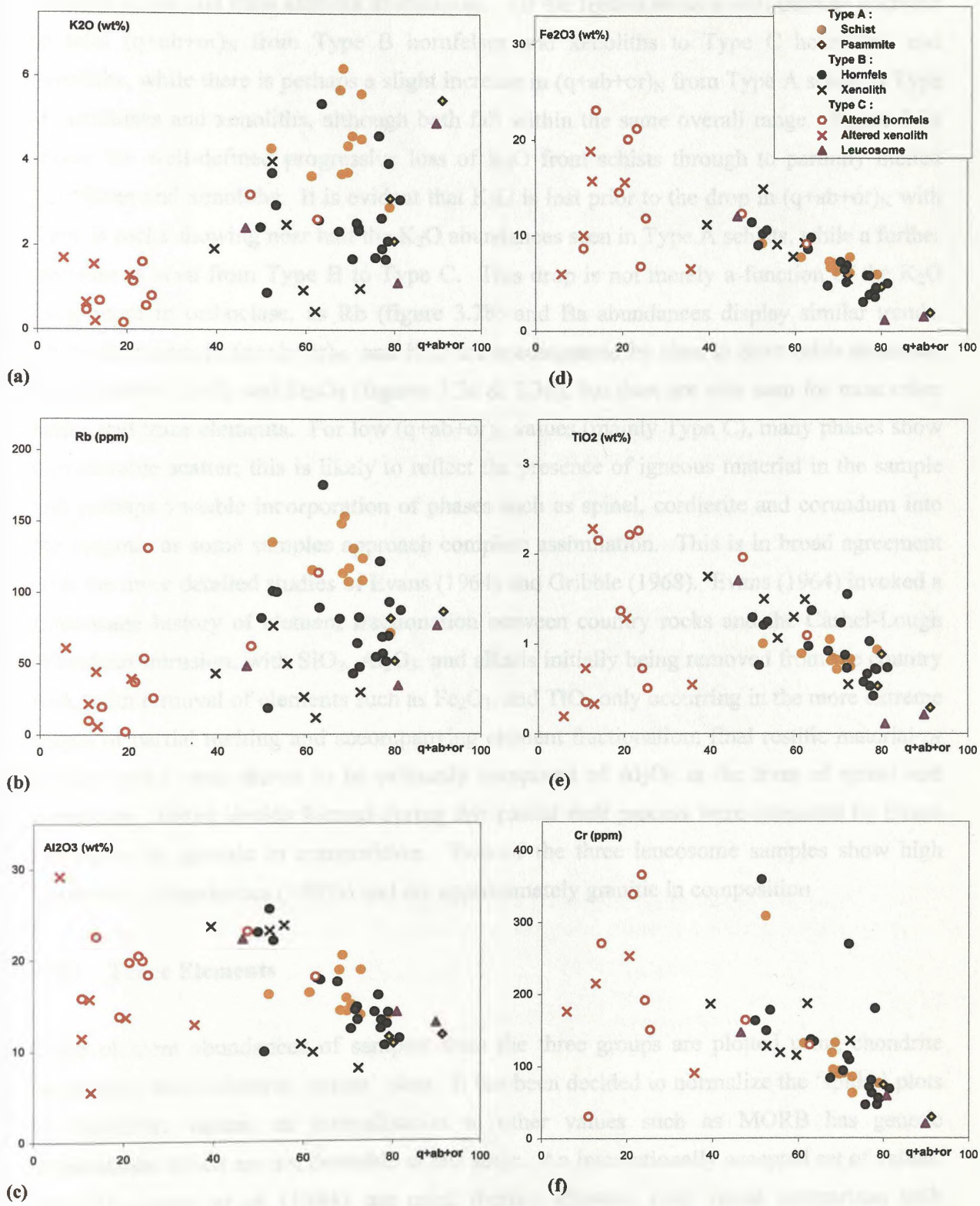


**Figure 3.3 Normative quartz + albite + orthoclase versus whole rock values for selected major and trace elements.**

selected major and trace element abundances. All the figures show a well-defined decrease in total $(q+ab+or)_N$ from Type B hornfelses and xenoliths to Type C hornfelses and xenoliths, while there is perhaps a slight increase in $(q+ab+or)_N$ from Type A schist to Type B hornfelses and xenoliths, although both fall within the same overall range. Figure 3.3a shows the well-defined progressive loss of $K_2O$ from schists through to partially melted hornfelses and xenoliths. It is evident that $K_2O$ is lost prior to the drop in $(q+ab+or)_N$ with Type B rocks showing near half the $K_2O$ abundances seen in Type A schists, while a further decrease is seen from Type B to Type C. This drop is not merely a function of the $K_2O$ component in orthoclase, as Rb (figure 3.2b) and Ba abundances display similar trends. These decreases in $(q+ab+or)_N$ and $K_2O$ are accompanied by rises in most other elements, most notably $Al_2O_3$ and $Fe_2O_3$ (figures 3.3c & 3.3d), but rises are also seen for most other major and trace elements. For low $(q+ab+or)_N$ values (mainly Type C), many phases show considerable scatter; this is likely to reflect the presence of igneous material in the sample and perhaps variable incorporation of phases such as spinel, cordierite and corundum into the magma, as some samples approach complete assimilation. This is in broad agreement with the more detailed studies of Evans (1964) and Gribble (1968). Evans (1964) invoked a three-stage history of element fractionation between country rocks and the Cashel-Lough Wheelaun intrusion, with $SiO_2$, $Al_2O_3$, and alkalis initially being removed from the country rock, with removal of elements such as $Fe_2O_3$, and $TiO_2$ only occurring in the more extreme stages of partial melting and accompanying element fractionation; final restitic material or 'emery rocks' was shown to be primarily composed of $Al_2O_3$ in the form of spinel and corundum. Initial liquids formed during this partial melt process were estimated by Evans (1964) to be granitic in composition. Two of the three leucosome samples show high $(q+ab+or)_N$ abundances (>80%) and are approximately granitic in composition.

### 3.3.3 Trace Elements

Trace element abundances of samples from the three groups are plotted using chondrite normalised multi-element 'spider' plots. It has been decided to normalize the 'spider' plots to chondritic values, as normalisation to other values such as MORB has genetic implications which are not desirable at this stage. An internationally accepted set of values, from Thompson *et al.* (1984), are used, thereby allowing easy visual comparison with 'spider' diagrams from published work. These normalisation values are given in Appendix B.6. These diagrams will be used in greater detail in Chapters 5 and 6 to examine the igneous rocks and their evolution. Here, these 'spider' plots, shown in figures 3.4 to 3.10, show the characteristic shapes of the pelitic material, as well as the country rock material. It

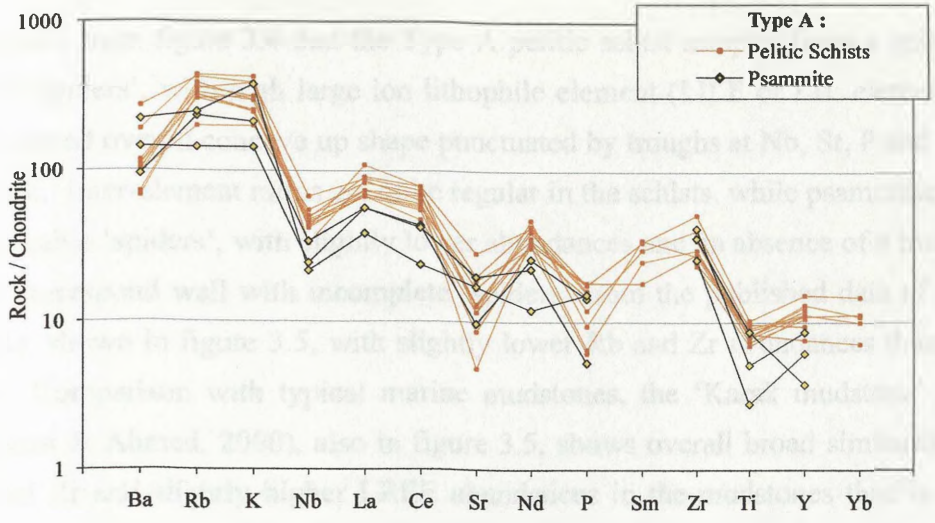


**Figure 3.4 'Spider' plots of Dalradian pelitic and psammitic schists. Normalization of this and subsequent 'spider' plots is to the chondrite normalized values of Thompson *et al.* (1984),which are given in Appendix B.6.**

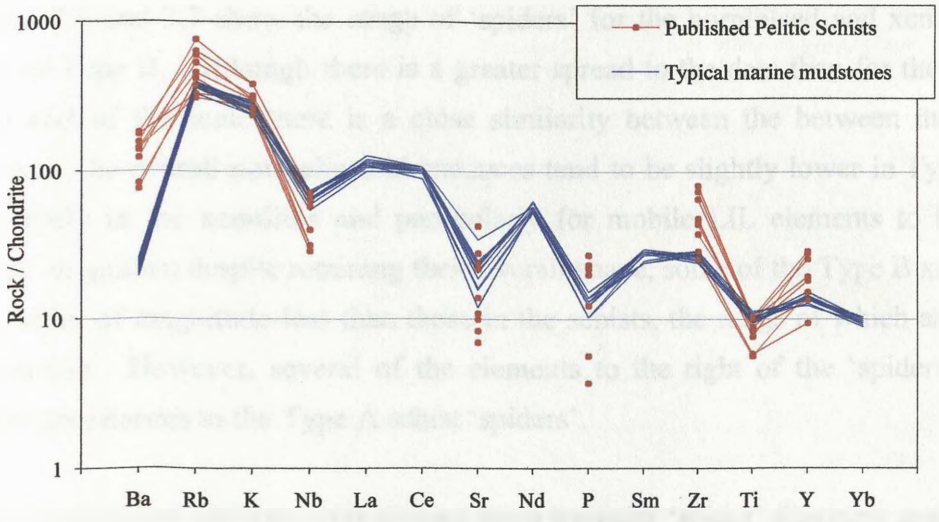


**Figure 3.5 'Spider' plots of published pelitic schists from the Dalradian (Lambert *et al.*, 1981), and of typical marine mudstones (Saleemi & Ahmed, 2000)**

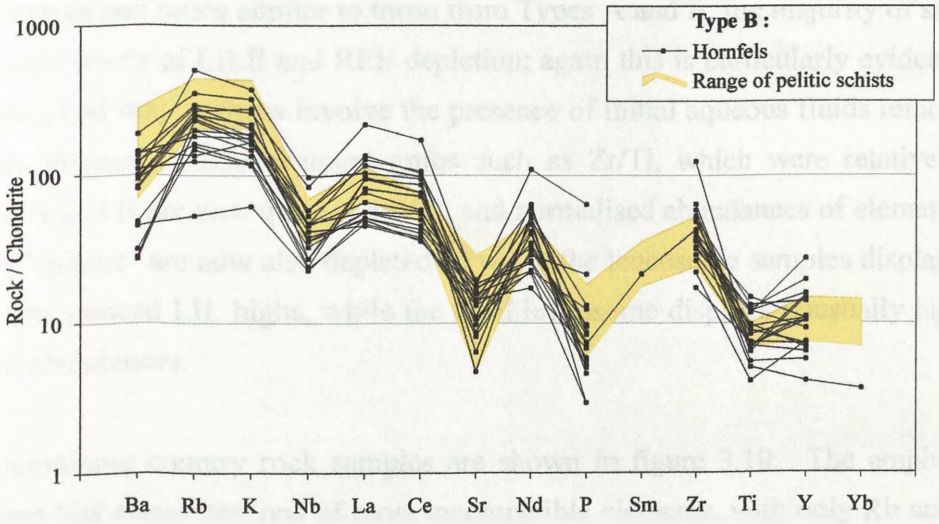


**Figure 3.6 'Spider' plots of hornfelses from intrusive margins, in which evidence for desilication or partial melting is minimal.**

is evident from figure 3.4 that the Type A pelitic schist samples form a quite well defined set of 'spiders', with high large ion lithophile element (LILE or LIL element) abundances and a broad overall concave up shape punctuated by troughs at Nb, Sr, P and Ti and a slight Zr peak. Inter-element ratios are quite regular in the schists, while psammitic samples show comparable 'spiders', with slightly lower abundances and an absence of a trough at Sr. The plots correspond well with incomplete 'spiders' from the published data of Lambert *et al.* (1981), shown in figure 3.5, with slightly lower Rb and Zr abundances than the published data. Comparison with typical marine mudstones, the 'Karak mudstone' from Pakistan (Saleemi & Ahmed, 2000), also in figure 3.5, shows overall broad similarities, with lower Ba and Zr and slightly higher LREE abundances in the mudstones than in the Dalradian schists; the Ba values in the Dalradian schists are up to an order of magnitude higher than in the muds.

Figures 3.6 and 3.7 show the range of 'spiders' for the hornfelsed and xenolithic country rocks of Type B. Although there is a greater spread to the data than for the pelites, at the upper end of the scale there is a close similarity between the between the two groups. However, the overall normalised abundances tend to be slightly lower in Type B samples, particularly in the xenoliths and particularly for mobile LIL elements to the left of the 'spider' diagrams; despite retaining their overall shape, some of the Type B xenoliths are up to an order of magnitude less than those in the schists, the range of which are included for comparison. However, several of the elements to the right of the 'spiders' still display similar abundances to the Type A schist 'spiders'.

Type C hornfelses and xenoliths display more irregular 'spider' diagrams and inter-element ratios, shown in figures 3.8 and 3.9. Although some samples still contain normalised abundances and ratios similar to those from Types A and B, the majority of samples display increased levels of LILE and REE depletion; again this is particularly evident in xenolithic samples, and may perhaps involve the presence of initial aqueous fluids removing the more mobile elements. Inter-element ratios such as Zr/Ti, which were relatively constant in Types A and B are now quite irregular, and normalised abundances of elements on the right of the 'spiders' are now also depleted. Two of the leucosome samples display flat 'spiders' with pronounced LIL highs, while the third leucosome displays unusually high normalised LREE abundances.

The remaining country rock samples are shown in figure 3.10. The amphibolite sample displays low concentrations of most incompatible elements, with only Rb and Sr above 10

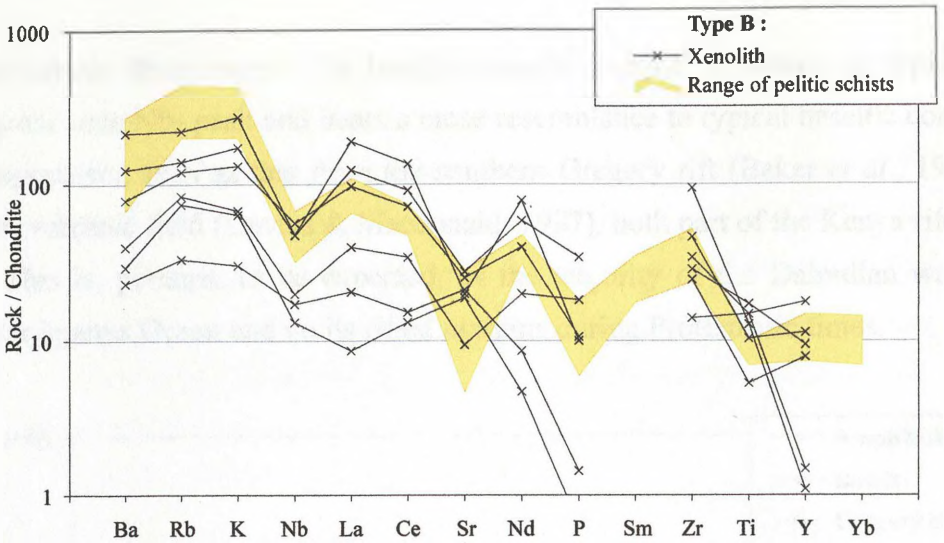


**Figure 3.7 'Spider' plots of xenoliths within the intrusions in which evidence for desilication or partial melting is minimal.**

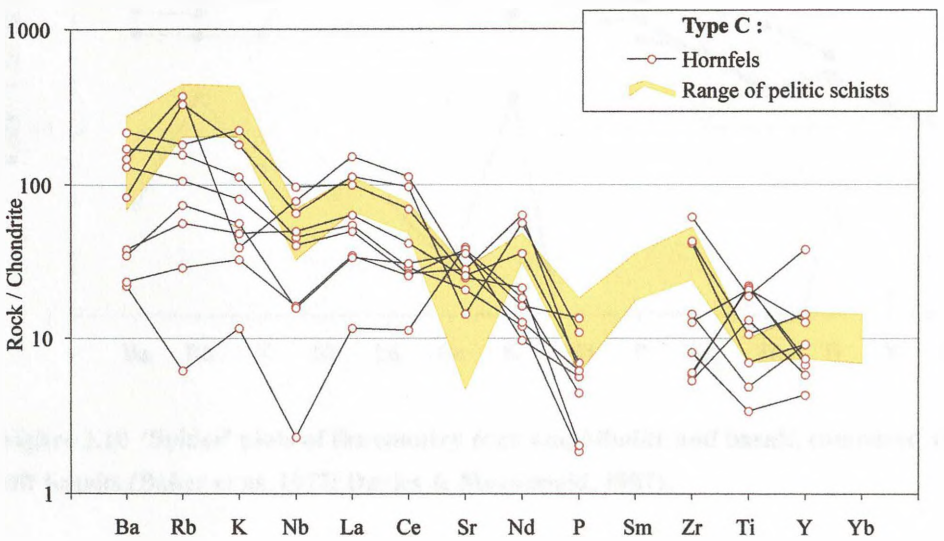


**Figure 3.8 'Spider' plots of hornfelsed samples showing evidence for desilication or partial melting**

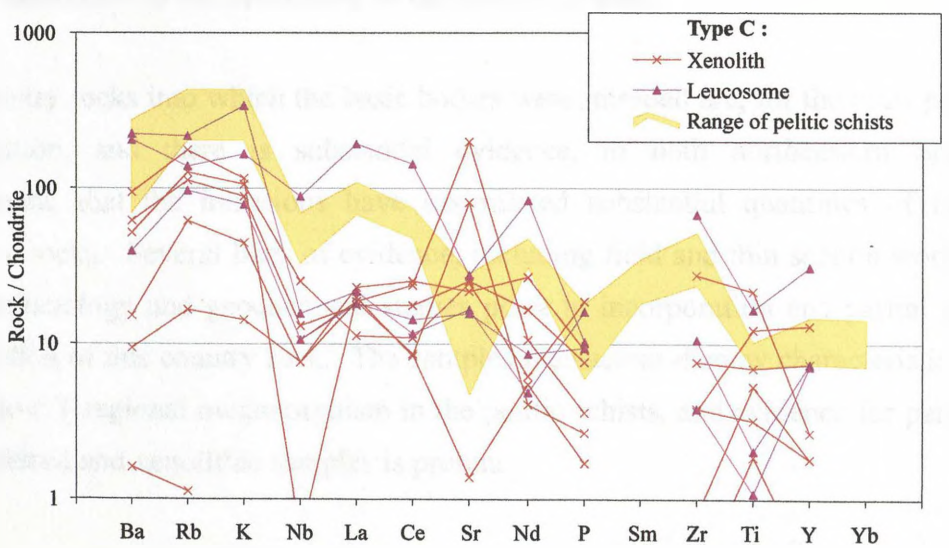


**Figure 3.9 'Spider' plots of xenolithic samples showing evidence for desilication or partial melting**

times chondritic abundances. The basaltic sample displays a convex- up 'spider' pattern, with a pronounce Nb- peak and bears a close resemblance to typical basaltic continental rift zone magmatism, such as that from the southern Gregory rift (Baker *et al.*, 1977) and the Naivasha volcanic field (Davies & Macdonald, 1987), both part of the Kenya rift (see figure 3.10). This is, perhaps, to be expected, as the majority of the Dalradian was deposited within the Iapetus Ocean and on its rifted margins during Proterozoic times.

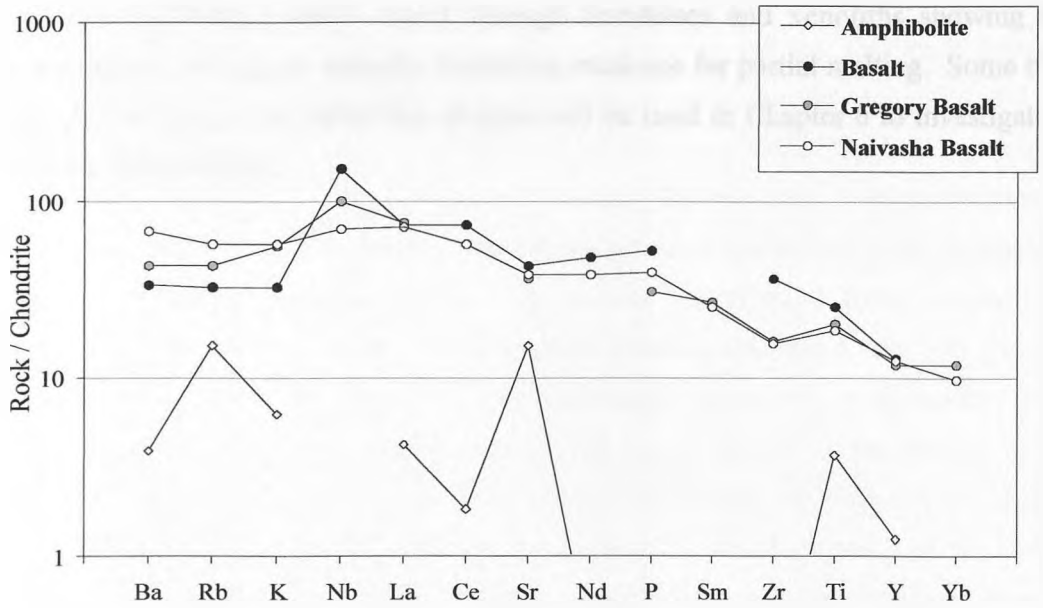


**Figure 3.10 'Spider' plots of the country rock amphibolite and basalt, compared with Kenyan rift basalts (Baker et al, 1977; Davies & Macdonald, 1987).**

## 3.4 Summary of the chemistry of the country rocks

The country rocks into which the basic bodies were intruded are, for the most part pelitic in composition, and there is substantial evidence, in both northeastern Scotland and Connemara, that the intrusions have assimilated substantial quantities of these pelitic envelope rocks. Several lines of evidence, including field and thin section work as well as phase mineralogy and geochemical studies point to incorporation and partial to complete assimilation of this country rock. The samples themselves display characteristics typical of high P low T regional metamorphism in the pelitic schists, and evidence for partial melting in hornfelsed and xenolithic samples is present.

Chemically, the pelites contain high levels of $SiO_2$ and alkalis, with many of the hornfelsed and xenolithic samples displaying depletion in these elements, and associated enrichment in other elements such as $Al_2O_3$ and $Fe_2O_3$. The pelites display steeply sloped 'spider' patterns, with high LIL concentrations and troughs at Sr, P and the HFSE, while depletion of these incompatible elements is most pronounced, initially for the mobile LIL elements, perhaps suggesting the influence of an aqueous phase, and becomes increasing irregular as the degree of melting increases. All of these trends are gradational, with an overall sequence from unaffected pelitic schist through hornfelses and xenoliths showing little evidence for partial melting to samples displaying evidence for partial melting. Some of the major and trace element data from this chapter will be used in Chapter 6 to investigate the contamination of the bodies.

# Chapter 4 Petrography and mineralogy of the Intrusions

## 4.1 Introduction

This chapter will concentrate on the petrographic and mineralogical properties of the 'Younger' Gabbros of the Grampian Highlands and Connemara. For reasons that will be discussed in Section 4.3, the suite has been divided into five groups, with each discussed separately. The form and petrography of the individual intrusions are described and their characteristic mineralogy examined. Descriptions of this form and of the internal structure of the bodies are based largely on published material by previous workers because, as mentioned in Chapter 1, field mapping is beyond the scope of this thesis, while petrographic descriptions have been supplemented by thin section descriptions from, among other sources, the BGS and the University of Birmingham teaching collection. An understanding of the petrography and mineralogy of the individual intrusions is necessary to aid understanding and interpretation of the whole rock geochemistry of the bodies in later chapters. For some of the groups, there are certain limitations on what can be obtained because of such factors as extensive alteration, which is found in some of the bodies, notably the Morven Cabrach mass. In addition, despite its relatively complete sequence, only selected mineralogical work has been undertaken on the Insch body, as published studies (Wadsworth; 1986, 1988) have already provided a thorough examination of its characteristic silicate mineralogy.

## 4.2 Previous work

The earliest work on the 'Younger' Gabbros of north-east Scotland was undertaken as part of regional BGS mapping in the area and led to the publication of 1:50,000 geological sheets and associated memoirs (Wilson, 1886; Hinxman, 1896; Hinxman & Wilson, 1902). Further BGS mapping by H.H. Read in the 1920s and 1930s led to a map and memoir of the Banff, Huntly and Turriff areas and several associated publications (Read, 1919, 1921, 1923a, 1923b, 1924, 1935). Subsequent regional work has included gravity and magnetic studies of the intrusions (McGregor & Wilson, 1967) and a Scottish Journal of Geology Special Publication in 1970 on the 'Younger' Basic igneous complex. More recently, the BGS, in collaboration with the University of Aberdeen have remapped extensively in the area leading to a better understanding of the bodies and, in particular, their intrusive

contacts and relation to the series of shear zones running through the area. Specific work on the individual intrusions will be discussed separately when those intrusions are described in upcoming sections.

## 4.3 Grouping of Bodies

The intrusions have been divided into five groups and these are shown in figure 4.1, while the sample coverage is outlined in Table 4.1. Several workers have noted slight variations to certain aspects of the bodies across the Grampian Highlands, most notably in the contamination of the northeastern bodies (Gribble, 1967) and the absence of complete stratigraphic sequences in all but the Insch and Boganclogh masses. In addition, petrological and geophysical studies have suggested that several of the bodies are likely to be linked at depth (Stewart & Johnson, 1960; McGregor & Wilson, 1967; Ashcroft *et al.*, 1984; Wadsworth, 1991). The five groups have been created based on some of these systematic variations such as petrological and geochemical similarities, and on the spatial relations between the intrusions; this will aid identification of geochemical trends within the suite as a whole and any possible variations within or between these trends. Despite this, it should be emphasised that these groups do not imply, at this stage, any structural or genetic link between the bodies within these groups, nor does it imply any larger scale variations between the groups: they are simply for subdividing the suite as a whole at this stage.

## 4.4 Sampling

A number of factors have influenced the sampling technique for this thesis. Because of the large geographical range and poorly exposed nature to many of the intrusions in the Grampian Highlands, a field season collecting samples for analysis was felt to be unfeasible. Consequently, samples were obtained from several previously acquired collections. The bulk of the samples were acquired from the British Geological Survey sample collection in Keyworth, Nottingham and from the University of Aberdeen and University of Cambridge museum collections. Additional samples were also obtained from the University of Manchester and University of Birmingham archive collections. The Connemara bodies, in contrast, are quite well exposed and were sampled during two brief field seasons.

One potential problem arising from this sampling approach is that, originally, the samples were not necessarily collected with similar study objectives in mind, and consequently may

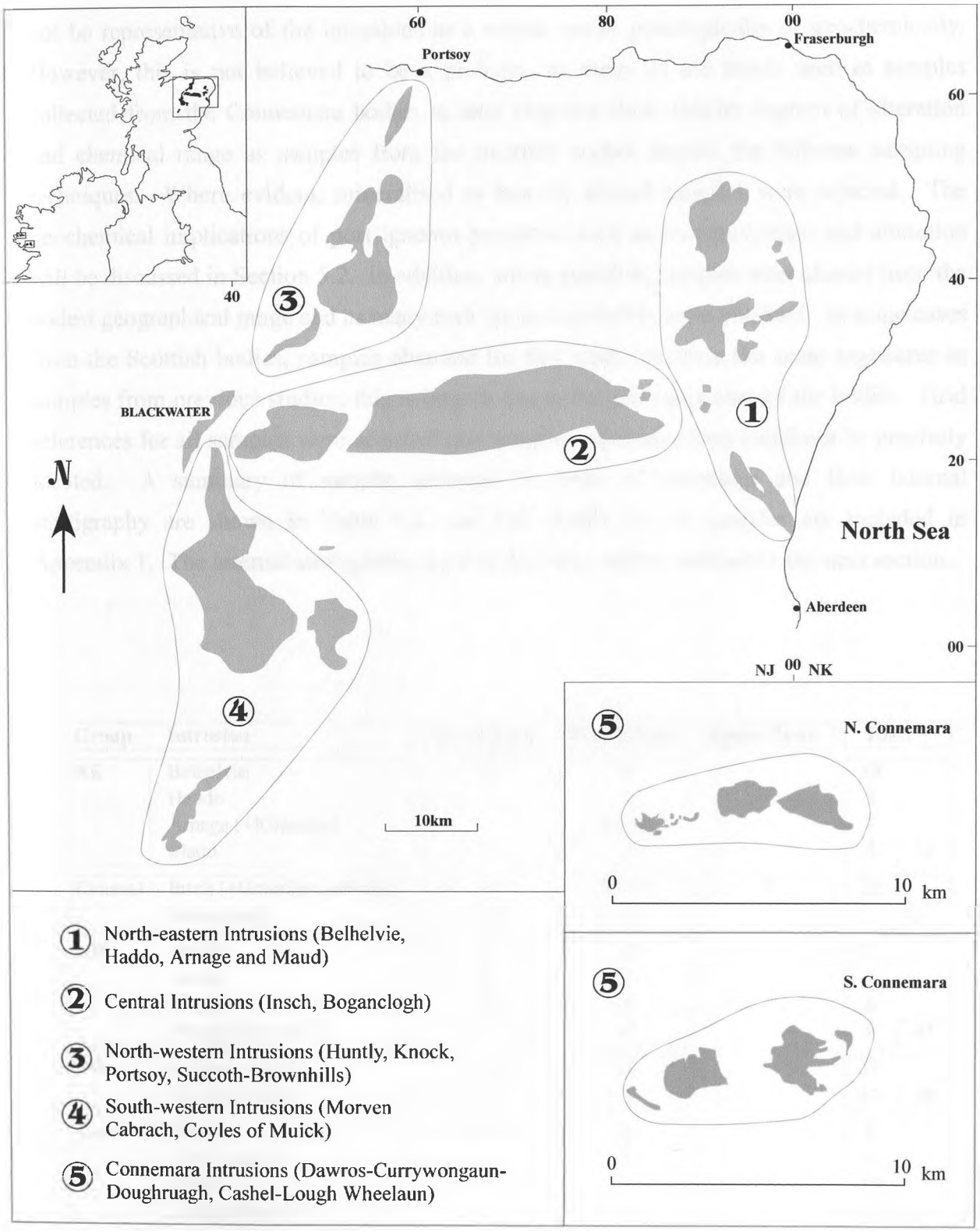


**Figure 4.1 Location of the five groups into which the intrusions have been divided.**

not be representative of the intrusions as a whole, either petrologically or geochemically. However, this is not believed to be a problem, as many of the trends seen in samples collected from the Connemara bodies in later chapters show similar degrees of alteration and chemical range as samples from the Scottish bodies despite the different sampling techniques. Where evident, mineralised or heavily altered samples were rejected. The geochemical implications of post igneous processes such as metamorphism and alteration will be discussed in Section 5.2. In addition, where possible, samples were chosen from the widest geographical range and as many rock types as possible were obtained. In some cases from the Scottish bodies, samples obtained for this study are from the same exposures as samples from previous studies; this is largely due to the poor exposure of the bodies. Grid references for all samples were acquired and samples rejected if they could not be precisely located. A summary of sample coverage in terms of intrusions and their internal stratigraphy are shown in Table 4.1, and full details for all samples are included in Appendix 1. The internal stratigraphy used in this table will be defined in the next section.

| Group | Intrusion | Lower Zone | Middle Zone | Upper Zone | Total | |
|---|---|---|---|---|---|---|
| NE | Belhelvie | 12 | 6 | | 18 | |
| | Haddo | | 4 | | 4 | |
| | Arnage (+Kinnadie) | | 8 (+1) | | 9 | |
| | Maud | | 3 | | 3 | **34** |
| Central | Insch (+Granular Gabbros) | 1 | 7 (+7) | 7 | 22 | |
| | Boganclogh | 8 | 6 | 1 | 15 | **37** |
| NW | Huntly | 12 | 10 | | 22 | |
| | Knock | 6 | 2 | | 8 | |
| | Portsoy | 4 | 4 | | 8 | |
| | Succoth Brownhills | 3 | 6 | | 9 | **47** |
| SW | Morven Cabrach | 6 | 13 | | 19 | |
| | Coyles of Muick | 8 | 3 | | 11 | **30** |
| Conn. | Dawros | 4 | 2 | | 6 | |
| | Currywongaun | | 5 | | 5 | |
| | Cashel | 1 | 9 | | 10 | |
| | Lough Wheelaun | 2 | 11 | | 13 | **34** |
| | | | | | | **182** |

**Table 4.1 Summary by group and zone of sample coverage from the Scottish and Irish bodies.**

## 4.5 Outline and form of the bodies

Although many of the details of the outline and form of the individual bodies vary from intrusion to intrusion, there are still many properties of the petrology, petrography and mineralogy, which are common to all the bodies. Faulting and shearing have disrupted the internal layout of the rock types to varying degrees; one feature common to many of the intrusions is the absence of the original intrusive contacts in almost all instances, with any possible chilled margins removed by this faulting and shearing. In addition, many of the more detailed field relations of the intrusions are not fully understood due to their poorly exposed nature. For the Scottish intrusions, the descriptions of the form and outline of the bodies are based on published work, while those for the Connemara bodies are based on a combination of limited field mapping and published work.

When attempting to divide and systematically classify these bodies, several problems arise. The obvious framework to use for this division and classification is the classic division into Lower, Middle and Upper Zones first proposed by Wager & Brown (1968) for the Skaergaard Intrusion, and several attempts have been made to do this for the intrusions individually (Allan, 1970; Clarke & Wadsworth; 1970; Boyd, 1972; Wadsworth, 1986) and as a whole (Wadsworth, 1982, Fletcher, 1989); the resultant division bears a strong resemblance to that of Wager & Brown for the Skaergaard and other layered basic intrusions. This system involves the division of the stratigraphy into three zones and several sub-zones, as shown in figure 4.2, based on the presence or absence of the main silicate minerals as cumulus phases.

While these bodies may represent a single phase of igneous activity, and possibly even a single intrusion originally, they are now present as several large intrusions and numerous smaller ones. Consequently, the problem arises that much of the mapping of these bodies was undertaken by a variety of authors over a period of several decades, resulting in a certain degree of inconsistency in the divisions into which the individual intrusions have been divided in the literature. Varying exposure levels from intrusion to intrusion also mean that certain bodies are divided and subdivided in far greater detail than others; for example, published BGS maps of the Maud intrusion display only one lithology, while the Huntly and Knock bodies have been divided into 6 and more divisions (Fletcher, 1989). Nevertheless, the zonal classification scheme of Wager & Brown has been adhered to as closely as possible for the overall descriptions of the bodies, although, as will be discussed

in Chapter 5, there are difficulties in using this classification when examining the whole rock chemistry of the bodies.

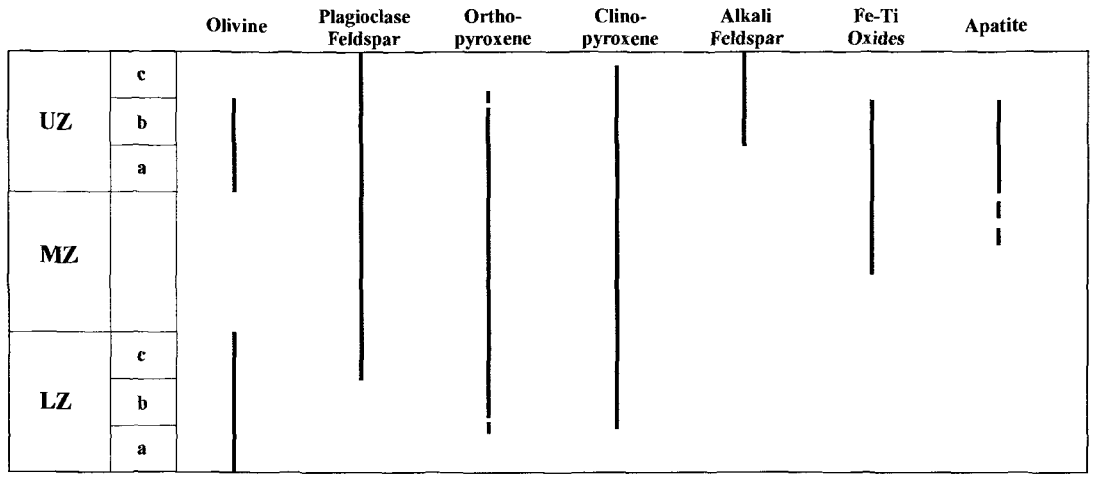


**Figure 4.2 Subdivision of the igneous stratigraphy of the 'Younger' Basics (based on the work of Wadsworth (1982, 1986, 1988), Munro (1984), Kneller (1987), Fletcher (1989), Stephenson & Gould (1995), Gunn *et al.* (1996) and Gould (1997). Vertical scale does not correspond to stratigraphic height.**

### 4.5.1 North-Eastern Bodies: Belhelvie, Arnage, Haddo, Kinnadie and Maud.

#### Previous work

Other than limited early work by Heddle (1882), Bonney (1885), and Gibb (1908, 1912), little detailed work was carried out on Belhelvie until its petrography, internal layering and overall structure were comprehensively described by Stewart (1946). Wadsworth *et al.* (1966) reclassified the internal divisions of the layered sequence and investigated some of the cryptic variation, while van Breemen & Boyd (1972) dated a pegmatite crosscutting the body at 472±5 Ma. Further work by Ashcroft (1970), Ashcroft & Boyd (1976), and Boyd & Munro (1978), redefined the contacts of the intrusion by means of boreholes and magnetic surveys. More recently, Wadsworth (1991) has published probe data of the silicate minerals in the layered units.

Read (1923a, 1923b, 1935) and Read & Farquhar (1952, 1956) have presented detailed descriptions of the geology of the Arnage and Haddo areas. These intrusions are considered to have undergone substantial contamination by their largely pelitic envelope rocks,

although this has also been interpreted as pre-intrusive migmatization (Read & Farquhar, 1956). Detailed work on their crystallisation history by Gribble (1967, 1968, 1970) and Sr-isotope data (Pankhurst, 1969) has shown that contamination is more likely and probably resulted from assimilation and partial melting of the Arnage and Haddo country rocks as discussed in Chapter 3, while the Kinnadie body has had no specific work on it and generally tends to be described as a faulted eastern extension of the Arnage body.

Maud is the most poorly exposed and studied of the 'Younger' Basic intrusions. It was briefly described as a dioritic body during the early regional BGS mapping of the region (Wilson, 1886), but the only subsequent published investigations have been as part of regional geophysical and magnetic surveys (McGregor & Wilson, 1967).

**Belhelvie**

The Belhelvie intrusion, shown in figure 4.3, is an elongate northwest-southeast trending body, ~ 25 $km^2$ in size, situated 5-10 km north of Aberdeen. Much of the form and internal detail of the intrusion has been established using aeromagnetic and borehole data as, over large portions of the intrusion, exposure is poor, particularly in the south and east of the intrusion. It consists mainly of layered peridotites, troctolites, norites and gabbros, with one fault, the Belhelvie fault cutting across the southeastern portion of the intrusion. A narrow hornfelsed country rock septum runs from the northeastern contact and divides the intrusion into two sequences to the east and west of the septum. Magnetic data have been used to model the three-dimensional form of the intrusion using the strong positive anomalies associated with the ultramafic units. This modelling suggests that the intrusion has steeply dipping margins and internal contacts extending to a depth of approximately 1 km, and has also shown that the intrusion extends further southeast, into the North Sea, for at least 5km. Igneous layering is found throughout the intrusion from the macro-scale (0.5-1 km thick dunitic cumulate units) down to the centimetre scale. Typically, the layering is irregular to lensoid in shape and is, in general, parallel to the length of the body, dipping steeply, roughly parallel to the margins of the intrusion.

The petrology of the Belhelvie intrusion has been subdivided into three main rock types, Lower Zone ultramafic rocks, Lower Zone troctolitic rocks, and Middle Zone gabbroic and noritic rocks. The *ultramafic rocks* are largely dunitic in composition, and are found mainly in the southern part of the mass, but also as major units running up the east and west sequences of the northern part of the body and as layers within the other units. The

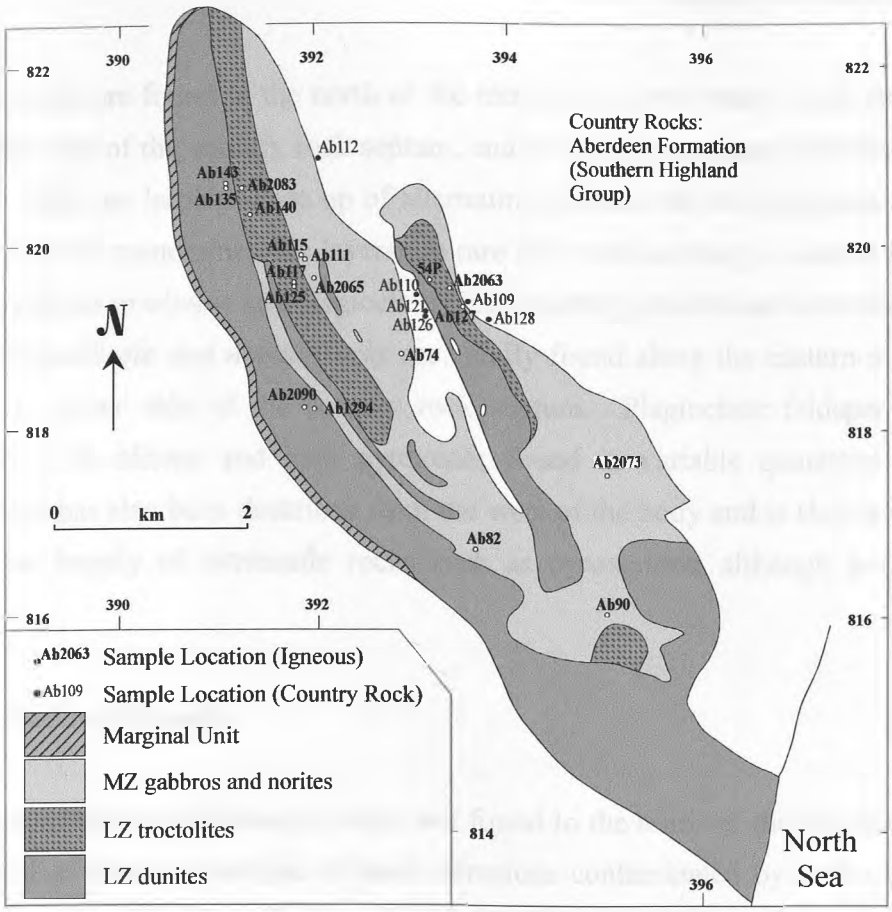


**Figure 4.3 Lithological units and location of samples within the Belhelvie intrusion (based on Boyd, 1972)**

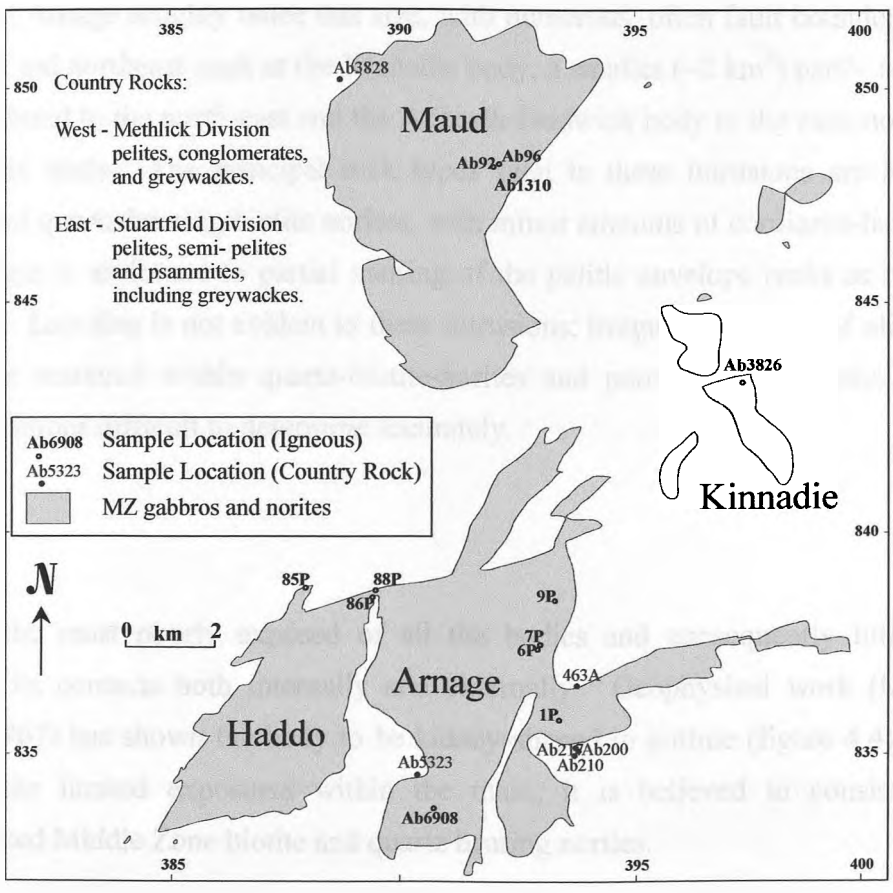


**Figure 4.4 Location of samples within the Haddo, Arnage, Kinnadie and Maud intrusions (based on BGS map)**

*troctolitic rocks* are found in the north of the intrusion, as two main bands running north-south, either side of the country rock septum, and in isolated outcrops elsewhere within the intrusion. They are largely made up of alternating olivine-rich and plagioclase-rich layers although extreme monominerallic layers are rare and most layering is caused by variations in the proportions of olivine and plagioclase with generally gradational contacts between the layers. The *gabbroic and noritic rocks* are chiefly found along the eastern margins of the intrusion, to either side of the country rock septum. Plagioclase feldspar is the main constituent, with olivine and both pyroxenes found in variable quantities. A narrow marginal unit has also been described from the west of the body and is shown in figure 4.3; this consists largely of ultramafic rocks such as pyroxenites, although norites are also common.

**Arnage / Haddo, Kinnadie**

The Arnage, Haddo and Kinnadie bodies are found to the north of the Belhelvie mass and are regarded as classic examples of basic intrusions contaminated by their country rocks. Irregular in shape, these intrusions are largely fault bounded (figure 4.4) and are dissected by the series of shear zones discussed in Chapter 2 (see figure 2.6). Haddo is about 13 $km^2$ in size and Arnage roughly twice this size, with numerous, often fault bounded, extensions to the east and northeast such as the Kinnadie body, a smaller (~2 $km^2$) partly fault bounded intrusion found to the north-east and the Arthrath-Dudwick body to the east, not sampled as part of this study. The principal rock types seen in these intrusions are Middle Zone olivine- and quartz-bearing biotite norites, with minor amounts of cordierite-bearing norites whose origin is attributed to partial melting of the pelitic envelope rocks as mentioned in Chapter 3. Layering is not evident in these intrusions; irregular outcrops of olivine-biotite-norites are scattered within quartz-biotite-norites and poor exposure makes the precise internal relations difficult to determine accurately.

**Maud**

Maud is the most poorly exposed of all the bodies and consequently little is known regarding its contacts both internally and externally. Geophysical work (McGregor & Wilson, 1967) has shown the body to be kidney-shaped in outline (figure 4.4) and, on the basis of the limited exposures within the mass, it is believed to consist mainly of contaminated Middle Zone biotite and quartz bearing norites.

### 4.5.2 Central Intrusions

**Previous work**

The Insch-Boganclogh mass represents the largest intrusive complex of the 'Younger' Basic suite of the northeast Grampian Highlands, and also represents the widest range of rock types found within the suite, ranging from peridotites, dunites and harzburgites through a variety of gabbros and norites to late stage differentiates such as syeno-diorites and syenites. As a consequence of this relatively complete sequence, these bodies are the most studied intrusions in the region, despite variable exposure.

Earliest investigations of the intrusions were by Hinxman (1896), Read (1923a), and Whittle (1936), but these were incomplete or cursory examinations. Since the 1950s, Read and co-workers have examined various aspects of the two intrusions in detail (Read, 1956; Read & Haq, 1963; Sadashivaiah, 1954a, 1954b; Read *et al.*, 1961, 1965) while McGregor & Wilson (1967) have examined geophysical aspects of the bodies, notably their margins and outline and have suggested the intrusions are probably connected beneath the younger igneous and sedimentary rocks which separate the intrusions on the surface.

Investigations by Clarke & Wadsworth (1970) and Busrewil *et al.* (1973) have provided the main systematic descriptions of the Insch and Boganclogh masses using modern layered basic intrusive nomenclature. More recent work has concentrated on various structural aspects of the bodies and their margins (Ashcroft & Munro, 1978; Leslie, 1984; Munro, 1986a), while Wadsworth (1986, 1988) has conducted detailed investigations of the compositional trends in the silicate minerals from the Middle and Upper Zones of the Insch body. Despite the considerable evidence that they are connected at depth (McGregor & Wilson, 1967), for convenience the bodies will be described separately.

**Insch**

The Insch mass, shown in figure 4.5, is an elongate E-W trending body, ~ 30 km by 10 km in size, and is the largest of the 'Younger' Basic intrusions. An overlying Devonian sedimentary sequence, the Rhynie outlier, and the younger, igneous Kennethmont complex, represent the westernmost margins of the body; both contacts are largely faulted, while intrusive contacts over the remainder of the body are extensively sheared, with both hornfelsed country rocks and any possible chilled margins removed by this shearing.

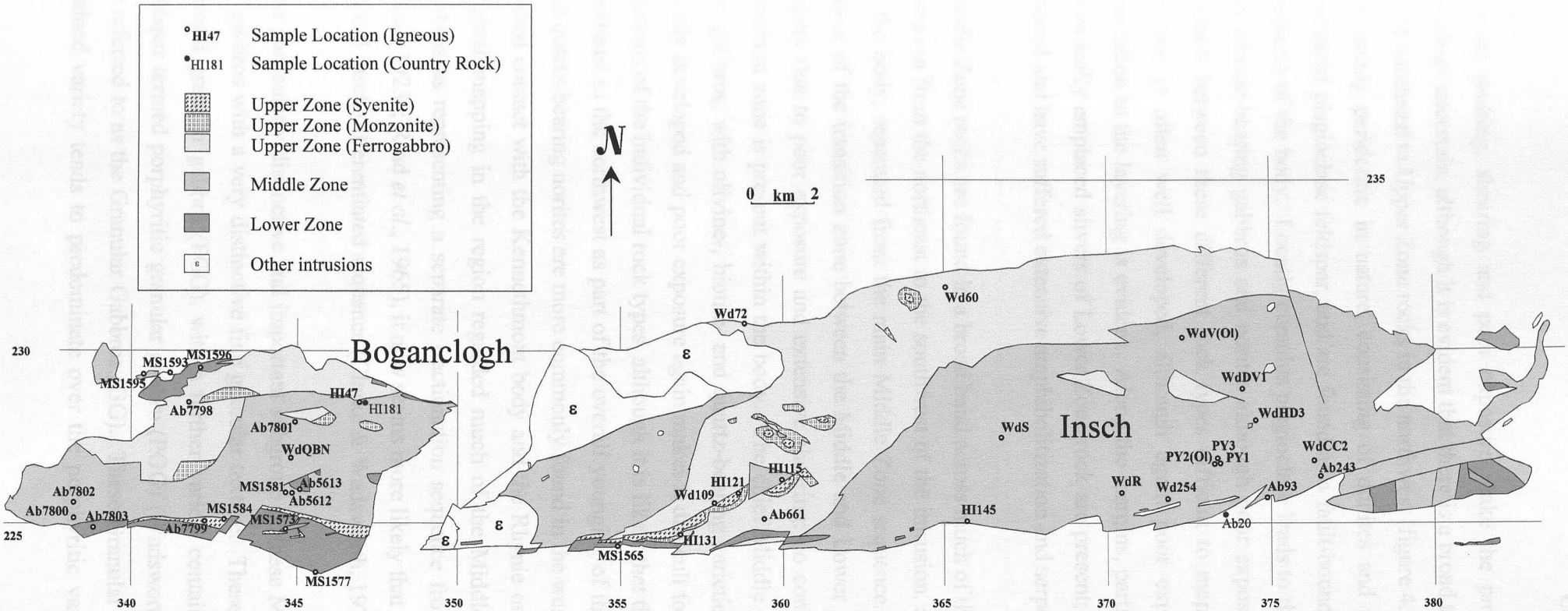


**Figure 4.5 Sample location in the Insch and Boganclogh intrusions**

Internal faulting, shearing and poor exposure make the precise details of the internal petrology uncertain, although it is evident that there is a broad trend from Lower Zone rocks in the southeast to Upper Zone rocks in the northwest (figure 4.5). These Lower Zone rocks are mainly peridotitic in nature, consisting of dunites and pyroxenites with occasional interstitial plagioclase feldspar, and are found as a fault-bounded extension to the east and southeast of the body. Locally cumulus plagioclase leads to the development of troctolites and olivine-bearing gabbros and norites although poor exposure makes the relations and contacts between these different rock types difficult to map out accurately. Rhythmic layering is often well developed, although again poor exposure means no consistent orientation to the layering is evident. Along the margins, particularly the southern margin, tectonically emplaced slivers of Lower Zone rock are present; these tend to be quite badly sheared and have suffered extensive amphibolitization and serpentinization.

Middle Zone rocks are found in a broad band across much of the central region of the Insch intrusion from the northeast to the southwest of the intrusion, and also to the extreme west of the body, separated from the main Middle Zone sequence by Upper Zone rocks. The nature of the transition zone between the Middle and Lower Zones is poorly understood, largely due to poor exposure and extensive shearing: no continuous section through this transition zone is present within the body. The chief Middle Zone rock types are norites, and gabbros, with olivine-, biotite- and quartz-bearing varieties present. Layering is only locally developed and poor exposure again makes it difficult to map out the precise internal relations of the individual rock types, although it is likely that the sequence youngs from the southeast to the northwest as part of the overall younging of the body. In addition, biotite- and quartz-bearing norites are more commonly found in the western parts of the intrusion in faulted contact with the Kennethmont body and the Rhynie outlier to the west. Although original mapping in the region regarded much of the Middle Zone hypersthene-bearing gabbros as representing a separate fractionation sequence from the main Insch sequence (Read, 1923a; Read *et al.*, 1965), it now seems more likely that these gabbros are part of the overall Insch differentiated sequence (Clarke & Wadsworth, 1970).

One particularly distinctive and important subgroup of these Middle Zone rocks is a series of gabbros with a very distinctive fine granular texture. These have been termed the fine-grained granular gabbro (FGG), with a further variety containing porphyritic plagioclase feldspar termed porphyritic granular gabbro (PGG) (Wadsworth, 1988), and will hereafter be referred to as the Granular Gabbros (GG). These Granular Gabbros, in which the fine-grained variety tends to predominate over the porphyritic variety, are found extensively

throughout the Middle Zone in the eastern part of the Insch mass, often in close association with cumulate Middle Zone gabbros and norites. Poor exposure, combined with the close association with the cumulate Middle Zone in the field means the mapping out of the Granular Gabbros as a separate unit has proved impossible. Read & Haq (1963), Clarke & Wadsworth, 1970), Thy & Esbensen (1982), and Wadsworth (1988) have all speculated at length regarding the possible origin and significance of these granular gabbros and they will be discussed in greater detail in Chapters 5 and 6.

Olivine ferrogabbros grading through to olivine monzonites and syenites are the principal rock types found in Upper Zone sequence of the Insch body. They are found as a broad 3-4 km thick band to the north and west of the Middle Zone, along the northern margin and down through the western regions of the body. The transition from the Middle Zone appears to be generally concordant and relatively good exposure has enabled the division of the Upper Zone into 3 sub-zones, UZa, UZb and UZc (Clarke & Wadsworth, 1970). Incoming cumulus olivine, alkali feldspar and zircon and the disappearance of cumulus olivine and orthopyroxene are the basis for this subdivision, in accordance with the classic divisions of layered basic intrusions (Wager & Brown, 1968). Again layering is rare, and occasional granular gabbros are seen within UZa. Faulting and shearing has led to several blocks of Upper Zone rocks cropping out within Middle Zone gabbros and also Lower Zone peridotites adjacent to Upper Zone syenites in the south-west of the body.

Several minor basic to ultra-basic bodies are found to the southeast and east of the Insch mass, including a fault bounded ultramafic mass at Lawel Hill to the southeast and a gabbroic body at Udny-Pitmedden to the east; neither have been sampled as part of this study.

**Boganclogh**

The Boganclogh body, also shown in figure 4.5, is roughly rectangular in outline and is located immediately to the east of the Rhynie outlier. It is approximately 15 by 10 km wide and is likely to be connected to the Insch mass beneath the Rhynie outlier; consequently, many of the rock types present in the Insch mass are also present in the Boganclogh body. The contacts to the west are also partly with Devonian sedimentary outliers while, as with the Insch body, the northern and southern margins are largely fault bounded, with shear zones again obliterating contact features. The sequence of rocks is again from ultramafics

through to olivine ferrogabbros and syenites, with the Lower Zone rocks generally to the south and the Middle and Upper Zone rocks to the north.

The Lower Zone rocks are mainly extensively altered and deformed dunites and harzburgites along the sheared southern margin. Primary layering is not evident, but this fact is likely to be the result of the extensive shearing and deformation rather than a non-cumulate origin for these rocks. Isolated, fault bounded outcrops of slightly less deformed and altered ultramafic rocks are found within Middle Zone rocks in the centre of the Boganclogh mass and tectonically emplaced pods of ultramafics are also found along the northeastern and northwestern margins; again deformation and serpentinization are extensive. An isolated outcrop of olivine norite is found just to the northwest of the body, but Gould (1997) suggests this is unrelated to the main Boganclogh mass.

Middle Zone quartz-biotite norites comprise most of the central regions of the Boganclogh mass. Little variation in composition is evident in these norites with no layering evident, although grain size is variable. Contacts with the Lower Zone rocks, where present are faulted while concordant contacts with the Upper Zone rocks appear to be present in places, although faulted contacts are also found.

Upper Zone rocks are relatively well exposed in the Boganclogh intrusion and, as in the Insch intrusion, the chief lithologies are olivine ferrogabbros, monzonites and syenites. A similar subdivision of Insch into UZa, UZb and UZc, based on the phase mineralogy, has been proposed (Busrewil *et al.*, 1973); these are mainly found in the northern parts of the intrusion (see figure 4.5). Several isolated outliers of Upper Zone olivine monzonites are found within Middle Zone quartz-biotite norites in the central parts of the mass and thin, tectonically emplaced, slivers of Upper Zone syenite are found juxtaposed with Lower and Middle Zone rocks along the southern margin.

### 4.5.3 North-Western Bodies: Huntly, Knock, Portsoy and Succoth Brownhills

#### Previous work

Watt (1914) undertook the earliest study of the Huntly-Knock-Portsoy intrusive suite and this was followed by regional BGS surveys of the region resulting in the publications of Read (1923a, 1924). Other than Shackleton (1948), little work was carried out on the intrusion until the 1970s when Weedon (1970), Fettes (1970), Munro (1970; 1984), Munro

& Gallagher (1984), Fletcher (1989) and Fletcher & Rice (1989) reassessed the bodies, resulting in a far greater understanding of the outline and internal form of the bodies, in particular the effects shearing associated with the Portsoy Lineament has had upon the bodies. The intrusions are poorly exposed and several of these latter publications have drawn on geophysical surveys and extensive trench and borehole work to clarify many of the features of the bodies. Nevertheless, there are significant discrepancies between various published maps of the bodies. The Succoth-Brownhills mass possesses better exposure than the other bodies and has been mapped in detail using geophysical and field data (Gunn *et al.*, 1996).

**Huntly, Knock, Portsoy**

The Huntly, Knock and Portsoy bodies, shown in figure 4.6, form part of a southwestern-northeastern trending suite of mafic and ultramafic rocks that have been heavily deformed and dismembered by faulting and shearing. These shear zones, which are related to the Portsoy Lineament immediately to the west (see figure 2.6) have separated the suite into three separate masses, with the largest, Huntly, to the south, Knock immediately to its north, and Portsoy further north, adjacent to the Banffshire coast. The Huntly mass is 50-60 $km^2$ in size and, broadly speaking, youngs from west to east, with layering, where evident, vertical or steeply dipping to the east. The western margins consist of Lower Zone peridotitic and troctolitic cumulates, with minor amounts of Lower Zone cumulates also found along parts of the eastern margin. Numerous, minor, badly altered and deformed peridotitic and amphibolitic bodies associated with the main intrusion are also found within the heavily sheared Dalradian country rocks immediately to the west of the mass.

The Middle Zone cumulates consist mainly of olivine-gabbros, gabbronorites and rare norites and are found throughout the remainder of the body. In the field, these cumulate Middle Zone rocks are again found in very closely association with a series of granular gabbros, which bear a strong resemblance to those found within the eastern parts of the Inch mass. As is the case in Insch, the precise relationship between the cumulate and non-cumulate gabbros is uncertain due to conflicting field relations and poor exposure; thin section evidence combined with outcrop and borehole evidence in the field, can be used to show that there is a gradation between the two rock types. Transitional gabbro varieties, containing both granular and cumulate aspects to their texture are also common. No Granular Gabbros samples from the Huntly body have been sampled as part of this study. Contaminated and xenolithic gabbros are widespread within the Middle Zone, as is the

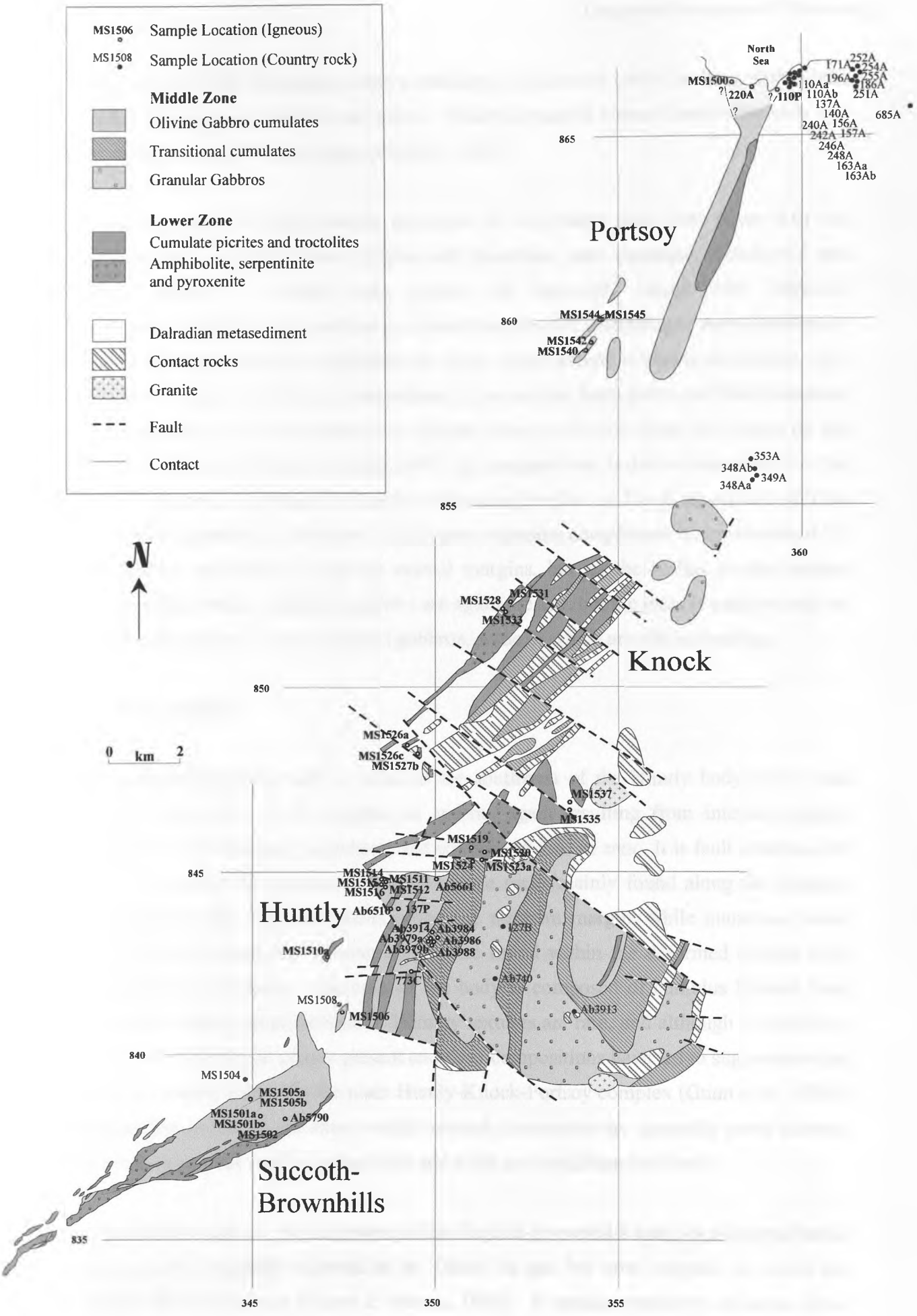


**Figure 4.6 Location of samples in the Huntly, Knock, Portsoy and Succoth- Brownhills intrusions (based on Fletcher (1989), Munro (1984) and Gunn et al (1996)**

presence of xenolithic fragments, often containing evidence for partial melting within both cumulate and granular Middle Zone rocks. Minor amount of Upper Zone rocks have also been reported form the Huntly mass (Fletcher, 1989).

The Knock mass is a fault bounded extension of the Huntly mass (see figure 4.6) and consists mainly of Lower Zone picrites and troctolites, and cumulate, transitional and granular varieties of Middle Zone gabbro, all intricately mixed with Dalradian metasediment, hornfels and xenoliths in a heavily tectonised assemblage. Amphibolites are also found along the western margins of the body. Precise field relations are unclear, with poor exposure again resulting in uncertainty as to precise boundaries and field relations. The Portsoy body is an elongate mass running inland from the town of Portsoy on the Banffshire coast for 8-10 km (see figure 4.6). Its elongate form is due to its proximity to the Portsoy Lineament, and numerous smaller associated bodies are found associated with the Portsoy body, especially to the west. Again poor exposure complicates interpretation of the field relations, particularly along the coastal margins, but all the bodies display intense shearing and alteration. Granular gabbros are again present, but the mass is mainly made up of serpentinized Lower Zone rocks and gabbros, some of which are olivine bearing.

**Succoth-Brownhills**

The Succoth-Brownhills mass is found to the southwest of the Huntly body and is also shown in figure 4.6. It is elongate in outline, again resulting from intense shearing associated with the Portsoy Lineament, and covers ~15 $km^2$ in area. It is fault bounded and heavily deformed with serpentinized Lower Zone rocks mainly found along the southern and eastern margins, but also locally along the northern margin, while numerous minor 'pods', primarily ultramafic in composition, are found within the deformed country rock adjacent to the main mass. The bulk of the body is composed of cumulus Middle Zone gabbros, now largely amphibolitized. Primary textures are rare, and although the intrusion is extensively altered, the phases present and their compositions have led to suggestions that they are not closely related to the main Huntly-Knock-Portsoy complex (Gunn *et al.*, 1996); orthopyroxene is rare in the mass, while mineral chemistries are generally more extreme (higher clinopyroxene mg#'s; higher Fo% and An% contents) than in Huntly.

The Blackwater mass, to the southwest of the Succoth-Brownhills body, is a sheared basic-ultrabasic body, originally believed to be 'Older' in age, but now accepted as one of the 'Younger' Basic intrusions (Fettes & Munro, 1989). It consists primarily of Lower Zone

peridotitic material and Middle Zone gabbros and olivine-gabbros and has not been sampled as part of this study.

### 4.5.4 South-Western Bodies: Morven Cabrach, Coyles of Muick

**Previous work**

Little published work has been undertaken on the southwestern bodies. The earliest work of Hinxman (1896) assigned it to the 'Older' Basic suite of bodies within the region. Allan (1970) published the only complete account of the body, and showed it was more likely to be of 'Younger' affinity. With the exception of BGS regional mapping, no specific accounts of the Coyles of Muick body have been published.

**Morven Cabrach**

The Morven Cabrach mass, shown in figure 4.7, is the westernmost of the main 'Younger' Basics masses, again found adjacent to the Portsoy Lineament. It is an elongate body, ~130km$^2$ in size, irregular in shape, narrowing towards its northern margins, which are close to the Boganclogh and Succoth-Brownhills masses (see figure 4.1). It is composed primarily of a variety of Middle Zone gabbros and norites, which are quite badly altered in the southern parts of the body. Possible Lower Zone serpentinites are found along the southern and parts of the western margins, although these may predate the main intrusion and consequently be 'Older' in age. Broadly speaking, the Middle Zone norites and gabbros can be divided into two groups in the north and in the south. In the south, norites, hypersthene-gabbros and ferrogabbros are found, displaying well-developed layering, which dips moderately to the north- northeast; poor exposure makes the boundaries between these individual units difficult to map precisely.

Further north, quartz-biotite-norites predominate; these are quite similar to those seen in the Boganclogh mass to the immediate northeast displaying little internal variation, except in the immediate north of the body, where they grade sharply into more dioritic compositions. Hornfelsed pelitic xenoliths are increasingly common towards the northern margins of the body. In the south, two isolated outcrops of Upper Zone syenogabbro are found, containing olivine and abundant apatite and oxide material; poor exposure again makes their relationship to the surrounding Middle Zone rocks unclear.

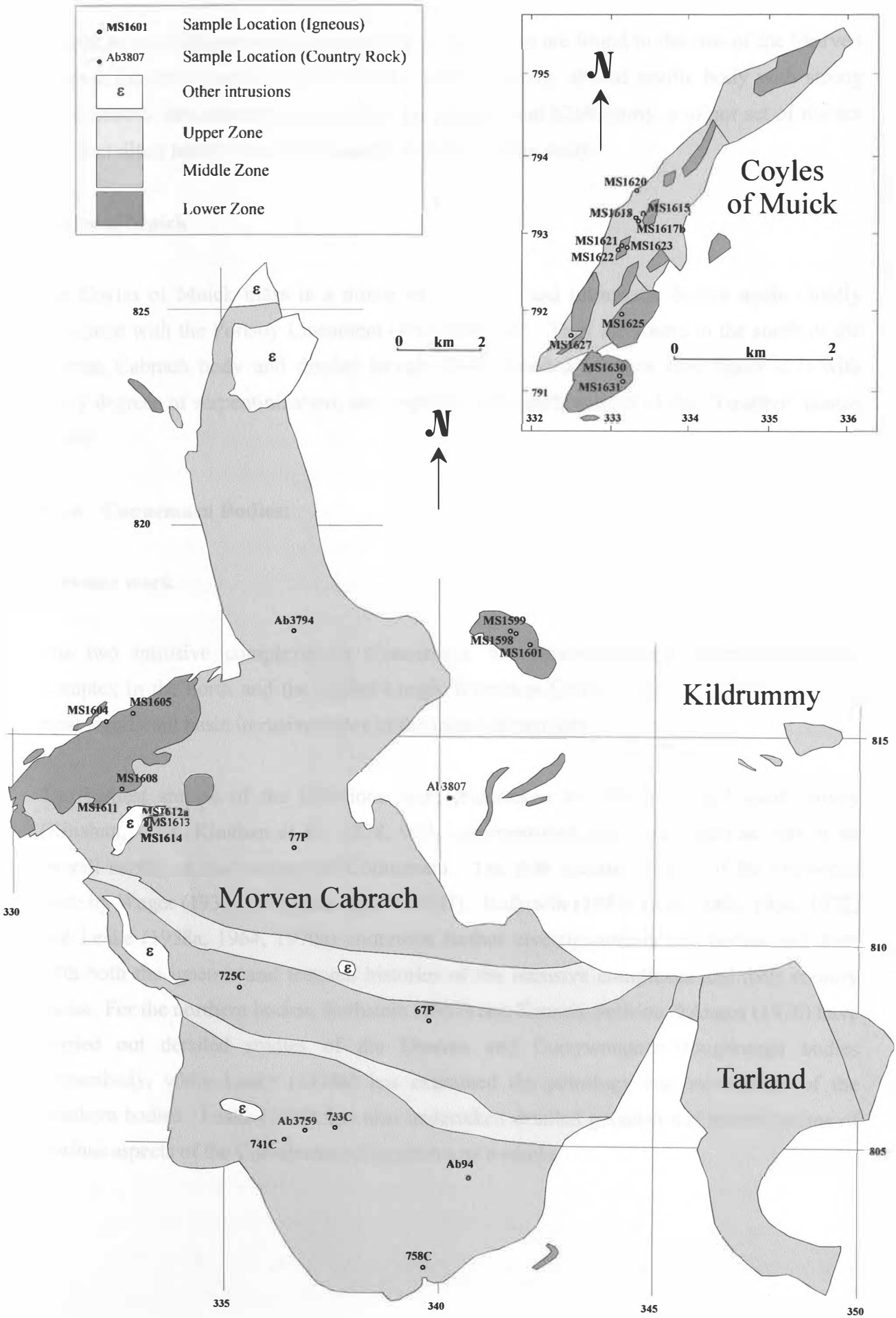


**Figure 4.7 Location of samples in the Morven Cabrach and Coyles of Muick intrusions (inset).**

Several minor fault bounded basic and ultrabasic bodies are found to the east of the Morven Cabrach intrusion, including the Tarland mass, a heavily altered noritic body with strong similarities to the southern parts of Morven Cabrach and Kildrummy, a minor set of norites and troctolites; neither have been sampled as part of this study.

**Coyles of Muick**

The Coyles of Muick mass is a minor set of mafic and ultramafic bodies again closely associated with the Portsoy Lineament (see figure 4.1). They are found to the south of the Morven Cabrach body and display largely fault bounded contacts (see figure 4.7) with heavy degrees of serpentinization; they represent the southernmost of the 'Younger' Basics bodies.

### 4.5.4 Connemara Bodies:

**Previous work**

The two intrusive complexes in Connemara, the Dawros-Currywongaun-Doughruagh Complex in the north and the Cashel-Lough Wheelaun Complex in the south are the two most significant basic intrusive suites in the Irish Caledonides.

The earliest studies of the intrusions were undertaken by the Irish Geological Survey (Kinahan, 1874; Kinahan *et al.*, 1878, with accompanying one inch maps) as part of an overall survey of the geology of Connemara. The first specific studies of the intrusions were by Wager (1932, 1939) and Ingold (1937). Rothstein (1957, 1958, 1961, 1964, 1972) and Leake (1958a, 1964, 1970a) undertook further investigations of the bodies and dealt with both the igneous and tectonic histories of the intrusive complexes and their country rocks. For the northern bodies, Rothstein (1957) and Kanaris-Sotiriou &Angus (1976) have carried out detailed studies of the Dawros and Currywongaun-Doughruagh bodies respectively, while Leake (1958a) has examined the petrology and mineralogy of the southern bodies. Leake (1989) has also undertaken detailed geochemical investigations of various aspects of the Connemara metagabbros as a whole.

**Dawros-Currywongaun-Doughruagh**

The Dawros-Currywongaun-Doughruagh Complex, shown on figure 4.8, is a series of well-exposed minor intrusions found intruded into Dalradian metasediments in the northwest of the Connemara inlier. The westernmost Dawros mass is slightly less than 1 $km^2$ in size and consists largely of layered Lower Zone peridotites with rare interstitial plagioclase feldspar. Despite having undergone extensive deformation and alteration, it retains many primary layered textures and structures, such as graded and cross bedding.

Middle Zone rocks are found chiefly in the Currywongaun body, which is found to the east of the Dawros body and tectonically separated from it. It is ~3 $km^2$ in size and comprises chiefly norites with local pyroxenites and anorthosites where layering is evident, although layering is poorly developed or absent over much of the body. In the eastern parts of the body, quartz-bearing norites are found. Several smaller, related noritic bodies are also found between the Currywongaun and Dawros bodies and within the Dawros mass. The slightly larger Doughruagh body immediately to the east consists of unlayered norites and extensive acid gneisses, which occur mainly as pegmatites injected within the Doughruagh body and locally within the Currywongaun mass. Contacts between the bodies are faulted or sheared and there is considerable internal disruption due to local shearing. With the exception of these acid pegmatites, Upper Zone rocks are not found within the complex.

**Cashel-Lough Wheelaun**

This suite of meta-gabbroic bodies is found along the southern margins of the Connemara region. Faulting and shearing have broken up the complex into several separate intrusions, shown in figure 4.9, with the Cashel intrusion forming the westernmost intrusion. It is ~2 $km^2$ in size and roughly oval in shape with variable exposure and the principal rock types are hornblende-bearing peridotites and gabbros. Broadly speaking, the Lower Zone peridotites are found in the north and west of the intrusion with hornblende-bearing Middle Zone gabbros and norites found to the southeast. Layering is poorly developed, and only found on the northern and western margins of the body. The Lough Wheelaun body is ~2.5 $km^2$ in size and quite poorly exposed with layering again only weakly developed. Lower Zone rocks are confined to northern parts of the intrusion, although isolated peridotitic areas are found in the south of the body, which is mainly composed of Middle Zone gabbros and norites with ever-present hornblende. Several tectonically separate, minor bodies are also

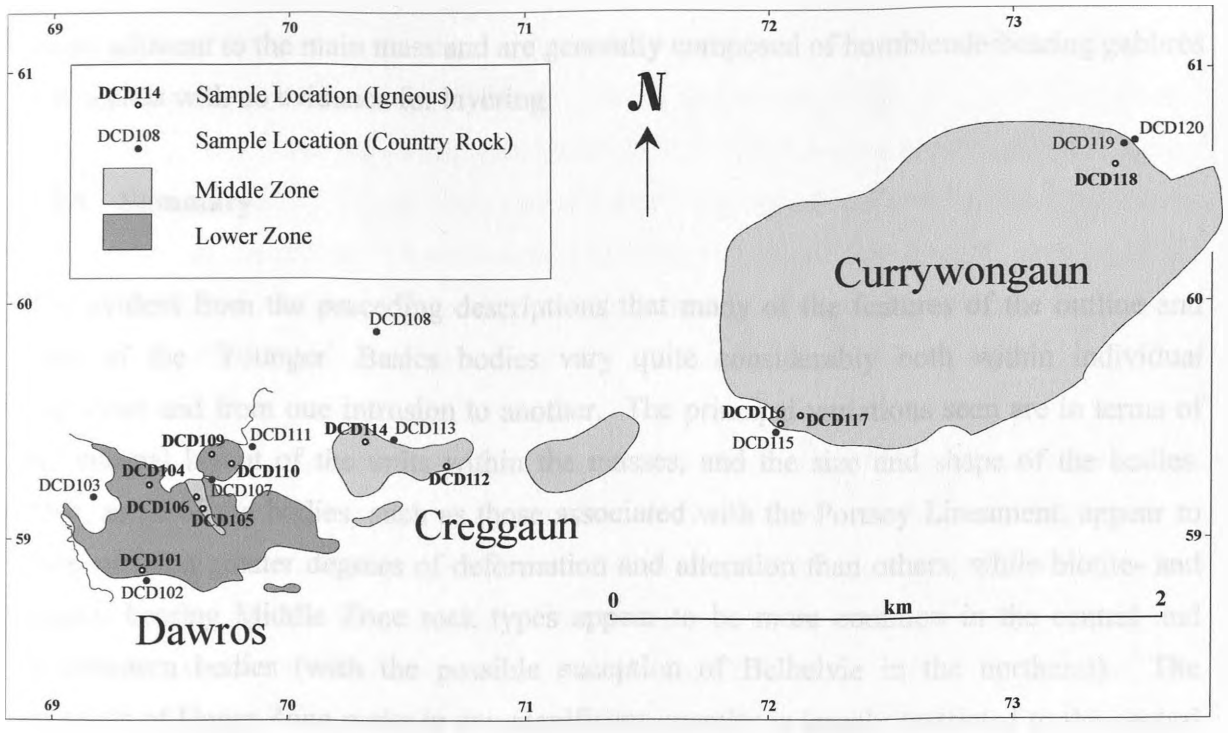


**Figure 4.8 Location of samples in the Dawros and Currywongaun intrusions.**

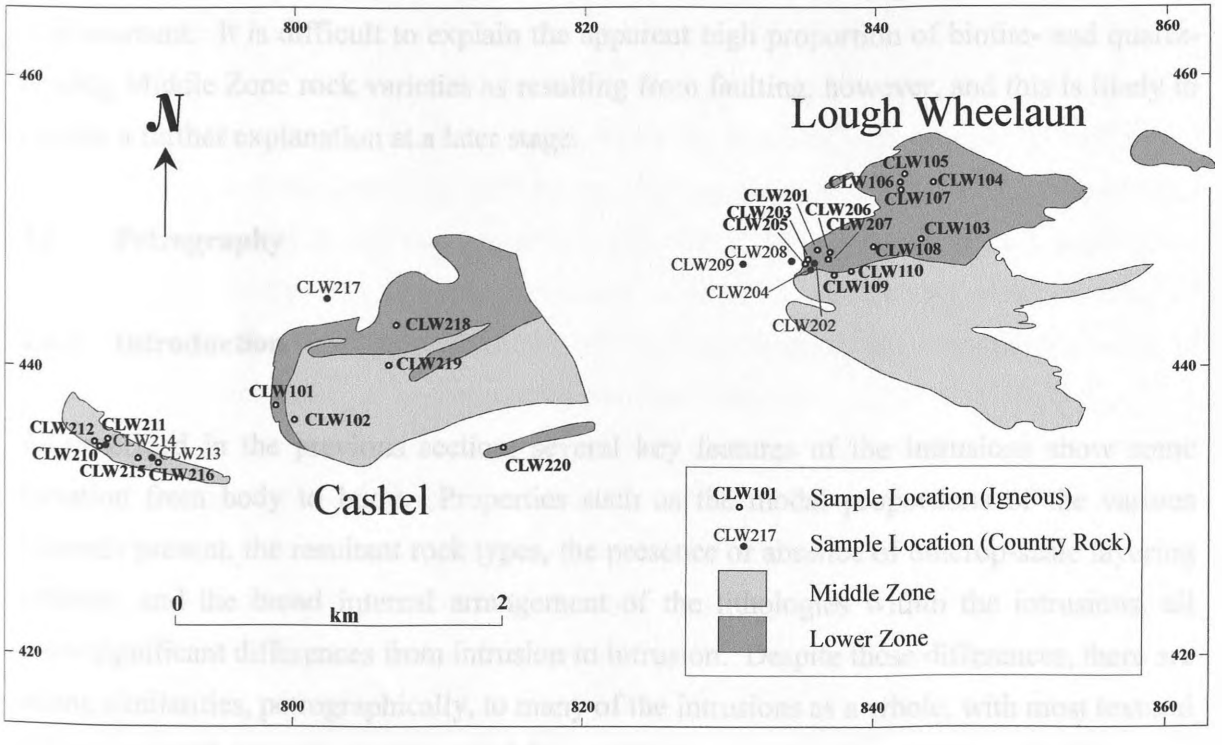


**Figure 4.9 Location of samples in the Cashel and Lough Wheelaun intrusions.**

found adjacent to the main mass and are generally composed of hornblende-bearing gabbros and norites with no evidence for layering.

### 4.5.5 Summary

It is evident from the preceding descriptions that many of the features of the outline and form of the 'Younger' Basics bodies vary quite considerably both within individual intrusions and from one intrusion to another. The principal variations seen are in terms of the internal layout of the units within the masses, and the size and shape of the bodies. Also, some of the bodies, such as those associated with the Portsoy Lineament, appear to have suffered greater degrees of deformation and alteration than others, while biotite- and quartz- bearing Middle Zone rock types appear to be more common in the central and northeastern bodies (with the possible exception of Belhelvie in the northeast). The presence of Upper Zone rocks in any significant quantity is largely restricted to the central Insch and Boganclogh bodies, while the relative proportions of Lower to Middle Zone rocks in the northeastern masses is quite variable. The majority of these variations can be satisfactorily explained as resulting from possible variations in volume at the time of emplacement, and shearing and alteration associated with the regional lineaments after emplacement. It is difficult to explain the apparent high proportion of biotite- and quartz-bearing Middle Zone rock varieties as resulting from faulting, however, and this is likely to require a further explanation at a later stage.

## 4.6 Petrography

### 4.6.1 Introduction

As described in the previous section, several key features of the intrusions show some variation from body to body. Properties such as the modal proportions of the various minerals present, the resultant rock types, the presence or absence of outcrop-scale layering features, and the broad internal arrangement of the lithologies within the intrusions, all show significant differences from intrusion to intrusion. Despite these differences, there are strong similarities, petrographically, to many of the intrusions as a whole, with most textural properties, both in hand specimen and thin section, consistent from intrusion to intrusion. Indeed, many of the textural features seen in the suite as a whole, and described below are similar to those commonly seen in classic layered basic intrusions. Also, although the overall stratigraphic sequence is far from complete in all but the Insch and Boganclogh

bodies, each intrusion or intrusive complex can be assigned to part of the division of layered basic bodies proposed by Wager & Brown (1968) and shown in figure 4.2. It is as a result of these similarities that the petrographic descriptions in this section are grouped into Lower Zone, Middle Zone and Upper Zone, rather than on a geographical or intrusion-by-intrusion basis, to avoid repetition. Nevertheless, important variations are present, such as in the Insch and Huntly masses, where samples with partial or non-cumulate textures are present, and these are described accordingly.

Irvine (1982) defined a cumulate as 'an igneous rock characterized by a cumulus framework of touching mineral crystals or grains that were evidently formed and concentrated primarily through fractional crystallization' and emphasized that crystal settling is not implied by use of the term 'cumulate'. Crystal settling, however, is traditionally associated with the term, although in this section, no genetic implications are inferred from the textures described. This study is not concerned with the precise mode of formation of the cumulate samples either in this case, or in general, nor is it concerned with the precise mechanics of the fractionation of these 'cumulates' from their parent magmas: there are far more suitable intrusions for such studies than these bodies. In addition, Irvine (1982) defined postcumulus material as a 'texturally later generation ... that appears to have crystallized from the intercumulus liquid in the interstices or pores of the intercumulus framework' (see Plates 4.5 & 4.16). Orthocumulates contain abundant (mostly interstitial) postcumulus materials with the cumulus minerals ideally exhibiting much of their original crystallization outlines, while adcumulates are defined as 'having only minor discrete postcumulate material' (Irvine, 1982), and consequently a significant degree of overgrowth on primary cumulate phases. As such, orthocumulates and adcumulates are end members in terms of cumulus mineral overgrowth, with mesocumulates representing the intermediate between these two end members. It is commonly believed (Wager *et al.*, 1960, Campbell, 1978; Irvine, 1982) that various genetic implications such as rate of crystal accumulation may be inferred from the degree of adcumulus mineral growth although this will not be investigated further. Postcumulus material, also called interstitial or intercumulus material, is not a cumulus phase, although postcumulus growth may result in overgrowth on cumulus crystals, where it is part of adcumulate growth.

### 4.6.2 Significance of cotectic phases

Distinguishing between cotectic and non-cotectic phases and identifying changes in these phases and assemblages of these phases is important for understanding fractionation trends

seen within the whole rock chemical data. In volcanic rocks, minerals at or near the cotectic point can be easily identified; they are present as phenocryst phases within the groundmass. In order to identify cotectic minerals in intrusive rocks, in this case cumulates, a distinction needs to be made between primary cumulate minerals and late stage interstitial or postcumulate minerals, as only the cumulate minerals will have formed at or near the cotectic point. In order to make this distinction, careful petrographic examination and interpretation of textures developed in thin section must be undertaken. For example, in layered troctolites with regular interbanding of olivine- and plagioclase-rich units, both olivine and plagioclase are considered to be cotectic phases, while a norite with euhedral cumulate plagioclase and olivine and late interstitial orthopyroxene (e.g. see Plate 4.2) would be considered to have a cotectic assemblage of clinopyroxene and plagioclase but not orthopyroxene. Again, late- and post-cumulus processes such as adcumulate growth and interstitial fluid crystallisation must be recognised and taken into account when assessing these assemblages. This poses difficulties for certain phases, notably apatite, where it can be difficult to distinguish between cumulate and non-cumulate varieties.

### 4.6.3 Overall Petrography

As mentioned above, there are many petrographic features in common throughout the 'Younger' Basics as a whole. Although varying degrees of alteration and replacement are present throughout the bodies, the majority of samples show cumulate textures, with the exception of the Insch and Huntly Granular Gabbros, and the most badly deformed and sheared samples. Internal crystal zoning is variably developed; in much of the Boganclogh intrusion, internal zoning of crystals is quite well developed, while in other bodies it may be weak or absent entirely. Plagioclase feldspar is the only phase to display zoning where it is evident, with zoning in olivine or pyroxene not observed. Perthitic textures are seen in some Upper Zone syenites from the Insch body, but otherwise, the internal textures of individual crystals are largely uniform or constant. As will be seen in the next section, this lack of zoning in thin section is also evident chemically, in the probe analyses of these phases.

Textural evidence for the presence of postcumulus features such as crystal overgrowth or adcumulate growth is variable. In many instances the absence of zoning makes identification of adcumulate growth quite difficult, as original crystal outlines are not as well defined as they would be where zoning is evident in thin section; despite this, it is still evident that adcumulate growth, usually most clearly evident as overgrowths on euhedral

plagioclase feldspar laths is weakly developed or absent in most samples, leading to their overall classification as orthocumulates, although individual samples may be classified as mesocumulates and, in one or two cases, as adcumulates. As a result of this minor degree of adcumulate overgrowth, characteristic euhedral outlines for plagioclase feldspar and pyroxenes are common (see Plates 4.2 & 4.15) and there is substantial development of interstitial or postcumulus growth of non-cotectic phases such as biotite, hornblende and pyroxene (see Plates 4.5 & 4.6). This results in extensive development of classic intercumulus textures such as ophitic or poikilitic growth (see Plates 4.2, 4.4 & 4.16).

### 4.6.4 Lower Zone

Lower Zone rocks are found, in varying quantities, in all the intrusions, with the exception of the northeastern bodies of Arnage, Haddo, Kinnadie and Maud, where Lower Zone rocks are largely absent. For two main reasons, the Lower Zone rocks tend to be quite badly deformed and altered. Firstly, by their very nature, they are commonly found at the margins of the bodies, and consequently suffer from extensive deformation due to faulting and shearing, and secondly, the susceptibility of olivine, the dominant Lower Zone mineral, to alteration means that most Lower Zone rocks display high degrees of alteration, most commonly serpentinization. Nevertheless, samples that have escaped extensive alteration and deformation do exist and, in addition, many of the textural features of these rocks can still be deciphered from less fresh samples.

Lower Zone ultramafic rocks from both the Scottish and Irish bodies are composed largely of quite coarse-grained olivine and pyroxene bearing units; these units display cumulate textures despite common alteration, with poikilitic pyroxenes and sub-euhedral olivines common. Olivine and clinopyroxene are generally present as cumulate phases, with orthopyroxene occasionally present as a cumulate phase, but more commonly as an intercumulate or poikilitic phase (see Plates 4.2, 4.15 & 4.16). In several cases, orthopyroxene is found as clusters of crystals in an olivine groundmass. As is to be expected in samples of a cumulate nature, mineral proportions are variable, but olivine is the predominant phase and olivine-rich dunites, wehrlite and lherzolites tend to predominate. Accessory minerals are mainly spinel and opaques while plagioclase, where present, is late and intercumulus (see Plate 4.1).

Towards the top of the Lower Zone, the incoming of plagioclase as a cumulate phase leads to rock types such as troctolites (see Plate 4.3), olivine-gabbros (see Plate 4.2) and

Plate 4.1 (a) PPL

Plate 4.1 (b) XPL

**Plate 4.1 Sample Ab82, a Lower Zone sample from the Belhelvie mass. Orthoyroxene is the main cumulus phase and is surrounded by interstitial plagioclase feldspar (top) and abundant biotite. Vertical scale = 3.0 mm.**

Plate 4.2 (a) PPL

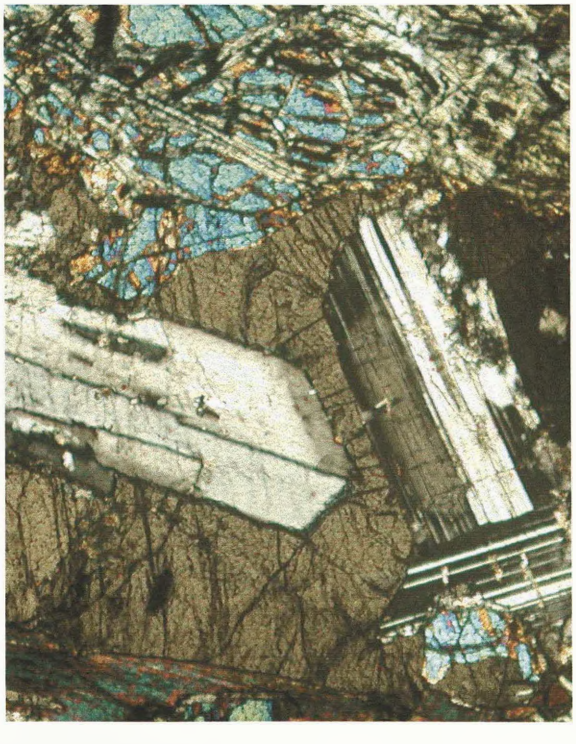

Plate 4.2 (b) XPL

**Plate 4.2 Sample MS1595 from the Boganclogh intrusion, showing euhedral cumulus plagioclase feldspar laths enclosed within postcumulus or poikilitic orthopyroxene. Some of the feldspars display weak zoning (centre in XPL). Cumulus olivine at the top of the view shows minor corona development. Vertical scale = 1.6 mm.**

Plate 4.3 (a) PPL

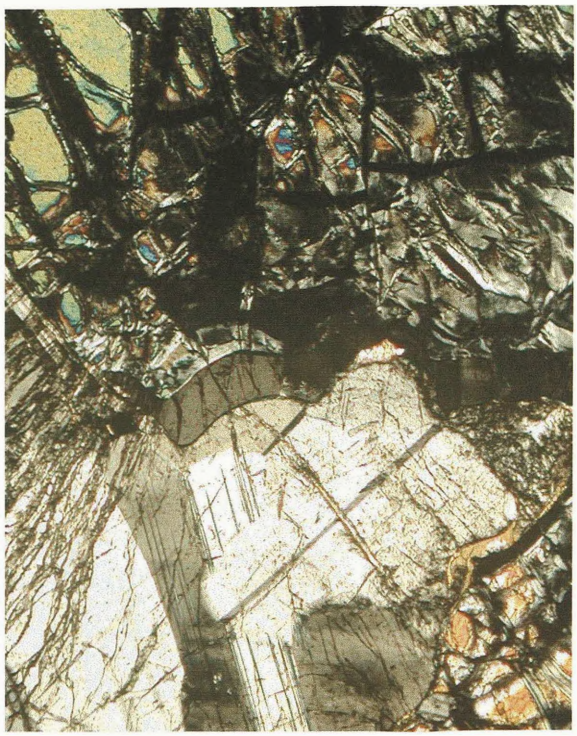

Plate 4.3 (b) XPL

**Plate 4.3 Sample Ab140, a troctolite from the Lower Zone of the Belhelvie mass. Cumulus olivine (partly serpentinized; top right) and cumulus plagioclase feldspar showing typical expansion cracks. An orthopyroxene corona between these two phases is also present. Vertical scale = 3.0 mm.**

Plate 4.4 (a) PPL

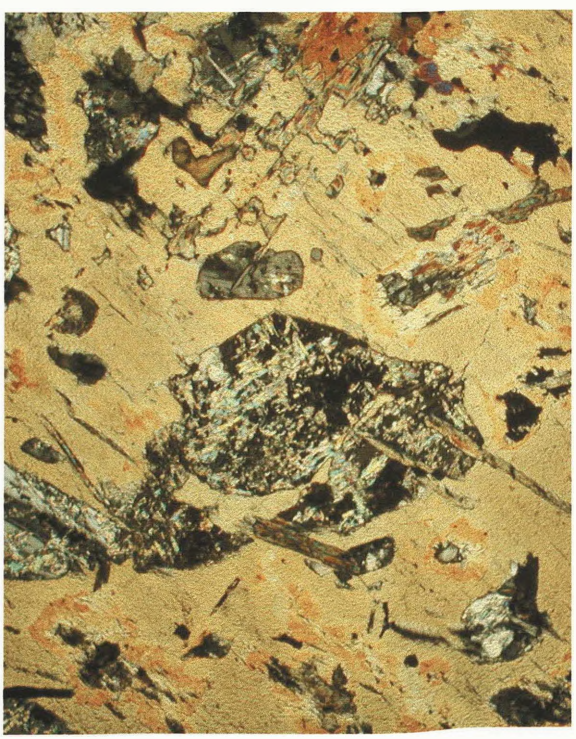

Plate 4.4 (b) XPL

**Plate 4.4 Sample CLW206 from the Lough Wheelaun body. Poikilitic hornblende encloses biotite, opaques and heavily altered plagioclase feldspar. Vertical scale = 3.0 mm.**

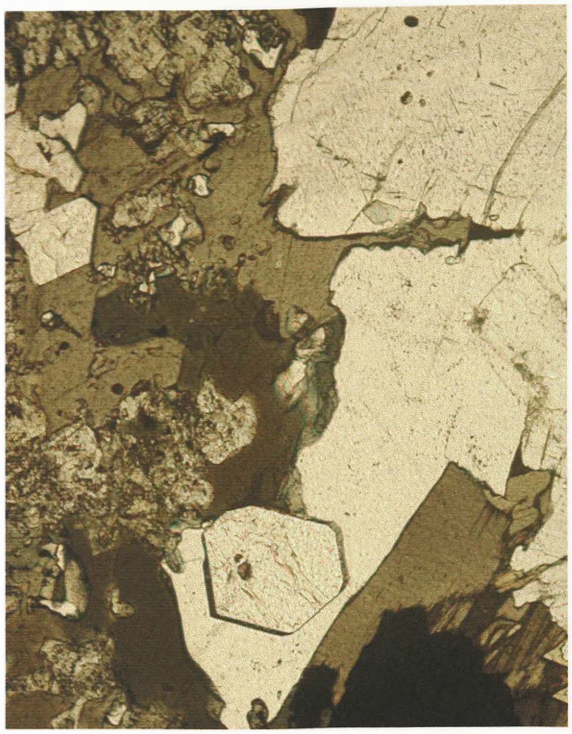

Plate 4.5 (a) PPL

Plate 4.5 (b) XPL

**Plate 4.5 Sample Ab92, a biotite- hornblende- gabbro from the Maud mass. Cumulus apatite and clear interstitial hornblende and quartz are present. Orthopyroxene partly replaced by secondary amphibole, and biotite by chlorite. Vertical scale = 1.6 mm.**

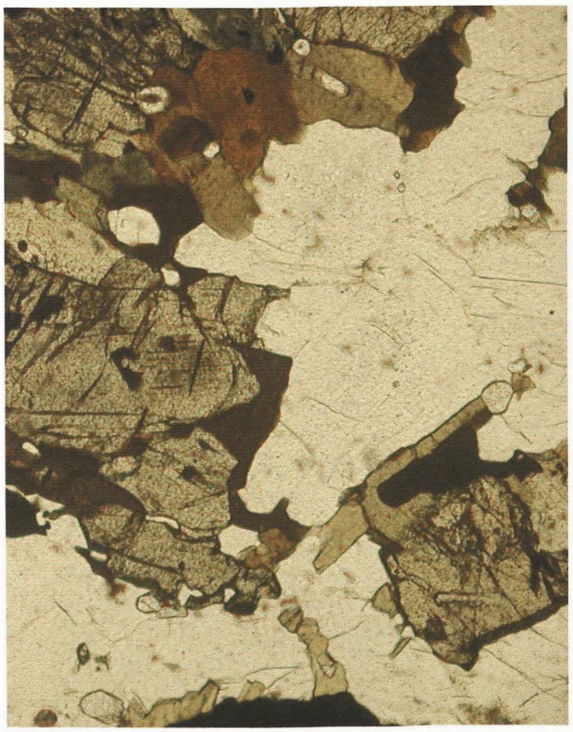

Plate 4.6 (a) PPL

Plate 4.6 (b) XPL

**Plate 4.6 Ab1310 from the Maud body. Abundant interstitial biotite and amphibole as mantles on ilmenite and orthopyroxene. Again cumulus apatite and late quartz present. Weak feldspar zoning present in several crystals. Vertical scale = 1.6 mm.**

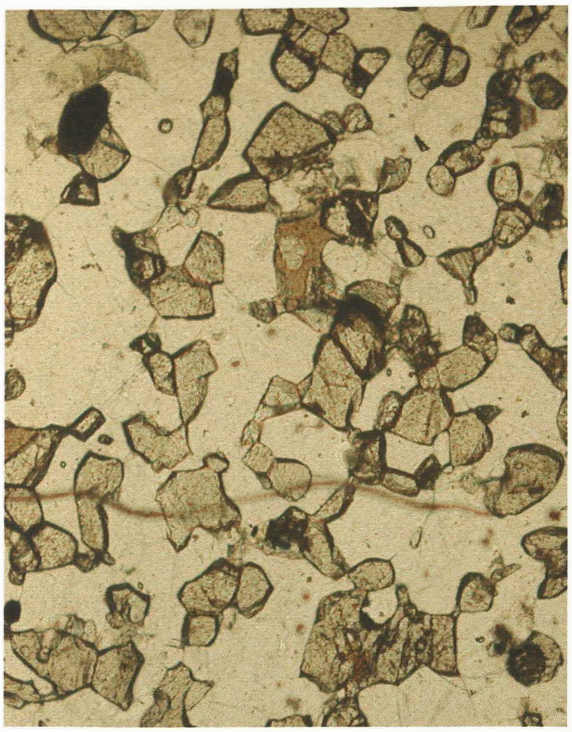

Plate 4.7 (a) PPL

Plate 4.7 (b) XPL

**Plate 4.7 Granular Gabbro sample V(Ol) from the Insch intrusion displaying an equigranular mosaic of olivine, both pyroxenes and plagioclase. Some opaques and interstitial amphibole are also present. Vertical scale = 1.6 mm.**

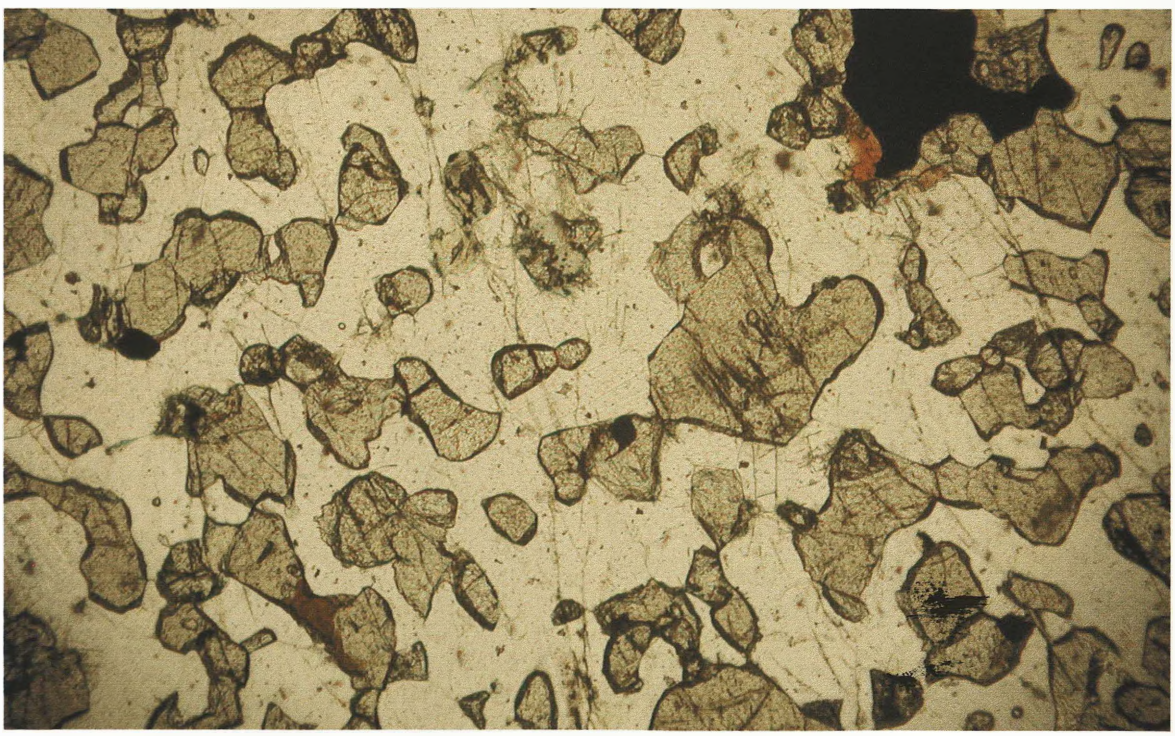

Plate 4.8 PPL

**Plate 4.8 Sample PY2, a similar Granular Gabbro from the Insch mass, with orthopyroxene, clinopyroxene, plagioclase feldspar and some late biotite and opaque material. Vertical scale = 1.6 mm.**

Plate 4.9 (a) PPL

Plate 4.9 (b) XPL

**Plate 4.9 Sample S, a Granular Gabbro from the Insch body. Consists of slightly altered orthopyroxene and clinopyroxene in an equigranular arrangement with plagioclase feldspar. Vertical scale = 1.6 mm.**

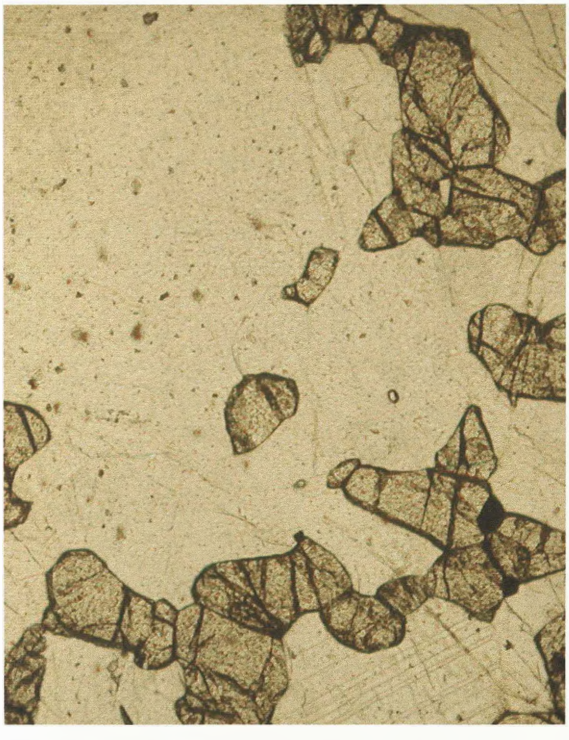

Plate 4.10 (a) PPL

Plate 4.10 (b) XPL

**Plate 4.10 Sample PY3, a Granular Gabbro from the Insch intrusion containing both porphyritic and granular plagioclase feldspar. Granular olivine, ortho- and clinopyroxene are also present. Vertical scale = 1.6 mm.**

gabbronorites; again layering is generally quite well developed in these rocks and, in thin section, the troctolites in particular display excellent cumulate textures with euhedral aligned plagioclase and olivine crystals both of which are cumulate in nature. Adcumulate growth is seen in several of these troctolitic samples. Pyroxene is not usually cumulate and tends to be present as minor intercumulus crystals, usually of orthopyroxene (see Plate 4.2), while accessories are rare, although occasional interstitial biotites (see Plate 4.2), amphiboles, and opaques are seen. Where the pyroxene is cumulate, olivine-gabbros and gabbronorites are developed, with similar petrographic properties to the troctolites. Corona growth on olivine is very common in these types of rock; these coronas are commonly formed of several layers of orthopyroxene and amphiboles mantles on the olivine resulting from post-cumulus reaction between the olivine and plagioclase feldspar (see Plates 4.2 & 4.3).

The Lower Zone rocks from the individual intrusions, where present display little variation in petrography. The troctolitic units from the upper regions of the Lower Zone are not always present, and the transition from Lower Zone to Middle Zone is commonly absent, perhaps due to shearing at the transition, or a hiatus in crystallisation, or a combination of both. The only notable variation is found in the Cashel-Lough Wheelaun Complex body in Southern Connemara, where the Lower Zone units contains several areas of ultramafic rock in which large quantities of intercumulus or poikilitic hornblende are found (see Plate 4.4). In addition, within these units, layering is poorly developed.

### 4.6.5 Middle Zone

The chief rock types of Middle Zone affinity are gabbros and norites, although olivine-bearing gabbros are common and troctolites, anorthosites and pyroxenites often occur where layering is well developed. Several of the intrusions, such as Belhelvie, do not contain a complete Middle Zone sequence, and as such, are not included in the following descriptions. With the exception of the Granular Gabbros, the degree of development of layering is particularly variable and Middle Zone rocks can display excellent layering in one outcrop and no evidence for layering in an adjacent outcrop. Typically, samples display well-developed, coarse-grained, cumulate textures with euhedral plagioclase usually the earliest and most abundant crystallizing phase, accompanied by one or both of the pyroxenes. Orthopyroxene, where present is typically elongate in shape, but is also commonly present as an intercumulus or poikilitic phase while clinopyroxene, when it occurs, tends only to be as a cumulate phase. In general, orthopyroxene is slightly more

abundant than clinopyroxene, although in any one sample, abundances can vary quite dramatically. Some of the orthopyroxene seen in the Middle Zone displays textural evidence to suggest that it has exsolved or inverted from an original pigeonite composition, with large clinopyroxene lamellae commonly found exsolved along cleavage planes within the orthopyroxene.

Towards the top of the Middle Zone, Fe-Ti oxides, predominantly ilmenite, are often present as a minor cumulate phase with distinctive lath shaped outlines (see Plate 4.13), while biotite, amphibole, apatite and quartz are common as minor late intercumulus phases (see Plate 4.5 & 4.6). Apatite appears to be generally postcumulus through much of the Middle Zone, although it may become cumulus towards the top of the Middle Zone (see Plate 4.14); as mentioned however, it can be quite difficult to distinguish between cumulus and postcumulus apatite in many instances due to its euhedral outline and apparent interstitial nature in both cases. The late biotite, and primary amphibole, where present, is commonly found as overgrowths on pyroxenes or Ti-oxides (see Plate 5.2), while late stage quartz is more common in the upper parts of the Middle Zone in some intrusions (see Plates 4.5 & 4.6). Although the development of cumulate textures is generally quite good, and alignment of lath-shaped crystals such as plagioclase feldspar and orthopyroxene is often found, outcrop scale layering is considerably less well developed than in the Lower Zone and is commonly absent.

The modal proportions of the individual phases are clearly dependent on cumulus processes and, as such, vary quite a great deal even within individual hand specimens; nevertheless, general variations are evident. The northeastern intrusions of Arnage, Haddo, Kinnadie and Maud have considerably more biotite, primary amphibole and quartz than Middle Zone rocks from other bodies (see Plate 4.5 & 4.6). Biotite can commonly reach 10% or more modally, and quartz up to 15%. The Insch and Boganclogh bodies rarely contain postcumulus quartz, while it is rare or absent in other bodies such as the Cashel-Lough Wheelaun and Huntly intrusions. Also, apatite concentrations, although still minor, are more abundant in the Middle Zone of the northeastern bodies than in other Middle Zone rocks, while orthopyroxene tends to predominate over clinopyroxene to a greater extent than in other Middle Zone rocks. The modal proportions of the bodies will be discussed in more detail in Section 4.7.9. Plagioclase feldspar zoning is seen in several samples from Boganclogh (see Plate 4.2); however, it is only found in occasional crystals and is poorly developed, with no evidence for other cumulate textures such as zoning in other crystals or secondary cumulate growth.

The Granular Gabbros from the Insch and Huntly masses form a quite distinctive set of rocks texturally. Their granular texture has led to considerable debate as to their origins, with both cumulate (Thy & Esbensen, 1982) and non-cumulate origins (Wadsworth, 1988) proposed. As mentioned earlier, Wadsworth (1988) proposed the names fine-grained granular gabbro (FGG) for the main type of Granular Gabbros, with a variety containing porphyritic plagioclase feldspar (PGG). As the names suggest, these gabbros are finer grained than their cumulate counterparts are, with a distinctive non-cumulate texture in thin section. Triple point or 120° equilibration textures are common (see Plate 4.7 & 4.8) and grain size is generally < 1 mm in size and quite uniform within individual samples (with the exception of porphyritic granular gabbros: see Plate 4.10). Fabrics are weak to absent in thin section; where present, the fabric takes the form of weak alignment of plagioclase feldspar or orthopyroxene. Occasional plagioclase feldspar zoning is seen, while interstitial hornblende and biotite is present in most samples (see Plates 4.7 & 4.8). Mixed fabrics are not uncommon in thin sections of Granular Gabbros samples from both Huntly and Insch; it is not unusual for individual thin sections to contain elements of both cumulate and granular textures.

In the field, the relationship between the Granular Gabbros and the established cumulate Middle Zone is unclear. The transition between the two Middle Zone rock types is accompanied by a decrease in grain size and, in some cases, a gradual transition can be detected from clearly cumulate to granular over the scale of 1-2 metres, with intermediate varieties containing aspects of both granular and cumulate textures. In other instances, however, the transition is quite sharp, but nevertheless the relationship with the cumulate Middle Zone is unclear, and poor exposure makes the precise relationship between the two rock types additionally difficult to interpret (see discussion in Wadsworth, 1988). The Granular Gabbros are markedly fresh in thin section, with sericitization of plagioclase feldspar and hydration of mafic phases largely absent.

### 4.6.6 Upper Zone

As Upper Zone rocks are mainly only found in the Insch and Boganclogh masses, the petrographic descriptions are of these rocks only and should not be considered representative of the whole gabbroic suite. Minor amounts of Upper Zone rocks are also found locally in the Morven Cabrach and Huntly intrusions and in some bodies, such as Currywongaun in North Connemara, as late acid pegmatite dykes, but in general, Upper Zone rocks are not found other than in the Insch and Boganclogh masses. In general,

grainsize is particularly coarse, occasionally reaching 10mm, with layering or crystal alignment rare. Cumulate textures are not as well developed as in Lower and Middle Zone samples and many of the more syenitic and dioritic samples display textures similar to those seen in granites. Nevertheless, minerals of cumulate and post-cumulate origin can be identified, with the base of the Upper Zone marked by the reappearance of cumulus olivine. Alkali-feldspar is also found, firstly as an intercumulus phase and then as a cumulus phase (see Plate 4.12), while isolated hornblende crystals of possible cumulate origin are seen towards the top of the Upper Zone (see Plate 4.17). Some of this early intercumulus alkali-feldspar displays strong perthitic textures in thin section (see Plate 4.12 & 4.17), while cumulus apatite and zircon are also present in the Upper Zone.

### 4.6.7 Alteration

All three zones have suffered alteration to varying degrees. In the Lower Zone, extensive replacement of olivine by iddingsite and serpentine is seen throughout (see Plates 4.2 & 4.3), while plagioclase feldspar displays varying degrees of sericitization, particularly in troctolitic units, where extensive sericitization is found along expansion cracks associated with the hydration and alteration of the olivines (see Plate 4.3). Alteration of pyroxene is also variable and, where present, is in the form of replacement by amphibole. Middle Zone rocks display similar alteration, with pyroxenes again replaced to varying degrees by amphiboles (see Plate 4.11 & 5.2), which also display varying textures. This amphibolitization varies as much within an individual thin section as it does from sample to sample. Although complete replacement is commonly seen in individual crystals, it is rarely seen throughout except in the most altered samples.

Biotite is generally fresh although frayed margins and alteration to chlorite are occasionally seen (see Plate 4.5) while oxide rims are occasionally present. Alteration of ilmenite and other associated Ti-oxides to marcasite and other sulphides or hydrous minerals is occasionally seen. As mentioned, the Granular Gabbros are noticeably fresher, presumably due to their granular nature making them less susceptible to hydrothermal alteration. Upper Zone rocks remain relatively fresh, with again amphibolitization of pyroxenes common and evidence, in some cases, for localised fluid movement and associated metasomatism.

### 4.6.8 Summary and Conclusions

One of the main features evident from studies of the petrography of the bodies is the broad overall similarity in the cumulate sequences from body to body. Similar cumulus phases occur in similar sequential orders with broadly similar textural relations between the individual mineral types. Notable differences are in the abundance of hornblende in Lower Zone rocks from the Cashel-Lough Wheelaun Complex and the occurrence of the Granular Gabbros in Insch and related rocks in Huntly. In addition, the abundance of quartz, biotite and apatite in Middle Zone rocks from the northeastern bodies is distinctive, as is the fact that Upper Zone rocks are only found in the Insch and Boganclogh masses. Adcumulate growth is generally only slight, resulting in extensive growth of postcumulus phases such as hornblende and biotite, while zoning is variably developed, suggesting that, perhaps, some form of chemical re-equilibration may have operated within the bodies, resulting in the weakly developed zoning features from many samples. The most likely causes of this re-equilibration are either slow cooling or metamorphism, or a combination of both. In addition, the growth of well-developed coronas of orthopyroxene and amphibole as reaction rims between olivine and plagioclase feldspar in many troctolitic units, the presence of inverted pigeonite in Middle Zone units, and the perthitic textures in Upper Zone alkali feldspars, all suggest a prolonged period of cooling and re-equilibration. Such a slowly cooling and crystallising magma chamber is necessary for the formation of features such as layering and development of zones based on phase assemblages; all of these features are consistent with the PT estimates for the emplacement of these intrusions at mid crustal levels (Ashworth & Chinner, 1978; Droop & Charnley, 1985)

## 4.7 Mineralogy

### 4.7.1 Introduction

Probework was carried out on polished thin sections of selected samples using a wavelength dispersive electron microprobe at the BGS, Keyworth, Nottingham. Details of analytical procedures and accuracy are given in Appendix B. Unless stated, analyses given in tables or in the text are mean values for a thin section, formed from an overall average of averages of individual crystals. As such, most analyses are an average of a minimum of 4-5 individual microprobe analyses, usually from the crystal core, although when referring to internal crystal zoning, individual microprobe analyses are given.

This section will examine various aspects of the mineral chemistry of the silicate phases found in the 'Younger' Basics, and their compositional variation with progressive evolution of the bodies. Summarised olivine, pyroxene and feldspar analyses are shown in Tables 4.2 to 4.5 and overall compositional trends for these main silicate phases are shown in figures 4.10 to 4.12. Both whole rock mg# and mineral mg# are used in this section, with the whole rock mg# values representing a fractionation index for the intrusions as will be discussed in the next chapter. Cationic mg# is used to describe $mg:fe^{2+}$ ratios in ferromagnesian silicate phases, where mg and $fe^{2+}$ are the cationic proportions present in the mineral. Where no other components (e.g. tephroite in olivine) are present, then the forsterite (Fo) and enstatite (En) components are the same as, or very similar to, the mineral mg#.

### 4.7.2 Possible modification of phase compositions

As discussed in the previous section, crystal zoning is, in general, weakly developed, with only plagioclase feldspar showing optical signs of internal compositional variation. Textural re-equilibration during a prolonged cooling and crystallisation history is a likely origin for this absence of zoning and it is possible that this textural re-equilibration may have been accompanied by a chemical re-equilibration. Local equilibrium between individual phases and between these phases and the intercumulus liquid can cause the initial composition of the phases to change as the rock cools; this change is known as the 'trapped liquid shift' (Barnes, 1986). This 'trapped liquid shift' is especially relevant for orthocumulates, where interstitial liquid is likely to be abundant, whereas for adcumulates, interaction between the interstitial liquid and the main magma chamber can result in a degree of re-equilibrium between the crystals and its interstitial liquid. The main effect on ferromagnesian minerals would be to make them more iron rich (lower Fo, En and mg# values), while plagioclase feldspar would become more sodic (lower An%), as the intercumulus liquid would be enriched in those elements depleted in the original cumulate phase. Similarly, levels of compatible elements, such as nickel in olivine, would drop upon re-equilibration, as the intercumulus liquid would be depleted in such elements. Barnes (1986) suggested that, depending on the modal proportions of the phases present, and the amount of intercumulus liquid present, shifts of up to 10 mol.% in mineral mg# could occur, and proposed that these 'trapped liquid shifts' could be greater than any potential fractionation trends within the phases, and indeed could be responsible for reverse cryptic variations, such as seen in the Upper Critical Zone of the Bushveld Complex.

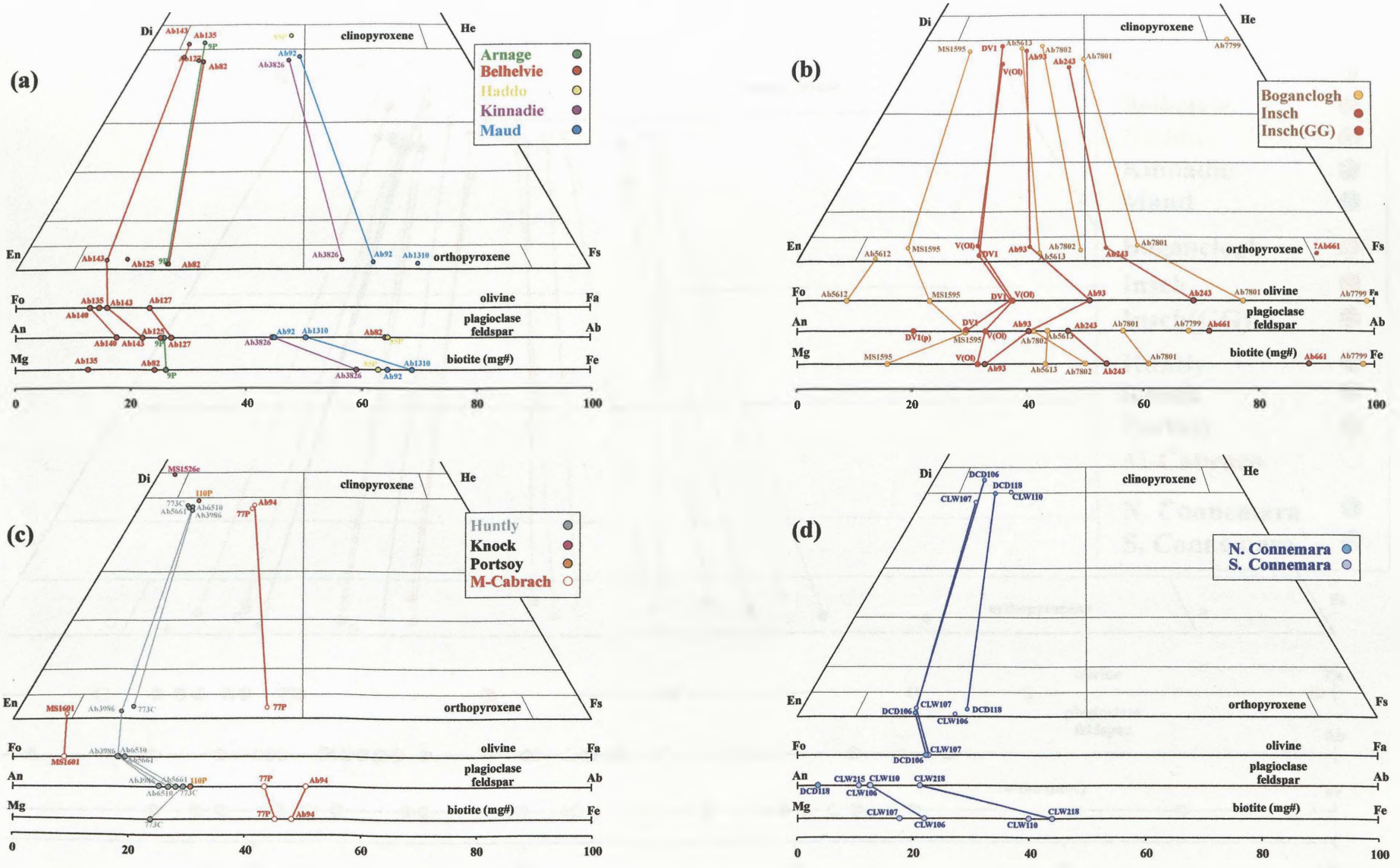


**Figure 4.10 Summary of compositional variation in the main silicate phases from (a) the northeastern bodies, (b) the Central Intrusions (c) the western bodies and (d) the Connemara bodies. Tie lines are shown for coexisting phases in the same thin section.**

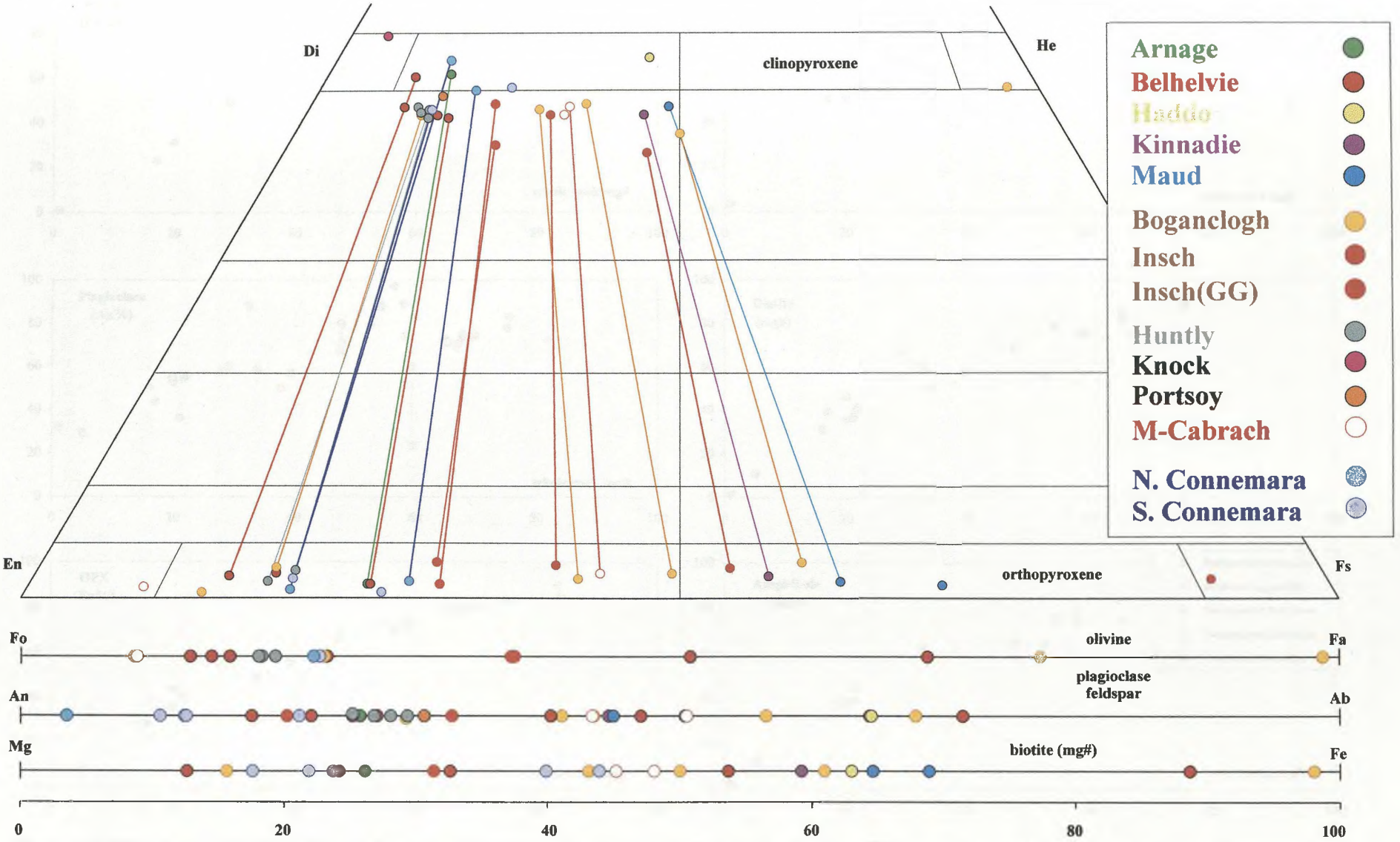


**Figure 4.11 Compositional variation in the main silicate minerals through the 'Younger Basic' bodies. Tie lines shown for co-existing pyroxenes only.**

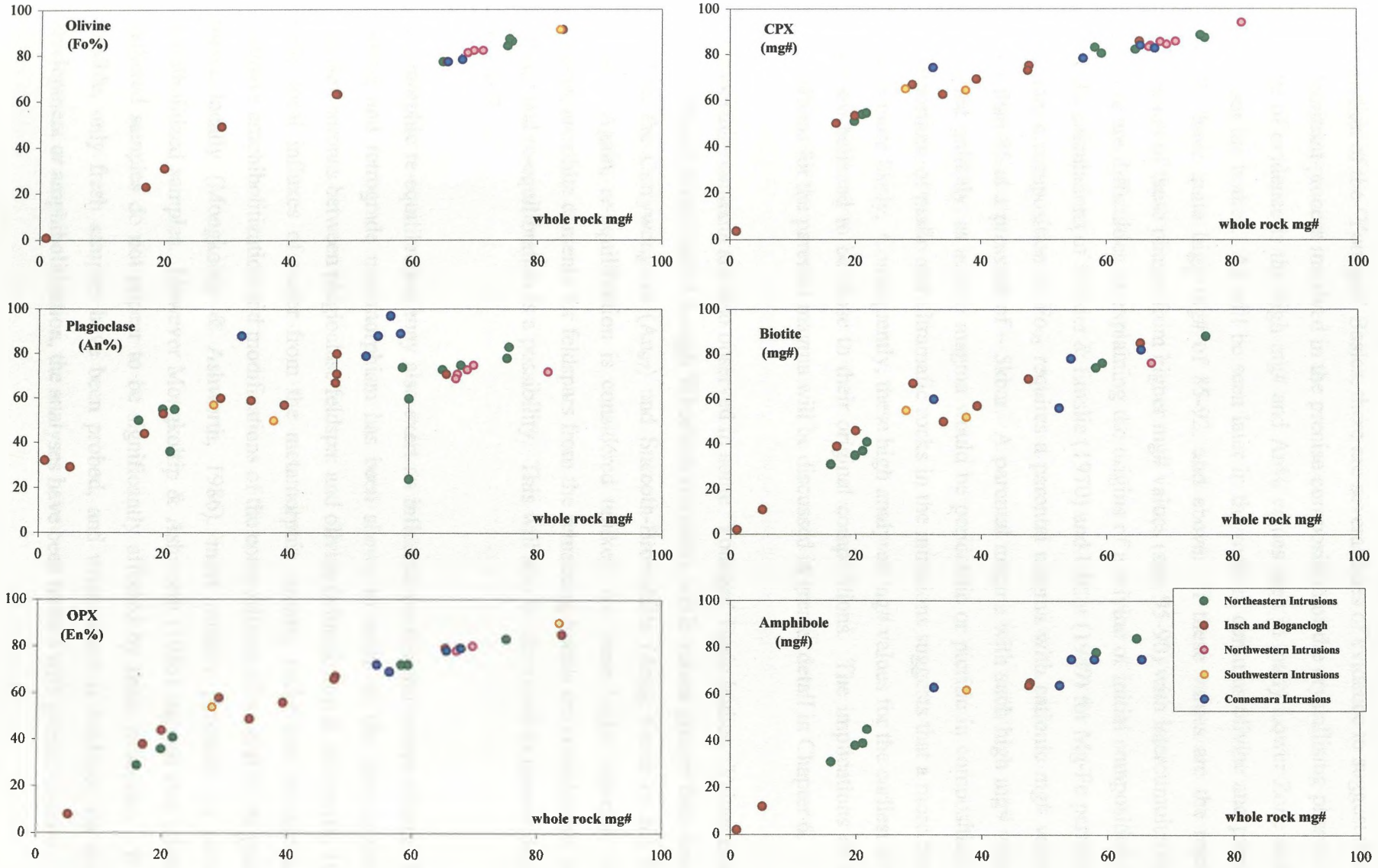


**Figure 4.12 Plots of compositional variation in the major silicate minerals against their whole rock mg# values. The jumps in several trends (most notably orthopyroxene) at mg#'s of 30-35 are as a result of the presence of cumulate ilmenite, which will be discussed in more detail in Section 5.3. Tie lines shown for zoned crystals.**

Although it is likely that a degree of chemical re-equilibration accompanied textural re-equilibration of the 'Younger' Basics, there are several lines of evidence to suggest that it is not a dominant process involved in the precise composition of the crystallising phases. The first line of evidence is the high mg# and An% values seen in many Lower Zone samples throughout the bodies. As will be seen later in the section, cumulus olivine and pyroxene generally have quite high mg# of 85-92, and above. If these values are the result of equilibration of these phases from higher mg# values (say, 95-90) with intercumulus liquid, then there are difficulties in explaining the origins of a olivine of initial composition $Fo_{95}$. Using the calculations of Roeder & Emslie (1970) and Ulmer (1989) for Mg-Fe partitioning in olivine, a composition of $Fo_{95}$ requires a parental magma with cationic mg# values of greater than 85 at a pressure of ~ 5kbar. A parental magma with such high mg# values is considered unlikely, as such a magma would be peridotitic or picritic in composition, and the proportions of mafic and ultramafic rocks in the intrusions suggests that a more basaltic parent is more likely. Consequently, these high analysed mg# values for the earliest silicate phases are believed to be close to their original compositions. The implications of these compositions for the parental magma will be discussed in greater detail in Chapter 6.

High anorthite contents are also observed in some 'Younger' Basic bodies. Values close to $An_{90}$ are found in the Cashel-Lough Wheelaun intrusion, while values greater than $An_{95}$ are found in the Currywongaun ($An_{97}$) and Succoth-Brownhills ($An_{99}$; Gunn *et al.*, 1996) masses. Again, re-equilibration is considered unlikely for these highly anorthic cases; however, anorthite contents for feldspars from the remaining bodies are considerably lower (~$An_{80}$) and re-equilibration is a possibility. This will also be discussed in greater detail in Chapter 7.

Metamorphic re-equilibration may also exert an influence on mineral compositions. Slow cooling and retrograde metamorphism has been shown to result in the development of complex coronas between plagioclase feldspar and olivine (Mongkoltip & Ashworth, 1983), while local influxes of water from the metamorphic country rocks has brought about extensive amphibolitization and modifications of the compositions of several of the primary phases locally (Mongkoltip & Ashworth, 1986), most notably pyroxene in partially amphibolitized samples. However Mongkoltip & Ashworth (1986) suggest that relatively unaltered samples do not appear to be significantly affected by these processes. Where possible, only fresh samples have been probed, and where there is evidence for corona development or amphibolitization, the analyses have been treated with greater caution.

### 4.7.3 Olivine

As discussed in the previous section, the occurrence of olivine is largely restricted to the Lower Zone peridotitic and troctolite units of the intrusive suite. It is occasionally found in minor quantities in Middle Zone gabbros and norites and is also a component of Upper Zone ferro- and syeno-gabbros from the Insch and Boganclogh intrusions. Despite variable degrees of serpentinization, sufficient fresh olivine for probing was found in virtually all samples where olivine was present. In total, olivine was probed in eighteen samples and summary data is shown in Table 4.2. Core to rim traverses were undertaken in olivines from all samples analysed, and although slight internal variations are occasionally present, no definitive evidence for chemical zoning was found in olivine from any sample. This is consistent with previous studies from the Belhelvie and Huntly bodies (Mongkoltip & Ashworth, 1983; Wadsworth, 1991).

Compositions typically range from $Fo_{91.4}$ to $Fo_{84.1}$ (mg# = 91.4 to 84.1) in Lower Zone samples from all intrusive groups, with the most forsteritic samples found in the Boganclogh and Morven Cabrach bodies. These olivines contain up to 0.32% NiO. Olivine is not common in the Middle Zone and is only present as a intercumulus phase; Middle Zone olivines from Huntly typically have values of $Fo_{82.0}$ to $Fo_{80.7}$, while olivines from the Middle Zone of the Boganclogh, Belhelvie, Dawros and Lough Wheelaun bodies all fall in the narrow range $Fo_{77.8}$ to $Fo_{76.8}$. Granular Gabbro samples V and DV1 from Insch show very similar compositions of $Fo_{62.8}$ and $Fo_{62.6}$. The reappearance of olivine in the Upper Zone is present only in the Insch and Boganclogh bodies, where it ranges from $Fo_{49.2}$ upon its reappearance to $Fo_{1.2}$ as an intercumulus phase towards the top of the Upper Zone.

NiO, $TiO_2$ and $Cr_2O_3$ abundances are all found in minor quantities in the most forsteritic samples, but drop to below detection quite quickly as Fo values drop. MnO abundances, in contrast rise steadily from <0.1% to over 1.0% in the Upper Zone (see figure 4.13), and as high as >2.4% in the most fayalitic samples, resulting in an olivine with a tephroite content of 3.5. This is typical of fayalitic olivines from the extreme Upper Zone of layered basic intrusions such as the Skaergaard.

Olivine has been probed in four samples from the Belhelvie mass, Ab135 and Ab143 from the ultramafic units, Ab140 from the troctolites and Ab127 from an olivine-bearing gabbro. They vary in composition from $Fo_{87.4}$ to $Fo_{76.7}$, which is in good agreement with published values varying from $Fo_{86.5}$ to $Fo_{77.0}$ (Wadsworth, 1991). Perhaps unusually, it is the olivines

| | Belhelvie | | | | Boganclogh | | | |
|---|---|---|---|---|---|---|---|---|
| Sample | Ab 127 | Ab 135 | Ab 143 | Ab 140 | Ab 5612 | Ab 7799 | Ab 7801 | MS 1595 |
| Rock type | Ol. Gabbro | Websterite | Websterite | Troctolite | Dunite | Syenite | Monzonite | Ol Bio Norite |
| SiO2 | 39.84 | 40.04 | 40.03 | 40.96 | 42.12 | 30.26 | 32.90 | 38.53 |
| TiO2 | 0.04 | 0.00 | 0.05 | 0.00 | 0.00 | 0.00 | 0.00 | 0.01 |
| Al2O3 | 0.00 | 0.00 | 0.00 | 0.06 | 0.00 | 0.00 | 0.00 | 0.04 |
| Cr2O3 | 0.00 | 0.00 | 0.00 | 0.08 | 0.00 | 0.00 | 0.00 | 0.03 |
| FeO | 21.53 | 13.36 | 14.66 | 12.32 | 8.38 | 67.70 | 58.47 | 20.44 |
| MnO | 0.26 | 0.20 | 0.22 | 0.10 | 0.07 | 2.42 | 1.18 | 0.14 |
| MgO | 40.48 | 45.13 | 44.37 | 47.46 | 50.39 | 0.49 | 9.79 | 38.72 |
| NiO | 0.00 | 0.06 | 0.03 | 0.03 | 0.14 | 0.00 | 0.00 | 0.00 |
| Total | 102.28 | 98.81 | 99.41 | 101.02 | 101.10 | 101.17 | 102.72 | 97.91 |
| Formula | | | | | | | | |
| Si | 1.007 | 1.009 | 1.009 | 1.003 | 1.012 | 1.010 | 1.010 | 1.013 |
| Ti | 0.001 | 0.000 | 0.001 | 0.000 | 0.000 | 0.000 | 0.000 | 0.000 |
| Al | 0.000 | 0.000 | 0.000 | 0.002 | 0.000 | 0.000 | 0.000 | 0.001 |
| Cr | 0.000 | 0.000 | 0.000 | 0.001 | 0.000 | 0.000 | 0.000 | 0.001 |
| Fe(ii) | 0.455 | 0.281 | 0.309 | 0.252 | 0.168 | 1.890 | 1.501 | 0.449 |
| Mn | 0.005 | 0.004 | 0.005 | 0.002 | 0.001 | 0.070 | 0.031 | 0.003 |
| Mg | 1.525 | 1.695 | 1.667 | 1.733 | 1.804 | 0.020 | 0.448 | 1.518 |
| Ni | 0.000 | 0.001 | 0.001 | 0.001 | 0.003 | 0.000 | 0.000 | 0.000 |
| Ca | 0.001 | 0.000 | 0.000 | 0.000 | 0.000 | 0.000 | 0.000 | 0.000 |
| TOTAL | 2.993 | 2.991 | 2.990 | 2.995 | 2.988 | 2.990 | 2.990 | 2.986 |
| Fo | 76.81 | 85.58 | 84.17 | 87.19 | 91.40 | 1.23 | 22.63 | 77.03 |
| Fa | 22.91 | 14.21 | 15.60 | 12.70 | 8.53 | 95.33 | 75.82 | 22.81 |
| Tp | | | | | | 3.45 | 1.55 | |

| | Insch | | | | Huntly | | | Morven Cabrach | Lough Wheelaun | Dawros |
|---|---|---|---|---|---|---|---|---|---|---|
| Sample | Ab93 | DV1 | V | Ab 243 | Ab 5661 | Ab 3986 | Ab 6510 | MS 1601 | CLW 107 | DCD 106 |
| Rock type | Ol. Gabbro | (Granular) Bio Gabbro | (Granular) Ol Norite | Bio Gabbro | Ol Gabbro | Bio Qtz Norite | Ol Gabbro | Harz- burgite | Hbl Harz-burgite | Ol. Gabbro |
| SiO2 | 35.08 | 35.99 | 37.44 | 33.13 | 40.24 | 40.03 | 40.01 | 42.04 | 39.27 | 39.28 |
| TiO2 | 0.00 | 0.00 | 0.00 | 0.00 | 0.00 | 0.00 | 0.00 | 0.00 | 0.00 | 0.04 |
| Al2O3 | 0.00 | 0.00 | 0.00 | 0.00 | 0.00 | 0.00 | 0.00 | 0.00 | 0.00 | 0.00 |
| Cr2O3 | 0.00 | 0.00 | 0.00 | 0.00 | 0.00 | 0.00 | 0.00 | 0.00 | 0.00 | 0.00 |
| FeO | 41.21 | 31.14 | 31.92 | 52.61 | 17.13 | 16.53 | 17.69 | 8.53 | 20.57 | 20.25 |
| MnO | 0.45 | 0.49 | 0.48 | 0.96 | 0.13 | 0.31 | 0.27 | 0.08 | 0.20 | 0.29 |
| MgO | 22.62 | 29.73 | 30.71 | 13.60 | 43.25 | 43.02 | 42.21 | 50.43 | 39.90 | 40.35 |
| NiO | 0.00 | 0.00 | 0.00 | 0.00 | 0.00 | 0.05 | 0.05 | 0.32 | 0.00 | 0.00 |
| Total | 99.47 | 97.36 | 100.66 | 100.54 | 100.76 | 99.89 | 100.22 | 101.40 | 99.94 | 100.21 |
| Formula | | | | | | | | | | |
| Si | 1.012 | 1.008 | 1.014 | 1.009 | 1.010 | 1.011 | 1.013 | 1.009 | 1.011 | 1.008 |
| Ti | 0.000 | 0.000 | 0.000 | 0.000 | 0.000 | 0.000 | 0.000 | 0.000 | 0.000 | 0.001 |
| Al | 0.000 | 0.000 | 0.000 | 0.000 | 0.000 | 0.000 | 0.000 | 0.000 | 0.000 | 0.000 |
| Cr | 0.000 | 0.000 | 0.000 | 0.000 | 0.000 | 0.000 | 0.000 | 0.000 | 0.000 | 0.000 |
| Fe(ii) | 0.994 | 0.730 | 0.723 | 1.340 | 0.360 | 0.349 | 0.374 | 0.171 | 0.443 | 0.434 |
| Mn | 0.011 | 0.012 | 0.011 | 0.025 | 0.003 | 0.007 | 0.006 | 0.002 | 0.004 | 0.006 |
| Mg | 0.972 | 1.242 | 1.239 | 0.617 | 1.618 | 1.620 | 1.593 | 1.804 | 1.531 | 1.543 |
| Ni | 0.000 | 0.000 | 0.000 | 0.000 | 0.000 | 0.001 | 0.001 | 0.006 | 0.000 | 0.000 |
| Ca | 0.000 | 0.000 | 0.000 | 0.001 | 0.000 | 0.000 | 0.000 | 0.000 | 0.000 | 0.000 |
| TOTAL | 2.988 | 2.992 | 2.986 | 2.992 | 2.990 | 2.989 | 2.987 | 2.991 | 2.989 | 2.992 |
| Fo | 49.19 | 62.62 | 62.82 | 31.15 | 81.71 | 82.00 | 80.74 | 91.27 | 77.40 | 77.78 |
| Fa | 50.26 | 36.79 | 36.62 | 67.60 | 18.15 | 17.67 | 18.97 | 8.65 | 22.38 | 21.90 |
| Tp | 0.56 | | | | | | | | | |

**Table 4.2 Summary of olivine compositions for samples probed.**

from the troctolites that are the most Mg-rich, with values of $Fo_{87.4}$ to $Fo_{87.0}$ while the ultramafic samples vary from $Fo_{85.9}$ to $Fo_{83.2}$. Although olivine is present in the Arnage mass, it has not been sampled in this study.

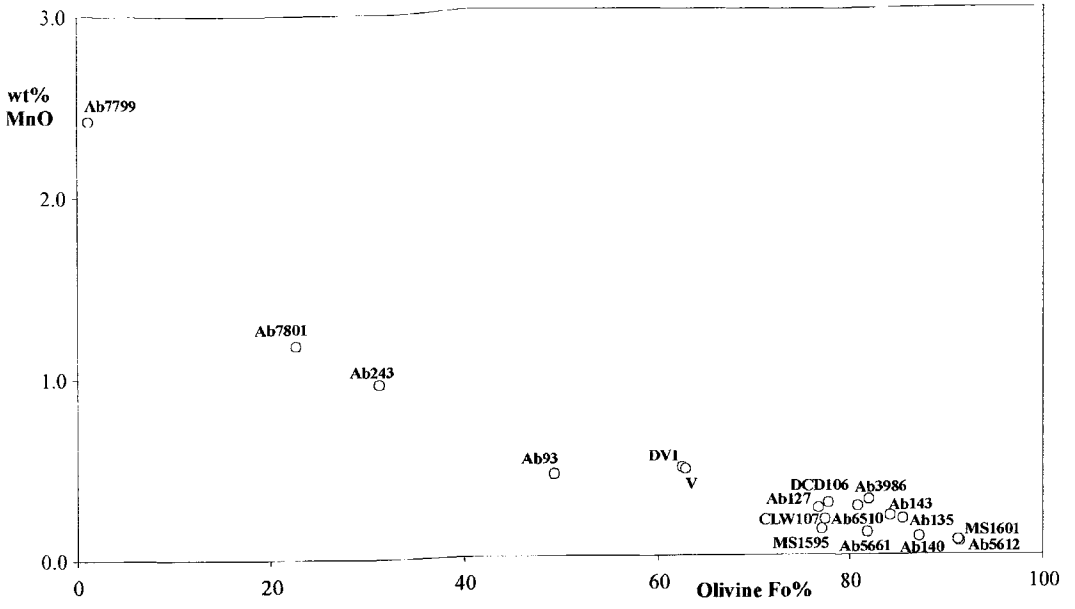


**Figure 4.13 Wt% MnO in olivine versus Fo% in all olivine samples**

The full range of Lower Zone olivine compositions for the Insch and Boganclogh bodies have not been determined as only one sample, a Boganclogh dunite with a $Fo_{91.4}$ composition has been analysed. This is considerably more forsteritic than the range established by Ashcroft & Munro, (1978) for Lower Zone rocks from the eastern parts of the Insch ($Fo_{87}$ to $Fo_{76}$), but quite similar to the $Fo_{92.4}$ to $Fo_{89.3}$ range for ultramafic samples from Boganclogh established by Stephenson & Gould (1995). Indeed these high forsterite contents ($Fo_{>90}$) from Boganclogh are as high as the highest published forsterite compositions from the 'Younger' Basics ($Fo_{92\text{-}88}$ for the Succoth-Brownhills mass (Gunn *et al.*, 1996). The implications of these highly forsteritic compositions for possible parental magmas will be discussed in the next chapter. Middle Zone olivines from Insch are only found in the Granular Gabbros, where the limited range from $Fo_{62.8}$ to $Fo_{62.6}$, is well within the range established by Wadsworth (1988) of $Fo_{63.9}$ to $Fo_{57.2}$. However, the composition of the most fayalitic cumulus olivine observed in the Upper Zone is outside the range proposed by Wadsworth (1986). Upper Zone olivine ranges up to $Fo_{01.2}$ in a Boganclogh syenite, which is somewhat more fayalitic than that put forward by Wadsworth (1986), who

proposed an Upper Zone range from $Fo_{46.7}$ to $Fo_{05.5}$. This extremely fayalitic olivine is the sample with the significant tephroite component ($Tp_{3.5}$) mentioned previously. The full range of olivine compositions from the 'Younger' Basics are shown in figures 4.10 and 4.11 and summarised in figure 4.20.

### 4.7.4 Pyroxene

Both Ca-rich (clino-) and Ca-poor (ortho-) pyroxenes are found throughout the 'Younger' Basics. Both begin to fractionate in the Lower Zone after olivine, and are present as cumulus phases throughout the remainder of the Lower Zone, and all the Middle Zone, before gradually losing cumulus status in the Upper Zone; they are also commonly found as overgrowths and as postcumulus or interstitial phases. Although the proportions in any one sample tend to be quite variable, there is an overall tendency for orthopyroxene to predominate over clinopyroxene. Alteration is widespread, with partial replacement by amphibole common, but only in the most altered cases is the entire pyroxene replaced. There appears to be a tendency for clinopyroxene to be preferentially replaced over orthopyroxene.

#### Orthopyroxene

In general, orthopyroxene tends to become a cumulate phase slightly before clinopyroxene, although poor exposure in many Lower Zone areas means that this relationship cannot be ascertained in all the bodies. In Lower Zone rocks, it is commonly present as both a cumulate and a postcumulate phase, and is found poikilitically and interstitially in troctolites, displaying occasional Ca-rich exsolution lamellae. Orthopyroxene is also present in the troctolites as layers within corona overgrowths on olivines. In Middle Zone gabbros and norites, orthopyroxene is predominantly cumulate in nature and tends to display distinctive elongate euhedral shapes with occasional bleb-like lamellae of clinopyroxene present. A summary of orthopyroxene probe analyses is shown in Table 4.3.

As shown in figure 4.11, the majority of orthopyroxenes analysed fall within the range $Wo_{03}$-$En_{79}$-$Fs_{18}$ to $Wo_{02}$-$En_{37}$-$Fs_{61}$ (mg# = 82 to 38), although compositions range to as high as $Wo_{01}$-$En_{90}$-$Fs_{09}$ (mg# = 92) in a Morven Cabrach ultramafic sample (figure 4.10) and as low as $Wo_{02}$-$En_{29}$-$Fs_{69}$ (mg# = 30) in a quartz-biotite norite from the Maud body. It is believed that orthopyroxene ceases to crystallize in the Upper Zone, with the most Fe-rich orthopyroxene recorded being of $Wo_{03}$-$En_{23}$-$Fs_{74}$ composition in UZb (Wadsworth, 1986).

| | Arnage | Belhelvie | | | Kinnadie | Maud | | Boganclogh | | | | | Insch | | | | | Huntly | | Morven Cabrach | | Lough Wheelaun | | North Connemara | |
|---|---|---|---|---|---|---|---|---|---|---|---|---|---|---|---|---|---|---|---|---|---|---|---|---|---|
| Sample | 9P | Ab82 | Ab 125 | Ab 143 | Ab 3826 | Ab 1310 | Ab92 | Ab 5612 | Ab 5613 | Ab 7801 | Ab 7802 | MS 1595 | Ab93 | Ab 661 | DV1 | V | Ab 243 | 773C | Ab 3986 | MS 1601 | 77P | CLW 106 | CLW 107 | DCD 106 | DCD 118 |
| SiO2 | 53.92 | 55.65 | 54.72 | 54.82 | 50.41 | 50.33 | 50.70 | 59.63 | 51.13 | 51.61 | 51.88 | 54.59 | 52.06 | 49.34 | 54.13 | 53.43 | 50.81 | 54.81 | 54.46 | 57.28 | 52.19 | 54.11 | 54.92 | 54.61 | 53.62 |
| TiO2 | 0.11 | 0.20 | 0.20 | 0.10 | 0.03 | 0.17 | 0.00 | 0.00 | 0.13 | 0.17 | 0.23 | 0.29 | 0.25 | 0.00 | 0.30 | 0.66 | 0.27 | 0.48 | 0.27 | 0.00 | 0.16 | 0.00 | 0.04 | 0.00 | 0.00 |
| Al2O3 | 1.00 | 1.13 | 1.91 | 2.71 | 0.46 | 0.56 | 0.48 | 0.00 | 0.73 | 0.66 | 0.68 | 1.21 | 1.08 | 0.44 | 1.45 | 1.95 | 0.69 | 2.15 | 1.92 | 1.66 | 1.02 | 1.82 | 2.14 | 2.98 | 2.48 |
| Cr2O3 | 0.13 | 0.09 | 0.14 | 0.52 | 0.00 | 0.00 | 0.00 | 0.00 | 0.01 | 0.00 | 0.00 | 0.17 | 0.00 | 0.00 | 0.00 | 0.00 | 0.00 | 0.31 | 0.00 | 0.59 | 0.00 | 0.05 | 0.07 | 0.17 | 0.09 |
| FeO | 16.15 | 16.28 | 11.33 | 9.27 | 31.72 | 40.54 | 35.61 | 7.92 | 24.61 | 34.53 | 29.16 | 11.39 | 23.62 | 42.34 | 19.32 | 18.45 | 30.70 | 12.47 | 11.22 | 5.64 | 26.17 | 17.01 | 12.57 | 12.60 | 17.93 |
| MnO | 0.36 | 0.28 | 0.26 | 0.16 | 0.97 | 0.99 | 1.35 | 0.38 | 0.62 | 0.94 | 0.64 | 0.21 | 0.50 | 2.66 | 0.49 | 0.36 | 0.90 | 0.21 | 0.36 | 0.06 | 0.59 | 0.37 | 0.26 | 0.28 | 0.36 |
| MgO | 26.10 | 26.13 | 28.51 | 30.30 | 13.55 | 9.67 | 12.05 | 29.24 | 19.03 | 13.19 | 16.83 | 28.59 | 19.88 | 2.32 | 23.91 | 23.42 | 14.85 | 28.48 | 28.96 | 34.24 | 18.94 | 25.91 | 28.58 | 28.43 | 24.82 |
| CaO | 0.85 | 0.85 | 1.39 | 1.25 | 1.06 | 0.78 | 0.88 | 0.45 | 0.99 | 1.72 | 1.28 | 1.57 | 1.58 | 0.78 | 0.86 | 1.80 | 1.43 | 1.48 | 0.91 | 0.71 | 1.27 | 0.44 | 1.06 | 0.57 | 1.01 |
| Na2O | 0.07 | 0.15 | 0.06 | 0.06 | 0.26 | 0.25 | 0.30 | 0.00 | 0.21 | 0.27 | 0.21 | 0.00 | 0.00 | 0.34 | 0.00 | 0.19 | 0.14 | 0.00 | 0.00 | 0.00 | 0.00 | 0.00 | 0.00 | 0.00 | 0.00 |
| K2O | 0.00 | 0.00 | 0.02 | 0.00 | 0.00 | 0.00 | 0.00 | 0.00 | 0.01 | 0.02 | 0.00 | 0.00 | 0.00 | 0.00 | 0.00 | 0.05 | 0.00 | 0.00 | 0.00 | 0.00 | 0.00 | 0.00 | 0.00 | 0.00 | 0.00 |
| Total | 98.69 | 100.77 | 98.54 | 99.25 | 98.46 | 103.37 | 101.36 | 97.61 | 97.45 | 103.10 | 100.92 | 98.03 | 99.01 | 98.21 | 100.44 | 100.34 | 99.79 | 100.40 | 98.11 | 100.18 | 100.39 | 99.73 | 99.64 | 99.64 | 100.31 |
| Formula | | | | | | | | | | | | | | | | | | | | | | | | | |
| Si | 1.977 | 1.993 | 1.966 | 1.939 | 2.008 | 1.985 | 1.997 | 2.101 | 1.986 | 1.984 | 1.984 | 1.974 | 1.978 | 2.089 | 1.975 | 1.954 | 1.986 | 1.944 | 1.962 | 1.967 | 1.977 | 1.966 | 1.959 | 1.945 | 1.948 |
| Ti | 0.003 | 0.005 | 0.005 | 0.003 | 0.001 | 0.005 | 0.000 | 0.000 | 0.004 | 0.005 | 0.007 | 0.008 | 0.007 | 0.000 | 0.008 | 0.018 | 0.008 | 0.013 | 0.007 | 0.000 | 0.005 | 0.000 | 0.001 | 0.000 | 0.000 |
| Al | 0.043 | 0.048 | 0.081 | 0.113 | 0.022 | 0.026 | 0.022 | 0.000 | 0.033 | 0.030 | 0.031 | 0.052 | 0.048 | 0.022 | 0.062 | 0.084 | 0.032 | 0.090 | 0.082 | 0.067 | 0.046 | 0.078 | 0.090 | 0.125 | 0.106 |
| Cr | 0.004 | 0.003 | 0.004 | 0.015 | 0.000 | 0.000 | 0.000 | 0.000 | 0.000 | 0.000 | 0.000 | 0.005 | 0.000 | 0.000 | 0.000 | 0.000 | 0.000 | 0.009 | 0.000 | 0.016 | 0.000 | 0.001 | 0.002 | 0.005 | 0.003 |
| Fe(ii) | 0.495 | 0.487 | 0.340 | 0.274 | 1.057 | 1.337 | 1.173 | 0.233 | 0.799 | 1.110 | 0.932 | 0.344 | 0.750 | 1.499 | 0.590 | 0.564 | 1.004 | 0.370 | 0.338 | 0.162 | 0.829 | 0.517 | 0.375 | 0.375 | 0.545 |
| Mn | 0.011 | 0.008 | 0.008 | 0.005 | 0.033 | 0.033 | 0.045 | 0.011 | 0.020 | 0.031 | 0.021 | 0.006 | 0.016 | 0.095 | 0.015 | 0.011 | 0.030 | 0.006 | 0.011 | 0.002 | 0.019 | 0.011 | 0.008 | 0.008 | 0.011 |
| Mg | 1.427 | 1.395 | 1.527 | 1.598 | 0.805 | 0.569 | 0.707 | 1.536 | 1.102 | 0.756 | 0.959 | 1.541 | 1.126 | 0.146 | 1.301 | 1.277 | 0.865 | 1.506 | 1.555 | 1.752 | 1.070 | 1.403 | 1.520 | 1.510 | 1.345 |
| Ca | 0.033 | 0.033 | 0.053 | 0.047 | 0.045 | 0.033 | 0.037 | 0.017 | 0.041 | 0.071 | 0.052 | 0.061 | 0.064 | 0.035 | 0.034 | 0.071 | 0.060 | 0.056 | 0.035 | 0.026 | 0.052 | 0.017 | 0.040 | 0.022 | 0.039 |
| Na | 0.005 | 0.010 | 0.004 | 0.004 | 0.020 | 0.019 | 0.023 | 0.000 | 0.016 | 0.020 | 0.016 | 0.000 | 0.000 | 0.028 | 0.000 | 0.013 | 0.011 | 0.000 | 0.000 | 0.000 | 0.000 | 0.000 | 0.000 | 0.000 | 0.000 |
| K | 0.000 | 0.000 | 0.001 | 0.000 | 0.000 | 0.000 | 0.000 | 0.000 | 0.000 | 0.001 | 0.000 | 0.000 | 0.000 | 0.000 | 0.000 | 0.002 | 0.000 | 0.000 | 0.000 | 0.000 | 0.000 | 0.000 | 0.000 | 0.000 | 0.000 |
| TOTAL | 4.00 | 3.98 | 3.99 | 4.00 | 3.99 | 4.01 | 4.00 | 3.90 | 4.00 | 4.01 | 4.00 | 3.99 | 3.99 | 3.91 | 3.99 | 3.99 | 4.00 | 3.99 | 3.99 | 3.99 | 4.00 | 3.99 | 3.99 | 3.99 | 4.00 |
| Wo | 1.69 | 1.72 | 2.76 | 2.45 | 2.36 | 1.70 | 1.93 | 0.95 | 2.11 | 3.67 | 2.68 | 3.13 | 3.30 | 2.08 | 1.77 | 3.71 | 3.11 | 2.90 | 1.82 | 1.34 | 2.67 | 0.88 | 2.07 | 1.15 | 2.02 |
| En | 72.99 | 72.85 | 79.53 | 83.27 | 42.21 | 29.35 | 36.88 | 86.00 | 56.75 | 39.03 | 49.36 | 79.19 | 58.04 | 8.69 | 67.58 | 66.79 | 44.84 | 77.95 | 80.65 | 90.31 | 54.84 | 72.43 | 78.55 | 79.18 | 69.73 |
| Fs | 25.32 | 25.43 | 17.71 | 14.28 | 55.43 | 68.95 | 61.19 | 13.05 | 41.14 | 57.31 | 47.97 | 17.68 | 38.66 | 89.23 | 30.65 | 29.50 | 52.05 | 19.15 | 17.53 | 8.35 | 42.49 | 26.69 | 19.38 | 19.66 | 28.25 |
| mg# | 74.2 | 74.1 | 81.8 | 85.4 | 43.2 | 29.9 | 37.6 | 86.8 | 58 | 40.5 | 50.7 | 81.8 | 60 | 8.9 | 68.8 | 69.4 | 46.3 | 80.3 | 82.1 | 91.5 | 56.3 | 73.1 | 80.2 | 80.1 | 71.2 |

**Table 4.3 Summary of orthopyroxene compositions for samples probed.**

However, a possible orthopyroxene of ferrosilite composition has been probed in a quartz syenite, Ab661, from zone UZc in the western part of the Insch mass. The analysis, shown in Table 4.3, corresponds to a composition of $Wo_{02}$-$En_{08}$-$Fs_{89}$ (mg# = 09). The crystal in question is shown in Plate 4.17, and can be seen to be overgrown by primary ferro-hornblende, with minor quantities of nearby secondary ferro-edenitic amphibole. Optically this crystal contains many features typical of orthopyroxene including faint pleochroism and near 90° cleavage. The probe analysis also contains appreciable amounts of MnO and $Na_2O$.

Orthopyroxenes have been probed from two Granular Gabbros samples and contain a limited compositional range from $Wo_{02}$-$En_{68}$-$Fs_{31}$ to $Wo_{04}$-$En_{67}$-$Fs_{30}$ (mg# ~ 69), within the overall compositional range for 'Younger' Basic orthopyroxenes. Analyses of Belhelvie orthopyroxene (see figure 4.14) fall within the ferroan enstatite field and range from $Wo_{03}$-$En_{83}$-$Fs_{14}$ to $Wo_{02}$-$En_{73}$-$Fs_{25}$ (mg# = 85 to 74), similar to that of Wadsworth (1988), except for sample Ab82, which has a significantly lower En% ($En_{72.9}$; mg# = 74.1) content than those published ($En_{78.6}$) (although optical 2V determinations (Wadsworth *et al*, 1966) have yielded orthopyroxene compositions of $En_{68\text{-}69}$). An orthopyroxene from an olivine corona from sample Ab140 is also shown in figure 4.14, and is similar to published orthopyroxene coronas from similar troctolitic rocks from the Belhelvie body (Mongkoltip & Ashworth, 1983). Orthopyroxene from the northeastern bodies range from $Wo_{02}$-$En_{73}$-$Fs_{25}$ (mg# = 74) in Arnage to $Wo_{02}$-$En_{29}$-$Fs_{69}$ (mg# = 30) in Maud; the Haddo and Arnage results are similar to those of Gribble (1967), although much of his data was obtained optically. The range in Insch and Boganclogh is similar to that identified by Wadsworth (1986, 1988), with the possible exception of the ferrosilitic sample described above. The remainder of the bodies show a limited spread, most displaying compositions in the range $Wo_{02}$-$En_{81}$-$Fs_{18}$ to $Wo_{02}$-$En_{70}$-$Fs_{28}$ (mg# = 82 to 71) (see figure 4.10 and 4.11)

There are apparent variations evident between orthopyroxene compositions from the Central Intrusions and the northeastern intrusions (see figure 4.12), with orthopyroxene and other ferromagnesian phases from Insch and Boganclogh displaying consistently higher mg# values than those from Haddo, Kinnadie and Maud. For example, sample Ab92 from Maud has orthopyroxene of $En_{36}$ composition, while sample Ab243 from Insch has orthopyroxene of $En_{44}$ composition; both have whole rock mg# values of 19.9 (see figure 4.12). Figure 4.15a, however, shows that coexisting orthopyroxene and biotite do not reveal this trend. It is believed that this variation is the result of the use of whole rock mg# as a fractionation index; the presence of cumulus ilmenite distorts the whole rock mg#, as will be discussed in

the next chapter, resulting in the misleading trends for many phases in figure 4.12. The 'kick' in compositions at mg# values of ~ 30, which is most clearly seen in the orthopyroxene data in Figure 4.12, is also as a result of the presence of ilmenite as a cumulus phase in these samples.

**Clinopyroxene**

Clinopyroxene, where present in the Lower Zone, is generally cumulate, although again interstitial clinopyroxene is found occasionally. In Middle Zone rocks it is present mainly as a primary cumulate phase but occasionally as larger poikilitic crystals; exsolved lamellae of Ca-poor pyroxene of varying size and orientation are commonly developed. Also, very fine lamellae of an exsolved oxide phase, probably ilmenite, are occasionally found. These tend to be quite fine and too thin for probe analysis. Summarised clinopyroxene probe data are shown in Table 4.4.

The majority of clinopyroxene fall within the range $Wo_{47}$-$En_{47}$-$Fs_{06}$ (mg# = 88) in a Belhelvie lherzolite to $Wo_{44}$-$En_{29}$-$Fs_{27}$ (mg# = 52) in a Maud norite. One higher composition, $Wo_{50}$-$En_{47}$-$Fs_{02}$ (mg# = 95) is found in a Morven Cabrach ultramafic sample, while a clinopyroxene from a Boganclogh syenite has the extreme hedenbergite composition $Wo_{46}$-$En_{02}$-$Fs_{52}$ (mg# = 04). These values are broadly similar to published analyses, although considerable scatter is present, with Ca contents varying quite significantly within samples and even within individual crystals (see figure 4.14). Ca-rich pyroxenes from the Belhelvie mass range from ferroan diopside ($Wo_{48}$-$En_{46}$-$Fs_{06}$) to Mg-rich augite ($Wo_{43}$-$En_{46}$-$Fs_{11}$) in composition; this trend is complicated by a significant number of analyses with lower Ca contents, which will be discussed below. These ranges are quite similar to values from Wadsworth *et al.* (1966) and Wadsworth (1991).

Clinopyroxene analyses from the northeastern bodies of Maud, Arnage, Kinnadie and Haddo are similar to those analysed by Gribble (1967), ranging from $Wo_{47}$-$En_{44}$-$Fs_{09}$ in Arnage to $Wo_{44}$-$En_{29}$-$Fs_{27}$ in Maud. Insch and Boganclogh show the widest range of clinopyroxene compositions from $Wo_{44}$-$En_{48}$-$Fs_{08}$ to $Wo_{46}$-$En_{02}$-$Fs_{52}$, similar to the range identified by Wadsworth (1986, 1988). Clinopyroxene from the Huntly mass have a limited compositional range (~$Wo_{44}$-$En_{48}$-$Fs_{08}$), while Connemara clinopyroxenes range from $Wo_{49}$-$En_{43}$-$Fs_{08}$ to $Wo_{46}$-$En_{40}$-$Fs_{14}$, although the values are somewhat scattered.

| | Arnage | Belhelvie | | | | Haddo | Kinnadie | Maud | Boganclogh | | | | | Insch | |
|---|---|---|---|---|---|---|---|---|---|---|---|---|---|---|---|
| Sample | 9P | Ab 82 | Ab 127 | Ab135 | Ab143 | 85P | Ab 3826 | Ab92 | Ab 5613 | Ab 7799 | Ab 7801 | Ab 7802 | MS 1595 | Ab93 | DV1 |
| SiO2 | 52.67 | 53.16 | 52.86 | 51.25 | 51.36 | 53.03 | 51.14 | 52.09 | 51.36 | 48.74 | 52.57 | 52.46 | 51.95 | 51.55 | 51.72 |
| TiO2 | 0.35 | 0.55 | 0.54 | 0.54 | 0.49 | 0.09 | 0.06 | 0.29 | 0.19 | 0.35 | 0.19 | 0.33 | 0.64 | 0.64 | 0.81 |
| Al2O3 | 1.28 | 2.42 | 3.61 | 3.97 | 3.93 | 0.66 | 0.72 | 0.95 | 1.01 | 0.99 | 1.21 | 1.35 | 2.41 | 2.11 | 2.82 |
| Cr2O3 | 0.31 | 0.32 | 0.79 | 1.03 | 0.92 | 0.13 | 0.04 | 0.08 | 0.12 | 0.04 | 0.09 | 0.07 | 0.45 | 0.10 | 0.14 |
| FeO | 5.65 | 6.56 | 6.02 | 4.12 | 3.80 | 14.51 | 15.35 | 16.57 | 10.49 | 29.62 | 18.01 | 12.80 | 5.12 | 11.28 | 8.41 |
| MnO | 0.00 | 0.34 | 0.13 | 0.07 | 0.09 | 0.60 | 0.50 | 0.41 | 0.22 | 0.91 | 0.47 | 0.24 | 0.06 | 0.27 | 0.13 |
| MgO | 15.52 | 15.87 | 16.25 | 16.46 | 15.89 | 9.80 | 10.57 | 9.92 | 13.21 | 0.73 | 10.16 | 12.15 | 16.54 | 13.10 | 14.41 |
| CaO | 22.91 | 20.59 | 20.71 | 20.54 | 21.89 | 23.25 | 20.33 | 20.97 | 20.65 | 20.20 | 20.03 | 21.20 | 20.63 | 20.58 | 21.00 |
| Na2O | 0.32 | 0.64 | 0.41 | 0.53 | 0.53 | 0.48 | 0.33 | 0.41 | 0.34 | 0.45 | 0.41 | 0.38 | 0.46 | 0.09 | 0.33 |
| K2O | 0.00 | 0.15 | 0.00 | 0.00 | 0.00 | 0.00 | 0.00 | 0.00 | 0.00 | 0.00 | 0.00 | 0.00 | 0.00 | 0.00 | 0.00 |
| Total | 99.35 | 100.61 | 101.33 | 98.51 | 98.94 | 102.56 | 99.03 | 101.68 | 97.60 | 102.05 | 103.16 | 100.98 | 98.23 | 99.76 | 99.78 |
| Formula | | | | | | | | | | | | | | | |
| Si | 1.960 | 1.945 | 1.913 | 1.897 | 1.897 | 1.987 | 1.982 | 1.975 | 1.975 | 1.969 | 1.970 | 1.967 | 1.934 | 1.942 | 1.924 |
| Ti | 0.010 | 0.015 | 0.015 | 0.015 | 0.014 | 0.003 | 0.002 | 0.008 | 0.005 | 0.011 | 0.005 | 0.009 | 0.018 | 0.018 | 0.023 |
| Al | 0.056 | 0.104 | 0.154 | 0.173 | 0.171 | 0.029 | 0.033 | 0.042 | 0.046 | 0.047 | 0.053 | 0.060 | 0.106 | 0.094 | 0.124 |
| Cr | 0.009 | 0.009 | 0.023 | 0.030 | 0.027 | 0.004 | 0.001 | 0.002 | 0.004 | 0.001 | 0.003 | 0.002 | 0.013 | 0.003 | 0.004 |
| Fe(ii) | 0.176 | 0.201 | 0.182 | 0.128 | 0.117 | 0.455 | 0.497 | 0.525 | 0.337 | 1.001 | 0.564 | 0.401 | 0.159 | 0.355 | 0.262 |
| Mn | 0.000 | 0.011 | 0.004 | 0.002 | 0.003 | 0.019 | 0.016 | 0.013 | 0.007 | 0.031 | 0.015 | 0.008 | 0.002 | 0.009 | 0.004 |
| Mg | 0.861 | 0.866 | 0.877 | 0.908 | 0.875 | 0.547 | 0.611 | 0.561 | 0.757 | 0.044 | 0.568 | 0.679 | 0.918 | 0.736 | 0.799 |
| Ca | 0.913 | 0.807 | 0.803 | 0.814 | 0.866 | 0.933 | 0.844 | 0.852 | 0.851 | 0.874 | 0.804 | 0.852 | 0.823 | 0.831 | 0.837 |
| Na | 0.023 | 0.045 | 0.029 | 0.038 | 0.038 | 0.035 | 0.025 | 0.030 | 0.025 | 0.035 | 0.030 | 0.028 | 0.033 | 0.007 | 0.024 |
| K | 0.000 | 0.007 | 0.000 | 0.000 | 0.000 | 0.000 | 0.000 | 0.000 | 0.000 | 0.000 | 0.000 | 0.000 | 0.000 | 0.000 | 0.000 |
| TOTAL | 4.01 | 4.01 | 4.00 | 4.01 | 4.01 | 4.01 | 4.01 | 4.01 | 4.01 | 4.01 | 4.01 | 4.01 | 4.01 | 3.99 | 4.00 |
| Wo | 46.82 | 43.06 | 43.13 | 44.00 | 46.61 | 48.22 | 43.24 | 43.96 | 43.75 | 45.54 | 41.53 | 44.10 | 43.32 | 43.24 | 44.10 |
| En | 44.15 | 46.21 | 47.10 | 49.08 | 47.09 | 28.27 | 31.30 | 28.95 | 38.92 | 2.29 | 29.34 | 35.14 | 48.32 | 38.29 | 42.10 |
| Fs | 9.03 | 10.73 | 9.77 | 6.92 | 6.30 | 23.51 | 25.46 | 27.09 | 17.33 | 52.16 | 29.13 | 20.76 | 8.37 | 18.47 | 13.80 |
| mg# | 83.0 | 81.2 | 82.8 | 87.6 | 88.2 | 54.6 | 55.1 | 51.7 | 69.2 | 4.2 | 50.2 | 62.9 | 85.2 | 67.5 | 75.3 |

| | Insch | | Huntly | | | | Knock | Portsoy | Morven Cabrach | | Lough Wheelaun | | North Connemara | |
|---|---|---|---|---|---|---|---|---|---|---|---|---|---|---|
| Sample | V | Ab 243 | 773C | Ab 5661 | Ab 3986 | Ab 6510 | MS 1526c | 110P | Ab94 | 77P | CLW 107 | CLW 110 | DCD 106 | DCD 118 |
| SiO2 | 51.70 | 50.91 | 51.94 | 52.24 | 52.30 | 52.25 | 55.14 | 51.26 | 53.30 | 52.00 | 52.86 | 52.05 | 51.69 | 51.26 |
| TiO2 | 0.74 | 0.41 | 0.53 | 0.63 | 0.64 | 0.60 | 0.00 | 0.74 | 0.19 | 0.42 | 0.14 | 0.18 | 0.38 | 0.53 |
| Al2O3 | 3.05 | 1.47 | 3.79 | 3.75 | 3.17 | 3.53 | 0.70 | 2.25 | 1.20 | 2.17 | 2.25 | 2.15 | 4.24 | 4.63 |
| Cr2O3 | 0.11 | 0.03 | 1.12 | 0.78 | 0.67 | 0.55 | 0.11 | 0.38 | 0.04 | 0.00 | 0.50 | 0.03 | 0.33 | 0.13 |
| FeO | 9.49 | 16.65 | 5.35 | 4.92 | 6.12 | 5.18 | 1.64 | 5.57 | 12.21 | 11.87 | 5.78 | 8.70 | 5.15 | 7.13 |
| MnO | 0.15 | 0.46 | 0.03 | 0.07 | 0.10 | 0.02 | 0.00 | 0.03 | 0.29 | 0.28 | 0.06 | 0.14 | 0.14 | 0.10 |
| MgO | 15.04 | 11.16 | 16.26 | 16.39 | 18.71 | 16.63 | 17.65 | 15.50 | 12.93 | 12.86 | 16.71 | 13.86 | 14.92 | 14.76 |
| CaO | 19.32 | 18.76 | 20.78 | 20.78 | 17.22 | 20.98 | 26.03 | 21.14 | 21.56 | 20.64 | 21.47 | 21.84 | 23.02 | 21.64 |
| Na2O | 0.39 | 0.19 | 0.41 | 0.28 | 0.17 | 0.35 | 0.00 | 0.30 | 0.36 | 0.29 | 0.05 | 0.34 | 0.23 | 0.20 |
| K2O | 0.00 | 0.00 | 0.00 | 0.00 | 0.00 | 0.00 | 0.00 | 0.02 | 0.02 | 0.00 | 0.00 | 0.04 | 0.00 | 0.00 |
| Total | 99.98 | 100.06 | 100.18 | 99.91 | 99.16 | 100.10 | 101.28 | 97.24 | 102.10 | 100.55 | 99.87 | 99.33 | 100.10 | 100.37 |
| Formula | | | | | | | | | | | | | | |
| Si | 1.920 | 1.954 | 1.899 | 1.910 | 1.917 | 1.909 | 1.978 | 1.937 | 1.971 | 1.948 | 1.942 | 1.952 | 1.898 | 1.886 |
| Ti | 0.021 | 0.012 | 0.015 | 0.017 | 0.018 | 0.016 | 0.000 | 0.021 | 0.005 | 0.012 | 0.004 | 0.005 | 0.010 | 0.015 |
| Al | 0.133 | 0.067 | 0.163 | 0.162 | 0.137 | 0.152 | 0.030 | 0.100 | 0.052 | 0.096 | 0.097 | 0.095 | 0.183 | 0.201 |
| Cr | 0.003 | 0.001 | 0.032 | 0.023 | 0.019 | 0.016 | 0.003 | 0.011 | 0.001 | 0.000 | 0.015 | 0.001 | 0.010 | 0.004 |
| Fe(ii) | 0.295 | 0.534 | 0.164 | 0.150 | 0.188 | 0.158 | 0.049 | 0.176 | 0.378 | 0.372 | 0.178 | 0.273 | 0.158 | 0.219 |
| Mn | 0.005 | 0.015 | 0.001 | 0.002 | 0.003 | 0.001 | 0.000 | 0.001 | 0.009 | 0.009 | 0.002 | 0.004 | 0.004 | 0.003 |
| Mg | 0.833 | 0.639 | 0.886 | 0.893 | 1.023 | 0.906 | 0.944 | 0.873 | 0.713 | 0.718 | 0.915 | 0.775 | 0.817 | 0.810 |
| Ca | 0.769 | 0.772 | 0.814 | 0.814 | 0.676 | 0.821 | 1.001 | 0.856 | 0.854 | 0.828 | 0.845 | 0.877 | 0.906 | 0.853 |
| Na | 0.028 | 0.014 | 0.029 | 0.020 | 0.012 | 0.025 | 0.000 | 0.022 | 0.026 | 0.021 | 0.004 | 0.025 | 0.016 | 0.014 |
| K | 0.000 | 0.000 | 0.000 | 0.000 | 0.000 | 0.000 | 0.000 | 0.001 | 0.001 | 0.000 | 0.000 | 0.002 | 0.000 | 0.000 |
| TOTAL | 4.01 | 4.01 | 4.00 | 3.99 | 3.99 | 4.00 | 4.01 | 4.00 | 4.01 | 4.00 | 4.00 | 4.01 | 4.00 | 4.00 |
| Wo | 40.54 | 39.69 | 43.67 | 43.83 | 35.82 | 43.55 | 50.20 | 44.93 | 43.91 | 43.17 | 43.60 | 45.56 | 48.17 | 45.32 |
| En | 43.91 | 32.85 | 47.53 | 48.09 | 54.21 | 48.06 | 47.34 | 45.83 | 36.66 | 37.43 | 47.21 | 40.26 | 43.43 | 43.04 |
| Fs | 15.55 | 27.46 | 8.80 | 8.08 | 9.96 | 8.38 | 2.46 | 9.24 | 19.43 | 19.40 | 9.18 | 14.18 | 8.40 | 11.64 |
| mg# | 73.8 | 54.5 | 84.4 | 85.6 | 84.5 | 85.2 | 95.1 | 83.2 | 65.4 | 65.9 | 83.7 | 74.0 | 83.8 | 78.7 |

**Table 4.4 Summary of clinopyroxene compositions for samples probed.**

**Composition of exsolution lamellae**

As mentioned, a variety of exsolution lamellae are present in pyroxenes from all intrusions and, where possible, they, and their host pyroxenes, have been analysed, with examples shown in figure 4.14. Lamellae are found in both orthopyroxene and clinopyroxene; those in orthopyroxenes, shown in figure 4.14b, tend to be quite bleb-like in nature and are either diopsidic or augitic in composition. Lamellae in clinopyroxene tend to be much finer and usually too thin for probe analysis; however where they have been probed they appear to be a Ca-poor pyroxene, which is likely to be orthopyroxene. In some samples, orthopyroxene hosts display Ca-rich pyroxene exsolved along two cleavage planes characteristic of inverted pigeonite; however, these are irregularly developed and where present are not found in all orthopyroxene from the sample.

One prominent feature of the pyroxenes from these bodies is the considerable range in Ca-content of clinopyroxenes, from individual samples. For example, clinopyroxenes from Belhelvie sample Ab135 vary from $Wo_{49}$-$En_{46}$-$Fs_{05}$ to $Wo_{35}$-$En_{56}$-$Fs_{09}$, (see figure 4.14), while clinopyroxenes from the Kinnadie sample (Ab3826), range from $Wo_{45}$ to $Wo_{35}$. This trend is not believed to be a compositional zoning feature as there is no obvious pattern to these changes within individual pyroxenes (for example, see figure 4.14d). There are several possible explanations for this scatter. One is the presence of very fine exsolution lamellae of low-Ca pyroxene within the clinopyroxene being inadvertently analysed as part of the clinopyroxene host; this would produce analyses with lower CaO than the actual host clinopyroxene composition by dragging the analysis towards the composition of the Ca-poor pyroxene lamellae.

Another possibility is the presence of very fine exsolution lamellae of a Fe-Ti oxide, probably ilmenite, again moving the clinopyroxenes analyses slightly away from their true composition. Very fine sets of opaque lamellae are commonly present in clinopyroxenes from all the intrusions described, although analyses inadvertently containing a Fe-Ti oxide component should be dragged towards the ferrosilite end member, which does not tend to be the case (see figure 4.14a). A third possibility is alteration of the pyroxenes. Secondary amphibole is occasionally present, and it is possible that chemical alteration, not visible in thin section, may have affected some crystals. While every effort was made to probe only fresh host crystals, none of the above factors can be discounted, although the presence of fine Ca-poor lamellae is considered the most likely reason, as they are pervasive throughout the clinopyroxenes seen in the northeastern bodies. As a result, when calculating average

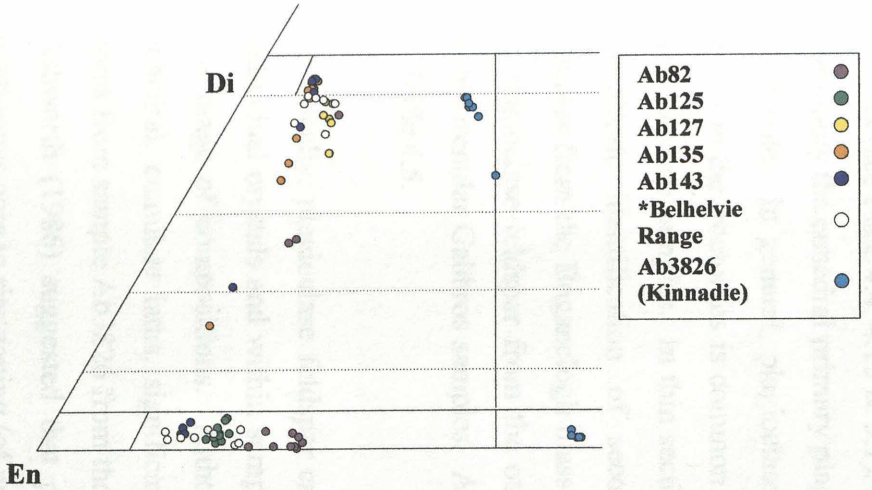


a. Individual analyses of Ca- rich and Ca-poor pyroxenes for selected Belhelvie and Kinnadie samples. Published Belhelvie data from Wadsworth et al (1991)

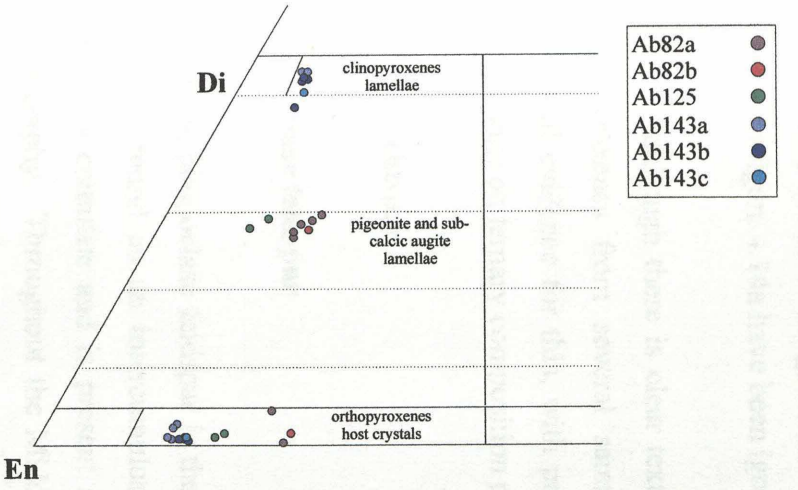


b. Pyroxene exsolution lamellae from the Belhelvie intrusion

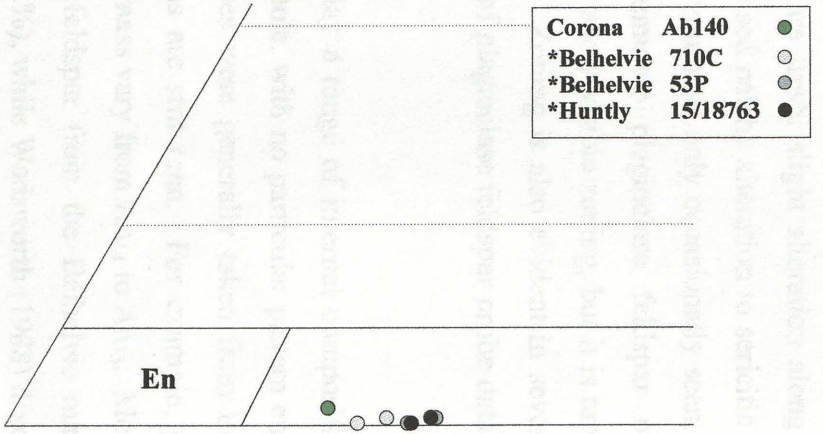


c. Pyroxenes from olivine corona from the Belhelvie Intrusion.
*Published data from Mongkoltip & Ashworth (1983).

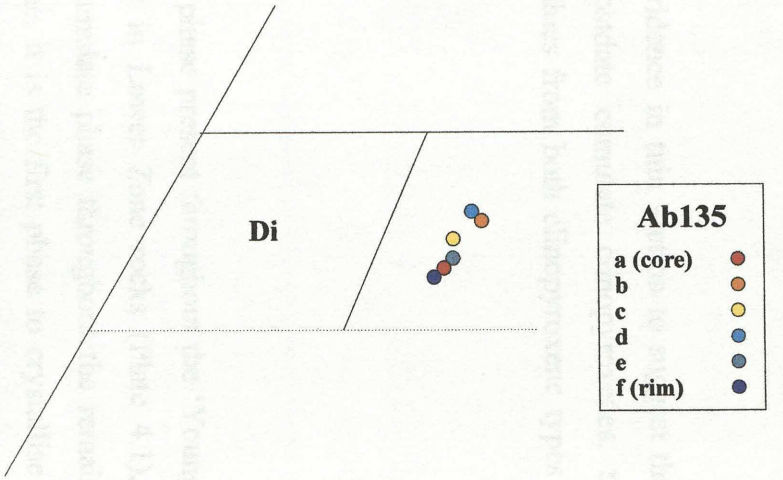


d. Core to rim analysis of a clinopyroxene from Ab135, a wehrlite from the Belhelvie intrusion

**Figure 4.14 Pyroxenes from the Belhelvie intrusion**

values for plots such as figures 4.10 to 4.12, values such as the low Ca analyses for sample Ab135 in figure 4.14a have been ignored.

Finally, although there is clear textural evidence in thin section to suggest that poikilitic clinopyroxenes from several samples postdate cumulate clinopyroxenes, there is no chemical evidence for this, with probe values from both clinopyroxene types plot in the same range on ternary composition plots.

### 4.7.5 Feldspar

#### Plagioclase feldspar

Modally, plagioclase feldspar is the main phase present throughout the 'Younger' Basics. Initially found as an intercumulus phase in Lower Zone rocks (Plate 4.1), it quickly becomes cumulate and is present as a cumulate phase throughout the remainder of the stratigraphy. Throughout the Middle Zone, it is the first phase to crystallise along with orthopyroxene and sometimes clinopyroxene, and usually displays excellent lath shaped outlines (see Plate 4.4, 4.15 & 5.1). Secondary overgrowth is occasionally present but more commonly the euhedral primary plagioclase crystals are outlined by late pyroxene, biotite or amphibole. In general, plagioclase feldspars are fresh; slight alteration along expansion cracks in the troctolites is common while localised patchy alteration to sericitic material is seen in some samples. In thin section, visible zoning is only occasionally seen, which can complicate identification of secondary adcumulate plagioclase feldspar overgrowth; samples from the Boganclogh mass commonly show visible zoning, but it is rare or absent in plagioclase feldspar from the other bodies. Zoning is also evident in several crystals from Granular Gabbros samples. A summary of plagioclase feldspar probe data are shown in Table 4.5.

Chemically, plagioclase feldspar crystals display a range of internal compositions within individual crystals and within samples as a whole, with no particular pattern emerging for this range of compositions. Although analyses were generally taken from the cores of euhedral, cumulate laths, significant variations are still seen. For example, plagioclase cores from sample Ab3826 from the Kinnadie mass vary from $An_{54}$ to $An_{33}$. Mongkoltip & Ashworth (1986) suggested that plagioclase feldspar from the Belhelvie mass showed continuous core to rim zoning (of up to 12 mol.%), while Wadsworth (1988) described such variation, seen specifically in the Insch mass, as 'patchy' and believed it to be the result of

| Plagioclase Feldspar | Arnage | Belhelvie | | | | | Haddo | Kinnadie | Maud | | Boganclogh | | | | | Insch | | | | | |
|---|---|---|---|---|---|---|---|---|---|---|---|---|---|---|---|---|---|---|---|---|---|
| Sample | 9P | Ab82 | Ab125 | Ab127 | Ab143 | Ab140 | 85P | Ab3826 | Ab1310 | Ab92 | Ab5613 | Ab7799 | Ab7801 | Ab7802 | MS1595 | Ab93 | Ab661 | DV1 | DV1(por) | V | Ab243 |
| SiO2 | 49.48 | 60.51 | 48.88 | 51.17 | 47.90 | 47.87 | 61.21 | 54.06 | 58.08 | 55.76 | 53.10 | 61.83 | 59.32 | 54.20 | 49.66 | 53.56 | 61.98 | 51.41 | 49.12 | 52.35 | 55.67 |
| Al2O3 | 30.30 | 24.74 | 30.16 | 31.29 | 30.68 | 32.11 | 25.22 | 27.28 | 27.53 | 28.30 | 27.04 | 24.34 | 26.51 | 28.69 | 29.73 | 27.93 | 23.48 | 30.40 | 31.71 | 29.83 | 27.32 |
| FeO | 0.00 | 0.14 | 0.14 | 0.00 | 0.05 | 0.10 | 0.00 | 0.07 | 0.29 | 0.13 | 0.13 | 0.14 | 0.17 | 0.10 | 0.00 | 0.14 | 0.00 | 0.21 | 0.21 | 0.24 | 0.16 |
| CaO | 14.96 | 7.43 | 14.90 | 15.13 | 15.61 | 16.78 | 7.49 | 11.23 | 10.44 | 11.56 | 11.30 | 6.83 | 9.17 | 12.19 | 14.11 | 12.00 | 5.89 | 14.40 | 16.38 | 13.87 | 10.82 |
| Na2O | 2.81 | 7.38 | 2.76 | 3.09 | 2.43 | 1.97 | 7.39 | 4.88 | 5.79 | 5.13 | 4.61 | 7.83 | 6.27 | 4.58 | 3.22 | 4.34 | 8.05 | 3.30 | 2.26 | 3.67 | 5.16 |
| K2O | 0.09 | 0.06 | 0.02 | 0.00 | 0.00 | 0.00 | 0.23 | 0.19 | 0.11 | 0.14 | 0.29 | 0.21 | 0.50 | 0.16 | 0.00 | 0.18 | 0.16 | 0.00 | 0.03 | 0.09 | 0.24 |
| BaO | 0.00 | 0.00 | 0.00 | 0.00 | 0.00 | 0.00 | 0.00 | 0.00 | 0.00 | 0.00 | 0.00 | 0.00 | 0.05 | 0.00 | 0.00 | 0.00 | 0.00 | 0.00 | 0.00 | 0.00 | 0.00 |
| Total | 97.63 | 100.28 | 96.90 | 100.67 | 96.72 | 98.86 | 101.61 | 97.71 | 102.23 | 101.02 | 96.49 | 101.17 | 101.99 | 99.92 | 96.75 | 98.20 | 99.55 | 99.78 | 99.78 | 100.07 | 99.48 |
| Formula | | | | | | | | | | | | | | | | | | | | | |
| Si | 9.242 | 10.757 | 9.209 | 9.259 | 9.062 | 8.883 | 10.742 | 9.984 | 10.216 | 9.962 | 9.944 | 10.881 | 10.436 | 9.810 | 9.342 | 9.862 | 11.038 | 9.381 | 9.022 | 9.512 | 10.092 |
| Al | 6.669 | 5.182 | 6.697 | 6.672 | 6.840 | 7.020 | 5.216 | 5.937 | 5.706 | 5.960 | 5.968 | 5.047 | 5.497 | 6.119 | 6.591 | 6.061 | 4.928 | 6.538 | 6.864 | 6.388 | 5.837 |
| Fe(ii) | 0.000 | 0.021 | 0.022 | 0.000 | 0.008 | 0.015 | 0.000 | 0.010 | 0.042 | 0.020 | 0.020 | 0.020 | 0.026 | 0.016 | 0.000 | 0.022 | 0.000 | 0.032 | 0.032 | 0.036 | 0.024 |
| Ca | 2.993 | 1.414 | 3.008 | 2.933 | 3.163 | 3.336 | 1.409 | 2.222 | 1.967 | 2.212 | 2.268 | 1.288 | 1.729 | 2.364 | 2.844 | 2.367 | 1.124 | 2.815 | 3.223 | 2.700 | 2.101 |
| Na | 1.017 | 2.543 | 1.008 | 1.084 | 0.891 | 0.707 | 2.514 | 1.746 | 1.976 | 1.777 | 1.674 | 2.670 | 2.138 | 1.608 | 1.174 | 1.549 | 2.779 | 1.167 | 0.805 | 1.293 | 1.814 |
| K | 0.021 | 0.014 | 0.004 | 0.000 | 0.000 | 0.000 | 0.051 | 0.044 | 0.025 | 0.032 | 0.070 | 0.048 | 0.112 | 0.036 | 0.000 | 0.042 | 0.036 | 0.000 | 0.007 | 0.021 | 0.055 |
| Ba | 0.000 | 0.000 | 0.000 | 0.000 | 0.000 | 0.000 | 0.000 | 0.000 | 0.000 | 0.000 | 0.000 | 0.000 | 0.004 | 0.000 | 0.000 | 0.000 | 0.000 | 0.000 | 0.000 | 0.000 | 0.000 |
| TOTAL | 19.943 | 19.930 | 19.949 | 19.947 | 19.964 | 19.961 | 19.933 | 19.943 | 19.932 | 19.963 | 19.944 | 19.954 | 19.940 | 19.952 | 19.950 | 19.903 | 19.906 | 19.934 | 19.952 | 19.951 | 19.924 |
| An | 74.24 | 35.61 | 74.82 | 73.02 | 78.02 | 82.51 | 35.45 | 55.39 | 49.59 | 55.01 | 56.54 | 32.15 | 43.45 | 58.99 | 70.77 | 59.80 | 28.53 | 70.69 | 79.88 | 67.27 | 52.93 |
| Ab | 25.23 | 64.04 | 25.07 | 26.98 | 21.98 | 17.49 | 63.25 | 43.52 | 49.79 | 44.19 | 41.73 | 66.66 | 53.74 | 40.12 | 29.23 | 39.14 | 70.55 | 29.31 | 19.94 | 32.21 | 45.68 |
| Or | 0.53 | 0.34 | 0.11 | 0.00 | 0.00 | 0.00 | 1.29 | 1.09 | 0.62 | 0.79 | 1.73 | 1.20 | 2.80 | 0.89 | 0.00 | 1.07 | 0.92 | 0.00 | 0.17 | 0.52 | 1.40 |

| Plagioclase Feldspar | Huntly | | | | Portsoy | Morven Cabrach | | Cashel | | Lough Wheelaun | | Currywongaun |
|---|---|---|---|---|---|---|---|---|---|---|---|---|
| Sample | 773C | Ab5661 | Ab3986 | Ab6510 | 110P | Ab94 | 77P | CLW218 | CLW215 | CLW106 | CLW110 | DCD118 |
| SiO2 | 50.59 | 50.78 | 49.56 | 49.33 | 50.61 | 57.23 | 54.93 | 49.17 | 52.77 | 45.91 | 46.14 | 44.35 |
| Al2O3 | 29.93 | 30.30 | 30.59 | 30.19 | 29.45 | 27.14 | 28.08 | 31.36 | 30.21 | 32.61 | 32.49 | 34.38 |
| FeO | 0.10 | 0.03 | 0.02 | 0.15 | 0.03 | 0.06 | 0.02 | 0.26 | 0.08 | 0.47 | 0.29 | 0.04 |
| CaO | 14.35 | 14.65 | 15.19 | 14.91 | 14.03 | 10.39 | 11.77 | 16.05 | 16.54 | 17.69 | 17.68 | 19.81 |
| Na2O | 3.26 | 3.14 | 2.82 | 3.01 | 3.39 | 5.78 | 4.82 | 2.34 | 1.08 | 1.38 | 1.39 | 0.39 |
| K2O | 0.05 | 0.01 | 0.00 | 0.02 | 0.05 | 0.12 | 0.22 | 0.04 | 0.00 | 0.00 | 0.02 | 0.00 |
| BaO | 0.00 | 0.05 | 0.00 | 0.00 | 0.00 | 0.00 | 0.00 | 0.08 | 0.00 | 0.01 | 0.00 | 0.00 |
| Total | 98.39 | 99.03 | 98.20 | 97.65 | 97.61 | 100.73 | 99.91 | 99.28 | 100.74 | 98.09 | 98.05 | 98.97 |
| Formula | | | | | | | | | | | | |
| Si | 9.372 | 9.344 | 9.208 | 9.228 | 9.435 | 10.214 | 9.935 | 9.068 | 9.499 | 8.634 | 8.673 | 8.294 |
| Al | 6.534 | 6.570 | 6.699 | 6.656 | 6.470 | 5.708 | 5.984 | 6.817 | 6.408 | 7.228 | 7.196 | 7.577 |
| Fe(ii) | 0.015 | 0.005 | 0.003 | 0.024 | 0.004 | 0.009 | 0.003 | 0.039 | 0.012 | 0.074 | 0.046 | 0.006 |
| Ca | 2.848 | 2.888 | 3.024 | 2.988 | 2.803 | 1.987 | 2.279 | 3.170 | 3.189 | 3.564 | 3.560 | 3.969 |
| Na | 1.171 | 1.121 | 1.015 | 1.090 | 1.224 | 2.000 | 1.691 | 0.837 | 0.377 | 0.504 | 0.505 | 0.141 |
| K | 0.012 | 0.003 | 0.000 | 0.004 | 0.012 | 0.027 | 0.052 | 0.010 | 0.000 | 0.000 | 0.004 | 0.000 |
| Ba | 0.000 | 0.003 | 0.000 | 0.000 | 0.000 | 0.000 | 0.000 | 0.006 | 0.000 | 0.001 | 0.000 | 0.000 |
| TOTAL | 19.952 | 19.933 | 19.949 | 19.990 | 19.948 | 19.945 | 19.945 | 19.947 | 19.485 | 20.005 | 19.984 | 19.988 |
| An | 70.66 | 71.99 | 74.88 | 73.20 | 69.40 | 49.49 | 56.67 | 78.92 | 89.43 | 87.60 | 87.48 | 96.56 |
| Ab | 29.05 | 27.94 | 25.12 | 26.71 | 30.30 | 49.83 | 42.04 | 20.83 | 10.57 | 12.40 | 12.42 | 3.44 |
| Or | 0.29 | 0.07 | 0.00 | 0.09 | 0.29 | 0.68 | 1.29 | 0.25 | 0.00 | 0.00 | 0.11 | 0.00 |

| Alkali Feldspar | Insch | Boganclogh | |
|---|---|---|---|
| Sample | Ab661 | Ab7799 | Ab7801 |
| SiO2 | 64.24 | 66.56 | 65.53 |
| Al2O3 | 18.32 | 18.66 | 18.92 |
| FeO | | 0.00 | 0.00 |
| CaO | 0.06 | 0.45 | 0.09 |
| Na2O | 1.33 | 2.68 | 1.31 |
| K2O | 14.10 | 12.90 | 14.69 |
| BaO | 2.11 | 0.38 | 2.11 |
| Total | 100.15 | 101.63 | 102.62 |
| Formula | | | |
| Si | 11.949 | 11.995 | 11.910 |
| Al | 4.016 | 3.963 | 4.050 |
| Fe(ii) | | 0.000 | 0.000 |
| Ca | 0.012 | 0.087 | 0.020 |
| Na | 0.480 | 0.938 | 0.460 |
| K | 3.345 | 2.966 | 3.410 |
| Ba | 0.154 | 0.027 | 0.150 |
| TOTAL | 19.956 | 19.975 | 20.000 |
| An | 0.30 | 2.16 | 0.43 |
| Ab | 12.02 | 23.32 | 11.44 |
| Or | 83.83 | 73.85 | 84.40 |
| Cn | 3.85 | 0.67 | 3.72 |



**Table 4.5 Summary of feldspar compositions for samples probed.**

partial re-equilibration during the late stages of crystallisation. Even in the plagioclase crystals that do display optical zoning in thin section, microprobe data suggests that the associated chemical variations are not straightforward core to rim zoning. Despite this 'patchy' internal variation, patterns are seen in average compositions through the bodies, although scatter is greater in these trends than it is for other silicate phases; this scatter is largely as a result of this large compositional variation within individual samples.

Although the sample database is relatively limited, one feature that emerges quite strongly is that plagioclase feldspars from Connemara display systematically higher An contents than those in the Grampian Highlands. This can be seen in Table 4.5 and figure 4.12, where it is evident that, for a given whole rock mg#, anorthite contents in Connemara plagioclase feldspar are $An_{20-30}$ greater than in Scottish ones. The trend of decreasing anorthite content with fractionation, which is evident in the Scottish samples is not well defined in Connemara, largely due to the aforementioned scatter and the limited amount of samples probed. However, the pattern of plagioclase feldspar with more highly calcic compositions is evident, with anorthite contents as high as $An_{96.6}$ seen in Connemara; individual microprobe analyses from this sample (shown in Plate 4.11) as high as $An_{97.4}$, while the overall anorthite range in Connemara is $An_{97}$ to $An_{79}$. All five of the samples analysed are from the Middle Zone, and four of these samples have compositions of $An_{88}$ or greater, which is significantly higher than the calcic plagioclase seen in most of the Scottish bodies.

Plots of An% versus the mg# of coexisting ferromagnesian phases also reveals this trend (see figure 4.15b+c), suggesting that it is not merely an artefact of the use of whole rock mg# as a fractionation index. The most anorthic plagioclase feldspars from the Grampian Highlands probed as part of this study are from the Lower Zone of Belhelvie and Huntly, and range from $An_{83}$ to $An_{69}$, with Middle Zone crystals generally in the range $An_{60}$ to $An_{40}$. Upper Zone feldspars from Insch and Boganclogh possess compositions ~$An_{30}$, although, as mentioned above, the trend is not as well defined as for the ferromagnesian phases, with considerable scatter present. However, highly calcic plagioclase feldspar has been identified from some of the minor Scottish bodies such as in Succoth-Brownhills ($An_{99-80}$; Gunn *et al.*, 1996) and in the Kildrummy mass ($An_{88-81}$; Gould, 1997). This trend for high An plagioclase feldspar does not appear be reflected in the other silicate phase compositions from the Connemara bodies (see figure 4.15a). The significance of these highly anorthic plagioclase feldspar will be discussed in Chapter 7.

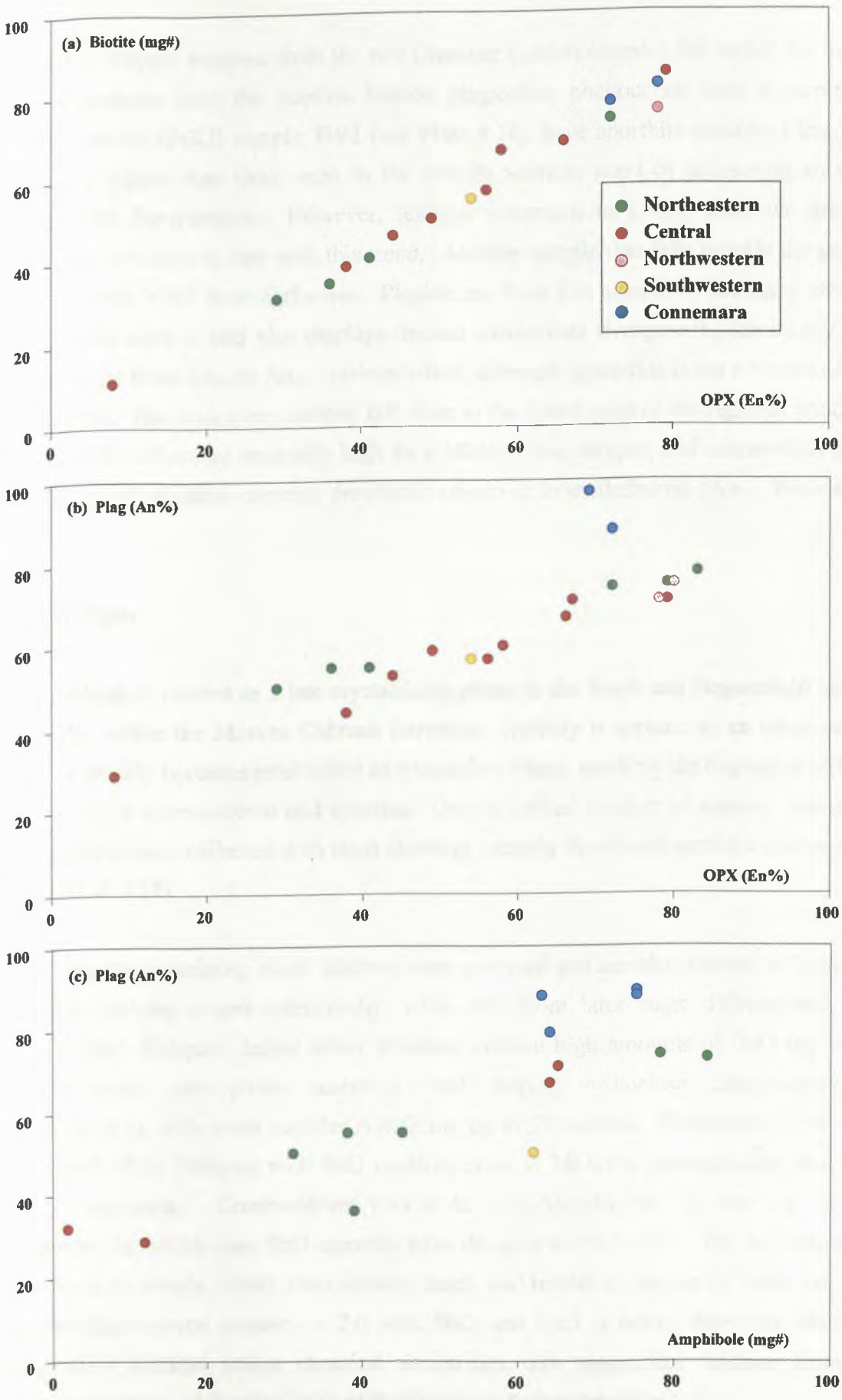


**Figure 4.15 Selected bivariate plots of coexisting silicate phases. (a) Biotite (mg#) versus Orthopyroxene (En%); (b) Plagioclase (An%) versus Orthopyroxene (En%); and (c) Plagioclase (An%) versus Amphibole (mg#)**

Plagioclase feldspar analyses from the two Granular Gabbro samples fall within the overall range of analyses from the Scottish bodies; plagioclase phenocrysts from a porphyritic Granular Gabbro (PGG) sample, DV1 (see Plate 4.10), have anorthite contents ($An_{80}$) that are slightly higher than those seen in the overall Scottish trend of decreasing anorthite contents with fractionation. However, feldspar compositions ($An_{71}$) from the granular groundmass are more in line with this trend. Another sample that falls outside the general trend is sample Ab82 from Belhelvie. Plagioclase from this sample is unusually strongly zoned in thin section, and also displays limited adcumulate overgrowth; chemically their contents range from $An_{60}$ to $An_{24}$ in composition, although again this is not a simple core to rim variation. The $An_{60}$ compositions fall close to the lower parts of the regional trend, but the more sodic values are unusually high for a Middle Zone sample, and substantially lower than the lowest anorthite contents previously observed from Belhelvie ($An_{71}$; Wadsworth, 1991).

**Alkali-feldspar**

Alkali feldspar is present as a late crystallising phase in the Insch and Boganclogh masses and locally within the Morven Cabrach intrusion. Initially it appears as an intercumulus phase but quickly becomes established as a cumulate phase, marking the beginning of UZb, and is found in syenogabbros and syenites. Only a limited number of samples containing alkali feldspar were collected with most showing variably developed perthitic textures (see Plates 4.12 & 4.17)

Only 3 samples containing alkali feldspar were analysed and are also shown in Table 4.5; one alkali feldspar occurs interstitially, while two from later stage differentiates with cumulus alkali feldspar. Initial alkali feldspars contain high amounts of BaO (up to 2.6 wt% in some microprobe analyses), and display orthoclase compositions of $An_0Ab_{12}Or_{84}Cn_4$, with some samples containing up to 5% celsian. Wadsworth (1986) has documented alkali feldspars with BaO contents close to 7.0 wt%, corresponding to a $Cn_{13}$ celsian component. Compositions evolve to $An_{02}Ab_{23}Or_{74}Cn_1$ by the top of the stratigraphy, by which time BaO contents have dropped to <0.5 wt%. The microperthites were probed in sample Ab661 from western Insch, and results are shown in Table 4.6. The host orthoclase crystal contains ~ 2.0 wt% BaO and CaO is below detection while the microperthite displays strong chemical similarities with plagioclase feldspar from the sample, containing ~ 5.0 wt% CaO and BaO contents below detection.

Plate 4.11 (a) PPL

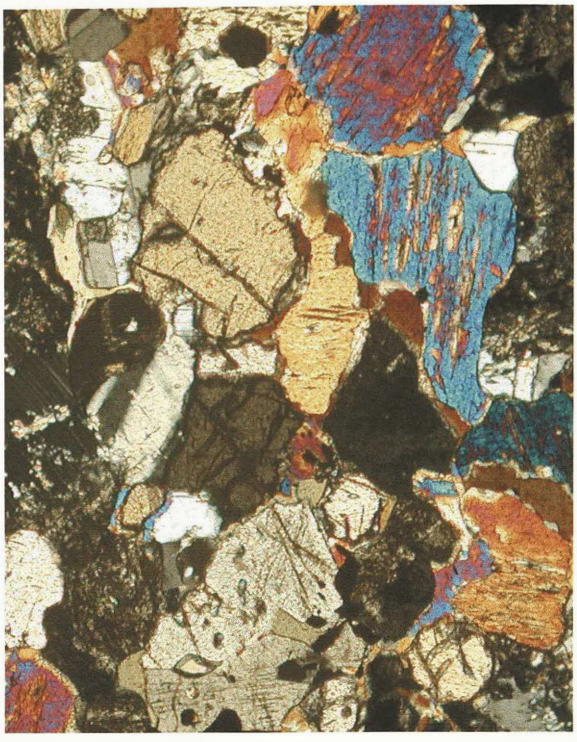

Plate 4.11 (b) XPL

**Plate 4.11 Sample DCD118 from the Currywongaun body, containing cumulus orthopyroxene, clinopyroxene and plagioclase feldspar. Interstitial opaques and primary amphibole are also present. Clinopyroxene is locally replaced by amphibole, while sericite after feldspar is variably developed; plagioclase feldspar from this sample has compositions up to $An_{97}$. Vertical scale = 1.6 mm.**

Plate 4.12 (a) PPL

Plate 4.12 (b) XPL

**Plate 4.12 Sample Ab661 from the Upper Zone of the Insch intrusion. Perthitic alkali feldspar, primary amphibole, cumulus apatite and late intercumulus quartz are evident. Heavily sericitized plagioclase feldspar is also present. Vertical scale = 1.6 mm.**

Plate 4.13 Ab7801 (PPL)

Plate 4.13 Lath-shaped cumulus ilmenite in a gabbroic sample from Boganclogh. Cumulus apatite is also present. Vertical scale = 1.6 mm.

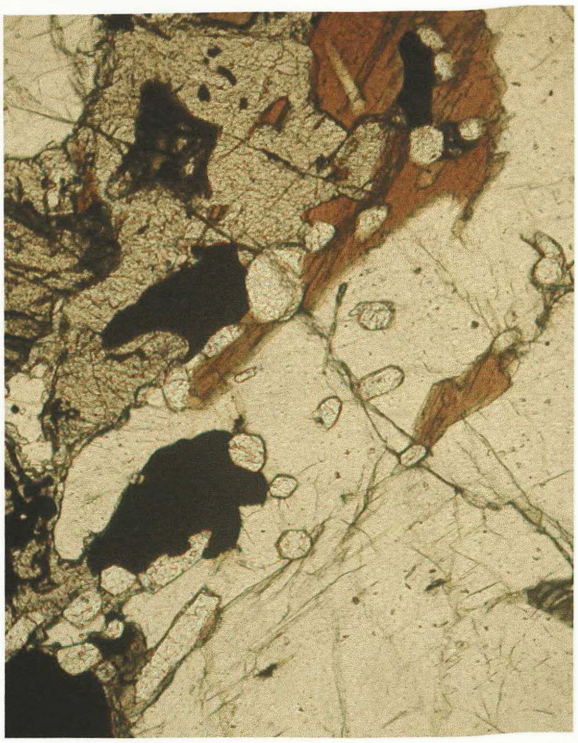

Plate 4.14 60W (PPL)

Plate 4.14 Cumulus apatite in a biotite-gabbro from the Insch mass. Vertical scale = 1.6 mm.

Plate 4.15 Ab3986 (PPL)

Plate 4.15 Poikilitic orthopyroxene from the Huntly intrusion enclosing cumulus plagioclase feldspar and olivine. Vertical scale = 3.0 mm.

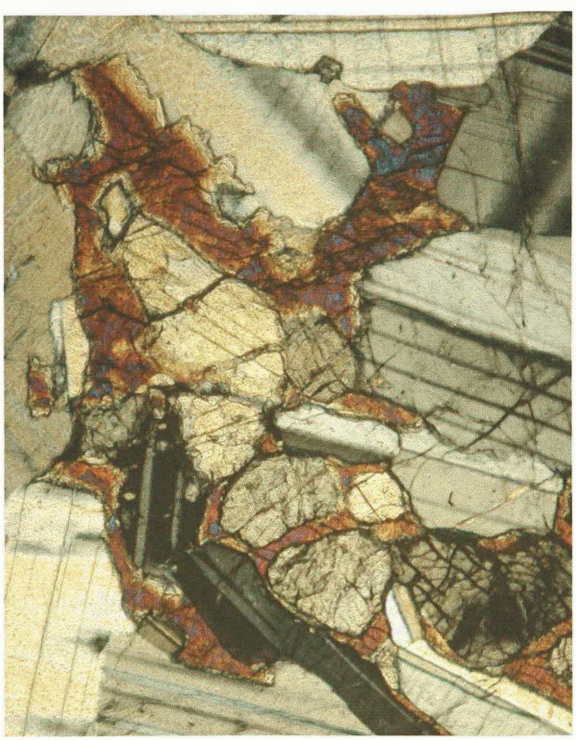

Plate 4.16 Ab2073 (XPL)

Plate 4.16 A Belhelvie gabbro, with postcumulus clinopyroxene enclosing cumulus plagioclase and orthopyroxene. Vertical scale = 1.6 mm.

Plate 4.17 (a) PPL

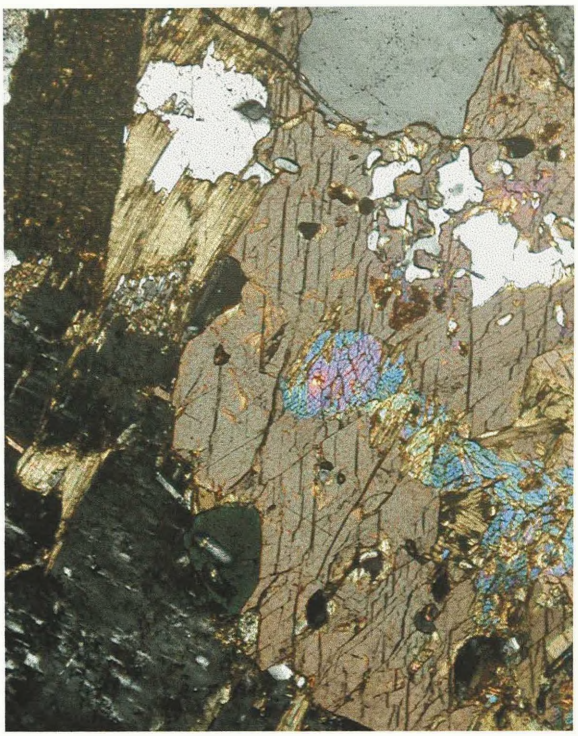

Plate 4.17 (b) XPL

**Plate 4.17 Sample Ab661 from the Upper Zone of the Insch intrusion. Euhedral primary hornblende is seen surrounding a possible orthopyroxene (centre, high birefringence); the analysis is shown in Table 4.3. Secondary amphibole is also seen to the bottom right of this pyroxene. Apatite, biotite, quartz and perthitic alkali feldspar are also present. Vertical scale = 1.6 mm.**

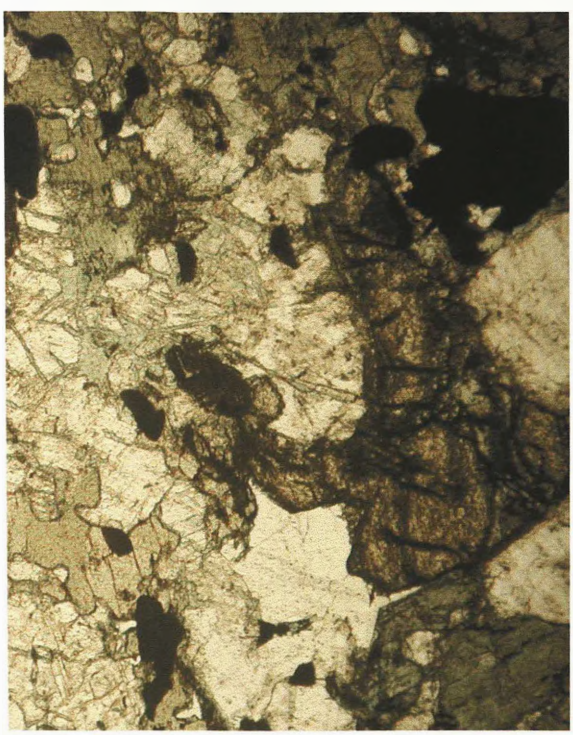

Plate 4.18 (a) PPL

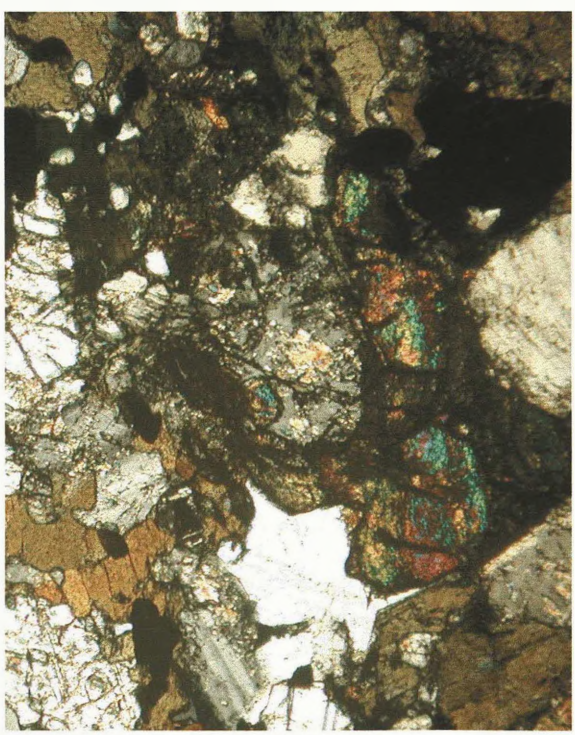

Plate 4.18 (b) XPL

**Plate 4.18 Sample CLW219 from the Cashel intrusion, displaying a cluster of cumulus zircon (high relief and birefringence). Euhedral primary hornblende (bottom right), sericitized plagioclase, secondary amphibole and interstitial quartz are also present. Vertical scale = 1.6 mm.**

| Sample : Ab661<br>Analysis name | kfel1a | kfel1b | per-kfel1 | plag3 | plag4 |
|---|---|---|---|---|---|
| SiO2 | 64.07 | 64.30 | 62.73 | 63.17 | 62.32 |
| Al2O3 | 18.25 | 18.39 | 22.92 | 22.99 | 23.02 |
| CaO | b.d. | b.d. | 5.32 | 5.13 | 5.16 |
| Na2O | 1.07 | 1.60 | 8.06 | 8.57 | 8.45 |
| K2O | 14.29 | 13.88 | 0.48 | 0.15 | b.d. |
| BaO | 1.93 | 2.18 | b.d. | b.d. | b.d. |
| Total | 99.62 | 100.36 | 99.50 | 100.01 | 98.95 |
| Formula | | | | | |
| Si | 11.97 | 11.94 | 11.17 | 11.18 | 11.14 |
| Al | 4.02 | 4.02 | 4.81 | 4.79 | 4.85 |
| Ca | 0.00 | 0.00 | 1.01 | 0.97 | 0.99 |
| Na | 0.39 | 0.58 | 2.78 | 2.94 | 2.93 |
| K | 3.41 | 3.29 | 0.11 | 0.03 | 0.00 |
| Ba | 0.14 | 0.16 | 0.00 | 0.00 | 0.00 |
| Total | 19.92 | 19.98 | 19.88 | 19.91 | 19.90 |
| An | - | - | 25.98 | 24.64 | 25.23 |
| Ab | 9.85 | 14.32 | 71.23 | 74.50 | 74.77 |
| Or | 86.56 | 81.74 | 2.79 | 0.86 | - |
| Cn | 3.59 | 3.94 | - | - | - |

**kfel1 a+b** : host alkali feldspar  b.d. : below detection
**per-kfel1** : microperthite in kfel1
**plag 3+4** : coexisting plagioclase feldspars

**Table 4.6 Microprobe analyses of alkali and plagioclase feldspars from sample Ab661, from western Insch (see Plate 4.12 & 4.17).**

### 4.7.6 Biotite

Biotite is a widespread constituent phase within the 'Younger' Basics, in both Connemara and the Grampian Highlands. It is a virtually ubiquitous accessory phase throughout the Middle and Upper Zones, but is also found within Lower Zone samples. In samples from the northeastern intrusions of Arnage, Haddo, Kinnadie and Maud, it is not uncommon for biotite to form 10-15% of the rock. It also forms a significant component of gabbros and norites locally in other bodies, especially Boganclogh. Typically, biotite is a late crystallising phase, only occasionally displaying its characteristic euhedral lath shaped outlines; it is also commonly found as a late overgrowth, especially on Fe-Ti oxide phases such as ilmenite (see Plates 4.6, 4.8 & 5.2), but also on pyroxenes. More rarely, it is present

as a poikilitic phase enclosing earlier cumulus phases. In such samples it can be found in association with earlier crystallising, more lath shaped, biotites. In general, biotite tends to be quite fresh, with only occasional frayed margins and alteration to chlorite.

Although the boundaries between the principal biotite components are not precisely defined, the majority of samples fall within the field for commonly occurring biotites (Figure 4.16). Lower Zone biotites from Belhelvie, Boganclogh, Huntly and Lough Wheelaun all display high mg# values of 87.5 to 82.4, and consequently have a significant phlogopite component. Mg#s decrease with fractionation and biotites from the most evolved syenitic samples from the Insch and Boganclogh bodies display the lowest mg#'s of 11.3 to 2.0, and consequently possess significant annite components. Biotite analysed from one Granular Gabbros sample (see Figure 4.16) falls within the range of the other samples, with a mg# value of 68.7. No zoning is evident either optically or in core to rim probe analyses. In addition, within individual samples, there is no apparent chemical difference between biotites of a poikilitic or late, intercumulus nature.

### 4.7.7 Amphibole

Both primary and secondary amphiboles are present in the 'Younger' Basics. In the majority of samples, primary amphibole is only present in minor quantities; where present it is as a late, postcumulus phase, displaying classic intercumulus outlines (see Plate 4.4), or as late overgrowths on cumulus phases such as pyroxene (see Plate 4.5 & 4.6). Only in the Lower Zone in the Cashel-Lough Wheelaun intrusion is amphibole found in significant quantities where large poikilitic amphiboles are found enclosing earlier phases including biotite (see Plate 4.4). However, there is no evidence for the fractionation of amphibole as a cumulus phase anywhere in the 'Younger' Basics. The other form in which primary amphibole is found is as part of corona overgrowths on olivines, which are quite common in troctolites from several of the intrusions. Secondary amphibole is far more abundant than primary amphibole, and results from replacement of pyroxenes, especially clinopyroxene, by late stage fluids; this can be seen to varying degrees in many of the plates in this chapter. In many cases, secondary amphibole displays several features in common with primary amphibole, such as distinct, euhedral crystal outlines, which appear optically to be single, discrete crystals; this results in difficulties in differentiating between primary and secondary amphibole in some samples. This replacement of primary pyroxene is especially common in samples from intrusions adjacent to the regional shear zones discussed previously,

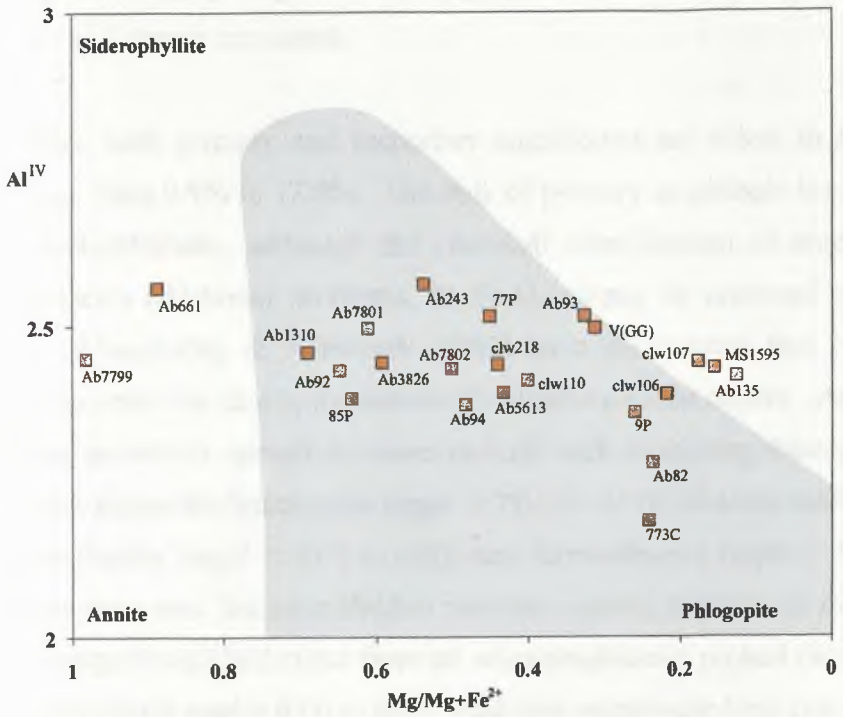


**Figure 4.16 Composition of biotites from the 'Younger' Basics. The shaded field is the region in which most 'commonly occurring biotites' fall (Deer *et al.*, 1992)**

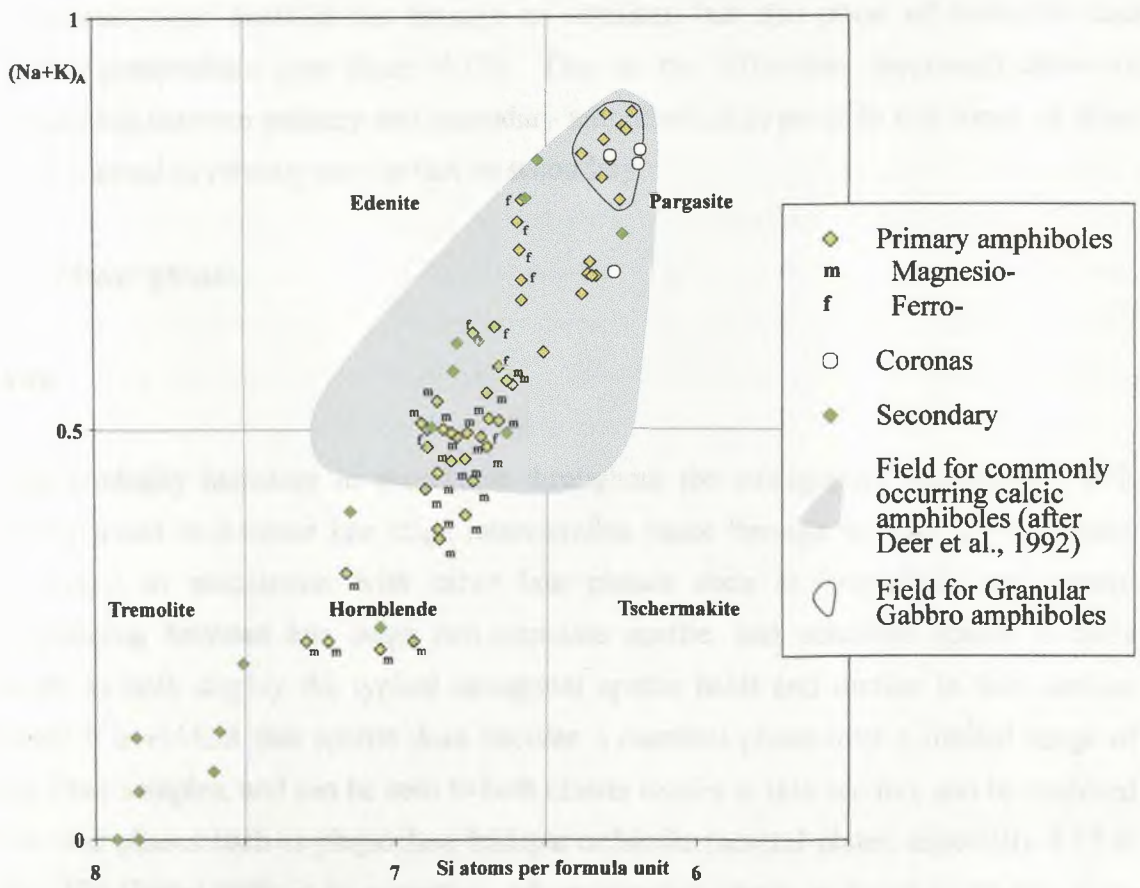


**Figure 4.17 Classification of both primary and secondary calcic amphibole analyses from the 'Younger' Basics**

resulting in secondary amphibole being particularly common in the Huntly-Knock-Portsoy and Morven Cabrach intrusions.

Chemically, both primary and secondary amphiboles are calcic in nature, with a limited CaO range, from 9.9% to 12.8%. The bulk of primary amphibole is classified as magnesio- and ferro-hornblendes, although the chemical classification of amphiboles (after Leake, 1978) presents additional problems, as $Fe_2O_3$ cannot be analysed using the microprobe. However, Mongkoltip & Ashworth (1983) have commented that $Fe_2O_3$ abundances are likely to be quite low due to the non-oxidised nature to the bodies. As with biotite, primary amphibole shows an overall decrease in mg# with increasing fractionation; compositions range from magnesio-hornblende (mg# = 79.1 to 45.0) in more mafic samples through to ferro-hornblendes (mg# = 45.3 to 4.8), and ferro-edenites (mg# = 39.3 to 1.7). Primary amphibole from two Granular Gabbro samples contain particularly high alkali abundances, and are compositionally distinct from all other amphiboles probed (see figure 4.17), plotting as pargasites, with mg# = 67.0 to 63.4. Poikilitic amphibole from one sample in the Cashel-Lough Wheelaun intrusion plots as pargasite (mg# = 76.2 to 73.8), but with lower $(Na+K)_A$ abundances, while corona amphiboles from Belhelvie, Insch and Huntly also plot as pargasites (mg# = 87.2 to 55.7). Secondary amphibole also contains a wide variety of compositions, from hornblendes through to edenites, but also some of tremolitic and actinolitic composition (see figure 4.17). Due to the difficulties mentioned above in distinguishing between primary and secondary amphibole, it is possible that some of those analyses classed as primary may in fact be secondary.

### 4.7.8 Minor phases

#### Apatite

Apatite gradually increases in abundance throughout the stratigraphic succession. It is generally found as a minor late stage intercumulus phase through most of the intrusions, often found in association with other late phases such as amphibole and quartz. Distinguishing between late stage non-cumulate apatite, and cumulate apatite is quite difficult, as both display the typical hexagonal apatite habit and outline in thin section; however it is evident that apatite does become a cumulus phase over a limited range of Upper Zone samples, and can be seen to both cluster locally in thin section, and be enclosed within later phases such as plagioclase feldspar or biotite (several plates, especially 4.12 & 4.14). The Cashel body is an exception, where cumulus apatite is found in Middle Zone

rocks, and also in several samples from the Maud body in the northeast where apatite also appears to be cumulate in nature. In cumulate samples apatite can reach 2-3 % modally, but when present interstitially is usually only present in very minor amounts (<<1%). Towards the top of the Upper Zone, apatite ceases to be a cumulate phase and is again only found in minor quantities.

**Oxides**

Detailed reflected light microscopy has not been carried out on the opaque minerals seen in the 'Younger' Basics as part of this study. However, a limited number of samples have been examined in polished thin section and also probed in some cases. Several oxide phases have been identified as crystallising in different parts of the stratigraphy. In some Lower Zone rocks, chrome spinel is found locally in the field, such as in the Dawros body in North Connemara, where narrow chrome spinel horizons are seen in ultramafic rocks; it is evident, both in the field and in thin section, that chrome spinel is briefly cumulate in nature in the Lower Zone. Through the Lower Zone, primary oxide phases are rare, with opaque alteration products after olivine, probably haematite or goethite, present in heavily altered samples. Through the Middle Zone, late stage opaque minerals are common, usually making up 1-2 % of the rock modally. Occasionally lath shaped outlines or partial outlines are evident and reflected light microscopy suggests that, in many cases, these are mainly ilmenite; occasional magnetite twinned with ilmenite or exsolving ilmenite is also found, and other forms of Fe-Ti oxides such as titaniferous magnetite are also likely to be present; the majority of samples analysed by microprobe are ilmenite. Marginal alteration to limonite is occasionally seen, as are occasional sulphides such as marcasite, pyrrhotite and pentlandite. Symplectic ilmenite textures are seen in one sample from the Morven Cabrach intrusion, with ilmenite mantled by sphene. However, the majority of opaque minerals present are ilmenite or closely related Fe-Ti oxides. These can be seen in thin section to become a cumulate phase towards the top of the Middle Zone, with crystal outlines becoming more consistently lath-shaped in outline (see Plate 4.13), and reaching 5-6% modally in abundance. Oxide abundances drop in the Upper Zone, and are only found interstitially in the most fractionated samples.

**Quartz**

Where present, quartz is invariably a late stage phase, often displaying textural evidence that it crystallised after both amphibole and apatite (see Plates 4.5 & 4.12). Quartz is

abundant in the gabbros from the northeastern bodies of Arnage, Haddo and Maud, commonly making up 10-15% of the rock modally, but is less common in most of the other bodies; it is found occasionally in the Upper Zone syenites and syenogabbros of the Insch and Boganclogh bodies, and also locally in Upper Zone Morven Cabrach rocks.

**Zircon**

Zircon is a minor accessory phase seen primarily in the Upper Zone of Insch and Boganclogh. Occasionally isolated crystals are present in very minor amounts in some Middle Zone samples, but it is in the Upper Zone that zircon is briefly present as an apparent cumulate phase, where it can be seen to form irregular clusters, usually enclosed within late phases such as amphibole (see Plate 4.18). As with apatite, the Cashel body in South Connemara, displays cumulus zircon in Middle Zone samples (see Plate 4.18). Zircon is also possibly present as a cumulate phase in some samples from the northeastern bodies, especially Maud. As will be seen in the next chapter, there is whole rock chemical evidence to suggest that zircon may fractionate at different stages in the Insch and Boganclogh masses. The very fine-grained nature to these zircons means that their textural relationship to the remainder of the sample is quite difficult to determine precisely (although they do appear to be a late crystallising phase). Consequently, caution must be exercised when interpreting clusters of zircon, such as those seen in Plate 4.1, as being cumulus in origin. This will also be discussed briefly in Section 6.3.2.

### 4.7.9 Modal Abundances

The nature of cumulate rocks and their formation means that the modal abundances of individual phases can vary quite substantially. Fractionation processes and postcumulate growth, combined with the coarse-grained nature to most samples means that precise modal abundances are quite difficult to ascertain precisely and, consequently detailed modal abundances have not been determined. Approximate modal abundances have nevertheless been ascertained, and averages for individual zones are shown on an intrusion-by-intrusion basis in Table 4.7. As mentioned, the modes vary quite substantially within a single coarse-grained thin section and consequently, norm abundances have also been included. Clearly, direct comparisons cannot be made between modal and norm abundances due to the absence of hydrous phases in the norm, but several features emerge from both sets of data.

The most obvious of these features is the high modal amounts of amphibole, biotite and quartz (and norm quartz) in the Middle Zone of the northeastern bodies compared to the

| Intrusion | Zone | (n) | Approximate modal abundances | | | | | | | | | | |
|---|---|---|---|---|---|---|---|---|---|---|---|---|---|
| | | | Oliv | Plag | OPX | CPX | Hbl | Biot | Opaq | K-fel | Ap | Qz | Alt. |
| Belhelvie | LZ | 12 | 18 | 51 | 10 | 17 | 0 | 0 | 1 | 0 | 0 | 0 | 3 |
| Insch | LZ | 2 | 50 | 35 | 4 | 8 | 0 | 0 | 4 | 0 | 0 | 0 | 0 |
| Boganclogh | LZ | 8 | 76 | 0 | 10 | 14 | 0 | 0 | 1 | 0 | 0 | 0 | 0 |
| Huntly | LZ | 12 | 40 | 39 | 1 | 14 | 0 | 0 | 1 | 0 | 0 | 0 | 7 |
| Knock | LZ | 6 | 77 | 0 | 1 | 6 | 0 | 0 | 5 | 0 | 0 | 0 | 12 |
| Portsoy | LZ | 4 | 62 | 21 | 6 | 8 | 0 | 1 | 3 | 0 | 0 | 0 | 0 |
| S. Brownhills | LZ | 3 | 47 | 10 | 0 | 13 | 0 | 0 | 2 | 0 | 0 | 0 | 28 |
| M. Cabrach | LZ | 5 | 86 | 0 | 8 | 0 | 0 | 0 | 4 | 0 | 0 | 0 | 2 |
| C. of Muick | LZ | 8 | 54 | 10 | 6 | 5 | 1 | 0 | 3 | 0 | 0 | 0 | 22 |
| Dawros | LZ | 4 | 56 | 0 | 15 | 25 | 0 | 0 | 4 | 0 | 0 | 0 | 0 |
| Cashel | LZ | 1 | 0 | 40 | 0 | 20 | 15 | 2 | 2 | 0 | 2 | 5 | 15 |
| L. Wheelaun | LZ | 2 | 10 | 15 | 15 | 5 | 15 | 1 | 0 | 0 | 0 | 1 | 38 |
| Arnage | MZ | 4 | 0 | 58 | 18 | 9 | 2 | 7 | 2 | 0 | 1 | 5 | 0 |
| Haddo House | MZ | 3 | 0 | 43 | 5 | 12 | 15 | 8 | 3 | 0 | 0 | 13 | 0 |
| Kinnadie | MZ | 1 | 0 | 55 | 10 | 0 | 10 | 10 | 8 | 0 | 2 | 5 | 0 |
| Maud | MZ | 3 | 0 | 51 | 10 | 0 | 13 | 12 | 3 | 0 | 4 | 7 | 0 |
| Belhelvie | MZ | 6 | 0 | 57 | 27 | 10 | 0 | 3 | 1 | 0 | 1 | 2 | 0 |
| Insch | MZ | 4 | 0 | 63 | 10 | 18 | 0 | 4 | 3 | 0 | 1 | 1 | 0 |
| Insch | GG | 6 | 3 | 55 | 15 | 19 | 1 | 2 | 5 | 0 | 0 | 0 | 0 |
| Boganclogh | MZ | 5 | 6 | 52 | 14 | 16 | 2 | 7 | 2 | 0 | 1 | 1 | 0 |
| Huntly | MZ | 5 | 22 | 27 | 0 | 4 | 0 | 0 | 0 | 0 | 0 | 0 | 47 |
| Knock | MZ | 2 | 0 | 55 | 0 | 3 | 0 | 0 | 3 | 0 | 0 | 0 | 40 |
| Portsoy | MZ | 2 | 0 | 43 | 0 | 0 | 0 | 1 | 5 | 0 | 2 | 5 | 45 |
| S. Brownhills | MZ | 5 | 0 | 53 | 0 | 0 | 0 | 0 | 0 | 0 | 0 | 0 | 47 |
| M. Cabrach | MZ | 12 | 0 | 59 | 3 | 5 | 1 | 4 | 5 | 0 | 2 | 1 | 20 |
| C. of Muick | MZ | 3 | 0 | 17 | 0 | 0 | 0 | 0 | 5 | 0 | 0 | 0 | 78 |
| Dawros | MZ | 2 | 5 | 43 | 5 | 20 | 0 | 0 | 0 | 0 | 0 | 0 | 28 |
| Currywongaun | MZ | 2 | 0 | 40 | 15 | 3 | 18 | 3 | 3 | 0 | 0 | 0 | 20 |
| Cashel | MZ | 9 | 0 | 44 | 0 | 0 | 6 | 0 | 2 | 0 | 0 | 3 | 45 |
| L. Wheelaun | MZ | 11 | 0 | 46 | 10 | 7 | 6 | 3 | 3 | 0 | 1 | 3 | 23 |
| Insch | UZ | 6 | 3 | 29 | 6 | 14 | 6 | 4 | 5 | 29 | 3 | 2 | 0 |
| Boganclogh | UZ | 1 | 5 | 10 | 0 | 15 | 0 | 0 | 2 | 60 | 2 | 6 | 0 |
| All | LZ | 67 | 50 | 21 | 6 | 11 | 1 | 0 | 2 | 0 | 0 | 0 | 8 |
| All | MZ | 79 | 2 | 49 | 7 | 6 | 3 | 3 | 3 | 0 | 1 | 2 | 24 |
| All | UZ | 7 | 4 | 26 | 5 | 14 | 5 | 3 | 4 | 34 | 3 | 2 | 0 |

| Zone | (n) | *Norm abundances* | | | | | | | |
|---|---|---|---|---|---|---|---|---|---|
| | | *ol* | *ab+an* | *hy* | *di* | *il* | *or* | *ap* | *q* |
| LZ | 12 | *20* | *51* | *11* | *14* | *0.3* | *0* | *0* | *0* |
| LZ | 2 | *31* | *31* | *29* | *2* | *2.9* | *1* | *0* | *0* |
| LZ | 8 | *61* | *3* | *22* | *11* | *0.1* | *0* | *0* | *0* |
| LZ | 12 | *32* | *37* | *13* | *13* | *0.4* | *0* | *0* | *0* |
| LZ | 6 | *54* | *2* | *30* | *11* | *0* | *0* | *0* | *0* |
| LZ | 4 | *44* | *24* | *24* | *4* | *0.2* | *0* | *0* | *0* |
| LZ | 3 | *33* | *18* | *30* | *12* | *1.7* | *1* | *0.4* | *0* |
| LZ | 5 | *66* | *0* | *29* | *0* | *0* | *0* | *0* | *0* |
| LZ | 8 | *50* | *15* | *27* | *4* | *0.2* | *0* | *0* | *0* |
| LZ | 4 | *57* | *4* | *16* | *19* | *0.1* | *0* | *0* | *0* |
| LZ | 1 | *0* | *32* | *33* | *25* | *0.9* | *5* | *0.1* | *1* |
| LZ | 2 | *11* | *15* | *33* | *33* | *0.6* | *4* | *0* | *1* |
| MZ | 4 | *0* | *53* | *25* | *9* | *1.9* | *4* | *0.1* | *5* |
| MZ | 3 | *0* | *47* | *23* | *8* | *4.2* | *8* | *0.6* | *6* |
| MZ | 1 | *0* | *48* | *23* | *8* | *6.3* | *5* | *0.8* | *5* |
| MZ | 3 | *0* | *50* | *21* | *5* | *4.8* | *7* | *1.9* | *8* |
| MZ | 6 | *2* | *50* | *30* | *12* | *0.7* | *2* | *0.1* | *1* |
| MZ | 6 | *4* | *54* | *18* | *5* | *4.5* | *5* | *0.5* | *3* |
| GG | 6 | *4* | *56* | *16* | *18* | *2.1* | *1* | *0* | *1* |
| MZ | 6 | *8* | *48* | *19* | *13* | *3.4* | *4* | *0.8* | *1* |
| MZ | 9 | *17* | *47* | *13* | *19* | *0.4* | *0* | *0* | *0* |
| MZ | 2 | *4* | *50* | *16* | *22* | *2.6* | *2* | *0.3* | *0* |
| MZ | 3 | *0* | *61* | *16* | *12* | *2.6* | *2* | *0.4* | *2* |
| MZ | 5 | *3* | *62* | *20* | *13* | *0.2* | *0* | *0* | *0* |
| MZ | 13 | *3* | *56* | *18* | *8* | *5.1* | *5* | *0.6* | *2* |
| MZ | 3 | *24* | *37* | *3* | *21* | *6.3* | *2* | *0.2* | *0* |
| MZ | 2 | *18* | *41* | *5* | *27* | *0.3* | *7* | *0* | *0* |
| MZ | 2 | *3* | *40* | *33* | *14* | *1.3* | *3* | *0.1* | *1* |
| MZ | 9 | *8* | *49* | *17* | *13* | *1.7* | *5* | *0.6* | *2* |
| MZ | 11 | *6* | *45* | *29* | *8* | *1.0* | *4* | *0.1* | *2* |
| UZ | 7 | *4* | *38* | *12* | *7* | *3.4* | *24* | *1.4* | *5* |
| UZ | 1 | *0* | *36* | *9* | *7* | *1.6* | *38* | *0.4* | *4* |
| LZ | 67 | *41* | *22* | *21* | *11* | *0.4* | *0* | *0* | *0* |
| MZ | 88 | *6* | *50* | *20* | *12* | *2.6* | *4* | *0.4* | *2* |
| UZ | 8 | *4* | *37* | *12* | *7* | *3.2* | *25* | *1.2* | *5* |

Alt. = Alteration products (mainly secondary amphibole and serpentine)
(n) = No of samples (thin sections not available for all samples)

**Table 4.7 Modal and norm abundances by zone and intrusion.**

Middle Zones from other groups. This is likely to result from assimilation of hydrous LIL-element bearing country rocks and chemical evidence for this will be discussed in Section 6.3.3. Ilmenite and apatite can be seen to rise from Lower to Middle to Upper Zones, for both modal and norm abundances, despite indications that neither phase is cumulus in the Upper Zone. High amounts of amphibole are also seen in Lower Zone rocks from south Connemara as mentioned; however, the data in this table should be treated with great caution as cumulate processes combined with low numbers of samples for individual zones is likely to make the data unreliable (e.g. the absence of olivine in the Cashel Lower Zone is based on only one sample) and, as such, this table is only presented to show up broad trends, such as those mentioned above.

## 4.8 Cotectic assemblages

Using this detailed thin section analysis of the mineralogy and textures seen in the rocks as discussed in Section 4.6.2, cotectic assemblages have been determined both for the suite as a whole and for the individual groups. These assemblages are shown plotted against whole rock mg# values in figure 4.18, and from this the sequence of fractionating minerals has been established. Whole rock mg# coverage is quite good over the bulk of the stratigraphy, but is lacking in key Upper Zone rocks with mg# values of 5 to 15; as a result, precise Upper Zone relations cannot be determined satisfactorily. It is evident from figure 4.18 that there are only minor variations between the assemblages from group to group, with key phase changes such as the disappearance of olivine at the top of the Lower Zone quite well constrained at mg# values of ~ 65 for most of the groups.

The most notable variation is the absence of olivine at mg# values of 10-30 in the northeastern bodies, compared with the Insch and Boganclogh intrusions. Olivine-bearing Upper Zone rocks are only present in Insch and Boganclogh, but there is overlap between these rocks and the Middle Zone rocks from the northeastern bodies, in terms of their whole rock mg# values, as discussed previously. Another feature seen is the relative order of initial fractionation of plagioclase and pyroxene at high mg# values, which appears to vary slightly from group to group. It is also evident that, for some of the intrusions, such as the southwestern bodies, the range of rock compositions is insufficient for the assemblage to be fully established. Because of this, and the overall similarities in the trends for the suite as a whole, the assemblage shown in figure 4.18f, for the entire set of intrusions, has been assumed to be applicable to all the data. Although this is a slight simplification, it is the most satisfactory approach to account for these gaps in the data range. This overall assemblage is again shown in figure 4.19 with available probe data, and again shows the

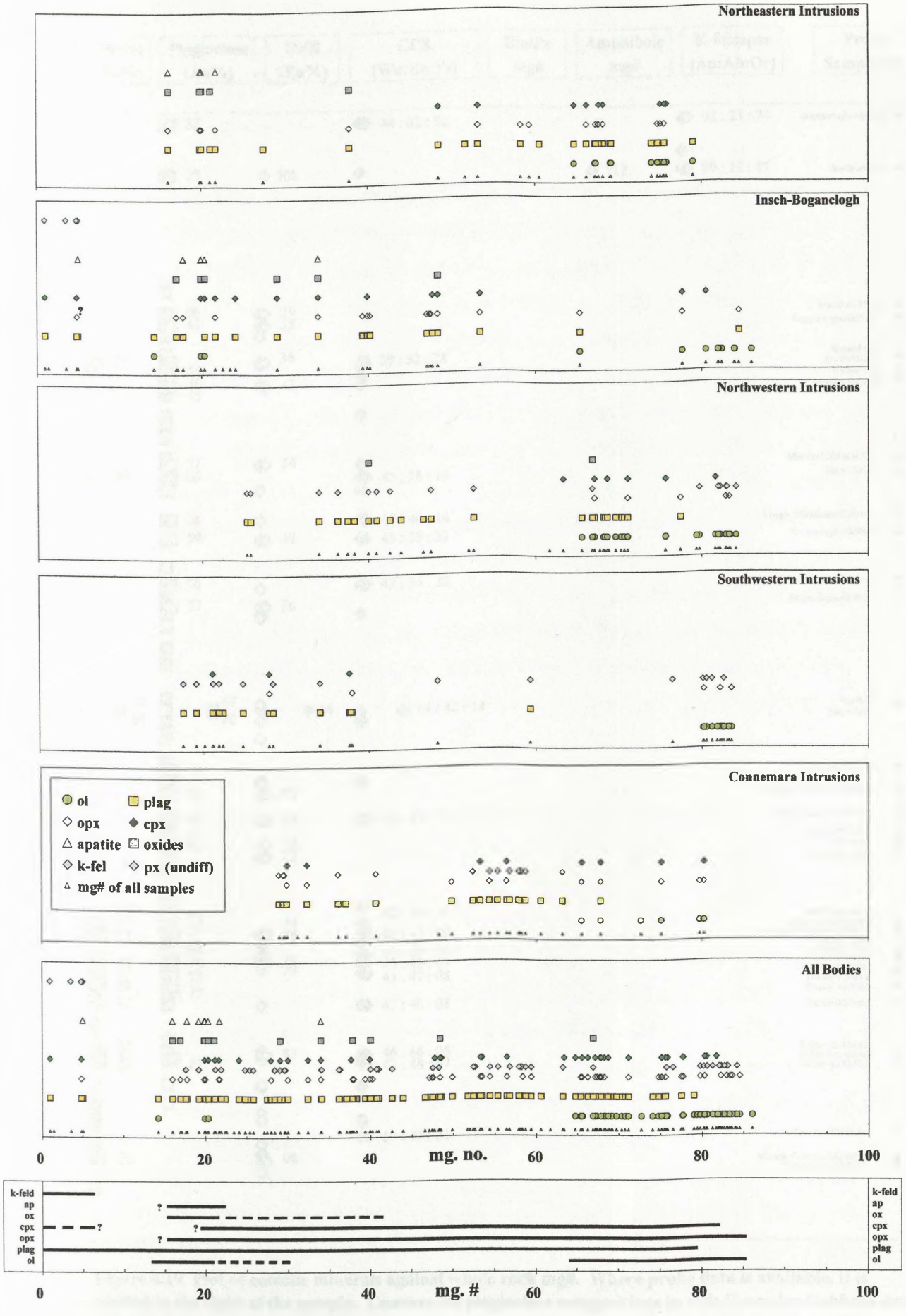


**Figure 4.18 Cotectic assemblages plotted against mg. number for the individual groups (a-e) and for the igneous suite as a whole (f and g)**

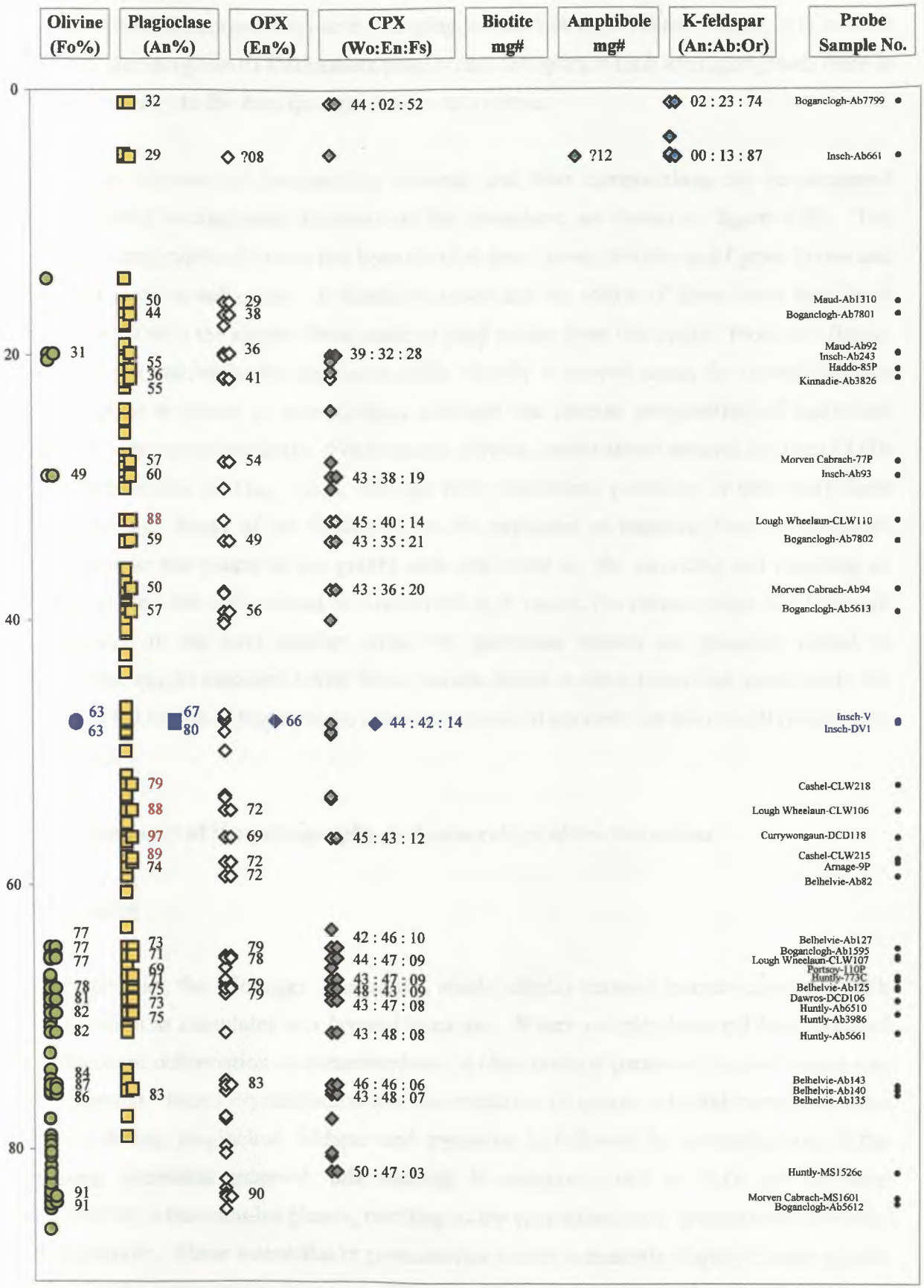


**Figure 4.19 Plot of cotectic minerals against whole rock mg#. Where probe data is available, it is plotted to the right of the sample. Connemara plagioclase compositions in red; Granular Gabbros data offset and shown in blue. Fe-Ti oxides and apatite omitted as no significant probe data is available.**

change in mineral compositions with changing whole rock mg# values. Again, it is evident that, with the exception of Connemara plagioclase feldspars, which are highlighted, there is a broad similarity to the data from the bodies as a whole.

Finally, the sequence of fractionating minerals and their compositions can be compared with published stratigraphic divisions of the intrusions, as shown in figure 4.20. The published stratigraphic division has been divided into Lower, Middle and Upper Zones and sub-zones as discussed earlier. It should be noted that the widths of these zones have been adjusted to fit with the simple linear scale of mg# values from this study. From this figure, it can be seen that while the sequences differ slightly in several areas, the overall cotectic crystallization sequence is very similar, although the precise composition of individual phases can vary quite markedly. For example, olivine compositions towards the top of UZb have compositions of $Fo_{06}$, while olivines from equivalent positions in this study have values of $Fo_{23}$. Many of the variations can be explained as resulting from the different scales used on the y-axis of the graph; both are based on the incoming and outgoing of cumulus phases, but one is based on whole rock mg# values, the shortcomings of which will be discussed in the next section, while the published studies are generally linked to stratigraphic height associated with these phases, which is often imprecise, particularly for fault bounded blocks. Despite these minor variations, it appears that the overall patterns are quite similar.

## 4.9 Summary of the petrography and mineralogy of the intrusions

### Petrography

Petrographically, the 'Younger' Basics as a whole, display textural features consistent with crystallization as cumulates in a layered intrusion. Where samples have not been affected by subsequent deformation or metamorphism, a clear textural pattern of crystallization can be recognized. Initial crystallisation and accumulation of coarse euhedral cumulus phases such as olivine, plagioclase feldspar and pyroxene is followed by crystallization of the remaining interstitial material; this material is commonly rich in $H_2O$ and elements incompatible in the cumulus phases, resulting in the crystallisation of phases such as biotite and amphibole. These interstitial or postcumulus phases commonly display classic ophitic and poikilitic intercumulus textures, 'filling in the gaps' between the cumulus phases. Secondary adcumulate growth on cumulus phases is minor and internal crystal zoning is weak or absent.

Lower Zone rocks predominantly contain cumulus olivine with orthopyroxene, clinopyroxene and plagioclase feldspar becoming cumulus through the Lower Zone; resultant rock types include dunites, lherzolites, troctolites and olivine-gabbros. Other phases such as spinel, opaques, biotite and amphibole are minor volumetrically, with the exception of the Cashel-Lough Wheelaun intrusion where abundant intercumulus hornblende occurs. Layering is generally quite well developed, although Lower Zone rocks tend to be quite badly altered and deformed. The base of the Middle Zone is marked by the disappearance of olivine as a cumulate phase although it may be found occasionally as a minor interstitial phase. Cumulus orthopyroxene, clinopyroxene and plagioclase feldspar are the main Middle Zone phases, resulting in gabbros and norites predominating; again, hornblende and biotite are found interstitially, but generally in greater abundances than in the Lower Zone, and especially so for the northeastern intrusions in which these two phases, combined with intercumulus quartz can make up over 30% of the rock. Ilmenite and apatite are also present as minor intercumulus phases through much of the Middle Zone; both become cumulus towards the top of the Middle Zone.

Granular gabbroic rocks are also found in the Insch and Huntly bodies. These are non-cumulate in origin and finer grained than their cumulate equivalents. Texturally, they are quite distinctive with equigranular pyroxene, plagioclase feldspar and occasionally olivine, present; other phases are rare or absent. They are found within the cumulate Middle Zone from both bodies, but their relationship to these cumulates is unclear in the field. Upper Zone rocks are restricted largely to the Insch and Boganclogh bodies, where olivine becomes a cumulate phase again. Apatite, ilmenite, alkali feldspar and zircon all occur as cumulate phases in the Upper Zone, while quartz is occasionally found as a minor late intercumulus phase.

**Mineralogy**

A broad summary of the mineralogy is shown in figure 4.20. The ferromagnesian minerals olivine, orthopyroxene and clinopyroxene all show progressive decreases in Mg with respect to Fe (mg#) with increasing fractionation of the intrusions; plagioclase feldspar shows a concomitant decrease in An% content, while the minor phases biotite and amphibole also display decreases in mg# which parallel the trends seen in the main silicate phases. There are apparent variations evident between ferromagnesian phases from different groups; these are considered likely to be an artefact of the whole rock mg# being used as the x-axis, as plots of coexisting mineral phases do not reveal this variation. There

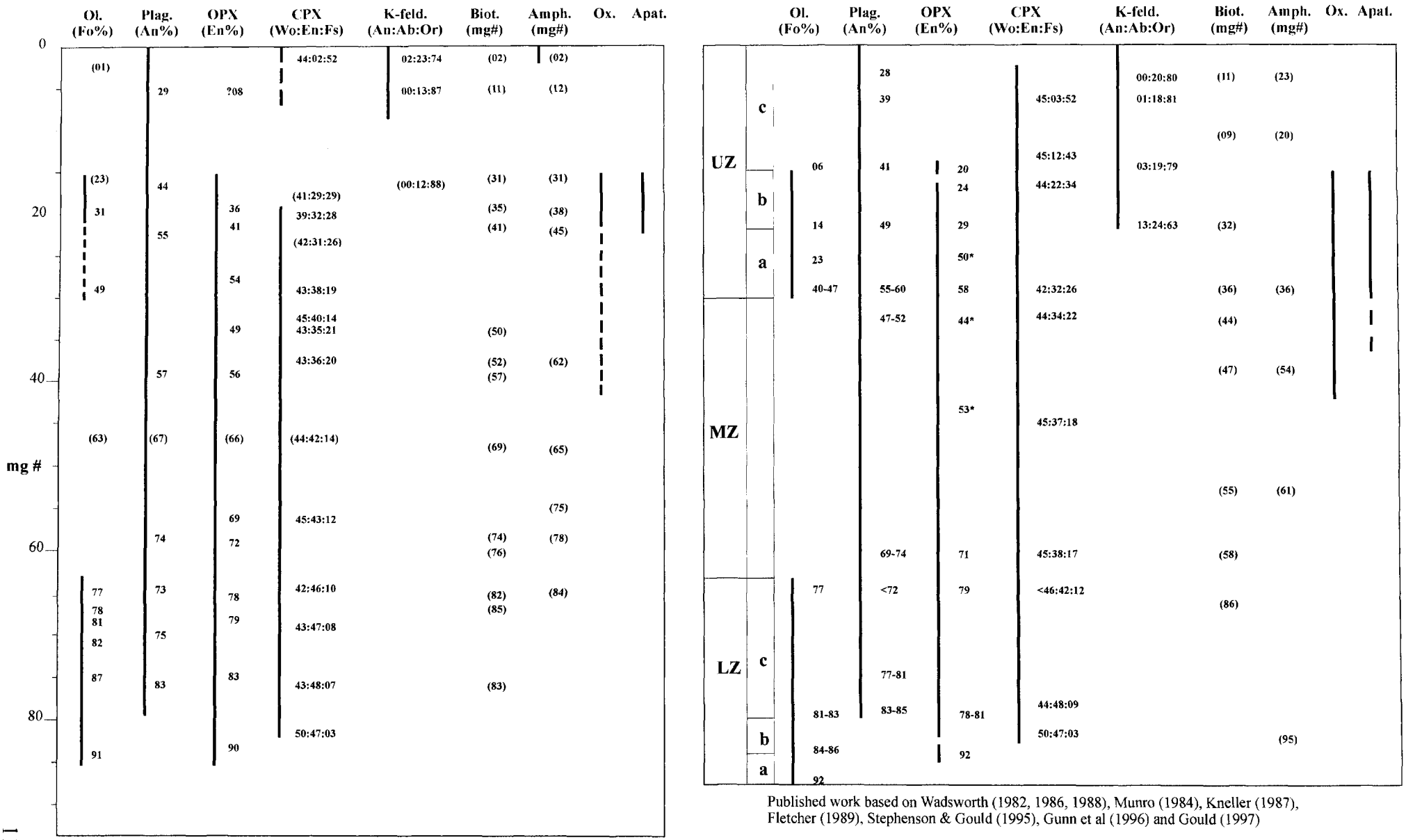


Published work based on Wadsworth (1982, 1986, 1988), Munro (1984), Kneller (1987), Fletcher (1989), Stephenson & Gould (1995), Gunn et al (1996) and Gould (1997)

**Figure 4.20 Comparison of mineral compositions plotted against whole rock mg# values for this study with published mineral compositions plotted against approximate stratigraphic height. Non- cotectic mineral compositions are shown in brackets. Inverted pigeonite values are marked by an asterisk**

is some scatter to clinopyroxene and plagioclase feldspar compositions; these are likely to be due to fine exsolution lamellae and partial re-equilibration respectively. Zoning is largely absent in silicate phases, both optically and in microprobe data.

Four main differences are seen within the petrography and mineralogy of the suite as a whole:

1. Modally, biotite, amphibole and quartz are more abundant in the northeastern bodies of Arnage, Haddo, Kinnadie and Maud as a whole than in the other bodies, although these phases may be abundant locally in several intrusions.

2. Plagioclase feldspars from both Connemara intrusive suites display anorthite contents that are significantly higher than those seen in the majority of bodies from the Grampian Highlands. Although the trend is poorly defined, Connemara plagioclase feldspars are generally $An_{88}$ or greater in composition, while Scottish bodies are mainly below $An_{75}$. This trend is not reflected in any other silicate phase.

3. Interstitial amphiboles from the Granular Gabbros in Insch are appreciably higher in total alkali content than primary amphiboles in the other bodies. Most primary amphiboles from the other bodies are hornblende in composition, while those from the Granular Gabbros are pargasitic in composition.

4. Variations in the order and range of fractionating phases are not particularly common but several examples are seen. Cumulus Upper Zone olivine is seen in the Insch and Boganclogh masses, while northeastern bodies with similar whole rock mg# values do not show cumulus olivine. Apatite and zircon appear to fractionate in Middle Zone rocks from the Cashel body in Southern Connemara, and possibly also in the Maud mass. Elsewhere, cumulate apatite and zircon are generally restricted to the Upper Zone.

# Chapter 5 Whole rock chemistry of the intrusions.

## 5.1 Introduction

In this chapter, the major and trace element characteristics of the intrusions and their chemical evolution are presented. As in Chapter 4, the intrusions have been divided into groups based on their petrology and spatial relations. The potential effects of alteration and cumulate processes on the whole rock chemistry are assessed, and a whole rock fractionation index proposed. The individual rock types and evolutionary trends are examined and classified using conventional geochemical classifications, binary plots of selected elements, and trace element 'spider' and REE diagrams.

## 5.2 Effects of alteration on chemistry

A significant proportion of the samples analysed chemically for this study display varying degrees of alteration in both hand specimen and thin section. Despite every effort being made to exclude heavily altered samples from the database, the complex post-emplacement history of the intrusions and the susceptibility of several major phases, such as olivine and plagioclase feldspar, to alteration means that a certain degree of alteration is unavoidable. Thin section evidence shows that the main alteration products are serpentine, sericite and amphibole after olivine, plagioclase feldspar and pyroxene respectively. These hydrated alteration products suggest that late stage hydrous fluids, associated with slow retrograde metamorphism related to the cooling of the bodies is likely to be the primary cause of this alteration. This is especially true for those intrusions in the Grampian Highlands adjacent to the Portsoy Lineament such as Morven Cabrach, where alteration in widespread in the south of the body. Postcumulus magmatic alteration is locally present, such as is found in troctolites from Belhelvie and Huntly where coronas are developed at olivine-plagioclase feldspar interfaces, while weathering can generally be eliminated during sample preparation.

In order to investigate the effects of this alteration on the accuracy of the geochemical data, an alteration index has been created, based on the type and grade of alteration observed in thin section. Due to the variety of lithologies present, inherent difficulties lie in comparing, say, a gabbro with a dunite, where no minerals are common to both rocks. In addition,

difficulties lie in the fact that olivine-bearing samples are likely to be preferentially classified as being more altered than olivine-free samples due to this susceptibility of olivine to alteration relative to other minerals. Nevertheless, the index can provide a guide to the effects of alteration on sample chemistry.

**Alteration index**

**Group 1** All minerals fresh with no visible signs of alteration.
No veining or staining.
Olivine fresh including along fractures.

**Group 2** Slight alteration:
- plagioclase partly sericitized;
- variable (but incomplete) alteration of olivine to iddingsite, or serpentine (particularly along internal fractures);
- other mafics fresh, except occasional marginal amphibolitization.

**Group 3a** Olivine heavily to completely serpentinized
Feldspars substantially sericitized.
Partial alteration of other mafics, particularly amphibolitization of pyroxenes.

**Group 3b** Feldspars partly sericitized.
All mafics heavily to completely altered or replaced by secondary amphiboles.

**Group 4** Fresh olivine rare.
Feldspars heavily sericitized.
Mafic minerals heavily altered or replaced.

**Group 5** All minerals heavily altered.
Abundant secondary products:
- olivine → iddingsite, serpentine;
- other mafics → amphiboles;
- feldspar → sericite, clays;

Difficult to identify individual mineral phases.

Comparisons of these alteration groups are shown in selected binary plots of mobile versus immobile elements (Figure 5.1) and versus mg# (Figure 5.2). Examination of plots such as $K_2O$, Ba, and Sr versus Zr and Y shows no obvious differences between the different alteration groups for these elements. On the plots of CaO and Sr versus mg#, a slight clustering of more altered samples (Group 5) can be seen around mg# values of 80-85. As mentioned, this is largely due to the easily altered nature of the olivine in these ultramafic

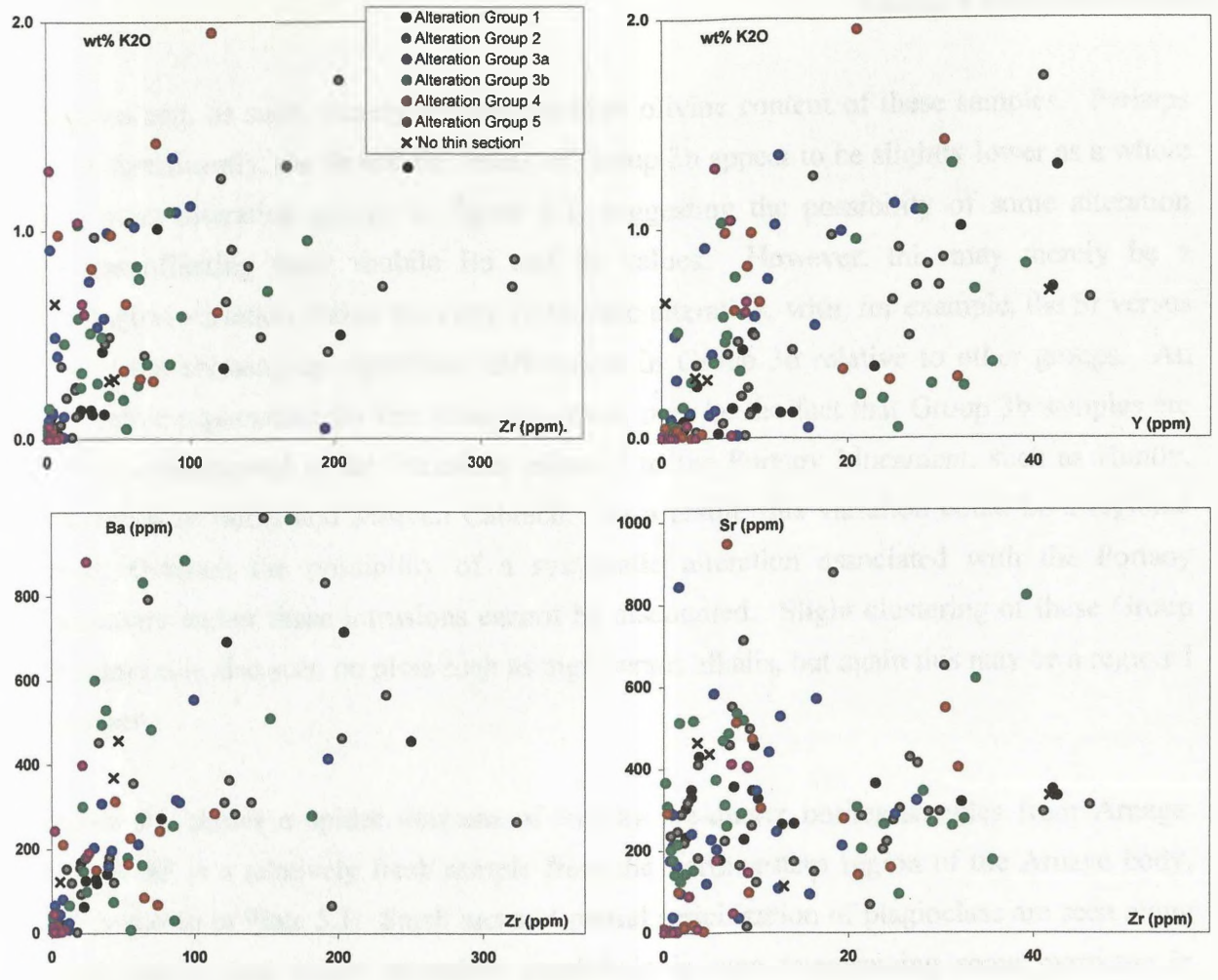


**Figure 5.1 Selected binary plots of mobile and immobile trace elements.**

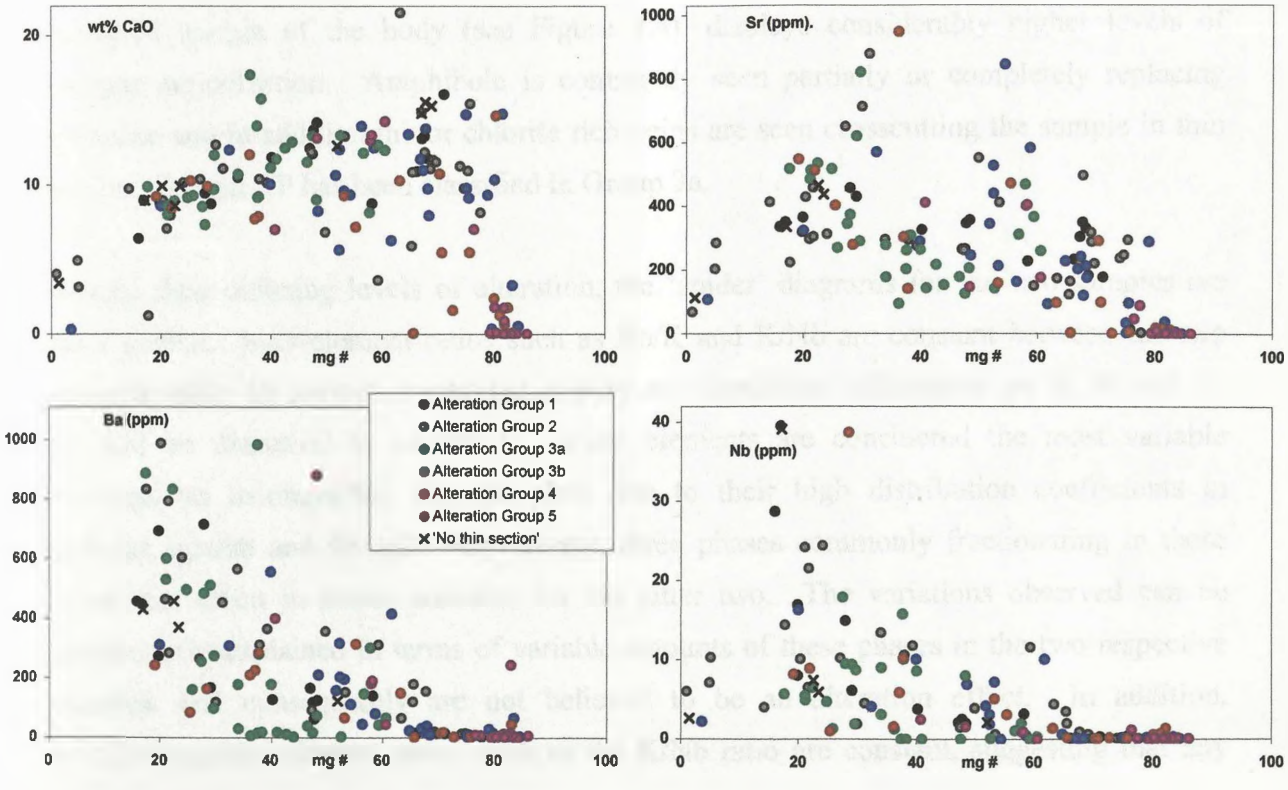


**Figure 5.2 Binary plots of mg# versus selected major and trace elements**

samples and, as such, merely reflects the high olivine content of these samples. Perhaps more significantly, the Sr and Ba values of Group 3b appear to be slightly lower as a whole than other alteration groups in figure 5.2, suggesting the possibility of some alteration process affecting these mobile Ba and Sr values. However, this may merely be a lithological variation, rather than any systematic alteration, with, for example, the Sr versus Y plot not showing up significant differences in Group 3b relative to other groups. An alternative explanation for this trend, however, may be the fact that Group 3b samples are largely concentrated in the intrusions adjacent to the Portsoy Lineament, such as Huntly, Succoth-Brownhills and Morven Cabrach. As a result, this variation could be a regional trend, although the possibility of a systematic alteration associated with the Portsoy Lineament and/or these intrusions cannot be discounted. Slight clustering of these Group 3b samples is also seen on plots such as mg# versus alkalis, but again this may be a regional variation.

Figure 5.3 shows a spider diagram of two biotite-quartz norites samples from Arnage. Sample 9P is a relatively fresh sample from the northwestern region of the Arnage body, and is shown in Plate 5.1. Small areas of partial sericitization of plagioclase are seen along minor cracks, and minor secondary amphibole is seen overgrowing some pyroxene in places. Biotite displays no visible alteration and the sample has been classified in Group 1. In contrast, sample 1P, shown in Plate 5.2, located 2.7 km south of sample 9P and near the southeast margin of the body (see Figure 4.4), displays considerably higher levels of feldspar sericitization. Amphibole is commonly seen partially or completely replacing pyroxene and in addition minor chlorite rich veins are seen crosscutting the sample in thin section. Sample 1P has been classified in Group 3a.

Despite their differing levels of alteration, the 'spider' diagrams for the two samples are quite similar. Inter-element ratios such as Rb/K and K/Nb are constant between the two samples while the only elements that display any significant differences are Sr, P, and Ti. As will be discussed in section 5.3, these elements are considered the most variable elements on incompatible element plots due to their high distribution coefficients in feldspar, apatite and ilmenite respectively, three phases commonly fractionating in these intrusions, albeit in minor amounts for the latter two. The variations observed can be satisfactorily explained in terms of variable amounts of these phases in the two respective samples, and consequently are not believed to be an alteration effect. In addition, mobile/immobile element ratios such as the K/Nb ratio are constant, suggesting that any

Plate 5.1 (a) PPL

Plate 5.1 (b) XPL

**Plate 5.1 Sample 9P from the Arnage body showing fresh euhedral plagioclase, pyroxene and late intercumulus hornblende (top left). Minor patches of sericitization are seen locally (centre) and slight replacement of orthopyroxene by amphibole along cracks is observed; this sample has been assigned to Alteration Group 1. Vertical scale = 1.6 mm.**

Plate 5.2 (a) PPL

Plate 5.2 (b) XPL

**Plate 5.2 Sample 1P, also from the Arnage mass, displaying more extensive sericitization and replacement of pyroxene by amphibole. Primary amphibole is present overgrowing pyroxene (now replaced), and biotite mantles are found on ilmenite (top left). Alteration Group 3a. Vertical scale = 0.8 mm.**

Plate 5.3 DCD106 XPL

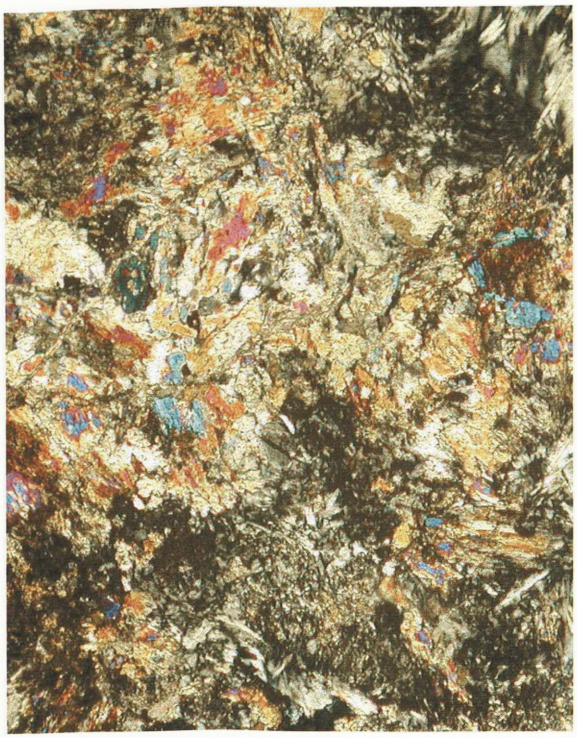

Plate 5.4 DCD105 XPL

**Contrasting degrees of alteration in adjacent samples from the Dawros body. DCD106 shows partial replacement of pyroxene by amphibole, and some serpentinization. Minor veining runs diagonally across the plate; this sample has been classed in Alteration Group 3a. In conrast, DCD105 has been assigned to Group 5. It is heavily altered, with the identity of original mineral phases unclear; abundant secondary amphibole, sericite and chlorite veining (top right) are present. Vertical scale = 1.6 mm for both plates.**

Plate 5.5 Sample 1P (PPL)

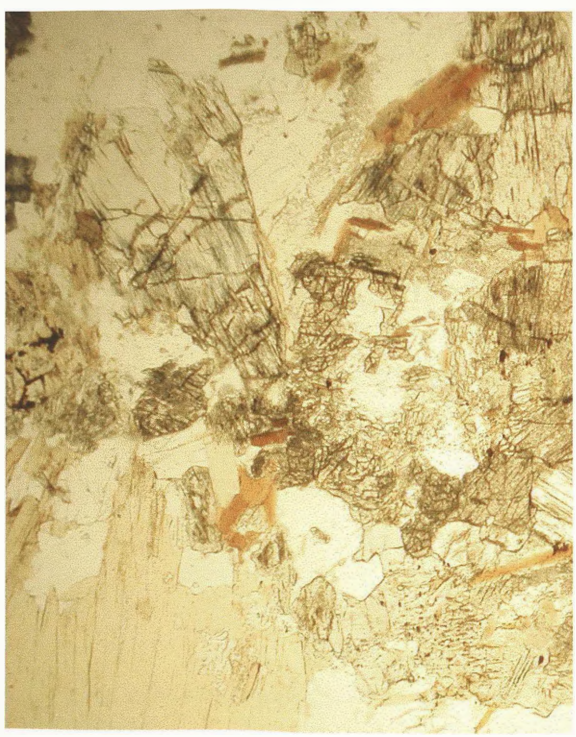

Plate 5.6 Sample 7P (PPL)

**Variation in degree of intercumulus development. Both sample contain cumulus plagioclase feldspar and orthopyroxene. Sample 1P contains moderate postcumulus growth of hornblende and biotite, while sample 7P shows extensive postcumulus hornblende and biotite in particular. Spider diagrams of these two samples are shown in Figure 5.5. Vertical scale = 3.0 mm for both plates.**

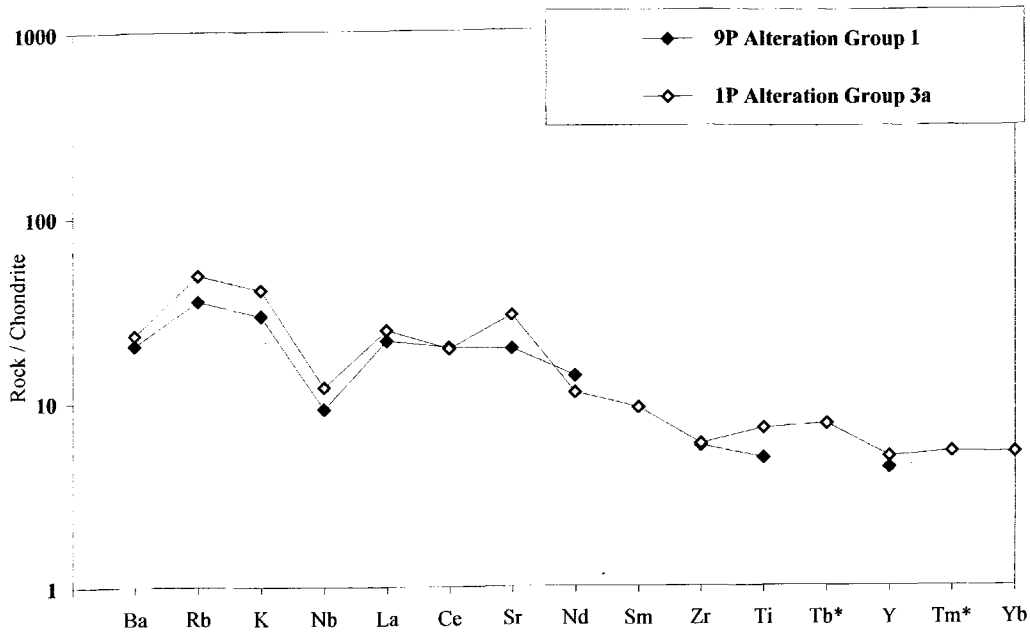


**Figure 5.3 Spider diagram of two samples from the Arnage mass assigned to two different alteration groups. Tb* and Tm* values in this and future plots represent values which have been interpolated from REE data.**

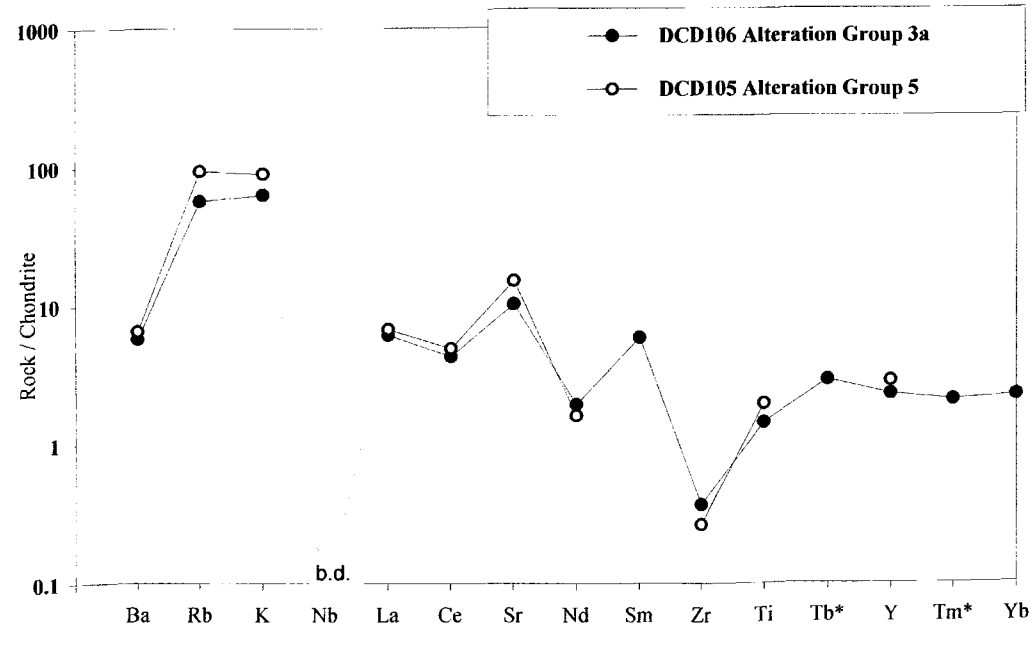


**Figure 5.4 Spider diagram of two samples from the Dawros intrusion assigned to two different alteration groups (Niobium values below detection).**

alteration affecting these rocks does not appear to have changed mobile element concentrations significantly.

This lack of change in element concentrations and ratios can also be seen to hold true for more extremely altered samples. Plates 5.3 & 5.4 show two altered gabbroic samples from the Dawros body in Connemara, specifically sampled to investigate the influence of alteration on the rock chemistry. Sample DCD106, shown in Plate 5.3, is taken from a relatively fresh outcrop of olivine gabbro; minor quantities of partially altered olivine are present, while partial sericitization of plagioclase feldspar and minor replacement of pyroxene with amphibole is present, along with some recrystallization. This sample has been classed in Alteration Group 3a. Sample DCD105, shown in Plate 5.4, was taken from a visibly sheared and broken up block of gabbro, 15 to 20 metres away within the same outcrop. It has been assigned to Alteration Group 5, with extensive plagioclase feldspar sericitization and replacement of pyroxene, probably mainly clinopyroxene, by abundant secondary amphiboles.

As is evident in Plate 5.4, chlorite and calcite veins crosscut the sample and it is difficult to distinguish between the individual phases. Despite this, there is a strong similarity to the 'spider' plots of both samples, shown in figure 5.4; Nb is below detection in both samples while most normalized element abundances are quite similar. Although LIL element concentrations are higher in sample DCD105 (e.g. Rb abundances: 32.5 ppm in DCD105 compared to 19.8 ppm in DCD106), inter-element ratios, particularly those involving the LIL elements, are quite constant between the two samples, suggesting any minor variations between the two plots may be as a result of slight modal variations in the abundances of minerals, rather than from addition of elements to the more altered sample. Again, inter-element ratios, especially those involving mobile elements, are generally quite uniform, suggesting that while metamorphism and associated alteration has taken place, there does not appear to be any systematic addition of an extra component, such as a LILE-enriched fluid, accompanying this metamorphism and distorting these ratios.

## 5.3 Problems associated with the geochemistry of layered intrusions

### 5.3.1 Introduction

For both major and trace elements, the understanding and interpretation of whole rock data from samples of a cumulate nature raise a number of important problems. The fundamental

origin of these problems lies in the fact that a cumulate sample, and its whole rock chemistry, *do not* necessarily represent the liquid from which the sample has crystallised. These cumulate processes have different effects on different types of elements, notably compatible and incompatible trace elements, while differing cumulate processes, such as postcumulus overgrowth, also have varying effects on the whole rock chemistry. Because of this, the identification of samples of a cumulate nature, and the various cumulus processes involved in their formation, are important when assessing the significance of the whole rock data. This is particularly important for assessing the fractionation of the bodies, as a whole rock major element ratio (mg#) has been used as a fractionation index.

### 5.3.2 The effect of cumulate processes on whole rock chemistry

The accumulation of a cumulus phase in a sample results in the abundance of elements compatible with this phase being higher in the phase than in the parental liquid. For example, a dunite with nickel concentrations >2000 ppm containing cumulus olivine evidently contains higher Ni values than will have been present in the parental liquid from which it crystallised and fractionated. Consequently, any trends within nickel or any other compatible element are likely to be a reflection of their concentration within cumulus phases and the degree of accumulation of these cumulus phases rather than any fractionation trends within the magma. This also applies to major element data, where for example, CaO and $Al_2O_3$ abundances are to a large extent controlled by the amount of plagioclase feldspar in a sample. Another example, shown in Figure 5.10, are samples containing over 3.0 wt% $TiO_2$, found in three of the groups; most of these samples contain cumulate ilmenite, but the liquid they crystallized from is unlikely to have contained $TiO_2$ in sufficiently high concentrations to yield over 3.0 wt% $TiO_2$ without this accumulation of cumulus ilmenite. Because of this, the difference between magmatic or liquidus trends, and the trends seen in the whole rock analyses of the resultant cumulates is one of the main difficulties arising during interpretation of the whole rock data.

Plots such as the normalised di-ol-hy tetrahedral plot and AFM plots are affected by the cumulate nature of samples. Cumulates with, say, high amounts of forsteritic olivine, will tend to be pushed towards the ol and M apices of these plots respectively, and as a result will not plot where the liquids from which they crystallized would plot; in particular, the normalised di-ol-hy plot is not applicable to strongly cumulate samples. Despite these difficulties, approximate magmatic fractionation trends can often be inferred from the whole rock data. The presence of, say, cumulus apatite or ilmenite in a sample can be seen in the

whole rock data by high $P_2O_5$ and $TiO_2$ concentrations respectively. Rising $P_2O_5$ and $TiO_2$ levels in the magma prior to the fractionation of these phases are likely, while a relative decrease in their levels in the magma after fractionation is also expected.

As a result, it is important to identify the degree to which cumulate processes have influenced a cumulate sample. The difficulty is that, with the exception of the Insch Granular Gabbros, virtually all of the samples have been influenced by cumulate processes to a lesser or greater extent. Consequently, a subgroup of 'strongly cumulate' or 'layered' samples have been identified for plots such as the di-ol-hy and AFM plots; these samples are commonly composed entirely of cumulate phases. They are most easily identified in hand specimen and thin section by examination of the phases present and their textures, commonly displaying features such as crystal alignment, and are occasionally monominerallic and with little interstitial material. 'Layered' samples can also be recognised by patterns of whole rock chemistry, with for example the samples with high nickel concentrations or samples with high strontium concentrations likely to represent samples containing accumulated olivine or plagioclase feldspar respectively.

Accordingly, samples of a strongly cumulate or layered nature have been identified, using hand specimen and thin section evidence, in combination with major and trace element data, and these samples have been assigned a separate symbol to distinguish them from those samples which display no evidence for actual crystal accumulation, either geochemically or in thin section, but are still regarded as cumulates texturally (i.e. they possess cumulate textures in thin section). While the dividing line between these two sets of samples is somewhat ambiguous and arbitrary, it does serve to lessen scatter on many plots, by eliminating samples with more extreme chemistry. A third group of samples, the Granular Gabbros are also labelled separately as they are considered likely to have a different origin to the cumulate samples and, as will be discussed in Chapter 6, may represent liquid compositions. These three groups have been called the 'layered', 'cumulate' and 'granular' groups respectively, although it should be noted that no genetic connotations are implied by these names. On several of the plots in Section 5.4, it can be seen that the layered samples display considerably greater scatter than either the granular or cumulate samples.

### 5.3.3 Effects on incompatible trace elements abundances and 'spider' diagrams

As mentioned previously, a key problem arising from cumulate processes is the effect cumulus and post-cumulus processes have on the absolute and relative abundances of whole

rock data, particularly compatible element data. The effect of cumulate processes on incompatible elements is also critical. The possibility exists that the modal abundances of individual phases such as olivine, plagioclase, and pyroxene are the main influence on the total incompatible element budget for any individual sample, and that any 'spider' or REE plot of this sample is simply a reflection of these major phases and their relative proportions. Fortunately, however, as will be seen in greater detail in Chapter 6, studies such as Cawthorn (1996), Mathez *et al.* (1997), and particularly Tribuzio *et al.* (1999a) have shown that the influence of cumulus phases on incompatible elements is far less than that of late intercumulus or post-cumulus crystallisation. Partition coefficient data for olivine, plagioclase and orthopyroxene are all extremely low for the incompatible elements on these 'spider' (with the exception of Sr in plagioclase feldspar) and REE plots (see table 6.4), while clinopyroxene partition coefficients for these elements are higher, but still considerably less that those for the commonly occurring interstitial phases such as biotite, primary amphibole, Fe-Ti oxide and apatite.

Consequently, the majority of the incompatible elements found in a sample are likely to be present within these accessory phases formed from interstitial 'trapped liquid'. In addition, Tribuzio *et al.* (1999a) have shown that amphibole is a very versatile phase and is capable of incorporating high levels of elements that have extremely low compatibility with the other phases; as the 'trapped liquid' becomes enriched in incompatible elements abundances, due to exclusion from the main phases, amphibole can accordingly accommodate significantly higher amounts of these incompatible elements. Consequently, the abundances of incompatible elements in a whole rock analysis are likely to be, for the most part, controlled by the level of development of intercumulus phases, such as biotite, Fe-Ti oxides, apatite and primary amphibole. In addition, irrespective of their ability to incorporate these so-called 'incompatible elements', intercumulus phases such as hornblende can only incorporate what is actually present in the 'trapped liquid'.

One important consequence of this is that, while the absolute abundances of these incompatible elements are controlled by the amount of 'trapped liquid' and the resultant intercumulus phases, the relative abundances are not. As a result, incompatible element ratios, such as in normalised incompatible element 'spider' diagrams are, to a large extent, independent of these cumulate processes. In other words, the *height* (normalized abundances) of the 'spider' diagrams is controlled by the amount of 'trapped liquid' in the sample, but the *shape* (sequence or pattern of interelement ratios across the 'spider') is controlled by the composition of the 'trapped liquid'.

As will be seen in Section 6.7, great care must be taken when any of the phases which accommodate these elements enriched in the intercumulus pore spaces is present as a cumulate phase (especially apatite and Fe-Ti oxide) as this will cause many of the so-called 'incompatible elements' ($P_2O_5$ and the REE for apatite; MnO, $TiO_2$ and V for ilmenite,) to effectively behave compatibly. This will consequently affect their total and relative abundances in the same way as described above for nickel in olivine. This affects strontium data from virtually all samples, as cumulus plagioclase feldspar is present throughout the fractionation of the bodies from the Lower Zone onwards; this will affect the LILE to a lesser extent (moderate $K_D$ values) and Eu for REE data.

An underlying assumption in much of the above is that there is little or no re-equilibration of the enriched 'trapped liquid' with less enriched liquid in the main magma chamber; while there is no definite evidence for this, the largely orthocumulate nature to samples from the bodies suggests that such re-equilibration was not extensive. However, the effects of such interaction between the liquids in these pore spaces and the main magma chamber and accompanying adcumulate overgrowth on cumulus phases such as olivine, pyroxene and plagioclase feldspar must still be accounted for. Although the overgrowths themselves will not contribute significantly to the incompatible element abundances of the rock, they will have the effect of 'squeezing out' the interstitial liquids, which are rich in incompatible elements. Again, it should be emphasised that, in general, while the *absolute* abundances of such incompatible elements are likely to be less as a result, the abundances of these elements *relative* to each other, such as found in the overall shape and slope of 'spider' diagrams are unlikely to change significantly, irrespective of the degree of liquid interaction and adcumulate overgrowth.

An example of this is shown in figure 5.5, where 'spiders' of two samples (1P and 7P) with varying degrees of intercumulus mineral growth are presented. Both samples are biotite-quartz-norites from the Arnage body from the northeastern group and possess similar mg# values (mg# = 51.73 for 1P and = 53.24 for 7P). Sample 1P contains some adcumulate growth and moderate intercumulus development (see Plate 5.5), while sample 7P possesses substantial intercumulus development of hornblende and biotite (Plate 5.6). This variation is reflected in the height of the 'spider' plots in figure 5.5; both samples have similar inter-element ratios and overall 'spider' shapes and slopes, but the normalized abundances for sample 7P are approximately twice those seen in sample 1P. Very similar niobium troughs are visible in both samples, while only normalized Zr abundances show any significant variation between the two samples. One consequence of this is that care should be taken to

avoid over-interpretation of trace element abundances and ratios in samples where intercumulus phases are limited, and elemental abundances are close to detection limits. Fortunately, however, intercumulus phases are well developed in the vast majority of samples collected, and as a result incompatible element ratios can be taken to represent those of the liquid from which the sample crystallised, although not the absolute abundances, which are, as mentioned above, likely to be a function of the amount of intercumulus phase development. As a result, ratios of these incompatible trace elements are a useful technique when assessing the whole rock chemistry of samples of a cumulate origin.

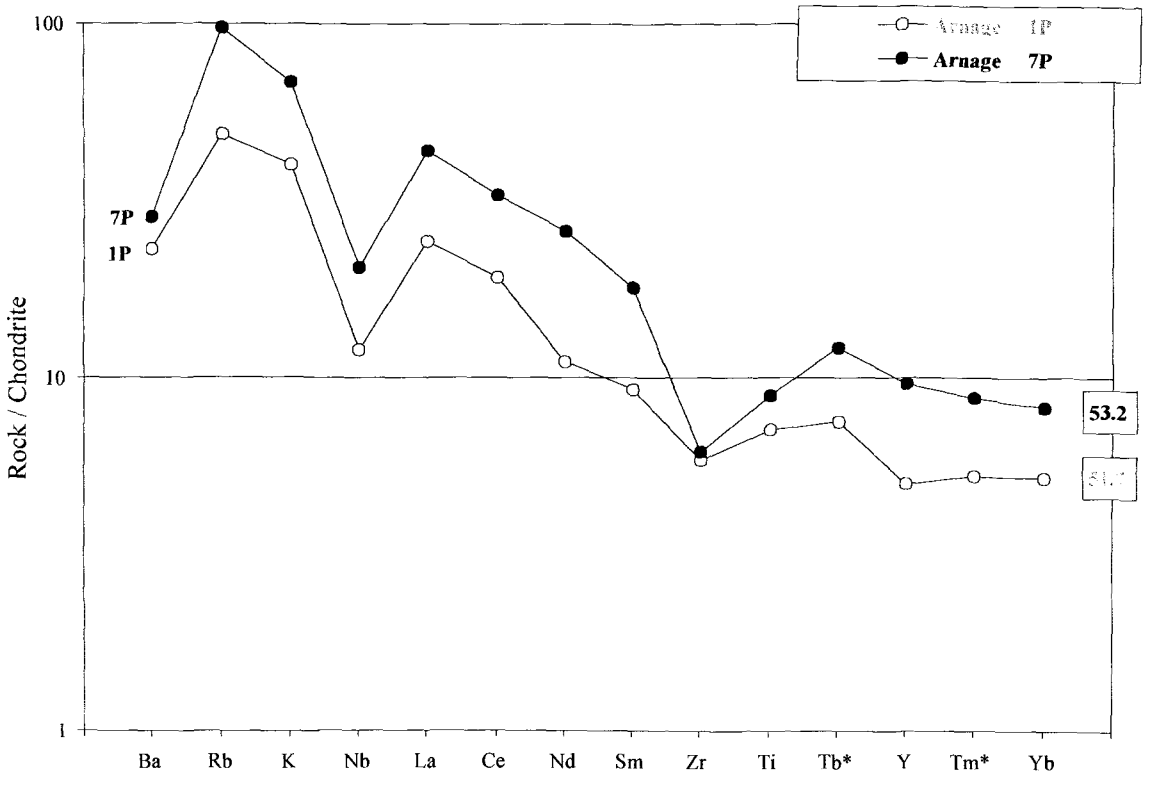


**Figure 5.5 'Spider' plots of samples with varying degrees of intercumulus growth. Sample 1P, shown in Plate 5.5, contains moderate postcumulus growth while sample 7P, shown in Plate 5.6 contains abundant postcumulus phase growth. Whole rock mg# for the individual samples is boxed at the right.**

Cumulate processes also necessitate modifications of conventional spider diagrams. The incompatible element spider diagrams used in this chapter are based on Thompson *et al.* (1984), with both their element order and normalizing values used. Three elements used in

these plots (Th, Ta, and Hf) were not analysed as part of this study and as a result are absent from the majority of plots; however, where published data containing these elements are used, then they are included. In addition, as seen in Chapter 4, plagioclase feldspar, ilmenite and apatite are common fractionating phases in these intrusions. Sr, Ti and P values, which are generally considered to be incompatible in these plots, are affected by the presence or absence of these minerals as cumulus phases in the crystal assemblage to a much greater extent than in, say, basaltic samples. In many cases where plagioclase feldspar, ilmenite and apatite are cumulus, the peaks are simply recording the amount of each phase in the rock. The problem is more limited for ilmenite and apatite than for plagioclase feldspar, which, although commonly present, are only cumulate in nature over a limited mg# range. As a result, strontium has been removed from the majority of plots and titanium and phosphorus removed from plots where it is evident that ilmenite and apatite are fractionating in significant quantities. This also poses problems for REE data as the REE, especially the LREE, are quite compatible in apatite. In addition, in some spider diagrams from the Insch and Boganclogh intrusions, Zr has been omitted for similar reasons, with zircon occurring as a fractionating accessory phase in some Upper Zone rocks. Nevertheless, these elements are still quite useful in identifying cumulate samples in certain instances, particularly cumulus apatite, which can be difficult to distinguish from postcumulus apatite.

### 5.3.4 Fractionation Index

In examining the evolutionary trends seen within the intrusive suites, it has been necessary to formulate a fractionation index against which the evolution of the rocks can be examined. Conventionally, as discussed in Section 4.5, layered basic intrusions are divided into Lower, Middle and Upper Zones based the presence or absence of key cumulate phases. While this stratigraphic approach has been used in the previous chapter for general petrological and petrographical descriptions, a number of problems arise when attempting to use this system for evaluating whole rock data. Firstly, poor exposure and extensive faulting and shearing mean that the precise position of any one sample within the stratigraphic framework is very uncertain. Although the mineralogy present in the sample may be used to assign it to a particular zone or sub-zone, its stratigraphic position within that zone, relative to other samples is largely unknown. In ideal circumstances, mineral compositions from probe data can be used to add detail to the stratigraphy, but only for those samples probed. Probing of every single sample was considered unfeasible, and consequently, a fractionation index based on the whole rock chemistry was sought.

The whole rock mg number or mg# ( $= \frac{100 \times MgO}{(MgO + Fe_2O_3)}$ ), already introduced in Chapter 5, has been chosen as the fractionation index. Several other possible indices including $SiO_2$, MgO and NiO were considered, but mg# was chosen for several reasons. Firstly, from the petrographic evidence described in Chapter 4, it is clear that mafic minerals (along with plagioclase feldspar and ilmenite) are the dominant fractionating phases from the parent magma. The compositions of these ferromagnesian minerals change systematically from Mg-rich to Fe-rich with progressive fractionation, as seen in Chapter 4.

The cumulate nature to many of the samples means that MgO and NiO are not suitable for use as a fractionation index. Both are compatible in mafic phases and consequently their abundances in a sample are largely controlled by the amounts of these mafic phases contained in the sample. As a result, MgO and NiO are largely a reflection of the varying amounts of these phases in a sample, rather than being a record of the degree of fractionation present. $SiO_2$ is not particularly suitable as a fractionation index either, due to the fact that there are not likely to be significant differences between the $SiO_2$ contents of the fractionating phases and the magma from which they are fractionating. For example, removal of olivine with a $SiO_2$ content of ~40% and pyroxene with an $SiO_2$ content of ~52% from a basaltic magma with ~48% $SiO_2$ will not change the silica content of the remaining magma significantly or in a systematic way; consequently trends plotted using $SiO_2$ as a fractionation index are not well defined.

An index based on Mg/Fe ratios, however, shows up fractionation more markedly than an index such as $SiO_2$ or MgO, with the relative quantities of the main crystallizing minerals not affecting this ratio. Progressive fractionation changes this ratio in a regular fashion, and, as seen in figure 4.12, displays a good correlation with the compositions of the silicate mineralogy (although plagioclase feldspar does display considerable scatter). One important potential distortion of this ratio, as mentioned in Chapter 4, is the crystallisation and fractionation of oxides, particularly ilmenite, which will affect the Fe-content of the rock and consequently the mg# values. However, ilmenite is a minor phase in these rocks, rarely reaching over 5% modally, and simple calculations show that for each additional percentage of cumulus ilmenite modally, mg# values decrease by approximately one. Consequently, for example, a typical Middle Zone sample with no ilmenite and an mg# of 25 would possess an mg# of 20 if 5% of ilmenite was added.

This can be seen quite nicely on figure 4.12, where orthopyroxene compositions as a whole are shifted to the left between mg# values of 20 and 35, where cumulate ilmenite is found. Ilmenite-rich samples with low abundances of ferromagnesian minerals, such as anorthosites, will shift the mg# even further, but such samples are rare, and most distortions are believed to be below 5%. Adding in a correction factor for the presence of ilmenite based on modal percentages or $TiO_2$ abundances was felt to be unfeasible, as modal percentages were considered insufficiently accurate, and whole rock abundances do not take into consideration the presence of $TiO_2$ in other phases, particularly pyroxenes, and also the possible presence of minor quantities of other oxide phases, such as magnetite. In addition, ilmenite tends to become a cumulate phase at a similar point in the stratigraphy (based on the En% values of co-existing orthopyroxenes from samples in three of the groups) and consequently any deviation in mg# values will be roughly similar in all samples, resulting in only the precise shape and position of inflection points for all data varying slightly in the mg# range of 20 to 40.

Figure 5.6 shows a trend from the northeastern bodies plotted using the fractionation indexes $SiO_2$, MgO, NiO and mg#. It is evident that using mg# as the fractionation index show up this trend most clearly. Scatter is less pronounced and the inflection point at $TiO_2$ ~ 3.2% is most clearly defined using mg# as the fractionation index. There are, however, limitations to the use of mg# as a fractionation index. For example, samples with low quantities of ferromagnesian minerals such as anorthosites, or samples with high amounts of Fe-Ti oxides, may not be accurately represented using mg# as a fractionation index. There is no easy solution to this problem, however, as anorthosites will not plot accurately using any of the other indexes either. In addition, there is a degree of overlap between Upper Zone samples from the Central Intrusions and Middle Zone samples from Maud and Haddo in terms of mg# (see figure 4.18). This is likely to be as a result of increased levels of contamination in the northeastern bodies; however, it means that mg# values may not be used to precisely identify the boundary between the Middle and Upper Zones. Nevertheless, despite these potential shortcomings, mg# does appear to be the most satisfactory index to use as a record of fractionation in the bodies.

## 5.4 Whole rock chemistry of the bodies

As before, the intrusions have been divided into groups, largely on a geographical basis, to simplify comparison between the individual groups in an effort to discover if there are any regional geochemical variations. Although this may be an oversimplification of the data,

with, for example, the Belhelvie mass in the northeastern Grampian Highlands likely to be unrelated to the adjacent Haddo and Arnage bodies, it is a useful starting point from where more detailed examinations can be carried out. Initially, the samples will be looked at and classified using conventional major and trace element plots, before more detailed examinations of the fractionation of the bodies will be examined. From Chapter 4, the main subdivision identified within the data is the presence of the Granular Gabbros in the Insch intrusion, and these have accordingly been assigned a separate symbol to the remainder of the Central Intrusions throughout this chapter.

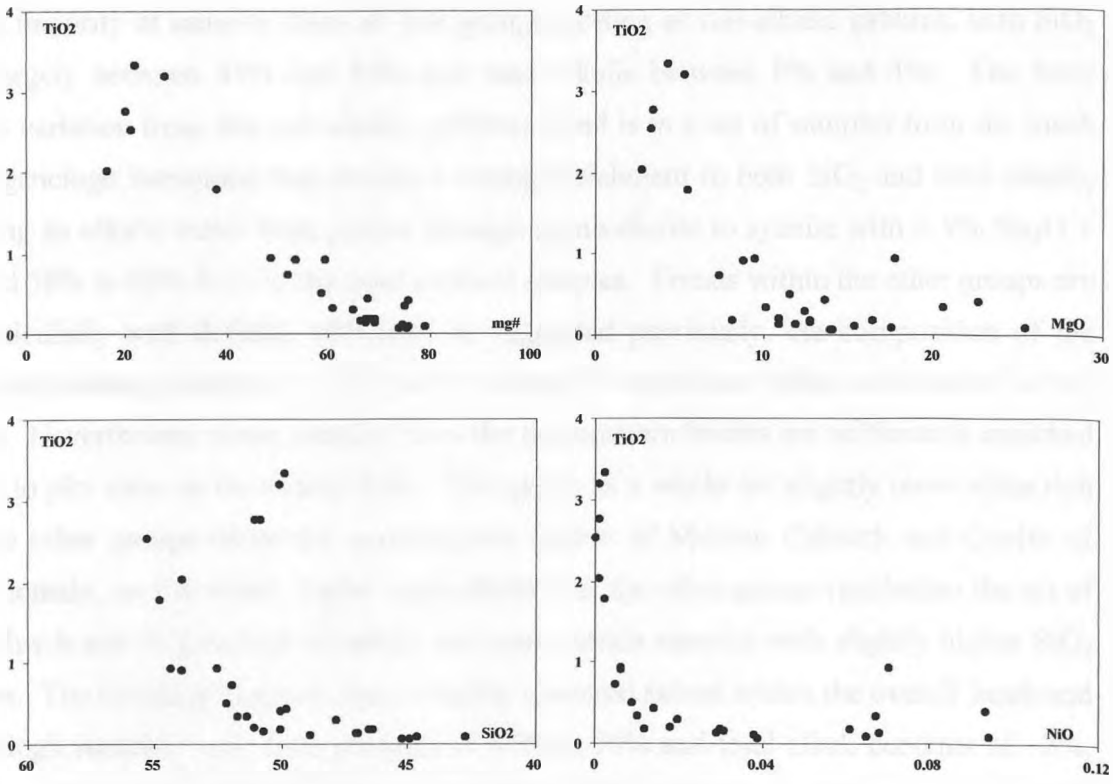


**Figure 5.6 Comparison of mg#, MgO, $SiO_2$ and NiO as fractionation indexes against $TiO_2$ values for samples from the northeastern bodies.**

Major, trace and REE element data are given in Appendix C, and analytical techniques and accuracy data given in Appendix B. Slight discrepancies are present in two specific sets of data and are mentioned here. Firstly, whole rock $P_2O_5$ data for samples with low abundances (<0.05%) display considerable scatter (see Appendix B) and are considered unreliable. This is particularly important for the Granular Gabbros, where published data suggests $P_2O_5$ values are somewhat higher. Secondly, data for one batch of samples

prepared for REE analysis appear to show some contamination for the elements Gd, Ho and Er (see Appendix B). These likely errors are most pronounced for samples with low REE abundances, and again, these include the Granular Gabbros. Details of both these inaccuracies are given in Appendix B, and where they affect the trends in the data, particularly for 'spider' and REE plots, they are noted.

### 5.4.1 Major element chemistry

Figure 5.7a and 5.7b show conventional TAS plots of the whole rock data. Although there are slight differences between the individual groups, there is a large degree of overlap, with the vast majority of samples from all five groups plotting as sub-alkalic gabbros, with $SiO_2$ totals largely between 43% and 53% and total alkalis between 0% and 4%. The most obvious variation from this sub-alkalic gabbroic trend is in a set of samples from the Insch and Boganclogh intrusions that display a strong enrichment in both $SiO_2$ and total alkalis, following an alkalic trend from gabbro through syeno-diorite to syenite with > 9% $Na_2O$ + $K_2O$ and 58% to 63% $SiO_2$ in the most evolved samples. Trends within the other groups are not particularly well defined, although, as suggested previously, the composition of the main fractionating minerals is not likely to lead to significant silica enrichment in the magma. Nevertheless, some samples from the northeastern bodies are sufficiently enriched in $SiO_2$ to plot close to the diorite field. This group as a whole are slightly more silica rich than the other groups while the southwestern bodies of Morven Cabrach and Coyles of Muick contain, on the whole, higher total alkalis than the other groups (excluding the set of alkalic Insch and Boganclogh samples), and also contain samples with slightly higher $SiO_2$ contents. The Granular Gabbros form a tightly clustered subset within the overall Insch and Boganclogh samples, with $SiO_2$ contents of 47% to 50% and total alkali contents of ~2%. For the northwestern and Connemara bodies only slight enrichment of silica or total alkalis is seen.

For the AFM plot in figure 5 8a, the samples showing textural or obvious chemical evidence for 'layering' have been omitted from the plot, where a tholeiitic trend for the majority of the samples is evident. Although this trend is not particularly well defined, it is clearer than with the layered samples included. All five divisions display the initial Fe-enrichment trend characteristic of tholeiitic samples, while only samples from the Insch and Boganclogh bodies show a subsequent alkali enrichment trend. Differences between the five groups are minor; figure 5.8b shows the range of the groups to be quite similar. There are, however, two minor variations to this trend; the most apparent is in the Insch Granular Gabbro

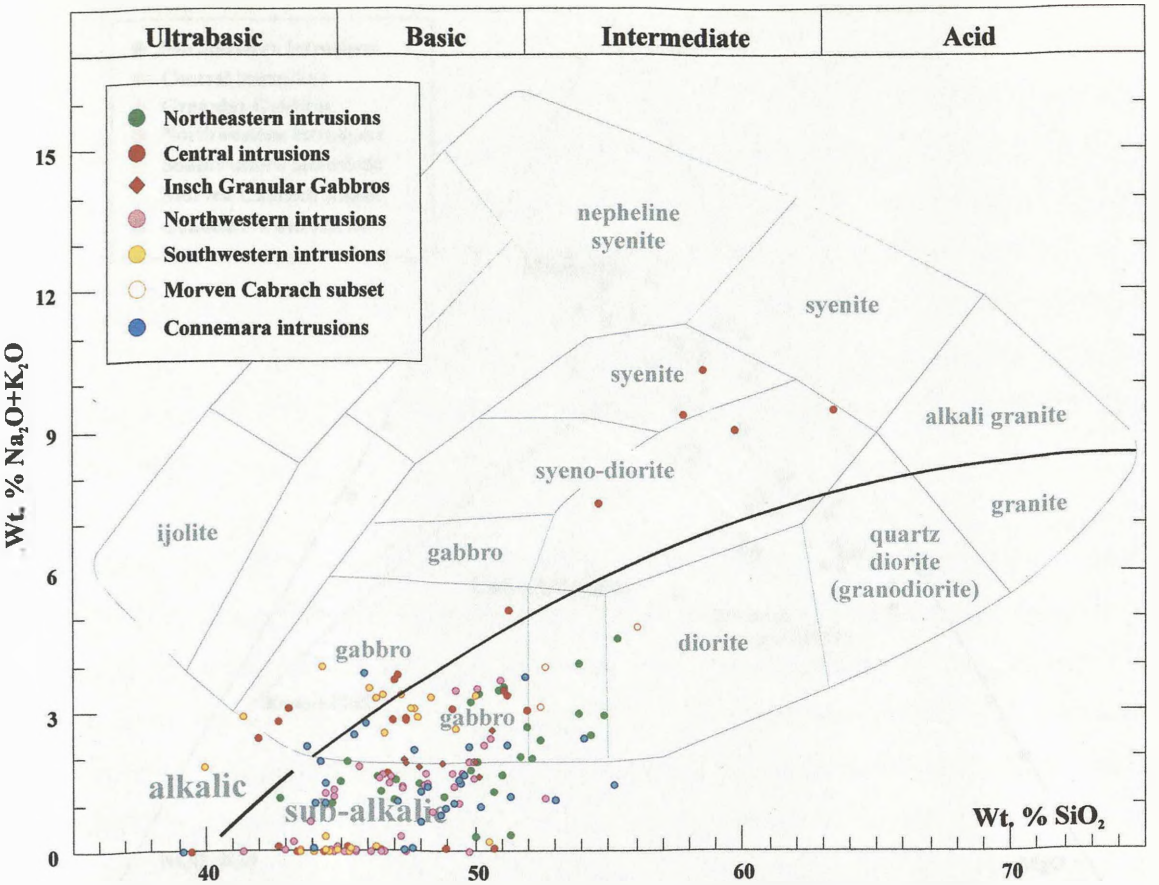


**Figure 5.7a Total alkalis versus silica (TAS) for all samples, divided into the 5 groups**

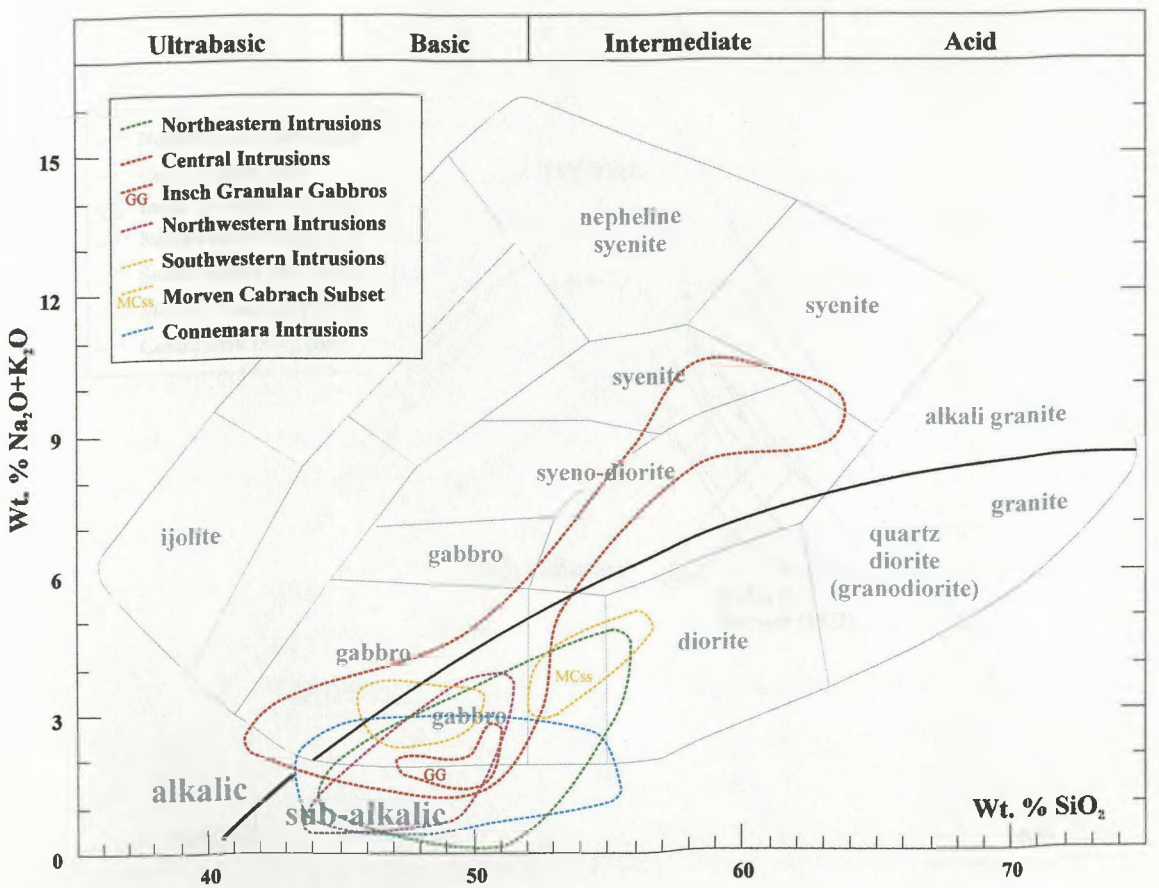


**Figure 5.7b Outline of the sample range for the TAS plot for each of the 5 groupings. Samples with low total alkali content in figure 5.7a are not included in these sample ranges.**

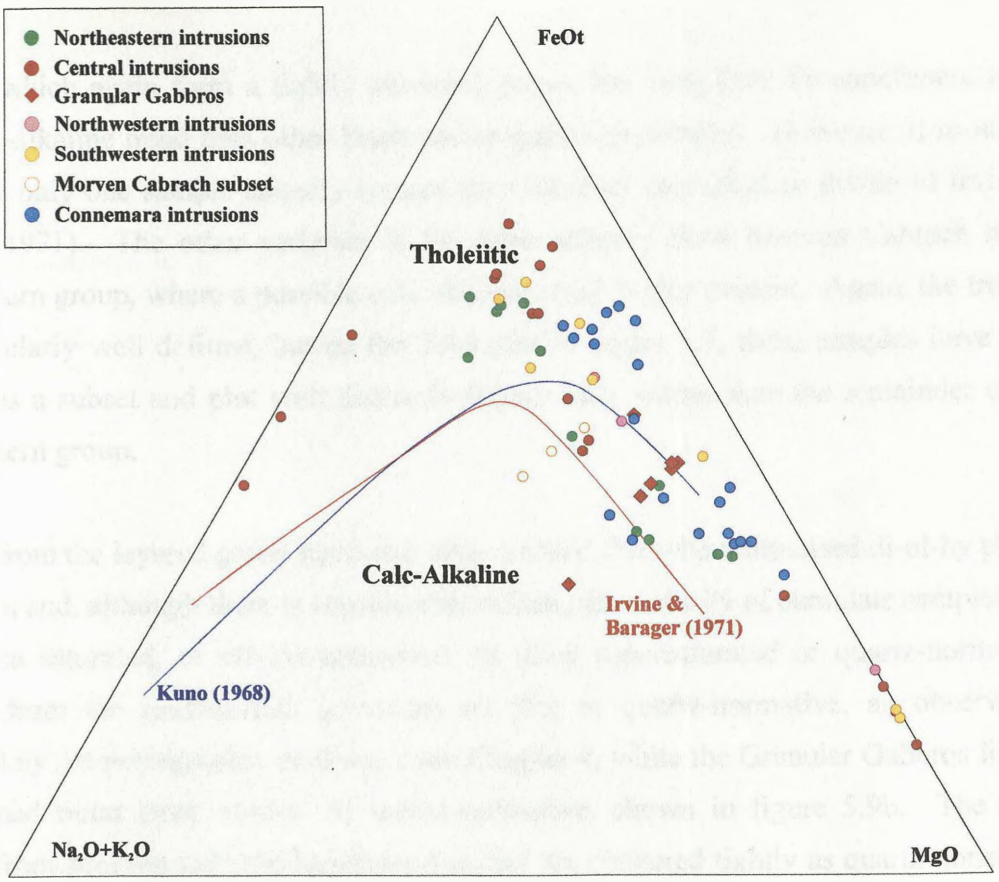


**Figure 5.8a AFM plot for non-layered samples from the groups as discussed in the text. Lines separating tholeiitic and calc-alkaline trends are shown.**

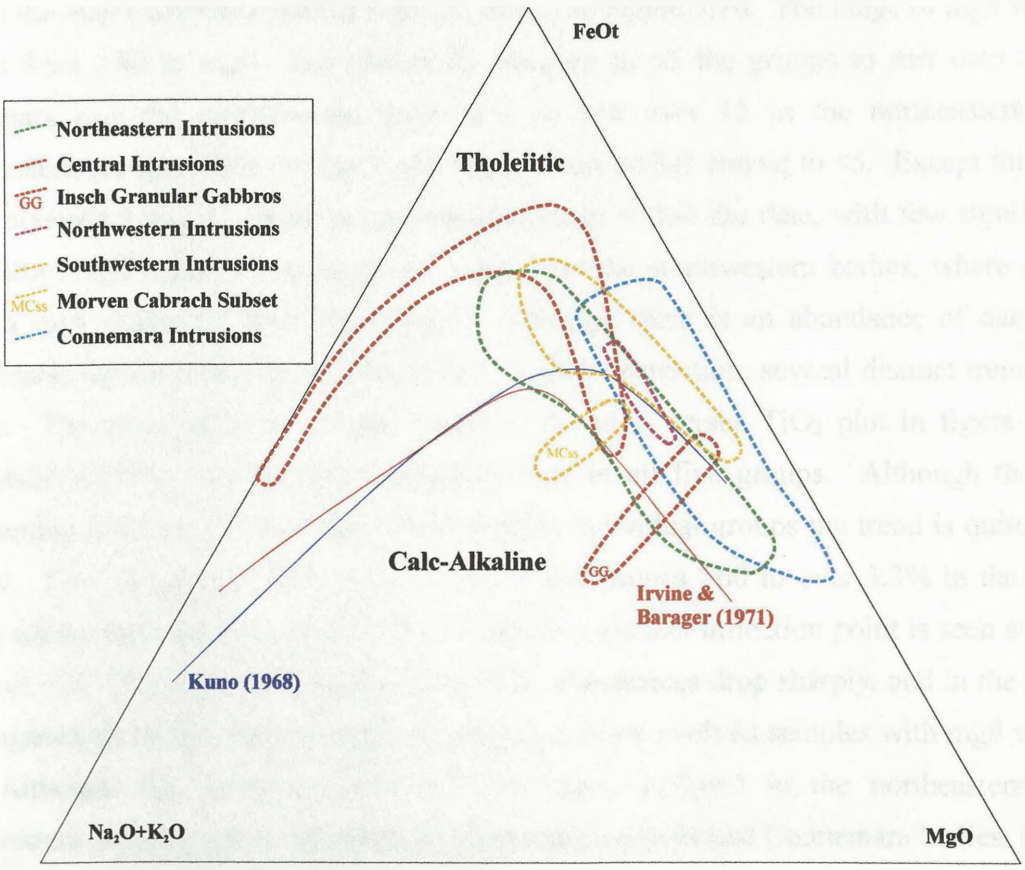


**Figure 5.8b Outline of the sample range on an AFM plot for non-layered samples. Lines separating tholeiitic and calc-alkaline trends are shown.**

samples, which again form a tightly clustered group, but with little Fe-enrichment and a more calc-alkaline trend than other Insch and Boganclogh samples. However, it should be noted that only one sample actually crosses the tholeiitic/ calc-alkaline divide of Irvine & Barager (1971). The other variation is for three samples from Morven Cabrach in the southwestern group, where a possible calc-alkaline trend is also evident. Again, the trend is not particularly well defined, but on the TAS plot in figure 5.7, these samples have been grouped as a subset and plot with distinctly higher $SiO_2$ values than the remainder of the southwestern group.

Samples from the layered group have also been omitted from the normalised di-ol-hy plot in figure 5.9a and, although there is considerable scatter, the majority of cumulate samples plot from silica saturated, or olivine-normative, to silica supersaturated or quartz-normative. Samples from the northeastern intrusions all plot as quartz-normative, an observation supported by the petrographic evidence from Chapter 4, while the Granular Gabbros form a well-defined trend from olivine- to quartz-normative, shown in figure 5.9b. The three samples from Morven Cabrach highlighted earlier are clustered tightly as quartz-normative samples, close to the di-hy join.

Plots of the major elements against mg# are shown in Figure 5.10. The range of mg# values extends from >80 in mafic and ultramafic samples in all the groups to just over 25 in Connemara and the northwestern intrusions, to just over 15 in the northeastern and southwestern groups, while the Insch and Boganclogh bodies extend to <5. Except for mg# values between 5 and 15, there is a continuous range within the data, with few significant gaps within mg# ranges for each group, apart from the southwestern bodies, where a gap between mg# values of 38 to 76 is seen. Although there is an abundance of data and considerable scatter on each individual plot, on close inspection, several distinct trends are evident. The most obvious of these trends is the mg# versus $TiO_2$ plot in figure 5.10. Enrichment of $TiO_2$ is seen with decreasing mg# in all five groups. Although there is considerable scatter to the data as a whole, within individual groups the trend is quite well defined. $TiO_2$ values rise from below 0.5% at mg# values >60 to over 3.3% in the three groups whose mg# values extend below 25, where a distinct inflection point is seen at mg# values of ~22. Beyond this inflection point $TiO_2$ abundances drop sharply, and in the Insch and Boganclogh bodies, rapidly reach <1.0% in the most evolved samples with mg# values <5. Although this inflection point is only just developed in the northeastern and southwestern samples and is not observed in the northwestern and Connemara bodies, this is

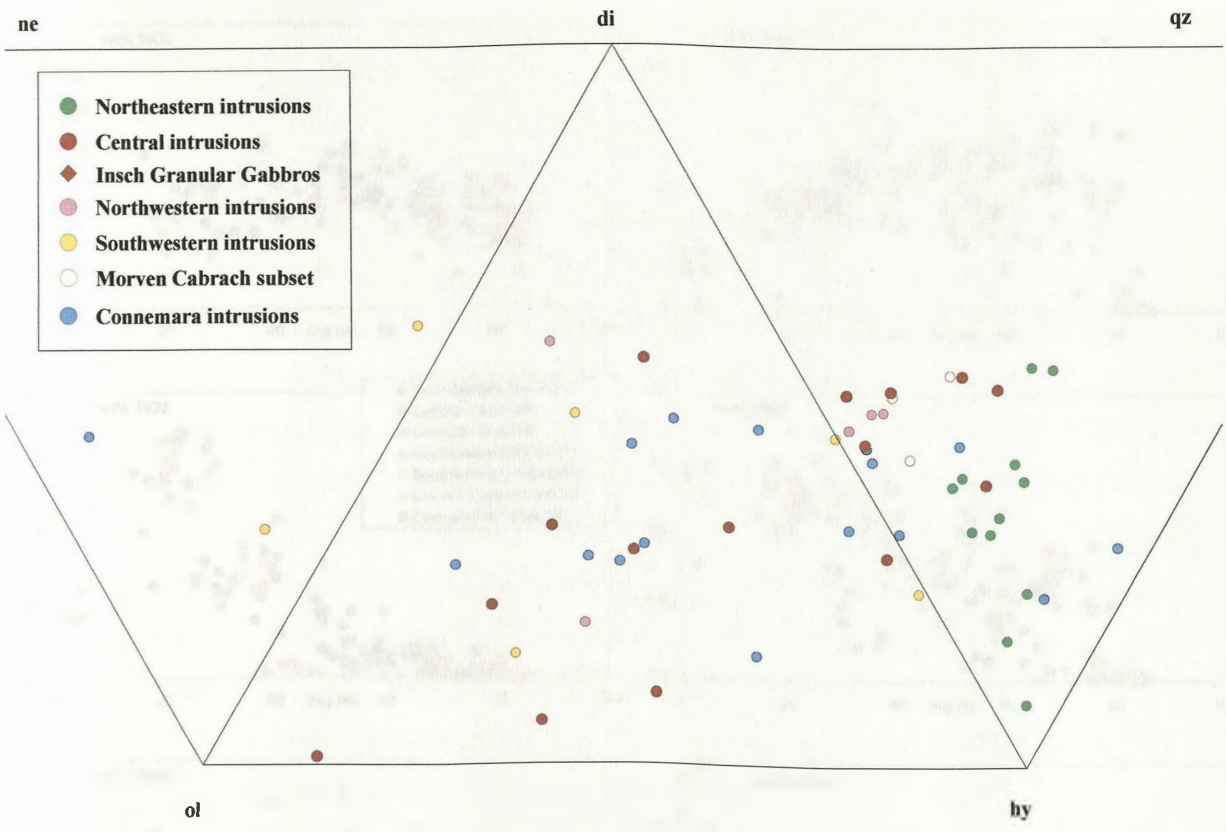


**Figure 5.9a Normative di-ol-hy plot for non-layered samples from the groups as discussed in the text.**

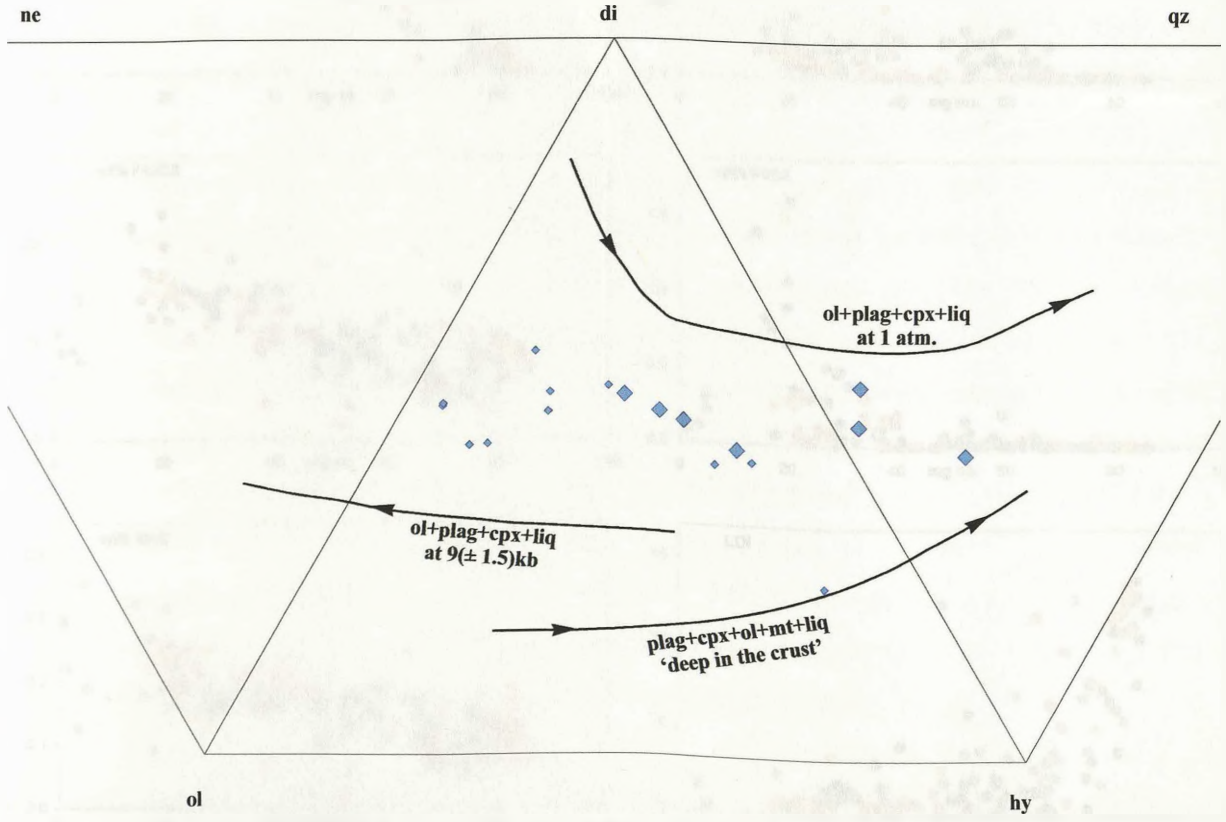


**Figure 5.9b Normative di-ol-hy plot for granular gabbro samples from the Insch intrusion. Published granular gabbro data (Hutchinson, 1965; Clarke & Wadsworth, 1970 and Thompson et al, 1984) included for comparison, with norms for all data calculated fixing $Fe_2O_3 = 1.5$.**

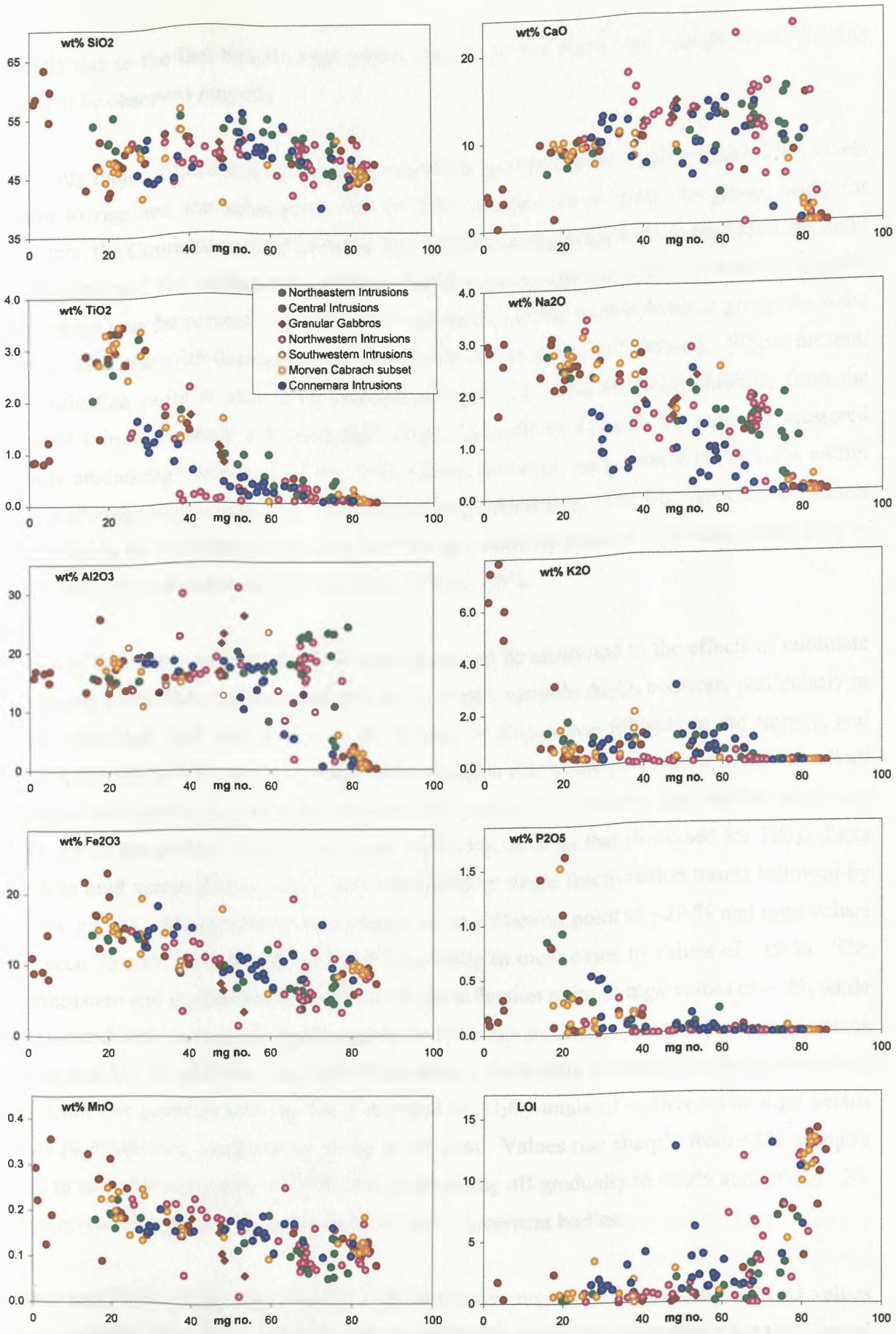


**Figure 5.10 Plots of major elements against mg# for all samples**

largely due to the fact that the mg# values simply do not reach low enough levels for this trend to be observed properly.

The only major differences between the individual groups are the mg# at which $TiO_2$ levels begin to rise and the subsequent rate of $TiO_2$ increase from group to group, with, for example, the Connemara trend showing less $TiO_2$ enrichment for a given mg# than the trend for Central and the northeastern groups. Northwestern samples show evidence to suggest two trends may be present. Despite these variations, within each individual group the same steady $TiO_2$ rise with decreasing mg# is present and is quite well defined. Where present, the inflection point is also quite constant at mg# ~22. The Granular Gabbros from the Central Intrusions show a limited mg# range, from 40 to 53 with the majority clustered tightly around mg# values of 47-48. $TiO_2$ values, however, vary from 0.1% to 1.7% within this mg# range, again with $TiO_2$ increasing as mg# decreases. The Morven Cabrach subset identified in the southwestern bodies also has an extremely limited mg# range, from 37.6 to 37.9, with $TiO_2$ abundances varying form 1.2% to 1.6%.

Much of the scatter seen on many of these plots can be attributed to the effects of cumulate processes within the magma chambers; for example, variable $Al_2O_3$ contents, particularly in those with high mg# values, due to the amount of plagioclase feldspar in the sample, and high $K_2O$ and $P_2O_5$ in some low mg# value samples due to the presence of cumulate alkali feldspar and apatite respectively. Despite this scatter, it is evident that similar trends are seen for all the groups, albeit with minor variations, such as that discussed for $TiO_2$. Plots such as mg# versus $Al_2O_3$, $Fe_2O_3$, and MnO display single fractionation trends followed by all the groups. $Al_2O_3$ contents rise sharply to an inflection point at ~20 % and mg# values between 75 and 55, before dropping off gradually in most cases to values of ~15 %. The northeastern and northwestern bodies reach the inflection point at mg# values of ~ 75, while the Central and Connemara bodies appear to have this inflection point at lower mg# values of around 55. In addition, the Connemara bodies show little evidence for the gradual drop off from this point, remaining fairly constant at $Al_2O_3$ totals of ~ 18%. The mg# versus CaO plot follows a similar trend to the $Al_2O_3$ plot. Values rise sharply from <3% at mg#'s >80 to up to 15% at mg#'s of 70-80, before dropping off gradually to <10% at mg#'s of ~20. Again, scatter is extensive, particularly for the Connemara bodies.

MnO and $Fe_2O_3$ values rise steadily with decreasing mg# for all the groups. MnO values rise gradually from 0.1% to 0.2%, with considerable scatter at lower mg#'s for the Central Intrusions, while $Fe_2O_3$ values rise from less than 10% to ~ 15% at mg#'s of ~ 20, with the

Central Intrusions reaching as high as 23%, before falling off sharply to values around 10% at low mg#'s (although, of course, an inverse relationship between $Fe_2O_3$ and mg# is to be expected, resulting from the presence of $Fe_2O_3$ in the formula used to calculate the mg#).

$SiO_2$ trends display considerable scatter, with totals varying by around 10% at any given mg#. There is a gentle overall rise from 45% at high mg#'s, to 50% at mg#'s of 40-60, followed by a gentle fall back to 45% at mg#'s of 20-30. The Central Intrusions show this pattern most clearly, with $SiO_2$ dropping to <43% at mg#'s of ~20, before rising sharply to >60% at low mg#'s. In contrast, the northeastern bodies have slightly higher $SiO_2$ totals throughout the mg# range, and do not follow this gentle decrease, resulting in $SiO_2$ totals up to 55% at mg#'s of ~20. $P_2O_5$ levels are generally quite low, below 0.1% for much of the mg# range, and, as mentioned, much data below 0.05% $P_2O_5$ may be considered unreliable. At mg#'s of <40 a sharp rise is seen in some of samples, rising to over 1% in several samples at mg#'s of ~20. A sharp inflection point and subsequent drop to <0.3% is seen in data from the Central Intrusions.

Data for $Na_2O$ and $K_2O$ show the greatest variation of the major element data, which is most pronounced for the Connemara Intrusions. $Na_2O$ values are consistently lower for the Connemara bodies than for the bodies from the Grampian Highlands. For these four Scottish groupings, $Na_2O$ values rise quite sharply, from close to 0% at high mg#'s of ~80, to ~1.5% at mg#'s of ~70, before rising gently to close to 3.0% at low mg#'s. The Connemara bodies, on the other hand, only show a slow rise from a similar starting point to <1.7% at mg#'s of 25-30. Variation is also seen for the Connemara bodies in $K_2O$ values, which are consistently higher than in the Grampian Highlands, except at low mg#'s, where samples from the Central Intrusions contain high $K_2O$ abundances up to over 6.0%. The northeastern intrusions also display similar levels of $K_2O$ to Connemara at mg#'s lower than 55, while the remainder of the groups only show $K_2O$ totals above 0.5% at low mg#'s of ~20, where the low mg# samples from the Central Intrusions rise sharply to over 5.0%. Loss on Ignition ranges from above 10% at high mg#'s, to generally below 2.0% for the remainder of the mg# range.

On several of these mg# versus major element plots in figure 5.10, the Granular Gabbros plot as part of the overall Insch and Boganclogh trend, as do the Morven Cabrach subset from the southwestern bodies. However, on plots such as $Al_2O_3$, $Fe_2O_3$ and MnO, the range within the Granular Gabbros as a group is quite large and difficult to envisage as part of the overall Insch and Boganclogh trend. $Al_2O_3$ values of up to 25% in the Granular Gabbros

are generally larger than other Insch and Boganclogh samples at similar mg#'s, while $Fe_2O_3$ and MnO concentrations drop below those expected within the Insch and Boganclogh trend. In addition, although they fit into the overall trend, CaO totals are higher in the Granular Gabbros than in the remainder of the Insch and Boganclogh trend, while the trend seen in the $Na_2O$ concentrations for the Granular Gabbros is somewhat different from that seen in the Central Intrusions as a whole. The Morven Cabrach subset fits into trends from the remainder of the southwestern group for most elements, with the notable exception of $K_2O$. These $K_2O$ values range from 0.8 to 1.9 % are well above those from the main group trend of ~ 0.3%, while $SiO_2$ totals are slightly higher (52.5 to 56.0%) than the remainder of the group (<51.0%).

### 5.4.2 Trace element chemistry

The cumulate nature to the majority of samples from the 'Younger' Basics means that many conventional classifications based on trace element abundances either cannot be used, or must be used with extreme caution. As discussed in Section 5.3, however, ratios of incompatible elements, such as in 'spider' and REE plots, may be used to examine the chemistry of the samples. Nevertheless, plots of trace elements against the fractionation index, mg#, can be used to examine the overall fractionation trends in the bodies and plots of mg# versus selected trace elements are shown in Figure 5.11.

Many of the features seen in the major element data are replicated, with trends within individual groups quite well defined, and any scatter within the data as a whole resulting from slight differences between the trends in these individual groups. Again, single fractionation trends are evident for most of the trace elements. Well-defined compatible element trends are seen for Ni and Cr, dropping from over 2500 and 4000 ppm respectively at mg#'s of ~80 to below 25 ppm at lower mg#'s; high Ni contents are not seen in the northeastern intrusions, where concentrations above 800 ppm are not present. Cu data show a poorly defined trend for most groups, with only the northeastern bodies showing a compatible element trend.

Zn values rise gradually from below 50 ppm at high mg# values to over 100 ppm at mg#'s of around 20. Central Intrusion levels reach up to 150 ppm before dropping sharply to ~50 ppm at low mg#'s. Scatter is considerable for trends in the Sc data, with values rising from ~10 ppm to ~50 ppm with decreasing mg#, with Connemara samples appearing, on average, to contain slightly higher abundances than the Scottish groups.

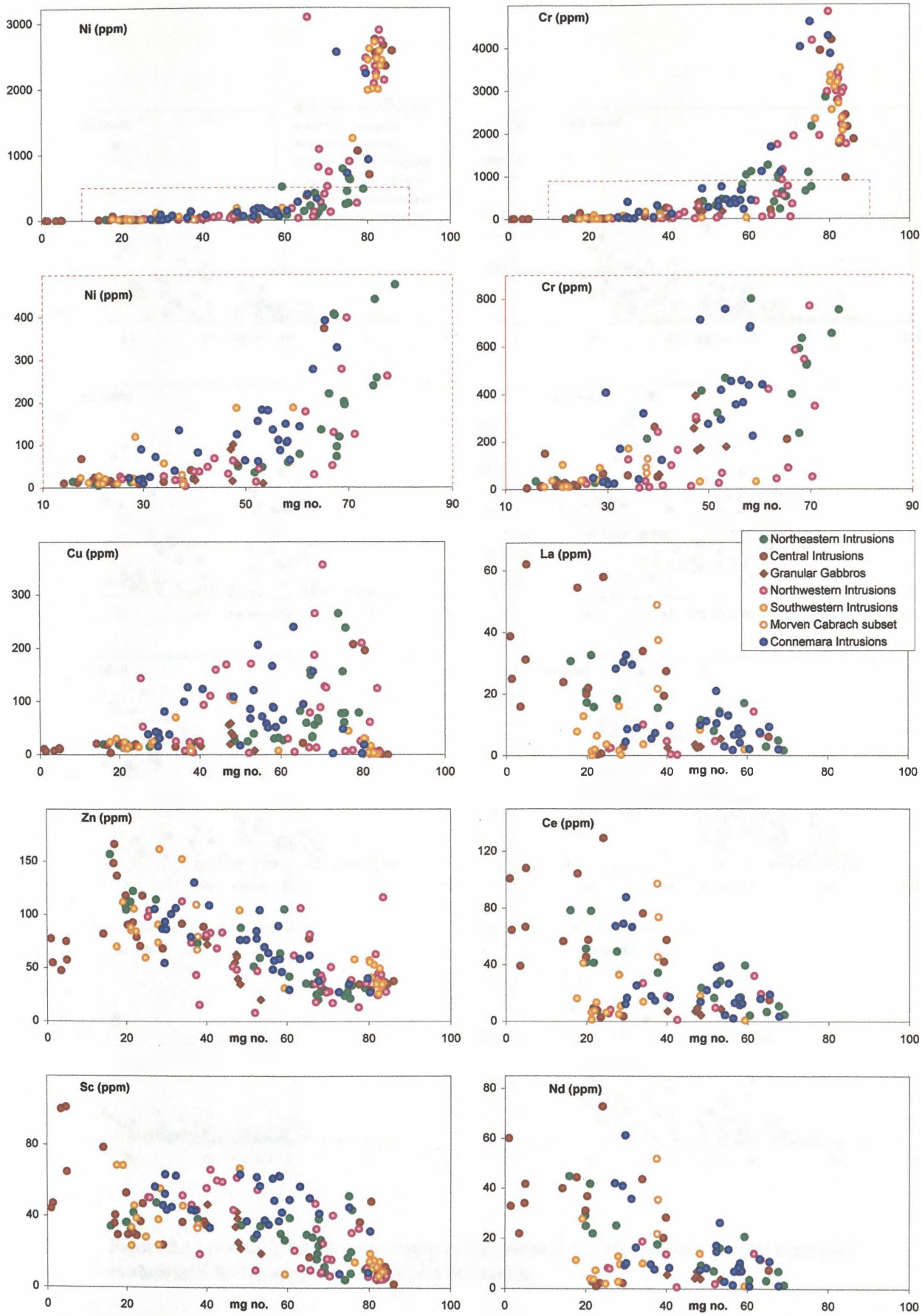


**Figure 5.11 Plots of trace elements against mg# for all samples. High mg# samples not analysed for REE Ni and Cr plots expanded to show trends for lower Ni and Cr abundances.**

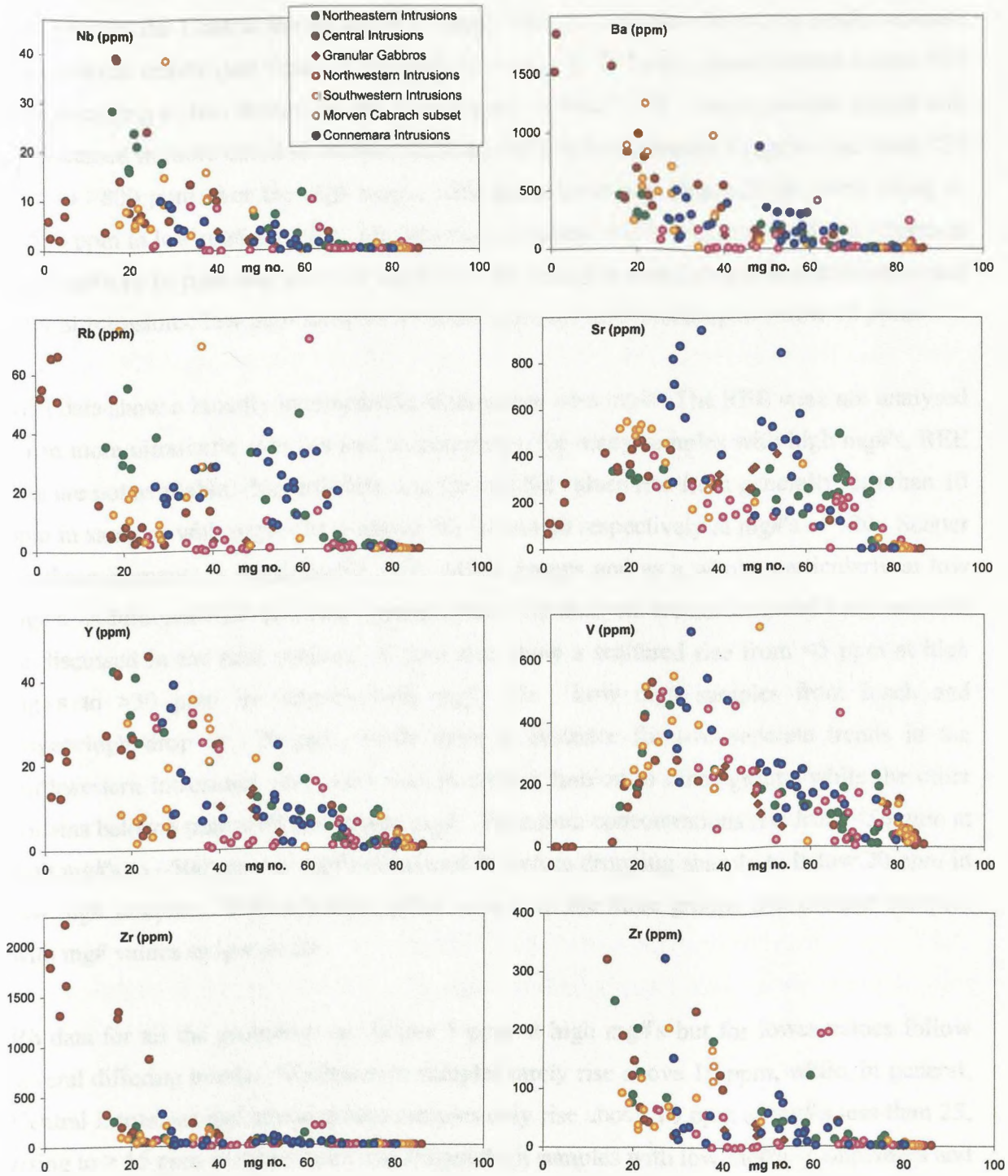


**Figure 5.11 (cont.) Plots of trace elements against mg# for all samples. Zr plot expanded to show trends for samples with lower abundances.**

Zr values rise irregularly from below 10 ppm at high mg#'s to over 200 ppm in samples at mg# ~ 20; Insch and Boganclogh samples rise rapidly to >1500 ppm at low mg# values, while within the Central Intrusions as a whole, there is evidence for two possible separate fractionation trends (see figure 5.11) with increases in Zr from concentrations below 100 ppm occurring in two distinct trends at mg#'s of ~ 40 and ~ 25. These possible trends will be discussed in more detail in the next section. Ba displays a similar irregular rise from <30 ppm to >800 ppm over the mg# range, with again Insch and Boganclogh levels rising to >1500 ppm in low mg# samples. Nb data show a steady rise in most groups from <2ppm at high mg#'s to 10 ppm and above at mg#'s of ~20, reaching over 20 ppm in northeastern and Central Intrusions; low mg# samples from the Central Intrusions drop to below 10 ppm.

REE data show a broadly incompatible relationship with mg#. The REE were not analysed for in more ultramafic samples and consequently, for many samples with high mg#'s, REE data are not available. Nevertheless, La, Ce and Nd values rise from generally less than 10 ppm in samples with mg# ~70 to above 30, 50 and 40 respectively at mg#'s of ~20. Scatter for these elements is considerable, both within groups and as a whole, particularly at low mg#'s. Additional REE analyses obtained from ICP analysis are not included here, and will be discussed in the next section. Y data also show a scattered rise from <5 ppm at high mg#'s to >30 ppm in samples with mg# ~20. Low mg# samples from Insch and Boganclogh drop to ~20 ppm, while there is evidence for two separate trends in the northwestern intrusions; one trend rises in similar fashion to other groups while the other remains below 5 ppm with decreasing mg#. Vanadium concentrations rise from <50 ppm at high mg#'s to ~500 ppm at mg#'s of around 25 before dropping sharply to below 20 ppm in low mg# samples. This inflection point is seen in the three groups that contain samples with mg# values as low as 20.

Rb data for all the groupings are below 5 ppm at high mg#'s but for lower values follow several differing trends. Northeastern samples rarely rise above 10 ppm, while, in general, Central Intrusions and southwestern samples only rise above 10 ppm at mg#'s less than 25, rising to > 65 ppm in some Insch and Boganclogh samples with low mg#'s. Connemara and northeastern samples, in contrast, are generally between 10 and 30 ppm below mg#'s of <70. Sr data show a gradual rise from below 10 ppm at high mg#'s to 400 to 500 ppm at mg# ~ 20 for the Scottish groups with Insch and Boganclogh samples dropping to less than 100 ppm at low mg#'s, while the Connemara bodies show scattered Sr totals ranging from 100 to 1000 ppm.

As with the major element data, the Morven Cabrach subset and the Granular Gabbros plot within the overall southwestern, and Central trends quite well in most cases, but on several plots, it is difficult to reconcile both sets of data. In particular, the limited trends within the Granular Gabbros data are usually different to those in the group as a whole. They display considerable variation over their limited mg# range for many of the trace elements measured. The Granular Gabbros show consistently higher levels of Ni, Cr and Cu than samples from the remainder of the Insch and Boganclogh trend at similar mg#'s. Ni levels range from 10 to 100 ppm, while the main trend has levels of 30-40 ppm; Cu values range from 10 to 60 ppm, compared to <25 in the rest of the intrusion. Cr abundances are generally 200 to 250 ppm in the main trend, while they reach up to 400 ppm in the Granular Gabbros. Although the totals are not substantially different from those in the main trend, the Granular Gabbros sub-trend for trace elements such as Zn, Sc, Y, V and Sr does not appear to fit in with the main trend, while values for Zr, Ba, Nb, Rb and the REE are quite low, similar to those from the main trend. This data will be considered in more detail in the next section.

The Morven Cabrach subset displays little internal variation in concentrations of the compatible elements Ni, Cu and Cr, and does not vary significantly from the southwestern trend as a whole for these elements. Although Zn, Nb, Ba, Sr, Y and V display a range of abundances, they all fall within or close to the southwestern trend as a whole, while Zr, Rb and the REE all contain abundances somewhat higher than those for the main trend. Zr totals range from 110 to 170 ppm, while the main trend has values around 50 to 60 ppm, while Rb totals range from 20 to 70 ppm where typical concentrations at similar mg#'s are generally less than 20 ppm. Finally, La, Ce and Nd data range from 20 to 50 ppm, 40 to 100 ppm and 20 to 50 ppm respectively in the main Morven Cabrach subset while concentrations in the main southwestern trend at similar mg#'s are typically 10 to 15 ppm for all three REE.

### 5.4.3 Insch and Boganclogh subtrends

A combination of thin section and preliminary geochemical evidence suggests more than one magmatic component in the Insch and Boganclogh intrusions, with three separate trends recognized. The Granular Gabbros from the Insch body have been identified from thin section evidence in Chapter 4 and have been shown to form a well-defined and often quite tightly clustered sub-group on the majority of plots. However, in addition to these Granular Gabbros, a second sub-division of samples in the Insch and Boganclogh masses has been

identified. On the plot of mg# versus Zr, shown in figure 5.11, and reproduced here in figure 5.16, there is evidence for two separate trends. A rise in Zr abundances from generally less than 50 ppm occurs at mg#'s of ~40 and ~25 resulting in two similar but discrete trends, here named Trend 1 and Trend 2. Assigning separate symbols to the samples from these two trends and plotting them geographically (figure 5.12) shows them to have a clear spatial relationship, with samples of Trend 1 association found in Boganclogh and the southwestern parts of the Insch body, while Trend 2 samples are restricted to the eastern parts of the main Insch mass where they are found in association with the Granular Gabbros. In addition, the limited available published whole rock data have been added to each of these two trends, on the basis of their location geographically.

Both trends are plotted in figure 5.13 and 5.14 for TAS and AFM plots and in figure 5.15 and 5.16 for fractionation plots, with Granular Gabbro data also included for comparison; published data sources contain only limited trace element data accounting for the absence of additional points on some graphs. It is evident in the TAS plot in figure 5.13 that Trend 1 extends to higher $SiO_2$ and total alkali values than Trend 2; a similar situation is seen in the AFM plot in figure 5.14, where Trend 2 samples only display a slight alkali enrichment after Fe-enrichment, while the Trend 1 data shows a well-defined Fe-enrichment and subsequent alkali enrichment trends.

On most of the major element plots in figure 5.15 the two trends are quite similar, with published data in good agreement with data from this study. Trend 1 is the more complete trend, with mg#'s ranging from over 80 to less than 5, while the majority of Trend 2 samples have mg#'s of between 15 and 30. Many of these plots do not necessarily suggest the presence of two separate trends, merely that samples from Boganclogh and the southwestern parts of Insch (generally Middle and Upper Zone) are more fractionated than samples from eastern Insch. However, plots of mg# versus $K_2O$ and $Na_2O$ highlight the differences between the two trends while it is trace element data, especially incompatible elements (figure 5.16) which show up these differences most clearly. The two trends follow slightly different trends on the majority of these trace element plots, particularly versus Zn, Nb, Ba, Rb, Y, V and of course Zr, where the trend was first identified. These separate trends are not merely a function of using mg# as a fractionation index; plots using MgO alone as an index also reveal the differences between the two trends, albeit with more scatter.

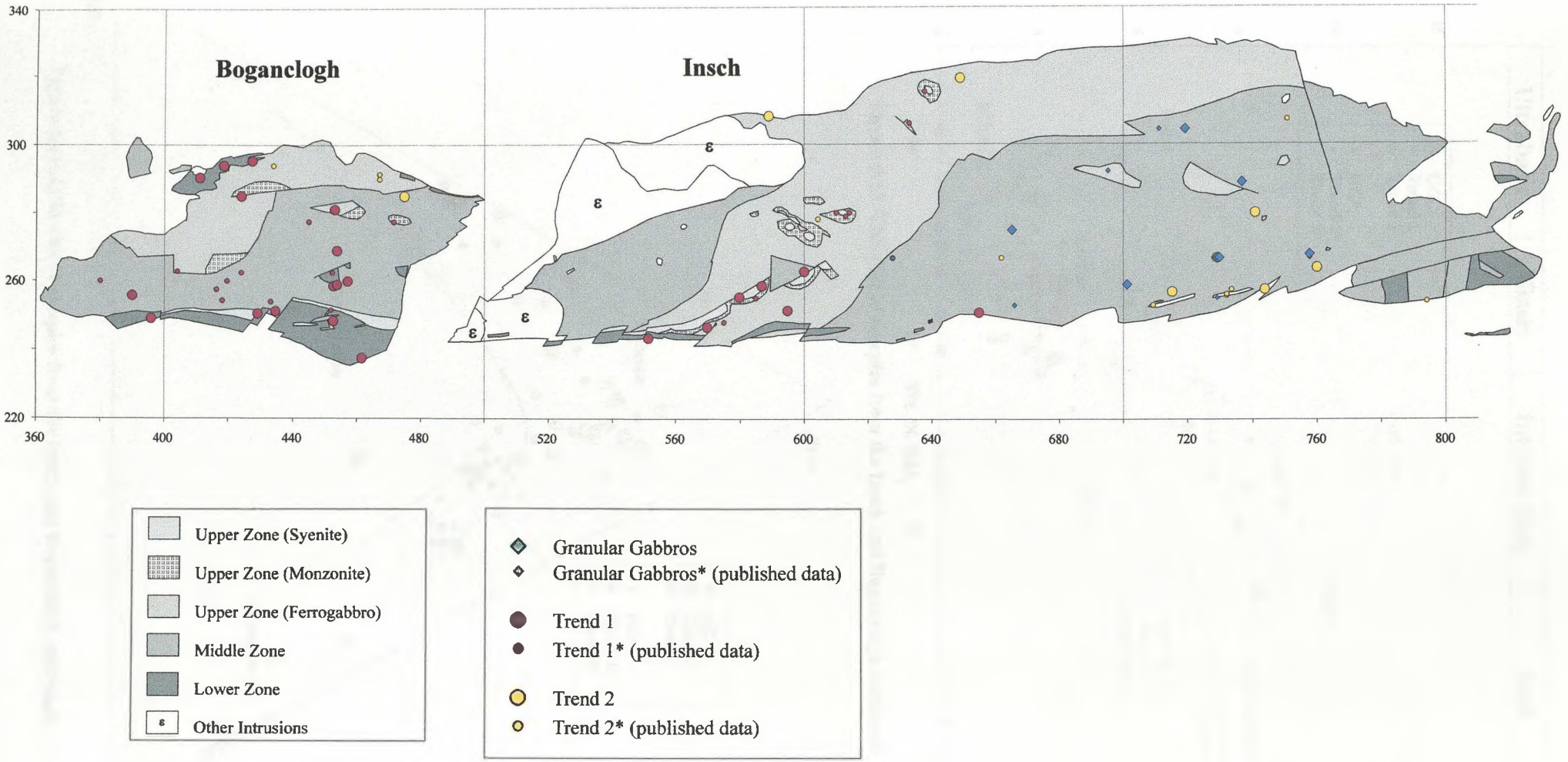


**Figure 5.12 Location from samples in the Insch and Boganclogh intrusions, divided into 3 groups as discussed in the text.**

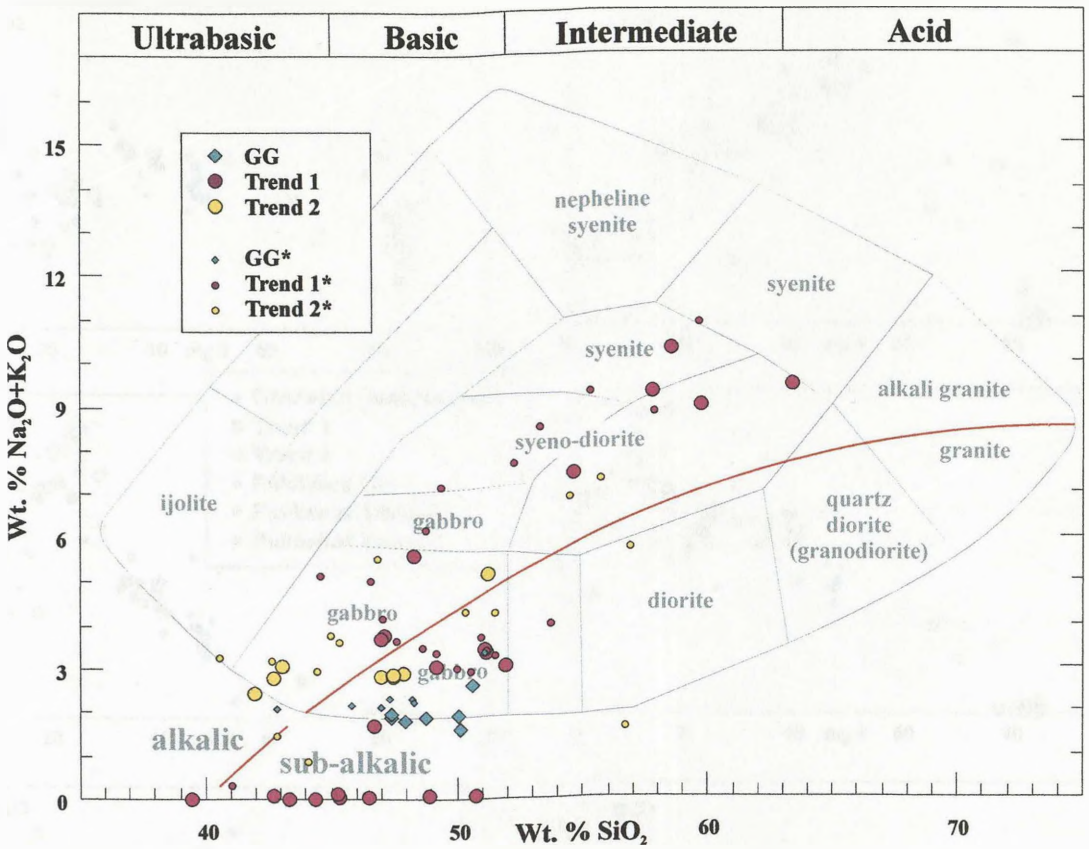


**Figure 5.13 TAS plot of samples from the Insch and Boganclogh subtrends**

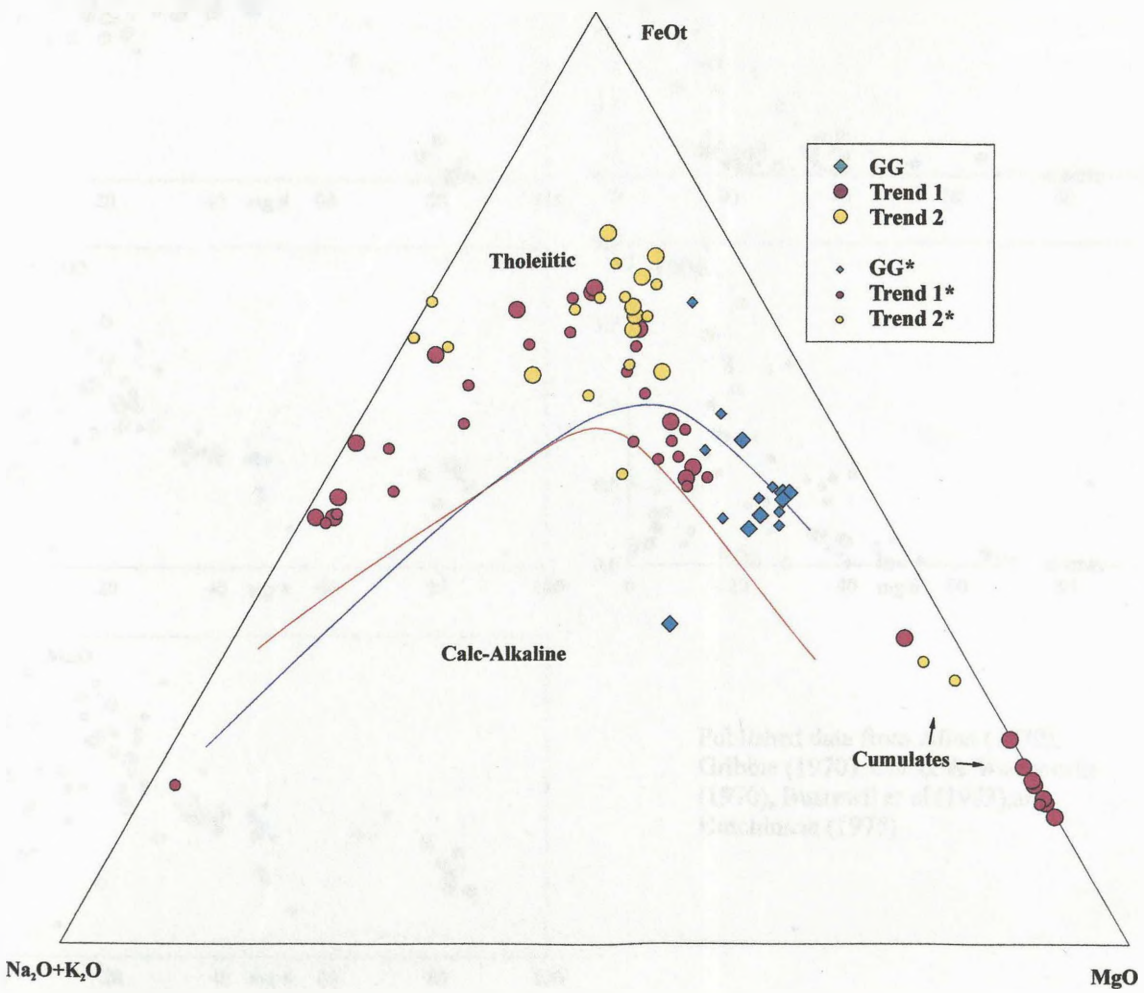


**Figure 5.14 AFM plot of samples from the Insch and Boganclogh subtrends**

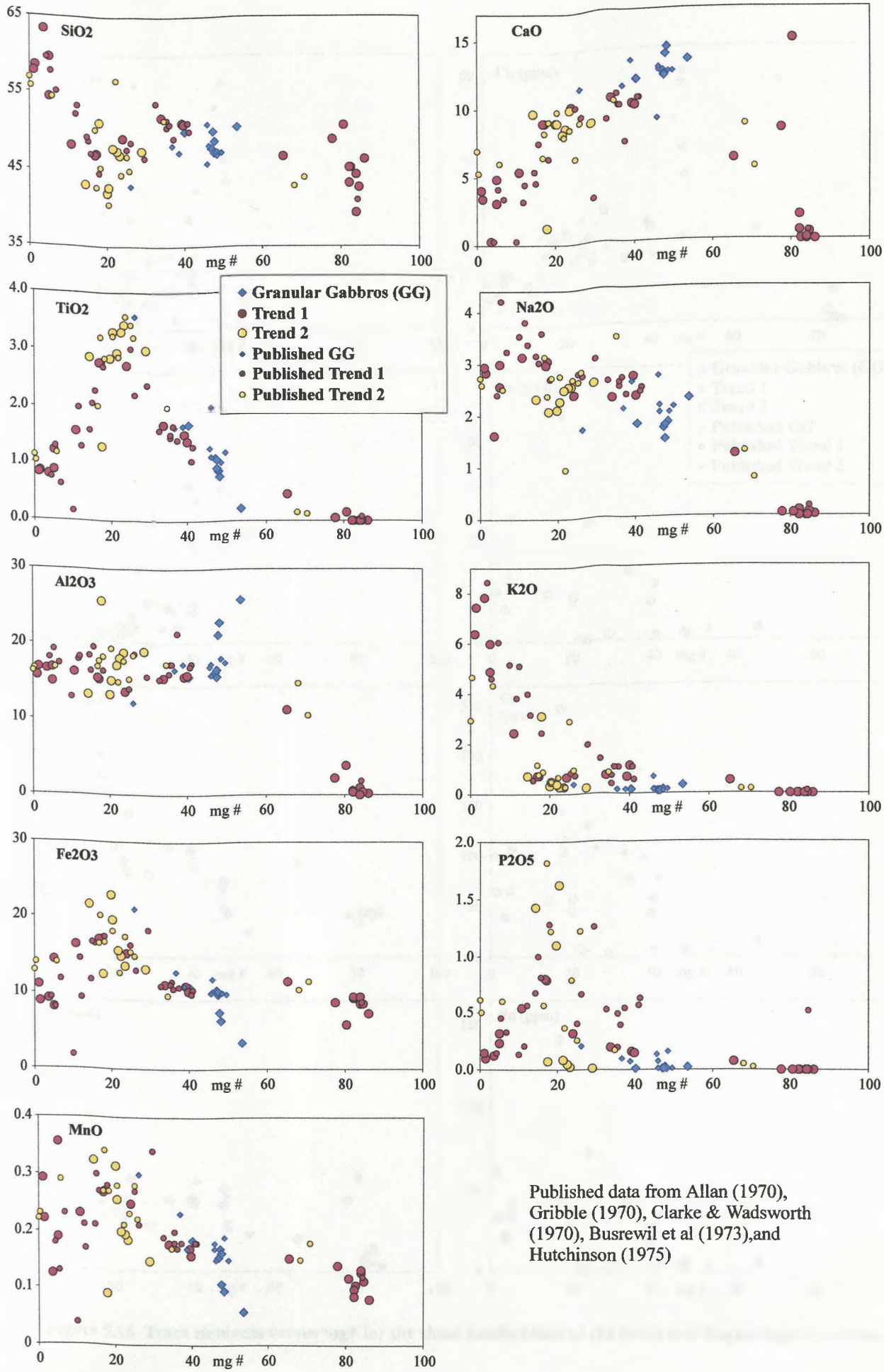


**Figure 5.15 Major elements versus mg# for the three subdivisions of the Insch and Boganclogh intrusions.**

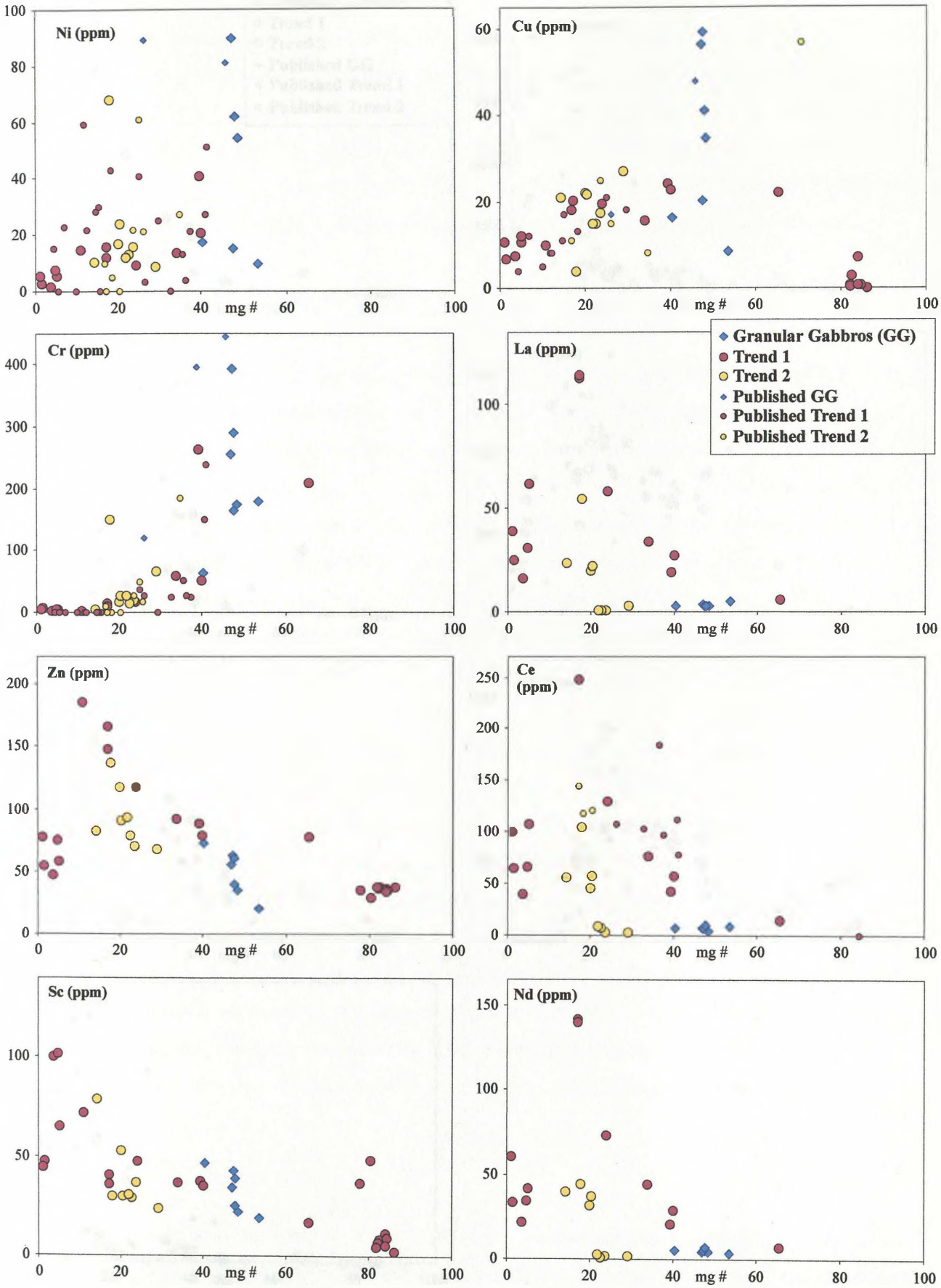


**Figure 5.16 Trace elements versus mg# for the three subdivisions of the Insch and Boganclogh intrusions.**

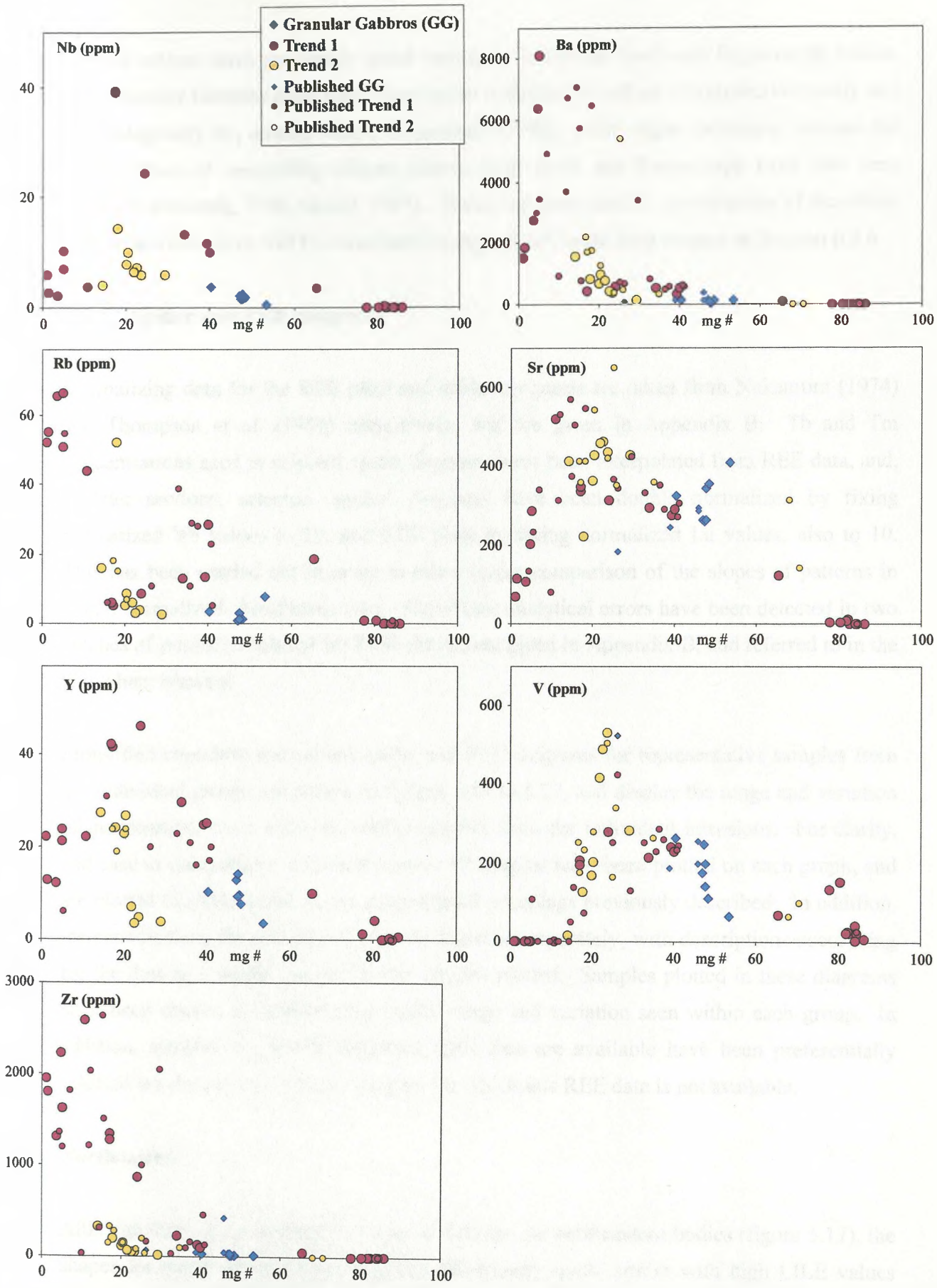


**Figure 5.16 (cont.) Trace elements versus mg# for the three subdivisions of the Insch and Boganclogh intrusions.**

Several authors have previously noted variations within the Insch and Boganclogh bodies. The Granular Gabbros have been observed as a distinctive subset of samples texturally and mineralogically by, among others, Wadsworth (1988), while slight variations between the compositions of co-existing silicate phases from Insch and Boganclogh have also been noted (Wadsworth, 1988; Gould, 1997). These variations and the implications of the whole rock trends seen here will be considered in more detail in the next chapter in Section 6.2.6.

### 5.4.4 Spider and REE diagrams

Normalizing data for the REE plots and spider diagrams are taken from Nakamura (1974) and Thompson *et al.* (1984) respectively, and are given in Appendix B. Tb and Tm concentrations used in selected spider diagrams have been interpolated from REE data, and, in later sections, selected 'spider' diagrams have been double normalized by fixing normalized Yb values to 10, and REE plots by fixing normalized Lu values, also to 10. This has been carried out in order to allow easier comparison of the slopes of patterns in which normalized abundances vary. Significant analytical errors have been detected in two batches of samples analysed for REE; details are given in Appendix B, and referred to in the text where relevant.

Simplified chondrite normalised spider and REE diagrams for representative samples from the individual groups are shown in figures 5.17 to 5.27, and display the range and variation of incompatible trace elements within samples from the individual intrusions. For clarity, and ease of comparison, a limited number of samples have been plotted on each graph, and are plotted together based on the geographical groupings previously described. In addition, for convenience, the groups will also be described separately, with descriptions accounting for the data as a whole, not just those samples plotted. Samples plotted in these diagrams have been chosen to represent the typical range and variation seen within each group. In addition, samples for which additional REE data are available have been preferentially selected for display over similar samples for which this REE data is not available.

#### Northeastern

Although there is a considerable range of data for the northeastern bodies (figure 5.17), the shapes for many of the spider diagrams are broadly quite similar with high LILE values (particularly Rb and K), with, generally, $Rb_N > K_N$ and $\gg Ba_N$, a pronounced, though variable, Nb-trough for most samples, quite constant LREE data and variable Zr and Ti

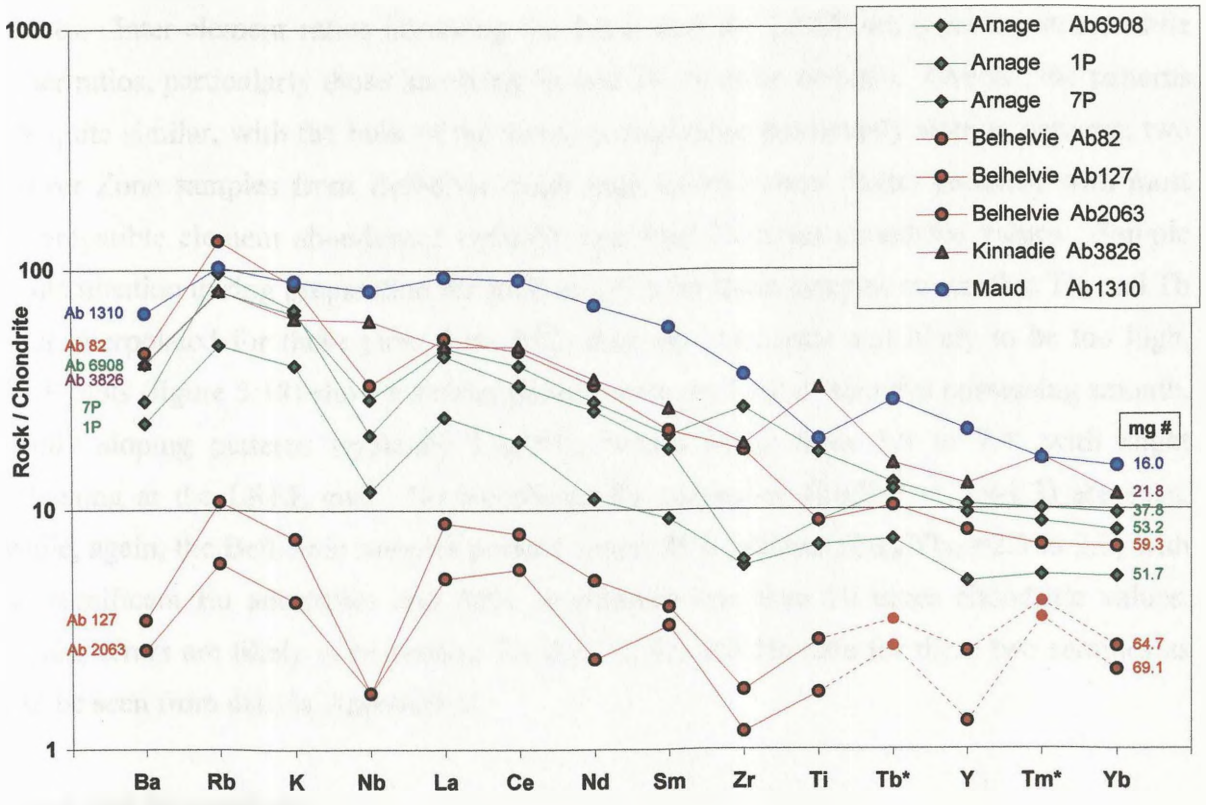


**Figure 5.17 Chondrite normalized spider diagram with selected samples from the northeastern intrusions. Interpolated Tb and Tm data for samples Ab127 and Ab2063 are likely to contain slight errors due to contamination.**

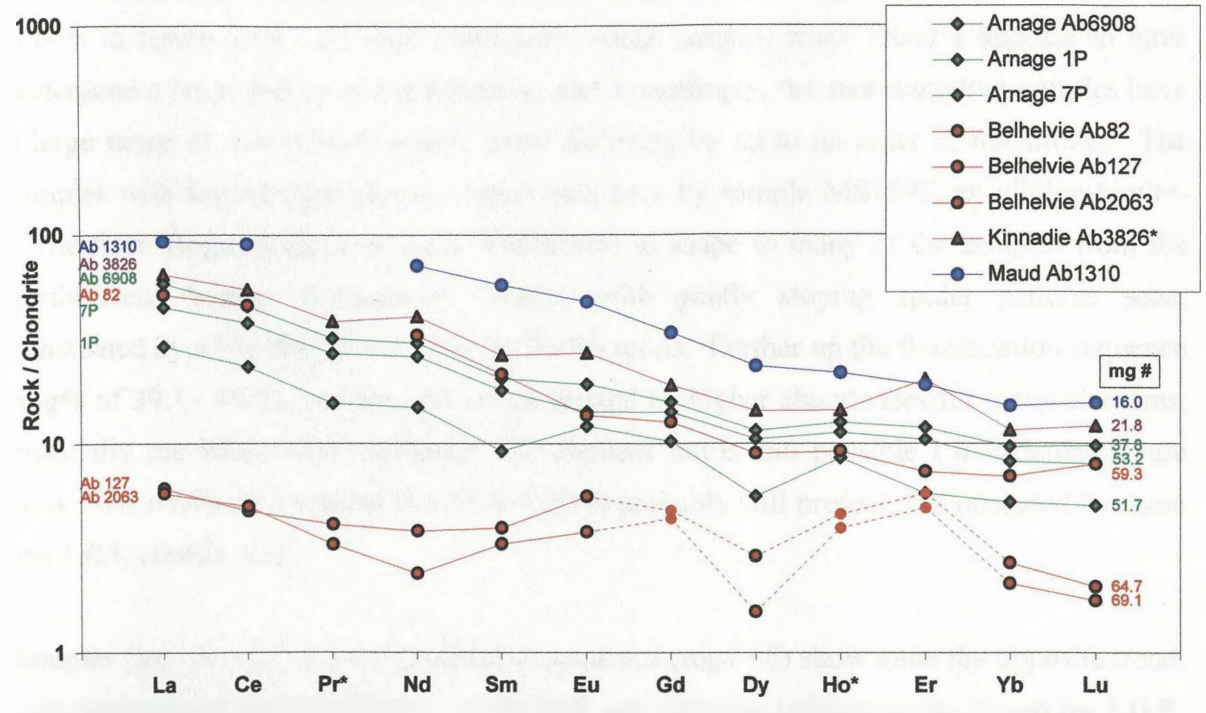


**Figure 5.18 Chondrite normalized REE plot of samples from the northeastern bodies. Gd, Ho and Er values for samples Ab127 and Ab2063 are likely to be too high due to errors resulting from sample contamination. Ab3826*: Partial analysis**

values. Inter-element ratios involving the LILE and the LREE are quite constant, while other ratios, particularly those involving Zr and Ti are quite variable. Overall, the patterns are quite similar, with the bulk of the samples displaying moderately sloping patterns; two Lower Zone samples from Belhelvie (high mg# values) show flatter patterns, with most incompatible element abundances typically less than 10 times chondritic values. Sample contamination during preparation for REE analysis for these samples means that Tm and Tb data interpolated for these plots from REE data are inaccurate and likely to be too high. REE plots (figure 5.18) show a similar pattern, with the bulk of samples possessing smooth, gently sloping patterns (typically $La_N/Yb_N$ values range from 5.5 to 7.4) with slight flattening at the LREE end. No significant Eu anomalies (Eu/Eu* = 0.9-1.3) are seen, while, again, the Belhelvie samples possess flatter REE patterns ($La_N/Yb_N$ =2.3 to 2.7) with no significant Eu anomalies and REE abundances less than 10 times chondritic values. Again, errors are likely to be present for the Gd, Er, and Ho data for these two samples as can be seen from data in Appendix B.

**Insch and Boganclogh**

Chondrite normalised spider diagrams for the Insch and Boganclogh intrusions have been broken down into three groups as discussed in section 5.4.3. Selected Trend 1 samples are shown in figure 5.19. As seen previously, some samples from Trend 1 appears to have undergone a large degree of fractionation, and accordingly, the representative samples have a large range of normalized values, many differing by up to an order of magnitude. The samples with lowest abundances, represented here by sample MS1595, an olivine-biotite-norite from Boganclogh have close similarities in shape to many of the samples from the northeastern bodies, particularly Arnage, with gently sloping spider patterns seen, punctuated by a Nb-trough and variable Ba/Rb ratios. Further up the fractionation sequence (mg#s of 39.3 - 16.9), 'spiders' are characterized by higher abundances for many elements, especially the REE, while irregular LIL element ratios and possible LILE depletion are seen; Nb/La ratios <1 suggest the Nb-trough is probably still present, but obscured by these low LILE abundances.

Samples from the end of the fractionation sequence (mg# <5) show quite the opposite trend, with decreases in the abundances of the REE and extreme enrichment in Zr and the LILE. Normalized Nb abundances are among the lowest seen in the Central Intrusions, resulting in very large Nb-troughs. REE plots of the data (Figure 5.20) show a similar trend as the spider diagrams, with smooth plots, with slight LREE flattening, as with the northeastern

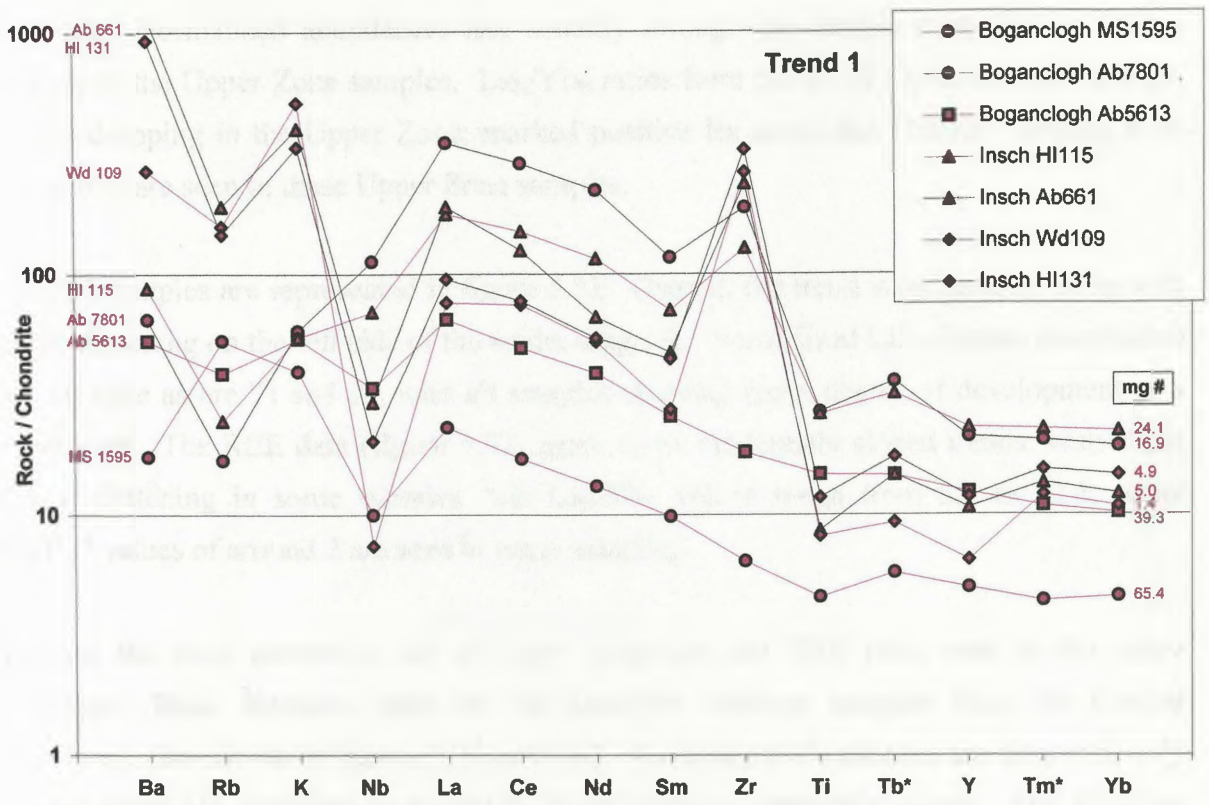


**Figure 5.19 Chondrite normalized spider diagram with selected Trend 1 samples from the Insch and Boganclogh intrusions**

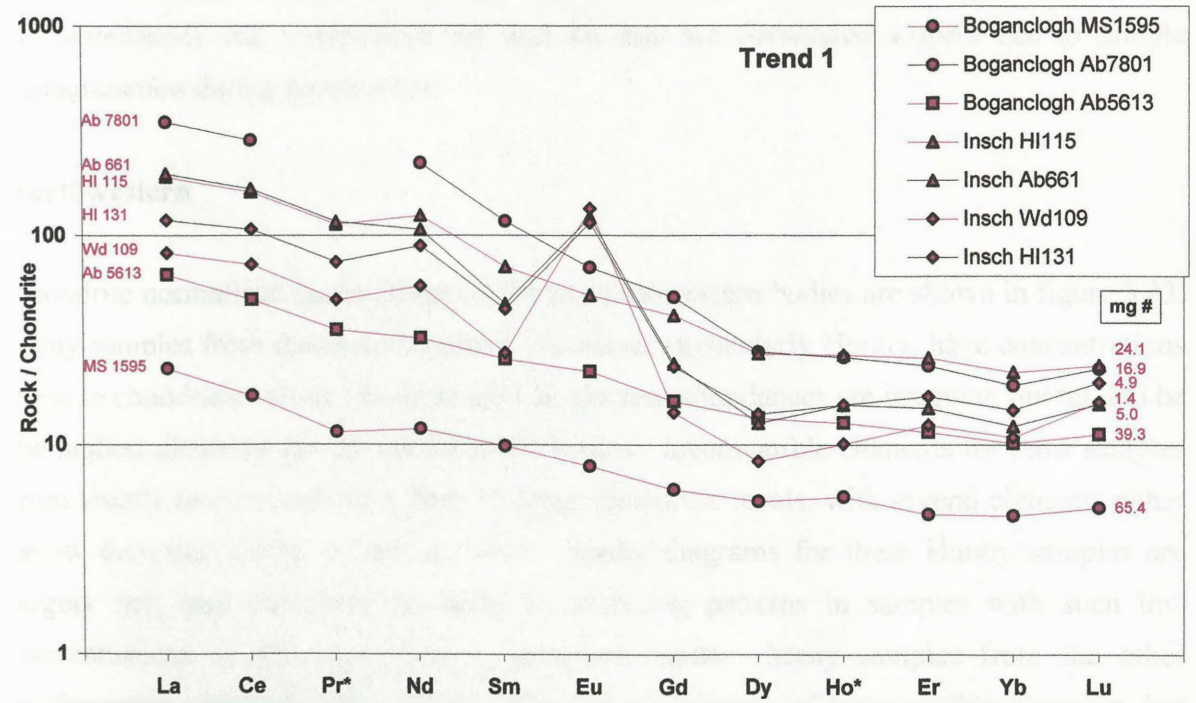


**Figure 5.20 REE plot of Trend 1 samples from the Insch and Boganclogh intrusions**

samples. Normalized abundances rise steadily through the sample range before falling sharply in the Upper Zone samples. $La_N/Yb_N$ ratios from 5.0 to 18.1 with decreasing mg#, before dropping in the Upper Zone; marked positive Eu anomalies (Eu/Eu* ranging from 3.6 to 6.9) are seen in these Upper Zone samples.

Trend 2 samples are represented in figure 5.21. Overall, the trend is moderately steep with slight flattening on the left side of the spider diagram. Normalized LIL element abundances are variable as are Ti and Zr, with all samples showing some degree of development of a Nb-trough. The REE data (figure 5.22) again show moderately sloped trends, with slight LREE flattening in some samples, and $La_N/Yb_N$ values range from 8.7 to 32.1, while Eu/Eu* values of around 2 are seen in some samples.

Perhaps the most distinctive set of spider diagrams and REE plots seen in the entire 'Younger' Basic intrusive suite are the Granular Gabbros samples from the Central Intrusions, also shown in figures 5.21 and 5.22. Normalized abundances are low, with only Ti and some LIL elements occasionally above 10 times chondritic values. The Granular Gabbros are very well clustered, with only slight Nb-troughs and Sr (not shown) and Ti peaks. In figure 5.22, the Granular Gabbros can be seen to have flat REE patterns ($La_N/Yb_N$ = 1.4-2.7) and consistently positive Eu anomalies (Eu/Eu* = 1.7-2.7). Again, Gd, Er and Ho abundances and interpolated Tm and Tb data are considered suspect due to sample contamination during preparation.

**Northwestern**

Chondrite normalised spider diagrams for the northwestern bodies are shown in figure 5.23. Many samples from these northwestern intrusions, particularly Huntly, have concentrations close to chondritic values. Normalized LIL element abundances are irregular, but tend to be the highest elements for the northwestern bodies. Incompatible elements for most samples from Huntly rarely reach more than 10 times chondritic levels, with several elements either below detection limits, or not analysed. Spider diagrams for these Huntly samples are largely flat, and care must be taken in analysing patterns in samples with such low concentrations as they are close to detection limits. Many samples from the other northwestern intrusions also contain quite low abundances of incompatible elements, but some samples with sufficiently high abundances are also found. These normalized abundances are generally in the range of 4 - 40, with LILE, Zr and Ti abundances and ratios quite variable. Again, most of these spiders display rather flat patterns with perhaps slight

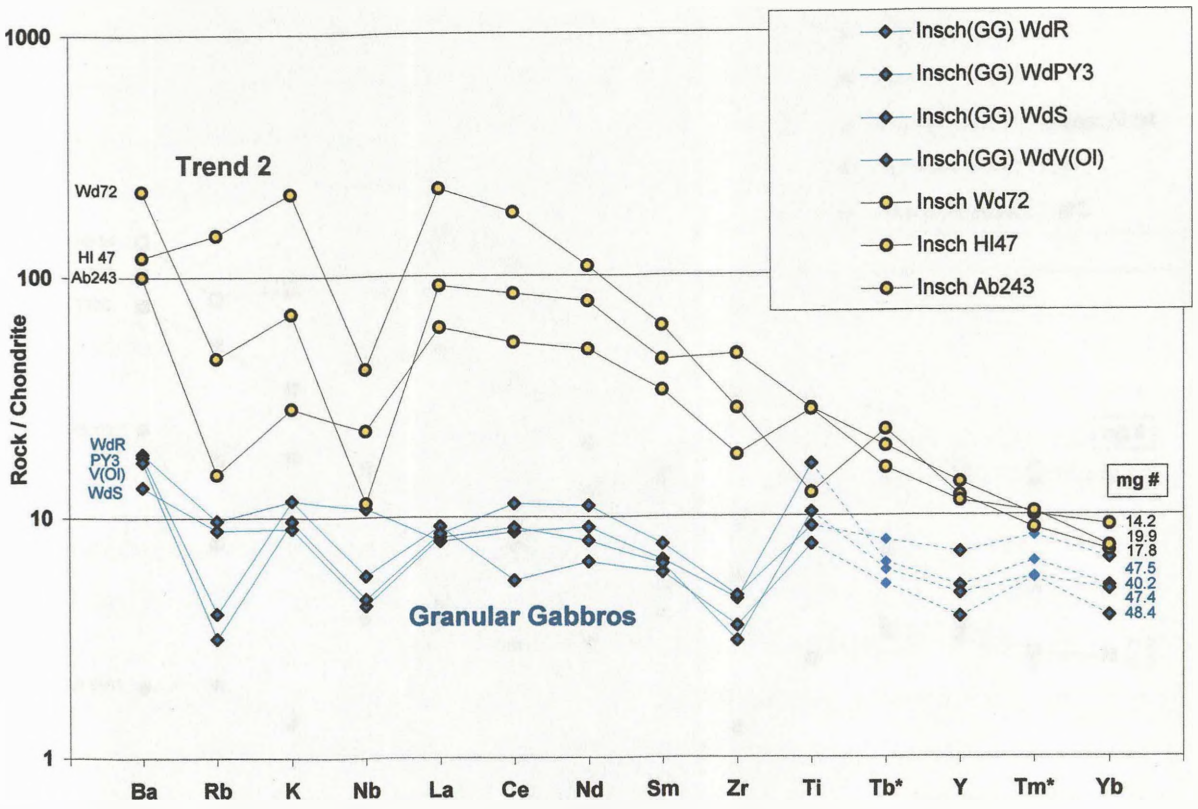


**Figure 5.21 Chondrite normalized spider diagram of Trend 2 and Granular Gabbro samples from the Insch and Boganclogh intrusions. Interpolated Tb and Tm data for Granular Gabbros samples are likely to be too high as a result of sample contamination.**

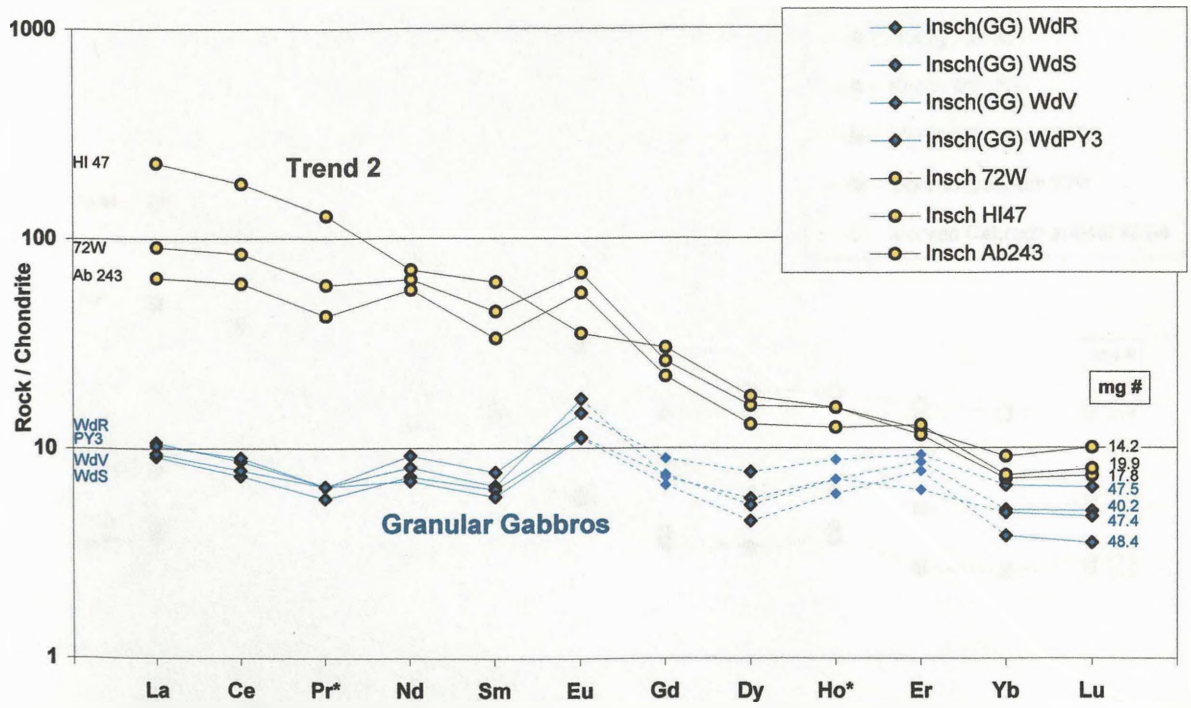


**Figure 5.22 Chondrite normalized REE plots of Trend 2 and Granular Gabbro samples from the Insch and Boganclogh masses. Gd, Ho and Er data for the Granular Gabbros samples are likely to be too high due to sample contamination.**

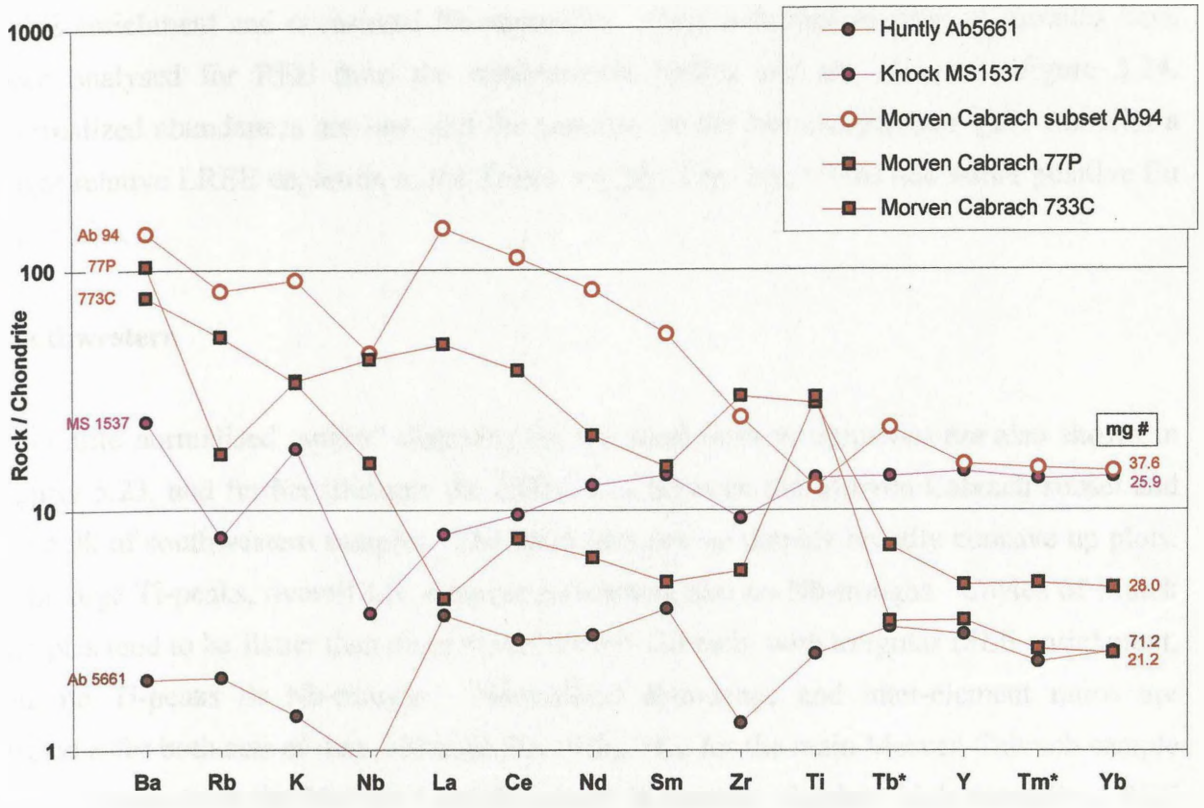


**Figure 5.23 Chondrite normalized spider diagram with selected samples from the northwestern and southwestern intrusions**

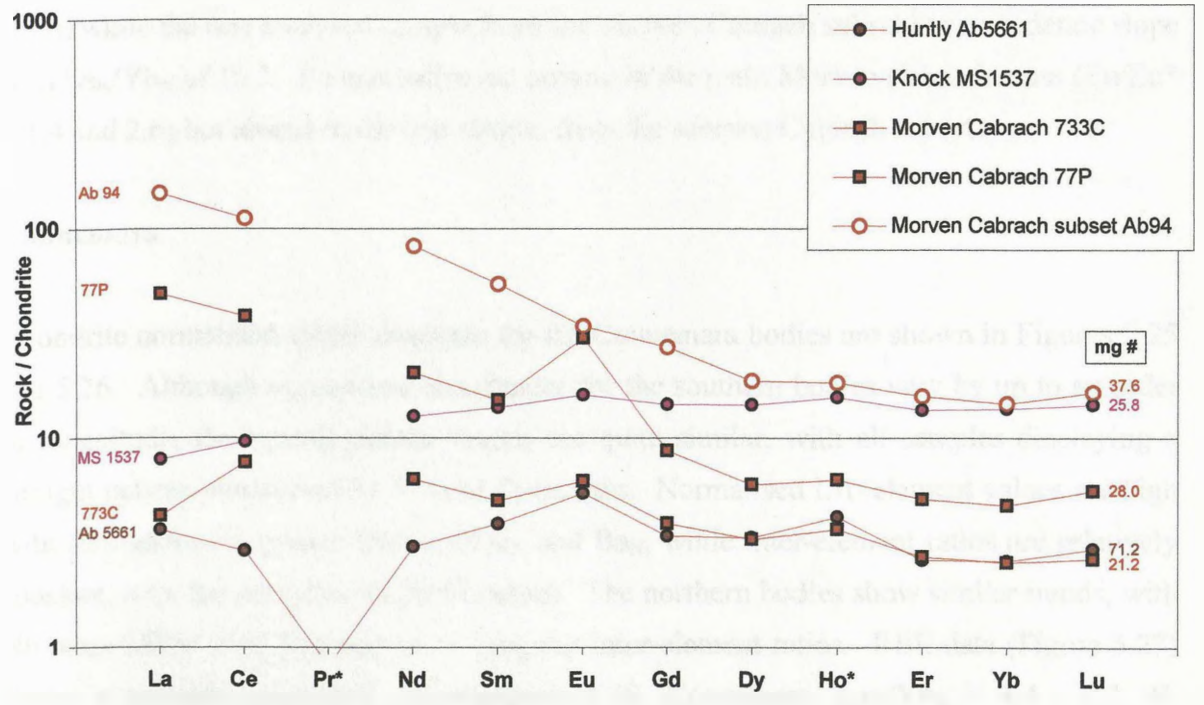


**Figure 5.24 REE plot of samples from the northwestern and southwestern intrusions**

LILE enrichment and occasional Nb-anomalies. Only a limited number of samples have been analysed for REE from the northwestern bodies and are shown in figure 5.24. Normalized abundances are low, and the patterns for the two samples are quite flat with a slight relative LREE depletion in the Knock sample ($La_N/Yb_N$ = 0.6) and minor positive Eu anomalies.

**Southwestern**

Chondrite normalised 'spider' diagrams for the southwestern intrusions are also shown in figures 5.23, and further illustrate the differences between the Morven Cabrach subset and the bulk of southwestern samples. The main samples set display broadly concave up plots, with large Ti-peaks, overall LIL element enrichment and no Nb-troughs. Coyles of Muick samples tend to be flatter than those from Morven Cabrach, with irregular LILE enrichment, and no Ti-peaks or Nb-troughs. Normalized abundance and inter-element ratios are irregular for both sets of data, although $Ba_N > Rb_N > K_N$ for the main Morven Cabrach sample set. Samples from the Morven Cabrach subset, in contrast, displays high normalised REE values with a concave upward spider plot, pronounced Nb-troughs and slight flattening at the LILE end. Again a limited number of REE analyses are available (Figure 5.24) and show shallow to flat slopes for the main Morven Cabrach samples ($La_N/Yb_N$ = 1.7 and 10.3), while the one analysed sample from the Morven Cabrach subset has a moderate slope with $La_N/Yb_N$ of 10.2. Eu anomalies are present in the main Morven Cabrach mass (Eu/Eu* = 1.4 and 2.6) but absent in the one sample from the Morven Cabrach subset.

**Connemara**

Chondrite normalised spider diagrams for the Connemara bodies are shown in Figures 5 25 and 5.26. Although normalized abundances for the southern bodies vary by up to an order of magnitude, the overall pattern shapes are quite similar, with all samples displaying a straight pattern punctuated by Nb-and Zr-troughs. Normalised LIL element values are high with $Rb_N$ generally greater than both $K_N$ and $Ba_N$, while inter-element ratios are relatively constant, with the exception of Zr/Ti values. The northern bodies show similar trends, with Nb often below detection and more irregular inter-element ratios. REE data (Figure 5.27) shows a smooth, moderately sloping pattern (S. Connemara: $La_N/Yb_N$ = 4.4 - 9.2; N. Connemara: $La_N/Yb_N$ = 2.7-3.9), again with slight flattening at the LREE end, while Eu anomalies are negligible (Eu/Eu* = 0.8-1.1).

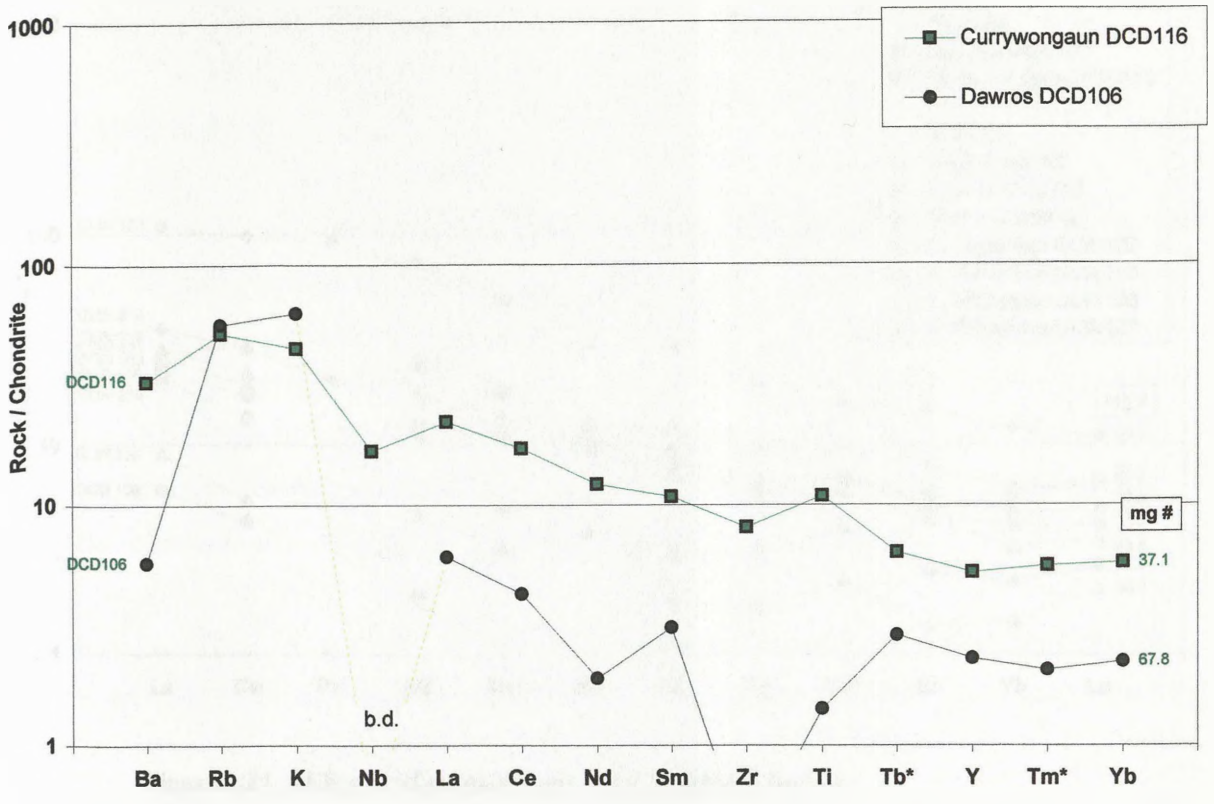


**Figure 5.25 Chondrite normalized spider diagram with selected samples from North Connemara (b.d. : below detection)**

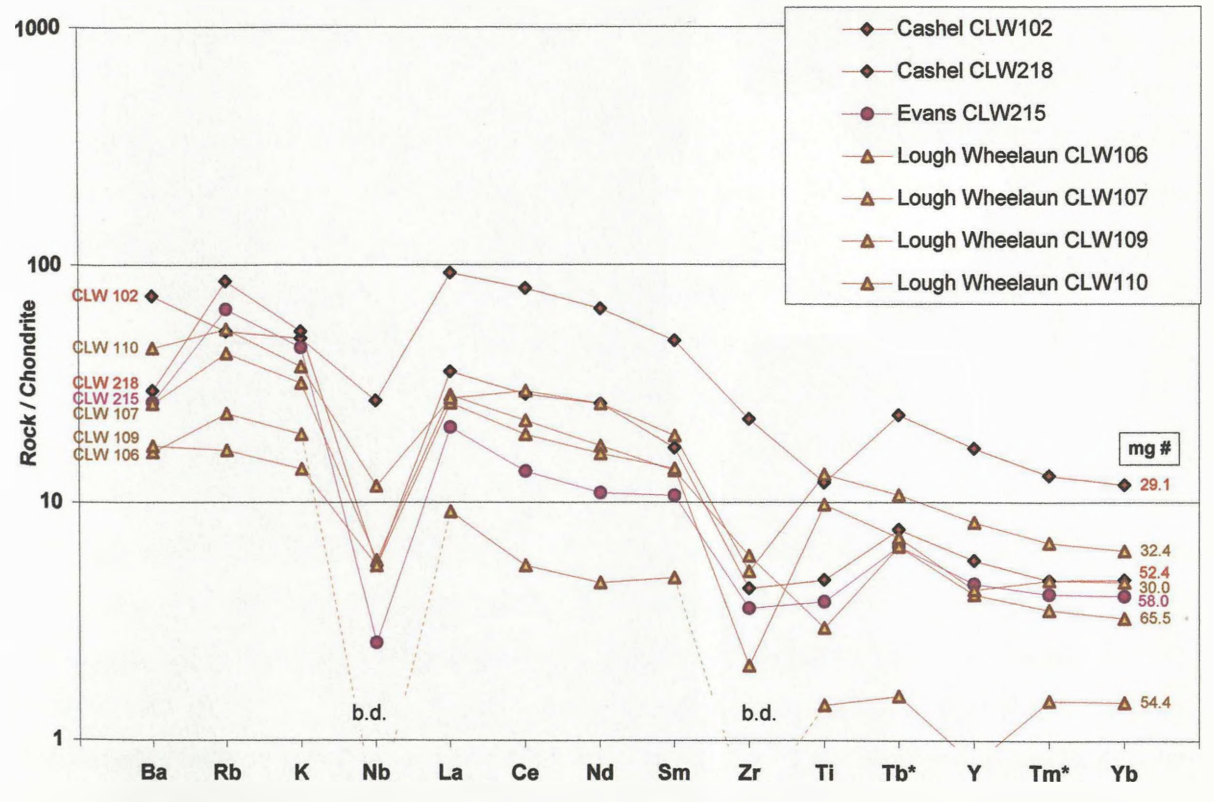


**Figure 5.26 Chondrite normalized spider diagram with selected samples from South Connemara (b.d. : below detection)**

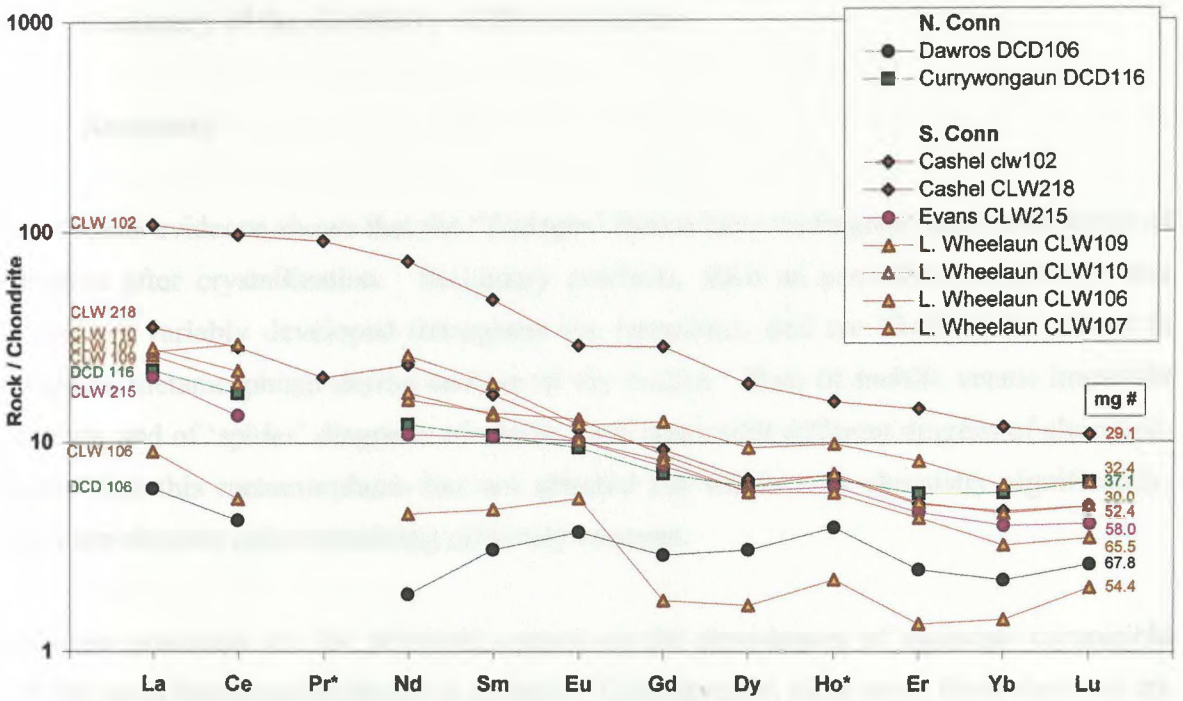


**Figure 5.27 REE plot of samples from the Connemara bodies**

## 5.5 Summary of the chemistry of the intrusions

## 5.5 Summary

Thin section evidence shows that the 'Younger' Basics have undergone significant levels of alteration after crystallization. Secondary products, such as serpentine, amphibole and sericite are variably developed throughout the intrusions, and are likely to be related to retrograde metamorphism during cooling of the bodies. Plots of mobile versus immobile elements, and of 'spider' diagrams of similar rock types with different degrees of alteration, suggest that this metamorphism has not affected the whole rock chemistry significantly, with inter-element ratios remaining relatively constant.

Cumulate processes are the principal control on the abundances of elements compatible with the main fractionating phases in samples. Consequently, plots using these elements are likely to have poorly defined trends with considerable scatter. Elements incompatible with cumulate phases are likely to be concentrated in postcumulus or interstitial phases. The absolute abundances of these elements are controlled by cumulate processes, but their abundances relative to each other are controlled by their relative abundances in the magma at the time of crystallisation.

Whole rock mg# has been chosen as a fractionation index. The effects of cumulus processes on mg# are less than other possible indices and as a result it defines trends seen in the data most clearly. Comparison of the whole rock mg# with the mg# of fractionating ferromagnesian phases suggests that it is an adequate substitute for an index based on stratigraphic height or the mg# of a selected ferromagnesian phase.

**Major element chemistry**

Although scatter is considerable, trends can be seen for most of the individual groupings and for the 'Younger' Basics as a whole. The majority of samples from all groups plot as sub-alkalic gabbros on a TAS plot, with only slight enrichment in $SiO_2$ and ($Na_2O + K_2O$) evident. One exception is a set of samples from Insch and Boganclogh, which show strong enrichment in both alkalis and $SiO_2$, and are syeno-dioritic to syenitic in composition. The Granular Gabbros also plot as sub-alkalic gabbros, forming a well-defined cluster within the overall trend for Insch and Boganclogh and the suite as a whole. AFM plots show tholeiitic-type Fe-enrichment for samples from all groups, with only samples from Insch

and Boganclogh showing subsequent alkali-enrichment. The Granular Gabbros and a minor subset from the Morven Cabrach intrusion show slightly different trends, with little or no Fe-enrichment. Normative di-ol-hy plots show considerable scatter as expected, but broad olivine- to quartz-normative trends are observed; this is particularly well defined for the Granular Gabbros. Samples from the northeastern bodies and the Morven Cabrach subset all plot as quartz-normative.

Plots of major elements against the fractionation index, mg#, show that trends within the individual groups are all quite similar, but display minor variations. Plots such as $P_2O_5$ and $TiO_2$ show gradual rises with decreasing mg# with inflection points at lower mg# values of ~ 20. $SiO_2$, $Fe_2O_3$, MnO, $K_2O$ and $Na_2O$ show gradual rises in content with decreasing mg# in all groups, although scatter is considerable, while CaO and $Al_2O_3$ show sharp rises at high mg#'s followed by gradual decreases with decreasing mg#. Samples from the Connemara bodies show the greatest variation, particularly for $Na_2O$, which is consistently lower, and $K_2O$, which is consistently higher than for the other groups. Very low mg# samples (<5) from the Central Intrusions show strong variations from Central Intrusions samples with higher mg# values (>15), including high $SiO_2$, $K_2O$, and low $Al_2O_3$, $Fe_2O_3$ and $P_2O_5$. The Granular Gabbro and Morven Cabrach subsets occur over a limited mg# range and the abundances and possible fractionation trends seen in these subsets are inconsistent with trends seen in the host intrusions for several elements; in particular, $Al_2O_3$, $Fe_2O_3$, $Na_2O$ and MnO for the Granular Gabbros and $SiO_2$ and $K_2O$ for the Morven Cabrach subset.

**Trace element chemistry**

Plots of trace elements against mg# show similar properties to the major element plots, with clear compatible element trends evident for Ni and Cr. Negative trends are evident for the incompatible elements Zn, Sc, Zr, Ba and Nb while more scattered negative trends are evident for the REE and Y. Vanadium displays a negative trend with a crude inflection point at mg# of 20 - 30, while the trends for Rb and Sr are less clear. Samples from the Connemara bodies show variation from the Grampian Highlands groups, with higher abundances of Rb, Sr and Sc over much of the mg# range. Again the Granular Gabbros and Morven Cabrach subset do not fit into fractionation trends seen within the main Central Intrusions and main Morven Cabrach trends, notably for Ni and Cr for the Granular Gabbros, and Zr, Rb and the REE for the Morven Cabrach subset.

Three separate fractionation trends are recognised within the Insch and Boganclogh bodies. In addition to the Granular Gabbros, the main cumulate sequence displays two slightly differing trends. The differences between these two trends are most clearly seen on plots of mg# versus certain incompatible trace element elements, such as Zr and the REE.

For the majority of samples from across the groups, 'spider' plots show consistently high LILE abundances, variable Sr, Ba, Ti and Zr contents and variable resultant inter-element ratios. Typically, samples contain a Nb-trough, consistent LREE abundances and slopes are generally straight with a slight flattening to the left of the pattern. Patterns from the Central Intrusions show the greatest variation, with Trend 1 samples varying considerably in normalized abundances, shape and inter-element ratios. The Granular Gabbros also display distinctive flat spider plots, with lower LILE and LREE abundances than for samples from the remainder of the Insch mass. REE data presents a similar picture, with smooth slopes ($La_N/Yb_N$ values generally between 5.0 and 10.0), also with slight flattening at the LREE end, and minor, usually positive Eu anomalies (Eu/Eu* values generally between 0.8 and 1.8). Again, the Granular Gabbros have distinctly different plots with flat slopes ($La_N/Yb_N$ values generally between 1.4 and 2.7) and positive Eu anomalies (Eu/Eu* = 1.7 to 2.7).

# Chapter 6 Origin and evolution of the bodies

## 6.1 Introduction

This chapter will examine the evolution of the 'Younger' Basics of northeastern Scotland and Connemara focusing on potential source rocks and on the evolution of the bodies by fractionation and country rock contamination. The Granular Gabbros from the eastern part of the Insch body are assessed as a potential parental magma source, and the relationship between the Granular Gabbros and the main cumulate sequence considered. The evolution of the intrusive suite as a whole is then examined, attempting to explain the trends seen in the major and trace element by fractionation of the phases discussed in Chapter 4. Finally AFC (assimilation and fractional crystallisation) processes are modelled for selected fractionation trends within the central and northeastern bodies.

## 6.2 The Granular Gabbros as parental magmas to the 'Younger' Basics?

### 6.2.1 Introduction

The role of the Granular Gabbros within the origin and evolution of the Insch and Boganclogh masses has been discussed in the literature and there are several lines of evidence to suggest that they may represent a composition approximating to a parental magma. However, some of the evidence, especially field evidence, is conflicting, and a number of other origins for the Granular Gabbros have also been proposed. Evidence from this study is largely geochemical, and favours the theory that the Granular Gabbros are similar in composition to the likely parental magmas.

Whittle (1936) was the first to discuss the possible origins of the Granular Gabbros, believing them to be older than the main Insch and Boganclogh mass, and metamorphosed by it during its intrusion. The idea of the Granular Gabbros as a potential parental magma was first proposed by Read & Haq (1963) and Read *et al.* (1965). They noted strong similarities between the composition of the parental magma proposed for the Skaergaard intrusion by Wager & Mitchell (1951), and their own geochemical data on the Granular Gabbros. They did not, however, believe that the Granular Gabbros, which they termed the *fine-grained granular hypersthene-gabbros* as part of a larger 'hypersthene-gabbro' suite,

were the parental magmas to the Insch and Boganclogh masses. They could not find any position for this 'hypersthene-gabbro' suite within the dunite to syenite fractionation sequence seen within the Insch and Boganclogh bodies as a whole, believing a separate set of olivine gabbros to be the parental material. Due to the presence of hypersthene, they suggested that the Granular Gabbros were contaminated at depth prior to emplacement and that their emplacement post-dated consolidation of the main Insch mass. They did however propose that the parent magma before this contamination might have resembled the source for the main Insch and Boganclogh series. Rb/Sr isotope work (Pankhurst, 1969), conversely, suggests that the 'fine-grained olivine-gabbros' are in fact the least contaminated rock type found in the Insch body. Although substantial levels of contamination, revealed by high $^{87}Sr/^{86}Sr$ ratios, are found within the Insch mass as a whole, initial $^{87}Sr/^{86}Sr$ ratios as low as 0.703 were obtained from the Granular Gabbros. These $^{87}Sr/^{86}Sr$ ratios, which are comparable to those of mantle derived magmas, are even lower than the values found in peridotites samples from the Lower Zone (see figure 6.1), appearing to rule out the role of contamination prior to emplacement. Pankhurst suggested these low $^{87}Sr/^{86}Sr$ ratios might represent an influx of fresh magma with low initial $^{87}Sr/^{86}Sr$ ratios during the crystallisation of the sequence as a whole.

Clarke & Wadsworth (1970) also proposed that the Granular Gabbros might be similar in composition to the parent magma of the intrusion. They recognised the main coarse-grained cumulate 'hypersthene-gabbro' suite of Read *et al.* (1961, 1965) as being a fundamental part of the overall Insch series while considering that, despite a complex field relationship with this coarse-grained hypersthene-gabbro, the fine-grained hypersthene-gabbro, and associated fine-grained olivine-hypersthene-gabbro, were 'probably not of close genetic significance'. They concluded, on field and textural evidence that the Granular Gabbros were most likely to represent a later intrusion, emplaced after solidification of the main Middle Zone 'hypersthene-gabbro' cumulates, thus explaining the closely mixed nature of the two rocks, while attributing the fine granular texture to chilling during emplacement. Their chemical data on 4 Granular Gabbros samples (Table 6.1) led them to believe the olivine-bearing Granular Gabbros were slightly more primitive than their hypersthene-bearing equivalents, and that these olivine-bearing Granular Gabbros gave the best available estimate of the parent magma, also noting it similarities to the source materials of other layered intrusions (Wager & Brown, 1968).

Thy & Esbensen (1982) expressed caution in the interpretation of fine-grained granular rocks as chilled magmas, particularly when found occurring internally in coarse-grained,

| | V(Ol) | S | PY2(Ol) | R | DV1 | PY3 | *avGG* (n=6) | 64067 | 40 | 13 | 161 | 5f | 1 | 2 | 3 | 4 | 5 | 2a | 4h | HR72 | TM52CP1 | TM51 | 1357* | TM47 |
|---|---|---|---|---|---|---|---|---|---|---|---|---|---|---|---|---|---|---|---|---|---|---|---|---|
| SiO2 | 48.76 | 50.14 | 47.92 | 50.06 | 47.41 | 47.39 | 48.61 | 47.66 | 48.10 | 51.55 | 46.71 | 45.44 | 47.15 | 47.42 | 46.70 | 47.09 | 48.00 | 47.71 | 49.19 | 49.97 | 51.88 | 48.39 | 49.62 | 48.94 |
| TiO2 | 0.938 | 1.071 | 1.106 | 1.694 | 0.883 | 0.789 | 1.080 | 1.160 | 2.20 | 1.280 | 1.640 | 1.970 | 1.21 | 1.10 | 1.01 | 1.11 | 1.63 | 0.67 | 1.83 | 0.48 | 0.42 | 1.21 | 1.60 | 2.50 |
| Al2O3 | 16.58 | 15.71 | 16.38 | 15.68 | 21.26 | 22.93 | 18.09 | 16.97 | 17.30 | 17.17 | 17.23 | 15.78 | 17.56 | 17.10 | 18.03 | 17.56 | 16.62 | 17.94 | 16.52 | 17.26 | 16.37 | 17.27 | 17.19 | 18.20 |
| Fe2O3 | | | | | | | | | 1.80 | 1.36 | 1.81 | 2.38 | 1.46 | 2.44 | 1.78 | 1.89 | 2.09 | 1.50 | 1.02 | | | | | |
| FeO | | | | | | | | | 9.00 | 8.03 | 8.16 | 8.46 | 7.60 | 6.90 | 7.53 | 7.34 | 9.73 | 7.26 | 10.75 | | | | | |
| Fe2O3' | 10.25 | 10.00 | 10.42 | 10.87 | 7.52 | 6.52 | 9.26 | 10.25 | | | | | | | | | | | | | | | | |
| MnO | 0.163 | 0.170 | 0.155 | 0.185 | 0.109 | 0.095 | 0.150 | 0.160 | 0.18 | 0.170 | 0.170 | 0.180 | 0.15 | 0.15 | 0.19 | 0.16 | 0.23 | 0.14 | 0.14 | 8.47 | 7.01 | 8.98 | 10.87 | 10.64 |
| MgO | 9.29 | 9.01 | 9.27 | 7.31 | 6.87 | 6.11 | 7.98 | 9.60 | 8.50 | 8.70 | 6.90 | 10.02 | 9.76 | 8.68 | 9.53 | 9.32 | 7.50 | 11.57 | 7.38 | 0.17 | 0.16 | 0.19 | 0.19 | 0.23 |
| CaO | 12.11 | 12.22 | 12.46 | 11.85 | 13.69 | 14.19 | 12.75 | 12.45 | 9.00 | 9.00 | 13.11 | 12.62 | 12.41 | 12.30 | 12.33 | 12.35 | 11.34 | 9.39 | 9.45 | 9.44 | 8.21 | 10.78 | 10.29 | 7.66 |
| Na2O | 1.76 | 1.49 | 1.69 | 1.77 | 1.77 | 1.81 | 1.72 | 2.00 | 2.60 | 2.71 | 2.55 | 1.99 | 2.10 | 2.09 | 2.00 | 2.06 | 2.07 | 1.99 | 2.12 | 11.87 | 11.08 | 12.09 | 10.52 | 10.22 |
| K2O | 0.12 | 0.11 | 0.12 | 0.14 | 0.12 | 0.14 | 0.13 | 0.13 | 0.30 | 0.68 | 0.15 | 0.15 | 0.18 | 0.18 | 0.11 | 0.16 | 0.15 | 0.47 | 0.11 | 2.03 | 1.91 | 1.77 | 1.90 | 1.50 |
| P2O5 | *0.015* | *0.009* | *0.011* | *0.012* | *0.027* | *0.015* | *0.010* | 0.100 | 0.06 | 0.130 | 0.070 | 0.070 | 0.01 | 0.01 | 0.16 | 0.06 | 0.10 | 0.08 | 0.21 | 0.04 | 0.05 | 0.00 | 0.17 | 0.08 |
| H2O | | | | | | | | | 0.33 | 0.470 | 0.620 | 0.970 | 0.76 | 1.17 | 0.83 | 0.92 | 0.54 | 0.76 | 1.34 | 0.00 | 0.00 | 0.00 | 0.05 | 0.04 |
| LOI | | | | | | | | | | | | | | | | | | | | 0.50 | 0.41 | 0.25 | 0.00 | 0.06 |
| mg# | 0.09 | 0.52 | 0.05 | 0.32 | 0.16 | 0.23 | 0.23 | | | | | | | | | | | | | | | | | |
| cationic mg# | 47.54 | 47.40 | 47.08 | 40.21 | 47.74 | 48.38 | 46.29 | 48.36 | 41.87 | 45.83 | 38.81 | 45.96 | 49.63 | 46.20 | 48.43 | 48.12 | 36.76 | 54.73 | 36.27 | 52.71 | 53.94 | 54.55 | 48.63 | 41.86 |
| Ba | 67.87 | 67.74 | 67.46 | 61.05 | 68.04 | 68.59 | 66.76 | 68.58 | 62.73 | 65.88 | 60.11 | 67.86 | 69.59 | 69.16 | 69.28 | 69.35 | 57.87 | 73.96 | 55.03 | 72.2 | 73.18 | 73.67 | 68.81 | 62.65 |
| Rb | 118.0 | 92.6 | 165.7 | 127.4 | 62.2 | 124.1 | 115.0 | 140.0 | 110 | 388.0 | 170.0 | 162.0 | | | | | 100 | 120 | 90 | | | | | |
| Sr | 1.1 | 3.1 | 0.8 | 3.4 | 1.3 | 1.4 | 1.9 | 2.8 | | | | | | | | | | 7 | 3 | | 0 | | 0 | 0 |
| Y | 265.2 | 260.9 | 263.7 | 325.7 | 345.6 | 355.4 | 302.8 | 257.0 | 300 | 293.0 | 246.0 | 287.0 | | | | | 300 | 242 | 260 | | 207 | | 232 | 246 |
| Zr | 14.1 | 9.5 | 12.8 | 10.2 | 9.6 | 7.6 | 10.6 | 13.0 | | | | | | | | | | | | | | | | |
| Nb | 32.0 | 20.8 | 40.2 | 31.1 | 22.8 | 24.0 | 28.5 | 42.0 | 47 | 430.0 | 44.0 | 53.0 | | | | | | | | | | | | |
| Zn | 1.6 | 1.5 | 2.1 | 3.8 | 2.5 | 2.0 | 2.3 | 1.5 | | | | | | | | | | | | | | | | |
| Cu | 60.7 | 62.8 | 55.3 | 72.4 | 40.1 | 35.0 | 54.4 | 59.0 | | | | | | | | | | | | | | | | |
| Ni | 59.3 | 20.1 | 56.6 | 16.3 | 41.2 | 34.8 | 38.1 | 53.0 | 10 | 48.0 | 75.0 | 95.0 | | | | | | | | | | | 77 | |
| Cr | 101.3 | 15.4 | 89.8 | 17.3 | 61.8 | 54.3 | 56.7 | 86.0 | 48 | 81.0 | 144.0 | 162.0 | | | | | | | | 6 | 0 | 7 | 14 | 7 |
| V | 291.0 | 393.5 | 256.3 | 63.0 | 165.1 | 174.5 | 223.9 | 273.0 | 70 | 445.0 | 395.0 | 490.0 | | | | | | | | | 2 | 25 | 11 | 6 |
| Sc | 198.8 | 249.3 | 174.3 | 264.2 | 140.5 | 109.3 | 189.4 | | 300 | 199.0 | 189.0 | 258.0 | | | | | | | | | 154 | 352 | 179 | 167 |
| Co | 38.8 | 42.5 | 34.2 | 46.8 | 25.3 | 22.0 | 34.9 | | | | | | | | | | | | | | 244 | 225 | 196 | 253 |
| Li | | | | | | | | | 55 | | | | | | | | | | | | | | | |
| Pb | | | | | | | | | | | | | | | | | | | | 42 | 39 | 46 | 32 | 32 |
| U | | | | | | | | 4 | | | | | | | | | | | | | | | | |
| Th | | | | | | | | <0.04 | | | | | | | | | | | | | | | | |
| Ta | | | | | | | | 0.02 | | | | | | | | | | | | | | | | |
| Hf | | | | | | | | | | | | | | | | | | | | | | | | |
| La | | | | | | | | 1.06 | | | | | | | | | | | | | | | | |
| Ce | | | | | | | | | | | | | | | | | | | | | | | | |
| Pr | 3.1 | 3.0 | 3.7 | 3.5 | 2.7 | 3.4 | 3.2 | 2.9 | | | | | | | | | | | | | | | | |
| Nd | 6.8 | 6.4 | 7.5 | 7.5 | 6.8 | 7.8 | 7.1 | 5.6 | | | | | | | | | | | | | | | | |
| Sm | 0.8 | 0.7 | | 0.8 | | 0.8 | 0.8 | 0.9 | | | | | | | | | | | | | | | | |
| Eu | 5.8 | 4.6 | 4.3 | 5.1 | 5.1 | 4.4 | 3.7 | 5.9 | | | | | | | | | | | | | | | | |
| Gd | 1.56 | 1.29 | | 1.34 | | 1.19 | 1.35 | 1.91 | | | | | | | | | | | | | | | | |
| Dy | 1.13 | 0.87 | | 1.32 | | 0.86 | 1.05 | 0.99 | | | | | | | | | | | | | | | | |
| Ho | *2.47* | *2.07* | | *2.01* | | *1.84* | *2.10* | 2.05 | | | | | | | | | | | | | | | | |
| Er | 2.64 | 1.84 | | 1.98 | | 1.54 | 2.00 | 2.16 | | | | | | | | | | | | | | | | |
| Yb | 0.67 | *0.54* | | *0.54* | | *0.46* | *0.55* | 0.42 | | | | | | | | | | | | | | | | |
| Lu | *2.09* | *1.42* | | *1.93* | | *1.75* | *1.80* | | | | | | | | | | | | | | | | | |
| Tb | 1.46 | 1.08 | | 1.12 | | 0.84 | 1.13 | 1.16 | | | | | | | | | | | | | | | | |
| Tm | 0.22 | 0.16 | | 0.17 | | 0.12 | 0.17 | 0.17 | | | | | | | | | | | | | | | | |
| | *0.41** | *0.32** | | *0.31** | | *0.27** | *0.33** | 0.37* | | | | | | | | | | | | | | | | |
| | *0.26** | *0.19** | | *0.25** | | *0.22** | *0.23** | 0.19* | | | | | | | | | | | | | | | | |

* Tm and Tb data interpolated from REE data

| | |
|---|---|
| **V(Ol)**, **S**, **PY2(Ol)**, **R**, **DV1**, **PY3** | Granular Gabbros, Insch |
| ***avGG* (n=6)** | Average of 6 Granular Gabbro samples, Insch (n=4 for REE data) |
| **64067** | Fine grained gabbro, Insch (Thompson et al., 1984) |
| **40** | Hypersthene Gabbro, Insch (Read, Sadashivaiah & Haq, 1965) |
| **13** | Granular gabbro, Insch (Hutchinson, 1965) |
| **161** | Ol-bearing granular hypersthene gabbro (Hutchinson, 1965) |
| **5f** | Olivine-pyroxene Granular gabbro (Hutchinson, 1965) |
| **1,2,3** | *Olivine bearing granular gabbro, Insch (Clarke & Wadsworth, 1970)* |
| **4** | Average of analyses 1, 2 & 3 (Clarke & Wadsworth, 1970) |
| **5** | Granular hypersthene gabbro, Insch (Clarke & Wadsworth, 1970) |
| **2a** | Average of 2 Arnage/Haddo House olivine norites (Gribble, 1967) |
| **4h** | Typical Huntly hypersthene gabbro (Weedon, 1970) |
| **HR72**, **TM52CP1**, **TM51**, **1357***, **TM47** | Modified Granular cumulates and granular Gabbronorites from the western area of the Huntly mass (Fletcher, 1989) |

**Table 6.1 Comparison of Insch Granular Gabbro analyses with other published analyses of fine grained gabbros from the 'Younger Basics' from northeastern Scotland. Data containing likely errors are italicized.**

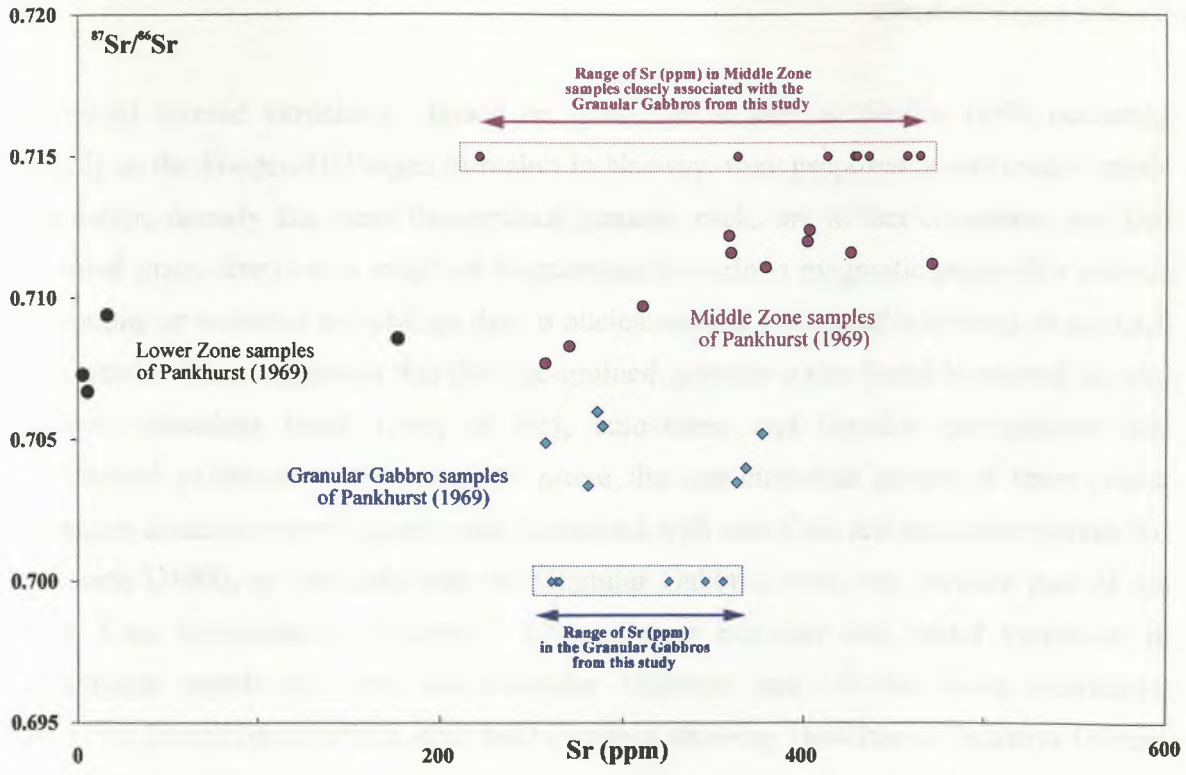


**Figure 6.1 $^{87}Sr/^{86}Sr$ data for samples from the Granular Gabbros and the Middle Zone of Insch (Pankhurst, 1969). Sr data from this study included simply to show that samples sets from this study and that of Pankhurst (1969) fall in the same range of Sr contents.**

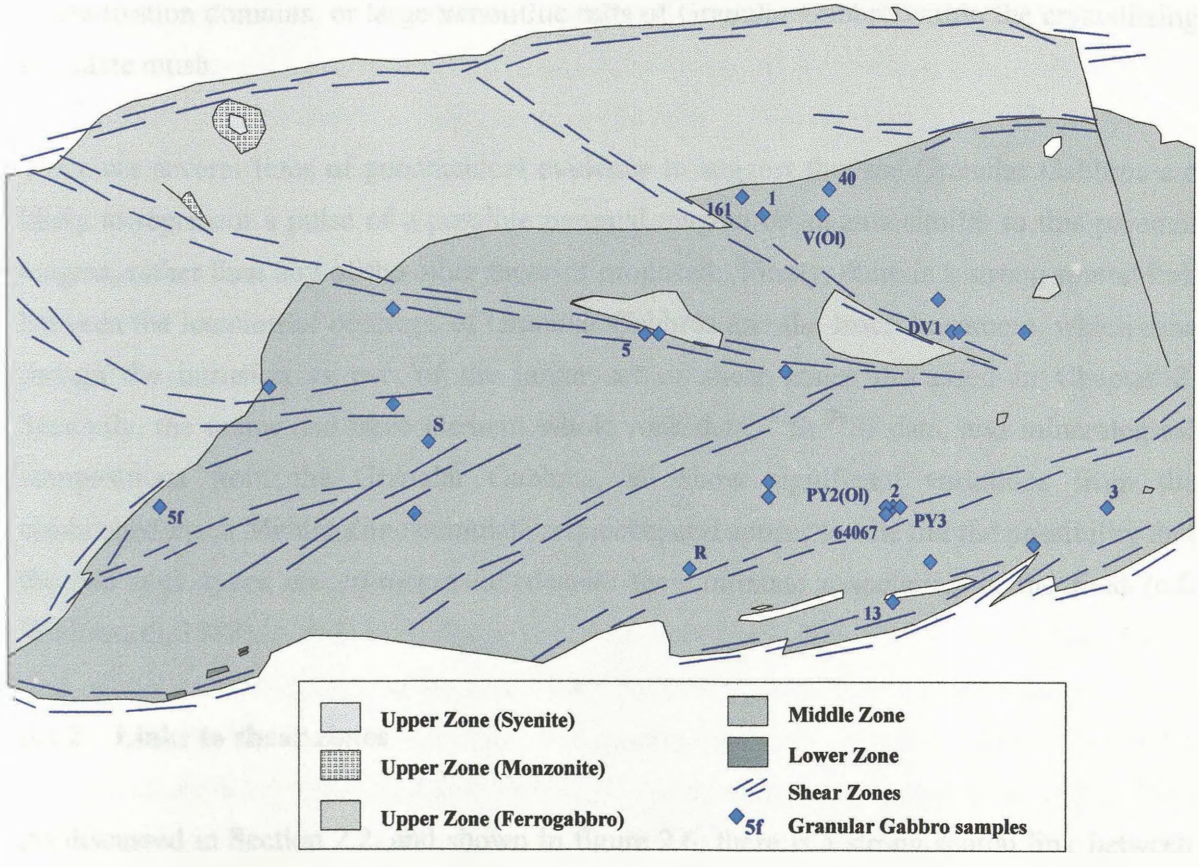


**Figure 6.2 Location of the Granular Gabbro samples in Table 6.1 within the Insch Middle Zone. Additional sample location data from Hutchinson (1965), Ashcroft & Munro (1978), Thompson et al. (1984), and Wadsworth (1988).**

fractionated layered intrusions. Based on grain size studies of similar rocks occurring internally in the Fongen-Hyllingen intrusion in Norway, they proposed an alternative mode of formation, namely that these fine-grained granular rocks are in fact cumulates, and that their small grain size is as a result of fluctuations in various magmatic properties such as supercooling or variation in volatiles due to nucleation and growth of a hydrous phase such as amphibole. They suggested that the fine-grained granular rocks found in several layered intrusions, including Insch were, in fact, cumulates, and detailed petrographic and mineralogical evidence was required to prove the non-cumulate nature of these rocks. Subsequent detailed mineralogical work, combined with new field and textural evidence led Wadsworth (1988), to conclude that the Granular Gabbros were 'an intrinsic part of the Middle Zone fractionation sequence'. Despite poor exposure and minor variations in mineralogical trends between the Granular Gabbros and Middle Zone cumulates, Wadsworth (1988) believed that new field evidence showing xenoliths of Granular Gabbro within these cumulates rocks ruled out the possibility that the Granular Gabbros intruded the cumulates, and that the granular and cumulate rocks were co-magmatic. He proposed that the intricate relationship between the two rock types both in the field and in mineral compositions, might be explained by either large scale block faulting, independent crystallisation domains, or large xenolithic rafts of Granular Gabbro within the crystallising cumulate mush.

There are several lines of geochemical evidence to suggest that the Granular Gabbros are likely to represent a pulse of a possible parental magma or magma similar to this parental magma, rather than any of the other theories proposed. Firstly, there is a strong spatial link between the location of outcrops of Granular Gabbros and the Insch lineament, which runs though the intrusion as part of the larger set of shear zones discussed in Chapter 2. Secondly, the major and trace element whole rock data, $^{87}Sr/^{86}Sr$ data, and mineralogical compositions from the Granular Gabbros, all show significant variations from the established Insch Middle Zone cumulate sequence, and appear to rule out the possibility that the two rock types are co-magmatic, despite their intimate association in the field (c.f. Wadsworth, 1988).

### 6.2.2 Links to shear zones

As discussed in Section 2.2, and shown in figure 2.6, there is a strong spatial link between the shear zones running through the area and the 'Younger' Gabbroic bodies themselves, which are concentrated on, or adjacent to, these shear zones. They were first identified by

Ashcroft *et al.* (1984) and Fettes *et al.* (1986), using a combination of structural and geophysical means and have been recognized as representing long-lived structural lineaments, which may have originated as far back as part of rifted fault systems associated with the late Proterozoic opening of the Iapetus Ocean (Ashcroft *et al.*, 1984; Fettes *et al.*, 1986; Goodman, 1994). Subsequent reactivation as a series of ductile shear zones occurred through the Caledonian Orogeny, during which time it is suggested the 'Younger' Basics exploited the shear zones as conduits for emplacement. Indeed, the idea that the 'Younger' Gabbros, as a whole, used these shear zones as a mode of emplacement has been suggested by several authors (Ashcroft *et al.*, 1984; Fettes *et al.*, 1986; Goodman, 1994), given the obvious spatial link between the shear zones and the majority of the bodies.

These lineaments are also believed to be related to variations in metamorphism (Harte & Hudson, 1979; Harte, 1988; Dempster *et al.*, 1995) and structural style (Ashcroft *et al.*, 1984; Fettes *et al.*, 1986) within the region, with shearing likely to have continued for some time after emplacement on many of these shear zones. In particular, the Portsoy-Duchray Hill lineament is associated with a series of smaller mafic and ultramafic bodies, which are likely to have been emplaced over a significant period of time (Fettes *et al.*, 1986), emphasizing the long-lived nature to these shear zones. Further evidence for this long-lived nature is the internal disruption and marginal shearing of the bodies, with both of these likely to have occurred after consolidation of the bodies. This is quite evident in the case of the Insch mass, which is transected by a lineament known as the Insch Lineament (Ashcroft *et al.*, 1984; Fettes *et al.*, 1986) and an associated series of shear zones. These shear zones have been responsible for extensive marginal shearing and internal disruption of lithological units within the mass (see Section 4.5.2 and figure 4.5), as well as sheared removal of hornfelsed country rocks by distances of up to several kilometres (Stephenson & Gould, 1995).

Figure 6.2 shows the location of shear zones associated with this lineament within the Insch mass as mapped by Ashcroft *et al.* (1984) and Gould (1997), in addition to the locations of Granular Gabbro samples from Table 6.1, with additional samples for which whole rock data is not available, but which have been shown texturally to be granular in nature (Hutchinson, 1965; Wadsworth, 1988). It is apparent that there is a strong link between the location of the shear zones and the Granular Gabbros within the eastern parts of the Insch mass.

This link further strengthens the possibility that the Granular Gabbros represent material emplaced along the shear zones at some stage after the emplacement of the main mass, exploiting the still active nature of the shear zones. The precise timing of this secondary emplacement is unclear; it is likely to be syn- or post-consolidation of the main mass, with the ongoing shearing activity resulting in the complex relationship seen in the field between the Granular Gabbros and the main Middle Zone. The fine-grained nature to the Granular Gabbros might be as a result either of chilling against the consolidated Middle Zone, or of crystallization in an actively shearing environment, although it should be noted that there is little evidence either in the field, or in thin section, for either of these origins. Both of these modes of formation could result in the low $^{87}Sr/^{86}Sr$ ratios for the Granular Gabbros (Pankhurst, 1969), with limited time for the change of these isotopic ratios by contamination. In addition, the complex field relations between the two rock types (Wadsworth, 1988) could perhaps be explained by this type of intrusive mechanism. Emplacement into partly consolidated Middle Zone rocks, while movement on the shear zone continues to take place, would disrupt these initially simple contact relationships, and result in quite complex and probable conflicting field evidence. The absence of shearing in the samples themselves suggests that they may represent the final pulses of magma into the shear zone: when shearing ceased, so too did magma emplacement, resulting in these final pulses not undergoing any subsequent shearing.

### 6.2.3 Chemistry of the Granular Gabbros

If the above is indeed the case, and the Granular Gabbros are, in fact, magmatic pulses that have crystallized relatively quickly, they may represent material originating deeper in the crust or in the mantle. There are several lines of evidence to suggest that these rocks have not fractionated significantly after emplacement, and consequently are likely to be close to their original composition. Table 6.1 shows the 6 Granular Gabbro samples analysed as part of this study compared to other published analyses from the 'Younger' Basics of northeastern Scotland. In addition to the fine-grained hypersthene- and olivine-bearing gabbros of Read *et al.* (1965) and Clarke & Wadsworth, (1970) discussed in the Section 6.2.1, analyses of additional granular samples from Insch (Hutchinson, 1965), Arnage/Haddo olivine-norites (Gribble, 1967) and a typical Huntly hypersthene-gabbro (Weedon, 1970) are included, as well as five 'modified granular cumulates' and 'granular gabbronorites' from the western area of the Huntly mass (Fletcher, 1989) which have been included due to their textural and chemical similarities. A fine-grained sample from Insch with detailed whole rock trace element data (Thompson *et al.*, 1984) is also included.

Thompson *et al.* (1984) describe this sample as an olivine-rich gabbro with a 'fine-grained (doleritic)' texture, and although doleritic textures were not evident in any Granular Gabbros samples examined as part of this study, a comparison of its location (figure 6.2) and chemistry (Table 6.1) with that of the Granular Gabbros samples leaves little doubt that they are from the same rock type.

Examination of the data in Table 6.1 shows that there is a remarkable similarity to the chemistry of granular gabbroic samples, notwithstanding the wide geographical range to their location within the region. Granular samples from Insch and Huntly have a relatively limited range of compositions over the majority of elements, with $TiO_2$, $P_2O_5$, Zr, Ba and Rb showing moderate variation while the highly compatible elements Ni, Cr and Cu show a significant range of values suggesting some degree of fractionation is likely to have taken place in situ. The range in the remaining elemental abundances is very limited, particularly for the incompatible elements, as can be seen from the 'spider' and REE plots in Chapter 5 and reproduced here in figure 6.3. In view of the possible mantle origin of the Granular Gabbros, the samples have been normalized to MORB values (given in Appendix B.6) in this and several subsequent plots. In addition to these whole rock chemical similarities, they also display low $^{87}Sr/^{86}Sr$ ratios (Pankhurst, 1969) at least for the Insch samples, and a limited range of silicate mineralogy compositions (Wadsworth, 1988).

It is suggested that the Granular Gabbros may represent material originating deeper in the crust or, more likely, in the mantle. Their low $^{87}Sr/^{86}Sr$ ratios and flat 'spider' diagrams point to such an origin, possibly as a partial melt of mantle material. These isotopic data, the flat 'spider' and REE plots and the limited variation in the whole rock chemistry and silicate mineralogy of the Granular Gabbros, suggest that they may represent magmatic pulses that have crystallized relatively quickly with only limited *in situ* fractionation having occurred. Petrographic evidence for this fractionation is present in the form of porphyritic plagioclase feldspar in some Granular Gabbros (see Plate 4.10) and chemical evidence is also present in the plots in Chapter 5, especially the range in Ni and Cr data, shown in figure 5.11; in general, Ni and Cr abundances fall with decreasing mg# and MgO, suggesting some fractionation may have taken place. This can also be seen in figure 6.3, where there is a correlation between the slope of individual and average REE plots and their MgO, Ni and Cr contents. The Granular Gabbros fall into two groups in terms of MgO content, those with ~ 9% MgO and those with 6-7% MgO (see Table 6.1). Average REE plots for these two MgO contents show a slight increase in slope with decreasing MgO, and also decreasing Ni and Cr contents. As will be seen in Section 6.4, large degrees of fractionation

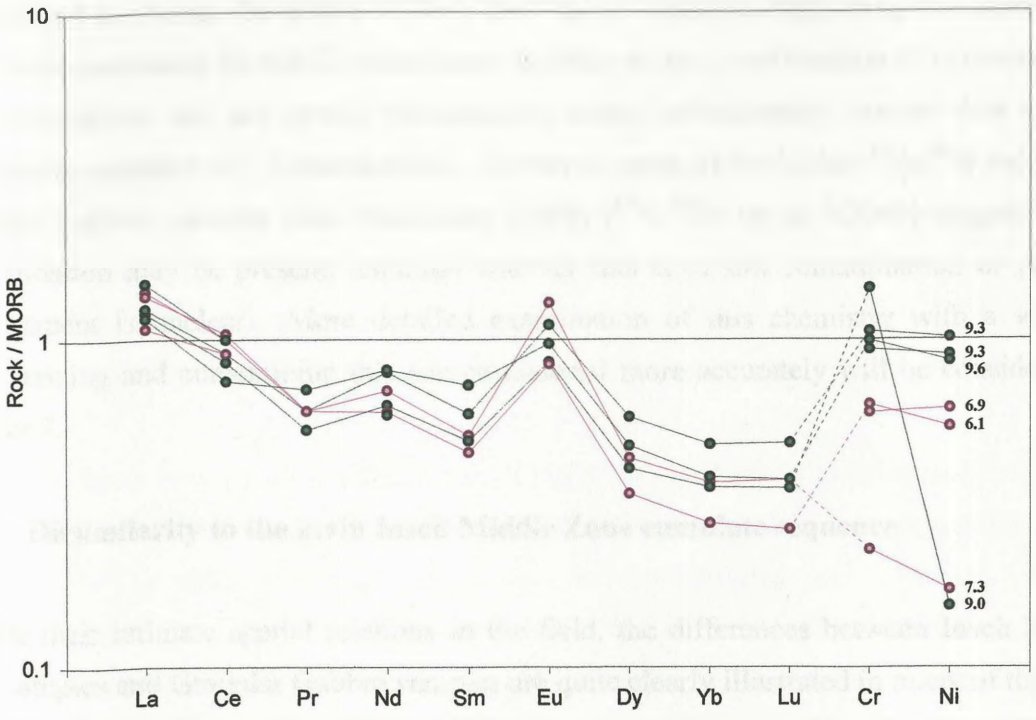


**Figure 6.3a MORB-normalized REE patterns for the Granular Gabbros. Green samples have I 9.0%, while pink samples have MgO < 7.3%. Gd, Ho and Er omitted due to sample contaminati Normalized Ni and Cr data also shown. MORB-normalizing values given in Appendix B.6.**

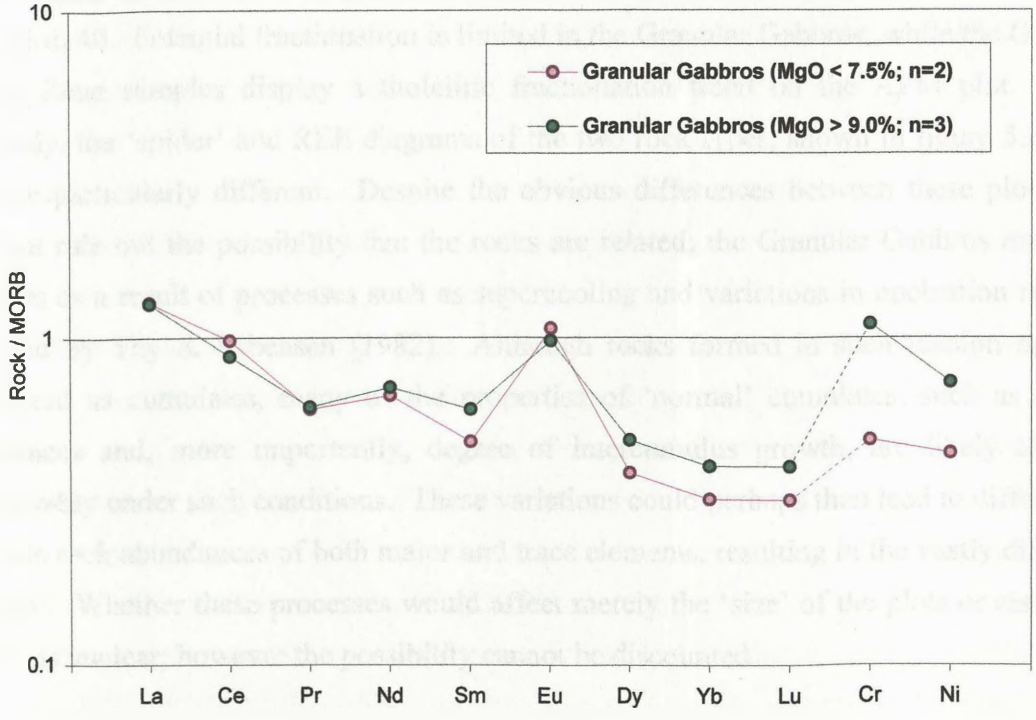


**Figure 6.3b Average MORB-normalized REE patterns from figure 6.3a for Granular Gabbro samples with different MgO contents.Gd, Ho and Er omitted due to sample contamination. Average Ni and Cr data also shown.**

are required to change the slopes of REE and 'spider' patterns suggesting this increase in slope with decreasing Ni and Cr abundances is likely to be a combination of contamination and fractionation and not merely fractionation alone; unfortunately isotope data are not available to constrain this contamination. However, some of the higher $^{87}Sr/^{86}Sr$ values for Granular Gabbro samples from Pankhurst (1969) ($^{87}Sr/^{86}Sr$ up to 0.7060) suggest slight contamination may be present, although whether this is *in situ* contamination or prior to emplacement is unclear. More detailed examination of this chemistry with a view to characterizing and constraining this source material more accurately will be considered in Chapter 7.

### 6.2.4 Dissimilarity to the main Insch Middle Zone cumulate sequence

Despite their intimate spatial relations in the field, the differences between Insch Middle Zone samples and Granular Gabbro samples are quite clearly illustrated in many of the plots in Section 5.4.3. Plots such as TAS, AFM and many of the mg# plots all suggest that the Granular Gabbros and Group 2 of the Middle Zone are unrelated. The mg# values of Group 2 Middle Zone samples in close outcrop proximity to Granular Gabbro samples range from 34 to 14 (and to less than 5 in published data), while those of the Granular Gabbros range from 53 to 40. Potential fractionation is limited in the Granular Gabbros, while the Group 2 Middle Zone samples display a tholeiitic fractionation trend on the AFM plot. Most obviously, the 'spider' and REE diagrams of the two rock types, shown in figure 5.21 and 5.22 are particularly different. Despite the obvious differences between these plots, this does not rule out the possibility that the rocks are related; the Granular Gabbros may still originate as a result of processes such as supercooling and variations in nucleation rates as proposed by Thy & Esbensen (1982). Although rocks formed in such fashion may be considered as cumulates, many of the properties of 'normal' cumulates, such as modal abundances and, more importantly, degree of intercumulus growth, are likely to vary considerably under such conditions. These variations could perhaps then lead to differences in whole rock abundances of both major and trace elements, resulting in the vastly differing 'spiders'. Whether these processes would affect merely the 'size' of the plots or also their 'shape' is unclear; however the possibility cannot be discounted.

Whether these variations would affect the composition of the silicate phases in the rock is also less clear. Thy & Esbensen (1982) proposed that these silicate compositions could be used to show if granular samples are indeed cumulate, suggesting that related coarse cumulate and fine granular samples should be indistinguishable in terms of mineral

composition. However, Wadsworth (1988; figures 3 & 4) has shown that this is not the case as, for a given orthopyroxene (En) composition, clinopyroxene (mg#) and plagioclase feldspar (An%) compositions are consistently greater in the Granular Gabbros than in the Middle Zone. This would appear to suggest that the granular samples are not simply fine-grained equivalents of the Middle Zone cumulates. In addition, as mentioned previously, despite the widespread occurrence of the Granular Gabbros in close association with the established Middle Zone, the range of mineralogical compositions in these Middle Zone rock is far greater than in the Granular Gabbros (see Chapter 4, and Wadsworth (1988)).

Further evidence to suggest that the Granular Gabbros are unlikely to be closely related to the Middle Zone fractionation sequence comes from the strontium isotope data of Pankhurst (1969). $^{87}Sr/^{86}Sr$ values of samples from the Granular Gabbros, and Lower and Middle Zone, shown in figure 6.1, reveal that the highest $^{87}Sr/^{86}Sr$ values of the Granular Gabbros (0.7055 to 0.7060) are less than the lowest values for the Middle Zone cumulate sequence (>0.7077), and form a distinct separate group. This isotopic variation again appears to suggest that the Granular Gabbros and the Middle Zone fractionation sequence are not closely related genetically. Unfortunately isotope analyses have not been undertaken as part of this study, but whole rock strontium abundances from this study have been included in the diagram merely to show the broad similarity between the whole rock strontium abundances from this study and from that of Pankhurst (see figure 6.1).

The possibilities of the outcrop patterns resulting from large scale block faulting, independent crystallisation domains, or large xenolith rafts of Granular Gabbro within the crystallising cumulate mush, as proposed by Wadsworth (1988) cannot be discounted, but are considered unlikely. Although large shear zones are known to transect the Insch mass (Ashcroft *et al.*, 1984; Fettes *et al.*, 1986), and have been used to explain variations in the detail of the cryptic variations within the mass (Wadsworth, 1988), little or no evidence for such block faulting is present, and does not seem to account for the chemical homogeneity of the Granular Gabbros and their isotopically distinct nature. Evidence for the existence of independent crystallisation domains is again absent, although such domains could perhaps explain the isotopic variations if the domains in which the Granular Gabbros crystallised were isolated chemically from the country rocks while contamination took place. The geometries and scales of such domains seem unlikely, given the intricate field relationships, and do not seem to account for the granular texture produced, while rafting of xenolithic granular samples perhaps from a roof zone, cannot, at present be ruled out, although, again, there is little or no evidence in support of this theory. Nevertheless, it can be said that the

two rock types are unlikely, at the very least, to have crystallized at the same time in the same close spatial associations now seen in the field.

### 6.2.5 Similarity of the Granular Gabbros to other 'Younger' Basics rocks

Texturally, the Insch Granular Gabbros are comparable to granular gabbros from the Huntly body as discussed in Chapter 5, and the limited geochemical data available (Table 6.1) also shows them to be similar. Geochemical comparisons of the Granular Gabbros with cumulate rocks are complicated by factors such as cumulate processes, fractionation and the likely contamination by country rock material. However, these factors can be minimized by comparison of the Granular Gabbros with cumulate samples that have undergone only slight fractionation, and are relatively uncontaminated. Lower Zone rocks from the Belhelvie body are believed to be relatively uncontaminated ($^{87}Sr/^{86}Sr$ ratios of 0.704 to 0.709; Pankhurst, 1969), and the troctolite samples chosen from Belhelvie are only slightly fractionated ($Fo_{77}$ and $An_{73}$ in sample Ab127). RE elements are strongly incompatible in olivine and plagioclase feldspar (see figure 6.4) and accordingly, any incompatible elements present in the troctolite are likely to be concentrated in phases crystallising from the intercumulus liquids. Consequently, while the absolute and normalized REE abundances are largely dependant on cumulate processes (in this case, the degree of postcumulus or interstitial mineral development), the *shape* of the REE plots of the troctolites should resemble those of the Granular Gabbro parent magma.

REE plots of the two Belhelvie troctolites are shown in figures 6.5a and 6.5b, along with the Insch Granular Gabbros. Concentrations in the troctolites are quite low, with all normalised abundances below those in the Granular Gabbros; as mentioned above this is, for the most part, controlled by the level of adcumulate growth, which limits the amounts of intercumulus phases. Only minor amounts of intercumulus material are present in these troctolites resulting in these low overall abundances of incompatible elements. Figure 6.5b shows that there is a strong similarity between the shapes of the two troctolite REE plots and those of the Granular Gabbro. Both display flat REE plots ($Ce_N/Yb_N$ = 2.0 for the troctolites, and 1.7 for the Granular Gabbros) with the Granular Gabbros containing more pronounced Eu peaks, although, as before, caution needs to be exercised due to the inaccuracies in the Gd, Ho and Er data for both sets of samples. As mentioned in Chapter 5 and Appendix B, this peak is likely to be as a result of contamination during preparation of a batch of REE samples. Further evidence to suggest this comes from the sample from Thompson *et al.* (1984); although it does not contain Er, normalised ratios of adjacent RE

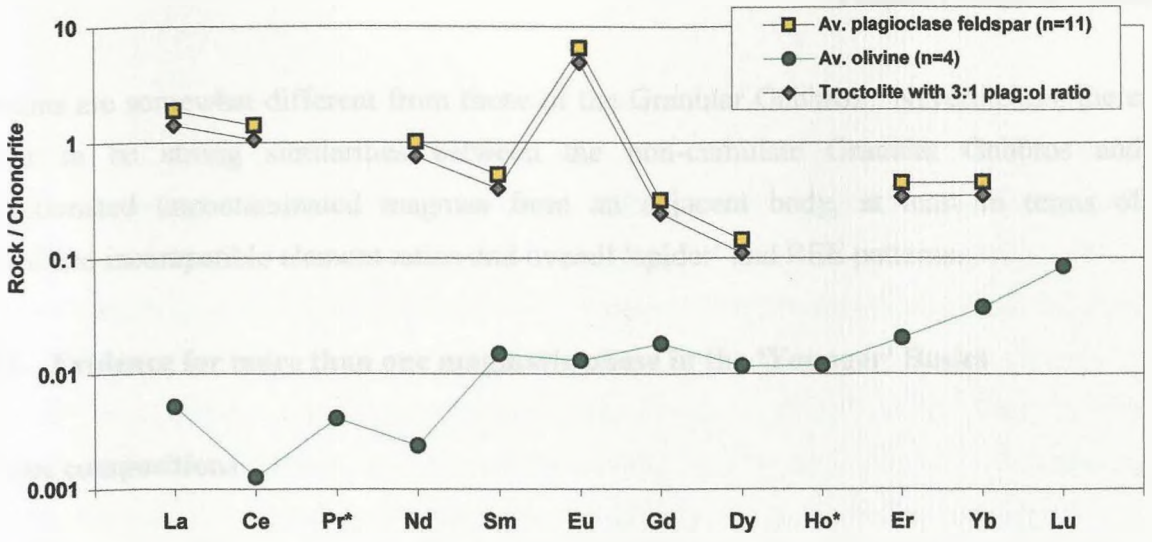


**Figure 6.4 REE plots of plagioclase and olivine from LA-ICPMS data (Tribuzio *et al.*, 1999a; Garrido *et al.*, 2000) and a theoretical troctolite composed of these two minerals with no interstitial material.**

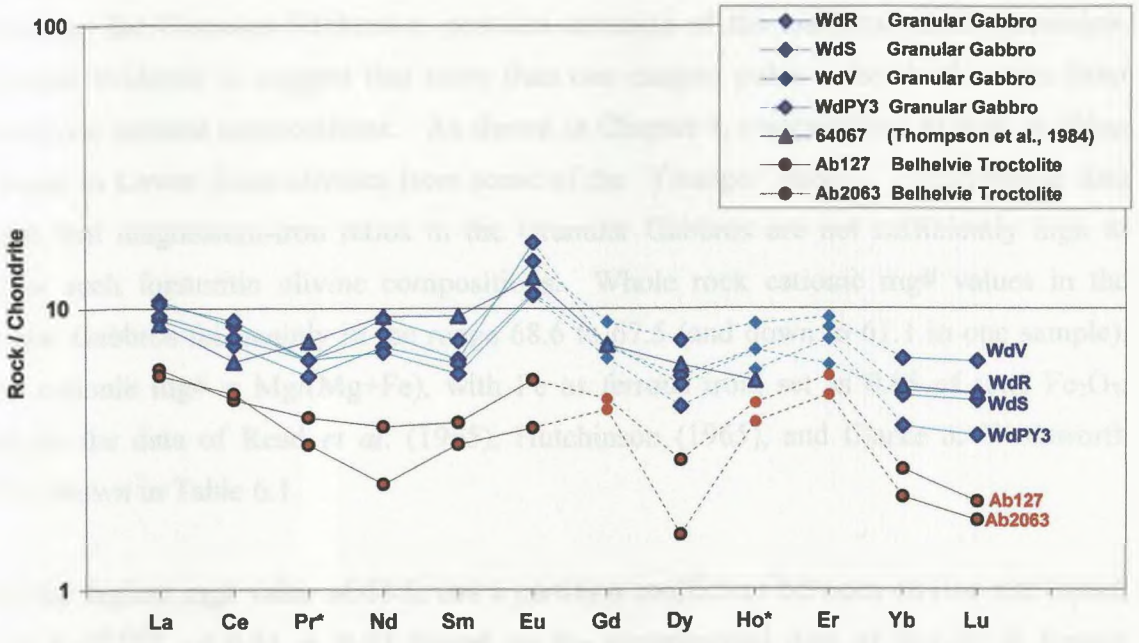


**Figure 6.5a REE plots of Insch Granular Gabbros compared to Lower Zone troctolites from Belhelvie. All samples contain Gd, Ho and Er values which are likely to be too high due to contamination.**

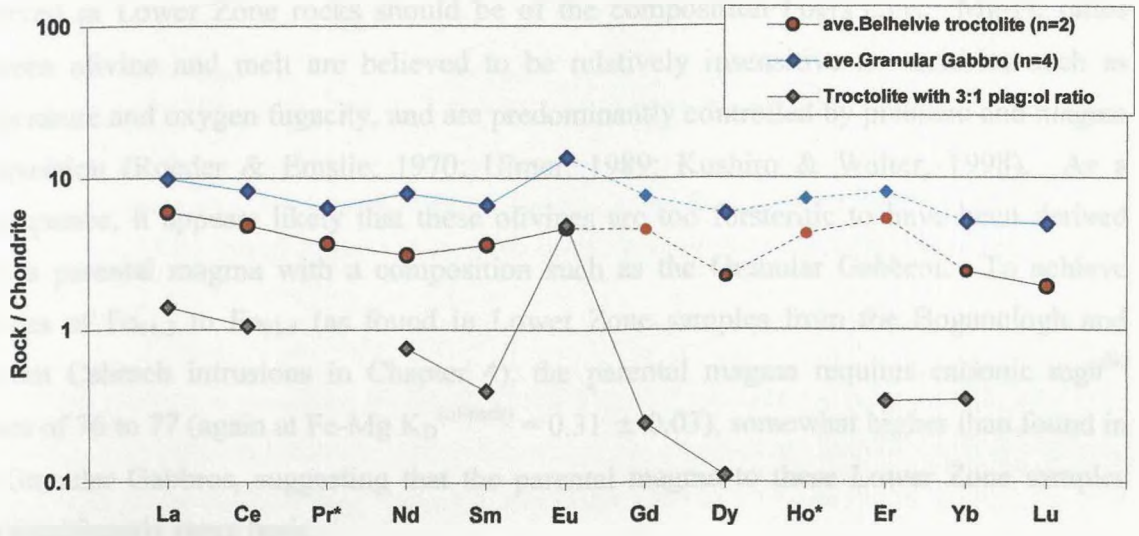


**Figure 6.5b REE plots of theoretical troctolite from figure 6.4 and average Granular Gabbro and Belhelvie troctolite 'spiders' from figure 6.5a.**

elements are somewhat different from those of the Granular Gabbros. Nevertheless, there appear to be strong similarities between the non-cumulate Granular Gabbros and unfractionated uncontaminated magmas from an adjacent body, at least in terms of normalized incompatible element ratios and overall 'spider' and REE patterns.

### 6.2.6 Evidence for more than one magmatic phase in the 'Younger' Basics

**Olivine compositions**

The suggestion that the Granular Gabbros may approximate to a parental magma for the 'Younger' Basics implies at least two phases of magmatic activity, as this suggestion necessitates the Granular Gabbros to postdate intrusion of the main cumulate succession. Additional evidence to suggest that more than one magma pulse is involved comes from Lower Zone mineral compositions. As shown in Chapter 4, compositions as high as $>Fo_{90}$ are found in Lower Zone olivines from some of the 'Younger' Basics. Experimental data suggest that magnesium-iron ratios in the Granular Gabbros are not sufficiently high to produce such forsteritic olivine compositions. Whole rock cationic mg# values in the Granular Gabbros fall mainly in the range 68.6 to 67.5 (and down to 61.1 in one sample), where cationic mg# = Mg/(Mg+Fe), with Fe as ferrous iron, set as 0.85 of total $Fe_2O_3$, based on the data of Read *et al.* (1965), Hutchinson (1965), and Clarke & Wadsworth (1970), shown in Table 6.1.

Using the highest mg# value of 68.6, and a partition coefficient between olivine and liquid, Fe-Mg $K_D^{(ol\text{-}melt)}$, of 0.31 ± 0.03 (based on the experimental data of Roeder & Emslie (1970) and Ulmer (1989), assuming a pressure of 5 kbar), the most forsteritic olivines observed in Lower Zone rocks should be of the composition $Fo_{87.6\ (\pm 1.1)}$. Mg-Fe ratios between olivine and melt are believed to be relatively insensitive to variables such as temperature and oxygen fugacity, and are predominantly controlled by pressure and magma composition (Roeder & Emslie, 1970; Ulmer, 1989; Kushiro & Walter, 1998). As a consequence, it appears likely that these olivines are too forsteritic to have been derived from a parental magma with a composition such as the Granular Gabbros. To achieve olivines of $Fo_{91.3}$ to $Fo_{91.4}$ (as found in Lower Zone samples from the Boganclogh and Morven Cabrach intrusions in Chapter 4), the parental magma requires cationic $mg\#^{liq}$ values of 76 to 77 (again at Fe-Mg $K_D^{(ol\text{-}melt)} = 0.31 \pm 0.03$), somewhat higher than found in the Granular Gabbros, suggesting that the parental magma to these Lower Zone samples was significantly more basic.

This picritic magma however, is not necessarily parental to the entire cumulate sequence. Olivines of compositions greater than $Fo_{90}$ appear to be restricted to certain intrusions, specifically the Lower Zones of the Boganclogh, Morven Cabrach and Succoth-Brownhills bodies (see Table 6.2). Detailed mineralogical studies of Belhelvie (Wadsworth, 1991), Huntly (Fletcher, 1989) and Insch (Ashcroft & Munro, 1978; Munro, 1986b) have failed to reveal olivine compositions greater than $Fo_{88}$ (see Table 6.2). The most magnesian pyroxene compositions are also systematically lower in these bodies than in the Boganclogh, Morven Cabrach and Succoth-Brownhills bodies (see Table 6.2). In addition, the most forsteritic compositions in the Belhelvie, Huntly and Insch bodies are generally in the range $Fo_{86-87}$, precisely that predicted for olivines in equilibrium with the Granular Gabbros (see above). This suggests that there may have been emplacement of an initial, more basic (?picritic), magma possessing a cationic mg# value of 76 to 77, with this magma responsible for the highly forsteritic compositions.

| | Olivine | | Orthopyroxene | | Clinopyroxene | |
|---|---|---|---|---|---|---|
| | this study | published | this study | published | this study | published |
| | Fo% | | En% | | mg# | |
| Belhelvie | 87.2 | 86.5 | 85.4 | 87.3 | 88.2 | 87.9 |
| Insch | | 87.0 | | | | |
| Kildrummy | | 81.6 | | 83.5 | | 83.9 |
| Huntly-Knock-Portsoy | 82.0 | 86.4 | | 86.3 | 85.6 | 88.5 |
| South Connemara | 77.4 | | 80.2 | | 83.7 | |
| North Connemara | 77.8 | | 80.1 | | 83.8 | |
| Boganclogh | 91.4 | 92.5 | 86.0 | 92.3 | 85.2 | 94.7 |
| Morven Cabrach | 91.3 | | 90.3 | | | |
| Succoth-Brownhills | | 92.0 | | | | 93.4 |

**Table 6.2 Summary of the most magnesian olivine, orthopyroxene and clinopyroxene compositions from the 'Younger' Basics (published data from Ashcroft & Munro, 1978; Munro, 1986b; Fletcher, 1989; Wadsworth, 1991; Gunn *et al.*, 1996; Gould, 1997).**

This initial magma is restricted to the most southwesterly bodies of Boganclogh, Succoth-Brownhills and Morven Cabrach, where these high Fo contents are found, while the second magma with lower cationic mg# values in the range 68.6 to 67.5, as found in the Granular

Gabbros, was then emplaced, and is found to the north (Huntly-Knock-Portsoy) and east (Insch and Belhelvie). Whether this second magmatic pulse was also emplaced into the Boganclogh, Succoth-Brownhills and Morven Cabrach masses after the initial more basic pulse is unclear. Faulting and metamorphism, combined with poor exposure, particularly in the Lower Zones of the intrusions make any field evidence in support of such a theory unlikely. However, the fact that the initial pulse is limited geographically and the similarity of the overall fractionation sequence in all the bodies suggests that the second magma may also be present in these bodies. In this scenario, the initial basic pulse is viewed as being minor volumetrically, and followed by the main magma pulse, of composition similar to the Granular Gabbros (at least in terms of whole rock Mg-Fe ratios). Interestingly, the bodies in which the Granular Gabbros themselves are found, Insch and Huntly, have olivine compositions consistent with those predicted by the Mg-Fe ratios of the Granular Gabbros. Caution should be taken, however, as ultramafic marginal rocks are disrupted in all of the bodies and the possibility exists that shearing may have removed Lower Zone units containing more magnesian olivine and pyroxene from those intrusions which do not exhibit these highly magnesian phases.

**Trace elements in ferromagnesian phases**

Using the trace element concentrations of these Lower Zone silicates, partition coefficients between potential parental magmas and these Lower Zone phases can be predicted. Figure 6.6 shows the concentrations of MnO, NiO and $Cr_2O_3$ in olivine and pyroxene, as well as in the Granular Gabbros. Data from the Boganclogh and Morven Cabrach intrusions have been assigned a separate symbol. Examination of the data reveals no systematic variation between data from the intrusions with high forsterite contents and low forsterite contents, with the exception of NiO content in olivine, which is slightly higher for the two samples from Boganclogh and Morven Cabrach (see Figure 6.6a). Approximate MnO, NiO and $Cr_2O_3$ trace elements abundances for the highest compositions of the three ferromagnesian phases have been estimated for the second magma from figure 6.6, as well as Mn, Ni and Cr in the least fractionated Granular Gabbros samples; these abundances have then been used to calculate approximate $K_D$ values for these phases coexisting with the Granular Gabbros source; these are shown in Table 6.3. Probe analyses of olivines and pyroxenes from the Granular Gabbros analyses are also plotted in figure 6.6 and, with the exception of MnO in olivine (as shown in figure 4.13), can be seen to fall within the trends established for the main cumulate sequence. Insufficient data has meant that precise $K_D$ values cannot be estimated for the possible initial picritic magma. Comparison with published $K_D$ values and

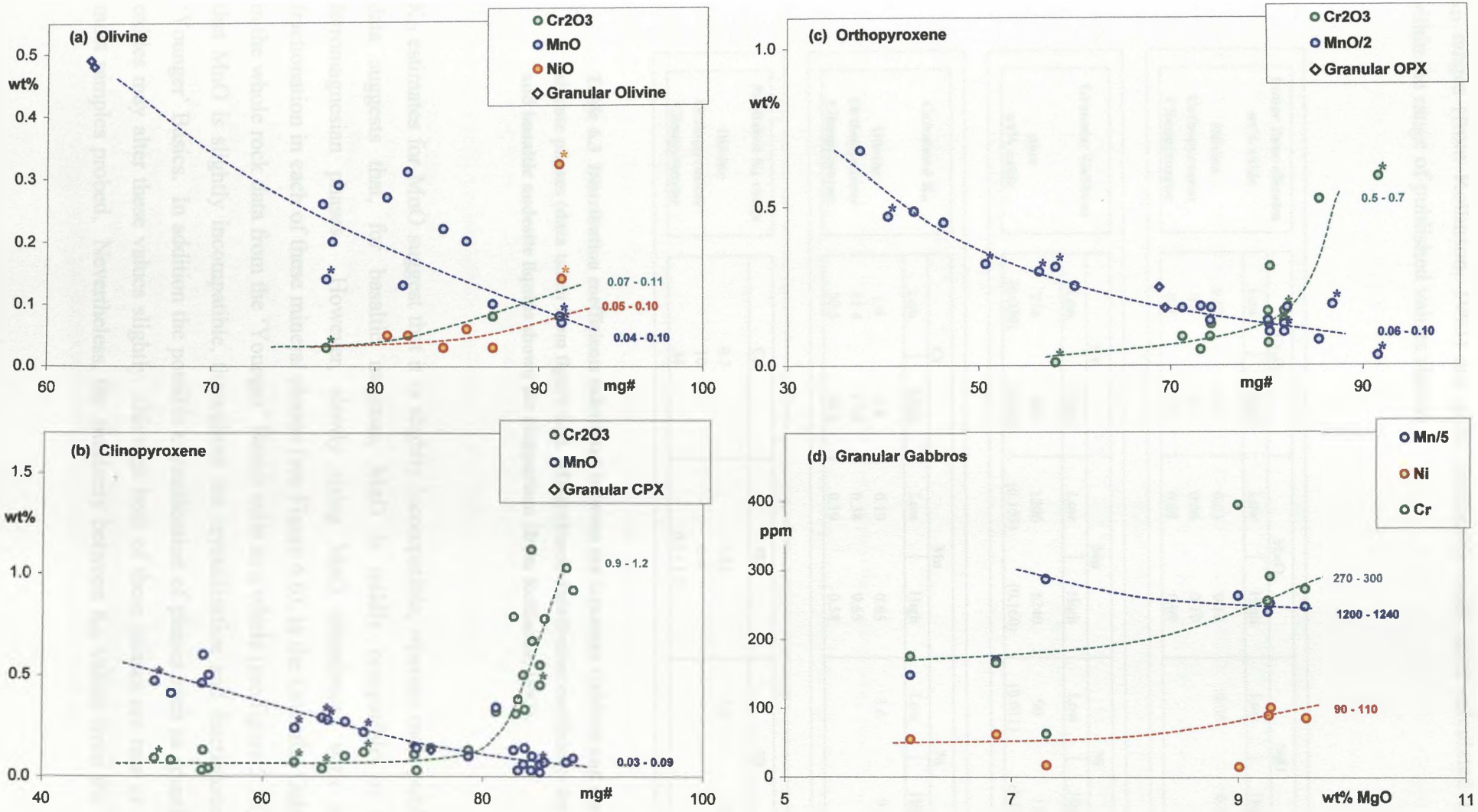


**Figure 6.6** Trace element abundances in (a) olivine, (b) clinopyroxene, (c) orthopyroxene and (d) the Granular Gabbros plotted against mineral mg#. Samples labelled * are from the Boganclogh and Morven Cabrach intrusions.

$K_D$ ranges (from Rollinson, 1993) are quite favourable with most calculated $K_D$ values within the range of published values shown.

| Lower Zone silicates wt% oxide | $Cr_2O_3$ | | MnO | | NiO | |
|---|---|---|---|---|---|---|
| | Low | High | Low | High | Low | High |
| Olivine | 0.07 | 0.11 | 0.03 | 0.10 | 0.05 | 0.10 |
| Orthopyroxene | 0.5 | 0.7 | 0.06 | 0.10 | | |
| Clinopyroxene | 0.9 | 1.2 | 0.03 | 0.09 | | |

| Granular Gabbros | Cr | | Mn | | Ni | |
|---|---|---|---|---|---|---|
| | Low | High | Low | High | Low | High |
| ppm | 270 | 300 | 1200 | 1240 | 90 | 110 |
| wt% oxide | (0.039) | (0.044) | (0.155) | (0.160) | (0.011) | (0.014) |

| Calculated $K_D$ | Cr | | Mn | | Ni | |
|---|---|---|---|---|---|---|
| | Low | High | Low | High | Low | High |
| Olivine | 1.6 | 2.8 | 0.19 | 0.65 | 3.6 | 9.1 |
| Orthopyroxene | 11.4 | 17.9 | 0.38 | 0.65 | | |
| Clinopyroxene | 20.5 | 30.8 | 0.19 | 0.58 | | |

| Published $K_D$ range | Cr | Mn | Ni | |
|---|---|---|---|---|
| Olivine | 0.7 | 1.45 | 5.9 | 29 |
| Orthopyroxene | 10 | 1.4 | | |
| Clinopyroxene | 34 | 0.3 - 1.2 | | |

**Table 6.3 Distribution coefficients calculated between the Granular Gabbros and the earliest silicate phases (data taken from figure 6.6). Mineral/melt distribution coefficients for basaltic and basaltic andesite liquids shown for comparison (from Rollinson, 1993).**

$K_D$ estimates for MnO suggest that it is slightly incompatible, whereas most published $K_D$ data suggests that, for basaltic magmas, MnO is mildly compatible in all three ferromagnesian phases. However, slowly rising MnO abundances with increasing fractionation in each of these mineral phases (see Figure 6.6), in the Granular Gabbros, and in the whole rock data from the 'Younger' Basics suite as a whole (see figure 5.10), suggest that MnO is slightly incompatible, throughout the crystallisation and fractionation of the 'Younger' Basics. In addition the possible crystallisation of phases such as spinel or Fe-Ti oxides may alter these values slightly, although both of these phases are rare or absent in most samples probed. Nevertheless, the similarity between $K_D$ values from the literature

and those between the Granular Gabbros and early silicate phases suggests that the abundances of these trace elements in the Granular Gabbros are quite similar to those present in the actual parental melt.

In addition, while the high olivine compositions in Lower Zone samples from the Boganclogh, Succoth-Brownhills and Morven Cabrach intrusions appear to require a slightly more basic parental magma, many other elemental abundances in this parental magma are likely to resemble those abundances found in the Granular Gabbros. The higher NiO contents (0.14-0.32 wt%) in olivines from Boganclogh and Morven Cabrach intrusion samples (see figure 6.6c) produce $K_D$ values in the range of 10-29 for equilibrium with Granular Gabbros parental magmas; again this is within the range of published $K_D$ data (see Table 6.3).

**Two Insch and Boganclogh trends**

As shown in Section 5.4.3, there is evidence from whole rock chemical data to suggest that there are at least three separate trends within the Insch and Boganclogh masses. One of these trends, seen in the Granular Gabbros, is also texturally distinct from the remaining trends, Trends 1 and 2. However, there is evidence that the difference between Trends 1 and 2 is not restricted to whole rock chemistry. Wadsworth (1988) first noticed a systematic difference between silicate phase compositions from Insch and Boganclogh. The mineral probe data of Wadsworth (1986, 1988) and Gould (1997) from the Insch and Boganclogh bodies reveal a systematic difference between the compositions of silicate phases along a broadly similar divide to that established for Trends 1 and 2 in the previous chapter. Figure 6.7a shows the location of all samples from the Insch and Boganclogh bodies for which probe data is available. They have been divided into three groups along the same lines established in the previous chapters. Granular Gabbros have been separated on a textural basis, while remaining samples have been divided into Trends 1 and 2 on a geographical basis, as in Section 5.4.3.

Figure 6.7b shows a plot of coexisting orthopyroxene and clinopyroxene from samples from the two bodies. Again it is clear that the data fall into three reasonably well defined trends; the clearest of these trends is for the Granular Gabbros, while, for a given En% content, clinopyroxene mg# values are consistently higher in Trend 1 than in Trend 2. Additional samples plotted in Gould (1997; fig. 14) also highlight the differences between these trends. Gould (1997) suggested that compositional overlap seen in probe data across the Middle to

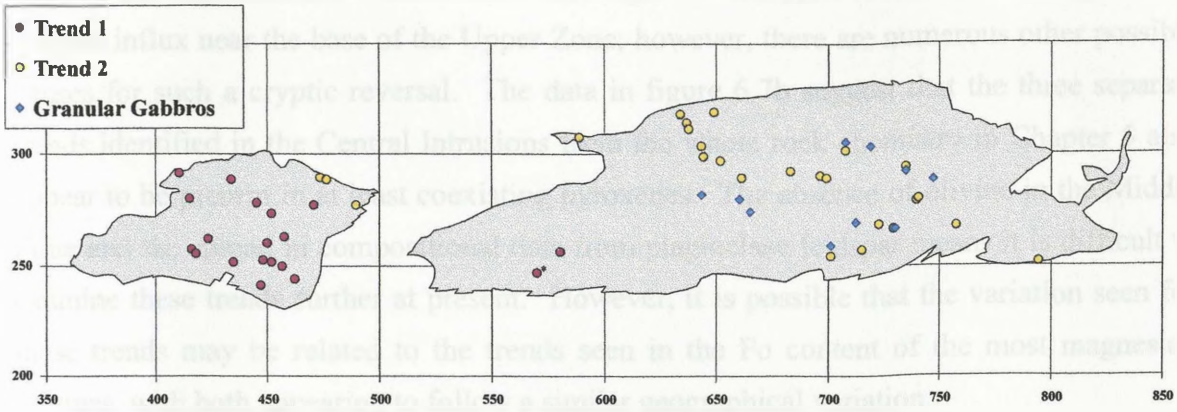


**Figure 6.7a Location of all samples for which probe data is available. The samples are divided into three groups as discussed in the text and the data includes this study, Wadsworth (1986, 1988), and Gould (1997).**

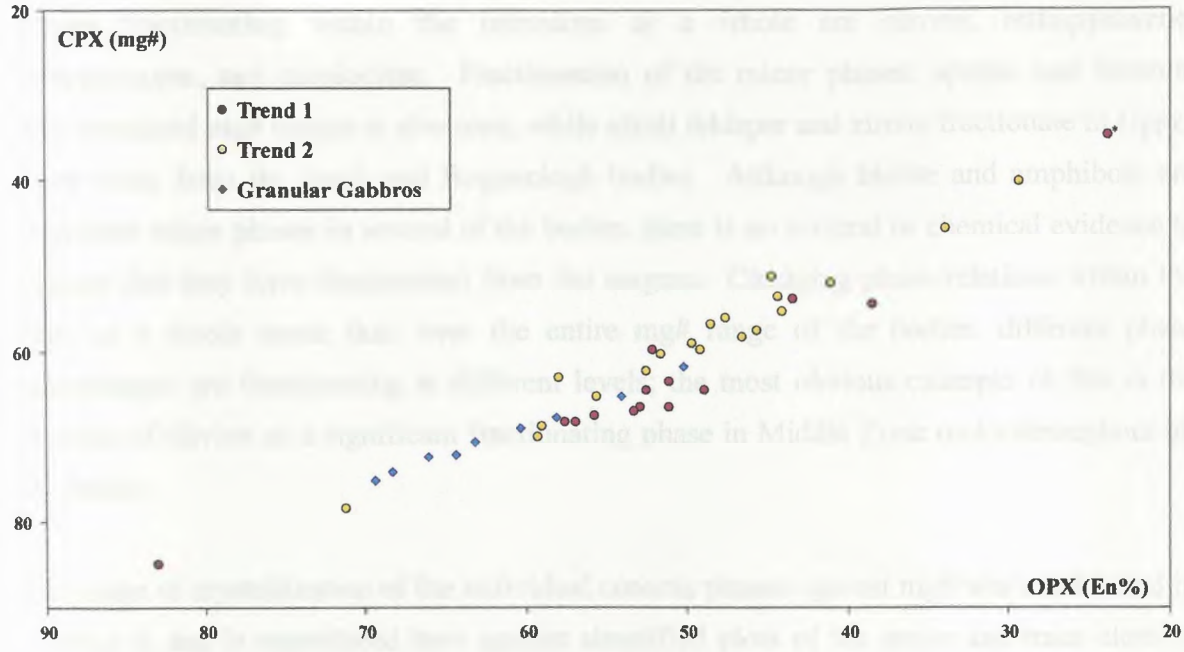


**Figure 6.7b Plot of orthopyroxene (En%) versus coexisting clinopyroxene (mg#) compositions for the three groups. The single Trend 1 sample with coexisting orthopyroxene and clinopyroxene from Insch is labelled with an asterisk. Some of the samples from figure 6.7a cannot be plotted as they do not contain coexisting orthopyroxene and clinopyroxene. Data sources as in figure 6.7a.**

Upper Zone transition in the Insch mass may represent a cryptic reversal indicating another magma influx near the base of the Upper Zone; however, there are numerous other possible causes for such a cryptic reversal. The data in figure 6.7b suggest that the three separate trends identified in the Central Intrusions from the whole rock chemistry in Chapter 5 also appear to be present in at least coexisting pyroxenes. The absence of olivine in the Middle Zone and the spread in compositional data from plagioclase feldspar means it is difficult to examine these trends further at present. However, it is possible that the variation seen for these trends may be related to the trends seen in the Fo content of the most magnesian olivines, with both appearing to follow a similar geographical variation.

## 6.3 Fractionation of the intrusions

### 6.3.1 Introduction

The mineralogical and textural evidence presented in Chapter 4 suggests that the main phases fractionating within the intrusions as a whole are olivine, orthopyroxene, clinopyroxene, and plagioclase. Fractionation of the minor phases, apatite and ilmenite over restricted mg# ranges is also seen, while alkali feldspar and zircon fractionate in Upper Zone rocks from the Insch and Boganclogh bodies. Although biotite and amphibole are important minor phases in several of the bodies, there is no textural or chemical evidence to suggest that they have fractionated from the magma. Changing phase relations within the suite as a whole mean that, over the entire mg# range of the bodies, different phase assemblages are fractionating at different levels; the most obvious example of this is the absence of olivine as a significant fractionating phase in Middle Zone rocks throughout all the bodies.

The range of crystallization of the individual cotectic phases against mg# was established in Chapter 4, and is reproduced here against simplified plots of the major and trace element data in figure 6.8; where well-defined fractionation trends are evident for individual groups or for the complex as a whole, they are displayed. As pointed out during discussions of the major element data, fractionation trends seen for the groups are all quite similar, with only minor variations in absolute abundances and in the angle of slopes and location of inflection points. Figures 6.8a and 6.8b shows plots of major and trace elements against mg# with fractionation paths superimposed. Although this is a simplification of the data, particularly in plots such as mg# versus $TiO_2$, where there are clear variations between individual groups, it does allow an approximate evaluation of the fractionation of the bodies as a

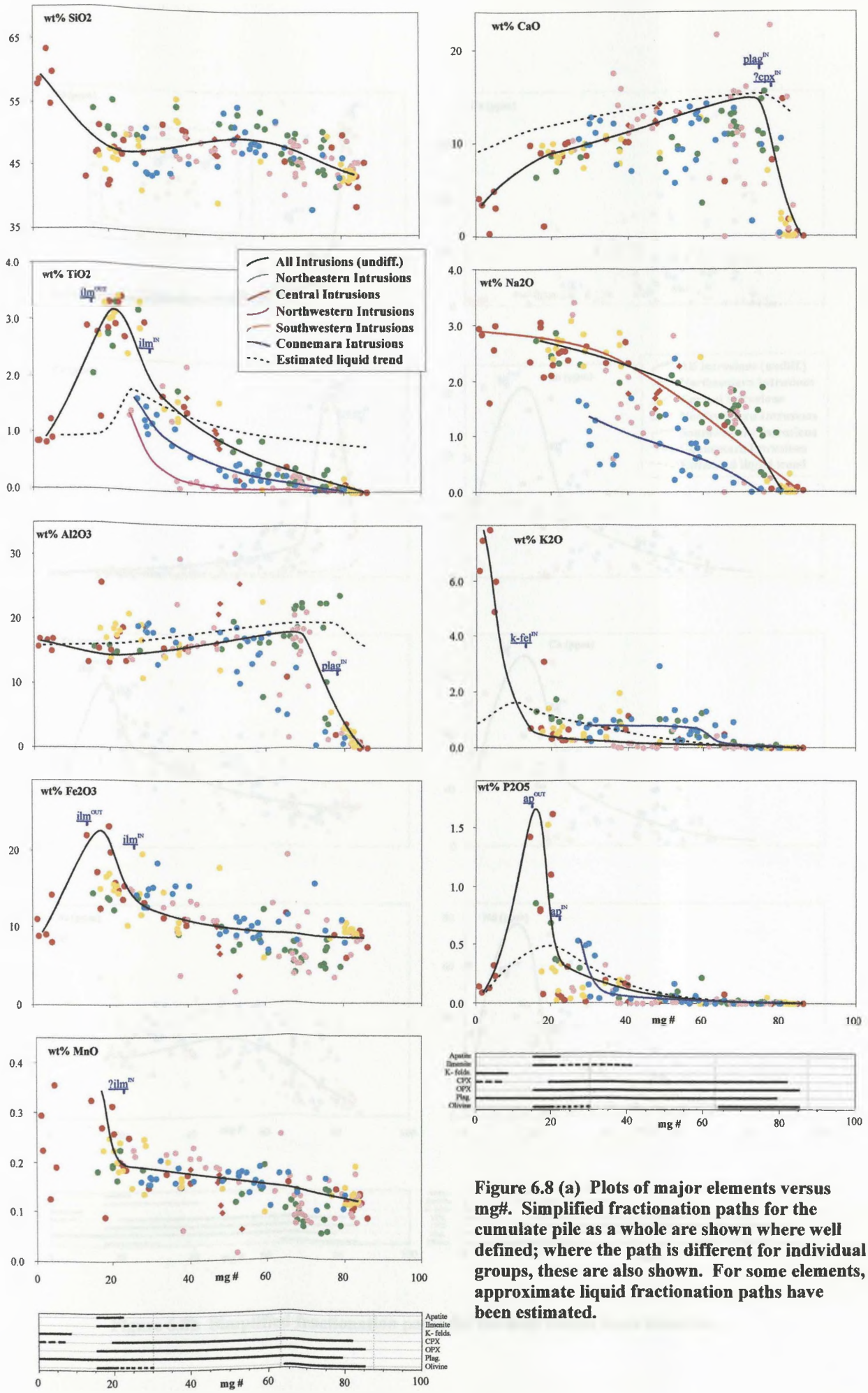


**Figure 6.8 (a) Plots of major elements versus mg#. Simplified fractionation paths for the cumulate pile as a whole are shown where well defined; where the path is different for individual groups, these are also shown. For some elements, approximate liquid fractionation paths have been estimated.**

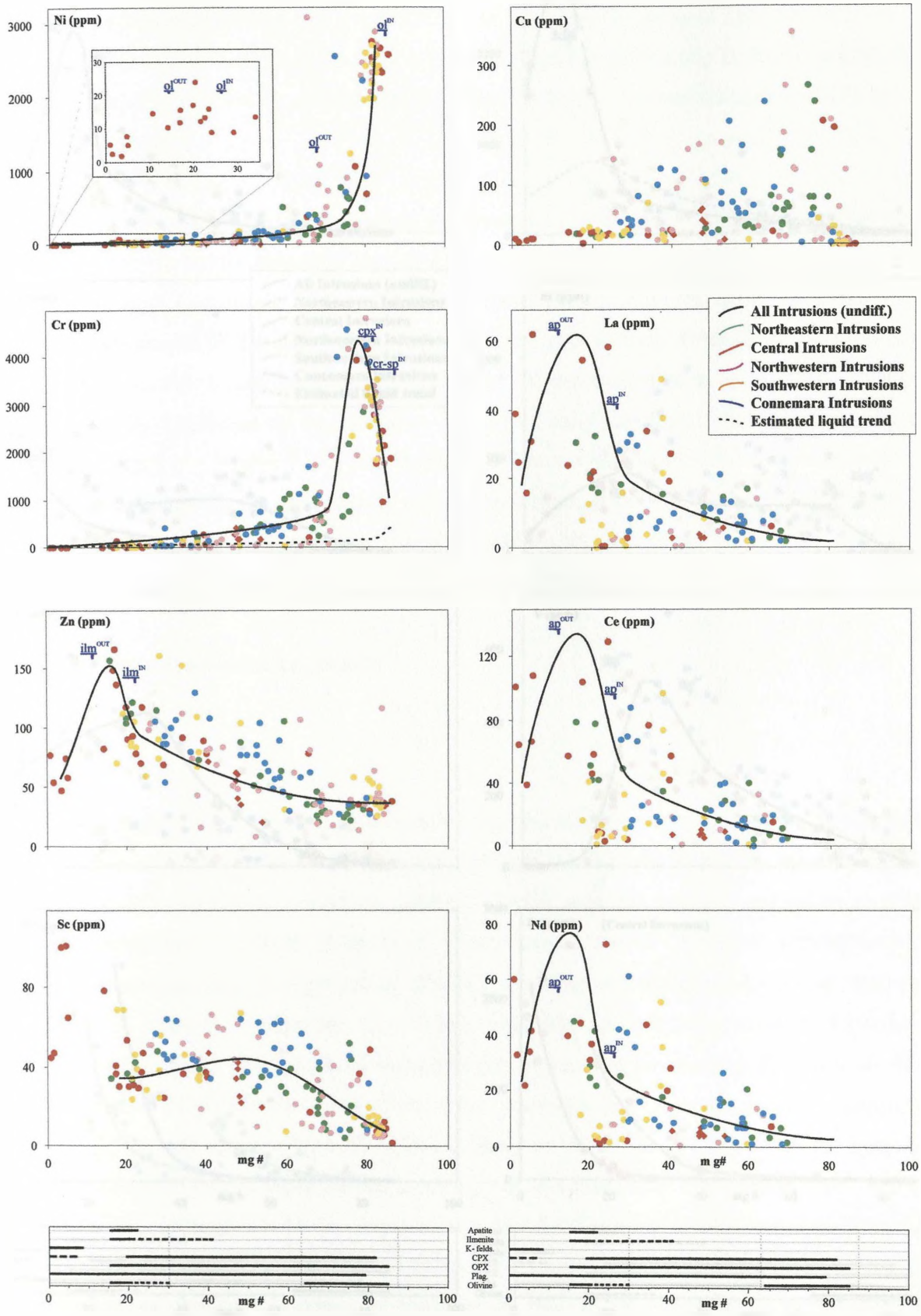


**Figure 6.8b Simplified fractionation paths for the mg# versus trace elements.**

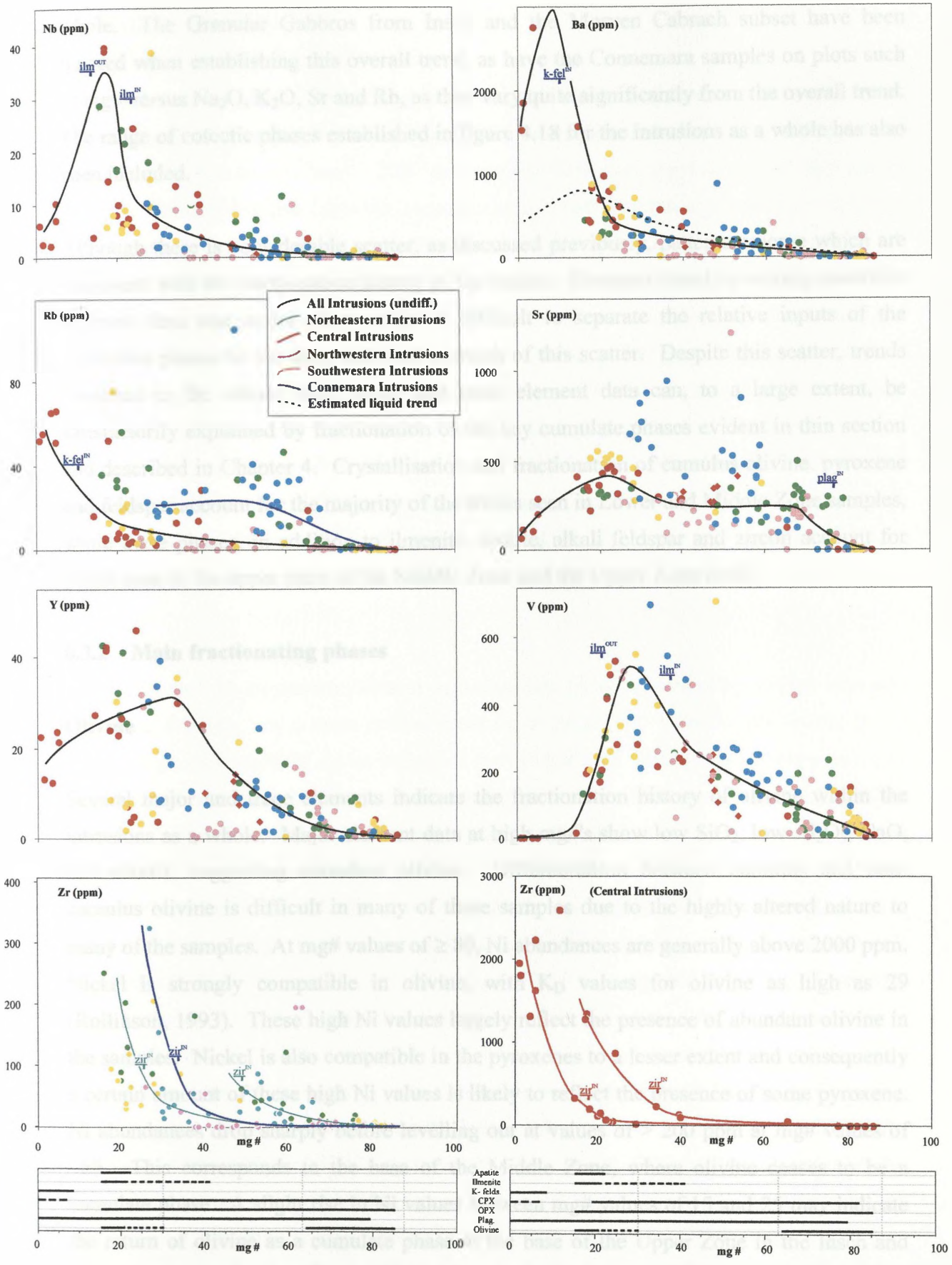


**Figure 6.8b (cont) Simplified fractionation paths for mg# versus trace elements.**

whole. The Granular Gabbros from Insch and the Morven Cabrach subset have been ignored when establishing this overall trend, as have the Connemara samples on plots such as mg# versus $Na_2O$, $K_2O$, Sr and Rb, as they vary quite significantly from the overall trend. The range of cotectic phases established in figure 4.18 for the intrusions as a whole has also been included.

Although there is considerable scatter, as discussed previously, patterns emerge which are consistent with the fractionation history of the bodies. Elements found in varying quantities in more than one major phase make it difficult to separate the relative inputs of the individual phases to the data, and lead to much of this scatter. Despite this scatter, trends observed in the whole rock major and trace element data can, to a large extent, be satisfactorily explained by fractionation of the key cumulate phases evident in thin section and described in Chapter 4. Crystallisation and fractionation of cumulus olivine, pyroxene and feldspar account for the majority of the trends seen in Lower and Middle Zone samples, while these phases, in addition to ilmenite, apatite, alkali feldspar and zircon account for trends seen in the upper parts of the Middle Zone and the Upper Zone itself.

### 6.3.2 Main fractionating phases

#### Olivine

Several major and trace elements indicate the fractionation history of olivine within the intrusions as a whole. Major element data at high mg#'s show low $SiO_2$, low $Al_2O_3$, CaO, and alkalis, suggesting abundant olivine. Differentiation between cumulus and non-cumulus olivine is difficult in many of these samples due to the highly altered nature to many of the samples. At mg# values of $\geq 80$, Ni abundances are generally above 2000 ppm. Nickel is strongly compatible in olivine, with $K_D$ values for olivine as high as 29 (Rollinson, 1993). These high Ni values largely reflect the presence of abundant olivine in the samples. Nickel is also compatible in the pyroxenes to a lesser extent and consequently a certain amount of these high Ni values is likely to reflect the presence of some pyroxene. Ni abundances drop sharply before levelling out at values of > 200 ppm at mg# values of ~65. This corresponds to the base of the Middle Zone, where olivine ceases to be a cumulate phase. A slight rise in Ni values between mg# values of 15 and 25 may indicate the return of olivine as a cumulate phase at the base of the Upper Zone in the Insch and Boganclogh samples (see figure 6.8b), although the high degree of compatibility of nickel with all mafic phases means abundances of nickel are quite low after the Lower Zone.

**Pyroxene**

The appearance of clinopyroxene as a major phase is most clearly seen on the plot of mg# versus Cr. Chromium has $K_D$ values up to 34 for clinopyroxene (Rollinson, 1993) and Cr values can be seen to rise from ~ 2000 ppm to over 4000 ppm quite sharply at mg# values of ~ 80. Some of this rise, however, may also be due to the presence of minor quantities of chrome spinel. Spinel was occasionally observed in the field and in thin section, although many of these samples tend to be quite badly altered, making precise identification of phases and their cumulate or non-cumulate nature difficult to establish, particularly for minor phases. Cr abundances then drop off to lower than 1000 ppm at mg# values of ~70 before dropping more slowly through the Middle and Upper Zones. In addition, CaO abundances rise sharply at mg# values of 75-80, although this rise is likely to be more as a result of incoming plagioclase feldspar than clinopyroxene. Scandium is found in both pyroxenes, but particularly clinopyroxene, and can be seen to broadly follow clinopyroxene fractionation, with an increase in abundance at mg#'s of ~70.

**Feldspar**

The appearance of plagioclase feldspar as a cumulate phase is marked by sudden increases in CaO, and $Al_2O_3$, and a more gradual increase in strontium. Considerable scatter in the CaO data possibly reflects the incoming of both plagioclase feldspar and clinopyroxene at slightly different mg# values, with the majority of the CaO content likely to reflect incoming plagioclase feldspar, although separating the relative roles of the two phases is difficult. Gradual decreases in the CaO content and corresponding increases in the $Na_2O$ content throughout the Middle Zone are likely to reflect the changing plagioclase composition from high to lower anorthite contents with continuing fractionation, while sharp rises in $K_2O$, Ba and Rb contents at mg# of <10 represent the incoming of cumulate alkali feldspar. Barium, in particular, reaches over 2.1% in some of the earliest crystallized alkali feldspars. $K_D$ values between Ba and plagioclase feldspar are generally <1, resulting in the gradual rise in Ba contents with decreasing mg# values, until the onset of cumulus alkali feldspar, in which Ba is strongly compatible ($K_D$ = 6-11 for high silica liquids; Rollinson, 1993). This results in sharp rises in Ba content, followed by a decrease as the magma is depleted in Ba. Sr values show substantial scatter, but generally rise from < 20 ppm to over 200 ppm at mg# values of 70-75. The exceptionally anorthic plagioclase feldspar seen in the Connemara bodies are likely to be the origin of the high $K_2O$ and low $Na_2O$ values seen for the whole rock chemistry of the Connemara bodies.

**Fe-Ti oxides (Ilmenite)**

The most obvious element to reflect ilmenite abundances is $TiO_2$. Although $TiO_2$ is also found in pyroxene, the gradual rise of $TiO_2$ values through the Middle Zone and the more sharp increase at mg# values of 25-20 is likely to reflect the presence of ilmenite as a cumulus phase. An inflection point and sharp falloff in $TiO_2$ abundances after this corresponds to the outgoing of ilmenite as a cumulus phase. This $TiO_2$ trend is mirrored in zinc, niobium and, to a lesser extent, vanadium data (all three are moderately to strongly compatible, with $K_D$ values up to and over 50), with Zn rising sharply to >150 ppm at mg# ~ 15, Nb abundances rising to >30 ppm at mg# of ~20 and V concentrations ~500 ppm at mg# ~ 25-20, before all three drop off sharply. The earlier rise in vanadium abundances may reflect the gradual incoming of cumulus ilmenite in the Middle Zone more clearly than the $TiO_2$, Zn or Nb data do. Plots of $TiO_2$ (wt%) versus Nb (ppm) show a good correlation (see figure 6.9), suggesting the whole rock niobium budget is primarily concentrated in ilmenite. This can also be seen in the 'spider' diagrams in Chapter 5, where the 'sizes' of Nb-troughs are related to Ti peaks; this can be best seen in figure 5.17, where sample Ab3826, from the Kinnadie mass possesses a Ti-peak while a Nb-trough is absent.

**Apatite**

$P_2O_5$ is strongly incompatible in all phases except apatite and consequently shows up the fractionation pattern of apatite quite well. $P_2O_5$ abundances remain very low (generally less than 0.1 wt%) throughout the Lower and Middle Zones, before rising sharply at mg# of 20-15. A well-defined inflection point causes the $P_2O_5$ values to drop considerably in Upper Zone rocks corresponding to the disappearance of apatite as a cumulus phase. This $P_2O_5$ trend is replicated to a certain extent by the REE data, with La, Ce and Nd abundances rising at mg# values of 20-15.

**Zircon**

Zirconium is also strongly incompatible in all of the phases fractionating in the Lower Zone and lower parts of the Middle Zone and consequently concentrations are low (generally <50 ppm). It can be seen in figure 6.8b that the apparent incoming of zircon as a cumulus phase is indicated by a sudden rise in Zr abundances. However, as discussed in Section 4.7.8, the precise role of zircon within the crystallisation history intrusions is quite difficult to determine, largely due to their fine-grained nature within samples.

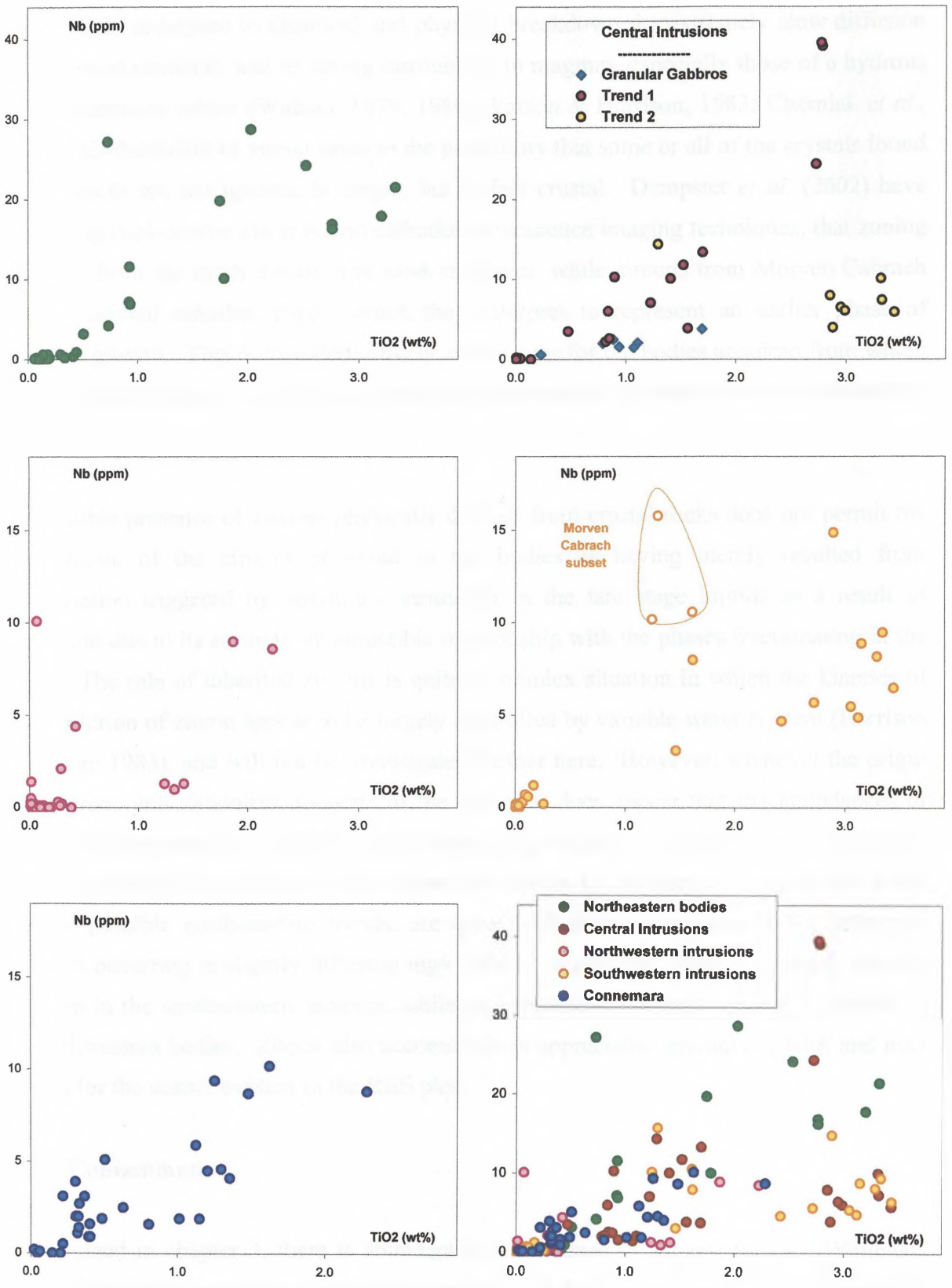


**Figure 6.9 $TiO_2$ (wt%) versus Nb (ppm) for the individual groups and for the 'Younger' Basics as a whole.**

Additional difficulties arise from the physical nature of zircons themselves. Zircon is well known for its resistance to chemical and physical breakdown, its extremely slow diffusion rates for most elements, and its strong insolubility in magmas, especially those of a hydrous and peraluminous nature (Watson, 1979, 1980; Watson & Harrison, 1983; Cherniak *et al.*, 1997). This durability of zircon leads to the possibility that some or all of the crystals found in these rocks are not igneous in origin, but in fact crustal. Dempster *et al.* (2002) have noted using back-scatter electron and cathodoluminescence imaging techniques, that zoning in zircons from the Insch intrusion is weak or absent, while zircons from Morven Cabrach show occasional euhedral cores, which they interpret to represent an earlier phase of magmatic growth. This is considered likely, as the ages for the bodies acquired from whole rock techniques appear to contain an inherited component of an earlier event or events (see Section 2.3).

The possible presence of zircons physically derived from crustal rocks does not permit the interpretation of the zircons observed in the bodies as having merely resulted from crystallisation triggered by zirconium saturation in the late stage liquids as a result of enrichment due to its strongly incompatible relationship with the phases fractionating in the bodies. The role of inherited zircons is quite a complex situation in which the kinetics of the dissolution of zircon appear to be largely controlled by variable water content (Harrison & Watson; 1983), and will not be investigated further here. However, whatever the origin of the zircon and zirconium contents of the bodies it does appear that the abundances of zircon and zirconium vary systematically from group to group. As discussed, the Central Intrusions display two separate trends; these two trends, in addition to a Connemara trend and two possible north-eastern trends, are quite well defined on figure 6.8b, inflection points all occurring at slightly differing mg# values. A possible, poorly scattered, trend is also seen in the southwestern samples, while no evidence for cumulus zircon is present in the northwestern bodies. Zircon also accommodates appreciable amounts of REE and may account for the scatter evident in the REE plots.

### 6.3.3 Contamination

As discussed in chapter 3, there is abundant field evidence to suggest that the 'Younger' Basics bodies have assimilated significant quantities of their predominantly pelitic envelope rocks during their fractionation and evolution. This field and thin section evidence, in addition to limited whole rock chemical and isotopic data suggest that the bodies have incorporated partial to complete melts of these Dalradian pelites, with a complete spectrum

of country rocks from schists to partially melted xenoliths present. As will be seen in the next section, attempts to model the fractionation of the 'Younger' Basics, from Granular Gabbros source rock to evolved Upper Zone rocks from Insch and Boganclogh require the input of some crustal material, as the 'spider' and REE plots of these evolved Upper Zone rocks cannot be achieved by fractional crystallization alone. However, as mentioned in Chapter 3, identification of contamination should be possible using relative mineral abundances, with the addition of $SiO_2$ and $Al_2O_3$ resulting in the formation of orthopyroxene and anorthitic plagioclase feldspar at the expense of olivine and clinopyroxene respectively, while additional $Na_2O$ and $K_2O$ result in the formation of additional biotite and/or amphibole. Consequently, samples or intrusions regarded as being significantly contaminated should possess different ratios of these minerals than those samples or intrusions regarded as being less contaminated. Although cumulate processes mean that this trend is not likely to be particularly well defined, it should be possible to distinguish between contaminated and uncontaminated intrusions on this basis.

To minimize any possible errors or scatter, only Middle Zone samples have been used for several reasons: firstly, a large proportion of Lower Zone samples display quite strongly layered textures, and are likely thus to contribute to the scatter evident in any trend; secondly, the outgoing of cumulus olivine at the phase transition from Lower Zone to Middle Zone may result in different ratios for the phases described above between samples from the two zones. Upper Zone samples are not included for the same reason, and also because they are only present from one group. As olivine is not present in the majority of Middle Zone samples, it has not been included for comparison. Samples in which the three phases selected, plagioclase feldspar, orthopyroxene and clinopyroxene form less than 60% of the rock have not been included either.

CIPW norm abundances of plagioclase feldspar, orthopyroxene and clinopyroxene have been calculated and are shown plotted in figures 6.10 for selected sets of samples, with the plagioclase feldspar and diopside abundances adjusted to plot in the approximate centre of the graph. In figure 6.10a, the classically contaminated northeastern bodies are compared with the northwestern bodies in which contamination is not believed to have played as significant a role in their development. It is evident that, as a whole, the northeastern bodies contain more normative plagioclase and hypersthene, consistent with the reactions outlined above. Whole rock $K_2O$ abundances have been plotted as labels in figure 6.10a; these $K_2O$ value are considered to represent an approximation of the amount of biotite present in samples, although care should be taken as the amount of biotite present in the sample is also

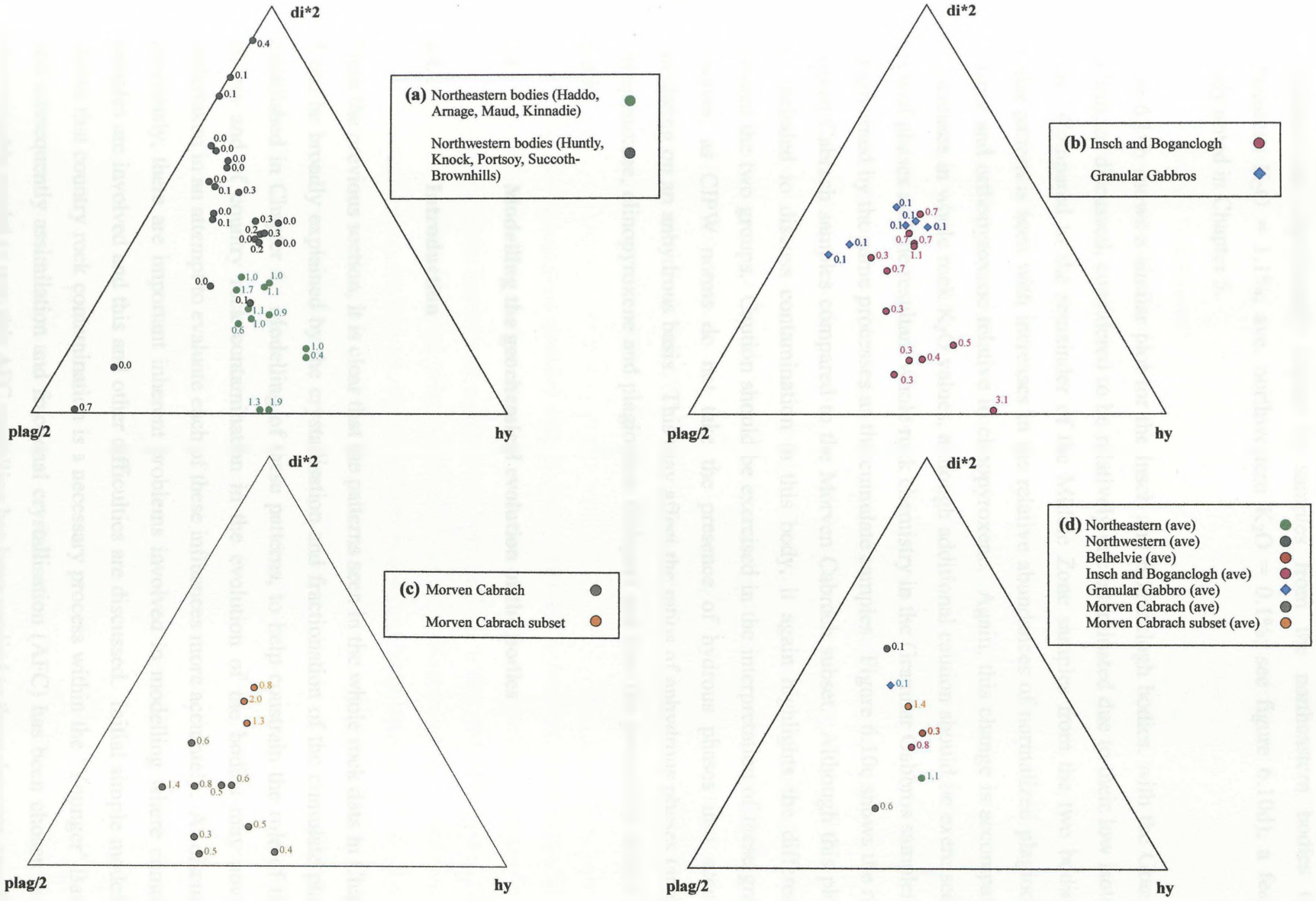


**Figure 6.10 Plots of normative plagioclase feldspar, diopside and hypersthene for selected Middle Zone sample groups as discussed in the text. Plagioclase values have been halved and diopside values doubled to move samples closer to the centre of the plot. Sample labels are whole rock $K_2O$ abundances.**

controlled by processes such as postcumulus growth. Nevertheless, it does appear that $K_2O$ abundances are significantly higher in samples from the northeastern bodies (ave. northeastern $K_2O$ = 1.1%; ave. northwestern $K_2O$ = 0.1%; see figure 6.10d), a feature already noted in Chapter 5.

Figure 6.10b shows a similar plot for the Insch and Boganclogh bodies, with the Granular Gabbros, as discussed, considered to be relatively uncontaminated due to their low isotopic ratios. Compared to the remainder of the Middle Zone samples from the two bodies, a similar pattern is seen with increases in the relative abundances of normalized plagioclase feldspar and orthopyroxene relative to clinopyroxene. Again, this change is accompanied by increases in whole rock $K_2O$ values, although additional caution should be exercised, as ratios of phases and the resultant whole rock chemistry in the Granular Gabbros samples are not governed by the same processes as the cumulate samples. Figure 6.10c shows the main Morven Cabrach samples compared to the Morven Cabrach subset. Although this plot is not included to discuss contamination in this body, it again highlights the differences between the two groups. Caution should be exercised in the interpretation of these graphs however, as CIPW norms do not take the presence of hydrous phases into account, calculating on an anhydrous basis. This may affect the ratios of anhydrous phases (such as orthopyroxene, clinopyroxene and plagioclase feldspar) and thus the potentially distort this graph.

## 6.4 Modelling the geochemical evolution of the bodies

### 6.4.1 Introduction

From the previous section, it is clear that the patterns seen in the whole rock data in Chapter 5 can be broadly explained by the crystallisation and fractionation of the cumulate phases established in Chapter 4. Modelling of these patterns, to help constrain the role of these phases and of country rock contamination in the evolution of the bodies may now be undertaken in an attempt to evaluate each of these influences more accurately. As discussed previously, there are important inherent problems involved in modelling where cumulate samples are involved and this and other difficulties are discussed. Initial simple modelling shows that country rock contamination is a necessary process within the 'Younger' Basics, and consequently assimilation and fractional crystallisation (AFC) has been chosen as the most suitable model to use; this AFC modelling has been applied to three datasets, two from the Central Intrusions and the third from the northeastern bodies for both major and trace

elements, using averaged sample analyses, probe data and published $K_D$ values. The results of these modelling procedures have then been compared to previous work, including isotopic studies.

### 6.4.2 Modelling constraints

#### The problem of cumulate processes

In attempting to model the evolution of the bodies, several unavoidable difficulties arise. The first and most significant problem is that the majority of these samples are, to a greater or lesser degree, of cumulate origin. As such, they do not precisely represent the liquid compositions from which they crystallised. This, however, as discussed previously, is a problem inherent to any samples containing appreciable amounts of cotectic phases, be they cumulates or phenocrysts-rich samples. As will be seen, the presence of cumulus phases is the primary cause of error in modelled results. However, there are some precautions which may be taken to minimize the effects which cumulate processes will have on the whole rock chemistry. The first of these is to use an average of several samples as 'parent' and 'daughter' analyses during modelling, thereby lessening the effects of any one cumulate process or any one sample on the results.

In addition, the omission of samples with strongly cumulate or layered textures can help to reduce the potential influence of cumulate processes on sample chemistry. In particular, samples with cumulate ilmenite or apatite have been omitted where possible. Many of the supposed incompatible elements behave compatibly in these phases and consequently using samples with cumulus ilmenite or apatite is likely to result in inaccurate modelling of many of these incompatible elements. Despite this, in the case of certain phases, most notably plagioclase feldspar, the effects of cumulate processes cannot be completely avoided, and consequently modelled strontium data should be treated with caution. Indeed, as will be seen, the main errors occurring in the trace element fractionation models are caused by the presence of cumulus phases, particularly apatite and ilmenite, in the observed daughter analysis and the compatibility of many of the so-called 'incompatible elements' in these phases.

Modelling has been attempted for both compatible and incompatible trace elements. Modelling of compatible elements, such as nickel and chromium, poses problems that are quite difficult to avoid. Both have high $K_D$ values for olivine, orthopyroxene and

clinopyroxene, as well as ilmenite and possibly chrome spinel. As a consequence, they are quite quickly removed from the melt (see figure 6.8b). In a cumulate sample, they are present in these ferromagnesian minerals, the abundances of which can vary quite considerably from sample to sample; accordingly, so do the compatible elements, making precise modelling difficult. In contrast, the incompatible trace elements are mainly found in the intercumulus material or 'trapped liquid' of a sample; their absolute abundances may vary, but their relative abundances should remain quite constant; this problem can be minimalized by double-normalisation of the data, which enables comparison of modelled values with actual rock abundances i.e. the *shape* of the real and modelled spider diagrams should be the same. To achieve this, spider diagrams of real and modelled values have been normalised with $Y_N$ values = 10, based on the convention of Thompson *et al.* (1984). Y has been chosen instead of Yb simply because yttrium data is available for all samples, while ytterbium data is only available for those samples analysed for REE.

Sample averages have been calculated in slightly different manners for major and trace elements. Major elements are straightforward averages of the total number of samples, which are also normalized to 100%. Trace element averages were calculated by normalizing each sample to a fixed value (the average yttrium composition of the samples), so that samples with high degrees of intercumulus material were not preferentially represented in the average. These values were then averaged to produce the overall average used in the modelling. This does not eliminate the over-representation of such samples, but reduces it somewhat. Trace element average abundances for the Granular Gabbro 'parent' analyses and the pelitic schist contaminants are straightforward averages, as cumulate processes are not responsible for their compositions. When comparing the modelled abundances of the trace elements selected with the actual abundances in the daughter analyses, it is necessary to double normalise the data, as single normalization of the data for spider diagrams does not take into account the role of 'trapped liquid' in determining the overall abundances of the trace elements. As a consequence of this 'trapped liquid' effect, the levels of fractionation and contamination predicted by the modelling should be regarded only as being approximate.

**The role of contamination**

As seen previously in Chapter 3 and Section 6.3, contamination of the evolving magma by country rocks is an important process that needs to be taken into consideration when attempting to model the evolution of the magmas. High degrees of country rock

assimilation by the magmas are likely to have occurred during the cooling and crystallisation of the bodies. Chemical evidence for this is shown in figures 6.11 and 6.12. 'Spider' and REE plots of the Granular Gabbros, Insch and Boganclogh Upper Zone samples, and typical northeastern samples are shown in figures 6.11a to 6.11f, with averages of these samples shown in figures 6.11g and 6.11h. It is evident from these plots that there is a substantial difference between the slopes of the 'spider' and REE plots of the parental (Granular Gabbro) samples ($La_N/Yb_N$ = 1.4 – 2.7; ave(n=4) = 2.0) and both the Insch and Boganclogh Upper Zone ($La_N/Yb_N$ = 8.6 – 32.1; ave(n=5) = 15.5) and the northeastern gabbros ($La_N/Yb_N$ = 5.5 – 7.4; ave(n=5) = 6.1). It is clear from these plots and from those in Section 5.4, that the fractionation and evolution of the bodies was accompanied by a progressive steepening of the slopes of both 'spider' and REE patterns. Any attempt to evaluate this fractionation and evolution must account for this continuing change from flat (Granular Gabbro) to steeply sloping (Insch and Boganclogh Upper Zone and northeastern gabbros) 'spider' and REE patterns.

Initially, simple (Rayleigh) fractional crystallization, using the distribution coefficients from Table 6.4 has been carried out for the main phases established as fractionating phases, and for a 'mixture' of these phases; this 'mixture' is an estimate based on the modal proportions of these phases in the 'Younger' Basics as a whole. Although ilmenite and apatite fractionate as minor phases in some parts of the Middle Zone, they are not considered to fractionate in sufficient quantities to affect these 'spider' and REE slopes significantly and have been omitted from this initial modelling. As the Central Intrusions range from peridotitic through to syenitic in composition, high amounts of fractionation are considered likely. Consequently, 90% fractional crystallisation of the individual phases olivine, orthopyroxene, clinopyroxene, plagioclase feldspar and hornblende has been carried out, and this is shown in figures 6.12a to 6.12c, along with a similar model for the 'mixture' of these phases in the proportions shown.

Although the modelled abundances may vary (figure 6.12a and 6.12b), the slopes of the patterns remain very similar to those of the Granular Gabbros (figure 6.12c), with only high amounts of fractionation of orthopyroxene, clinopyroxene, or amphibole changing the slope significantly. In particular, fractionation of hornblende can steepen the slope quite substantially ($La_N/Yb_N$ values rising from 2.0 for the Granular Gabbros to ~24.2 for 90% fractional crystallisation); however, fractionation of amphibole or either pyroxene or combinations of these three phases is strongly inconsistent with the petrographic and chemical data presented thus far. Indeed, there is no evidence to suggest the fractionation

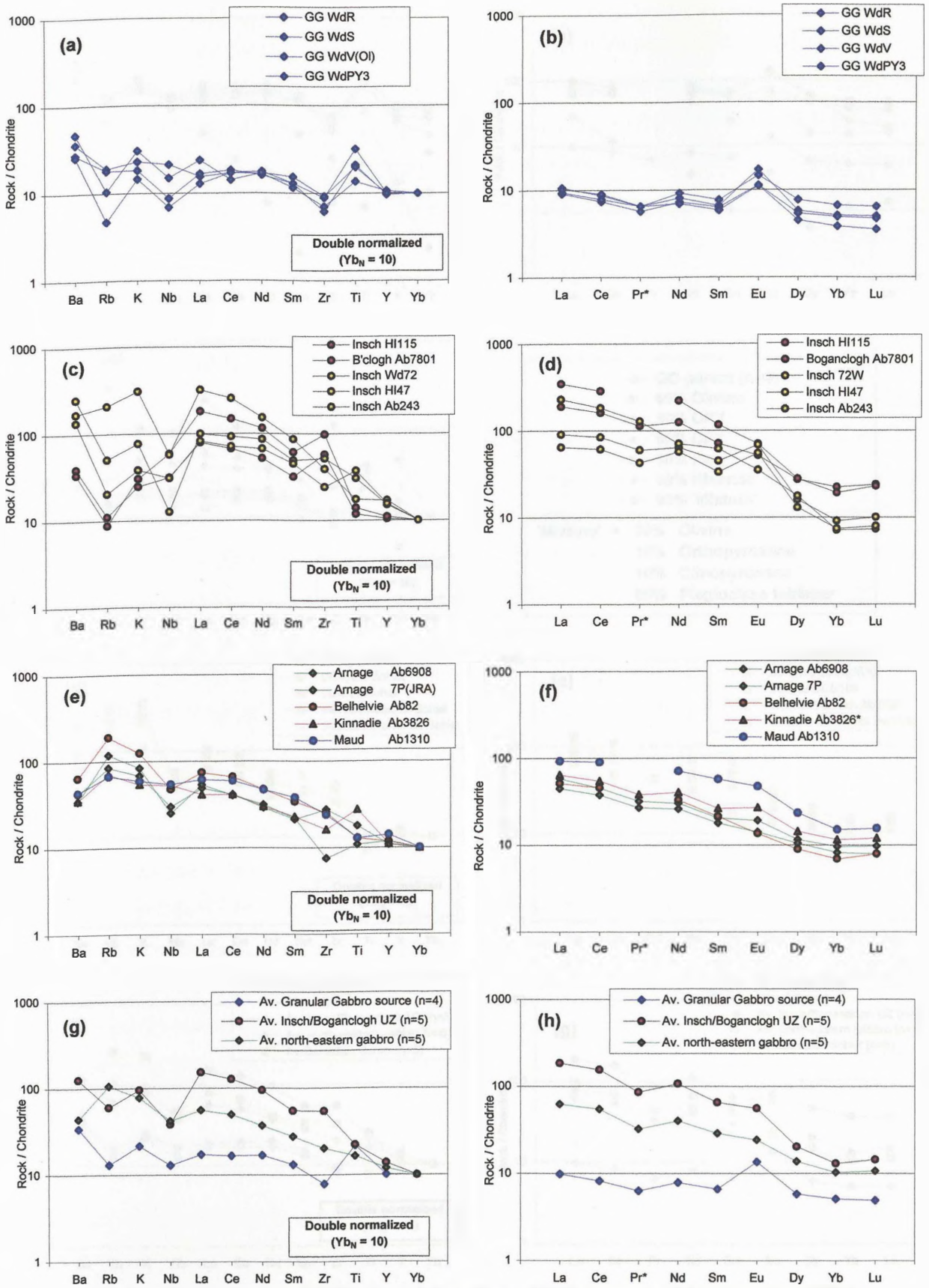


**Figure 6.11 Selected chondrite normalized 'spider' and REE plots for (a & b): the Granular Gabbros; (c & d): Upper Zone Insch and Boganclogh samples; (e & f): contaminated north-eastern gabbros; and (g & h): average analyses. Gd, Ho and Er data omitted from REE plots due to contamination Spider' plots are double normalized.**

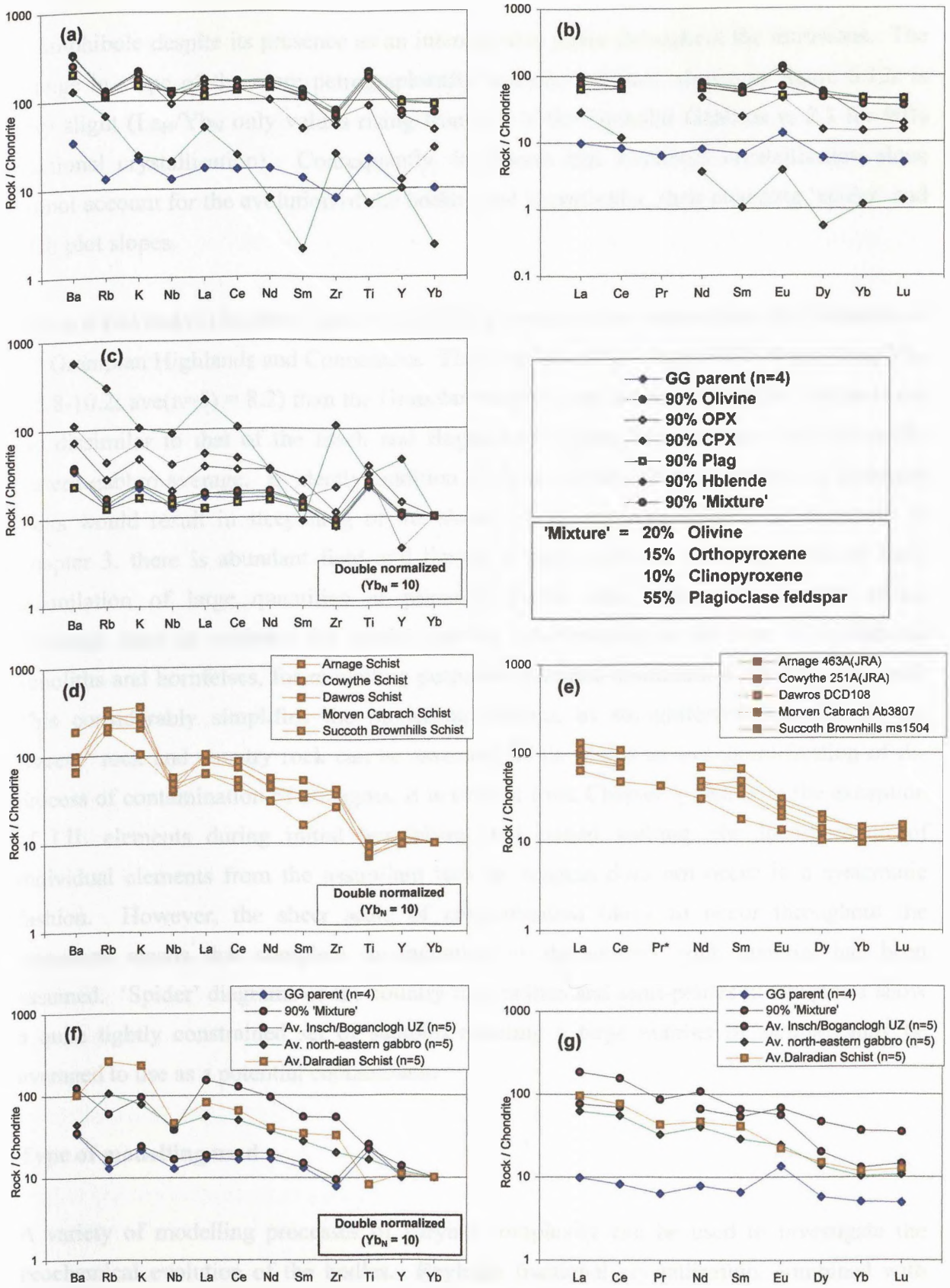


**Figure 6.12** **(a+b) 'Spider' and REE plots of the effects of high amounts of fractionation (90%) of individual phases and of a 'mixture', on the Granular Gabbro source;**
**(c) Double normalized 'spider' plot of the 'spiders' in plot (a);**
**(d+e) 'Spider' and REE plots of typical country rock schists;**
**(f+g) 'Spider' and REE plots of average samples from the above plots and from figure 6.11. 'Spiders' in plots c, d and f are double normalized.**

of amphibole despite its presence as an intercumulus phase throughout the intrusions. The change in slope of the more petrographically realistic 'mixture' shown in figure 6.12c is very slight ($La_N/Yb_N$ only values rising from 2.0 in the Granular Gabbros to 2.1 for 90% fractional crystallisation). Consequently, it appears that fractional crystallisation alone cannot account for the evolution of the bodies, and in particular, their changing 'spider' and REE plot slopes.

Figure 6.12d and 6.12e show 'spider' and REE plots of typical schists from the Dalradian of the Grampian Highlands and Connemara. They display much steeper REE slopes ($La_N/Yb_N$ = 5.8-10.2; ave(n=5) = 8.2) than the Granular Gabbros, and the overall 'spider' shape is not too dissimilar to that of the Insch and Boganclogh Upper Zone average and the north-eastern gabbro average. Evidently, addition of these schists either as a whole or as partial melts would result in steepening of the slopes of the resultant rocks. As discussed in Chapter 3, there is abundant field and limited isotope evidence pointing to whole scale assimilation of large quantities of primarily pelitic and semi-pelitic country rocks. Although there is evidence for partial melting contributions in the form of desilicated xenoliths and hornfelses, for modelling purposes complete assimilation has been assumed. This considerably simplifies the modelling process, as straightforward mixing of the 'parent' rock and country rock can be assumed; while this is an oversimplification of the process of contamination of a magma, it is evident from Chapter 3 that, with the exception of LIL elements during initial hornfelsing and partial melting, the incorporation of individual elements from the assimilant into the magma does not occur in a systematic fashion. However, the sheer scale of contamination likely to occur throughout the intrusions means that complete incorporation of the country rock material has been assumed. 'Spider' diagrams of the country rock pelites and semi-pelites in Chapter 3 show a quite tightly constrained set of samples meaning a large number of samples may be averaged to use as a potential contaminant.

**Type of modelling used**

A variety of modelling processes of varying complexity can be used to investigate the geochemical evolution of the bodies. Rayleigh fractional crystallisation, combined with assimilation of crustal material has been chosen as the model best suited to investigate the evolution for a variety of reasons. Equilibrium crystallisation was rejected on the basis that the presence of zoned crystals in most bodies, albeit weak in many cases, suggested that, while equilibrium crystallisation may take place locally, the re-equilibration of crystallising

phases with their parental melt as the dominant fractionating process would not lead to the degree of compositional variation seen within the 'Younger' Basics as a whole. The *in situ* crystallisation model of Langmuir (1989) has also been rejected, largely because many of the constraints required for this model, such as magma chamber mass and the fraction of magma returning to the magma chamber from the solidification zone at the chamber wall-magma interface would be quite difficult to define for these bodies; in reality the fractionation process is probably intermediate between Rayleigh and equilibrium fractionation, and may well approximate to this *in situ* model. On the basis of the evidence in Section 6.2, ideally one should attempt to model a more dynamic system of continuous fractionation with periodic addition and removal of magma (RTF) (O'Hara & Matthews, 1981), but insufficient data is present on parental magma compositions other than the Granular Gabbro, and little or no evidence is present for possible tapping of magma from the chamber, or the likely quantities of any of these processes.

Consequently, Rayleigh fractionation, combined with country rock contamination has been chosen as the most appropriate modelling approach; accordingly, assimilation and fractional crystallisation (AFC) modelling has been carried out on the trends identified, initially using 'least squares' mass balance modelling on the major element dataset. The results of this simple mixing have then been used as a guideline for more detailed trace element AFC modelling. Three distinct fractionation trends have been selected from the overall data trend for AFC modelling using both major and trace element data and are outlined in the next section.

'Least squares' mass balance modelling has been carried out on the major element dataset. Calculations were performed using 'IGPET Mixing', a Windows based 'least squares' mixing program. For whole rock major element data, the data were firstly averaged for the number of samples used, $Fe_2O_3$ abundances were then recalculated to FeO, and then the overall analysis total was normalized to 100%. Mineral probe data were also normalized to 100%, and attempts at straightforward major element mass balance modelling were undertaken in the three cases outlined below.

Trace element modelling is based on the equations of De Paolo (1981) and Powell (1984). Using the proportions of the fractionating phases, and degrees of fractionation and contamination calculated from the 'least squares' major element modelling, trace element modelling has been attempted, using a simple template or worksheet in Microsoft Excel. Distribution coefficients for the trace element modelling are based on the compilation of

Rollinson (1993) and are shown in Table 6.4. A wide range of $K_D$ data exist in the published literature, depending on the specific situation being investigated, the analytical techniques used, and a variety of controlling parameters such as temperature, magma composition and oxygen fugacity. Although the broad overall crystallising conditions of the 'Younger' Basics are known, the influence of many of these parameters, such as oxygen fugacity, on $K_D$ values is poorly constrained. Consequently, for this study, the distribution coefficient values chosen are values considered typical for equilibration between the fractionating phases and basaltic liquids, with more extreme $K_D$ values rejected. Several trace elements have not been modelled. Tb and Tm data have been omitted from the modelling for two reasons; firstly, the original Tm and Tb data in this study are not actual measured data, having been interpolated from other REE values merely for plotting purposes, and secondly, published distribution coefficients for Tb and Tm are quite limited. Phosphorus data (from major element $P_2O_5$ data) have also been omitted, as some lower $P_2O_5$ concentrations are potentially inaccurate, as discussed previously.

### 6.4.3 Trends selected for modelling

Any attempt to assess the role of fractionation of the various phases and of country rock assimilation in the dataset as a whole would prove quite difficult, chiefly because there is a substantial spread to the data. Because of this, reasonably well-defined data subsets have been selected for modelling purposes. Three main trends have been selected for modelling; these are outlined below, and are summarised in the flowchart in figure 6.13. The three trends are also shown in figures 6.14 and 6.22 plotted against whole rock mg#.

**Model 1**

From a Granular Gabbro source material to a typical Insch and Boganclogh Middle Zone composition by AFC processes. This has been modelled for both major and trace elements, using the whole rock and mineral probe data from Trend 1 of the Insch and Boganclogh bodies, shown in figure 6.14. There are several reasons for this selection; firstly, Trend 1 from Insch and Boganclogh is the most complete trend within the overall dataset, and is reasonably representative of the trends in the 'Younger' Basics as a whole. Secondly, the trend is quite well defined, with particularly low scatter, especially for samples with intermediate mg# values. In addition, the modelling can be compared with published isotope data from comparable rocks.

| Phase / KD values | Olivine | OPX | CPX | Plag. | Ilmenite* | Apatite | Alk feld. | Zircon |
|---|---|---|---|---|---|---|---|---|
| Ba | 0.0099 | 0.013 | 0.026 | 0.23 | 0.00034 | 0.05 | 20 | |
| Rb | 0.0098 | 0.022 | 0.031 | 0.071 | 0.1 | 0.4 | 0.4 | |
| K | 0.0068 | 0.014 | 0.038 | 0.17 | 0.045 | | 10 | |
| Nb | 0.01 | 0.15 | 0.05 | 0.01 | 2 | 0.1 | 0.04 | |
| La | 0.0067 | 0.002 | 0.056 | 0.022 | 0.098 | 14.5 | 0.129 | 4.18 |
| Ce | 0.006 | 0.02 | 0.092 | 0.016 | 0.11 | 21.1 | | 4.31 |
| Sr | 0.014 | 0.04 | 0.06 | 1.83 | 0.17 | 1.3 | 4 | |
| Nd | 0.0059 | 0.03 | 0.23 | 0.014 | 0.14 | 32.8 | 0.03 | 4.29 |
| Sm | 0.007 | 0.05 | 0.445 | 0.072 | 0.15 | 46 | 0.026 | 4.94 |
| Zr | 0.012 | 0.18 | 0.1 | 0.048 | 0.1 | 0.1 | 0.05 | 500 |
| Ti | 0.02 | 0.1 | 0.4 | 0.04 | 150 | 0.1 | | |
| Y | 0.01 | 0.18 | 0.9 | 0.03 | 0.2 | 40 | 0.02 | 71.4 |
| Yb | 0.02 | 0.34 | 0.542 | 0.056 | 0.17 | 15.4 | 0.03 | 527 |
| Ni | 9.3 | 5 | 4 | 0.06 | 3.8 | | 1.1 | |
| Cr | 0.7 | 10 | 13 | 0.02 | 6 | 9 | | 68.65 |
| V | 0.06 | 0.6 | 1.35 | | 26 | | | 189.5 |
| Sc | 0.17 | 1.2 | 3 | 0.01 | 1.8 | 0.22 | 0.029 | 1.52 |

**Table 6.4 Distribution coefficient values used for modelling in Section 6.5. The majority of the values used are from the compilation in Rollinson (1993).**

**Model 1**

| | OlLZ | CPXLZ | OPXLZ | PlagLZ |
|---|---|---|---|---|
| SiO2 | 41.72 | 53.17 | 55.79 | 52.34 |
| TiO2 | 0.00 | 0.35 | 0.30 | 0.00 |
| Al2O3 | 0.00 | 2.46 | 1.24 | 30.74 |
| FeO | 15.30 | 5.24 | 11.64 | 0.00 |
| MnO | 0.07 | 0.06 | 0.22 | 0.00 |
| MgO | 42.91 | 17.13 | 29.21 | 0.00 |
| CaO | 0.00 | 21.32 | 1.60 | 15.59 |
| Na2O | 0.00 | 0.27 | 0.00 | 1.33 |
| K2O | 0.00 | 0.00 | 0.00 | 0.00 |
| P2O5 | 0.00 | 0.00 | 0.00 | 0.00 |

**Model 2**

| | OlMZ | CPXMZ | OPXMZ | PlagMZ | IlmMZ | ApMZ |
|---|---|---|---|---|---|---|
| SiO2 | 35.31 | 52.69 | 52.59 | 55.05 | 0.18 | 0.00 |
| TiO2 | 0.00 | 0.19 | 0.25 | 0.00 | 52.73 | 0.00 |
| Al2O3 | 0.00 | 1.04 | 1.09 | 28.53 | 0.00 | 0.00 |
| FeO | 41.48 | 10.76 | 23.87 | 0.13 | 46.28 | 0.00 |
| MnO | 0.45 | 0.23 | 0.51 | 0.00 | 0.30 | 0.00 |
| MgO | 22.77 | 13.55 | 20.09 | 0.00 | 0.51 | 0.00 |
| CaO | 0.00 | 21.19 | 1.60 | 11.71 | 0.00 | 57.81 |
| Na2O | 0.00 | 0.35 | 0.00 | 4.28 | 0.00 | 0.00 |
| K2O | 0.00 | 0.00 | 0.00 | 0.30 | 0.00 | 0.00 |
| P2O5 | 0.00 | 0.00 | 0.00 | 0.00 | 0.00 | 42.19 |

**Model 3**

| | OlMZ | CPXMZ | OPXMZ | PlagMZ |
|---|---|---|---|---|
| SiO2 | 40.56 | 53.01 | 55.28 | 48.44 |
| TiO2 | 0.00 | 0.55 | 0.20 | 0.00 |
| Al2O3 | 0.00 | 2.41 | 1.12 | 32.49 |
| FeO | 13.53 | 6.54 | 16.17 | 0.10 |
| MnO | 0.20 | 0.34 | 0.28 | 0.00 |
| MgO | 45.71 | 15.83 | 25.96 | 0.00 |
| CaO | 0.00 | 20.53 | 0.84 | 16.98 |
| Na2O | 0.00 | 0.64 | 0.15 | 1.99 |
| K2O | 0.00 | 0.15 | 0.00 | 0.00 |
| P2O5 | 0.00 | 0.00 | 0.00 | 0.00 |

**Table 6.5 Typical mineral compositions from probe data used in 'least squares' modelling in Section 6.5**

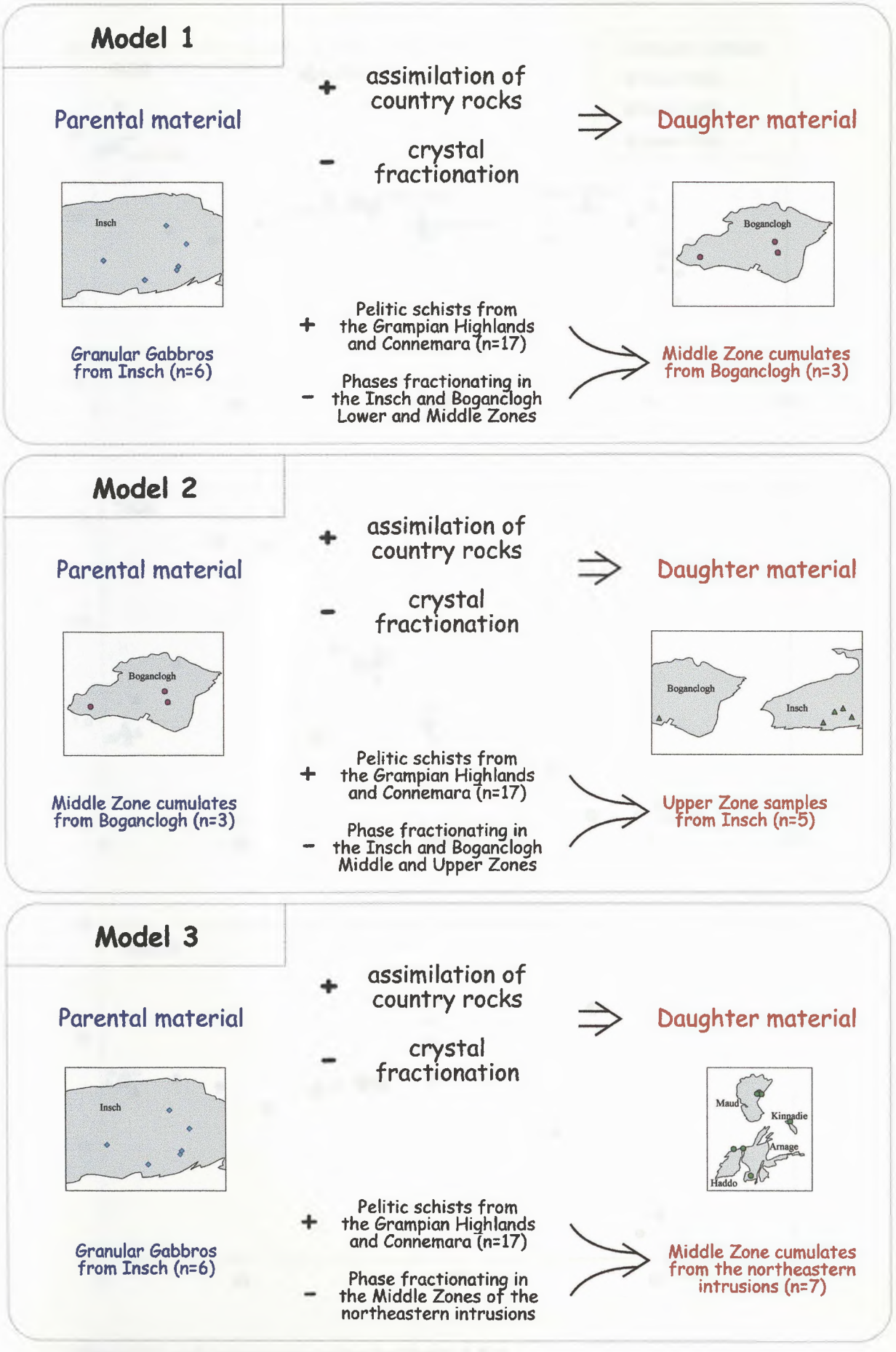


**Figure 6.13 Flow chart illustrating the three trends selected for modelling in Section 6.4. Maps are not to scale.**

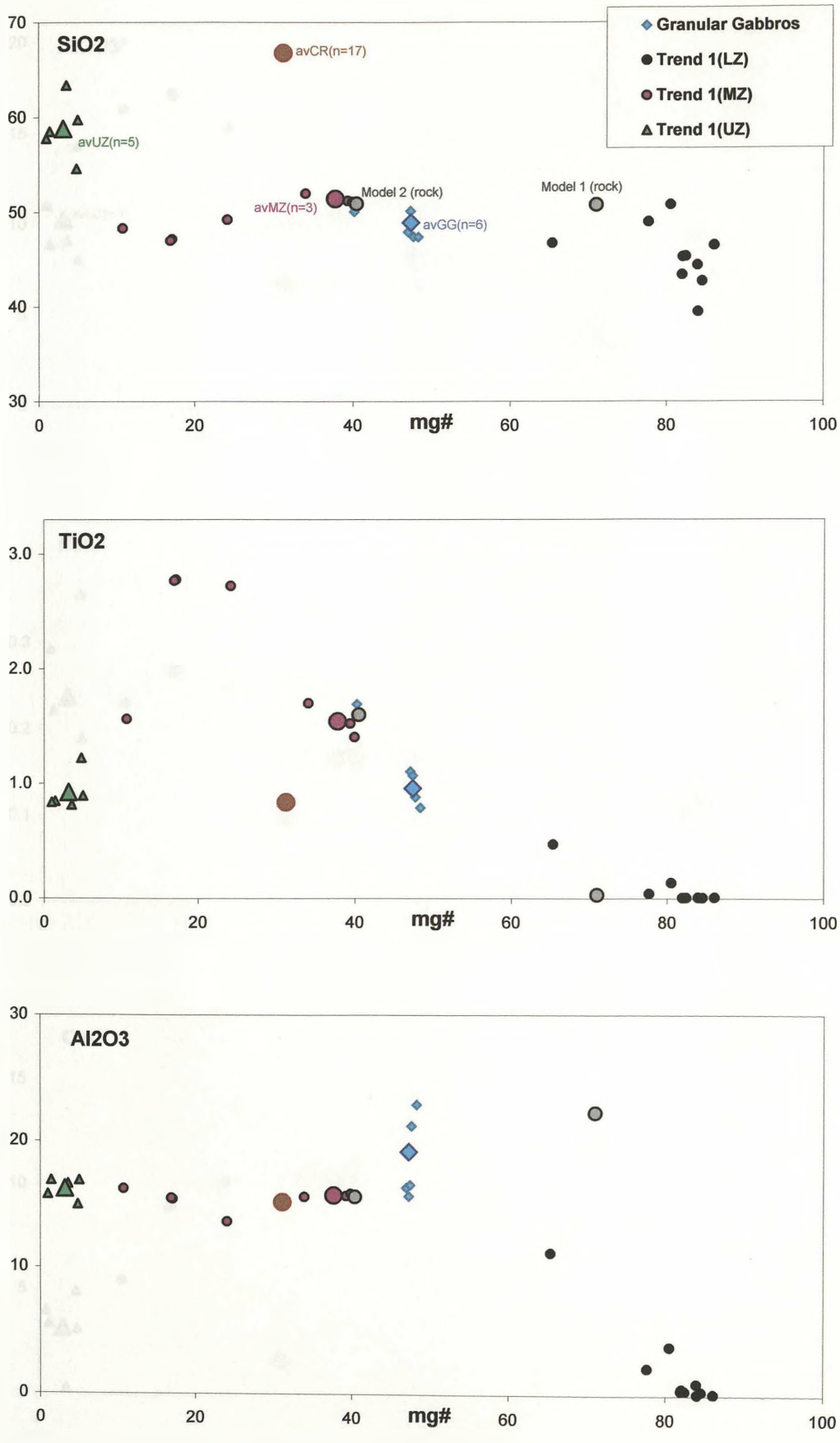


**Figure 6.14 mg# versus major oxides for Models 1 & 2**

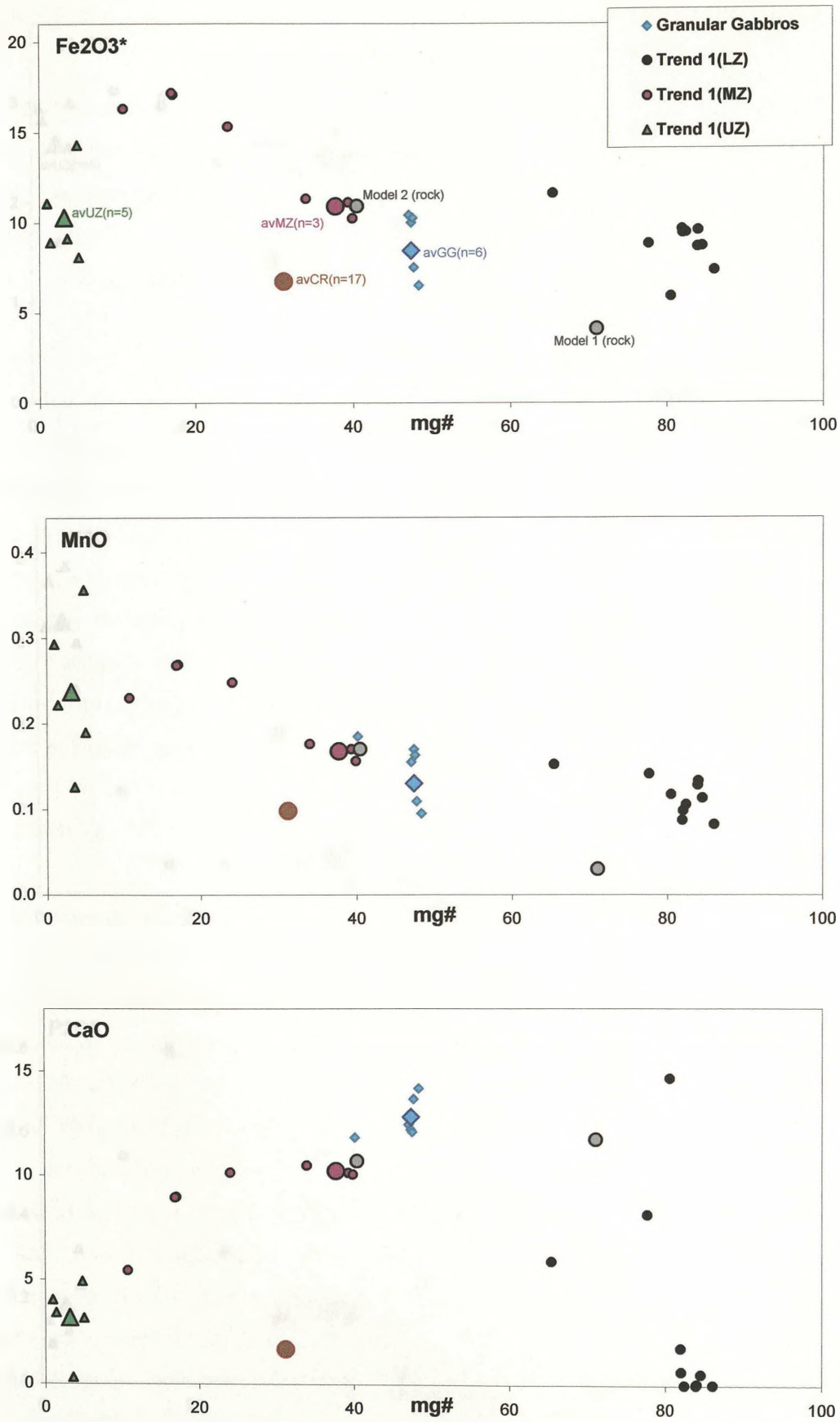


**Figure 6.14 (cont) mg# versus major oxides for Models 1 & 2**

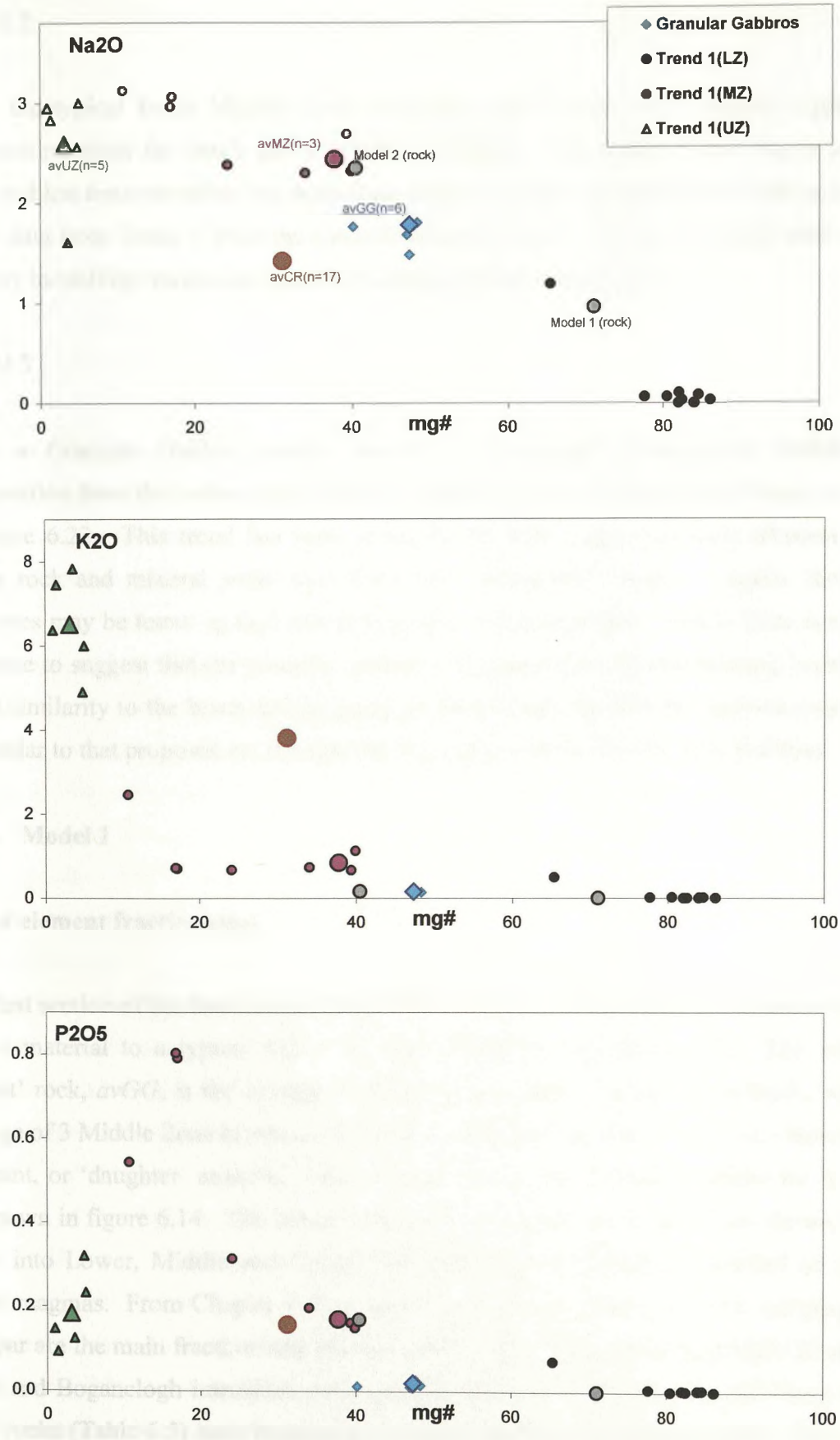


**Figure 6.14 (cont) mg# versus major oxides for Models 1 & 2**

**Model 2**

From the typical Insch Middle Zone composition in Model 1 to a typical Upper Zone composition from the Insch and Boganclogh bodies. This trend is also shown in figure 6.14, and has been modelled for both major and trace elements with whole rock and mineral probe data from Trend 1 from the Central Intrusions used. The trend is quite well defined, and any modelling results can again be tested published isotope data.

**Model 3**

From a Granular Gabbro source material to a typical contaminated Middle Zone composition from the northeastern bodies of Haddo, Arnage, Kinnadie and Maud, as shown in figure 6.22. This trend has been modelled for both major and trace elements, using whole rock and mineral probe data from the northeastern samples. Again, these AFC processes may be tested against previous studies and isotope data. While there is no direct evidence to suggest that the Granular Gabbros are parental to the northeastern bodies, their broad similarity to the Insch and Boganclogh bodies suggests that the parental magma will be similar to that proposed for the Central Intrusions, namely the Granular Gabbros.

### 6.4.4 Model 1

**Major element fractionation**

The first section of the fractionation path to be modelled is that from the 'Granular Gabbro' source material to a typical Insch and Boganclogh Middle Zone rock. The source or 'parent' rock, *avGG*, is the average of 6 Granular Gabbros samples from Insch, while the average of 3 Middle Zone biotite norite samples from Boganclogh, *avMZ*, was chosen as the resultant, or 'daughter' analysis. Plots of mg# versus major element oxides for this trend are shown in figure 6.14. The samples from Trend 1 used in this model are shown, broken down into Lower, Middle and Upper Zones the Granular Gabbros included as possible parent magmas. From Chapter 4, it is evident that olivine, both pyroxenes and plagioclase feldspar are the main fractionating phases in the Lower Zone and lower Middle Zone of the Insch and Boganclogh intrusions, and typical probe values from Lower and lower Middle Zone rocks (Table 6.5) have been used to model this early fractionation path. The country rock chosen as an assimilant is *avCR*, an average of 17 Dalradian pelitic and semi-pelitic

schists from throughout the Grampian Highlands and Connemara and this is also shown on figure 6.14.

The results of this 'least squares' mass balance modelling are shown in Table 6.6. The $R^2$ value of 0.288 is considerably lower than for modelling by fractional crystallisation alone ($R^2 \sim 1.8$), with the low CaO and high alkali content of the country rock helping to provide a good fit, while $Na_2O$ and $P_2O_5$ values are somewhat higher than predicted. The modelling suggests that approximately 40% of the parent magma has fractionated, with addition of just over 17% of country rock required to produce this Middle Zone rock. In addition, a theoretical rock composed of the phases olivine, orthopyroxene and clinopyroxene and plagioclase feldspar in the proportions predicted by the modelling would be roughly similar to those Lower Zone rocks observed in the Central Intrusions (see figure 6.14), while modal analyses of actual Insch Lower Zone rocks display similar proportions of olivine orthopyroxene and clinopyroxene to those modelled.

**Trace element fractionation**

Using the parameters calculated in the above 'least squares' modelling, trace element modelling was performed. 17.1% of the contaminant pelitic schist (*avCR*) has been added to the Granular Gabbro source rock, *avGG*, while olivine, clinopyroxene, orthopyroxene and plagioclase feldspar are removed in the proportions shown in Table 6.6. The results of the modelling are shown in figure 6.15a, with fractionation shown in 10% increments. The observed daughter, *avMZ* is shown in figure 6.15b alongside the modelled daughter, displaying 39.9% fractionation, and the problem caused by the presence of cumulus apatite is evident. In this graph, and in the double normalised equivalent (figure 6.15c), REE and Y abundances in the observed daughter are consistently higher than those modelled. This is due to the presence of a small amount (~1.5%) of cumulus apatite in the observed daughter sample. The influence of this apatite can be seen more clearly in figure 6.16a, where the difference in the REE and Y values of the observed and calculated daughter analyses is plotted with the concentrations in a typical apatite from a intrusive complex (Hoskin *et al.*, 2000). It is evident that 1.5% of this apatite corresponds closely to the REE and Y variation between the observed and modelled daughter analyses. The presence of additional apatite is also suggested by the mass balance modelling in Table 6.6, where the observed $P_2O_5$ value (0.17%) is somewhat higher than that predicted (0.04%).

| | Parent | Contaminant | Daughter | | |
|---|---|---|---|---|---|
| | avGG(n=6) | avCR(n=17) | avMZ(n=3) | | |
| | | | Obs. | Calc. | Misfit (R) |
| SiO2 | 49.17 | 67.23 | 51.97 | 51.96 | 0.01 |
| TiO2 | 1.09 | 0.84 | 1.56 | 1.45 | 0.11 |
| Al2O3 | 18.30 | 15.30 | 15.91 | 15.93 | -0.02 |
| FeO* | 8.43 | 6.11 | 9.90 | 10.00 | -0.10 |
| MnO | 0.15 | 0.10 | 0.17 | 0.19 | -0.02 |
| MgO | 8.07 | 3.30 | 6.67 | 6.64 | 0.03 |
| CaO | 12.90 | 1.69 | 10.34 | 10.36 | -0.02 |
| Na2O | 1.74 | 1.44 | 2.46 | 1.97 | 0.49 |
| K2O | 0.13 | 3.83 | 0.85 | 0.93 | -0.08 |
| P2O5 | 0.01 | 0.16 | 0.17 | 0.04 | 0.13 |
| **% of contaminant added:** | | 17.1 % | | $R^2$ = | 0.288 |
| **Fractionated Phases:** | | 16.3 % Olivine | | | |
| | | 1.7 % Orthopyroxene | | | |
| | | 9.7 % Clinopyroxene | | | |
| | | 72.3 % Plagioclase | | | |
| **% Fractionated** | | 39.9 % | | | |

**Table 6.6 'Least squares' mass balance modelling of contamination and fractionation in Model 1 from the Lower and Middle Zones of the Insch and Boganclogh intrusions**

| | Parent | Contaminant | Daughter | | |
|---|---|---|---|---|---|
| | avMZ(n=3) | avCR(n=17) | avUZ(n=5) | | |
| | | | Obs. | Calc. | Misfit (R) |
| SiO2 | 51.97 | 67.23 | 59.84 | 59.85 | -0.01 |
| TiO2 | 1.56 | 0.84 | 0.94 | 0.93 | 0.01 |
| Al2O3 | 15.91 | 15.30 | 16.52 | 16.49 | 0.03 |
| FeO* | 9.90 | 6.11 | 9.44 | 9.45 | -0.01 |
| MnO | 0.17 | 0.10 | 0.24 | 0.16 | 0.08 |
| MgO | 6.67 | 3.30 | 0.35 | 0.32 | 0.03 |
| CaO | 10.34 | 1.69 | 3.22 | 3.21 | 0.01 |
| Na2O | 2.46 | 1.44 | 2.64 | 2.76 | -0.12 |
| K2O | 0.85 | 3.83 | 6.62 | 6.56 | 0.06 |
| P2O5 | 0.17 | 0.16 | 0.19 | 0.20 | -0.01 |
| **% of contaminant added:** | | 3.4 % | | $R^2$ = | 0.027 |
| **Fractionated Phases:** | | 4.4 % Olivine | | | |
| | | 18.7 % Orthopyroxene | | | |
| | | 19.6 % Clinopyroxene | | | |
| | | 54.0 % Plagioclase | | | |
| | | 2.9 % Ilmenite | | | |
| | | 0.4 % Apatite | | | |
| **% Fractionated** | | 87.7 % | | | |

**Table 6.7 'Least squares' mass balance modelling of contamination and fractionation in Model 2 from the Middle and Upper Zones of the Insch and Boganclogh intrusions**

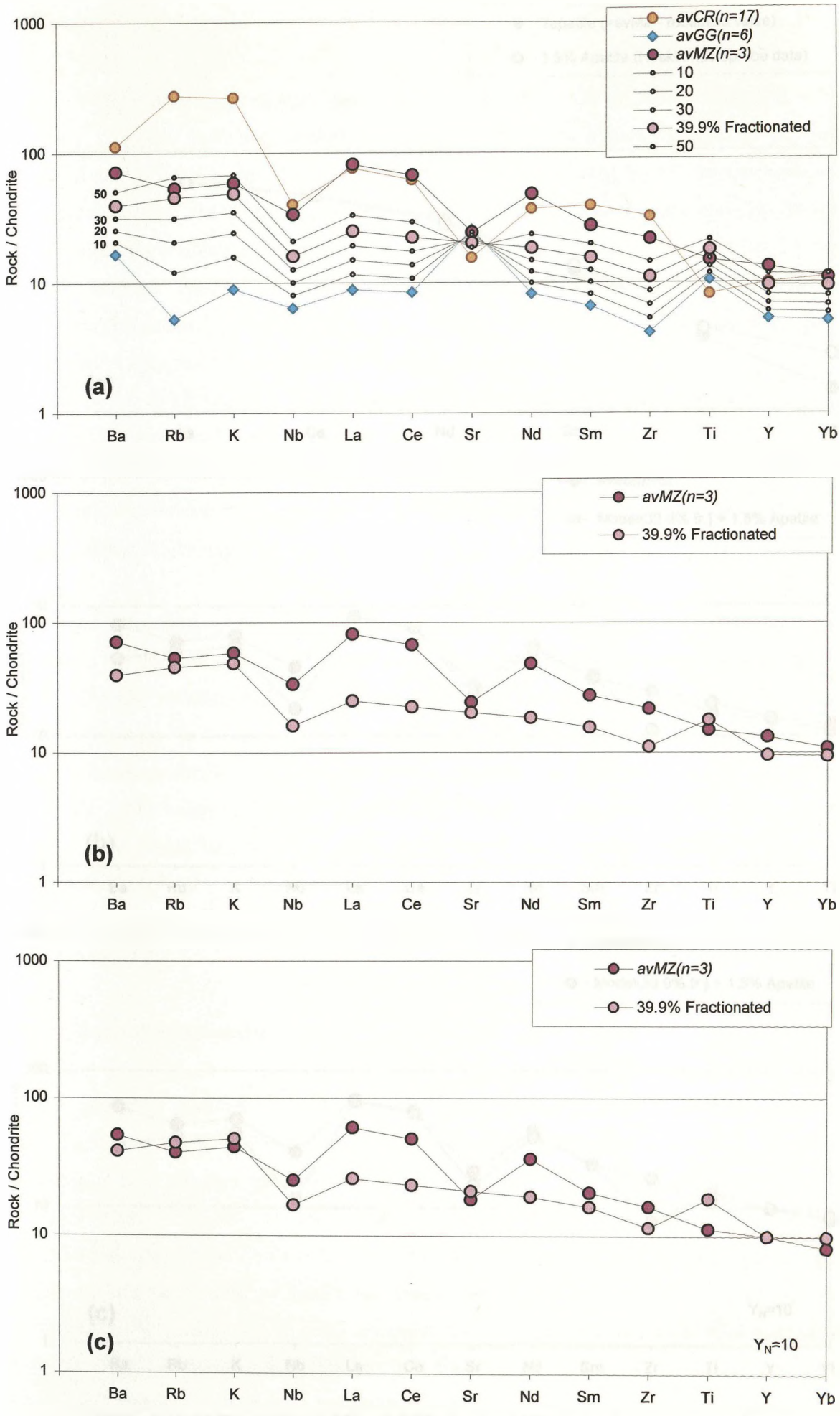


**Figure 6.15 'Spider' diagrams of modelled and actual data for Model 1**

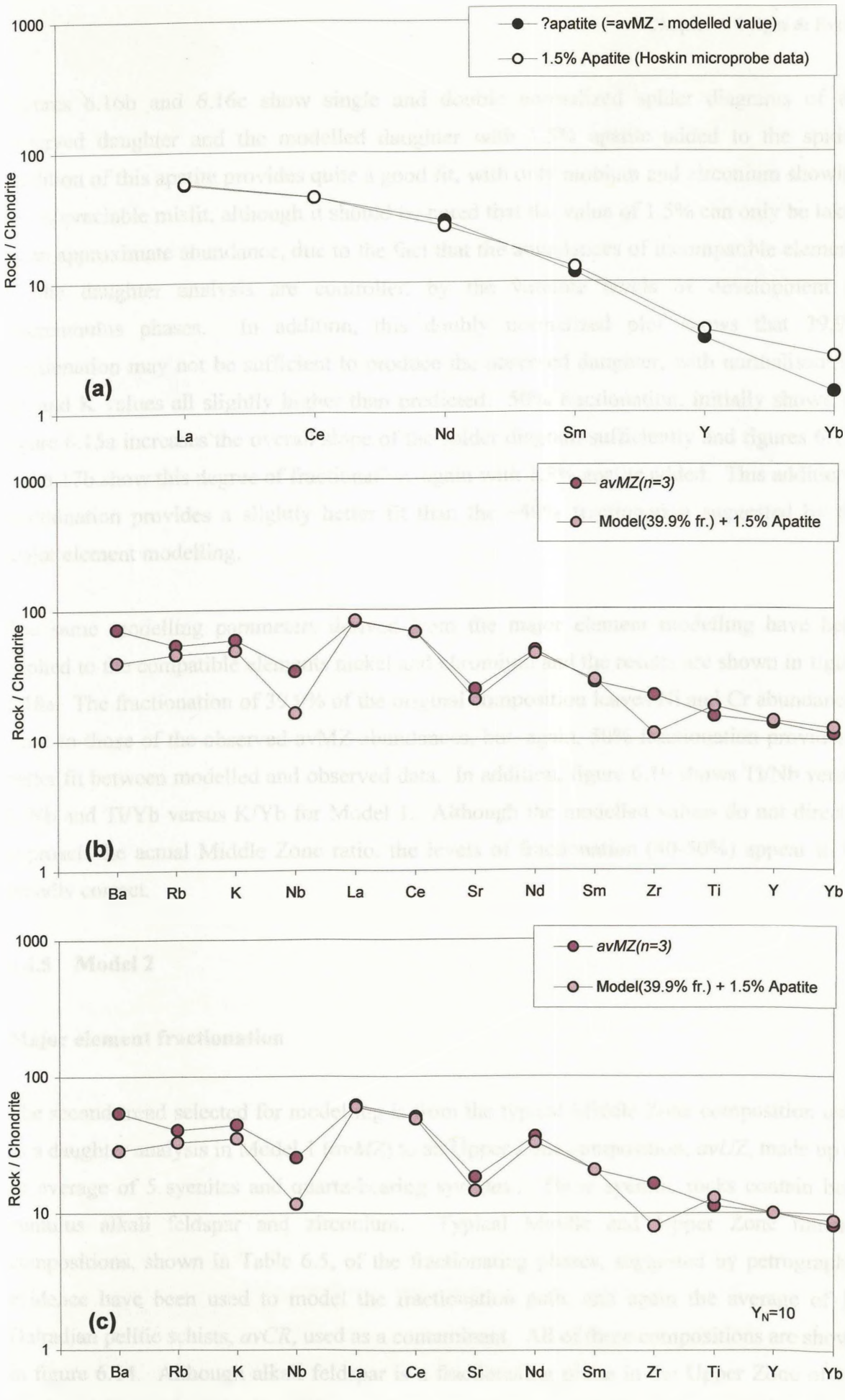


**Figure 6.16 (a) Comparison of Y and REE elements differences between the real and modelled data in figure 6.15b with abundances found in a typical intrusive apatite; (b+ c) 'Spider' diagrams of modelled data, with added apatite, and actual data for Model 1**

Figures 6.16b and 6.16c show single and double normalized spider diagrams of the observed daughter and the modelled daughter with 1.5% apatite added to the spider. Addition of this apatite provides quite a good fit, with only niobium and zirconium showing any appreciable misfit, although it should be noted that the value of 1.5% can only be taken as an approximate abundance, due to the fact that the abundances of incompatible elements in the daughter analysis are controlled by the variable levels of development of intercumulus phases. In addition, this doubly normalized plot shows that 39.9% fractionation may not be sufficient to produce the observed daughter, with normalised Ba, Rb and K values all slightly higher than predicted. 50% fractionation, initially shown on figure 6.15a increases the overall slope of the spider diagram sufficiently and figures 6.17a and 6.17b show this degree of fractionation, again with 1.5% apatite added. This additional fractionation provides a slightly better fit than the ~40% fractionation suggested by the major element modelling.

The same modelling parameters derived from the major element modelling have been applied to the compatible elements nickel and chromium and the results are shown in figure 6.18a. The fractionation of 39.9% of the original composition leaves Ni and Cr abundances close to those of the observed avMZ abundances, but, again, 50% fractionation provides a better fit between modelled and observed data. In addition, figure 6.19 shows Ti/Nb versus K/Nb and Ti/Yb versus K/Yb for Model 1. Although the modelled values do not directly approach the actual Middle Zone ratio, the levels of fractionation (40-50%) appear to be broadly correct.

### 6.4.5 Model 2

**Major element fractionation**

The second trend selected for modelling is from the typical Middle Zone composition used as a daughter analysis in Model 1 (*avMZ*) to an Upper Zone composition, *avUZ*, made up of an average of 5 syenites and quartz-bearing syenites,. These syenitic rocks contain both cumulus alkali feldspar and zirconium. Typical Middle and Upper Zone mineral compositions, shown in Table 6.5, of the fractionating phases, suggested by petrographic evidence have been used to model the fractionation path, and again the average of 17 Dalradian pelitic schists, *avCR*, used as a contaminant. All of these compositions are shown in figure 6.14. Although alkali feldspar is a fractionating phase in the Upper Zone of the Insch and Boganclogh bodies, it has not been used here, as it is found as a cumulate phase

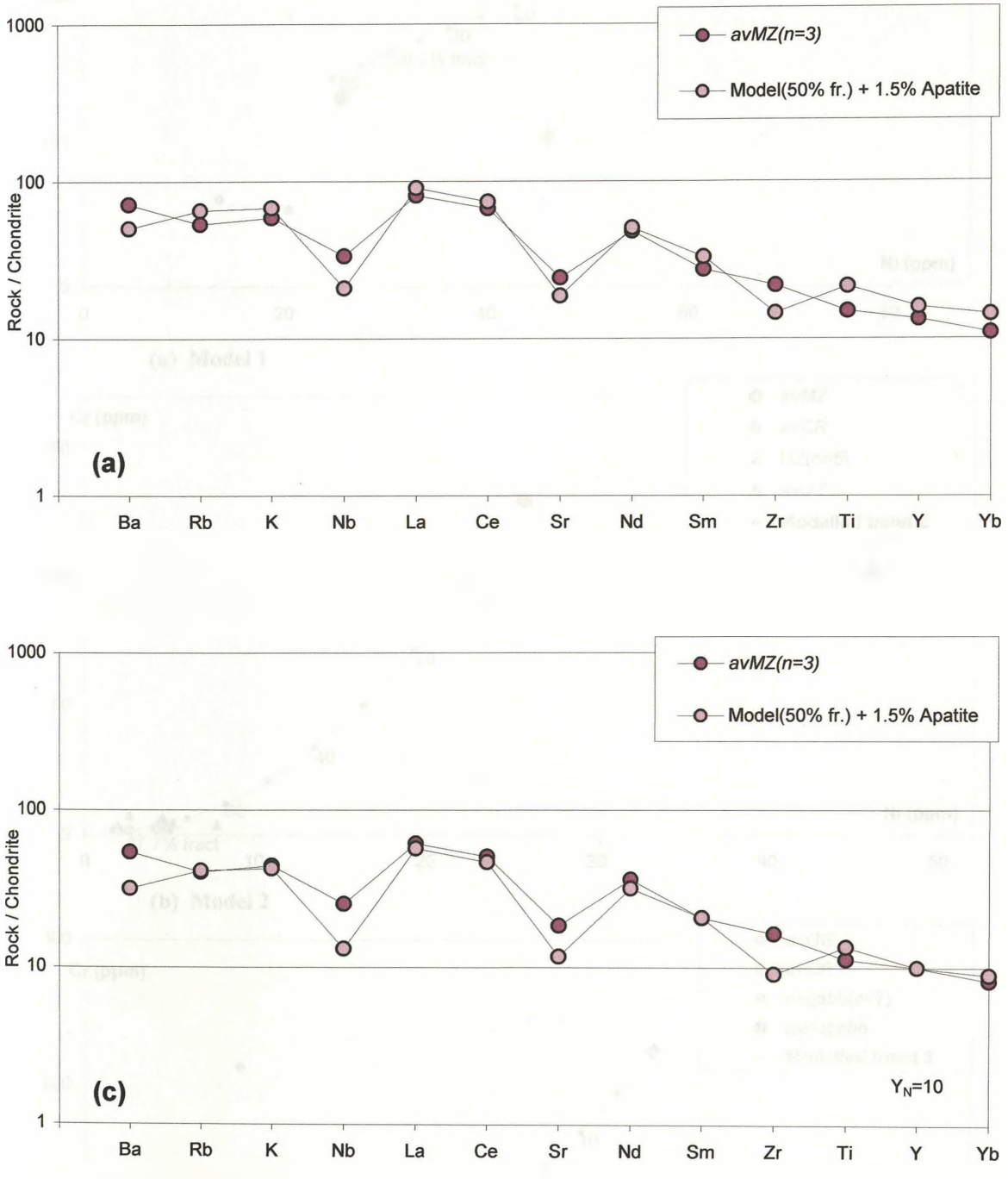


**Figure 6.17 'Spider' diagrams of modelled data, with added apatite, and actual data for Model 1**

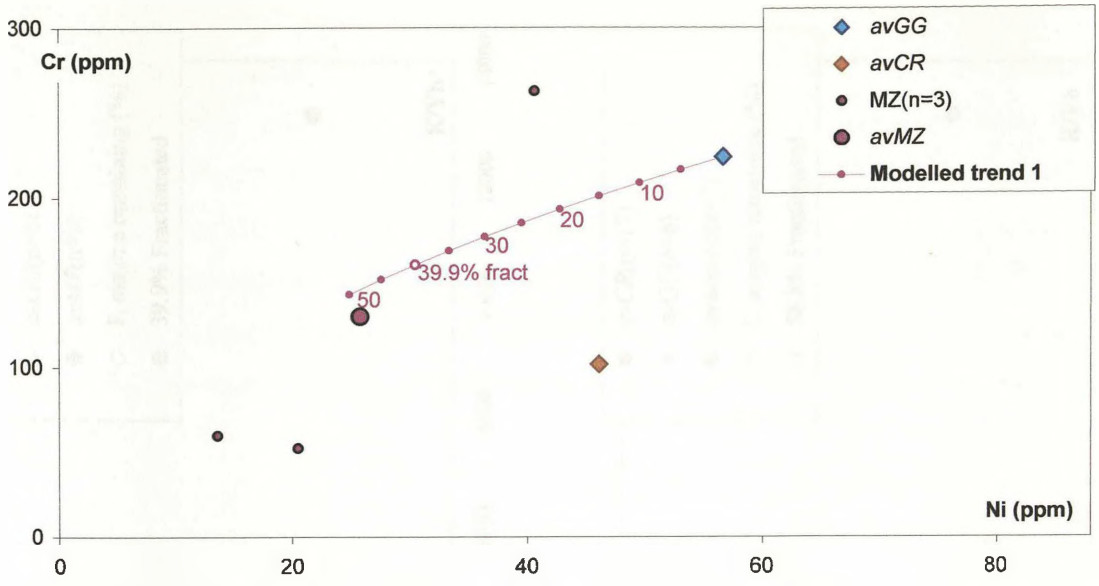


(a) Model 1

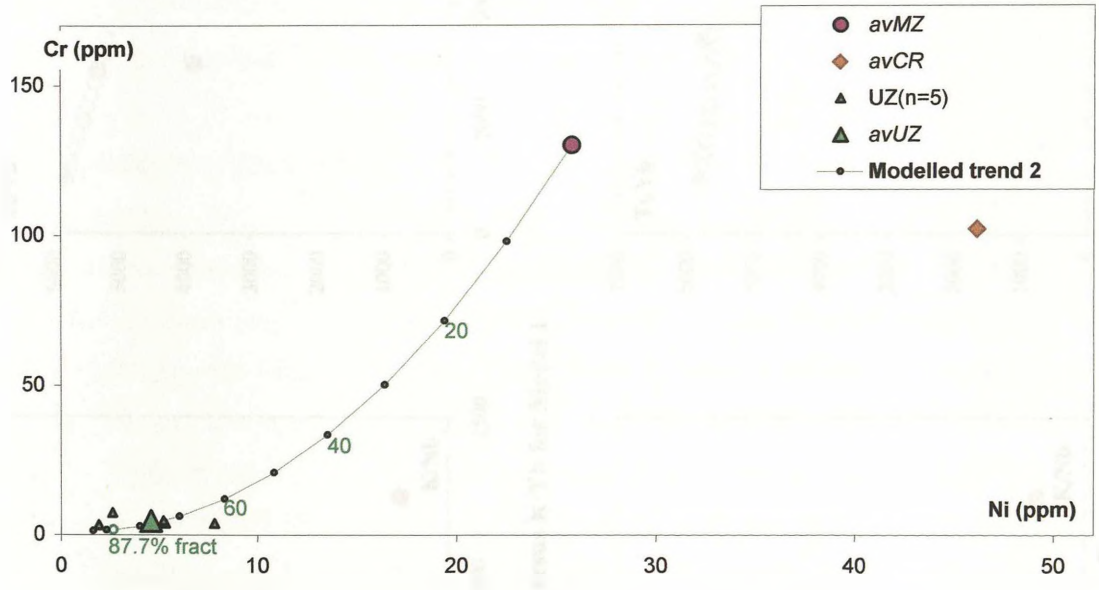


(b) Model 2

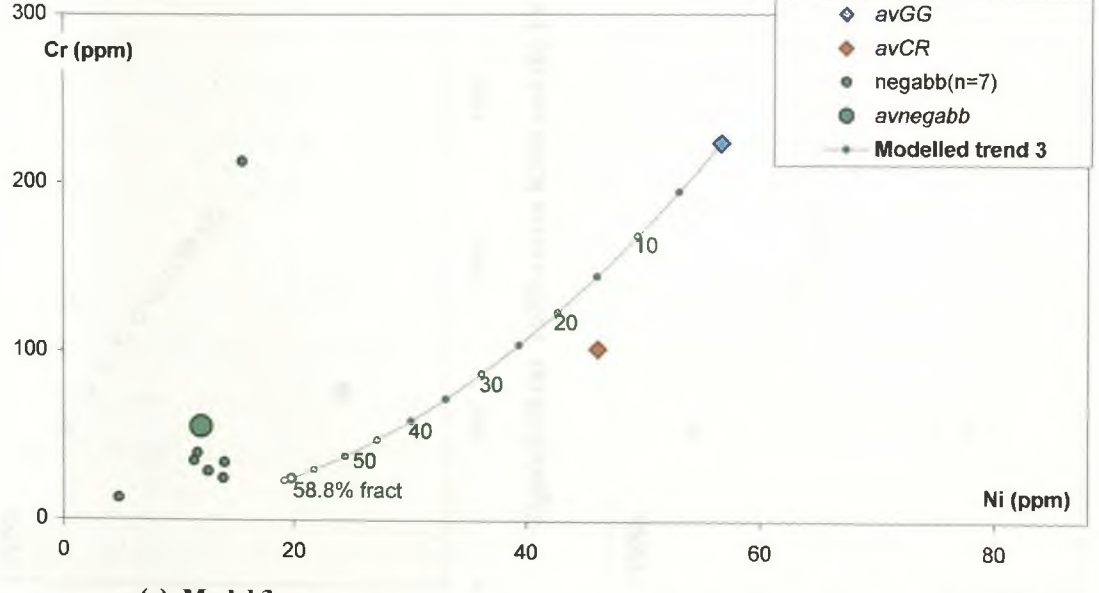


(c) Model 3

**Figure 6.18 Modelling paths for the compatible elements Ni and Cr**

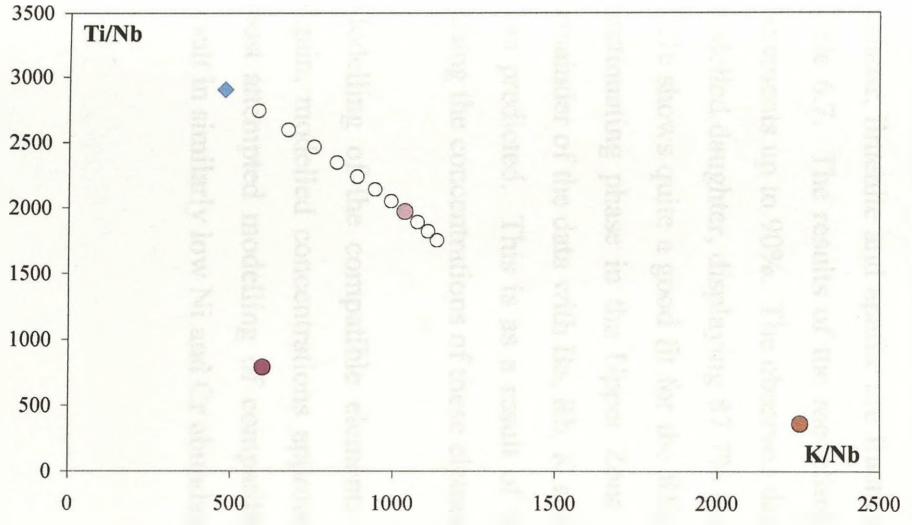


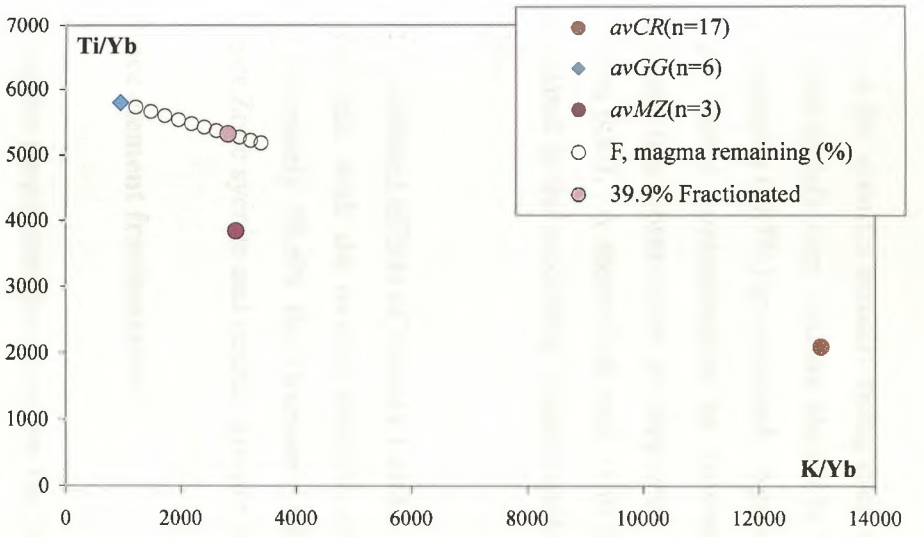


**Figure 6.19 (a) Ti/Nb versus K/Nb and (b) Ti/Yb versus K/Yb for Model 1**

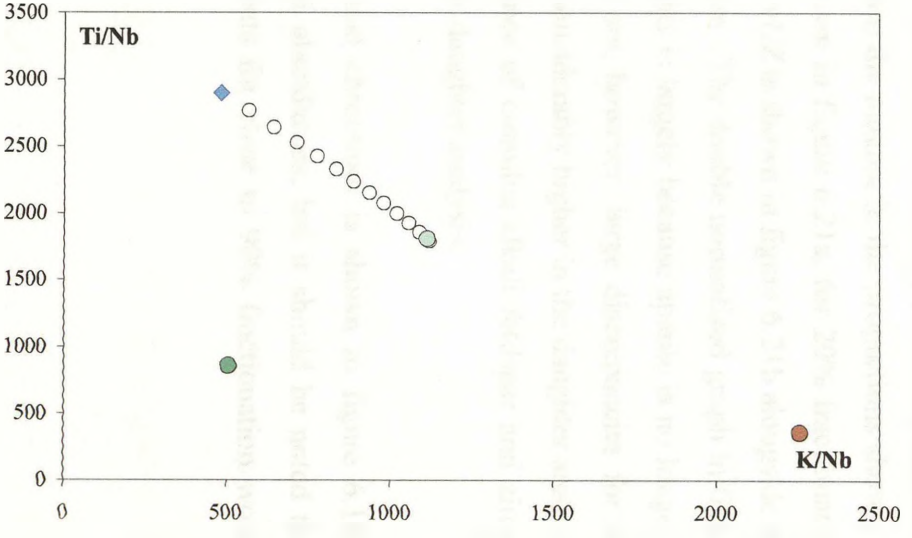


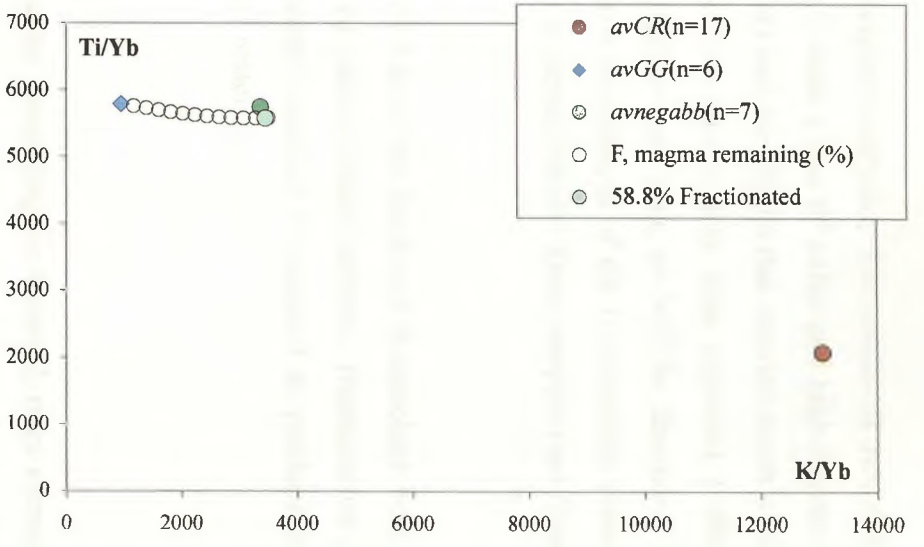


**Figure 6.20 (a) Ti/Nb versus K/Nb and (b) Ti/Yb versus K/Yb for Model 3**

only in the syenites actually being used as the daughter analyses. The results of modelling are quite satisfactory, and are shown in Table 6.7, with a low $R^2$ value and high degree of fractionation (>87%) as expected. Again it is CaO and the alkalis that provide much of the misfit, while contamination by country rocks is, perhaps, less than expected (<4%), although this observation is supported by limited isotope data, as will be discussed in Section 6.4.7. A theoretical rock with the relative abundances of the fractionating phases calculated in the modelling is again quite similar to actual Middle Zone samples (see figure 6.14).

The combined effects of models 1 and 2 for Trend 1 from the Insch and Boganclogh bodies mean that, with the overall addition of 8.6% of pelitic schist material, fractionation of approximately 92.6% the Granular Gabbro 'parent' material is required to produce the Upper Zone syenite and quartz- syenite 'daughter' material.

**Trace element fractionation**

Using the parameters generated by the 'least squares' modelling for Model 2, trace element modelling has been carried out on the data. 3.4% of the contaminant pelitic schist (*avCR*) has been added to the Middle Zone source rock (*avMZ*) while olivine, pyroxene, plagioclase feldspar, ilmenite and apatite are fractionated from the magma in the proportions shown in Table 6.7. The results of the modelling are shown in figure 6.21a, for 20% fractionation increments up to 90%. The observed daughter, *avUZ* is shown in figure 6.21b alongside the modelled daughter, displaying 87.7% fractionation. The double normalized graph in figure 6.21c shows quite a good fit for the REE data; this is largely because apatite is no longer a fractionating phase in the Upper Zone. There are, however, large discrepancies for the remainder of the data with Ba, Rb, K and Zr all considerably higher in the daughter analysis than predicted. This is as a result of the presence of cumulus alkali feldspar and zircon raising the concentrations of these elements in the daughter analysis.

Modelling of the compatible elements nickel and chromium is shown in figure 6.18b. Again, modelled concentrations approach actual abundances, but it should be noted that most attempted modelling of compatible elements for close to 90% fractionation would result in similarly low Ni and Cr abundances.

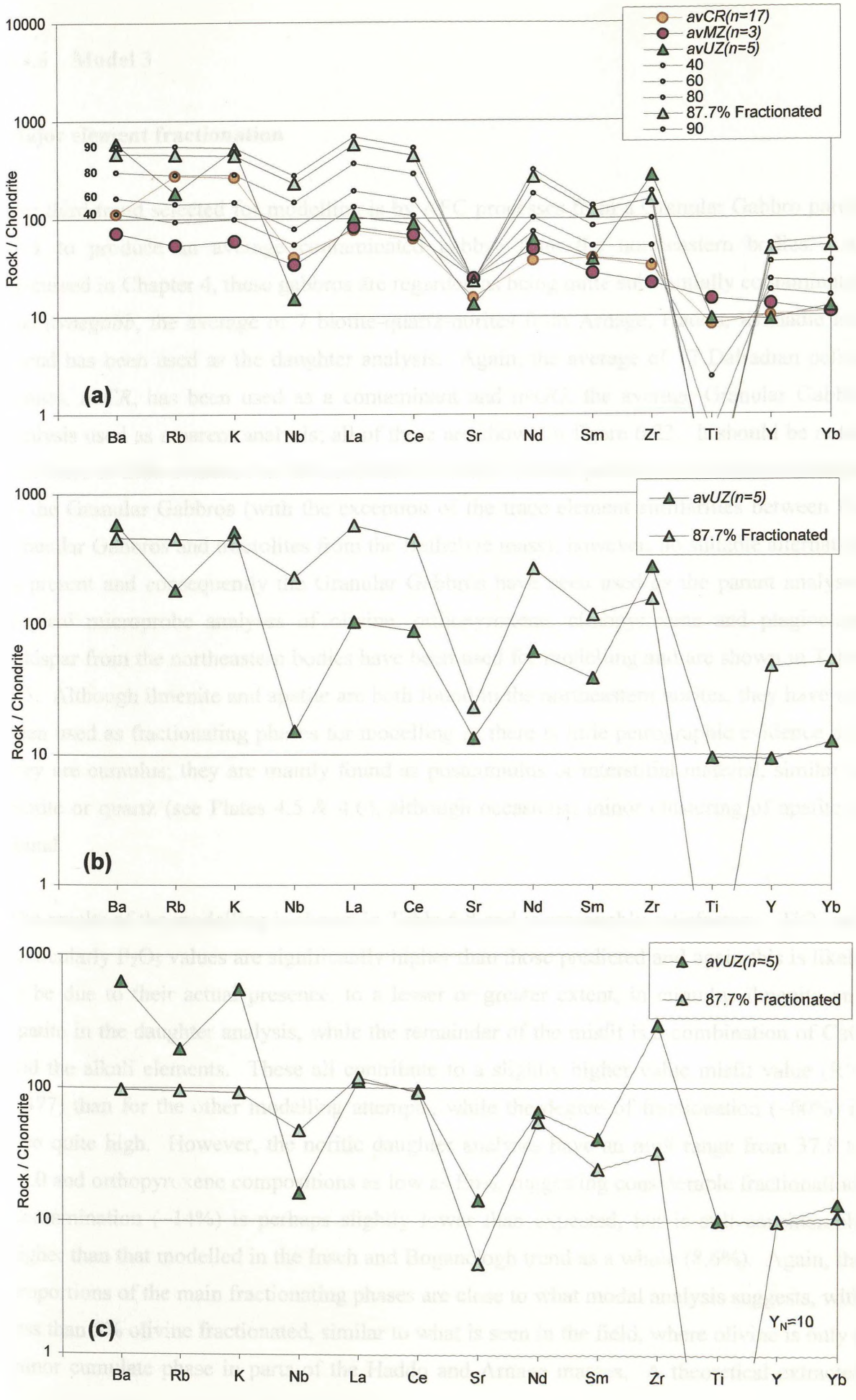


**Figure 6.21 'Spider' diagrams of modelled and real data for Model 2.**

### 6.4.6 Model 3

**Major element fractionation**

The third trend selected for modelling is by AFC processes from a Granular Gabbro parent rock to produce an average contaminated gabbro from the northeastern bodies. As discussed in Chapter 4, these gabbros are regarded as being quite substantially contaminated and *avnegabb*, the average of 7 biotite-quartz-norites from Arnage, Haddo, Kinnadie and Maud has been used as the daughter analysis. Again, the average of 17 Dalradian pelitic schists, *avCR*, has been used as a contaminant and *avGG*, the average Granular Gabbro analysis used as a parent analysis; all of these are shown in figure 6.22. It should be noted that there is little evidence in the northeastern bodies for the presence of rocks comparable to the Granular Gabbros (with the exception of the trace element similarities between the Granular Gabbros and troctolites from the Belhelvie mass); however, no suitable alternative is present and consequently the Granular Gabbros have been used as the parent analysis. Typical microprobe analyses of olivine, orthopyroxene, clinopyroxene and plagioclase feldspar from the northeastern bodies have been used for modelling and are shown in Table 6.5. Although ilmenite and apatite are both found in the northeastern norites, they have not been used as fractionating phases for modelling as there is little petrographic evidence that they are cumulus; they are mainly found as postcumulus or interstitial material, similar to biotite or quartz (see Plates 4.5 & 4.6), although occasional minor clustering of apatite is found.

The results of the modelling is shown in Table 6.8 and is reasonably satisfactory. $TiO_2$ and particularly $P_2O_5$ values are significantly higher than those predicted and again this is likely to be due to their actual presence, to a lesser or greater extent, in cumulus ilmenite and apatite in the daughter analysis, while the remainder of the misfit is a combination of CaO and the alkali elements. These all contribute to a slightly higher value misfit value ($R^2$= 0.477) than for the other modelling attempts, while the degree of fractionation (~60%) is also quite high. However, the noritic daughter analyses have an mg# range from 37.8 to 16.0 and orthopyroxene compositions as low as $En_{29}$, suggesting considerable fractionation. Contamination (~14%) is perhaps slightly lower than expected, but is still considerably higher than that modelled in the Insch and Boganclogh trend as a whole (8.6%). Again, the proportions of the main fractionating phases are close to what modal analysis suggests, with less than 5% olivine fractionated, similar to what is seen in the field, where olivine is only a minor cumulate phase in parts of the Haddo and Arnage masses. A theoretical extracted

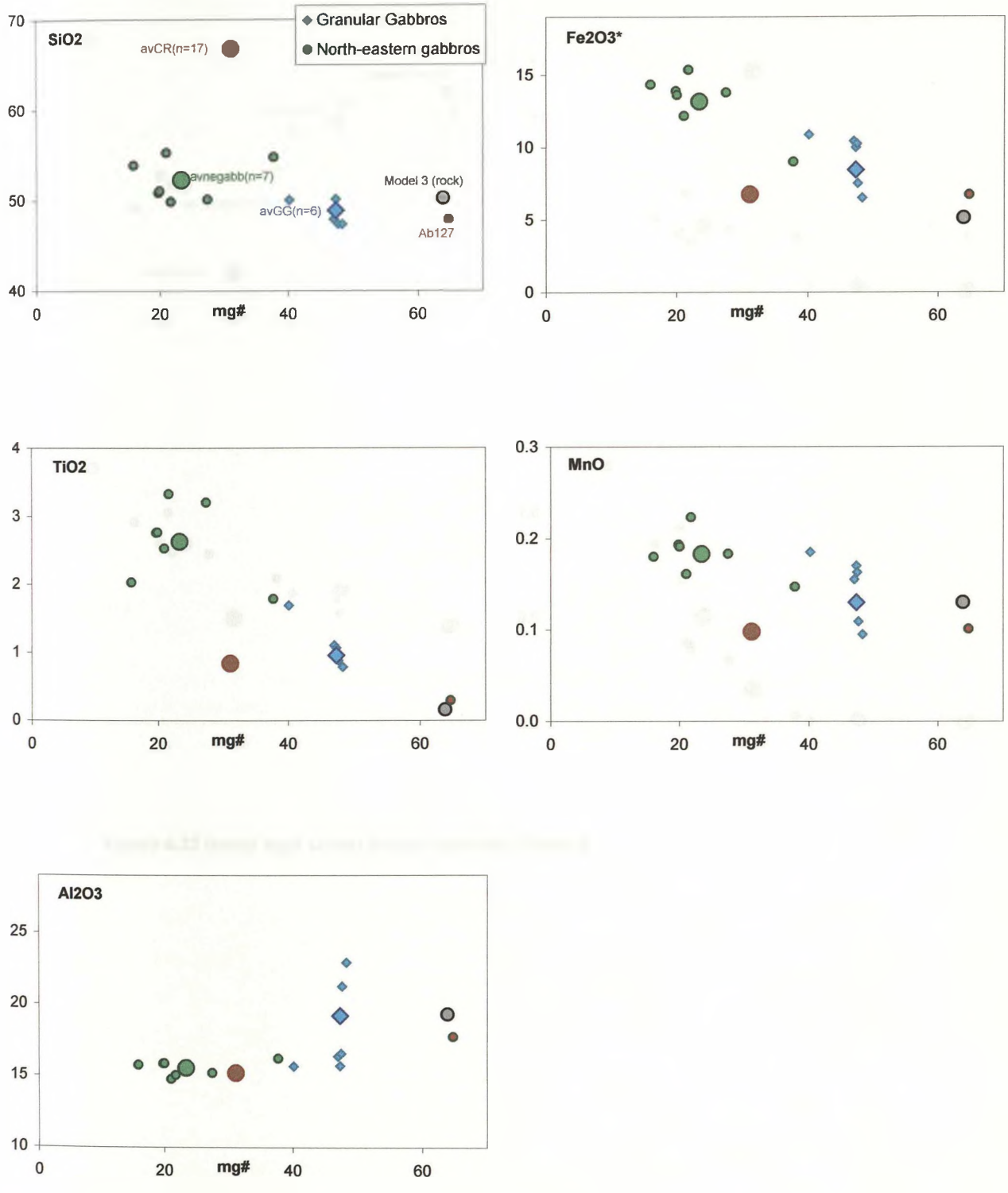


**Figure 6.22 mg# versus major oxides for Model 3**

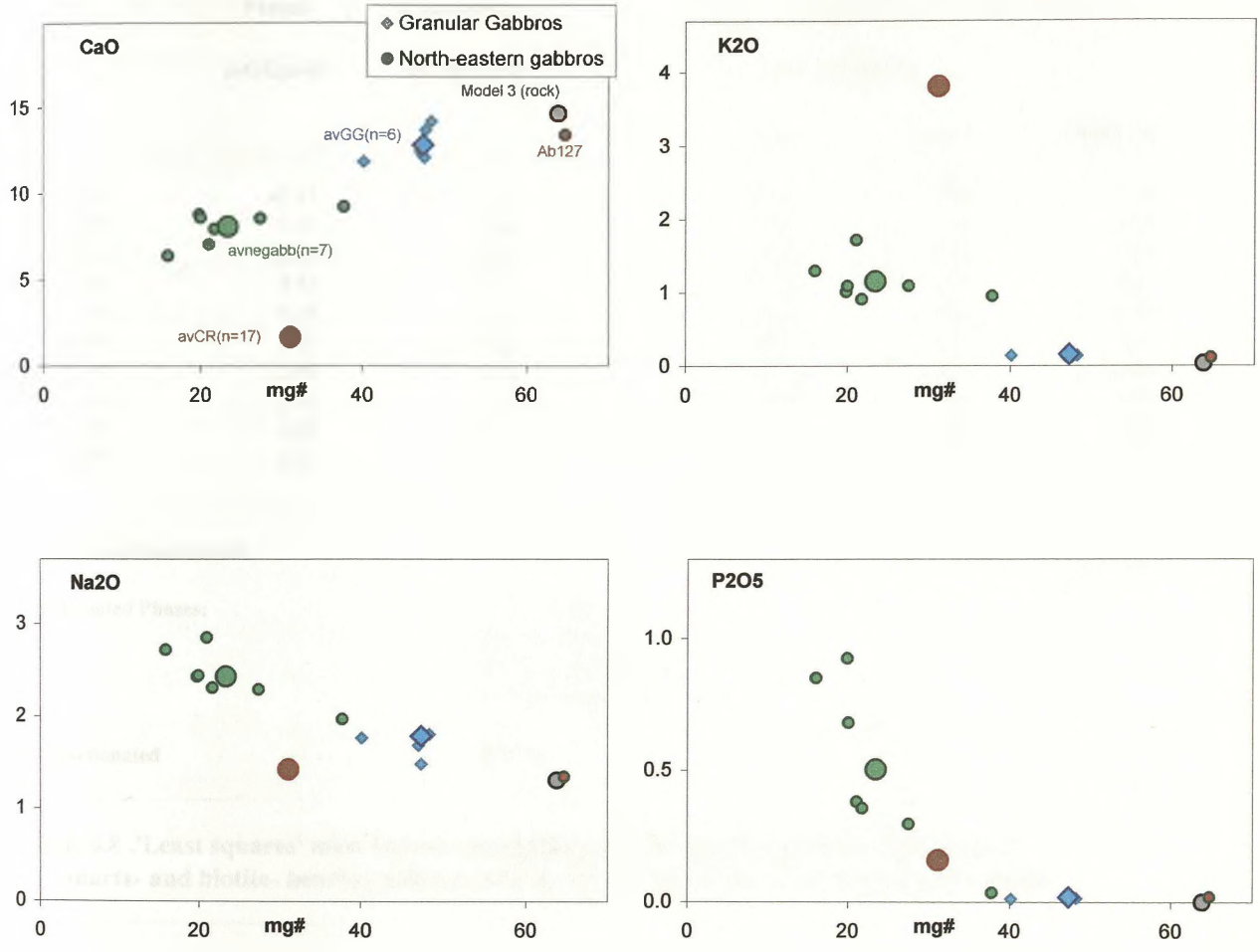


**Figure 6.22 (cont) mg# versus major oxides for Model 3**

| | Parent | Contaminant | Daughter | | |
|---|---|---|---|---|---|
| | avGG(n=6) | avCR(n=17) | avnegabb(n=7) | | |
| | | | Obs. | Calc. | Misfit (R) |
| SiO2 | 49.17 | 67.23 | 53.01 | 52.98 | 0.03 |
| TiO2 | 1.09 | 0.84 | 2.67 | 2.35 | 0.32 |
| Al2O3 | 18.30 | 15.30 | 15.75 | 15.78 | -0.03 |
| FeO* | 8.43 | 6.11 | 12.01 | 12.12 | -0.11 |
| MnO | 0.15 | 0.10 | 0.19 | 0.16 | 0.03 |
| MgO | 8.07 | 3.30 | 4.03 | 4.02 | 0.01 |
| CaO | 12.90 | 1.69 | 8.20 | 8.25 | -0.05 |
| Na2O | 1.74 | 1.44 | 2.46 | 2.28 | 0.18 |
| K2O | 0.13 | 3.83 | 1.17 | 1.53 | -0.36 |
| P2O5 | 0.01 | 0.16 | 0.51 | 0.08 | 0.43 |
| % of contaminant added: | | 14.1 % | | $R^2$ = | 0.477 |
| Fractionated Phases: | | 2.1 % | Olivine | | |
| | | 23.4 % | Orthopyroxene | | |
| | | 17.1 % | Clinopyroxene | | |
| | | 57.4 % | Plagioclase | | |
| % Fractionated | | 58.8 % | | | |

**Table 6.8 'Least squares' mass balance modelling of contamination and fractionation of the quartz- and biotite- bearing gabbros and norites of the north-eastern bodies (Model 3).**

rock, based on the modelled mineral proportions falls outside the range of any northeastern gabbros, but is quite similar to Ab127, an olivine gabbro sample from the nearby Belhelvie intrusion (see figure 6.22).

**Trace element fractionation**

Trace element fractionation modelling has again been carried out using the constraints provided by the major elements. 14.1% of contaminant *avCR* has been added to Granular Gabbro source, *avGG*, while fractionating olivine, pyroxene and plagioclase feldspar in the proportions shown in Table 6.8. Fractionation is shown in 10% increments up to and including 58.8% fractionation in figure 6.23a and again it is apparent from the single and double normalized spider plots in figure 6.23b and 6.23c, that a small amount of cumulus apatite is likely to be present in the observed daughter, *avnegabb*, with REE values consistently higher than predicted. Again, the addition of 0.5% apatite (Hoskin *et al.*, 2000) to the modelled values is required, and this produces the spider diagrams shown in figures 6.24a and 6.24b, which provide quite a good match between observed and modelled values. Niobium abundances are higher than predicted, while Ti values appear to be quite accurate despite the high misfit (0.32) in the 'least squares' modelling. Again, the addition of 0.5% apatite should be regarded as being only an approximation, due to variable intercumulus development in *avnegabb* samples resulting in variable abundances of the trace elements.

Compatible element modelling has again been carried out for nickel and chromium and the results are shown in figure 6.18c. Actual abundances are slightly different than predicted, but, as mentioned earlier, the compatible nature of nickel and chromium makes precise modelling in cumulate samples difficult. Figure 6.20 shows Ti/Nb versus K/Nb and Ti/Yb versus K/Yb for the data from Model 3. Again, the levels of fractionation appear to be quite close to those predicted, while the plot of Ti/Yb versus K/Yb provides quite a good fit to the data.

### 6.4.7 Comparison with isotope data

$^{87}Sr/^{86}Sr$ data from Insch and the northeastern bodies (Pankhurst, 1969) and regional Dalradian pelitic schists (Pankhurst, 1969; Dempster *et al.*, 1985) are shown in figures 6.25 and 6.26. In addition, the models of DePaolo (1981) for the behaviour of Rb, Sr and $^{87}Sr/^{86}Sr$ concentrations undergoing AFC processes are shown for comparison. Because the isotope data are not part of this study, it will not be examined in detail; however, broad

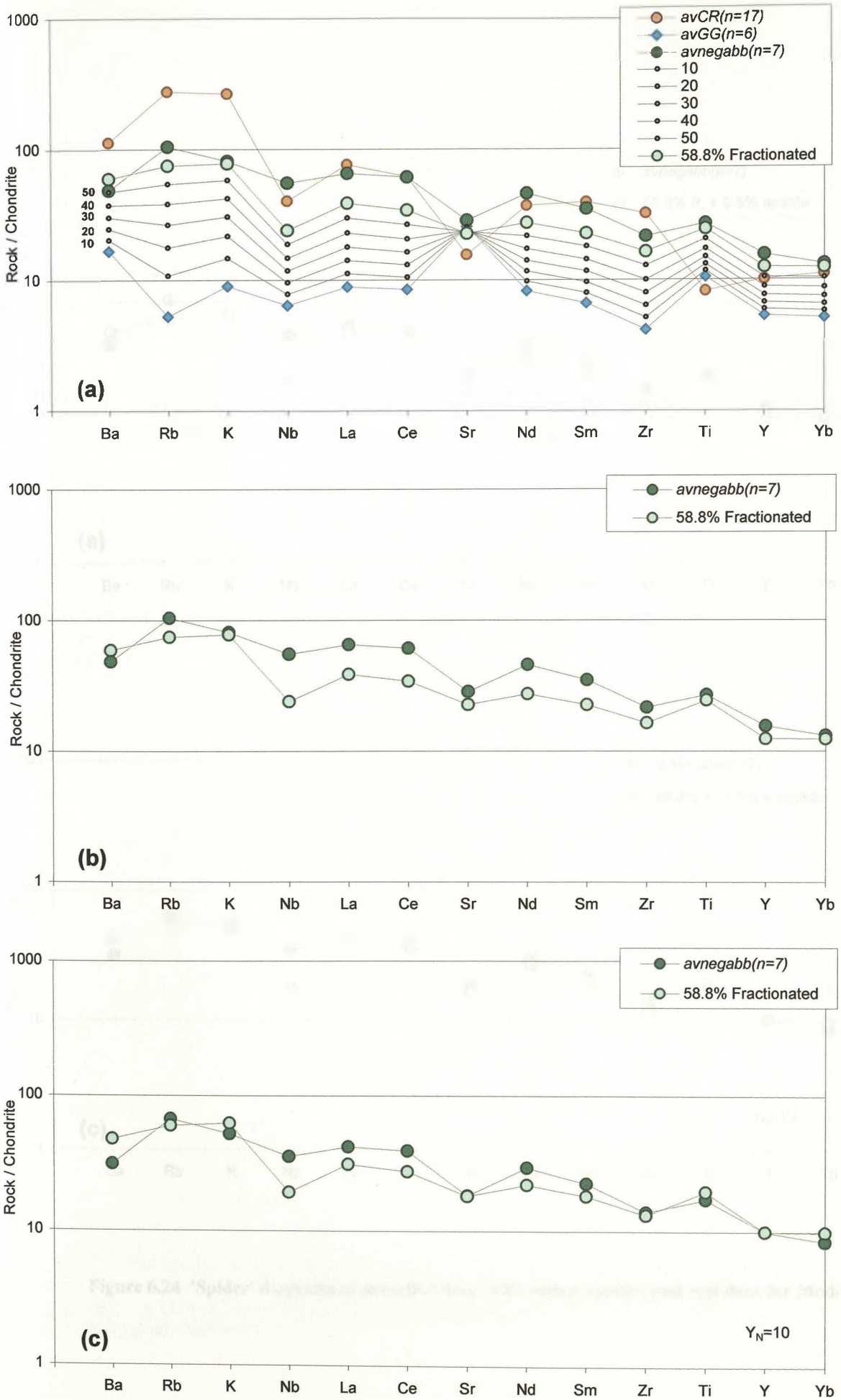


**Figure 6.23 'Spider' diagrams of modelled data and real data for Model 3.**

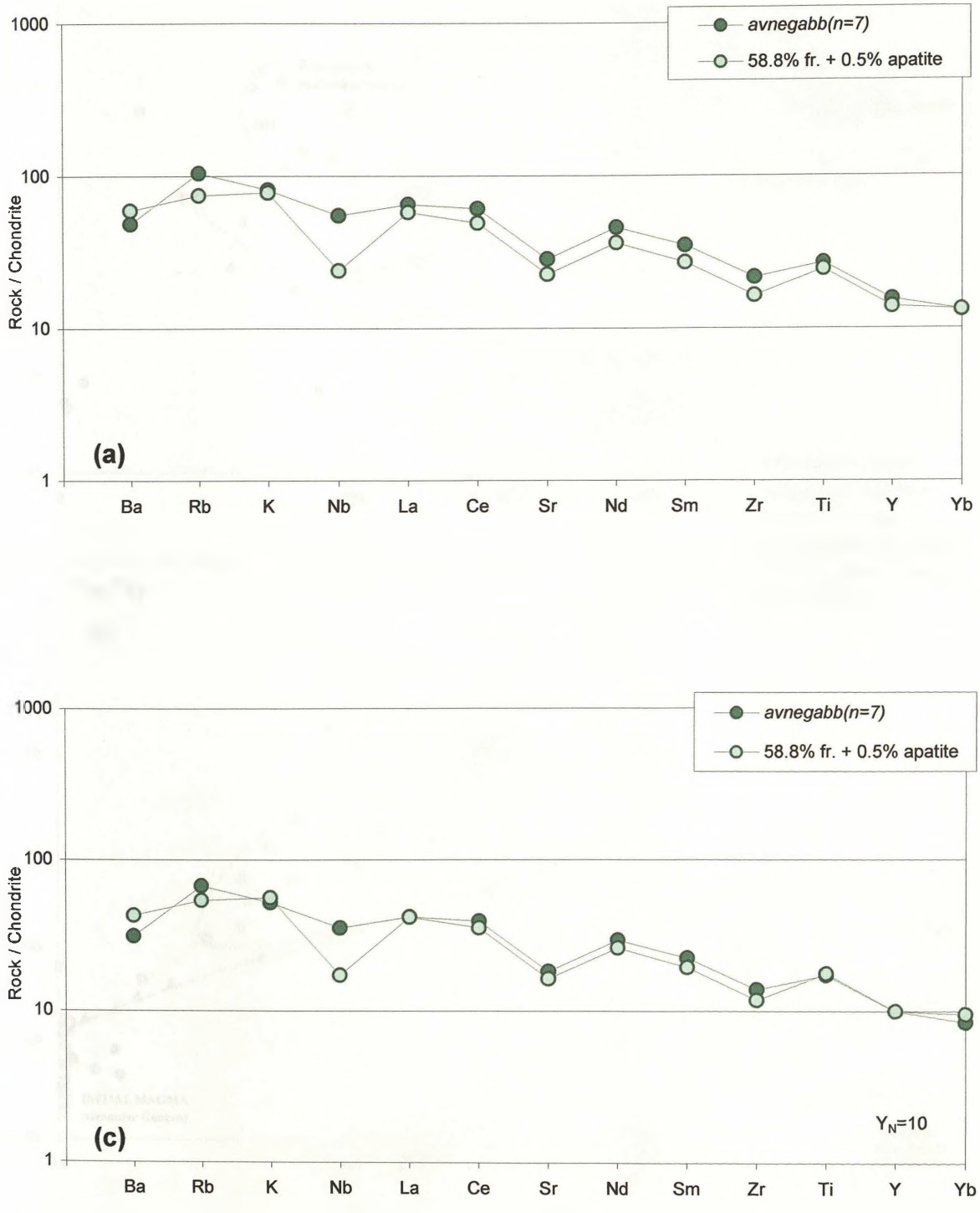


**Figure 6.24 'Spider' diagrams of modelled data, with added apatite, and real data for Model 3**

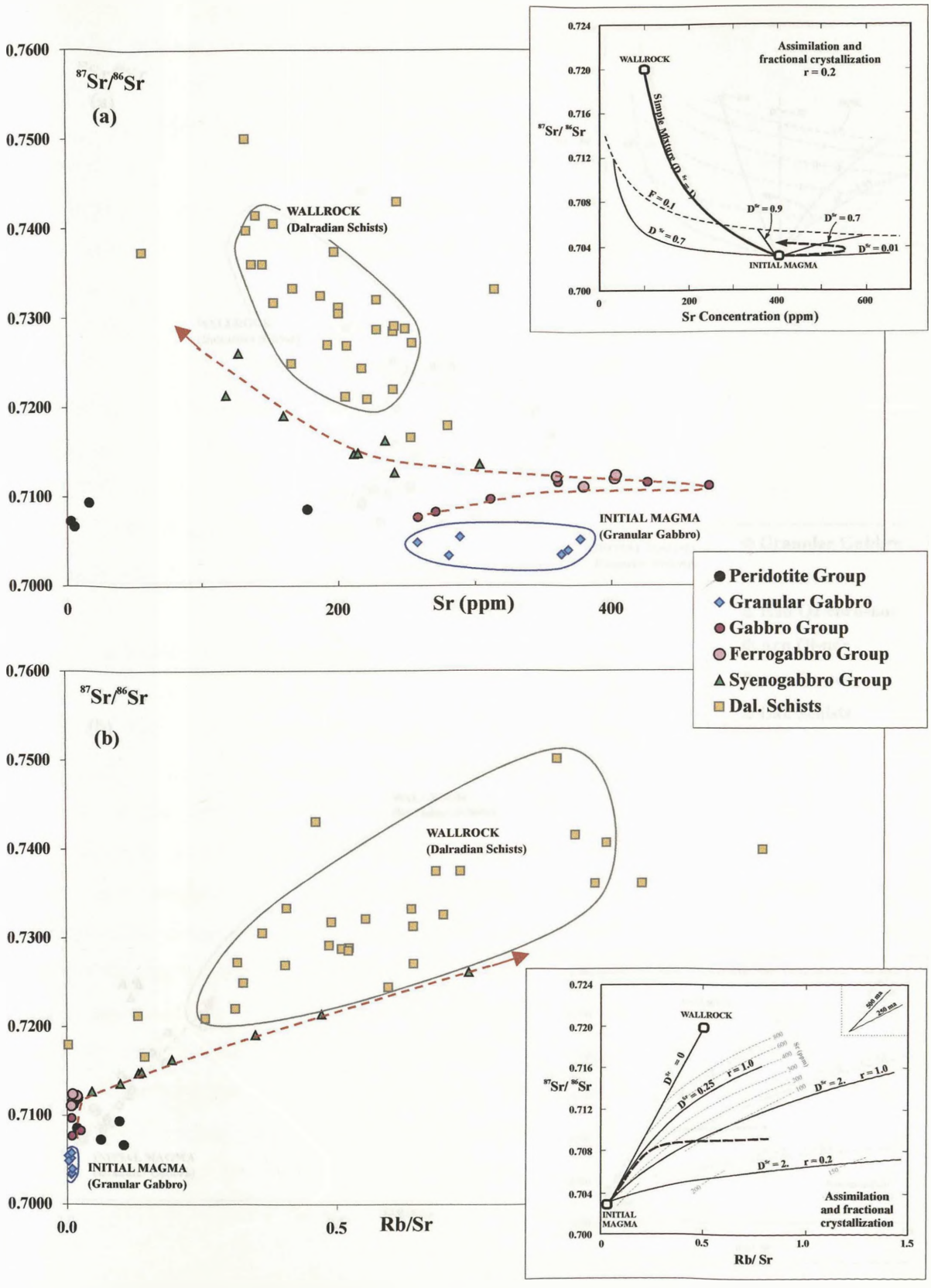


**Figure 6.25** $^{87}Sr/^{86}Sr$ **isotope data versus (a) Sr(ppm) and (b) Rb/Sr for samples from the Insch mass (Pankhurst, 1969) and associated country rocks (Pankhurst, 1969; Dempster *et al.*, 1995). The insets shows the predicted paths of a fractionating magma for approximately 20% contamination from DePaolo (1981) for comparison.**

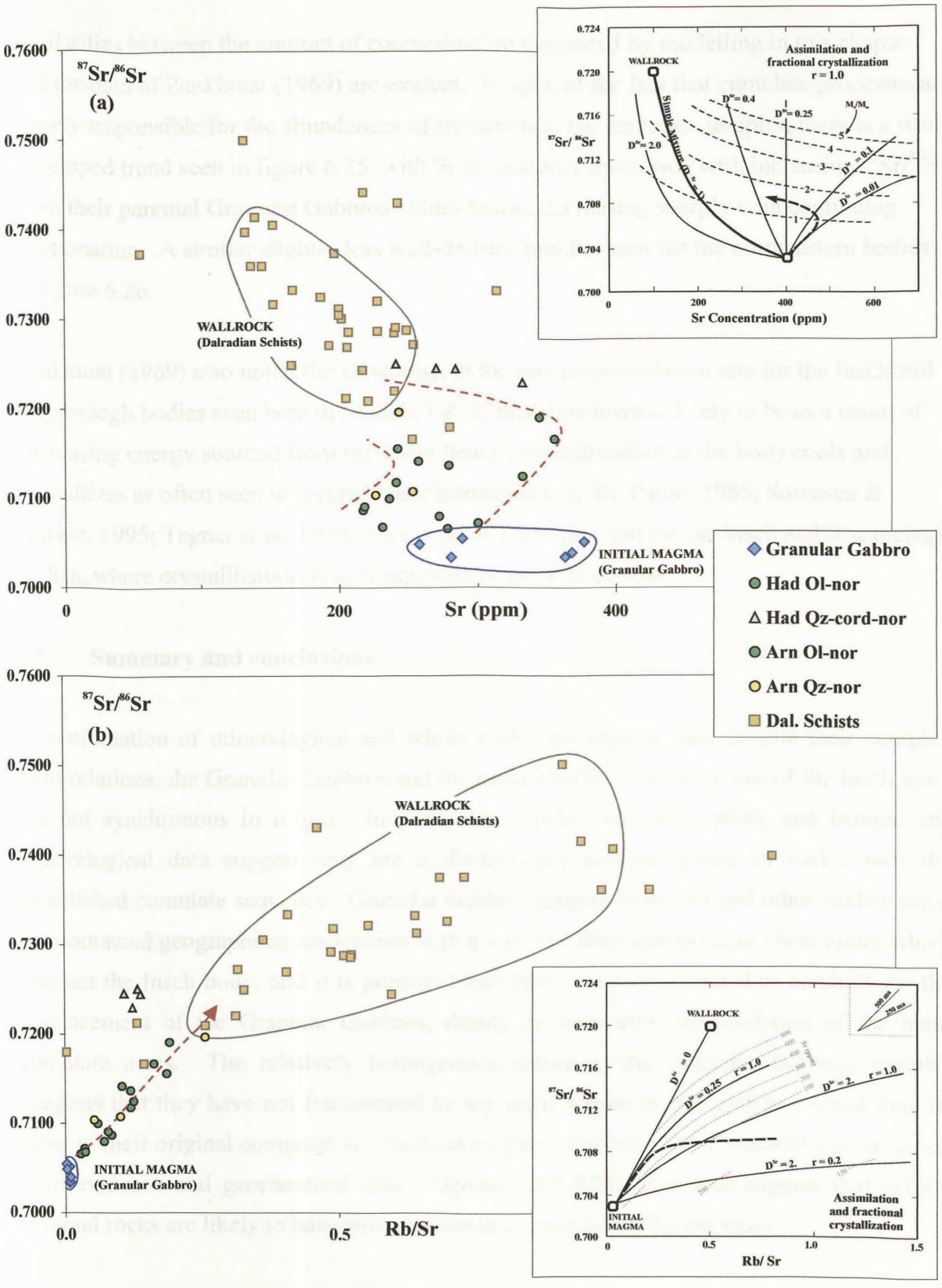


**Figure 6.26** $^{87}Sr/^{86}Sr$ **isotope data versus (a) Sr(ppm) and (b) Rb/Sr for samples from the Arnage and Haddo masses (Pankhurst, 1969) and associated country rocks (Pankhurst, 1969; Dempster *et al.*, 1995). The insets show the predicted paths of a fractionating magma with approximately 50% contamination from DePaolo (1981) for comparison.**

similarities between the amount of contamination suggested by modelling in this chapter and the data of Pankhurst (1969) are evident. In spite of the fact that cumulate processes are largely responsible for the abundances of strontium in the cumulate samples, there is a well-developed trend seen in figure 6.25, with Sr abundances increasing with increasing $^{87}Sr/^{86}Sr$ from their parental Granular Gabbros values before decreasing sharply with continuing fractionation. A similar slightly less well-defined trend is seen for the northeastern bodies in figure 6.26.

Pankhurst (1969) also noted the slowdown in the rate of assimilation rate for the Insch and Boganclogh bodies seen here in Models 1 & 2; this slowdown is likely to be as a result of decreasing energy sourced from the latent heat of crystallization as the body cools and crystallizes as often seen in layered basic intrusions (e.g. De Paolo, 1985; Sorensen & Wilson, 1995; Tegner *et al*, 1999); this is particularly relevant for the Insch and Boganclogh bodies, where crystallization is to completion or close to completion.

## 6.5 Summary and conclusions

A combination of mineralogical and whole rock data suggest that, despite their complex field relations, the Granular Gabbros and the main Middle Zone sequence of the Insch mass are not synchronous in origin. In particular, 'spider' and REE plots, and isotope and mineralogical data suggest they are a distinct and separate group of rocks from the established cumulate sequence. Granular Gabbro samples from this and other studies show a pronounced geographical association with a series of deep synchronous shear zones which transect the Insch body, and it is proposed that these shear zones acted as conduits for the emplacement of the Granular Gabbros, during or soon after consolidation of the main cumulate mass. The relatively homogenous nature to the Granular Gabbros samples suggests that they have not fractionated to any great degree *in situ*, and as a result may be close to their original composition. Such an origin is consistent with much of the published field evidence and geochemical data. 'Spider' and REE plots also suggest that similar parental rocks are likely to have been present in at least the Belhelvie mass.

Lower Zone samples in most of the bodies contain olivine Fe-Mg ratios, and trace element abundances that are consistent with derivation from a Granular Gabbro-like parent. Lower Zone rocks in several intrusions to the south and west contain more forsteritic olivines and consequently require more basic parental compositions than the Granular Gabbros; some trace element abundances of this source material are likely to be within similar ranges to

those found in the Granular Gabbros, and it is suggested that the two magmas are related. The evidence seen for three evolutionary paths in the Insch and Boganclogh bodies from whole rock chemistry in the previous chapter is also seen in probe data from this and other studies.

Trends seen in the plots of major and trace elements against the fractionation index, mg#, can be broadly explained by the crystallization and fractionation of the main cumulus phases identified in Chapter 4. Olivine, plagioclase feldspar and both pyroxenes are the main control on these trends, but apatite, ilmenite, alkali feldspar, and zircon also have significant control on certain elements. Contamination can be shown to have played a significant role in the evolution of bodies using 'spider', REE and plagioclase feldspar, orthopyroxene and clinopyroxene norms, with the northeastern bodies showing strong evidence for contamination as well as the main Insch and Boganclogh cumulates relative to the Granular Gabbros.

Caution is required when attempting to model AFC processes using cumulate samples; satisfactory results have been achieved by taking certain precautions. Samples with strong evidence for accumulation of phases are difficult to avoid, especially for plagioclase feldspar; however, averaging of samples can help to minimize the associated errors. A combination of 'least squares' mass balance modelling for major elements and Rayleigh fractional crystallisation combined with country rock assimilation for trace elements has been carried out for three selected trends. Results are variable, with all three models predicting levels of fractional crystallization and assimilation broadly consistent with the petrographic evidence and whole rock data from Chapters 4 & 5, as well as published isotope data. The presence of minor cumulus phases, in which the so-called incompatible elements are in fact compatible, has led to significant error in some of the trace element modelling. In particular, apatite and alkali feldspar cause substantial error to the REE and LILE respectively when present as cumulate phases.

# Chapter 7 Tectonic significance of the 'Younger' Basics

## 7.1 Introduction

In the previous chapters a composition likely to approximate to a parental magma for the 'Younger' Basics has been proposed, and their evolution subsequent to emplacement has been examined. This magmatic evolution involves fractionation, and contamination by pelitic country rocks and these, combined with cumulate processes have obscured many of the original properties of the parental magma. As a result, information regarding the tectonic setting of these bodies can only be obtained from these likely parental rocks, the Granular Gabbros.

This chapter will examine the chemistry of these Granular Gabbro parental rocks and evaluate them in terms of a likely tectonic setting. Although the dataset is quite limited, and isotope data is not available, an origin as partial melts associated with arc magmatism is proposed. Brief comparisons of their chemistry with other arc magmatism is attempted, including aspects of their mineral chemistry. Their position within the Grampian Orogeny is also assessed.

## 7.2 Origin of the Granular Gabbros

### 7.2.1 Introduction

As discussed in Section 6.2, the Granular Gabbros form a distinctive set of rocks, in terms of texture, mineral chemistry, whole rock major, trace and REE data, and published isotope data. Limited *in situ* fractionation is likely to have occurred, as shown by REE plots and Ni and Cr data. Despite this fractionation, the chemistry of the Granular Gabbros shows quite a narrow range of values, especially for incompatible element abundances, in spite of their wide geographical location; these features suggest that the Granular Gabbros as a group may have a common and uniform source.

### 7.2.2 Chemical affinities of the Granular Gabbros with island arc magmas

Whole rock major and trace element chemistry is available for six Granular Gabbro samples; four of these have been analysed for REE. In addition, sample 64067, from Thompson *et al.* (1984) contains analyses of extra elements including thorium, uranium and lead, and has been included with the six from this study. As discussed previously, slight but significant errors are present in whole rock $P_2O_5$ data and REE Gd, Ho and Er data for these samples.

As discussed in Section 6.2 and shown in Table 6.1, there is limited variation within the chemistry of Granular Gabbros samples from both Insch and Huntly taken as a whole, and including published data. There is a broad similarity to the data with most samples displaying a high alumina basaltic composition. These $Al_2O_3$ abundances are quite constant, varying from 16.2% to 18.2%, although abundances extend to almost 23.0% in those granular samples with porphyritic plagioclase feldspar. CaO is also quite constant, ranging from ~10.0% to 12.5%, again reaching higher values of over 14% in the same high $Al_2O_3$ samples with porphyritic plagioclase feldspar. MgO and $Fe_2O_3$ are variable, while $SiO_2$ values are limited to between 47.4% and 50.6%. $Na_2O$ and MnO contents are quite constant, as are $K_2O$ and $P_2O_5$ abundances except in one or two cases, while $TiO_2$ abundances are variable ranging from 0.7% to 1.7%. The compatible trace elements V, Ni, Cr and Cu show significant variation, while Ba, Rb, Y, Nb, and the REE are quite constant, although limited published data other than the sample from Thompson *et al.* (1984) are available for many elements. This similarity to the data is present despite the wide geographical variation to the sample locations, both in Insch and Huntly.

The fine-grained, non-cumulate nature to the Granular Gabbro samples means that they are likely to be close to their liquid compositions and consequently conventional discrimination diagrams may be used to examine their chemistry. Figures 7.1a to 7.1f show the Granular Gabbro data from Table 6.1 plotted on a series of classification and discrimination diagrams. The published data include the Granular Gabbros from Insch (Read *et al.*, 1965; Hutchinson, 1965; Clarke & Wadsworth, 1970; and Thompson *et al.*, 1984) and Huntly (Fletcher, 1989), and proposed parental magmas for Arnage and Haddo (Gribble, 1967). The two troctolites from Belhelvie discussed in Section 6.2.5 have also been included on certain plots, despite their cumulate nature. It is clear from the AFM and TAS plots in figures 7.1a and 7.1b that, chemically, these samples represent a tightly clustered set of low-K, sub-alkaline, tholeiitic basalts, although clustering on the AFM plot is such that the

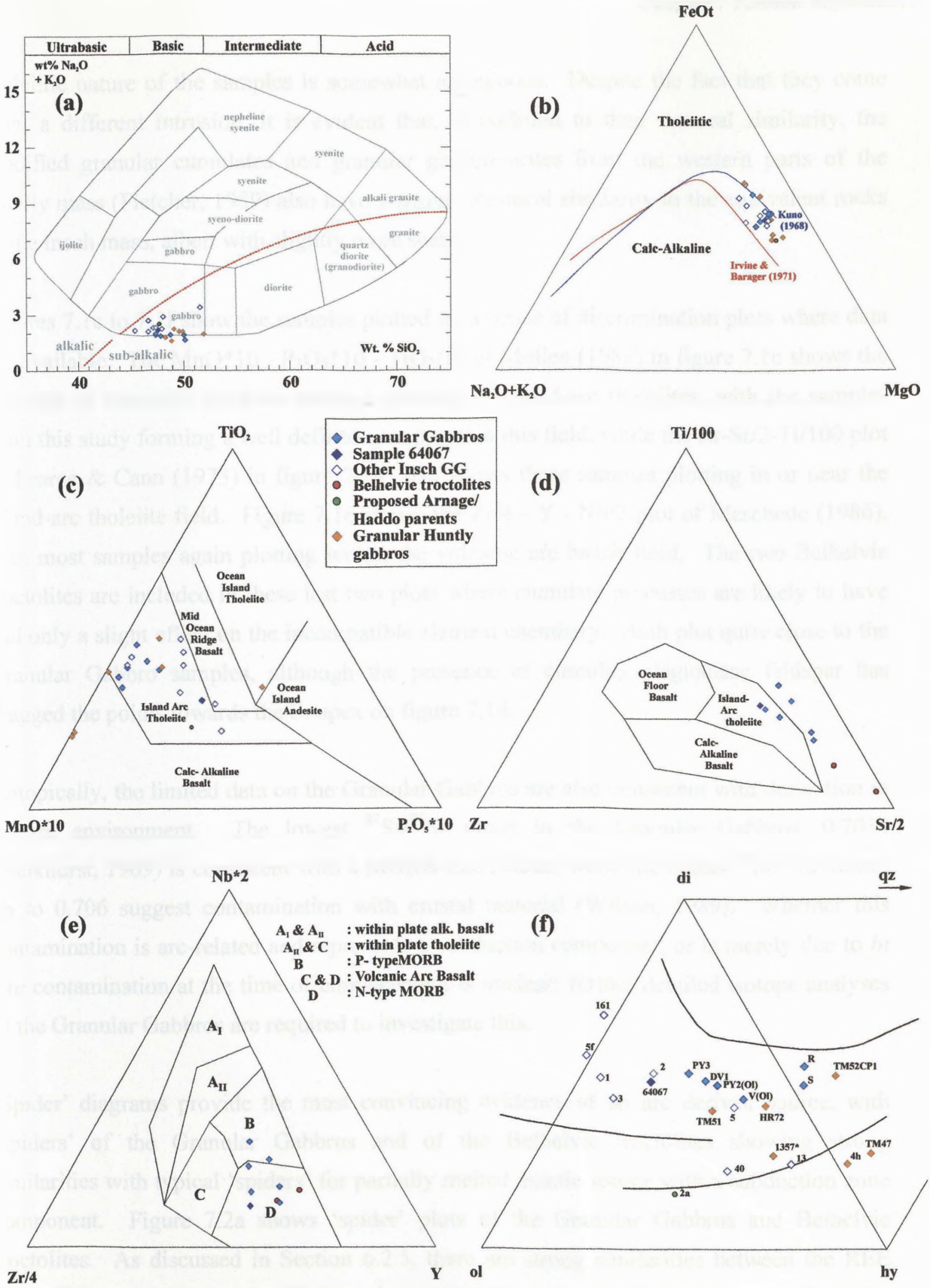


**Figure 7.1** **Selected classification and discrimination plots for proposed parental magmas to the 'Younger' Basics, including the Granular Gabbros from the Insch intrusion.**

**(a) TAS plot**
**(b) AFM plot**
**(c) MnO*10-$P_2O_5$*10-$TiO_2$/10 (Mullen, 1983)**
**(d) Zr-Sr/2-Ti/100 (Pearce & Cann, 1973)**
**(e) Zr/4-Y-Nb/2 (Meschede, 1986)**
**(f) normative di-ol-hy plot**

**Additional data from Read *et al.* (1965), Hutchinson (1965), Gribble (1967) Clarke & Wadsworth (1970), Weedon (1970) Thompson *et al.* (1984), and Fletcher (1989)**

tholeiitic nature of the samples is somewhat ambiguous. Despite the fact that they come from a different intrusion, it is evident that, in addition to their textural similarity, the modified granular cumulates and granular gabbronorites from the western parts of the Huntly mass (Fletcher, 1989) also have a strong chemical similarity to the equivalent rocks in the Insch mass, albeit with slightly more scatter.

Figures 7.1c to 7.1f show the samples plotted on a series of discrimination plots where data are available. The MnO*10 - $P_2O_5$*10 - $TiO_2$/10 of Mullen (1983) in figure 7.1c shows the majority of Granular Gabbros samples plotting as island-arc tholeiites, with the samples from this study forming a well defined group within this field, while the Zr-Sr/2-Ti/100 plot of Pearce & Cann (1973) in figure 7.1d, also shows these samples plotting in or near the island-arc tholeiite field. Figure 7.1e shows the Zr/4 - Y - Nb/2 plot of Meschede (1986), with most samples again plotting within the volcanic arc basalt field. The two Belhelvie troctolites are included in these last two plots where cumulate processes are likely to have had only a slight effect on the incompatible element chemistry. Both plot quite close to the Granular Gabbro samples, although the presence of cumulus plagioclase feldspar has dragged the points towards the Sr apex on figure 7.1d.

Isotopically, the limited data on the Granular Gabbros are also consistent with derivation in an arc environment. The lowest $^{87}Sr/^{86}Sr$ ratios in the Granular Gabbros, 0.7034 (Pankhurst, 1969) is consistent with a MORB-like source, while the higher $^{87}Sr/^{86}Sr$ values up to 0.706 suggest contamination with crustal material (Wilson, 1989). Whether this contamination is arc-related and represents a subduction component, or is merely due to *in situ* contamination at the time of emplacement is unclear; further detailed isotope analyses of the Granular Gabbros are required to investigate this.

'Spider' diagrams provide the most convincing evidence of an arc derived source, with 'spiders' of the Granular Gabbros and of the Belhelvie troctolites showing strong similarities with typical 'spiders' for partially melted mantle source with a subduction zone component. Figure 7.2a shows 'spider' plots of the Granular Gabbros and Belhelvie troctolites. As discussed in Section 6.2.5, there are strong similarities between the REE plots of the two rock types, while here the 'spider' plots can also be seen to be similar, with the troctolites again showing lower overall abundances. The main difference between the two 'spider' groups are these overall abundances, and normalized Ba/Rb ratios; other than these Ba/Rb ratios, the shapes of the two rock types are quite similar.

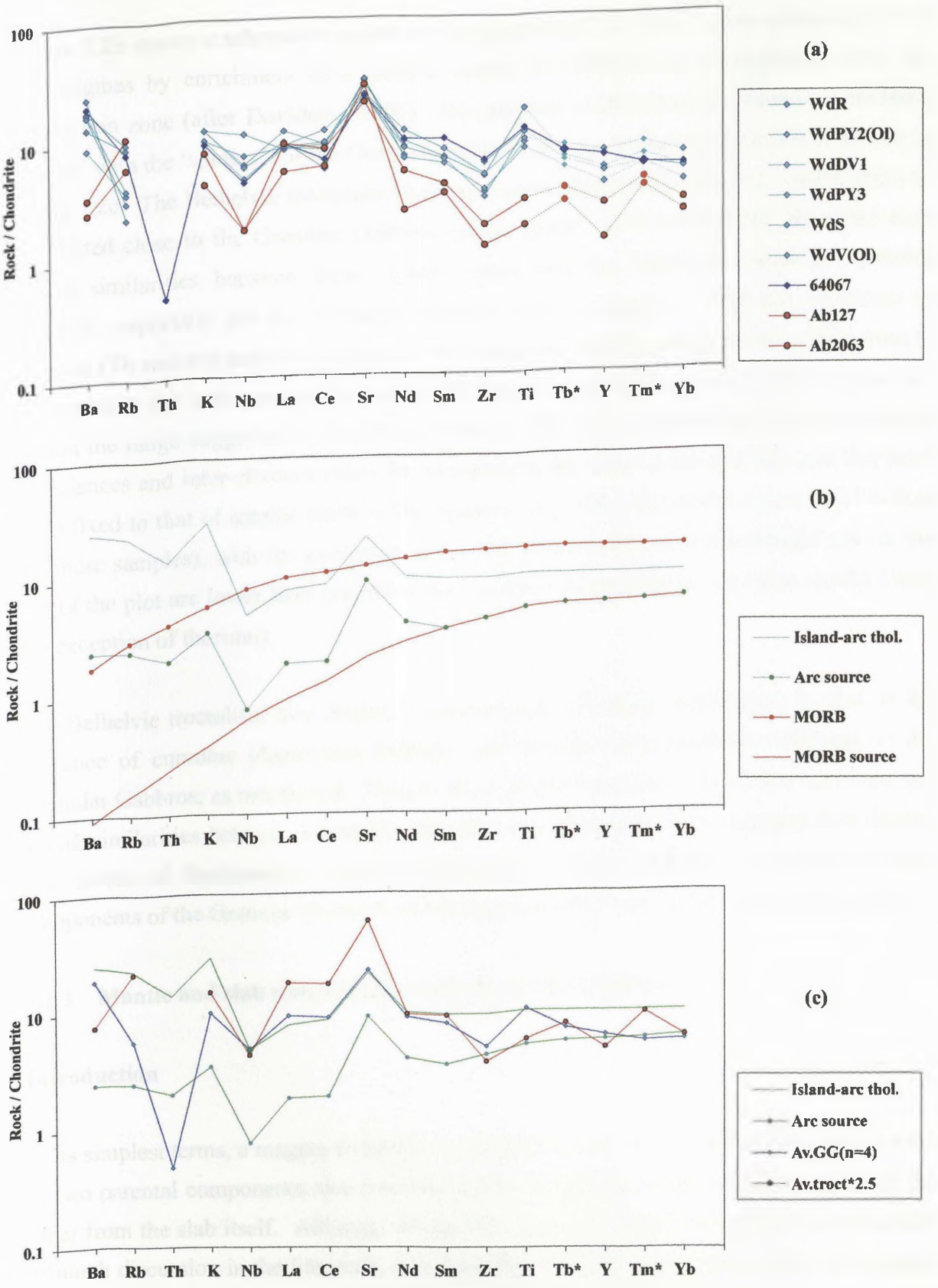


**Figure 7.2** **(a) Spider plots of Granular Gabbro and Belhelvie troctolite samples**
**(b) Generalized model for source of arc magmas from a partially melted MORB-source and an added subduction-zone component (from Davidson, 1996)**
**(c) Comparison of average Granular Gabbro samples with MgO >9.0% (n=4; Tb and Tm data fixed to that of sample 64067, as discussed in the text), and the average Belhelvie troctolite with the generalized model predicted in Davidson (1996)**

Figure 7.2b shows a schematic model for the generation of 'spider' plots characteristic of arc magmas by enrichment of a MORB source by addition of a component from the subduction zone (after Davidson, 1996). Comparison of this idealised island-arc tholeiite 'spider' with the 'spiders' for the Granular Gabbros and the Belhelvie troctolites is shown in figure 7.2c. The Belhelvie troctolites have been multiplied by 2½ simply to enable them to be plotted close to the Granular Gabbros on the graph. It is evident that there are very strong similarities between these 'spider' plots and the idealized island-arc tholeiite 'spiders', especially for the average Granular Gabbro analysis. With the exception of thorium (Th was not analysed as part of this study; as a result, sample 64067 (Thompson *et al.*, 1984) is the only sample for which Th data is available), all normalised values are within the range suggested by Davidson (1996), with strong resemblances for normalized abundances and inter-element ratios for elements to the right of the plot (Tb and Tm have been fixed to that of sample 64067 (Thompson *et al.*, 1984) due to the errors in REE data for these samples), with the exception of Ti. Normalized LIL-element abundances on the left of the plot are lower than predicted, but the inter-element ratios are quite similar (with the exception of thorium).

The Belhelvie troctolites also display a similar range of values with higher Sr (due to the presence of cumulus plagioclase feldspar) and Ba/Rb ratios markedly different to the Granular Gabbros, as mentioned. Despite these slight variations, it is evident that there are strong similarities between island-arc tholeiites and 'Younger' Basic samples that display low levels of fractionation and contamination. These MORB and subduction-zone components of the Granular Gabbros will be considered in more detail in the next section.

### 7.2.3 Mantle and slab components in the Granular Gabbros

#### Introduction

In its simplest terms, a magma formed in an arc setting may be considered to be the product of two parental components, one from the mantle wedge above the subducted slab and the other from the slab itself. Although the precise origin of the slab component is the subject of much discussion in the literature, it is generally believed to be sourced from an aqueous phase resulting from dehydration reactions occurring in the downgoing oceanic crust. This aqueous phase is primarily enriched in fluid-soluble elements (such as the LIL elements) and is transported from the slab to the overlying mantle wedge (Pearce, 1983; Arculus, 1994; Tatsumi & Eggins, 1995) where, possibly in combination with decompression

melting, it triggers partial melting of the overlying mantle MORB material. Although this is a simplification of what is an inevitably more complex system, the resultant arc magma can essentially be thought of as a partially melted MORB source with LILE enrichment from a subduction-related aqueous phase.

**Mantle Component**

To evaluate these mantle and slab components, the approach of Pearce (1983), and Pearce & Parkinson (1993) has been followed. The approach is based on the assumption that the concentrations of certain elements, such as Nb, Zr, Ti, Y and Yb are predominantly mantle derived, while the abundances of other elements, such as Pb and the LILE are sourced in the slab component. Normalization to MORB abundances should reveal MORB characteristics for the mantle-derived elements; these characteristics can then be extrapolated for the remaining elements, and abundances above these extrapolated values are likely to represent the slab-sourced contribution to the magma.

Figure 7.3a shows extended 'spider' plots for the two sets of Granular Gabbros samples identified in figure 6.3; those samples with slightly flatter REE patterns and higher MgO (> 9.0%), Ni and Cr contents are regarded as representing slightly less fractionated (?and also less contaminated) Granular Gabbros samples. Nb, Zr, Hf, Y and Yb data from these less fractionated samples have been used to estimate and constrain the mantle component, as shown in figure 7.3b. $TiO_2$ is generally regarded as being principally sourced from the mantle; here, however, $TiO_2$ values are outside the range of values suggested by the other mantle-derived elements and have consequently been ignored when establishing this mantle component. In addition the HREE peak at Ho and Er (and interpolated Tm and Tb) are likely to represent analytical error as discussed previously. As a result, the abundances for these elements have been fixed to those from sample 64067 from Thompson *et al.* (1984).

**Source of this mantle component**

Due to the limited dataset and inaccuracies in several elemental abundances, modelling of a possible partial melting source for this mantle component has not been attempted. Nevertheless, various general properties of this mantle source can be assessed. From plot 7.3b, it appears likely that Nb and elements to the right of Zr (with the possible exception of the MREE and $TiO_2$) have been derived primarily from the mantle. The gently sloping nature to the normalized REE data on figure 7.3a (ignoring those elements in which errors

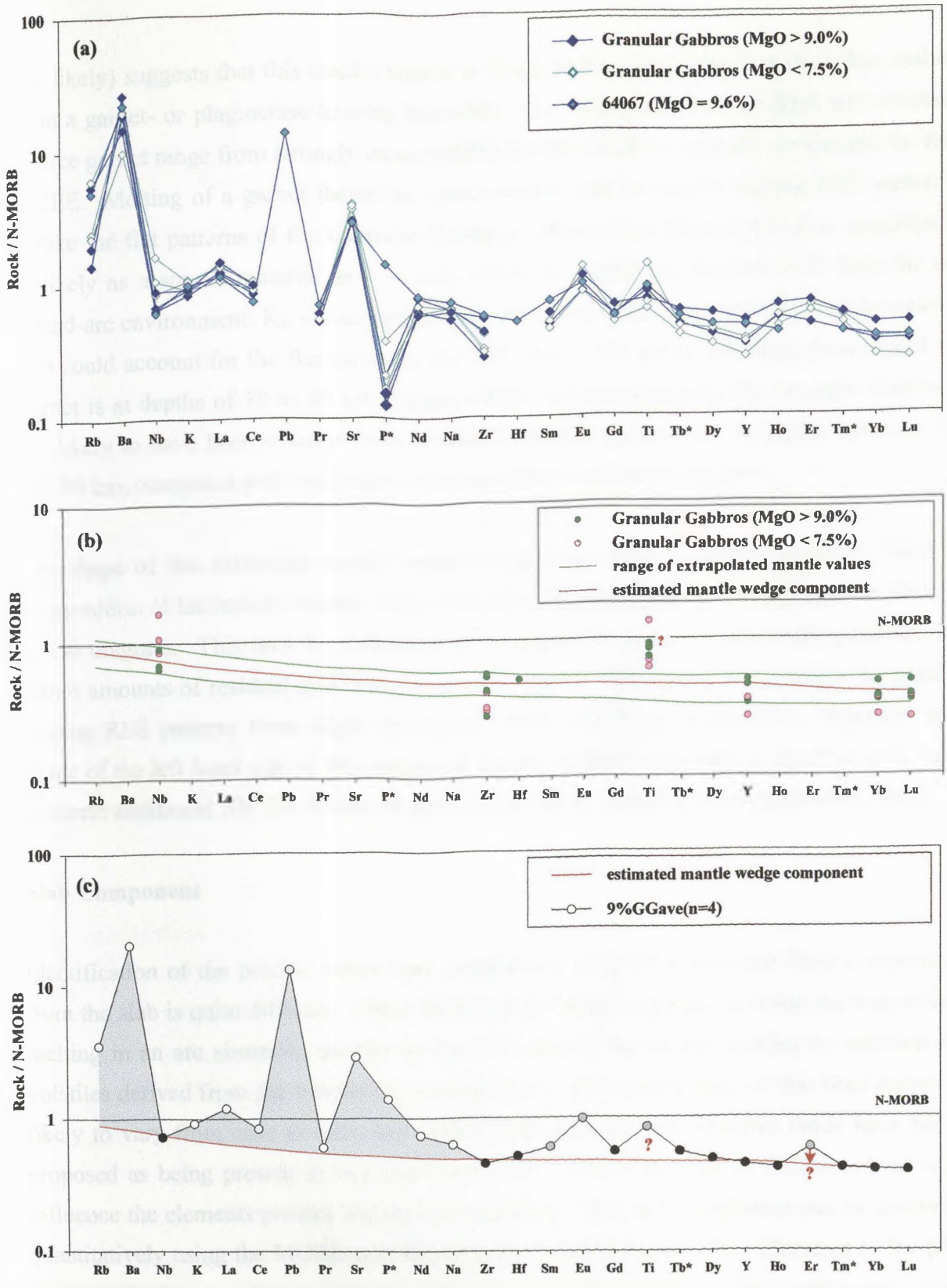


**Figure 7.3 (a) N-type MORB-normalized spider patterns for the Granular Gabbros. (b) Extrapolated mantle component for all elements based on values for Nb, Zr, Y, and Yb from Granular Gabbros with MgO > 9.0%. (c) N-type MORB-normalized spider patterns of the average Granular Gabbro (where MgO > 9.0 wt%; n=4). Solid circles represent those elements likely to be primarily sourced from the mantle, while the open circles represent those samples likely to have a significant additional slab contribution; the grey circles represent elements for which some uncertainty exists as discussed in the text. The shaded area above the extrapolated line representing this possible slab component. P, Tm, Tb, Gd, and Ho values fixed to those of sample 64067 (Thompson et al., 1984) for reasons outlined in the text; no Er data was available for this sample and the average value for the remaining samples has been used, and is likely to be too high. MORB-normalizing values are from Pearce & Parkinson (1993).**

are likely) suggests that this mantle source is likely to be a spinel-bearing lherzolite, rather than a garnet- or plagioclase-bearing lherzolite. $K_D$ values between the REE and residual source garnet range from strongly incompatible for the LREE to strongly compatible for the HREE. Melting of a garnet lherzolite source would lead to steeply sloping REE patterns unlike the flat patterns of the Granular Gabbros. Plagioclase lherzolite is also considered unlikely as a source material as it is only stable at depths too shallow (<30 km) for an island-arc environment; $K_D$ values between the REE and spinel are relatively even however, and could account for the flat nature to the REE data. The phase transition from spinel to garnet is at depths of 70 to 80 km (Ellam, 1992) and consequently, the Granular Gabbros are likely to have been sourced from a spinel-lherzolite partial melt at depths between 30 and 80 km, consistent with derivation in an arc-type tectonic environment.

The shape of this estimated mantle wedge component can also yield information on the composition of the mantle source; slight enrichment is seen in Nb, Zr and Hf data to the left of the diagram. This may be indicative of an enriched mantle source or the presence of minor amounts of residual garnet in the mantle source. This could also explain the gently sloping REE patterns from slight enrichment of the LREE on figure 7.3c. However, the shape of the left hand side of this estimated mantle wedge component is based on only one element; additional Nb, Ta, Zr and Hf data could help to constrain this mantle component.

**Slab Component**

Identification of the precise nature and composition of a LILE-enriched fluid component from the slab is quite difficult. These fluids are generally regarded as being the trigger for melting in an arc situation, usually by the lowering of the mantle solidus by addition of volatiles derived from the subducting oceanic crust. The composition of this fluid phase is likely to vary from case to case, and indeed both aqueous and siliceous fluids have been proposed as being present in this slab component; clearly the type of fluid involved will influence the elements present and their abundances. This slab component can be assessed quantitatively using the MORB-normalised plot shown in figure 7.3c. Elements to the left of Zr (with the exception of Nb) are likely to be derived from the slab component. The shaded region above the mantle wedge component estimated in the previous section represents this slab component. Pb (based on one sample) and the LIL elements Rb, Ba and Sr show the greatest enrichment, along with $P_2O_5$ (also based on only one sample due to the $P_2O_5$ inaccuracies) and positive enrichments in the LREE and MREE. $K_2O$ shows only slight enrichment, while the origin of the $TiO_2$ peak is unclear. The trend seen in this plot

for the Granular Gabbros is similar to that proposed for island-arc tholeiites by Pearce (1983), with the subduction-zone component mainly enriched in LIL elements, but also slightly enriched in P, Ti, the LREE and also the MREE.

## 7.3 Similarity of the 'Younger' Basics to other island arc magmas

### 7.3.1 Introduction

As seen in the previous section, the Granular Gabbros and certain unevolved cumulates show properties consistent with derivation in an arc environment. These Granular Gabbros are the only control on the original magma composition of the 'Younger' Basics with the majority of non-granular samples from the bodies displaying the chemical effects of contamination, fractionation and cumulate processes, thus obscuring any possible characteristic signatures from the original magma. Contamination in particular masks these parental attributes, causing changes to 'spider' and REE plots and to whole rock isotopic ratios. In this section, the Granular Gabbros will be briefly compared to arc magmas and the chemistry of the main silicate phases also compared to examples from arc settings.

### 7.3.2 Primitive/Primary arc volcanics

As a result of the limited dataset, only a brief discussion of the similarities between the Granular Gabbros and arc magmas will be undertaken. Table 7.1 shows a comparison of data from the Granular Gabbros and several samples from arc settings. These data are also shown on 'spider' diagrams in figure 7.4a & 7.4b; these plots reveal strong similarities between the Granular Gabbros and volcanic rocks of island-arc affinity, specifically island-arc tholeiites. The 'spiders' are flat, with slight enrichment at the LILE end, and display minor Nb-troughs and pronounced Sr-peaks. However, Nb-troughs are evident in most cumulate samples from the 'Younger' Basics; these are due to contamination by Nb-depleted country rocks. Isotopic data are required to evaluate if the Nb-troughs are arc-related or merely slight contamination by these Nb-depleted country rocks; the size of these troughs on figures 7.2 and 7.3 appears to be related to the sample MgO content, and as a result this may be the case.

| | avGG(n=6) | 64067 | 27857 | 27196 | 670 | i-a th (ppm) |
|---|---|---|---|---|---|---|
| SiO2 | 48.61 | 47.66 | 48.77 | 48.17 | 47.79 | |
| TiO2 | 1.08 | 1.16 | 0.86 | 0.73 | 0.54 | 3000 |
| Al2O3 | 18.09 | 16.97 | 16.86 | 18.04 | 16.49 | |
| Fe2O3 | | | | | 1.76 | |
| FeO | | | | | 8.80 | |
| $Fe2O3^T$ | 9.26 | 10.25 | 12.64 | 9.67 | 11.54 | |
| MnO | 0.15 | 0.16 | 0.21 | 0.16 | 0.20 | |
| MgO | 7.98 | 9.60 | 7.81 | 10.10 | 8.94 | |
| CaO | 12.75 | 12.45 | 12.00 | 11.19 | 13.24 | |
| Na2O | 1.72 | 2.00 | 1.28 | 2.55 | 1.78 | |
| K2O | 0.13 | 0.13 | 0.07 | 0.12 | 0.38 | 3240 |
| P2O5 | *0.01* | 0.10 | 0.04 | 0.06 | 0.09 | |
| LOI | 0.23 | | | | 0.59 | |
| mg# | 46.29 | 48.36 | 38.19 | 51.09 | 43.65 | |
| Ba | 115 | 140 | 98 | 59 | 120 | 110 |
| Rb | 1.85 | 2.8 | 1.9 | 2.6 | 6.2 | 4.6 |
| Sr | 302.75 | 257 | 183 | 212 | 378 | 200 |
| Y | 10.63 | 13 | 16 | 20 | 14.4 | 12 |
| Zr | 28.48 | 42 | 30 | 47 | 19 | 22 |
| Nb | 2.25 | 1.5 | 0.2 | 0.7 | 0.46 | 0.7 |
| Zn | 54.38 | 59 | 81 | 48 | | |
| Cu | 38.05 | 53 | 93 | 77 | | |
| Ni | 56.65 | 86 | 35 | 176 | | |
| Cr | 223.9 | 273 | 181 | 154 | | |
| V | 189.4 | | | | | |
| Sc | 34.93 | | | | | |
| Pb | | 4 | 9 | <2 | | |
| U | | <0.04 | 0.053 | 0.072 | 0.11 | |
| Th | | 0.02 | <0.12 | 0.2 | 0.26 | |
| Ta | | | 0.015 | 0.035 | | |
| Hf | | 1.06 | 0.72 | 0.88 | | |
| La | 3.23 | 2.9 | 1.61 | 2.06 | 2.78 | 1.3 |
| Ce | 7.13 | 5.6 | 2.63 | 3.79 | 7.03 | 3.7 |
| Pr | 0.78 | 0.93 | 0.6 | 0.8 | 0.94 | |
| Nd | 3.71 | 5.9 | 4.1 | 5 | 4.85 | 3.4 |
| Sm | 1.35 | 1.91 | 1.6 | 1.9 | 1.31 | 1.2 |
| Eu | 1.05 | 0.99 | 0.61 | 0.78 | 0.52 | |
| Gd | *2.1* | 2.05 | 2 | 2.4 | 1.65 | |
| Dy | 2 | 2.16 | 2.45 | 3.03 | 1.88 | |
| Ho | *0.55* | 0.42 | 0.51 | 0.66 | 0.39 | |
| Er | *1.8* | | 1.53 | 2.04 | 1.21 | |
| Yb | 1.13 | 1.16 | 1.51 | 2.14 | 1.07 | |
| Lu | 0.17 | 0.17 | 0.21 | 0.34 | | |

| | |
|---|---|
| 27857 | Olivine basalt, Atami, Japan (Thompson et al., 1984) |
| 27196 | Olivine basalt, Warner flow, California (Thompson et al., 1984) |
| 670 | Eastern Epi olivine basalt with phyric plag (30%), olivine (10%) & cpx (5%) (Gorton, 1977) |
| i-a th. | Island-arc tholeiite (Sun, 1982) |
| *0.55* | Italicized data is likely to contain analytical errors |

**Table 7.1 Comparison of Granular Gabbro data with samples from arc settings**

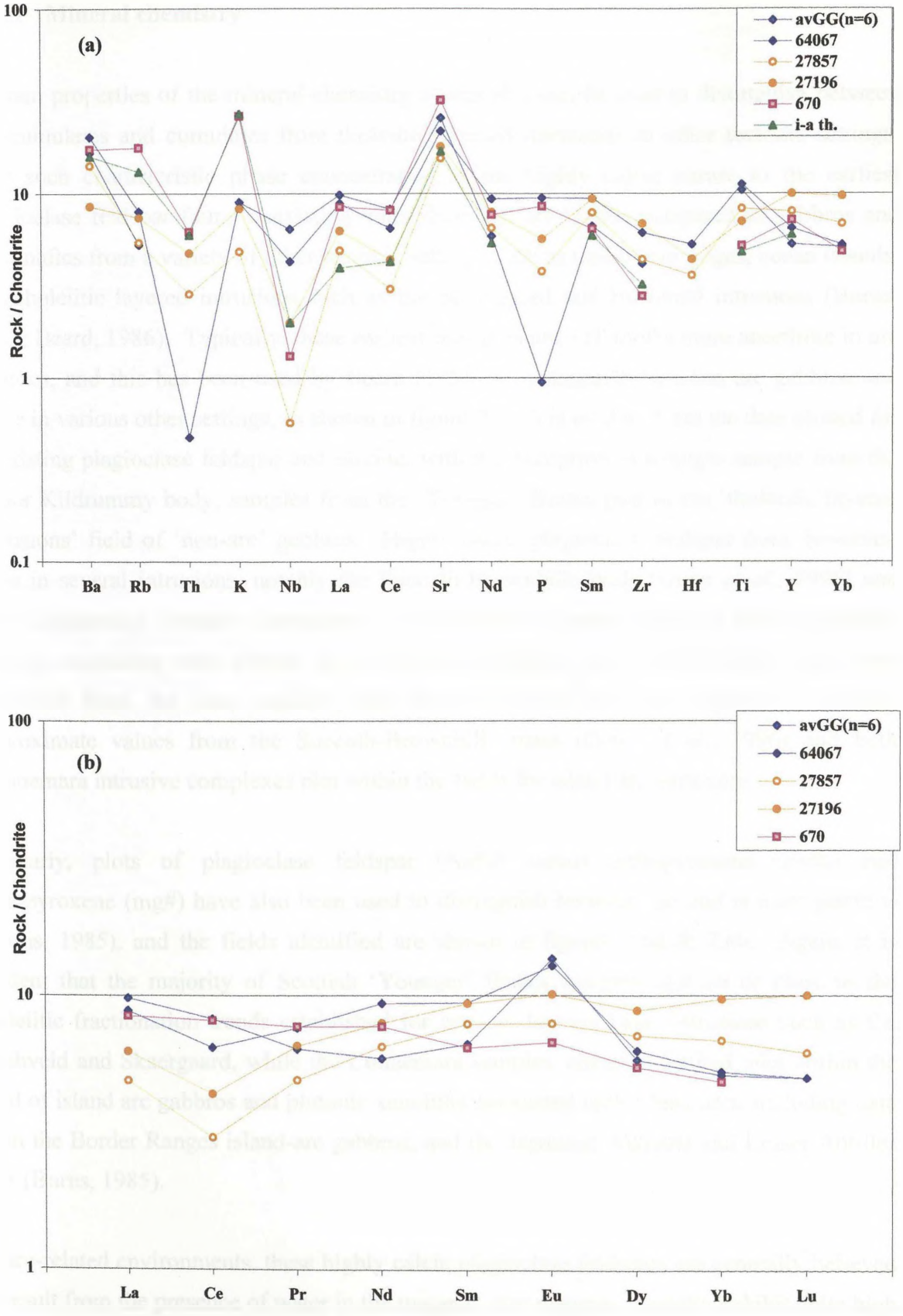


**Figure 7.4 Comparison of Granular Gabbro data with arc-type samples on samples on chondrite normalized (a) spider and (b) REE plots. Data given in Table 7.1. Gd, Ho and Er data omitted.**

### 7.3.3 Mineral chemistry

Certain properties of the mineral chemistry of samples can be used to distinguish between arc-cumulates and cumulates from tholeiitic layered intrusions in other tectonic settings. One such characteristic phase concentration is the highly calcic nature to the earliest plagioclase feldspar found coexisting with olivine in arc bodies compared to gabbros and ultramafics from a variety of other tectonic settings such as mid-ocean ridges, ocean islands, and tholeiitic layered intrusions such as the Skaergaard and Bushveld intrusions (Burns, 1985; Beard, 1986). Typically, these earliest feldspars are ~10 mol% more anorthitic in arc gabbros, and this has been used by Beard (1986) to distinguish between arc gabbros and those in various other settings, as shown in figure 7.5. It is evident from the data plotted for coexisting plagioclase feldspar and olivine, with the exception of a single sample from the minor Kildrummy body, samples from the 'Younger' Basics plot in the 'tholeiitic layered intrusions' field of 'non-arc' gabbros. Highly calcic plagioclase feldspar does, however, exist in several intrusions, notably the Succoth-Brownhills body (Gunn *et al.*, 1996) and both Connemara intrusive complexes. Unfortunately, probe data for this plagioclase directly coexisting with olivine have not been obtained; as a result, values have been estimated from the data available, and these are also shown in figure 7.5. These approximate values from the Succoth-Brownhills mass (Gunn *et al.*, 1996) and both Connemara intrusive complexes plot within the fields for island arc intrusions.

Similarly, plots of plagioclase feldspar (An%) versus orthopyroxene (En%) and clinopyroxene (mg#) have also been used to distinguish between arc and non-arc gabbros (Burns, 1985), and the fields identified are shown in figures 7.6a & 7.6b. Again, it is evident that the majority of Scottish 'Younger' Basics samples plot on or close to the tholeiitic fractionation trends established for non-arc layered basic intrusions such as the Bushveld and Skaergaard, while the Connemara samples, although limited, plot within the field of island arc gabbros and plutonic xenoliths associated with island arcs, including data from the Border Ranges island-arc gabbros, and the Japanese, Mariana and Lesser Antilles arcs (Burns, 1985).

In arc-related environments, these highly calcic plagioclase feldspars are generally believed to result from the presence of water in the magma. Arc-magmas typically exhibit quite high water content and experimental studies have shown that such high $H_2O$ leads to the lowering and flattening of both the liquidus and the solidus in the $NaAlSi_3O_8$ – $CaAlSi_2O_8$ binary system (Helz, 1973; Johannes, 1989). This flattening of the phase diagram leads to

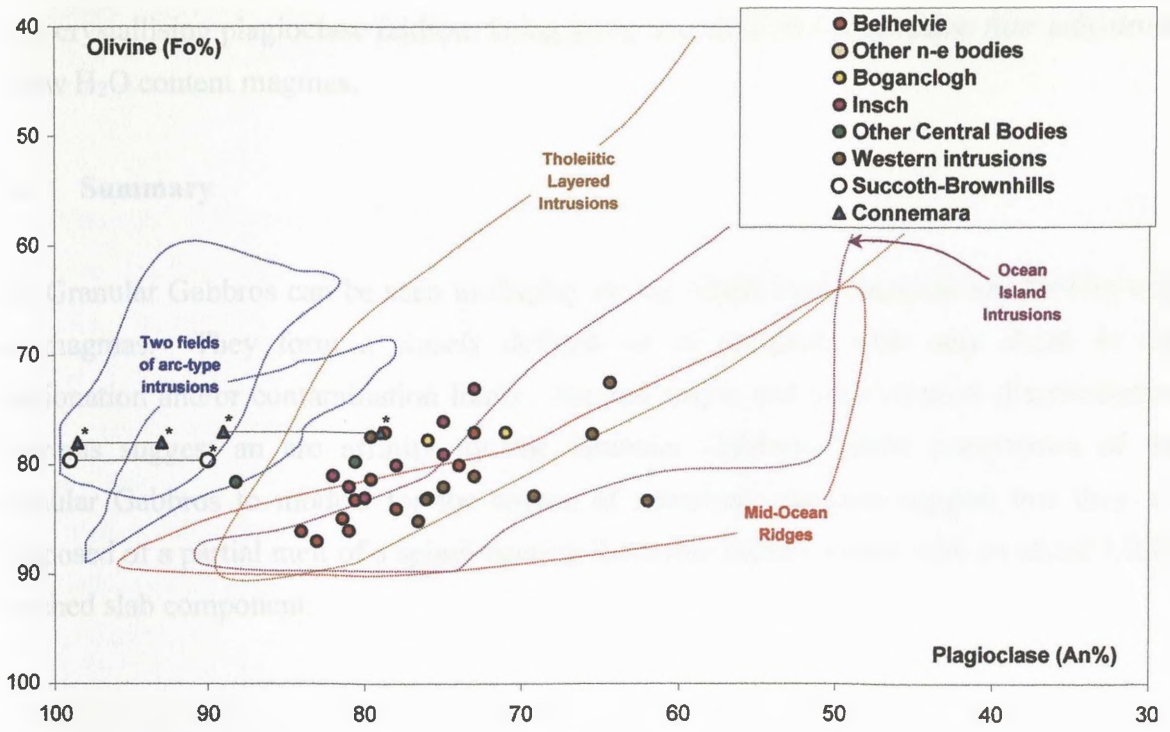


**Figure 7.5 Plagioclase feldspar anorthite content (An%) versus forsterite content (Fo%) of coexisting olivine for samples from the 'Younger' Basics. The fields for arc-related layered intrusions are from Beard (1986). Additional intrusions and non-arc tholeiitic data from Wadsworth et al. (1966), Ashcroft & Munro (1978), Fletcher (1989), Wadsworth (1991) and Gould (1997). Starred values are samples for which data for coexisting phases are not present and likely value ranges are shown. Where a range of data is available, the most anorthitic and forsteritic values were used.**

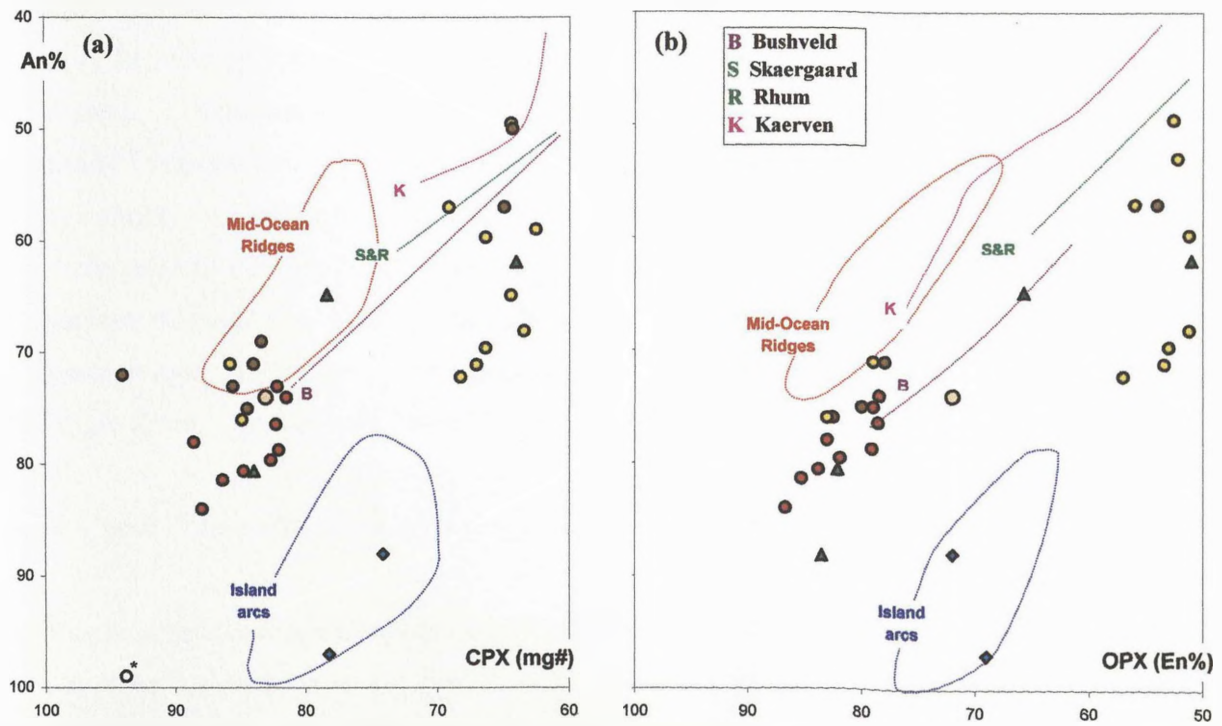


**Figure 7.6 Plagioclase feldspar anorthite content (An%) versus coexisting (a) clinopyroxene (mg#) and (b) orthopyroxene (En%) for samples from the 'Younger' Basics. The fields for arc-related intrusions and non-arc tholeiitic layered intrusions are from Burns (1985). Additional data from Wadsworth et al. (1966), Ashcroft & Munro (1978), Fletcher (1989), Wadsworth (1991), Gunn et al (1996) and Gould (1997). Symbols as for Figure 7.4 above.**

early crystallising plagioclase feldspar being more anorthitic in composition than anhydrous or low $H_2O$ content magmas.

## 7.4 Summary

The Granular Gabbros can be seen to display strong whole rock chemical similarities with arc magmas. They form a closely defined set of samples, with only slight *in situ* fractionation and/or contamination likely. Several major and trace element discrimination diagrams suggest an arc affinity for the Granular Gabbros, while comparison of the Granular Gabbros to models for the source of island-arc magmas suggest that they are composed of a partial melt of a spinel-bearing lherzolite mantle source with an added LILE-enriched slab component.

# Chapter 8 Conclusions and future work

The 'Younger' Basics of northeastern Scotland and Connemara are a suite of tectonically deformed and dismembered ultrabasic to basic intrusions, which were emplaced during the Grampian Orogeny in mid-Ordovician times. There are several lines of evidence to suggest that the 'Younger' Basics have been contaminated by Dalradian country rock material. Country rocks unaffected by the bodies are largely pelitic in nature and display steeply sloping 'spider' and REE patterns with pronounced Nb-troughs. Chemical evidence suggests that initially there was removal of LIL; evidence for partial melting and wholescale assimilation of this material is also seen, suggesting that this contamination is likely to be quite extensive.

## 8.1 Fractionation of the cumulate sequence

Despite their subsequent extensive internal disruption and shearing, the majority of the bodies display textural and mineralogical evidence consistent with having crystallized as cumulates. Those phases behaving cotectically can be identified from these cumulate textures, and, although a detailed stratigraphy cannot be constructed due to the poor exposure in most of the bodies, a coherent fractionation history for the bodies has been established. Ferromagnesian minerals typically show decreasing Mg:Fe ratios with increasing fractionation, while plagioclase feldspar becomes increasingly less anorthic. The disappearance and subsequent return of olivine as a cumulus phase is the key phase transition used to subdivide the bodies as a whole into Lower, Middle and Upper Zones. Plagioclase feldspar and both pyroxenes both become cumulus in the Lower Zone and remain cumulate throughout the stratigraphy, except for orthopyroxene, which disappears in the Upper Zone. Apatite and ilmenite are found as cumulus phases towards the top of the Middle Zone, while alkali feldspar and zircon take on cumulus status in the Upper Zone. These Upper Zone rocks are restricted to the Insch and Boganclogh bodies.

Biotite and amphibole are found in significantly greater quantities in the northeastern bodies than in other bodies such as the Huntly mass. These hydrous phases are found, commonly in association with late stage quartz; this assemblage suggests increased levels of contamination have occurred in these bodies, with rocks from the Insch and Boganclogh bodies which have undergone similar degrees of fractionation containing olivine bearing

assemblages. Exceptionally anorthitic plagioclase feldspar is found in certain intrusions, notably the Connemara bodies; this is the only phase to show any significant difference within the suite as a whole compositionally.

Alteration is quite common in samples from the 'Younger' Basics, with hydrous replacement products, notably secondary amphibole widespread especially in western bodies from the Grampian Highlands. However, it is likely that this alteration does not appreciably affect the whole rock chemistry. Cumulate processes are shown to exert a significant control over the abundances of element in the whole rock data; this has implications for the use of incompatible element plots and contributes to the significant scatter seen in the data.

Chemically, the majority of samples are sub-alkalic basalts in composition. Limited $SiO_2$ or alkali enrichment is seen in most bodies; samples from the Insch and Boganclogh bodies show evolution to syenitic compositions. AFM plots suggest a tholeiitic fractionation trend, with initial Fe-enrichment seen in all bodies, and subsequent alkali enrichment restricted to the Insch and Boganclogh bodies. Trends in whole rock major and trace element data against a whole rock mg# fractionation index show evidence for slight geographical variations; however all the bodies follow the same approximate fractionation path. Variations are recognized in whole rock fractionation patterns for samples from the Insch and Boganclogh bodies - these variations are also recognized in the compositions of certain silicate phases.

'Spider' and REE plots from all bodies display steepening slopes with increasing evolution. Fractionation of the phases seen in the bodies alone is insufficient to produce these slopes, which are largely as a result of increased assimilation of country rock material; the 'spiders' display LIL-element enrichment and Nb-troughs indicative of this. Modelling of selected trends within the Insch and Boganclogh, and northeastern bodies support this suggestion, and are consistent with petrographic and chemical data.

## 8.2 Parental magmas to the 'Younger' Basics

The parental magmas to the 'Younger' Basics are likely to resemble a set of distinctive granular gabbros from the Huntly and Insch masses. These Granular Gabbros are texturally, mineralogically and chemically distinct from the main cumulate pile and appear to be related to a series of deep seated shear zones which crosscut many of the bodies.

Limited fractionation in these samples is inconsistent with that seen in the main cumulate sequence from the same body, and estimates for equilibration between the Granular Gabbros and Lower Zone silicate phases from most of the bodies are consistent with a Granular Gabbros-type source for the bodies. However, exceptionally Mg-rich phases in certain intrusions suggests an initial, more picritic, magma may also have also been emplaced.

The chemistry of these Granular Gabbros bears a strong resemblance to arc-type magmas and identification of source mantle and slab components in these samples is possible. This arc chemistry, combined with the highly anorthitic plagioclase feldspar seen in some bodies are consistent with derivation of these bodies in an arc-type environment.

## 8.3 Future Work

It is evident from many of the discussions in Chapters 6 & 7 that the Granular Gabbros require more detailed and systematic geochemical analysis. Their precise relationship to the main Middle Zone sequence in Insch is poorly understood and the equivalent relationship in Huntly even less so. Detailed localized fieldwork, combined with textural analysis in these two bodies, combined with additional accurate geochemical analysis are required to describe fully this suite of rocks. In particular detailed trace element analysis, especially of incompatible elements such as Th, Hf and Ta, may help to identify the precise source of these bodies and also assess their *in situ* fractionation and any possible spatial variations between the two bodies. To this end, isotope analysis would be an invaluable tool in characterizing these parental rocks, as well as aiding in the investigation of their likely mantle source.

Although the Insch and Boganclogh bodies represent an excellent example of a tholeiitic layered basic intrusion undergoing AFC processes to completion, it seems likely that their poorly exposed nature prevents their examination as such as system in greater detail. However, the mineralogical and chemical evidence for the presence of several trends in these bodies and the variation in their initial forsterite compositions may possibly require further investigation. Detailed and systematic probework on Lower Zone samples from these bodies and indeed the bodies as a whole may well reveal systematic variations as suggested in Chapter 6, with these trends possibly linked to an initial more picritic magma. In addition, the Morven Cabrach subset, identified on the basis of only three samples, may require further investigation.

# References

Allan, W.C. (1970) The Morven-Cabrach intrusion. *Scottish Journal of Geology*, **6**, 53-72.

Anderton, R (1976) Tidal-shelf sedimentation: an example from the Dalradian. *Sedimentology*, **23**, 429-458.

Arculus, R.J. (1994) Aspects of magma genesis in arcs. *Lithos*, **33**, 189-208.

Ashcroft, W.A. (1970) Note on the contacts of the Belhelvie igneous intrusion. *Scottish Journal of Geology*, **6**, 73-74.

Ashcroft, W.A., Kneller, B.C., Leslie A.G., Munro, M. (1984) Major shear zones and autochthonous Dalradian in the northeast Scottish Caledonides. *Nature*, **310**, 760-762.

Ashcroft, W.A. & Boyd, R. (1976) The Belhelvie mafic igneous intrusion, Aberdeenshire - a reinvestigation. *Scottish Journal of Geology*, **12**, 1-14.

Ashcroft, W.A. & Munro, M. (1978) The structure of the eastern part of the Insch Mafic Intrusion, Aberdeenshire. *Scottish Journal of Geology*, **14**, 55-79.

Ashworth, J.R. (1975) The sillimanite zones of the Huntly-Portsoy area in the north-east Dalradian, Scotland. *Geological Magazine*, **112**, 113-224.

Ashworth, J.R. (1976) Petrogenesis of migmatites in the Huntly-Portsoy area, north-east Scotland. *Mineralogical Magazine*, **40**, 661-682.

Ashworth, J.R. & Chinner G.A. (1978) Coexisting garnet and cordierite in migmatites from the Scottish Caledonides. *Contributions to Mineralogy and Petrology*, **65**, 379-394.

Atherton, M.P. (1977) The metamorphism of the Dalradian rocks of Scotland. *Scottish Journal of Geology*, **13**, 331-370.

Atherton, M.P. & Brotherton, M.S. (1982) Major element composition of the pelites of the Scottish Dalradian. *Geological Journal*, **17**, 185-221.

Baker, B.H., Goles, G.G., Leeman, W.P. & Lindstrom, M.M. (1977) Geochemistry and petrogenesis of a basalt-benmoreite-trachyte suite from the southern part of the Gregory Rift, Kenya. *Contributions to Mineralogy and Petrology*, **64**, 303-332.

Barnes, S.J. (1986) The effect of trapped liquid crystallization on cumulus mineral compositions in layered intrusions. *Contributions to Mineralogy and Petrology*, **93**, 524-531.

Barrow, G. (1893) On an intrusion of muscovite-biotite gneiss in the southeastern Highlands of Scotland and its accompanying metamorphism. *Quarterly Journal of the Geological Society of London*, **49**, 330-358.

Barrow, G. (1912) On the geology of Lower Dee-side and the southern Highland Border. *Proceedings of the Geologists Association*, **23**, 268-273.

Beard, J.S. (1986) Characteristic mineralogy of arc-related cumulate gabbros: Implications for the tectonic setting of gabbroic plutons and for andesite genesis. *Geology*, **14**, 848-851.

Bonney, T.G. (1885) On bastite-serpentine and troktolite in Aberdeenshire, with a note on the rock of the Black Dog. *Geological Magazine*, **3**, 439.

Boyd, R. (1972) The geology of the Belhelvie mafic intrusion and its margins, Aberdeenshire. *University of Aberdeen PhD thesis (unpublished)*.

Boyd, R. & Munro, M. (1978) Deformation of the Belhelvie Mass, Aberdeenshire. *Scottish Journal of Geology*, **14**, 29-44.

Brasier, M.D. & Shields, G. (2000) Neoproterozoic chemostratigraphy and correlation of the Port Askaig glaciation, Dalradian Supergroup of Scotland. *Journal of the Geological Society of London*, **157**, 909-914.

Brown, P.E., Miller, J.A., Grasty, R.L., & Fraser, W.E. (1965) Potassium-argon ages of some Aberdeenshire granites and gabbros. *Nature*, **207**, 1287-1288.

Burns, L.E. (1985) The Border Ranges ultramafic and mafic complex, south-central Alaska: cumulate fractionates of island-arc volcanics. *Canadian Journal of Earth Sciences*, **22**, 1020-1038.

Busrewil, M.T., Pankhurst, R.J. & Wadsworth, W.J. (1973) The igneous rocks of the Boganclogh area, N.E. Scotland. *Scottish Journal of Geology*, **9**, 165-176.

Campbell, I.H. (1978) Some problems with the cumulus theory. *Lithos*, **11**, 311-323.

Cawthorn, G.R. (1996) Models for incompatible trace element abundances in cumulus minerals and their application to plagioclase and pyroxenes in the Bushveld Complex. *Contributions to Mineralogy and Petrology*, **123**, 109-115.

Cherniak, D.J., Hanchar, J.M. & Watson, E.B. (1997) Diffusion of tetravalent cations in zircon. *Contributions to Mineralogy and Petrology*, **127**, 383-390

Chinner, G.A. (1960) Pelitic gneisses with varying ferrous/ferric ratios from Glen Clova, Angus, Scotland. *Journal of Petrology*, **1**, 128-267.

Chinner, G.A. (1966) The distribution of pressure and temperature during Dalradiam metamorphism. *Quarterly Journal of the Geological Society of London*, **122**, 159-186.

Clarke, P.D. & Wadsworth, W.J. (1970) The Insch layered intrusion. *Scottish Journal of Geology*, **6**, 7-25.

Davidson, J.P. (1996) Deciphering mantle and crustal signatures in subduction zone magmatism. Subduction Top to Bottom. In: *Geophysical Monograph.*, American Geophysical Union. **96,,** 251-262.

Davies, G.R. & Macdonald, R. (1987) Crustal influences in the petrogenesis of the Naivasha basalt-rhyolite complex: combined trace element and Sr-Nd-Pb isotope constraints. *Journal of Petrology*, **28**, 1009-1031.

Deer, W.A., Howie, R.A. & Zussman, J. (1992) *An Introduction to the Rock Forming Minerals*, Longman Scientific & Technical.

Dempster, T.J. (1985) Uplift patterns and orogenic evolution of the Scottish Dalradian. *Journal of the Geological Society of London*, **142**, 111-128.

Dempster, T.J., Hudson, N.F.C. & Rogers, G (1995) Metamorphism and cooling of the NE Dalradian. *Journal of the Geological Society of London*, **152**, 383-390.

Dempster, T.J., Rogers, G., Tanner, P.G.W., Bluck, B.J., Muir, R.J., Redwood, S.D., Ireland, T.R. & Paterson, B.A. (2002) Timing of deposition, orogenesis and glaciation within the Dalradian rocks of Scotland: constraints from U-Pb zircon ages. *Journal of the Geological Society of London*, **159**, 83-94.

DePaolo, D.J. (1981) Trace element and isotopic effects of combined wallrock assimilation and fractional crystallization. *Earth and Planetary Science Letters*, **53**, 189-202.

DePaolo, D.J. (1985) Isotopic studies of processes in magma chambers: I The Kiglapait intrusion, Labrador. *Journal of Petrology*, **26**, 925-951.

Dewey, J.F.& Shackleton, R.M. (1984) A model for the evolution of the Grampian Tract in the early Caledonides and Appalachians. *Nature*, **312**, 115-121.

Downie, C., Lister, T.R., Harris, A.R., & Fettes, D.J. (1971) *A palynological investigation of the Dalradian rocks of Scotland*, Institute of Geological Sciences. 30pp.

Draut, A.E. & Clift, P.D. (2002) The origin and significance of the Delaney Dome Formation, Connemara, Ireland. *Journal of the Geological Society of London*, **159**, 95-103.

Droop, G.T.R. & Charnley, N.R. (1985) Comparative geobarometry of pelitic hornfelses associated with the Newer Gabbros: a preliminary study. *Journal of the Geological Society of London*, **122**, 53-62.

Ellam, R. M. (1992) Lithosphere thickness as a control on basalt geochemistry. *Geology*, **20**, 153-156.

Evans, B.W. (1964) Fractionation of elements in the pelitic hornfelses of the Cashel-Lough Wheelaun intrusion, Connemara, Eire. *Geochimica et Cosmochimica Acta*, **28**, 127-156.

Ferguson, C.C. & Al Ameen, S.I. (1986) Geochemistry of Dalradian pelites from Connemara, Ireland - new constraints on kyanite genesis and conditions of metamorphism. *Journal of the Geological Society of London*, **143**, 237-252.

Fettes, D.J. (1970) The structural and metamorphic state of the Dalradian rocks and their bearing on the age of emplacement of the basic sheet. *Scottish Journal of Geology*, **6**, 108-118.

Fettes, D.J., and six others (1985) Grade and time of metamorphism in the Caledonide Orogen of Britain and Ireland. In: *The nature and timing of orogenic activity in the Caledonian rocks of the British Isles.* (eds. Harris, A.L.), Memoir of the Geological Society of London No. **9,,** 41-43.

Fettes, D.J., Graham, C.M., Harte, B and Plant, J.A. (1986) Lineaments and basement domains; an alternative view of Dalradian evolution. *Journal of the Geological Society of London*, **143**, 453-464.

Fettes, D.J. & Munro, M. (1989) Age of the Blackwater mafic and ultramafic intrusion, Banffshire. *Scottish Journal of Geology*, **25**, 105-111.

Fletcher, T.A. (1989) The Geology, Mineralization (Ni-Cu-PGE) and isotope systematics of Caledonian mafic intrusions near Huntly, NE Scotland. *Unpublished PhD thesis, University of Aberdeen.*

Fletcher, T.A., & Rice, C.M. (1989) Geology, mineralization (Ni-Cu) and precious-metal geochemistry of Caledonian mafic and ultramafic intrusions near Huntly, northeast Scotland. *Transactions of the Institution of Mining and Metallurgy*, **B98**, 185-200.

Friedrich, A.M., Bowring, S.A., Martin, M.W., and Hodges, K.V. (1999a) Short-lived continental magmatic arc at Connemara, Western Irish Caledonides: Implications for the age of the Grampian Orogeny. *Geology*, **27**, 27-30.

Friedrich, A.M., Hodges, K.V., Bowring, S.A., & Martin, M.W. (1999b) Thermal evolution of the Connemara Caledonides, Western Ireland. *Journal of the Geological Society of London*, **156**, 1217-1230.

Garrido, C.J., Bodinier, J.L. & Alard, O. (2000) Incompatible trace element partitioning and residence in anhydrous spinel peridotites and websterites from the Ronda orogenic peridotite. *Earth and Planetary Science Letters*, **181**, 341-358.

Gast, P.W. (1968) Trace element fractionation and the origin of tholeiitic and alkaline magma types. *Geochimica et Cosmochimica Acta*, **32**, 1057-1086.

Gibb, A. W. (1908) The basic igneous rocks of Belhelvie. *Unpublished D.Sc. dissertation, University of Aberdeen.*

Gibb, A.W. (1912) On an actinolite-bearing rock allied to serpentine. *Report of the British Association, Dundee*. p. 468.

Goodman, S. (1994) The Portsoy-Duchray Hill Lineament: a review of the evidence. *Geological Magazine*, **130**, 407-415.

Gorton, M.P. (1977) The geochemistry and origin of quaternary volcanism in the New Hebrides. *Geochimica et Cosmochimica Acta*, **41**, 1257-1270.

Gould, D (1997) Geology of the country around Inverurie and Alford. *Memoir of the British Geological Survey, Sheets 76E and 76W (Scotland).*

Govindaraju, K. (1989) 1989 compilation of working values and sample description for 272 geostandards. *Geostandards Newsletter*, **13**, 1-113.

Gribble, C.D. (1966) The thermal aureole of the Haddo House norite in Aberdeenshire. *Scottish Journal of Geology*, **2**, 306-313.

Gribble, C.D. (1967) The basic intrusive rocks of Caledonian age in the Haddo House and Arnage districts, Aberdeenshire. *Scottish Journal of Geology*, **3**, 125-136.

Gribble, C.D. (1968) The cordierite-bearing rocks of the Haddo House and Arnage districts, Aberdeenshire. *Contributions to Mineralogy and Petrology*, **17**, 315-330.

Gribble, C.D. (1970) The role of partial fusion in the genesis of certain cordierite- bearing rocks. *Scottish Journal of Geology*, **6**, 75-82.

Gribble, C.D. & O'Hara, M.J. (1967) Interaction of basic magma and pelitic materials. *Nature*, **214**, 1198-1201.

Gunn, A.G., Styles, M.T., Rollin, K.E., & Stephenson, D. (1996) The geology of the Succoth-Brown Hill mafic-ultramafic intrusive complex, near Huntly, Aberdeeenshire. *Scottish Journal of Geology*, **32**, 33-49.

Hall, A (1996) *Igneous Petrology.*, Longman.

Halliday, A.N., Graham, C.M., Aftalion, M. & Dymoke, P. (1989) The depositional age of the Dalradian Supergroup: U-Pb and Sm-Nd isotopic studies of the Tayvallich Volcanics, Scotland. *Journal of the Geological Society of London*, **146**, 3-6.

Harrison, T.M. & Watson, E.B. (1983) Kinetics of zircon dissolution and zirconium diffusion in granitic melts of variable water content. *Contributions to Mineralogy and Petrology*, **84**, 66-72.

Harte, B (1988) Lower Palaeozoic metamorphism in the Moine-Dalradian belt of the British Isles. In: *The Caledonian-Appalachian Orogen.* (eds. Harris, A.L., & Fettes, D.J.), Special Publication of the Geological Society of London No. **38**, 123-134.

Harte, B. & Hudson, N.F.C. (1979) Pelitic facies series and the temperatures and pressures of Dalradiam metamorphism. In: *The Caledonides of the British Isles - reviewed.* (eds. Harris, A.L., Holland, C.H. & Leake, B.E.), Special Publication of the Geological Society of London No. **8**, 323-337.

Hawkesworth, C. J., Gallagher, K., Hergt, J. M. & McDermott, F. M. (1993) Trace element fractionation processes in the generation of island arc basalts. *Philosophical Transactions of the Royal Society of London, Series A*, **342**, 179-191.

Hawkesworth, C. J. & Norry , M.J. (Eds.) (1993) *Continental Basalts and Mantle Xenoliths.*, Shiva Publishing.

Heddle, M.F. (1882) Minerals new to Britain. *Mineralogical Magazine*, **1**, 1.

Helz, R.T. (1973) Phase relations of basalts in their melting range at PH2O = 5 kb as a function of oxygen fugacity. Part I. Mafic phases. *Journal of Petrology*, **14**, 249-302.

Hinxman, I.W. (1896) The geology of West Aberdeenshire and Banffshire with parts of Elgin and Inverness. *Memoir of the Geological Survey, Scotland, Sheet 75 (Scotland).*

Hinxman, I.W. & Wilson, J.S.G. (1902) The geology of Lower Strathspey. *Memoir of the Geological Survey, Scotland, Sheet 85 (Scotland).*

Hoskin, P.W.O., Kinny, P.D., Wyborn D., et al. (2000) Identifying accessory mineral saturation during differentiation in granitoid magmas: an integrated approach. *Journal of Petrology*, **41**, 1365-1396.

Huppert, H.E. & Sparks, R.S.J. (1985) Cooling and contamination of mafic and ultramafic magmas during ascent through continental crust. *Earth and Planetary Science Letters*, **74**, 371-386.

Hutchinson, C.D. (1965) Aspects of the petrology of the Insch mass, Aberdeenshire. *Unpublished MSc thesis. University of Cambridge.*

Ingold, L.M. (1937) The geology of the Currywongaun- Doughruagh area, Co. Galway. *Proceedings of the Royal Irish Academy*, **43B**, 135-159.

Irvine, T.N. (1982) Terminology for Layered Intrusions. *Journal of Petrology*, **23**, 127-162.

Irvine, T.N. & Baragar, W.R.A. (1971) A guide to the chemical classification of the common volcanic rocks. *Canadian Journal of Earth Sciences*, **8**, 523-548.

Jagger, M.D., Aftalion, M., Max, M.D. & Leake, B.E. (1988) U- Pb zircon ages of basic rocks and gneisses intruded into Dalradian rocks of Cashel, Connemara, western Ireland. *Journal of the Geological Society of London*, **132**, 485-508.

Johannes, W. (1989) Melting of plagioclase-quartz assemblages at 2-kbar water pressure. *Contributions to Mineralogy and Petrology*, **103**, 270-276.

Johannsen, A. (1931) *A Descriptive Petrography of the Igneous Rocks*, University of Chicago Press. 267pp.

Kanaris-Sotiriou, R. & Angus, N.S. (1976) The Currywongaun-Doughruagh syntectonic intrusion, Connemara, Ireland. *Journal of the Geological Society of London*, **132**, 485-508.

Kinahan, G.H. (1874) The geology of West Galway and SW Mayo, Ireland. *Geological Magazine*, **2**, 453-462.

Kinahan, G.H., Nolan, J., Leonard, H. & Cruise, R.J. (1878) *Explanation of Sheets 93 and 94.*

Kneller, B.C. (1987) A geological history of NE Scotland. In: *Excursion guide to the geology of the Aberdeen area.* (eds. Trewin, N.H., Kneller, B.C. & Gillen, C.), Geological Society of Aberdeen.

Kuno, H. (1968) Differentiation of basalt magmas. In: *Basalts: The Poldervaart treatise on rocks of basaltic composition.* (eds. Hess, H.H. & Poldervaart, A.), Vol.2. Interscience, New York, 623-688.

Kushiro, I. & Walter, M.J. (1998) Mg-Fe partitioning between olivine and mafic-ultramafic melts. *Geophysical Research Letters*, **25**, 2337-2340.

Lambert, R. St. J., & McKerrow, W.S. (1976) The Grampian orogeny. *Scottish Journal of Geology*, **12**, 271-292.

Lambert, R. St. J., Winchester, J.A. & Holland, J.G. (1981) Comparative geochemistry of pelites from the Moinian and Appin Group (Dalradian) of Scotland. *Geological Magazine*, **118**, 477-490.

Lambert, R. St. J., Holland, J.G. & Winchester, J.A. (1982) A geochemical comparison of the Dalradian Leven Schists and the Grampian Division Monadhliath Schists of Scotland. *Journal of the Geological Society of London*, **139**, 71-84.

Langmuir, C.H. (1989) Geochemical consequences of *in situ* crystallisation. *Nature*, **340**, 199-205.

Leake, B.E. (1958a) The Cashel-Lough Wheelaun intrusion, Co. Galway. *Proceedings of the Royal Irish Academy*, **598**, 155-203.

Leake, B.E. (1958b) Composition of pelites from Connemara, Co. Galway, Ireland. *Geological Magazine*, **100**, 44-46.

Leake, B.E. (1964) New Light on the Dawros Peridotite. *Geological Magazine*, **101**, 63-75.

Leake, B.E. (1970a) The fragmentation of the Connemara basic and ultrabasic intrusions. In: *Mechanisms of igneous intrusion.* (eds. Newall, G. & Rast, N.), Seel House Press, 103-122.

Leake, B.E. (1970b) The origin of the Connemara migmatites of the Cashel district, Connemara, Ireland. *Quarterly Journal of the Geological Society of London*, **125**, 219-276.

Leake, B. E. (1978) Nomenclature of amphiboles. *Canadian Mineralogist*, **63**, 1023–1053.

Leake, B.E. (1989) The metagabbros, orthogneisses and paragneisses of the Connemara Complex, Western Ireland. *Journal of the Geological Society of London*, **146**, 575-596.

Leake, B. E. & Skirrow, G (1960) The pelitic hornfelses of the Cashel-Lough Wheelaun intrusion, Co. Galway, Eire. *Journal of Geology*, **68**, 23-40.

Leake, B. E. & Tanner, P.G.W. (1994) *The geology of the Dalradian and associated rocks of Connemara, Western Ireland: a report to accompany the1:63660 geological map and cross sections.*, Royal Irish Academy.

Leslie, A.G. (1984) Field relations in the northeastern part of the Insch mafic igneous mass, Aberdeenshire. *Scottish Journal of Geology*, **20**, 215-235.

Mathez, E.A., Hunter, R.H. & Kinzler, R. (1997) Petrologic evolution of partially molten cumulate: the Atok Section of the Bushveld Complex. *Contributions to Mineralogy and Petrology*, **129**, 20-34.

McGregor, D.M. & Wilson, C.D.V. (1967) Gravity and magnetic surveys of the younger gabbros of Aberdeenshire. *Quarterly Journal of the Geological Society of London*, **123**, 99-123.

McKerrow, W.S., Mac Niocaill, C. & Dewey, J.F. (2000) The Caledonian Orogeny redefined. *Journal of the Geological Society of London*, **157**, 1149-1154.

Meschede, M. (1986) A method of discriminating between different types of mid-ocean ridge basalts and continental tholeiites with the Nb-Zr-Y diagram. *Chemical Geology*, **56**, 207-218.

Molyneux, S.G. (1998) An Upper Dalradian microfossil reassessed. *Journal of the Geological Society of London*, **155**, 741-743.

Mongkoltip, P. & Ashworth, J. R. (1983) Quantitative Estimation of an Open-system Symplectite-forming Reaction: Restricted Diffusion of Al and Si in Coronas around Olivine. *Journal of Petrology*, **24**, 635-661.

Mongkoltip, P. & Ashworth, J.R. (1986) Amphibolitization of metagabbros in the Scottish Highlands. *Journal of Metamorphic Geology*, **4**, 261-283.

Mullen, E.D. (1983) $MnO/TiO_2/P_2O_5$; a minor element discriminant for basaltic rocks of oceanic environments and its implications for petrogenesis. *Earth and Planetary Science Letters*, **62**, 53-62.

Munro, M. (1970) A reassessment of the younger basic igneous rocks between Huntly and Portsoy based on new

borehole evidence. *Scottish Journal of Geology*, **6**, 41-52.

Munro, M. (1984) Cumulate relations in the `Younger Basic' masses of the Huntly Portsoy area, Grampian region. *Scottish Journal of Geology*, **20**, 343-359.

Munro, M. (1986a) Mylonite zones in the Insch Younger Basic mass. *Scottish Journal of Geology*, **22** (1), 132-136.

Munro, M. (1986b) Geology of the country around Aberdeen. *Memoir of the British Geological Survey, Sheet 77 (Scotland)*.

Munro, M. & Gallagher, J.W. (1984) Disruption of the Younger Basic masses in the Huntly Portsoy area, Grampian region. *Scottish Journal of Geology*, **20**, 361-382.

Nakamura, N. (1974) Determination of REE, Ba, Fe, Mg, Na and K in carbonaceous and ordinary chondrites. *Geochimica et Cosmochimica Acta*, **38**, 757-775.

Oliver, G.J.H. (2001) Reconstruction of the Grampian episode in Scotland: its place in the Caledonian Orogeny. *Tectonophysics*, **332**, 23-49.

Oliver, G.J.H., Chen, F., Buchwaldt, R. & Hegner, E. (2001) Fast tectonometamorphism and exhumation in the type area of the Barrovian and Buchan zones. *Geology*, **28**, 459-462

O'Hara, M.J. & Matthews, R.E. (1981) Geochemical evolution in an advancing. periodically replenished, periodically tapped, continuously fractionated magma chamber. *Journal of the Geological Society of London*, **138**, 237-277.

Pankhurst, R.J. (1969) Strontium isotope studies applied to petrogenesis in the basic igneous province of North-East Scotland. *Journal of Petrology*, **10**, 116-145.

Pankhurst, R.J. (1970) The geochronology of the basic igneous complexes. *Scottish Journal of Geology*, **6**, 83-107.

Pearce, J.A. (1983) The role of sub-continental lithosphere in magma genesis at destructive plate margins. In: *Continental basalts and mantle xenoliths*. (eds. Hawkesworth, C. J., & Norry, M.J.), Nantwich: Shiva, 230-249.

Pearce, J.A. & Cann, J.R. (1973) Tectonic setting of basic volcanic rocks determined using trace element analysis. *Earth and Planetary Science Letters*, **19**, 290-300.

Pearce, J.A. & Parkinson, I.J. (1993) Trace element models for mantle melting: application to volcanic arc petrogenesis. In: *Magmatic processes and plate tectonics*. (eds. Prichard, H.M., Alabaster, T., Harris, N.B.W. & Neary, C.R.), Geological Society Special Publication. **76**, 373-403.

Phillips, W.E.A., Stillman, C.J., & Murphy, T. (1976) A Caledonian plate tectonic model. *Journal of the Geological Society of London*, **132**, 579-609.

Piasecki, M.A.J. & van Breemen, O. (1979) A Morarian age for the "younger Moines" of central and western Scotland. *Nature*, **278**, 734-736.

Pidgeon, R.T. & Aftalion, M. (1978) Cogenetic and inherited zircon U-Pb systems in granites: Palaeozoic granites of Scotland and England. In: Crustal evolution in north-west Britain and adjacent regions: *Geological Society of London Special Issue*, No **10**, 183-220.

Powell, R. (1984) Inversion of the assimilation and fractional crystallisation (AFC) equations: Characterization of contaminants from the isotope and trace element relationships in volcanic suites. *Journal of the Geological Society of London*, **141**, 447-52.

Prave, A.R. (1999) The Neoproterozoic Dalradian Supergroup of Scotland: an alternative hypothesis. *Geological Magazine*, **136**, 609-617.

Pringle, J. (1940) The discovery of Cambrian trilobites in the Highland border rocks near Callander, Perthshire. Adv. Sci. Lond., **1**, 252.

Pringle, I.R. (1972) Rb-Sr age determinations on shales associated with the Varanger Ice Age. *Geological Magazine*, **109**, 465-472.

Read, H.H. (1919) The two magmas of Strathbogie and Lower Banffshire. *Geological Magazine*, **56**, 364-371.

Read, H.H. (1921) The Contaminated Gabbro of Easter Saphock near Old Meldrum in Aberdeenshire. *Geological Magazine*, **58**, 177.

Read, H.H. (1923a) The geology of the country around Banff, Huntly and Turriff (Lower Banffshire, and North-west Aberdeenshire). *Memoir of the Geological Survey, Scotland, Sheets 86 & 96 (Scotland)*.

Read, H.H. (1923b) The petrology of the Arnage district in Aberdeenshire: a study of assimilation. *Quarterly Journal of the Geological Society of London*, **79**, 446-484.

Read, H.H. (1924) On certain xenoliths associated with the contaminated rocks of the Huntly mass, Aberdeenshire. *Geological Magazine*, **61**, 433-444.

Read, H.H. (1935) *British regional geology: the Grampian Highlands (1st edition)*, HMSO.

Read, H.H. (1956) The Dislocated South-Western Margin of the Insch Igneous Mass, Aberdeenshire. *Proceedings of the Geologists Association*, **67**, 73.

Read, H.H., Sadashivaiah, M.S., & Haq, B.T. (1961) Differentiation in the olivine-gabbro of the Insch mass, Aberdeenshire. *Proceedings of the Geologists Association*, **72**, 391-413.

Read, H.H., Sadashivaiah, M.S., & Haq, B.T. (1965) The hypersthene-gabbro of the Insch Complex, Aberdeenshire. *Proceedings of the Geologists Association*, **76**, 13-19.

Read, H.H. & Farquhar, O.C. (1952) The geology of the Arnage district (Aberdeenshire): a reinterpretation. *Quarterly Journal of the Geological Society of London*, **107**, 423-440.

Read, H.H. & Farquhar, O.C. (1956) The Buchan Anticline of the Banff Nappe of the Dalradian rocks in north-east Scotland. *Quarterly Journal of the Geological Society of London*, **112**, 131-156.

Read, H.H. & Haq, B.T. (1963) The Distribution of Trace Elements in the Dunite-Syenite Differentiated Series of the Insch Complex, Aberdeenshire. *Proceedings of the Geologists Association*, **74**, 203.

Roeder, P.D. & Emslie, R.F. (1970) Olivine-liquid equilibrium. *Contributions to Mineralogy and Petrology*, **29**, 275-289.

Rogers, G., Dempster, T.L., Bluck, B.J. & Tanner, P.W. (1989) A high-precision U-Pb age for the Ben Vuirich Granite: implications for the evolution of the Dalradian Supergroup. *Journal of the Geological Society of London*, **146**, 789-798.

Rogers, G., Paterson, B.A., Dempster, T.L. & Redwood, S.D. (1994). *U-Pb geochronology of the 'Newer' gabbros, NE Grampians*. Caledonian terrane relationships in Britain: British Geological Survey Programme with Abstracts, p. 8.

Rollinson, H. (1993) *Using Geochemical Data: evaluation, presentation, interpretation*, Longman Scientific & Technical.

Rothstein, A.T.V. (1957) The Dawros peridotite, Connemara, Eire. *Quarterly Journal of the Geological Society of London*, **113**, 1-25.

Rothstein, A.T.V. (1958) Pyroxenes from the Dawros peridotite and some comments on their nature. *Geological Magazine*, **95**, 456-462.

Rothstein, A.T.V. (1961) A synorogenic peridotite at Dawros, Connemara. *Acta Geodaetica et Geophysica Hungarica*, 7, 221-232.

Rothstein, A.T.V. (1964) New light on the Dawros Peridotite, Connemara. *Geological Magazine*, **101**, 283-285.

Rothstein, A.T.V. (1972) Spinels from the Dawros peridotite, Connemara, Ireland. *Mineralogical Magazine*, **38**, 957-960.

Sadashivaiah, M.S. (1954a) The form of the eastern end of the Insch mass, Aberdeenshire. *Geological Magazine*, **91**, 137-143.

Sadashivaiah, M.S. (1954b) The granite-diorite complex of the Insch Igneous Mass, Aberdeenshire. *Geological Magazine*, **91**, 286-292.

Saleemi, A.A. & Ahmed, Z. (2000) Mineral and chemical composition of Karak mudstone, Kohat Plateau, Pakistan: implications for smectite-illitization and provenance. *Sedimentary Geology*, **130** (3-4), 229-247.

Shackleton, R.M. (1948) Overturned rhythmic banding in the Huntly gabbro of Aberdeenshire. *Geological Magazine*, **85**, 358-360.

Soper, N.J., Ryan, P.D., & Dewey, J.F. (1999) Age of the Grampian orogeny in Scotland and Ireland. *Journal of the Geological Society of London*, **156** (1231-1236).

Sorensen, H.S. & Wilson, J.R. (1995) A strontium and neodymium isotope investigation of the Fongen-Hyllingen layered intrusion, Norway. *Journal of Petrology*, **36**, 161-187.

Stephenson, D. & Gould, D. (1995) *British Regional Geology. the Grampian Highlands (4th ed.)*, HMSO. 261pp.

Stewart, F.H. (1946) The gabbroic complex of Belhelvie in Aberdeenshire. *Quarterly Journal of the Geological Society of London*, **102**, 465-498.

Stewart, F.H. & Johnson, M.R.W. (1960) The structural problem of the younger gabbros of north-east Scotland. *Transactions of the Edinburgh Geological Society*, **18**, 104-112.

Stone, P. & Kimbell, G.S. (1995) Caledonian terrane relationships in Britain: an introduction. *Geological Magazine*, **132**, 461-464.

Sun, S. S. (1982) Chemical composition and origin of the Earth's primitive mantle. *Geochimica et Cosmochimica Acta*, **46**, 179–192.

Tanner, P.G.W. (1995) New evidence that the Lower Cambrian Leny Limestone at Callander, Perthshire, belongs to the Dalradian Supergroup and a re-assessment of the 'exotic' status of the Highland Border Complex. *Geological Magazine*, **132**, 473-483.

Tanner, P.G.W. & Bluck, B.J. (1999) Current controversies in the Caledonides. *Journal of the Geological Society of London*, **156**, 1137-1141.

Tatsumi, Y. & Eggins, S.M. (1995) *Subduction zone magmatism*, Blackwell.

Tegner, C., Robins, B., Reginiussen, H. & Grundvig, S. (1999) Assimilation of Crustal Xenoliths in a Basaltic Magma Chamber: Sr and Nd Isotopic Constraints from the Hasvik Layered Intrusion, Norway. *Journal of Petrology*, **40**, 363-380.

Thirlwall, M.F. (1981) Implications for Caledonian plate tectonic models of chemical data from volcanic rocks of the British Old Red Sandstone. *Journal of the Geological Society of London*, **138**, 123-138.

Thompson, R.N., Morrison, M.A., Dickin, A.P. & Hendry, G.L (1983) Continental flood basalts ... arachnids rule OK? In: *Continental Basalts and Mantle Xenoliths*. (eds. Hawkesworth, C. J. & Norry , M.J.), Shiva Publishing, 158-185.

Thompson, R.N., Morrison, M.A., Hendry, G.L. & Parry, S.J. (1984) An assessment of the relative roles of crust and mantle in magma genesis: an elemental approach. *Philosophical Transactions of the Royal Society of London, Series A*, **310**, 549-590.

Thy, P. & Esbensen, K.H. (1982) Origin of fine-grained granular rocks in layered intrusions. *Geological Magazine*, **119**, 405-412.

Tilley, C.E. (1925) A preliminary survey of metamorphic zones in the southern Highlands of Scotland. *Quarterly Journal of the Geological Society of London*, **81**, 100-112.

Tindle, A.G. & Pearce, J.A. (1983) Petrogenetic modelling of *in situ* fractional crystallisation in the zoned Loch Doon pluton, Scotland. *Contributions to Mineralogy and Petrology*, **78**, 196-207.

Tribuzio, R., Tiepolo, M., Vannucci, R. & Bottazzi, P. (1999a) Trace element distribution within olivine-bearing gabbros from the Northern Apennine ophiolites (Italy): evidence for post-cumulus crystallization in MOR type gabbroic rocks. *Contributions to Mineralogy and Petrology*, **134**, 123-133.

Tribuzio, R., Thirlwall, M.F. & Messiga, B. (1999b) Petrology, mineral and isotope geochemistry of the Sondalo gabbroic complex (Central Alps, Northern Italy): implications for the origin of post-Variscan magmatism. *Contributions to Mineralogy and Petrology*, **136**, 48-62.

Tuttle, O.F. & Bowen, N.L. (1958) The origin of granite in the light of experimental studies in the system $NaAlSi_3O_8$-$KAlSi_3O_8$-$SiO_2$-$H_2O$. *Memoir of the Geological Society of America, No 74.*

Ulmer, P (1989) The dependence of the $Fe^{2+}$-Mg cation-partitioning between olivine and basaltic liquid on pressure, temperature and composition: an experimental study to 30 kbars. *Contributions to Mineralogy and Petrology*, **101**, 261-273.

van Breemen, O & Boyd, R. (1972) A radiometric age for pegmatite cutting the Belhelvie mafic intrusion, Aberdeenshire. *Scottish Journal of Geology*, **8**, 115-120.

Wadsworth, W.J., Stewart, F.H. & Rothstein, A.T.V. (1966) Cryptic Layering in the Belhelvie intrusion, Aberdeenshire. *Scottish Journal of Geology*, **2**, 54-66.

Wadsworth, W.J. (1982) The basic plutons. In: *Igneous rocks of the British Isles*. (eds. Sutherland, D.), Wiley, 135-148.

Wadsworth, W.J. (1986) Silicate mineralogy in the later fractionation stages of the Insch intrusion, NE Scotland. *Mineralogical Magazine*, **50**, 583-595.

Wadsworth, W.J. (1988) Silicate mineralogy of the Middle Zone cumulates and associated gabbroic rocks from the Insch intrusion, NE Scotland. *Mineralogical Magazine*, **52**, 309-322.

Wadsworth, W.J. (1991) Silicate mineralogy of the Belhelvie cumulates, NE Scotland. *Mineralogical Magazine*, **55** (378), 113-119.

Wager, L.R. (1932) The Geology of the Roundstone district, Co. Galway. *Proceedings of the Royal Irish Academy*, **41B**, 46-72.

Wager, L.R. (1939) Outline of the geology of Connemara. *Proceedings of the Geological Association*, **50**, 346-351.

Wager, L.R., Brown, G.M., & Wadsworth, W.J. (1960) Types of igneous cumulates. *Journal of Petrology*, **1**, 73-85.

Wager, L. R. & Brown, G. M. (1968) *Layered Igneous Rocks.*, Oliver & Boyd. 588pp.

Wager, L. R. & Mitchell, R.L. (1951) The distribution of trace elements during strong fractionation of basic magma - a further study of the Skaergaard Intrusion, East Greenland. *Geochimica et Cosmochimica Acta*, **1**, 129-208.

Walsh, J.N., Buckley, F. & Barker, J. (1981) The simultaneous determination of the rare-earth elements in rocks using inductively coupled plasma source spectrometry. *Chemical Geology*, **33**, 141-153.

Watson, E.B. (1979) Zircon saturation in felsic liquids: experimental results and application to trace element geochemistry. *Contributions to Mineralogy and Petrology*, **70**, 407-419.

Watson, E.B. (1980) Some experimentally determined zircon/liquid partition coefficients for the rare-earth elements. *Geochimica et Cosmochimica Acta*, **44**, 895-897.

Watson, E.B. & Harrison, T.M. (1983) Zircon saturation revisited: temperature and composition effects in a variety of crustal magma types. *Earth and Planetary Science Letters*, **64**, 295-304.

Watt, W.R. (1914) Geology of the District around Huntly (Aberdeenshire). *Quarterly Journal of the Geological Society of London*, **70**, 266-293.

Weedon, D.S. (1970) The basic/ultrabasic rocks of the Huntly region. *Scottish Journal of Geology*, **6**, 26-40.

Wellings, S.A. (1998) Timing of deformation associated with the syn-tectonic Dawros-Currywongaun-Doughruagh Complex, NW Connemara, Western Ireland. *Journal of the Geological Society of London*, **155**, 25-37.

Whittle, G (1936) The eastern end of the Insch igneous mass, Aberdeenshire. *Proceedings of the Liverpool Geological Society*, **17**, 64-95.

Wilson, J.S.G. (1886) Explanation of Sheet 87, North-east Aberdeenshire and detached portions of Banffshire. *Memoir of the Geological Survey, Scotland.*

Wilson, M (1989) *Igneous Petrogenesis*, Unwin Hyman. 466pp.

Yardley, B.D.W., & Senior, A.L. (1982) Basaltic magmatism in Connemara, Ireland: evidence for a volcanic arc? *Journal of the Geological Society of London*, **139**, 67-70.

Yardley, B.D.W., Vine, F.J., & Baldwin, C.D. (1982) The plate tectonic setting of NW Britain and Ireland in late Cambrian and early Ordovician times. *Journal of the Geological Society of London*, **139**, 455-463.

# Appendix A - Sample location and description

## Appendix A Sample location and description.

**Sample prefixes:**

| | |
|---|---|
| **Ab** | Samples from the Aberdeen University archive |
| **CLW** | Samples collected from the Cashel-Lough Wheelaun Complex |
| **DCD** | Samples collected from the Dawros-Currywongaun-Doughruagh Complex |
| **HI** | Samples from C.D. Hutchinsons M.Phil in the Harker collection, provided by the University of Cambridge |
| **MS** | Samples provided by Mike Styles at the British Geological Survey, Keyworth, Nottingham |
| **PGD** | Samples from the British Geological Survey archive at Keyworth, Nottingham |
| **Wd** | Samples supplied by W.J. Wadsworth at the University of Manchester |

**Sample suffixes:**

| | |
|---|---|
| **A, C and P** | Samples from J.R. Ashworths PhD in the Harker collection, provided by the University of Cambridge, and from P. Mongkoltips PhD in the University of Birmingham |

Scottish grid references:
Irish grid references:

| Sample | Disc (XRF pellet No.) | Grid reference: Easting | Northing | Intrusion | Rock name |
|---|---|---|---|---|---|
| | | **Igneous Rocks:** | | | |
| **Ab6908** | 35386 | 390600 | 833700 | Arnage | Bio Qtz Hbl Norite |
| **1P** | 35556 | 393300 | 835700 | Arnage | Bio Qtz Norite |
| **7P** | 35558 | 393000 | 837400 | Arnage | Bio Qtz Norite |
| **9P** | 35559 | 393300 | 838400 | Arnage | Bio Qtz Norite |
| **Ab74** | 35333 | 392800 | 818750 | Belhelvie | Hbl Gabbro |
| **Ab82** | 35334 | 393600 | 816700 | Belhelvie | Bio Qtz Gabbro |
| **Ab90** | 35335 | 395000 | 816000 | Belhelvie | Troctolite |
| **Ab111** | 35342 | 391800 | 819800 | Belhelvie | Norite |
| **Ab115** | 35344 | 391800 | 819800 | Belhelvie | Norite |
| **Ab117** | 35345 | 391700 | 819550 | Belhelvie | Ol. Gabbro |
| **Ab125** | 35347 | 391700 | 819500 | Belhelvie | Norite |
| **Ab127** | 35349 | 393500 | 819300 | Belhelvie | Ol. Gabbro |
| **Ab135** | 35351 | 391100 | 820600 | Belhelvie | Websterite |
| **Ab140** | 35352 | 391350 | 820300 | Belhelvie | Troctolite |
| **Ab143** | 35353 | 391100 | 820620 | Belhelvie | Websterite |
| **Ab1294** | 35360 | 392000 | 818210 | Belhelvie | Troctolite |
| **Ab2063** | 35362 | 393400 | 819500 | Belhelvie | Troctolite |
| **Ab2065** | 35363 | 391900 | 819600 | Belhelvie | Gabbro |
| **Ab2073** | 35364 | 395000 | 817500 | Belhelvie | Ol. Norite |
| **Ab2083** | 35365 | 391250 | 820600 | Belhelvie | Ol Gabbro |
| **Ab2090** | 35366 | 391900 | 818220 | Belhelvie | Ol Gabbro |
| **54P** | 35565 | 393200 | 819600 | Belhelvie | Troctolite |
| **85P** | 35560 | 387700 | 838600 | Haddo House | Bio Qtz Norite |

| Sample | Disc (XRF pellet No.) | Grid reference: Easting | Northing | Intrusion | Rock name |
|---|---|---|---|---|---|
| **86P** | 35561 | 389400 | 838600 | Haddo House | Bio Gabbro |
| **88P** | 35562 | 389400 | 838700 | Haddo House | Bio Qtz Norite |
| **Ab3826** | 35370 | 397400 | 843150 | Kinnadie | Bio Qtz Hbl Norite |
| **Ab92** | 35336 | 392000 | 848000 | Maud | Bio Hbl Gabbro |
| **Ab96** | 35339 | 392100 | 848100 | Maud | Bio Hbl Gabbro |
| **Ab1310** | 35361 | 392400 | 847800 | Maud | Bio Qtz Norite |
| **Ab5612** | 35381 | 345400 | 825900 | Boganclogh | Dunite |
| **Ab5613** | 35382 | 345700 | 826000 | Boganclogh | Bio Norite |
| **Ab7798** | 35387 | 342400 | 828500 | Boganclogh | Gabbro |
| **Ab7799** | 35388 | 342900 | 825100 | Boganclogh | Qtz Syenite |
| **Ab7801** | 35390 | 345300 | 828100 | Boganclogh | Monzonite |
| **Ab7802** | 35391 | 339000 | 825600 | Boganclogh | Bio Gabbro |
| **Ab7803** | 35392 | 339600 | 824900 | Boganclogh | Ol Clinopyroxenite |
| **WdQBN** | 35434 | 345400 | 826900 | Boganclogh | Bio Gabbro |
| **MS1573** | 35439 | 345270 | 824850 | Boganclogh | Dunite |
| **MS1577** | 35440 | 346180 | 823540 | Boganclogh | Dunite |
| **MS1581** | 35441 | 345280 | 825880 | Boganclogh | Harzburgite |
| **MS1584** | 35442 | 343450 | 825140 | Boganclogh | Lherzolite |
| **MS1593** | 35443 | 341820 | 829380 | Boganclogh | Dunite |
| **MS1595** | 35444 | 341070 | 829340 | Boganclogh | Ol Bio Norite |
| **MS1596** | 35445 | 342740 | 829530 | Boganclogh | Dunite |
| **Ab93** | 35337 | 374400 | 825750 | Insch | Ol. Gabbro |
| **Ab243** | 35358 | 376000 | 826400 | Insch | Bio Gabbro |
| **Ab661** | 35359 | 359500 | 825200 | Insch | Qtz Syenite |
| **WdV(Ol)** | 35423 | 371900 | 830400 | Insch | Granular Ol Norite |
| **WdS** | 35424 | 366500 | 827500 | Insch | Granular Gabbro |
| **WdHD3** | 35425 | 374100 | 828000 | Insch | Gabbro |
| **Wd109** | 35426 | 358000 | 825600 | Insch | Syenite |
| **WdPY1** | 35427 | 372900 | 826700 | Insch | Gabbro |
| **WdCC2** | 35428 | 375800 | 826800 | Insch | Ol Gabbro |
| **WdPY3** | 35429 | 373000 | 826700 | Insch | Granular Ol Gabbro |
| **WdPY2** | 35430 | 372900 | 826700 | Insch | Granular Gabbro |
| **Wd72** | 35431 | 358900 | 830800 | Insch | Ol Ferrogabbro |
| **Wd60** | 35432 | 364900 | 831900 | Insch | Ol Ferrogabbro |
| **WdDV1** | 35433 | 373700 | 828900 | Insch | Granular Bio Gabbro |
| **Wd254** | 35435 | 371500 | 825700 | Insch | Bio Gabbro |
| **WdR** | 35436 | 370100 | 825900 | Insch | Granular Gabbro |
| **MS1565** | 35438 | 355150 | 824350 | Insch | Dunite |
| **HI115** | 35786 | 360000 | 826300 | Insch | Bio Gabbro |
| **HI121** | 35787 | 358700 | 825900 | Insch | Syenite |
| **HI47** | 35788 | 347500 | 828500 | Insch | Bio Norite |
| **HI131** | 35791 | 357000 | 824700 | Insch | Syenite |
| **PGD1209** | 35161 | 349822 | 843082 | Huntly | Gabbro |
| **PGD1215** | 35162 | 349822 | 843082 | Huntly | Gabbro |
| **PGD1229** | 35164 | 349822 | 843082 | Huntly | Gabbro |
| **PGD1232** | 35165 | 349822 | 843082 | Huntly | Gabbro |
| **Ab3914** | 35373 | 349910 | 843060 | Huntly | Troctolite |
| **Ab3979a** | 35375 | 349910 | 843060 | Huntly | Dunite |
| **Ab3979b** | 35376 | 349910 | 843060 | Huntly | Troctolite |
| **Ab3984** | 35377 | 349910 | 843060 | Huntly | Ol Gabbro |
| **Ab3986** | 35378 | 349910 | 843060 | Huntly | Ol Gabbro |
| **Ab3988** | 35379 | 349910 | 843060 | Huntly | Troctolite |
| **Ab5661** | 35383 | 350000 | 844800 | Huntly | Ol Gabbro |
| **Ab6510** | 35385 | 348800 | 844000 | Huntly | Ol Gabbro |
| **MS1511** | 35403 | 348500 | 844620 | Huntly | Gabbro |
| **MS1512** | 35404 | 348500 | 844620 | Huntly | Gabbro |
| **MS1514** | 35405 | 348440 | 844640 | Huntly | Gabbro |

| Sample | Disc (XRF pellet No.) | Grid reference: Easting | Northing | Intrusion | Rock name |
|---|---|---|---|---|---|
| **MS1515** | 35406 | 348440 | 844640 | Huntly | Lherzolite |
| **MS1519** | 35408 | 351240 | 845320 | Huntly | Gabbro |
| **MS1520** | 35409 | 351240 | 845320 | Huntly | Lherzolite |
| **MS1523a** | 35410 | 351240 | 845320 | Huntly | Gabbro |
| **MS1524** | 35411 | 351240 | 845320 | Huntly | Dunite |
| **773C** | 35578 | 349300 | 842300 | Huntly | Ol Gabbro |
| **MS1526a** | 35412 | 348920 | 847960 | Knock | Lherzolite |
| **MS1526c** | 35413 | 348920 | 847960 | Knock | Wehrlite |
| **MS1527b** | 35414 | 348920 | 847960 | Knock | Harzburgite |
| **MS1528** | 35415 | 351820 | 852100 | Knock | Harzburgite |
| **MS1531** | 35416 | 352050 | 852300 | Knock | Harzburgite |
| **MS1533** | 35417 | 351860 | 852050 | Knock | Dunite |
| **MS1535** | 35418 | 353640 | 846700 | Knock | Gabbro |
| **MS1537** | 35419 | 353630 | 846740 | Knock | Gabbro |
| **MS1500** | 35393 | 358100 | 866400 | Portsoy | Gabbro |
| **MS1540** | 35420 | 354120 | 859200 | Portsoy | Dunite |
| **MS1542** | 35421 | 354230 | 859400 | Portsoy | Harzburgite |
| **MS1544** | 35422 | 354410 | 860020 | Portsoy | Qtz Gabbro |
| **MS1545** | 35437 | 354430 | 860010 | Portsoy | Gabbro |
| **110P** | 35563 | 359300 | 866200 | Portsoy | Ol Gabbro |
| **137P** | 35564 | 349000 | 844000 | Portsoy | Troctolite |
| **220A** | 35785 | 358660 | 866260 | Portsoy | Gabbro |
| **Ab5790** | 35384 | 345900 | 838250 | Succoth Brownhills | Websterite |
| **MS1501a** | 35394 | 345180 | 838360 | Succoth Brownhills | Gabbro |
| **MS1501b** | 35395 | 345180 | 838360 | Succoth Brownhills | Gabbro |
| **MS1502** | 35396 | 345180 | 838360 | Succoth Brownhills | Gabbro |
| **MS1505a** | 35398 | 344960 | 838790 | Succoth Brownhills | Gabbro |
| **MS1506** | 35400 | 347360 | 841360 | Succoth Brownhills | Gabbro |
| **MS1510a** | 35402 | 347000 | 842650 | Succoth Brownhills | Lherzolite |
| **Ab7800** | 35389 | 339000 | 825200 | Morven Cabrach | Gabbro |
| **Ab94** | 35338 | 339400 | 804300 | Morven Cabrach | Biotite Gabbro |
| **Ab3759** | 35367 | 336100 | 805400 | Morven Cabrach | Bio Hbl Gabbro |
| **Ab3794** | 35368 | 335900 | 817600 | Morven Cabrach | Bio Hbl Gabbro |
| **MS1598** | 35446 | 340870 | 817270 | Morven Cabrach | Harzburgite |
| **MS1601** | 35448 | 341160 | 817020 | Morven Cabrach | Harzburgite |
| **MS1604** | 35449 | 332100 | 815350 | Morven Cabrach | Harzburgite |
| **MS1605** | 35450 | 332650 | 815550 | Morven Cabrach | Dunite |
| **MS1608** | 35451 | 332450 | 813570 | Morven Cabrach | Dunite |
| **MS1611** | 35452 | 332710 | 813120 | Morven Cabrach | Gabbro |
| **MS1612a** | 35453 | 332880 | 812980 | Morven Cabrach | Gabbro |
| **MS1614** | 35455 | 332980 | 812750 | Morven Cabrach | Gabbro |
| **67P** | 35566 | 338600 | 808100 | Morven Cabrach | Hbl Gabbro |
| **77P** | 35567 | 335900 | 812300 | Morven Cabrach | Bio Norite |
| **725C** | 35574 | 334800 | 808900 | Morven Cabrach | Gabbro |
| **733C** | 35575 | 336700 | 805500 | Morven Cabrach | Gabbro |
| **741C** | 35576 | 335700 | 805200 | Morven Cabrach | Gabbro |
| **758C** | 35577 | 338500 | 802100 | Morven Cabrach | Gabbro |
| **MS1615** | 35456 | 333350 | 793100 | Coyles of Muick | Gabbro |
| **MS1617b** | 35457 | 333300 | 793050 | Coyles of Muick | Harzburgite |
| **MS1618** | 35458 | 333300 | 793050 | Coyles of Muick | Gabbro |
| **MS1620** | 35459 | 333300 | 793350 | Coyles of Muick | Harzburgite |
| **MS1621** | 35460 | 333150 | 792750 | Coyles of Muick | Gabbro |
| **MS1622** | 35461 | 333150 | 792750 | Coyles of Muick | Peridotite |
| **MS1623** | 35462 | 333150 | 792750 | Coyles of Muick | Wehrlite |
| **MS1625** | 35463 | 333150 | 792000 | Coyles of Muick | Harzburgite |
| **MS1627** | 35464 | 332600 | 791750 | Coyles of Muick | Gabbro |
| **MS1630** | 35465 | 333120 | 791300 | Coyles of Muick | Harzburgite |

| Sample | Disc (XRF pellet No.) | Grid reference: Easting | Northing | Intrusion | Rock name |
|---|---|---|---|---|---|
| **MS1631** | 35466 | 333150 | 791240 | Coyles of Muick | Ol Norite |
| **CLW101** | 35546 | 7988 | 4377 | Cashel | Hbl Gabbro |
| **CLW102** | 35547 | 8004 | 4366 | Cashel | Qtz Hbl Gabbro |
| **CLW218** | 35762 | 8071 | 4432 | Cashel | Hbl Gabbro |
| **CLW219** | 35763 | 8069 | 4403 | Cashel | Hbl Gabbro |
| **CLW220** | 35764 | 8150 | 4332 | Cashel | Hbl Gabbro |
| **CLW210** | 35754 | | | Cashel | Gabbro |
| **CLW211** | 35755 | | | Cashel | Gabbro |
| **CLW212** | 35756 | | | Cashel | Gabbro |
| **CLW215** | 35759 | | | Cashel | Gabbro |
| **CLW216** | 35760 | | | Cashel | Hbl Gabbro |
| **CLW103** | 35548 | 8433 | 4490 | Lough Wheelaun | Hbl Gabbro |
| **CLW104** | 35549 | 8442 | 4528 | Lough Wheelaun | Gabbro |
| **CLW105** | 35550 | 8422 | 4534 | Lough Wheelaun | Gabbro |
| **CLW106** | 35551 | 8419 | 4528 | Lough Wheelaun | Norite |
| **CLW107** | 35552 | 8420 | 4524 | Lough Wheelaun | Hbl Harzburgite |
| **CLW108** | 35553 | 8401 | 4484 | Lough Wheelaun | Gabbro |
| **CLW109** | 35554 | 8374 | 4466 | Lough Wheelaun | Norite |
| **CLW110** | 35555 | 8385 | 4468 | Lough Wheelaun | Hbl Gabbro |
| **CLW201** | 35745 | 8362 | 4477 | Lough Wheelaun | Bio Qtz Gabbro |
| **CLW203** | 35747 | 8358 | 4473 | Lough Wheelaun | Gabbro |
| **CLW205** | 35749 | 8357 | 4472 | Lough Wheelaun | Gabbro |
| **CLW206** | 35750 | 8370 | 4480 | Lough Wheelaun | Gabbro |
| **CLW207** | 35751 | 8370 | 4477 | Lough Wheelaun | Bio Norite |
| **DCD101** | 35273 | 6941 | 5884 | Dawros | Harzburgite |
| **DCD104** | 35276 | 6943 | 5922 | Dawros | Dunite |
| **DCD105** | 35277 | 6966 | 5908 | Dawros | Gabbro |
| **DCD106** | 35278 | 6964 | 5913 | Dawros | Ol. Gabbro |
| **DCD109** | 35281 | 6971 | 5933 | Dawros | Lherzolite |
| **DCD110** | 35282 | 6978 | 5928 | Dawros | Lherzolite |
| **DCD116** | 35288 | 7206 | 5942 | Currywongaun | Norite |
| **DCD118** | 35299 | 7343 | 6048 | Currywongaun | Hbl Gabbro |
| | | **Country Rocks:** | | | |
| **Ab200** | 35355 | 393400 | 835600 | Arnage | Hornfels |
| **Ab210** | 35356 | 393400 | 835500 | Arnage | Hornfels |
| **Ab217** | 35357 | 393400 | 835600 | Arnage | Hornfels |
| **6P** | 35557 | 393000 | 837400 | Arnage | Hornfels |
| **463A** | 35783 | 393700 | 836500 | Arnage | Schist |
| **Ab109** | 35340 | 393550 | 819300 | Belhelvie | Hornfels |
| **Ab110** | 35341 | 393000 | 819400 | Belhelvie | Hornfels |
| **Ab112** | 35343 | 392000 | 820800 | Belhelvie | Hornfels |
| **Ab121** | 35346 | 393150 | 819250 | Belhelvie | Hornfels |
| **Ab126** | 35348 | 393150 | 819200 | Belhelvie | Hornfels |
| **Ab128** | 35350 | 393700 | 819150 | Belhelvie | Hornfels |
| **Ab5323** | 35380 | 390300 | 834400 | Haddo House | Xenolithic Bio Norite |
| **Ab3828** | 35371 | 389600 | 849800 | Maud | Hornfels |
| **Ab20** | 35332 | 373000 | 825400 | Insch | Xenolith |
| **HI181** | 35789 | 475 | 285 | Insch | Xenolith |
| **Ab3913** | 35372 | 353800 | 841200 | Huntly | Xenolith |
| **Ab740** | 35374 | 351600 | 842100 | Huntly | Hornfels |
| **MS1516** | 35407 | 348390 | 844660 | Huntly | Amphibolite |
| **127B** | 35793 | 351800 | 843500 | Huntly | Hornfels |
| **MS1504** | 35397 | 344800 | 839370 | Succoth Brownhills | Schist |
| **MS1508** | 35401 | 347360 | 841360 | Succoth Brownhills | Basalt |

| Sample | Disc (XRF pellet No.) | Grid reference: Easting | Northing | Intrusion | Rock name |
|---|---|---|---|---|---|
| **Ab3807** | 35369 | 339000 | 813550 | Morven Cabrach | Schist |
| **MS1613** | 35454 | 332910 | 812860 | Morven Cabrach | Hornfels |
| **348Aa** | 35777 | 587 | 559 | Whitehills | Hornfels |
| **348Ab** | 35778 | 587 | 559 | Whitehills | Hornfels |
| **349A** | 35779 | 587 | 559 | Whitehills | Hornfels |
| **353A** | 35780 | 587 | 559 | Whitehills | Hornfels |
| **685A** | 35781 | 635 | 657 | Whitehills | Schist |
| **137A** | 35736 | 359860 | 866530 | Cowythe | Schist |
| **140A** | 35737 | 359920 | 866550 | Cowythe | Hornfels |
| **156A** | 35738 | 360080 | 866760 | Cowythe | Hornfels |
| **157A** | 35739 | 360190 | 866850 | Cowythe | Hornfels |
| **163Aa** | 35740 | 6017 | 6684 | Cowythe | Hornfels |
| **163Ab** | 35741 | 6017 | 6684 | Cowythe | Hornfels |
| **171A** | 35742 | 6147 | 6655 | Cowythe | Schist |
| **186A** | 35743 | 361430 | 866190 | Cowythe | Schist |
| **110Aa** | 35766 | 5970 | 6646 | Cowythe | Hornfels |
| **110Ab** | 35767 | 5970 | 6646 | Cowythe | Hornfels |
| **196A** | 35768 | 6144 | 6626 | Cowythe | Schist |
| **240A** | 35769 | 5962 | 6636 | Cowythe | Schist |
| **242A** | 35770 | 5968 | 6645 | Cowythe | Hornfels |
| **246A** | 35771 | 5978 | 6643 | Cowythe | Hornfels |
| **248A** | 35772 | 5986 | 6654 | Cowythe | Schist |
| **251A** | 35773 | 6143 | 6619 | Cowythe | Schist |
| **252A** | 35774 | 6148 | 6636 | Cowythe | Schist |
| **254A** | 35775 | 6148 | 6637 | Cowythe | Schist |
| **255A** | 35776 | 6147 | 6637 | Cowythe | Schist |
| **CLW217** | 35761 | N.A. | N.A. | Cashel | Schist |
| **CLW213** | 35757 | N.A. | N.A. | Cashel | Xenolith |
| **CLW214** | 35758 | N.A. | N.A. | Cashel | Xenolith |
| **CLW202** | 35746 | 8358 | 4474 | Lough Wheelaun | Xenolith |
| **CLW204** | 35748 | 8357 | 4472 | Lough Wheelaun | Xenolith |
| **CLW208** | 35752 | 8370 | 4476 | Lough Wheelaun | Hornfels |
| **CLW209** | 35753 | 8311 | 4473 | Lough Wheelaun | Hornfels |
| **DCD102** | 35274 | 6943 | 5880 | Dawros | Hornfels |
| **DCD103** | 35275 | 6920 | 5918 | Dawros | Hornfels |
| **DCD108** | 35280 | 7027 | 5988 | Dawros | Schist |
| **DCD107** | 35279 | 6968 | 5923 | Dawros | Hornfels |
| **DCD111** | 35283 | 6985 | 5938 | Dawros | Schist |
| **DCD112** | 35284 | 7069 | 5929 | Dawros | Xenolith |
| **DCD113** | 35285 | 7046 | 5940 | Dawros | Hornfels |
| **DCD114** | 35286 | 7033 | 5942 | Dawros | Xenolith |
| **DCD115** | 35287 | 7205 | 5940 | Currywongaun | Hornfels |
| **DCD117** | 35298 | 7212 | 5944 | Currywongaun | Xenolith |
| **DCD119** | 35300 | 7348 | 6053 | Currywongaun | Xenolith |
| **DCD120** | 35301 | 7353 | 6055 | Currywongaun | Hornfels |

# Appendix B - Analytical techniques

## Appendix B: Analytical techniques

### B.1 Preparation of rock powders

Weathered surfaces and veining/alteration were removed from samples using a metal saw, and polished to remove any contamination. A minimum of 150g (except where limited by samples size) was crushed to sand grade using a metal press and ground to a fine powder for 3 – 5 minutes in an agate Tema®.

### B.2 Determination of Loss on Ignition (LOI)

1. Sample powders were measured into weighed ceramic crucibles and weighed.
2. The samples were then placed in a furnace at 1000°C for 2 hours.
3. Samples were weighed after cooling and LOI calculated as

$$\frac{(wt_i - wt_f)}{wt_f} \times 100$$

where $wt_i$ = initial weight and
$wt_f$ = post ignition weight

Weighing error: ± 0.0001g

### B.3 X- Ray Fluorescence analysis

X- Ray Fluorescence (XRF) was used to determine major and trace element analyses on fused discs and powder pellets respectively. Major elements were analysed on 46mm diameter fusion beads using a Phillips PW1400 automated wavelength dispersive XRF spectrophotometer at the University of Birmingham. Trace elements were analysed on 40mm pressed powder discs using a X-Ray Fluorescence Automated Philips PW2404 spectrometer at the Department of Geology and Geophysics, Grant Institute, University of Edinburgh. Major element checks were also carried out on 38 samples on this XRF.

#### B.3.1 Trace element powder pellet preparation

1. 12-13g of rock powder was weighed into a glass beaker
2. 12-15 drops of Mowiol binding agent was added and mixed thoroughly to a stiff paste
3. Sample was added to a 40mm polished stainless steel die and compressed to ~15 tonnes/inch$^2$
4. Sample was removed from die and dried overnight at 40°C

#### B.3.2 Major element fused disc preparation

1. 4.5000g (± Δg) Li- Metaborate flux (*spectroflux 100B*) was measured into a platinum crucible, where Δg is previously determined *LOI* for the flux
2. 0.9000 (±0.0001) g of ignited rock powder was added to the flux and carefully mixed
3. The sample was heated in the furnace to 1250°C for 5 minutes, stirring briefly half way through, before placing immediately on a rotating Bunsen Burner for 20 minutes
4. The sample was returned to the furnace for a further 5 minutes
5. The sample was immediately cast in a 46mm die and allowed to cool on a 250°C hotplate for 1 hour
6. The fused disc was labelled and stored in a desiccator until analysis

#### B.3.3 XRF accuracy

International geostandards were analysed with each sample run for both Birmingham and Edinburgh XRFs. Major element standards are shown in Table B.1. Major element checks for samples analysed at

the University of Edinburgh are shown in Table B.3. Accuracy is variable for $P_2O_5$ data below 0.05%, as can be seen in figure B.1. Trace element standards shown in Table B.3 and B.4

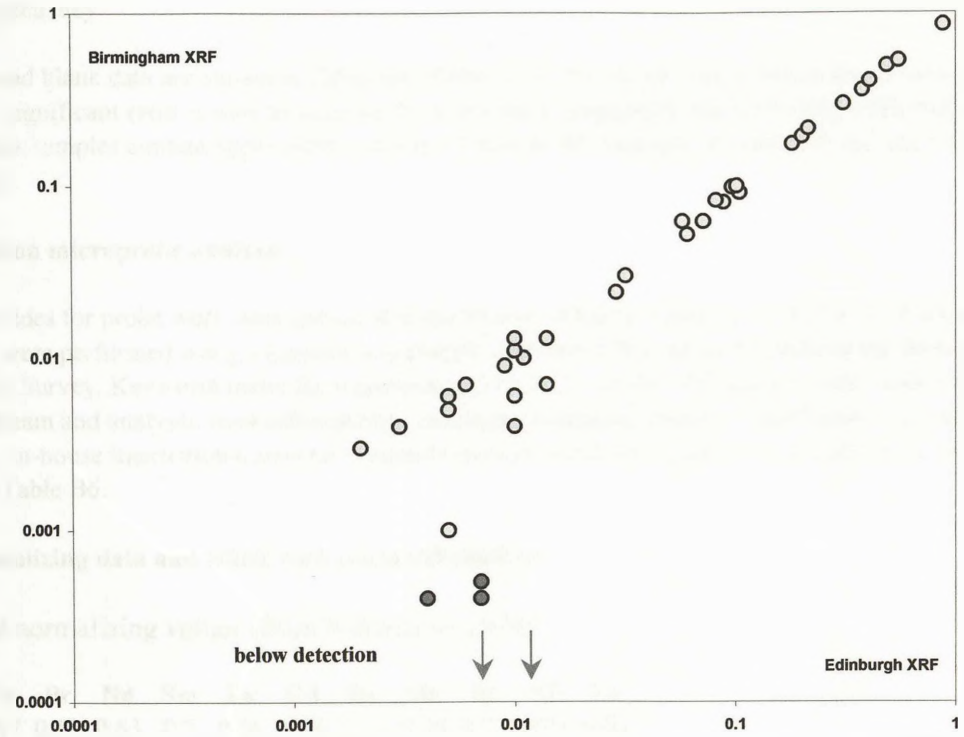


**Figure B.1 $P_2O_5$ data from samples analysed on both the Edinburgh and Birmingham XRFs**

## B.4 ICP analysis

REE were measured on an ICP-AES at The Department of Geology, Royal Holloway, University of London under the supervision of Dr. J.N. Walsh. The REE were extracted in several batches from whole rock solutions at Royal Holloway and at the University of Birmingham using the following technique, based on that of Walsh (1982):

### B.4.1 Rare Earth Element sample preparation

1. Place 0.5 (± 0.0001) g of dry sample into a PTFE crucible. Each sample run contains 6 samples, 1 standard and one blank.
2. Add 12 ml of a HF and $HClO_4$ mixture was each sample and leave on a hot sandbath until fully digested.
3. Add approx. 5ml concentrated HCl to each sample and allow to dissolve fully.
4. Place each sample in an ashless filter paper and filter overnight into a covered beaker. Rinse thoroughly with de-ionised water.
5. Place each filter paper in a silver crucible and heat to 800°C in 200°C steps. Leave at 800°C for 30 minutes
6. Remove crucibles from furnace and add 5 pellets of NaOH to each. Return to the furnace for a further 30 minutes.
7. Remove from furnace and allow to cool, swirling continuously.
8. Dissolve in 5 ml HCl and return to covered beaker.
9. Pour sample into ion-exchange column filled with Bio-rad analytical cation-exchange resin. Wash through with 500ml of 1.7M HCl, and discard this portion.

10. Wash through with 600ml of 4.0M HCl, collecting this portion.
11. Evaporate this sample to dryness on a hotplate and seal with clingfilm.
12. Sample is now ready for analysis at Royal Holloway.

### B.4.2 ICP accuracy

Standard and blank data are shown in Table B4. Error is low for samples prepared in Royal Holloway. However, significant error is seen in samples from one batch prepared in the University of Birmingham, where blank samples contain appreciable amounts of certain RE elements, notably Gd, Ho and Er (see Table B.5).

## B.5 Electron microprobe analysis

Polished slides for probe work were prepared in the School of Earth Sciences, University of Birmingham. Analyses were performed using a Cameca wavelength dispersive electron microprobe at the British Geological Survey, Keyworth under the supervision of Dr M.T. Styles. All analyses were with a fully focussed beam and analyses were subsequently calculated to mineral cationic abundances using computer software. In-house international mineral standards were checked for precision on a daily basis, and are shown in Table B6.

## B.6 Normalizing data and whole rock norm calculations

REE plot normalizing values (from Nakamura, 1974):

| La | Ce | Pr | Nd | Sm | Eu | Gd | Dy | Ho | Er | Yb | Lu |
|---|---|---|---|---|---|---|---|---|---|---|---|
| 0.33 | 0.87 | 0.12 | 0.63 | 0.2 | 0.08 | 0.28 | 0.34 | 0.08 | 0.23 | 0.22 | 0.03 |

Chondrite normalizing values for 'spider' diagrams (from Thompson *et al.*, 1984):

| Ba | Rb | Th | K | Nb | Ta | La | Ce | Sr | Nd | P | Sm | Zr | Hf | Ti | Tb | Y | Tm | Yb |
|---|---|---|---|---|---|---|---|---|---|---|---|---|---|---|---|---|---|---|
| 6.9 | 0.35 | 0.04 | 120 | 0.35 | 0.02 | 0.33 | 0.87 | 11.8 | 0.63 | 46 | 0.2 | 6.84 | 0.2 | 620 | 0.05 | 2 | 0.03 | 0.22 |

MORB normalizing values for 'spider' diagrams (from Pearce, 1983):

| Sr | $K_2O$ | Rb | Ba | Th | Ta | Nb | Ce | $P_2O_5$ | Zr | Hf | Sm | $TiO_2$ | Y | Yb |
|---|---|---|---|---|---|---|---|---|---|---|---|---|---|---|
| 120 | 0.15 | 2 | 20 | 0.2 | 0.18 | 3.5 | 10 | 0.12 | 90 | 2.4 | 3.3 | 1.5 | 30 | 3.4 |

Norms were calculated in accordance with the conventions of Thompson *et al.* (1983), fixing $Fe_2O_3$ at 1.5% of total $Fe_2O_3$ and converting the remaining $Fe_2O_3$ to FeO. A simple Excel spreadsheet based on the CIPW norm calculations of Johannsen (1931) was used.

**Major element run**

| | $SiO_2$ | $TiO_2$ | $Al_2O_3$ | FeO | $Fe_2O_3$ | MnO | MgO | CaO | $Na_2O$ | $K_2O$ | $P_2O_5$ | $H_2O+$ | $H_2O-$ | $CO_2$ | $Fe_2O_3^{(T)}$ | Total |
|---|---|---|---|---|---|---|---|---|---|---|---|---|---|---|---|---|
| AN-G | 46.30 | 0.220 | 29.80 | 2.24 | 0.87 | 0.04 | 1.80 | 15.90 | 1.63 | 0.13 | 0.01 | 0.61 | 0.11 | 0.13 | 3.36 | 100.04 |
| **AN-G** | 47.17 | 0.221 | 31.37 | | | 0.042 | 1.80 | 16.40 | 1.49 | 0.12 | 0.010 | | | | 3.35 | 101.97 |
| JA-1 | 64.06 | 0.87 | 14.98 | 4.08 | 2.42 | 0.15 | 1.61 | 5.68 | 3.86 | 0.78 | 0.16 | 0.8 | 0.26 | | 6.95 | 100.16 |
| **JA-1** | 63.98 | 0.821 | 15.10 | | | 0.148 | 1.57 | 5.7 | 3.96 | 0.72 | 0.149 | | | | 6.89 | 99.04 |
| NIM-S | 63.63 | 0.044 | 17.34 | 0.30 | 1.07 | 0.01 | 0.46 | 0.68 | 0.43 | 15.35 | 0.12 | 0.22 | | 0.09 | 1.40 | 99.77 |
| **NIM-S** | 62.46 | 0.043 | 17.47 | | | 0.11 | 0.39 | 0.64 | 0.07 | 15.39 | 0.105 | | | | 1.40 | 98.08 |
| PCC-1 | 41.67 | 0.013 | 0.67 | 5.06 | 2.72 | 0.119 | 43.43 | 0.52 | 0.027 | 0.007 | 0.002 | 4.71 | 0.44 | 0.15 | 8.25 | 100.01 |
| PCC-1(recalc) | 43.93 | 0.01 | 0.71 | 5.33 | 2.87 | 0.13 | 45.79 | 0.55 | 0.03 | 0.01 | 0.00 | | | 0.16 | 8.70 | 100.01 |
| **PCC-1** | 43.88 | 0.007 | 0.68 | | | 0.121 | 47.50 | 0.56 | < | 0.06 | < | | | | 8.94 | 101.75 |
| | $SiO_2$ | $TiO_2$ | $Al_2O_3$ | FeO | $Fe_2O_3$ | MnO | MgO | CaO | $Na_2O$ | $K_2O$ | $P_2O_5$ | $H_2O+$ | $H_2O-$ | $CO_2$ | $Fe_2O_3^{(T)}$ | Total |

**Major element analyses run in September 1999.**

Values in red are Geostandard Reference values
Data underlined are recommended values; other values are proposed.
Recalculated PCC-1 data involves removal of $H_2O$ values from actual PCC-1 for comparison with H2O free analysis, as analysis was carried out on fused powders

**Geostandard Samples for major and trace element accuracy**

| I.D. | Sample | Rock type |
|---|---|---|
| (004) | **BCR-1** | Basalt |
| (005) | **DTS-1** | Dunite |
| (008) | **PCC-1** | Peridotite |
| (009) | **BHVO-1** | Basalt |
| (017) | **BIR-1** | Basalt |
| (065) | **AN-G** | Anorthosite |
| (156) | **JA-1** | Andesite |
| (206) | **NIM-S** | Syenite |

(Geostandards Newsletter Vol. VIII, Special Issue, July 1984)

**Table B.1 Comparison of major element reference samples analyses with data obtained from XRF.**

| Sample | Ab210 | Ab217 | 7P | Ab74 | Ab117 | Ab143 | Ab2090 | 54P | Ab3826 | Ab1310 | Ab5612 | MS1581 | HD3 | Wd72 | Wd254 | PGD1209 | Ab3979b | MS1515 | MS1524 |
|---|---|---|---|---|---|---|---|---|---|---|---|---|---|---|---|---|---|---|---|
| SiO2 | 52.63 | 54.03 | 52.78 | 50.68 | 45.71 | 51.56 | 44.68 | 44.96 | 49.88 | 53.41 | 37.83 | 39.02 | 46.63 | 42.71 | 47.20 | 47.87 | 42.49 | 39.77 | 39.20 |
| TiO2 | 1.254 | 1.201 | 0.894 | 0.318 | 0.135 | 0.327 | 0.171 | 0.141 | 3.331 | 2.014 | 0.008 | 0.009 | 3.378 | 2.862 | 2.938 | 0.263 | 0.048 | 0.015 | 0.025 |
| Al2O3 | 22.63 | 21.70 | 16.18 | 16.97 | 21.17 | 5.07 | 16.03 | 22.96 | 15.31 | 15.81 | 0.18 | 0.43 | 19.07 | 13.98 | 17.93 | 16.71 | 20.80 | 0.95 | 2.53 |
| Fe2O3 | 11.21 | 10.29 | 7.53 | 6.39 | 5.09 | 6.70 | 7.67 | 5.14 | 15.39 | 14.28 | 8.57 | 7.45 | 13.54 | 22.35 | 16.01 | 5.09 | 5.59 | 7.81 | 9.16 |
| MnO | 0.169 | 0.157 | 0.139 | 0.105 | 0.071 | 0.138 | 0.111 | 0.065 | 0.237 | 0.190 | 0.122 | 0.100 | 0.188 | 0.343 | 0.212 | 0.091 | 0.080 | 0.111 | 0.124 |
| MgO | 3.43 | 3.62 | 8.50 | 9.86 | 10.55 | 20.22 | 15.82 | 11.40 | 4.31 | 2.74 | 45.40 | 41.27 | 4.13 | 3.71 | 4.52 | 11.48 | 13.05 | 37.59 | 36.32 |
| CaO | 2.13 | 1.81 | 9.39 | 12.06 | 12.54 | 14.27 | 10.57 | 11.29 | 7.87 | 6.30 | 0.08 | 0.49 | 9.74 | 9.68 | 8.06 | 14.85 | 10.09 | 0.03 | 0.11 |
| Na2O | 2.38 | 2.14 | 1.90 | 1.57 | 1.40 | 0.30 | 1.05 | 1.47 | 2.37 | 2.86 | -0.09 | -0.03 | 2.63 | 2.39 | 2.59 | 1.36 | 1.80 | -0.10 | -0.08 |
| K2O | 2.450 | 3.004 | 1.011 | 0.451 | 0.092 | 0.035 | 0.132 | 0.074 | 0.936 | 1.320 | -0.002 | -0.001 | 0.285 | 0.768 | 0.429 | 0.042 | 0.046 | -0.004 | 0.001 |
| P2O5 | 0.105 | 0.102 | 0.097 | 0.011 | 0.010 | 0.006 | 0.014 | 0.017 | 0.380 | 0.880 | 0.002 | 0.003 | 0.032 | 1.475 | 0.082 | 0.010 | 0.010 | 0.007 | 0.009 |
| LOI | 1.52 | 1.36 | 1.00 | 1.78 | 2.79 | 0.85 | 3.36 | 2.62 | 0.10 | -0.17 | 8.10 | 10.71 | -0.15 | -0.79 | -0.29 | 1.67 | 5.55 | 13.30 | 12.00 |
| TOTAL | 99.91 | 99.42 | 99.41 | 100.21 | 99.56 | 99.48 | 99.60 | 100.13 | 100.12 | 99.63 | 100.21 | 99.45 | 99.47 | 99.47 | 99.67 | 99.42 | 99.56 | 99.48 | 99.40 |

| Sample | MS1531 | MS1544 | 137P | MS1510a | Ab7800 | Ab94 | MS1608 | MS1630 | CLW102 | CLW218 | CLW219 | CLW220 | DCD114 | DCD101 | DCD105 | CLW109 | CLW203 | CLW206 | CLW207 |
|---|---|---|---|---|---|---|---|---|---|---|---|---|---|---|---|---|---|---|---|
| SiO2 | 39.95 | 49.99 | 72.56 | 39.98 | 47.53 | 52.08 | 39.83 | 38.81 | 48.65 | 48.33 | 44.88 | 42.59 | 71.09 | 39.87 | 45.07 | 43.05 | 49.90 | 48.18 | 53.72 |
| TiO2 | 0.010 | 2.210 | 0.551 | 0.021 | 2.991 | 1.280 | 0.014 | 0.035 | 1.198 | 0.463 | 1.578 | 1.161 | 1.258 | 0.047 | 0.192 | 0.997 | 0.210 | 0.296 | 0.304 |
| Al2O3 | 1.16 | 14.73 | 10.12 | 0.47 | 14.43 | 16.69 | 0.31 | 1.78 | 17.43 | 12.02 | 19.38 | 18.20 | 10.36 | 0.72 | 17.59 | 19.47 | 18.58 | 15.12 | 17.13 |
| Fe2O3 | 7.50 | 10.99 | 4.85 | 6.98 | 17.22 | 9.80 | 7.88 | 8.26 | 12.25 | 10.96 | 14.11 | 15.08 | 7.64 | 9.30 | 6.57 | 14.75 | 8.51 | 10.05 | 9.26 |
| MnO | 0.103 | 0.212 | 0.048 | 0.095 | 0.233 | 0.166 | 0.096 | 0.098 | 0.155 | 0.181 | 0.161 | 0.166 | 0.106 | 0.091 | 0.110 | 0.173 | 0.163 | 0.187 | 0.181 |
| MgO | 37.53 | 7.33 | 5.11 | 38.52 | 4.40 | 5.82 | 38.29 | 38.14 | 4.99 | 11.94 | 5.29 | 6.92 | 2.54 | 37.25 | 10.20 | 6.24 | 9.38 | 13.80 | 9.14 |
| CaO | 0.06 | 10.94 | 1.36 | 0.04 | 9.81 | 8.97 | 0.03 | 0.03 | 9.40 | 11.97 | 10.05 | 10.80 | 4.04 | 0.35 | 13.55 | 12.32 | 5.38 | 8.15 | 6.64 |
| Na2O | -0.06 | 2.15 | 1.42 | -0.10 | 2.56 | 2.68 | -0.08 | -0.09 | 1.62 | 0.44 | 1.66 | 1.16 | 0.39 | -0.06 | 1.06 | 0.76 | 2.43 | 0.54 | 1.26 |
| K2O | 0.000 | 0.211 | 2.412 | -0.002 | 0.722 | 1.339 | 0.004 | -0.001 | 0.726 | 0.778 | 0.901 | 0.988 | 0.937 | 0.028 | 1.251 | 0.232 | 1.358 | 1.021 | 1.095 |
| P2O5 | 0.004 | 0.216 | 0.095 | 0.010 | 0.312 | 0.202 | 0.005 | 0.007 | 0.492 | 0.072 | 0.556 | 0.411 | 0.014 | 0.005 | 0.005 | 0.061 | 0.182 | 0.058 | 0.029 |
| LOI | 13.24 | 0.52 | 1.68 | 13.40 | 0.10 | 0.80 | 13.04 | 12.57 | 2.50 | 2.30 | 1.70 | 1.90 | 1.07 | 11.16 | 3.80 | 1.42 | 3.94 | 2.68 | 1.23 |
| TOTAL | 99.49 | 99.51 | 100.21 | 99.42 | 100.31 | 99.84 | 99.43 | 99.63 | 99.41 | 99.45 | 100.27 | 99.37 | 99.45 | 98.76 | 99.41 | 99.47 | 100.03 | 100.10 | 99.98 |

**Table B.2 XRF data from the major element checks from the XRF, University of Edinburgh.**

| | Trace run 1 | | | | | Trace run 2 | | | | | | | REE run | | |
|---|---|---|---|---|---|---|---|---|---|---|---|---|---|---|---|
| | Nb | Rb | Sr | Y | Zr | Ba | Cr | Cu | Ni | Sc | V | Zn | La | Ce | Nd |
| | ppm | ppm | ppm | ppm | ppm | ppm | ppm | ppm | ppm | ppm | ppm | ppm | ppm | ppm | ppm |
| BHVO-1 | 19 | 11 | 403 | 27.6 | 179 | 139 | 289 | 136 | 121 | 31.8 | 317 | 105 | 15.8 | 39 | 25.2 |
| BHVO-1 | 19.7 | 8.7 | 398 | 27.1 | 176 | 137 | 290 | 135 | 116.2 | 33.8 | 312 | 101.1 | 14.9 | 39.7 | 25.6 |
| BHVO-1 | 19.8 | 8.9 | 397 | 27.3 | 176 | 133 | 292 | 135 | 115.9 | 33.5 | 311 | 102.2 | 14.2 | 41.3 | 26.4 |
| BHVO-1 | 19.8 | 9.0 | 397 | 27.1 | 175 | 133 | 290 | 135 | 115.9 | 33.8 | 321 | 101.6 | 11.4 | 38.7 | 26.2 |
| BHVO-1 | 19.8 | 9.1 | 397 | 27.4 | 174 | 139 | 293 | 136 | 115.9 | 33.5 | 317 | 102.1 | | | |
| BHVO-1 | 19.8 | 9.1 | 397 | 27.6 | 175 | 138 | 292 | 135 | 116.7 | 33.4 | 315 | 102.2 | | | |
| BHVO-1 | 19.8 | 8.8 | 398 | 27.7 | 176 | | | | | | | | | | |
| BHVO-1 | 19.8 | 8.6 | 397 | 27.0 | 176 | | | | | | | | 12.3 | 38.2 | 25.3 |
| BHVO-1 | 19.7 | 8.9 | 397 | 27.3 | 177 | | | | | | | | 14.1 | 37.9 | 25.8 |
| BHVO-1 | 19.8 | 8.9 | 398 | 27.3 | 177 | | | | | | | | | | |
| BCR-1 | 14 | 47.2 | 330 | 38 | 190 | 681 | 16 | 19 | 13 | 32.6 | 407 | 129.5 | 24.9 | 53.7 | 28.8 |
| BCR-1 | 13.2 | 47.2 | 345 | 38.4 | 197 | 681 | 12.4 | 18.8 | 13.5 | 34.7 | 401 | 126.5 | 22.7 | 51.2 | 28.1 |
| BCR-1 | 13.1 | 47.1 | 343 | 38.4 | 197 | 676 | 10.9 | 19.2 | 14.2 | 34.7 | 414 | 128.0 | 25.4 | 52.3 | 27.1 |
| BCR-1 | 13.0 | 47.2 | 342 | 38.1 | 196 | 672 | 12.1 | 19.2 | 13.1 | 35.2 | 407 | 127.2 | 24.2 | 54.1 | 29.1 |
| BCR-1 | 12.9 | 47.1 | 334 | 37.5 | 191 | | | | | | | | | | |
| BCR-1 | 12.8 | 47.0 | 338 | 37.9 | 193 | | | | | | | | | | |
| BCR-1 | 12.9 | 47.4 | 338 | 38.1 | 193 | | | | | | | | | | |
| BIR-1 | 2 | 1 | 108 | 16 | 22 | 7.7 | 382 | 126 | 166 | 44 | 313 | 71 | 0.88 | 2.5 | 2.5 |
| BIR-1 | 0.6 | 0.4 | 108 | 16.6 | 15.1 | 9.8 | 382 | 144 | 152 | 40.5 | 319 | 65 | 2.7 | 1.2 | 2.0 |
| BIR-1 | 0.3 | 0.3 | 108 | 16.3 | 15.4 | 12.3 | 382 | 143 | 152 | 38.7 | 317 | 67 | 2.1 | 4.7 | 2.2 |
| BIR-1 | 0.4 | 0.3 | 108 | 16.4 | 15.5 | 9.3 | 384 | 143 | 153 | 39.7 | 319 | 66 | 1.1 | 0.4 | 3.0 |
| BIR-1 | 0.4 | 0.3 | 108 | 16.3 | 15.5 | | | | | | | | | | |
| BIR-1 | 0.5 | 0.3 | 108 | 16.3 | 15.0 | | | | | | | | | | |
| BIR-1 | 0.6 | 0.2 | 108 | 16.5 | 15.4 | | | | | | | | | | |
| BIR-1 | 0.4 | 0.3 | 109 | 16.6 | 14.7 | | | | | | | | | | |
| BIR-1 | 0.6 | 0.0 | 109 | 16.3 | 15.0 | | | | | | | | | | |
| BIR-1 | 0.5 | 0.5 | 109 | 16.4 | 15.2 | | | | | | | | | | |
| DTS-1 | 2.2 | 0.06 | 0.32 | 0.04 | 4 | | | | | | | | | | |
| DTS-1 | 0.3 | -0.1 | 0.45 | -0.2 | 1.7 | | | | | | | | | | |
| DTS-1 | 0.1 | 0.3 | 0.35 | 0.0 | 2.0 | | | | | | | | | | |
| DTS-1 | 0.0 | 0.1 | 0.16 | -0.2 | 1.8 | | | | | | | | | | |
| DTS-1 | 0.1 | 0.0 | 0.60 | -0.3 | 1.2 | | | | | | | | | | |
| DTS-1 | 0.1 | 0.1 | 0.20 | -0.2 | 1.5 | | | | | | | | | | |
| DTS-1 | -0.1 | 0.1 | 0.10 | -0.1 | 1.6 | | | | | | | | | | |
| PCC1 | | | | | | 1.2 | 2730 | 10 | 2380 | 8.4 | 31 | 42 | | | |
| PCC1 | | | | | | 7.2 | 2824 | 9.0 | 2439 | 7.4 | 32.6 | 44.9 | | | |
| PCC1 | | | | | | 4.0 | 2820 | 8.4 | 2432 | 7.6 | 28.2 | 44.4 | | | |
| PCC1 | | | | | | 7.2 | 2822 | 8.0 | 2436 | 7.6 | 32.6 | 45.5 | | | |
| | Nb | Rb | Sr | Y | Zr | Ba | Cr | Cu | Ni | Sc | V | Zn | La | Ce | Nd |

**Trace element analyses run in May 2000.**

Values in red are Geostandard Reference values
Data underlined are recommended values; other values are proposed, except those in italics, which are information values
Sets of data grouped in boxes are data from individual XRF runs

## Table B.3 Comparison of reference samples analyses with data obtained from XRF.

| | Nb | Rb | Sr | Y | Zr | Ba | Cr | Cu | Ni | Sc | V | Zn | La | Ce | Nd |
|---|---|---|---|---|---|---|---|---|---|---|---|---|---|---|---|
| DCD116 - a | 5.9 | 18.2 | 303.8 | 10.5 | 55.3 | 225.6 | 319.5 | 126.7 | 134.2 | 43.2 | 379.6 | 130.4 | 14.90 | 7.3 | 7.7 |
| DCD116 - b | 5.8 | 18.3 | 304.1 | 10.4 | 49.2 | 224.3 | 320.2 | 127.8 | 135.1 | 44.0 | 387.2 | 131.5 | 16.10 | 8.3 | 7.0 |
| DCD116 - c | 5.8 | 18.3 | 303.7 | 10.3 | 50.0 | 221.5 | 318.7 | 126.9 | 133.9 | 44.4 | 380.1 | 130.0 | 18.50 | 7.4 | 8.1 |
| DCD116 - d | 5.9 | 18.2 | 301.8 | 10.6 | 64.5 | 228.6 | 318.1 | 127.6 | 135.5 | 43.6 | 380.8 | 131.0 | 16.70 | 9.1 | 7.9 |
| DCD116 - e | 5.8 | 18.2 | 302.2 | 10.2 | 57.9 | 228.0 | 323.9 | 126.8 | 134.1 | 43.1 | 379.8 | 131.2 | 17.90 | 8.9 | 8.4 |

## Table B.4 Multiple XRF runs to test the reproducability of the data

**RHBNC Laboratory Standard Rock Data**

| | La | Ce | Pr | Nd | Sm | Eu | Gd | Dy | Ho | Er | Yb | Lu |
|---|---|---|---|---|---|---|---|---|---|---|---|---|
| **KC10** | 4.3 | 9.2 | 1.6 | 6.8 | 1.7 | 0.75 | 1.9 | 2 | 0.43 | 1.25 | 1.1 | 0.16 |
| **KC11** | 23 | 49 | 5.9 | 26.5 | 5.2 | 1.4 | 5 | 4.45 | 1 | 2.7 | 2.2 | 0.32 |
| **KC12** | 37 | 70 | 7.2 | 27 | 3.3 | 1.1 | 2.1 | 1.2 | ('0.25) | 0.8 | 0.5 | 0.06 |
| **KC14** | 59 | 120 | 13 | 58 | 14 | 0.57 | 15 | 18 | 4 | 11.8 | 11.2 | 1.5 |
| **Comp.** | 100 | 200 | 20 | 100 | 20 | 10 | 20 | 10 | 10 | 10 | 10 | 10 |

**Batch 1**

**Prepared: Summer 1999** **Analysed: Summer 1999**

| | La | Ce | Pr | Nd | Sm | Eu | Gd | Dy | Ho | Er | Yb | Lu |
|---|---|---|---|---|---|---|---|---|---|---|---|---|
| **Comp.** | 102 | 209.8 | 20.21 | 97.6 | 20.03 | 10.11 | 20.42 | 10.22 | 9.76 | 9.9 | 10.18 | 9.95 |
| **Blank** | 0.2 | 0 | 0 | 0 | 0 | 0 | 0 | 0 | 0 | 0 | 0 | 0 |
| **KC12** | 39.7 | 74.59 | 8.02 | 26.49 | 3.46 | 1.09 | 2.01 | 1.17 | 0.19 | 0.46 | 0.42 | 0.06 |
| **Comp.** | 102 | 210.4 | 20.1 | 97.3 | 20.07 | 10.11 | 20.24 | 10.21 | 9.75 | 9.88 | 10.18 | 9.96 |
| **Blank** | 0.7 | 1.48 | 0.03 | 0.66 | 0.12 | 0.04 | 0.03 | 0 | 0 | 0 | 0 | 0 |
| **KC10** | 4 | 10.38 | 1.33 | 6.27 | 1.46 | 0.75 | 1.86 | 1.86 | 0.37 | 0.91 | 1.01 | 0.16 |
| **Comp.** | 103.8 | 214.31 | 20.35 | 97.6 | 20.38 | 10.25 | 20.64 | 10.27 | 9.83 | 9.98 | 10.33 | 10.14 |
| **Blank** | 0.1 | 0 | 0 | 0 | 0 | 0 | 0 | 0 | 0 | 0 | 0 | 0 |
| **KC10** | 4.5 | 10.2 | 1.26 | 5.97 | 1.64 | 0.75 | 1.79 | 1.97 | 0.37 | 1.13 | 1.07 | 0.15 |
| **KC11** | 25.1 | 55.39 | 6.66 | 25.41 | 5.05 | 1.47 | 4.68 | 4.39 | 0.84 | 2.44 | 2.15 | 0.32 |
| **KC12** | 40.4 | 76.71 | 8.21 | 26.67 | 3.59 | 1.12 | 2.1 | 1.23 | 0.2 | 0.51 | 0.43 | 0.06 |
| **KC14** | 58.7 | 132.12 | 14 | 51.08 | 12.49 | 0.51 | 13.17 | 18.07 | 3.77 | 11.72 | 12.37 | 1.77 |
| **Comp.** | 104 | 215.4 | 20.27 | 97.2 | 20.28 | 10.25 | 20.8 | 10.26 | 9.79 | 9.96 | 10.33 | 10.2 |

**Batch 2**

**Prepared: Nov.- Dec. 2000.** **Analysed: January 2001**

| | La | Ce | Pr | Nd | Sm | Eu | Gd | Dy | Ho | Er | Yb | Lu |
|---|---|---|---|---|---|---|---|---|---|---|---|---|
| **KC14** | 57.7 | 130.3 | 13 | 55.5 | 12.9 | 0.56 | 13.37 | 19.31 | 4.18 | 13.57 | 13.55 | 1.99 |
| **Blank** | 0.6 | 2.1 | 0.1 | 0.4 | 0.26 | 0.04 | 0.81 | 0.08 | 0.21 | 1.06 | 0.16 | 0.02 |
| **Blank** | 0.5 | 1.5 | 0.1 | 0.2 | 0.26 | 0.03 | 0.5 | 0.05 | 0.14 | 0.96 | 0.11 | 0 |
| **KC14** | 56.7 | 129.8 | 12.7 | 53.1 | 13.06 | 0.57 | 13.87 | 18.75 | 4.34 | 14.08 | 13.47 | 2.02 |
| **KC14** | 56.8 | 131.5 | 12.8 | 54.3 | 12.46 | 0.55 | 13.14 | 18.94 | 4.1 | 13.35 | 13.51 | 1.96 |
| **Blank** | 0.8 | 2.8 | 0.1 | 0.6 | 0.36 | 0.05 | 1.15 | 0.1 | 0.24 | 0.79 | 0.22 | 0.02 |

**Batch 3**

**Prepared: August 2001** **Analysed: September 2001**

| | La | Ce | Pr | Nd | Sm | Eu | Gd | Dy | Ho | Er | Yb | Lu |
|---|---|---|---|---|---|---|---|---|---|---|---|---|
| **Blank** | 0.4 | 0.7 | 0.1 | 0.1 | 0.15 | 0.01 | 0.17 | 0.03 | 0.04 | 0.06 | 0.03 | 0 |
| **KC12** | 36.5 | 68.3 | 6.8 | 26.3 | 3.71 | 1.08 | 1.98 | 1.26 | 0.32 | 0.55 | 0.45 | 0.08 |
| **Blank** | | | | | 0.2 | 0.03 | 0.25 | 0.07 | 0.09 | 0.08 | 0.05 | 0 |
| **KC14** | | | | | 14.36 | 0.71 | 13.41 | 19.46 | 4.4 | 12.82 | 13.7 | 2.08 |

## Table B.5 REE Standards

| Sample | Jadeite | | Olivine | | Al2O3 | Pyroxene | | Wollastonite | | Orthoclase | | Apatite | | E.S.Olivine | | Fayalite | |
|---|---|---|---|---|---|---|---|---|---|---|---|---|---|---|---|---|---|
| | Publ. | *Mar '01* | Publ. | *Mar '01* | *Mar '01* | Publ. | *Mar '01* | Publ. | *Mar '01* | Publ. | *Mar '01* | Publ. | *Mar '01* | Publ. | *Mar '01* | Publ. | *Mar '01* |
| SiO2 | 59.44 | *59.16* | 41.54 | *41.54* | | 49.625 | *49.77* | 51.62 | *53.01* | 65.14 | *66.67* | 0.11 | | 39.22 | *40.56* | 29.57 | *30.33* |
| TiO2 | | | | | | 0.835 | *0.99* | | | | | | | | | | |
| Al2O3 | 25.19 | *23.96* | | | *95.12* | 7.749 | *7.56* | | | 17.37 | *17.49* | | | | | | |
| Cr2O3 | | | | | | 0.019 | | | *0.21* | | | | | | | | |
| FeO | | | 6.78 | *6.42* | | 6.834 | *5.62* | | | 0.45 | *0.36* | 0.04 | | 18.83 | *18.72* | 66.41 | *66.96* |
| MnO | | | 0 | *0.22* | | 0.137 | | 0.4 | *0.37* | | | | | | | 2.14 | *2.24* |
| MgO | | | 51.03 | *50.41* | | 15.517 | *15.03* | | *0.15* | | | | | 42.31 | *42.85* | 0 | |
| CaO | | | 0 | | | 17.651 | *17.39* | 47.89 | *49.35* | | | 55.35 | *56.2* | | | | |
| Na2O | 15.21 | *14.76* | | | | 1.303 | *1.12* | | | 0.87 | *1.06* | | *0.16* | | | | *0.84* |
| K2O | | | | | | | | | | 15.52 | *15.76* | | | | | | |
| NiO | | | 0.38 | | | | | | | | | | | | | 0.13 | |
| P2O5 | | | | | | | | | | | | 41.93 | *40.38* | | | | |
| Total | 99.84 | *97.88* | 99.73 | *98.59* | *95.12* | 99.67 | *97.48* | 99.91 | *103.09* | 99.35 | *101.35* | 97.43 | *96.73* | 100.36 | *102.14* | 98.25 | *100.37* |

| Sample | Jadeite | | Olivine | | Al2O3 | Pyroxene | | Wollastonite | | Orthoclase | | Apatite | | E.S.Olivine | | Fayalite | |
|---|---|---|---|---|---|---|---|---|---|---|---|---|---|---|---|---|---|
| | Publ. | *Jul '01* | Publ. | *Jul '01* | *Jul '01* | Publ. | *Jul '01* | Publ. | *Jul '01* | Publ. | *Jul '01* | Publ. | *Jul '01* | Publ. | *Jul '01* | Publ. | *Jul '01* |
| SiO2 | 59.44 | *61.55* | 41.54 | *42.53* | | 49.625 | *51.73* | 51.62 | *52.4* | 65.14 | *65.89* | 0.11 | | 39.22 | *40.42* | 29.57 | *29.88* |
| TiO2 | | | | | | 0.835 | *0.85* | | | | | | | | | | |
| Al2O3 | 25.19 | *24.57* | | | | 7.749 | *7.81* | | | 17.37 | *17.11* | | | | | | |
| Cr2O3 | | | | | | 0.019 | | | *0.21* | | | | | | | | |
| FeO | | *0.24* | 6.78 | *6.78* | | 6.834 | *6.25* | | | 0.45 | *0.48* | 0.04 | | 18.83 | *18.97* | 66.41 | *67.18* |
| MnO | | | 0 | | | 0.137 | | 0.4 | *0.34* | | | | | | *0.23* | 2.14 | *2.33* |
| MgO | | | 51.03 | *51.86* | | 15.517 | *15.75* | | *0.2* | | | | | 42.31 | *42.96* | 0 | |
| CaO | | | 0 | | | 17.651 | *17.86* | 47.89 | *48.36* | | | 55.35 | *55.63* | | *0.14* | | |
| Na2O | 15.21 | *15.3* | | | | 1.303 | *1.14* | | | 0.87 | *0.99* | | *0.28* | | | | *0.75* |
| K2O | | | | | | | | | | 15.52 | *15.43* | | | | | | |
| NiO | | | 0.38 | *0.34* | | | | | | | | | | | | 0.13 | |
| P2O5 | | | | | | | | | | | | 41.93 | *40.42* | | | | |
| Total | 99.84 | *101.67* | 99.73 | *101.5* | *95.12* | 99.67 | *101.4* | 99.91 | *101.51* | 99.35 | *99.9* | 97.43 | *96.33* | 100.36 | *102.72* | 98.25 | *100.15* |

**Table B.6 Probe Standards**

# Appendix C.1 - Major and Trace Element data

| Igneous Rocks: | Ab6908 | 1P | 7P | 9P | Ab74 | Ab82 | Ab90 | Ab111 | Ab115 | Ab117 | Ab125 | Ab127 | Ab135 | Ab140 | Ab143 |
|---|---|---|---|---|---|---|---|---|---|---|---|---|---|---|---|
| **SiO2** | 54.79 | 51.94 | 53.91 | 52.16 | 51.68 | 54.31 | 42.75 | 51.04 | 50.72 | 47.05 | 50.07 | 47.89 | 50.05 | 45.23 | 51.34 |
| **TiO2** | 1.79 | 0.74 | 0.92 | 0.51 | 0.33 | 0.93 | 0.08 | 0.20 | 0.17 | 0.14 | 0.18 | 0.30 | 0.41 | 0.06 | 0.34 |
| **Al2O3** | 16.22 | 19.91 | 16.29 | 16.63 | 16.67 | 8.10 | 24.01 | 19.11 | 17.66 | 22.02 | 22.30 | 17.73 | 3.81 | 22.78 | 4.87 |
| **Fe2O3** | 9.00 | 6.83 | 7.71 | 8.24 | 6.55 | 12.15 | 4.67 | 5.07 | 6.46 | 5.29 | 3.87 | 6.72 | 7.22 | 4.57 | 6.83 |
| **MnO** | 0.15 | 0.12 | 0.13 | 0.14 | 0.11 | 0.19 | 0.07 | 0.10 | 0.12 | 0.07 | 0.08 | 0.10 | 0.14 | 0.06 | 0.14 |
| **MgO** | 5.47 | 7.32 | 8.78 | 11.52 | 10.05 | 17.73 | 17.55 | 10.89 | 12.67 | 10.86 | 8.10 | 12.33 | 22.63 | 14.04 | 20.61 |
| **CaO** | 9.24 | 10.66 | 9.63 | 8.77 | 12.34 | 3.61 | 9.33 | 11.78 | 10.91 | 13.11 | 13.28 | 13.40 | 15.45 | 10.95 | 14.73 |
| **Na2O** | 1.97 | 2.10 | 1.96 | 1.58 | 1.57 | 1.25 | 1.06 | 1.54 | 1.26 | 1.44 | 1.83 | 1.35 | 0.31 | 1.89 | 0.36 |
| **K2O** | 0.95 | 0.58 | 0.99 | 0.42 | 0.46 | 1.25 | 0.09 | 0.11 | 0.04 | 0.08 | 0.11 | 0.11 | 0.01 | 0.04 | 0.01 |
| **P2O5** | 0.035 | 0.063 | 0.098 | 0.043 | 0.010 | 0.215 | 0.007 | 0.001 | 0.004 | 0.011 | 0.014 | 0.019 | 0.011 | 0.007 | 0.007 |
| **BaO** | 0.044 | 0.023 | 0.027 | 0.016 | 0.011 | 0.042 | 0.002 | 0.003 | 0.004 | 0.002 | 0.002 | 0.005 | 0.003 | 0.004 | 0.006 |
| **Cr2O3** | 0.029 | 0.040 | 0.059 | 0.101 | 0.135 | 0.132 | 0.499 | 0.081 | 0.053 | 0.150 | 0.076 | 0.171 | 0.692 | 0.121 | 0.662 |
| **NiO** | 0.002 | 0.005 | 0.006 | 0.009 | 0.010 | 0.070 | 0.065 | 0.018 | 0.031 | 0.068 | 0.012 | 0.020 | 0.093 | 0.039 | 0.067 |
| **Total** | 99.61 | 100.25 | 100.42 | 100.01 | 99.77 | 99.73 | 99.61 | 99.83 | 100.01 | 100.07 | 99.83 | 99.95 | 100.04 | 99.62 | 99.22 |
| **mg#** | 37.80 | 51.73 | 53.24 | 58.30 | 60.54 | 59.34 | 78.98 | 68.23 | 66.23 | 67.24 | 67.67 | 64.72 | 75.81 | 75.44 | 75.11 |
| **LOI** | 0.84 | 0.95 | 0.62 | 0.13 | 1.26 | 0.55 | 6.81 | 0.32 | 0.20 | 2.26 | 0.57 | 1.33 | 3.26 | 7.82 | 0.42 |
| **Rb** | 28.5 | 17.0 | 34.0 | 12.3 | 11.4 | 46.2 | 1.8 | 1.1 | 0.7 | 1.9 | 1.4 | 3.8 | 1.6 | 1.3 | 1.2 |
| **Sr** | 306.2 | 344.8 | 213.0 | 227.3 | 260.2 | 149.5 | 289.3 | 330.6 | 232.6 | 303.3 | 348.9 | 227.7 | 14.4 | 294.6 | 34.8 |
| **Y** | 20.9 | 10.0 | 19.3 | 8.7 | 6.8 | 16.3 | 1.0 | 3.0 | 2.4 | 2.4 | 3.0 | 5.1 | 9.0 | 0.7 | 8.1 |
| **Zr** | 181.7 | 40.0 | 42.2 | 39.1 | 12.4 | 120.9 | 1.5 | 3.8 | 3.2 | 2.9 | 3.8 | 12.1 | 17.9 | 1.0 | 12.0 |
| **Nb** | 10.1 | 4.2 | 7.2 | 3.2 | 0.3 | 11.6 | 0.2 | 0.2 | 0.1 | 0.1 | 0.2 | 0.6 | 0.4 | 0.1 | 0.2 |
| **Zn** | 73.5 | 51.4 | 59.7 | 64.0 | 42.2 | 105.2 | 31.3 | 27.9 | 34.9 | 25.1 | 20.6 | 35.6 | 33.5 | 21.4 | 32.5 |
| **Cu** | 18.6 | 24.9 | 39.8 | 30.5 | 27.4 | 31.9 | 78.9 | 56.1 | 59.9 | 157.9 | 32.4 | 82.2 | 238.2 | 60.8 | 156.2 |
| **Ni** | 15.6 | 34.9 | 47.6 | 58.9 | 78.4 | 506.6 | 475.8 | 118.2 | 219.4 | 406.7 | 72.7 | 135.5 | 616.3 | 257.4 | 441.3 |
| **Cr** | 212.7 | 320.9 | 466.4 | 799.5 | 1111.8 | 1033.9 | 2844.4 | 633.0 | 399.6 | 1019.9 | 591.0 | 1254.8 | 5123.8 | 752.0 | 5114.7 |
| **V** | 252.6 | 132.7 | 173.9 | 138.7 | 173.3 | 134.7 | 37.1 | 102.0 | 108.4 | 54.9 | 91.6 | 103.9 | 193.9 | 11.2 | 232.5 |
| **Ba** | 279.5 | 158.4 | 195.8 | 139.7 | 66.1 | 311.1 | 28.6 | 22.3 | 16.7 | 26.1 | 23.3 | 23.9 | 2.4 | 9.7 | 8.5 |
| **Sc** | 38.5 | 27.8 | 34.5 | 30.2 | 39.2 | 26.7 | 10.2 | 26.9 | 28.4 | 16.1 | 23.7 | 29.8 | 43.6 | 7.9 | 51.5 |
| **La** | 15.5 | 8.0 | 14.4 | 7.0 | 2.1 | 17.0 | | | | | | 2.9 | | | |
| **Ce** | 34.5 | 16.7 | 28.6 | 17.1 | 4.3 | 39.7 | | | | | | 6.9 | | | |
| **Nd** | 17.7 | 7.0 | 16.3 | 8.6 | 3.6 | 20.8 | | | | | | 3.2 | | | |

| | Ab1294 | Ab2063 | Ab2065 | Ab2073 | Ab2083 | Ab2090 | 54P | 85P | 86P | 88P | Ab3826 | Ab92 | Ab96 | Ab1310 | Ab5612 | Ab5613 |
|---|---|---|---|---|---|---|---|---|---|---|---|---|---|---|---|---|
| **SiO2** | 44.98 | 46.37 | 49.83 | 48.88 | 44.69 | 46.52 | 46.97 | 55.29 | 52.48 | 50.13 | 49.86 | 50.87 | 51.06 | 53.89 | 39.46 | 51.19 |
| **TiO2** | 0.06 | 0.18 | 0.44 | 0.11 | 0.10 | 0.18 | 0.14 | 2.53 | 0.93 | 3.20 | 3.33 | 2.76 | 2.76 | 2.03 | 0.01 | 1.52 |
| **Al2O3** | 22.95 | 22.16 | 15.95 | 19.14 | 10.57 | 16.08 | 22.76 | 14.76 | 15.79 | 15.20 | 15.04 | 15.86 | 15.86 | 15.75 | 0.09 | 15.71 |
| **Fe2O3** | 4.87 | 5.67 | 6.46 | 5.18 | 8.23 | 7.95 | 5.25 | 12.17 | 10.03 | 13.78 | 15.36 | 13.89 | 13.63 | 14.34 | 9.55 | 11.11 |
| **MnO** | 0.05 | 0.07 | 0.14 | 0.08 | 0.11 | 0.11 | 0.07 | 0.16 | 0.16 | 0.18 | 0.22 | 0.19 | 0.19 | 0.18 | 0.13 | 0.17 |
| **MgO** | 13.90 | 12.68 | 13.55 | 15.34 | 25.44 | 16.41 | 11.81 | 3.25 | 9.46 | 5.23 | 4.27 | 3.44 | 3.41 | 2.73 | 50.16 | 7.20 |
| **CaO** | 11.26 | 11.48 | 12.19 | 9.77 | 9.14 | 10.99 | 11.67 | 7.05 | 8.26 | 8.56 | 7.95 | 8.79 | 8.60 | 6.39 | 0.06 | 10.14 |
| **Na2O** | 1.47 | 1.55 | 1.49 | 1.12 | 1.00 | 1.15 | 1.06 | 2.85 | 1.37 | 2.29 | 2.31 | 2.43 | 2.44 | 2.72 | 0.00 | 2.69 |
| **K2O** | 0.03 | 0.06 | 0.24 | 0.04 | 0.02 | 0.12 | 0.06 | 1.72 | 1.02 | 1.09 | 0.91 | 1.01 | 1.09 | 1.30 | 0.01 | 0.66 |
| **P2O5** | 0.006 | 0.022 | 0.018 | 0.003 | 0.007 | 0.013 | 0.014 | 0.380 | 0.073 | 0.296 | 0.356 | 0.924 | 0.679 | 0.849 | 0.003 | 0.163 |
| **BaO** | 0.000 | 0.003 | 0.017 | 0.003 | 0.001 | 0.002 | 0.003 | 0.063 | 0.025 | 0.045 | 0.046 | 0.042 | 0.047 | 0.061 | 0.004 | 0.045 |
| **Cr2O3** | 0.094 | 0.083 | 0.034 | 0.146 | 0.302 | 0.132 | 0.080 | 0.001 | 0.052 | 0.005 | 0.004 | 0.004 | 0.003 | 0.002 | 0.182 | 0.036 |
| **NiO** | 0.122 | 0.030 | 0.014 | 0.038 | 0.094 | 0.061 | 0.029 | 0.000 | 0.006 | 0.001 | 0.002 | 0.001 | 0.001 | 0.001 | 0.361 | 0.004 |
| **Total** | 99.58 | 100.24 | 100.31 | 99.67 | 99.30 | 99.52 | 99.80 | 100.16 | 99.58 | 99.96 | 99.61 | 100.17 | 99.72 | 100.18 | 99.46 | 100.56 |
| **mg#** | 74.05 | 69.10 | 67.72 | 74.76 | 75.56 | 67.36 | 69.23 | 21.08 | 48.54 | 27.51 | 21.75 | 19.85 | 20.01 | 15.99 | 84.01 | 39.32 |
| **LOI** | 7.00 | 3.77 | 3.13 | 2.30 | 7.97 | 3.16 | 2.22 | 0.29 | 1.99 | 0.75 | -0.01 | 0.26 | 0.47 | -0.14 | 7.85 | -0.02 |
| **Rb** | 1.2 | 2.1 | 4.7 | 1.9 | 1.3 | 2.1 | 1.7 | 55.9 | 33.2 | 38.9 | 28.7 | 29.9 | 33.4 | 35.9 | -0.1 | 13.5 |
| **Sr** | 236.8 | 317.9 | 496.5 | 246.8 | 96.6 | 241.9 | 288.6 | 295.6 | 245.9 | 344.8 | 303.3 | 318.9 | 322.9 | 334.5 | 0.4 | 274.9 |
| **Y** | 0.8 | 2.6 | 9.3 | 1.5 | 1.8 | 3.0 | 1.9 | 41.1 | 12.2 | 28.0 | 25.5 | 32.2 | 27.3 | 42.6 | 0.2 | 24.8 |
| **Zr** | 2.1 | 8.1 | 20.2 | 2.6 | 3.2 | 4.4 | 5.8 | 202.9 | 60.9 | 85.2 | 128.4 | 77.0 | 89.6 | 250.3 | 1.5 | 124.4 |
| **Nb** | 0.1 | 0.6 | 0.9 | 0.2 | 0.0 | 0.0 | 0.6 | 24.2 | 6.9 | 17.9 | 21.5 | 16.9 | 16.3 | 28.7 | 0.0 | 11.8 |
| **Zn** | 24.0 | 29.6 | 38.1 | 27.1 | 38.1 | 45.8 | 28.6 | 112.3 | 87.8 | 114.4 | 122.4 | 108.6 | 104.8 | 156.8 | 34.0 | 89.0 |
| **Cu** | 265.1 | 68.6 | 34.4 | 77.5 | 78.3 | 149.8 | 62.9 | 12.7 | 26.1 | 15.5 | 20.7 | 18.9 | 18.0 | 19.3 | 0.7 | 24.3 |
| **Ni** | 778.6 | 201.1 | 95.4 | 238.9 | 641.6 | 404.0 | 194.1 | 4.8 | 49.3 | 12.6 | 13.9 | 11.7 | 11.4 | 14.0 | 2660.3 | 40.6 |
| **Cr** | 653.8 | 521.5 | 235.2 | 1085.7 | 2164.2 | 952.0 | 526.7 | 12.9 | 413.8 | 28.9 | 24.8 | 39.7 | 35.1 | 34.1 | 959.6 | 262.6 |
| **V** | 11.6 | 30.9 | 191.6 | 48.1 | 61.9 | 73.0 | 26.5 | 302.6 | 186.1 | 458.5 | 425.4 | 191.9 | 188.5 | 130.3 | 5.1 | 241.6 |
| **Ba** | 12.5 | 17.9 | 155.4 | 14.3 | 7.0 | 19.6 | 19.8 | 462.7 | 210.7 | 255.3 | 283.5 | 272.4 | 310.9 | 455.5 | -2.0 | 363.9 |
| **Sc** | 4.3 | 11.7 | 38.6 | 16.9 | 20.1 | 19.2 | 8.5 | 33.0 | 35.0 | 47.7 | 42.1 | 36.5 | 36.5 | 34.4 | 5.7 | 37.3 |
| **La** | | 1.7 | 4.9 | | | | | 32.6 | 11.6 | 18.4 | 15.8 | 21.1 | 17.2 | 30.7 | | 19.4 |
| **Ce** | | 4.9 | 10.9 | | | | | 78.0 | 23.9 | 49.3 | 41.5 | 51.3 | 41.7 | 78.4 | | 42.2 |
| **Nd** | | 1.5 | 6.9 | | | | | 41.9 | 9.3 | 25.2 | 22.0 | 29.1 | 25.0 | 44.9 | | 20.3 |

| | Ab7798 | Ab7799 | Ab7801 | Ab7802 | Ab7803 | WdQBN | MS1573 | MS1577 | MS1581 | MS1584 | MS1593 | MS1595 | MS1596 | Ab93 | Ab243 | Ab661 |
|---|---|---|---|---|---|---|---|---|---|---|---|---|---|---|---|---|
| **SiO2** | 47.12 | 57.80 | 46.98 | 51.97 | 50.74 | 51.08 | 45.31 | 44.39 | 42.70 | 48.93 | 45.26 | 46.73 | 43.36 | 47.43 | 41.95 | 59.73 |
| **TiO2** | 2.78 | 0.84 | 2.77 | 1.70 | 0.14 | 1.41 | 0.01 | 0.01 | 0.01 | 0.04 | 0.01 | 0.47 | 0.01 | 2.99 | 2.85 | 0.90 |
| **Al2O3** | 15.43 | 15.79 | 15.50 | 15.62 | 3.83 | 15.88 | 0.35 | 0.93 | 0.30 | 2.14 | 0.52 | 11.24 | 0.37 | 19.10 | 13.27 | 16.90 |
| **Fe2O3** | 17.09 | 11.08 | 17.17 | 11.31 | 5.88 | 10.23 | 9.43 | 8.64 | 8.68 | 8.80 | 9.40 | 11.61 | 9.61 | 13.23 | 23.08 | 8.09 |
| **MnO** | 0.27 | 0.29 | 0.27 | 0.18 | 0.12 | 0.16 | 0.11 | 0.13 | 0.11 | 0.14 | 0.10 | 0.15 | 0.09 | 0.15 | 0.31 | 0.19 |
| **MgO** | 3.53 | 0.11 | 3.50 | 5.82 | 24.28 | 6.79 | 44.24 | 45.15 | 47.35 | 30.61 | 42.96 | 21.92 | 43.69 | 5.43 | 5.74 | 0.43 |
| **CaO** | 8.97 | 4.02 | 8.94 | 10.49 | 14.66 | 10.06 | 0.01 | 0.01 | 0.53 | 8.15 | 0.66 | 5.91 | 1.78 | 8.73 | 8.94 | 3.15 |
| **Na2O** | 3.06 | 2.95 | 2.96 | 2.30 | 0.06 | 2.32 | 0.03 | 0.00 | 0.08 | 0.06 | 0.10 | 1.19 | 0.00 | 2.60 | 2.10 | 3.00 |
| **K2O** | 0.70 | 6.37 | 0.72 | 0.73 | 0.02 | 1.12 | 0.00 | 0.00 | 0.01 | 0.01 | 0.00 | 0.49 | 0.00 | 0.25 | 0.34 | 6.00 |
| **P2O5** | 0.791 | 0.147 | 0.803 | 0.198 | 0.001 | 0.151 | 0.002 | 0.004 | 0.004 | 0.006 | 0.003 | 0.072 | 0.004 | 0.012 | 1.097 | 0.233 |
| **BaO** | 0.068 | 0.188 | 0.065 | 0.070 | 0.006 | 0.063 | 0.000 | 0.000 | 0.002 | 0.006 | 0.004 | 0.018 | 0.004 | 0.034 | 0.094 | 0.966 |
| **Cr2O3** | 0.000 | 0.000 | 0.000 | 0.008 | 0.549 | 0.006 | 0.368 | 0.419 | 0.395 | 0.622 | 0.599 | 0.031 | 0.506 | 0.010 | 0.001 | 0.000 |
| **NiO** | 0.001 | 0.001 | 0.000 | 0.001 | 0.092 | 0.002 | 0.351 | 0.326 | 0.325 | 0.143 | 0.344 | 0.051 | 0.381 | 0.001 | 0.000 | 0.001 |
| **Total** | 99.74 | 99.40 | 99.61 | 100.31 | 99.72 | 99.19 | 99.44 | 99.25 | 99.76 | 98.88 | 99.01 | 99.79 | 98.91 | 99.92 | 99.68 | 98.62 |
| **mg#** | 17.12 | 0.98 | 16.93 | 33.98 | 80.50 | 39.89 | 82.43 | 83.94 | 84.51 | 77.67 | 82.05 | 65.37 | 81.97 | 29.10 | 19.92 | 5.05 |
| **LOI** | -0.71 | -0.29 | -0.77 | 0.01 | 3.79 | 0.13 | 13.23 | 14.04 | 10.56 | 7.49 | 13.54 | 2.74 | 13.66 | -0.34 | -1.15 | 0.34 |
| **Rb** | 5.0 | 52.1 | 5.9 | 13.1 | 0.7 | 28.3 | 0.1 | -0.1 | 0.0 | 0.7 | 0.0 | 18.5 | -0.1 | 2.4 | 5.3 | 66.5 |
| **Sr** | 334.9 | 68.3 | 349.6 | 295.5 | 3.8 | 288.9 | 1.3 | 0.3 | 1.0 | 3.7 | 10.3 | 122.7 | 8.4 | 429.6 | 363.8 | 285.1 |
| **Y** | 41.7 | 22.3 | 42.1 | 29.8 | 4.3 | 25.0 | 0.0 | 0.2 | 0.1 | 1.2 | 0.0 | 10.0 | 0.1 | 3.8 | 22.9 | 21.4 |
| **Zr** | 1348.9 | 1944.7 | 1283.5 | 233.2 | 3.9 | 99.7 | 1.5 | 1.8 | 1.6 | 2.0 | 1.6 | 43.9 | 1.3 | 20.7 | 122.8 | 1615.0 |
| **Nb** | 39.1 | 6.0 | 39.5 | 13.4 | 0.0 | 10.1 | 0.0 | 0.0 | 0.1 | 0.1 | -0.1 | 3.5 | 0.2 | 6.1 | 8.0 | 10.3 |
| **Zn** | 166.4 | 77.5 | 148.4 | 91.7 | 29.3 | 79.1 | 37.6 | 36.6 | 34.9 | 34.6 | 36.2 | 78.0 | 37.5 | 68.4 | 118.0 | 57.7 |
| **Cu** | 20.3 | 10.7 | 18.2 | 15.5 | 195.6 | 22.8 | 3.0 | 7.0 | 0.6 | 207.0 | 0.7 | 21.9 | 0.3 | 26.9 | 22.0 | 10.8 |
| **Ni** | 15.6 | 5.3 | 11.9 | 13.6 | 692.5 | 20.5 | 2544.7 | 2359.8 | 2342.8 | 1053.7 | 2539.6 | 372.5 | 2748.3 | 8.9 | 17.1 | 5.2 |
| **Cr** | 15.1 | 3.9 | 11.0 | 59.9 | 4184.3 | 52.4 | 1763.4 | 2431.5 | 2151.6 | 3936.1 | 3013.3 | 210.0 | 2777.6 | 67.0 | 16.3 | 4.7 |
| **V** | 206.3 | 0.0 | 195.1 | 216.0 | 152.4 | 230.8 | 22.8 | 42.6 | 21.8 | 134.9 | 25.5 | 68.3 | 22.5 | 281.4 | 169.4 | 0.0 |
| **Ba** | 429.3 | 1523.0 | 446.5 | 564.8 | 2.3 | 555.1 | 4.2 | 2.7 | 4.7 | 1.8 | 11.3 | 120.2 | 6.4 | 167.5 | 691.5 | 8137.3 |
| **Sc** | 40.8 | 44.3 | 36.1 | 36.8 | 48.5 | 35.2 | 8.3 | 11.8 | 9.1 | 36.8 | 6.9 | 17.2 | 4.5 | 24.0 | 53.1 | 65.0 |
| **La** | 113.2 | 38.8 | 114.3 | 33.9 | | 27.4 | | | | | | 6.1 | | 3.0 | 20.0 | 62.1 |
| **Ce** | 247.4 | 100.9 | 247.3 | 76.4 | | 57.6 | | | | | | 15.3 | | 3.6 | 45.7 | 108.2 |
| **Nd** | 141.8 | 60.1 | 139.7 | 43.8 | | 28.5 | | | | | | 7.5 | | 2.2 | 31.2 | 41.8 |

| | WdV(Ol) | WdS | WdHD3 | Wd109 | WdPY1 | WdCC2 | WdPY3 | WdPY2 | Wd72 | Wd60 | WdDV1 | Wd254 | WdR | MS1565 | HI115 | HI121 |
|---|---|---|---|---|---|---|---|---|---|---|---|---|---|---|---|---|
| **SiO2** | 48.76 | 50.14 | 46.95 | 58.52 | 47.43 | 50.66 | 47.39 | 47.92 | 43.05 | 42.68 | 47.41 | 47.85 | 50.06 | 46.49 | 49.19 | 63.39 |
| **TiO2** | 0.94 | 1.07 | 3.44 | 0.85 | 3.33 | 0.23 | 0.79 | 1.11 | 2.88 | 3.32 | 0.88 | 2.95 | 1.69 | 0.01 | 2.72 | 0.81 |
| **Al2O3** | 16.58 | 15.71 | 18.80 | 16.91 | 18.18 | 25.94 | 22.93 | 16.38 | 13.36 | 15.12 | 21.26 | 17.30 | 15.68 | 0.10 | 13.65 | 16.62 |
| **Fe2O3** | 10.25 | 10.00 | 13.63 | 8.92 | 14.88 | 3.47 | 6.52 | 10.42 | 21.80 | 19.74 | 7.52 | 15.73 | 10.87 | 7.34 | 15.31 | 9.14 |
| **MnO** | 0.16 | 0.17 | 0.18 | 0.22 | 0.19 | 0.06 | 0.10 | 0.16 | 0.32 | 0.26 | 0.11 | 0.20 | 0.19 | 0.08 | 0.25 | 0.13 |
| **MgO** | 9.29 | 9.01 | 4.18 | 0.13 | 4.34 | 3.98 | 6.11 | 9.27 | 3.62 | 5.05 | 6.87 | 4.35 | 7.31 | 45.21 | 4.86 | 0.34 |
| **CaO** | 12.11 | 12.22 | 9.92 | 3.41 | 8.60 | 13.27 | 14.19 | 12.46 | 9.74 | 8.94 | 13.69 | 8.15 | 11.85 | 0.01 | 10.14 | 0.30 |
| **Na2O** | 1.76 | 1.49 | 2.53 | 2.83 | 2.53 | 2.26 | 1.81 | 1.69 | 2.33 | 2.28 | 1.77 | 2.49 | 1.77 | 0.03 | 2.38 | 1.61 |
| **K2O** | 0.12 | 0.11 | 0.28 | 7.45 | 0.29 | 0.35 | 0.14 | 0.12 | 0.73 | 0.49 | 0.12 | 0.40 | 0.14 | 0.00 | 0.67 | 7.83 |
| **P2O5** | 0.015 | 0.009 | 0.030 | 0.093 | 0.047 | 0.026 | 0.015 | 0.011 | 1.418 | 1.621 | 0.027 | 0.082 | 0.012 | 0.000 | 0.314 | 0.124 |
| **BaO** | 0.014 | 0.016 | 0.061 | 0.211 | 0.065 | 0.021 | 0.022 | 0.027 | 0.167 | 0.119 | 0.016 | 0.100 | 0.022 | 0.001 | 0.077 | 0.353 |
| **Cr2O3** | 0.039 | 0.054 | 0.003 | 0.000 | 0.003 | 0.025 | 0.025 | 0.039 | 0.000 | 0.002 | 0.025 | 0.002 | 0.008 | 0.413 | 0.002 | 0.000 |
| **NiO** | 0.014 | 0.002 | 0.001 | 0.001 | 0.001 | 0.002 | 0.009 | 0.014 | 0.000 | 0.002 | 0.010 | 0.001 | 0.002 | 0.352 | 0.000 | 0.000 |
| **Total** | 99.99 | 99.93 | 99.94 | 99.33 | 99.82 | 100.24 | 99.99 | 99.53 | 99.25 | 99.49 | 99.66 | 99.50 | 99.57 | 99.23 | 99.48 | 100.29 |
| **mg#** | 47.54 | 47.40 | 23.47 | 1.44 | 22.58 | 53.42 | 48.38 | 47.08 | 14.24 | 20.37 | 47.74 | 21.66 | 40.21 | 86.03 | 24.10 | 3.59 |
| **LOI** | 0.09 | 0.52 | -0.14 | -0.08 | -0.42 | 0.44 | 0.23 | 0.05 | -0.77 | -0.75 | 0.16 | -0.31 | 0.32 | 12.24 | -0.36 | 1.75 |
| **Rb** | 1.1 | 3.1 | 4.0 | 55.1 | 3.0 | 7.7 | 1.4 | 0.8 | 16.1 | 8.5 | 1.3 | 6.1 | 3.4 | 0.1 | 8.6 | 65.7 |
| **Sr** | 265.2 | 260.9 | 436.1 | 112.9 | 464.6 | 410.9 | 355.4 | 263.7 | 413.0 | 428.2 | 345.6 | 457.5 | 325.7 | 0.8 | 312.1 | 108.0 |
| **Y** | 14.1 | 9.5 | 4.9 | 13.0 | 3.6 | 3.7 | 7.6 | 12.8 | 27.4 | 26.6 | 9.6 | 7.1 | 10.2 | 0.7 | 46.1 | 12.4 |
| **Zr** | 32.0 | 20.8 | 43.7 | 1798.3 | 47.1 | 10.5 | 24.0 | 40.2 | 321.6 | 148.7 | 22.8 | 68.0 | 31.1 | 1.5 | 873.5 | 1318.7 |
| **Nb** | 1.6 | 1.5 | 5.9 | 2.6 | 7.4 | 0.6 | 2.0 | 2.1 | 4.0 | 10.1 | 2.5 | 6.5 | 3.8 | 0.1 | 24.4 | 2.2 |
| **Zn** | 60.7 | 62.8 | 70.7 | 54.8 | 79.1 | 20.5 | 35.0 | 55.3 | 82.3 | 90.6 | 40.1 | 92.9 | 72.4 | 37.7 | 118.1 | 47.5 |
| **Cu** | 59.3 | 20.1 | 17.4 | 6.7 | 15.0 | 8.4 | 34.8 | 56.6 | 21.0 | 21.6 | 41.2 | 14.9 | 16.3 | 0.1 | 19.7 | 7.5 |
| **Ni** | 101.3 | 15.4 | 16.0 | 2.6 | 13.3 | 9.9 | 54.3 | 89.8 | 10.5 | 24.0 | 61.8 | 12.2 | 17.3 | 2572.5 | 9.0 | 1.9 |
| **Cr** | 291.0 | 393.5 | 20.5 | 7.4 | 14.1 | 179.0 | 174.5 | 256.3 | 4.9 | 28.0 | 165.1 | 27.9 | 63.0 | 1865.2 | 16.1 | 3.3 |
| **V** | 198.8 | 249.3 | 530.7 | 0.0 | 490.1 | 65.7 | 109.3 | 174.3 | 14.7 | 204.2 | 140.5 | 416.9 | 264.2 | 8.4 | 278.8 | 0.0 |
| **Ba** | 118.0 | 92.6 | 369.2 | 1846.4 | 456.9 | 151.9 | 124.1 | 165.7 | 1565.5 | 985.8 | 62.2 | 791.8 | 127.4 | 7.5 | 603.0 | 2756.7 |
| **Sc** | 38.8 | 42.5 | 37.1 | 47.1 | 29.2 | 19.2 | 22.0 | 34.2 | 78.8 | 29.7 | 25.3 | 30.6 | 46.8 | 2.0 | 47.2 | 100.5 |
| **La** | 2.8 | 2.7 | 0.7 | 25.0 | 0.4 | 5.5 | 3.0 | 3.7 | 23.9 | 22.0 | 2.7 | 0.8 | 2.6 | | 58.0 | 15.9 |
| **Ce** | 9.8 | 7.8 | 2.9 | 64.5 | 8.0 | 9.0 | 4.7 | 7.5 | 56.7 | 57.7 | 6.8 | 9.3 | 7.5 | | 129.5 | 39.2 |
| **Nd** | 7.0 | 5.0 | 2.2 | 33.0 | 1.0 | 3.8 | 4.1 | 4.3 | 40.1 | 36.9 | 5.1 | 2.8 | 5.7 | | 72.9 | 22.0 |

| | HI47 | HI131 | PGD1209 | PGD1215 | PGD1229 | PGD1232 | Ab3914 | Ab3979a | Ab3979b | Ab3984 | Ab3986 | Ab3988 | Ab5661 | Ab6510 | MS1511 | MS1512 |
|---|---|---|---|---|---|---|---|---|---|---|---|---|---|---|---|---|
| **SiO2** | 51.28 | 54.60 | 48.12 | 49.22 | 49.15 | 49.55 | 44.77 | 41.38 | 45.71 | 43.24 | 46.58 | 44.45 | 49.98 | 46.81 | 47.29 | 48.18 |
| **TiO2** | 1.29 | 1.22 | 0.28 | 0.27 | 0.31 | 0.31 | 0.07 | 0.04 | 0.05 | 0.10 | 0.13 | 0.08 | 0.26 | 0.20 | 0.16 | 0.05 |
| **Al2O3** | 25.82 | 14.98 | 18.54 | 16.91 | 17.32 | 17.32 | 18.72 | 1.66 | 21.43 | 9.70 | 18.83 | 14.80 | 18.27 | 15.32 | 16.19 | 17.65 |
| **Fe2O3** | 12.50 | 14.30 | 5.46 | 5.22 | 5.06 | 5.06 | 8.02 | 19.27 | 5.88 | 11.82 | 6.21 | 9.81 | 3.88 | 7.55 | 13.40 | 8.73 |
| **MnO** | 0.09 | 0.36 | 0.09 | 0.09 | 0.09 | 0.09 | 0.10 | 0.17 | 0.08 | 0.16 | 0.09 | 0.12 | 0.07 | 0.11 | 0.23 | 0.16 |
| **MgO** | 2.70 | 0.73 | 11.14 | 11.55 | 10.65 | 10.65 | 17.22 | 36.76 | 13.95 | 28.61 | 14.29 | 21.24 | 9.57 | 16.57 | 9.30 | 9.69 |
| **CaO** | 1.22 | 4.92 | 14.81 | 15.30 | 15.56 | 15.56 | 9.74 | 0.08 | 10.76 | 5.48 | 11.54 | 7.96 | 16.07 | 11.08 | 11.74 | 13.34 |
| **Na2O** | 2.08 | 2.56 | 1.38 | 1.37 | 1.67 | 1.67 | 1.28 | 0.00 | 1.76 | 0.17 | 1.62 | 1.22 | 1.53 | 1.44 | 1.24 | 1.66 |
| **K2O** | 3.09 | 4.90 | 0.04 | 0.03 | 0.02 | 0.02 | 0.03 | 0.00 | 0.05 | 0.04 | 0.03 | 0.03 | 0.02 | 0.03 | 0.15 | 0.02 |
| **P2O5** | 0.072 | 0.320 | 0.013 | 0.006 | 0.013 | 0.013 | 0.011 | 0.021 | 0.006 | 0.009 | 0.001 | 0.008 | 0.006 | 0.013 | 0.001 | 0.010 |
| **BaO** | 0.107 | 0.751 | 0.000 | 0.006 | 0.004 | 0.004 | 0.002 | 0.002 | 0.002 | 0.003 | 0.006 | 0.001 | 0.000 | 0.003 | 0.003 | 0.000 |
| **Cr2O3** | 0.022 | 0.000 | 0.165 | 0.243 | 0.113 | 0.113 | 0.159 | 0.013 | 0.006 | 0.053 | 0.127 | 0.214 | 0.253 | 0.080 | 0.001 | 0.008 |
| **NiO** | 0.010 | 0.000 | 0.053 | 0.040 | 0.017 | 0.017 | 0.125 | 0.401 | 0.079 | 0.105 | 0.058 | 0.170 | 0.018 | 0.039 | 0.004 | 0.005 |
| **Total** | 100.14 | 98.89 | 99.87 | 99.97 | 99.84 | 100.24 | 99.96 | 99.38 | 99.67 | 99.33 | 99.32 | 99.72 | 99.66 | 99.12 | 99.70 | 99.48 |
| **mg#** | 17.76 | 4.86 | 67.11 | 68.87 | 67.79 | 67.79 | 68.23 | 65.61 | 70.35 | 70.76 | 69.71 | 68.41 | 71.15 | 68.70 | 40.97 | 52.61 |
| **LOI** | 2.36 | -0.55 | N/A | N/A | N/A | N/A | 6.62 | 11.79 | 5.28 | 9.76 | 3.37 | 6.48 | 0.82 | 3.49 | 0.82 | 0.71 |
| **Rb** | 52.1 | 51.0 | | | | | 0.8 | 0.2 | 0.8 | 1.5 | 0.6 | 0.6 | 0.7 | 0.4 | 6.8 | 0.7 |
| **Sr** | 222.9 | 203.3 | | | | | 212.6 | 3.4 | 291.5 | 99.5 | 220.1 | 176.9 | 177.6 | 182.9 | 143.2 | 141.7 |
| **Y** | 24.1 | 23.7 | | | | | 1.0 | 0.7 | 0.4 | 1.6 | 2.2 | 0.7 | 6.1 | 3.7 | 2.3 | 1.2 |
| **Zr** | 191.2 | 2226.8 | | | | | 1.0 | 2.8 | -0.6 | 3.5 | 3.1 | 0.7 | 8.9 | 5.3 | 1.8 | 1.3 |
| **Nb** | 14.4 | 7.1 | | | | | 0.0 | 0.2 | 0.1 | 0.1 | 0.1 | 0.1 | 0.3 | 0.0 | 0.0 | 0.1 |
| **Zn** | 136.7 | 75.0 | | | | | 33.9 | 81.8 | 28.1 | 51.1 | 27.2 | 43.3 | 17.3 | 39.5 | 83.2 | 47.3 |
| **Cu** | 3.8 | 12.2 | | | | | 187.1 | 1626.2 | 356.5 | 128.4 | 89.2 | 265.5 | 126.1 | 13.5 | 93.8 | 171.0 |
| **Ni** | 67.7 | 7.8 | | | | | 805.6 | 3081.2 | 514.3 | 737.0 | 398.0 | 1077.7 | 125.0 | 277.8 | 37.5 | 43.4 |
| **Cr** | 150.6 | 3.9 | | | | | 918.7 | 90.7 | 52.5 | 349.6 | 769.5 | 1154.2 | 1942.4 | 545.4 | 16.7 | 68.5 |
| **V** | 127.3 | 0.0 | | | | | 22.0 | 16.9 | 5.1 | 29.7 | 45.7 | 26.1 | 172.9 | 108.4 | 287.0 | 168.9 |
| **Ba** | 831.6 | 6393.2 | | | | | 12.7 | 3.0 | 15.0 | 17.8 | 12.2 | 9.5 | 13.5 | 12.4 | 18.0 | 3.3 |
| **Sc** | 29.6 | 101.5 | | | | | 8.3 | 9.9 | 6.6 | 15.8 | 16.2 | 8.9 | 40.6 | 24.9 | 66.4 | 55.0 |
| **La** | 54.5 | 31.2 | | | | | | | | | | | | | 0.5 | |
| **Ce** | 104.4 | 66.8 | | | | | | | | | | | | | -1.1 | |
| **Nd** | 44.5 | 34.1 | | | | | | | | | | | | | -0.8 | |

| | MS1514 | MS1515 | MS1519 | MS1520 | MS1523a | MS1524 | 773C | MS1526a | MS1526c | MS1527b | MS1528 | MS1531 | MS1533 | MS1535 | MS1537 | MS1500 |
|---|---|---|---|---|---|---|---|---|---|---|---|---|---|---|---|---|
| **SiO2** | 46.45 | 45.53 | 43.87 | 42.94 | 47.25 | 44.63 | 49.76 | 46.60 | 49.76 | 44.75 | 46.14 | 45.53 | 45.25 | 50.07 | 50.97 | 52.64 |
| **TiO2** | 0.20 | 0.01 | 1.24 | 0.02 | 0.07 | 0.02 | 0.30 | 0.01 | 0.01 | 0.02 | 0.02 | 0.01 | 0.02 | 1.33 | 1.42 | 0.42 |
| **Al2O3** | 16.09 | 0.84 | 15.70 | 3.10 | 14.95 | 2.42 | 20.87 | 0.74 | 0.75 | 1.27 | 0.73 | 1.12 | 1.97 | 13.99 | 13.74 | 8.24 |
| **Fe2O3** | 13.08 | 9.38 | 13.19 | 10.73 | 3.34 | 10.65 | 3.77 | 8.02 | 6.25 | 9.46 | 8.93 | 8.96 | 9.20 | 15.02 | 14.86 | 5.94 |
| **MnO** | 0.20 | 0.13 | 0.22 | 0.13 | 0.08 | 0.13 | 0.07 | 0.13 | 0.09 | 0.09 | 0.17 | 0.12 | 0.11 | 0.22 | 0.21 | 0.25 |
| **MgO** | 9.70 | 43.42 | 7.51 | 42.20 | 11.49 | 41.01 | 7.70 | 40.49 | 27.85 | 43.64 | 43.33 | 43.88 | 41.94 | 5.12 | 5.18 | 10.26 |
| **CaO** | 12.50 | 0.01 | 17.40 | 0.01 | 22.56 | 0.10 | 14.88 | 3.28 | 14.78 | 0.05 | 0.05 | 0.05 | 0.89 | 10.29 | 9.29 | 21.56 |
| **Na2O** | 1.52 | 0.00 | 0.60 | 0.03 | 0.25 | 0.04 | 1.86 | 0.00 | 0.00 | 0.00 | 0.00 | 0.04 | 0.00 | 3.19 | 3.40 | 0.72 |
| **K2O** | 0.05 | 0.00 | 0.05 | 0.00 | 0.06 | 0.00 | 0.07 | 0.01 | 0.00 | 0.00 | 0.01 | 0.00 | 0.00 | 0.29 | 0.26 | 0.42 |
| **P2O5** | 0.000 | 0.000 | 0.106 | 0.000 | 0.000 | 0.009 | 0.006 | 0.002 | 0.000 | 0.003 | 0.001 | 0.000 | 0.005 | 0.123 | 0.100 | 0.043 |
| **BaO** | 0.003 | 0.001 | 0.012 | 0.001 | 0.006 | 0.004 | 0.002 | 0.010 | 0.000 | 0.002 | 0.000 | 0.000 | 0.000 | 0.006 | 0.023 | 0.011 |
| **Cr2O3** | 0.014 | 0.625 | 0.001 | 0.785 | 0.242 | 0.484 | 0.229 | 0.566 | 0.432 | 0.481 | 0.383 | 0.430 | 0.440 | 0.005 | 0.003 | 0.006 |
| **NiO** | 0.006 | 0.340 | 0.001 | 0.317 | 0.036 | 0.323 | 0.019 | 0.401 | 0.265 | 0.327 | 0.354 | 0.320 | 0.315 | 0.001 | 0.000 | 0.004 |
| **Total** | 99.80 | 99.30 | 99.88 | 99.11 | 100.05 | 99.02 | 99.28 | 99.27 | 99.50 | 99.27 | 99.37 | 99.71 | 99.39 | 99.65 | 99.43 | 100.50 |
| **mg#** | 42.60 | 82.23 | 36.28 | 79.73 | 77.48 | 79.38 | 67.13 | 83.47 | 81.67 | 82.18 | 82.91 | 83.04 | 82.01 | 25.42 | 25.85 | 63.33 |
| **LOI** | 0.75 | 13.20 | 0.40 | 11.98 | 1.96 | 11.79 | 1.33 | 11.35 | 5.64 | 13.08 | 12.80 | 13.08 | 12.55 | 0.81 | 0.15 | 0.48 |
| **Rb** | 3.7 | 0.0 | 0.5 | 0.1 | 1.0 | 0.0 | 1.6 | 0.1 | 0.1 | 0.4 | -0.1 | 0.1 | 0.2 | 5.4 | 2.7 | 13.0 |
| **Sr** | 216.5 | 1.0 | 94.5 | 1.0 | 89.2 | 2.2 | 223.6 | 6.7 | 38.0 | 1.6 | 2.4 | 1.2 | 2.7 | 402.8 | 268.9 | 173.3 |
| **Y** | 1.5 | 0.2 | 25.4 | 0.3 | 2.7 | 1.4 | 6.6 | 0.2 | 1.0 | 0.1 | 0.2 | 0.1 | 0.7 | 31.8 | 29.0 | 14.1 |
| **Zr** | 0.0 | 1.5 | 55.4 | 1.9 | 1.8 | 2.1 | 9.9 | 2.2 | 2.7 | 2.8 | 1.6 | 1.3 | 1.4 | 65.0 | 63.6 | 195.8 |
| **Nb** | -0.2 | 0.1 | 1.3 | 0.0 | 0.1 | 0.0 | 0.2 | 0.3 | 0.5 | 1.4 | 0.1 | 0.1 | 0.2 | 1.0 | 1.3 | 4.4 |
| **Zn** | 68.6 | 44.5 | 74.1 | 38.2 | 13.2 | 35.5 | 18.3 | 116.3 | 63.0 | 24.6 | 36.5 | 39.7 | 40.4 | 98.3 | 104.2 | 106.3 |
| **Cu** | 110.8 | 0.5 | 7.8 | 209.5 | 8.1 | 25.3 | 79.3 | 124.8 | 61.4 | 1.1 | 5.5 | 0.6 | 5.7 | 144.2 | 53.1 | 5.5 |
| **Ni** | 48.6 | 2468.0 | 17.2 | 2464.2 | 261.8 | 2296.0 | 129.3 | 2725.2 | 2077.2 | 2234.1 | 2568.7 | 2363.8 | 2343.9 | 26.2 | 20.5 | 30.2 |
| **Cr** | 101.2 | 3272.7 | 7.2 | 4833.8 | 1945.5 | 2974.9 | 1741.8 | 3047.7 | 2987.9 | 2785.1 | 1887.2 | 2948.3 | 3415.2 | 38.7 | 24.1 | 45.3 |
| **V** | 459.0 | 37.8 | 449.0 | 40.4 | 111.4 | 27.1 | 152.0 | 23.6 | 38.5 | 31.5 | 28.2 | 39.9 | 59.2 | 479.3 | 500.6 | 145.5 |
| **Ba** | 11.9 | 5.1 | 7.6 | 0.7 | 8.5 | 0.8 | 20.6 | 65.9 | 13.1 | 7.3 | 16.4 | 5.3 | 3.5 | 84.9 | 161.2 | 65.6 |
| **Sc** | 60.3 | 10.5 | 46.5 | 6.2 | 33.1 | 11.2 | 33.0 | 4.8 | 5.1 | 11.5 | 9.9 | 10.3 | 12.0 | 50.7 | 50.6 | 11.0 |
| **La** | 0.3 | | | | | | | | | | | | | 2.4 | 2.6 | 7.1 |
| **Ce** | 1.4 | | | | | | | | | | | | | 5.8 | 8.3 | 19.6 |
| **Nd** | 0.7 | | | | | | | | | | | | | 8.3 | 8.0 | 11.7 |

| | MS1540 | MS1542 | MS1544 | MS1545 | 110P | 137P | 220A | Ab5790 | MS1501a | MS1501b | MS1502 | MS1505a | MS1506 | MS1510a | Ab7800 | Ab94 |
|---|---|---|---|---|---|---|---|---|---|---|---|---|---|---|---|---|
| **SiO2** | 44.86 | 45.10 | 50.34 | 50.60 | 49.96 | 44.77 | 49.30 | 47.43 | 47.28 | 46.86 | 49.39 | 48.22 | 48.41 | 46.48 | 47.74 | 52.63 |
| **TiO2** | 0.02 | 0.03 | 2.23 | 1.87 | 0.28 | 0.07 | 0.29 | 0.03 | 0.18 | 0.05 | 0.11 | 0.08 | 0.10 | 0.01 | 3.02 | 1.30 |
| **Al2O3** | 0.59 | 1.21 | 15.29 | 14.53 | 17.17 | 13.25 | 30.74 | 1.38 | 22.59 | 29.80 | 16.69 | 19.02 | 15.82 | 0.44 | 14.14 | 16.52 |
| **Fe2O3** | 9.03 | 8.89 | 11.11 | 12.60 | 6.28 | 12.95 | 1.54 | 10.88 | 9.44 | 3.66 | 11.20 | 10.76 | 10.93 | 8.36 | 17.01 | 9.87 |
| **MnO** | 0.48 | 0.07 | 0.21 | 0.22 | 0.13 | 0.14 | 0.02 | 0.16 | 0.15 | 0.06 | 0.19 | 0.19 | 0.18 | 0.11 | 0.23 | 0.17 |
| **MgO** | 43.99 | 44.45 | 7.40 | 6.50 | 12.68 | 20.86 | 1.67 | 33.88 | 5.66 | 2.27 | 8.77 | 9.38 | 9.89 | 44.42 | 4.31 | 5.95 |
| **CaO** | 0.01 | 0.02 | 11.17 | 10.74 | 11.74 | 6.28 | 12.64 | 5.48 | 13.97 | 15.79 | 12.90 | 11.55 | 13.33 | 0.03 | 9.94 | 9.17 |
| **Na2O** | 0.09 | 0.00 | 2.08 | 2.17 | 1.79 | 1.14 | 2.79 | 0.00 | 1.34 | 1.59 | 1.05 | 1.41 | 0.84 | 0.00 | 2.40 | 2.65 |
| **K2O** | 0.00 | 0.00 | 0.19 | 0.25 | 0.13 | 0.05 | 0.65 | 0.00 | 0.01 | 0.00 | 0.00 | 0.06 | 0.02 | 0.00 | 0.68 | 1.31 |
| **P2O5** | 0.002 | 0.001 | 0.214 | 0.320 | 0.002 | 0.014 | 0.011 | 0.001 | 0.005 | 0.006 | 0.000 | 0.005 | 0.008 | 0.004 | 0.297 | 0.192 |
| **BaO** | 0.034 | 0.001 | 0.032 | 0.027 | 0.006 | 0.006 | 0.011 | 0.001 | 0.002 | 0.003 | 0.003 | 0.007 | 0.003 | 0.000 | 0.070 | 0.107 |
| **Cr2O3** | 0.474 | 0.390 | 0.032 | 0.016 | 0.077 | 0.012 | 0.009 | 0.672 | 0.004 | 0.001 | 0.022 | 0.005 | 0.039 | 0.247 | 0.001 | 0.012 |
| **NiO** | 0.397 | 0.334 | 0.004 | 0.004 | 0.006 | 0.113 | 0.002 | 0.115 | 0.002 | 0.002 | 0.008 | 0.004 | 0.009 | 0.296 | 0.001 | 0.003 |
| **Total** | 99.06 | 99.78 | 100.23 | 99.79 | 100.16 | 99.52 | 99.65 | 99.24 | 100.61 | 100.09 | 100.30 | 100.67 | 99.53 | 99.86 | 99.77 | 99.75 |
| **mg#** | 82.97 | 83.33 | 39.98 | 34.03 | 66.88 | 61.70 | 52.02 | 75.69 | 37.48 | 38.28 | 43.92 | 46.57 | 47.50 | 84.16 | 20.22 | 37.61 |
| **LOI** | 12.91 | 12.84 | 0.42 | 0.29 | 2.14 | 7.17 | 1.54 | 7.86 | 0.66 | 0.56 | 0.62 | 1.33 | 0.58 | 13.06 | -0.45 | 0.51 |
| **Rb** | 0.1 | 0.1 | 2.3 | 2.8 | 1.8 | 71.5 | 9.8 | 0.3 | 0.6 | 0.1 | 0.4 | 0.6 | 0.3 | -0.1 | | 28.6 |
| **Sr** | 3.4 | 2.2 | 264.4 | 278.0 | 203.4 | 93.6 | 1211.3 | 6.1 | 202.6 | 308.4 | 152.6 | 177.6 | 125.6 | 0.5 | | 261.4 |
| **Y** | 1.4 | 0.6 | 23.8 | 32.5 | 5.7 | 15.8 | 0.4 | 0.5 | 0.8 | 0.4 | 3.2 | 1.0 | 1.8 | 0.2 | | 31.2 |
| **Zr** | 2.1 | 2.5 | 53.4 | 23.8 | 4.1 | 193.3 | 5.9 | 2.1 | 0.3 | -0.7 | 1.1 | 0.3 | 1.5 | 2.0 | | 167.0 |
| **Nb** | 0.1 | 0.1 | 8.6 | 9.0 | 0.1 | 10.1 | 2.1 | 0.1 | 0.0 | 0.0 | -0.1 | -0.2 | 0.0 | 0.2 | | 15.8 |
| **Zn** | 44.0 | 36.1 | 81.4 | 112.8 | 35.3 | 62.1 | 8.2 | 38.8 | 43.6 | 15.7 | 83.5 | 51.5 | 48.6 | 27.7 | | 109.6 |
| **Cu** | 2.0 | 1.6 | 25.4 | 25.5 | 14.0 | 30.3 | 3.6 | 6.7 | 23.8 | 5.0 | 159.8 | 169.6 | 109.5 | 4.4 | | 15.3 |
| **Ni** | 2888.0 | 2394.8 | 37.5 | 26.8 | 51.7 | 178.0 | 13.5 | 894.9 | 18.4 | 3.3 | 68.5 | 32.4 | 63.1 | 2128.8 | | 29.4 |
| **Cr** | 2203.1 | 2382.5 | 241.6 | 126.1 | 585.0 | 420.5 | 26.4 | 4169.4 | 35.1 | 10.2 | 165.8 | 14.3 | 304.5 | 1755.0 | | 92.9 |
| **V** | 19.1 | 32.2 | 343.6 | 258.1 | 431.1 | 112.9 | 22.5 | 74.0 | 229.4 | 61.0 | 251.4 | 247.0 | 187.3 | 20.0 | | 190.4 |
| **Ba** | 243.6 | 4.7 | 178.5 | 178.7 | 31.8 | 414.4 | 122.5 | 2.8 | 15.7 | 19.0 | 3.1 | 39.2 | 17.2 | 0.7 | | 982.3 |
| **Sc** | 4.7 | 9.2 | 55.9 | 51.8 | 47.3 | 21.0 | 9.7 | 30.8 | 43.6 | 18.9 | 59.5 | 43.6 | 61.9 | 6.7 | | 34.0 |
| **La** | | | 4.7 | 10.1 | | 14.3 | 4.7 | | | | | | | | | 48.9 |
| **Ce** | | | 18.1 | 27.1 | | 32.3 | 9.8 | | | | | | | | | 97.3 |
| **Nd** | | | 13.8 | 18.9 | | 14.1 | 2.0 | | | | | | | | | 52.0 |

| | Ab3759 | Ab3794 | MS1598 | MS1601 | MS1604 | MS1605 | MS1608 | MS1611 | MS1612a | MS1614 | 67P | 77P | 725C | 733C | 741C | 758C |
|---|---|---|---|---|---|---|---|---|---|---|---|---|---|---|---|---|
| **SiO2** | 52.48 | 56.04 | 44.88 | 44.56 | 44.41 | 44.02 | 45.33 | 49.27 | 46.07 | 46.55 | 46.30 | 48.35 | 50.06 | 47.61 | 47.24 | 44.34 |
| **TiO2** | 1.61 | 1.25 | 0.01 | 0.01 | 0.01 | 0.01 | 0.01 | 3.34 | 3.44 | 2.72 | 3.12 | 2.89 | 2.42 | 3.05 | 3.15 | 3.29 |
| **Al2O3** | 15.47 | 14.85 | 0.63 | 0.53 | 0.95 | 0.78 | 0.23 | 16.86 | 18.45 | 18.64 | 19.21 | 19.32 | 20.98 | 18.46 | 17.67 | 17.09 |
| **Fe2O3** | 10.67 | 9.33 | 9.07 | 8.85 | 9.64 | 9.11 | 9.42 | 14.49 | 14.45 | 15.06 | 15.65 | 11.67 | 10.32 | 14.89 | 15.33 | 16.58 |
| **MnO** | 0.16 | 0.15 | 0.19 | 0.12 | 0.13 | 0.11 | 0.11 | 0.25 | 0.18 | 0.23 | 0.18 | 0.14 | 0.15 | 0.20 | 0.24 | 0.25 |
| **MgO** | 6.52 | 5.66 | 44.48 | 45.01 | 44.53 | 45.28 | 44.04 | 5.63 | 4.18 | 3.22 | 4.22 | 4.54 | 3.41 | 4.00 | 4.31 | 3.94 |
| **CaO** | 10.40 | 7.91 | 0.01 | 0.11 | 0.01 | 0.01 | 0.01 | 7.35 | 8.93 | 9.87 | 8.01 | 9.45 | 9.16 | 8.61 | 8.44 | 9.22 |
| **Na2O** | 2.27 | 2.87 | 0.03 | 0.00 | 0.03 | 0.00 | 0.00 | 2.27 | 2.71 | 2.75 | 2.76 | 2.83 | 3.07 | 2.59 | 2.73 | 2.55 |
| **K2O** | 0.83 | 1.95 | 0.00 | 0.00 | 0.00 | 0.00 | 0.00 | 0.36 | 0.77 | 0.59 | 0.51 | 0.50 | 0.27 | 0.49 | 0.61 | 1.42 |
| **P2O5** | 0.192 | 0.166 | 0.001 | 0.000 | 0.001 | 0.001 | 0.001 | 0.061 | 0.335 | 0.277 | 0.026 | 0.124 | 0.039 | 0.277 | 0.103 | 1.519 |
| **BaO** | 0.040 | 0.042 | 0.006 | 0.000 | 0.000 | 0.000 | 0.002 | 0.082 | 0.116 | 0.113 | 0.083 | 0.086 | 0.072 | 0.079 | 0.151 | 0.039 |
| **Cr2O3** | 0.017 | 0.008 | 0.403 | 0.425 | 0.509 | 0.375 | 0.409 | 0.004 | 0.000 | 0.000 | 0.010 | 0.005 | 0.005 | 0.001 | 0.003 | 0.004 |
| **NiO** | 0.001 | 0.001 | 0.351 | 0.329 | 0.331 | 0.322 | 0.354 | 0.002 | 0.002 | 0.002 | 0.002 | 0.001 | 0.000 | 0.000 | 0.001 | 0.001 |
| **Total** | 100.60 | 100.17 | 99.26 | 99.19 | 99.71 | 99.32 | 99.14 | 99.88 | 99.52 | 99.90 | 99.99 | 99.81 | 99.88 | 100.18 | 99.82 | 100.20 |
| **mg#** | 37.93 | 37.76 | 83.06 | 83.57 | 82.20 | 83.25 | 82.38 | 27.98 | 22.44 | 17.61 | 21.24 | 28.01 | 24.84 | 21.18 | 21.95 | 19.20 |
| **LOI** | 0.06 | 1.90 | 13.04 | 12.98 | 13.21 | 13.27 | 12.86 | 3.41 | 0.88 | 0.57 | 0.84 | -0.22 | 0.62 | 0.42 | 0.44 | 0.72 |
| **Rb** | 19.6 | 69.6 | 0.1 | 0.1 | -0.1 | 0.0 | 0.3 | 9.2 | 21.5 | 13.0 | 10.9 | 6.0 | 3.5 | 18.4 | 20.4 | 75.5 |
| **Sr** | 294.4 | 141.5 | 1.7 | 0.6 | 0.7 | 0.7 | 0.9 | 373.4 | 534.6 | 517.4 | 512.6 | 456.3 | 517.3 | 485.1 | 512.0 | 547.7 |
| **Y** | 28.6 | 21.0 | 0.0 | 0.1 | 0.1 | 0.1 | 0.0 | 5.6 | 7.9 | 8.6 | 1.7 | 9.8 | 3.2 | 7.0 | 7.8 | 30.4 |
| **Zr** | 140.0 | 114.0 | 1.6 | 1.6 | 1.7 | 1.6 | 1.7 | 69.9 | 64.3 | 93.6 | 30.5 | 204.4 | 35.5 | 38.3 | 118.3 | 75.9 |
| **Nb** | 10.6 | 10.2 | 0.0 | 0.1 | 0.2 | 0.1 | 0.1 | 9.5 | 6.5 | 5.7 | 4.9 | 14.9 | 4.7 | 5.5 | 8.9 | 8.2 |
| **Zn** | 79.6 | 67.6 | 32.7 | 35.8 | 36.9 | 34.7 | 26.2 | 90.8 | 84.5 | 70.1 | 85.4 | 74.1 | 59.8 | 88.3 | 105.7 | 111.9 |
| **Cu** | 12.5 | 7.3 | 0.0 | 1.5 | 0.6 | 0.3 | 0.0 | 18.3 | 17.0 | 24.0 | 23.7 | 22.7 | 15.1 | 12.8 | 11.9 | 30.2 |
| **Ni** | 12.1 | 7.1 | 2574.8 | 2430.2 | 2181.8 | 2346.0 | 2452.7 | 21.4 | 20.2 | 23.4 | 27.0 | 13.6 | 9.3 | 8.9 | 9.3 | 11.8 |
| **Cr** | 128.7 | 68.7 | 2356.2 | 2154.9 | 2702.0 | 2069.0 | 1822.8 | 38.4 | 10.6 | 10.7 | 103.9 | 40.6 | 37.6 | 10.6 | 13.8 | 36.8 |
| **V** | 249.6 | 192.8 | 32.3 | 29.3 | 33.7 | 24.2 | 13.1 | 242.9 | 260.1 | 206.0 | 229.5 | 408.9 | 338.1 | 322.9 | 515.0 | 247.4 |
| **Ba** | 311.1 | 284.9 | 46.1 | 3.1 | 4.7 | 5.3 | 8.7 | 483.9 | 832.6 | 884.9 | 600.6 | 714.5 | 495.4 | 529.9 | 1249.0 | 242.9 |
| **Sc** | 35.5 | 33.5 | 8.8 | 9.2 | 11.5 | 8.9 | 6.7 | 38.3 | 39.1 | 68.8 | 23.5 | 24.0 | 28.5 | 33.7 | 46.0 | 68.7 |
| **La** | 37.5 | 21.7 | | | | | | 1.7 | 6.5 | 7.8 | 0.1 | 16.1 | 3.7 | 1.4 | 2.0 | 12.8 |
| **Ce** | 73.7 | 45.5 | | | | | | 5.2 | 13.5 | 16.3 | 1.4 | 33.0 | 6.3 | 6.6 | 7.8 | 41.3 |
| **Nd** | 35.6 | 21.9 | | | | | | 2.8 | 7.3 | 11.4 | -0.4 | 12.9 | 2.0 | 4.0 | 3.7 | 27.9 |

| | MS1615 | MS1617b | MS1618 | MS1620 | MS1621 | MS1622 | MS1623 | MS1625 | MS1627 | MS1630 | MS1631 | CLW101 | CLW102 | CLW218 | CLW219 | CLW220 |
|---|---|---|---|---|---|---|---|---|---|---|---|---|---|---|---|---|
| **SiO2** | 41.41 | 45.37 | 46.63 | 44.46 | 39.98 | 50.52 | 46.32 | 43.54 | 47.86 | 43.54 | 44.01 | 44.24 | 49.77 | 50.20 | 45.52 | 43.78 |
| **TiO2** | 6.84 | 0.09 | 0.04 | 0.07 | 1.62 | 0.17 | 0.12 | 0.03 | 1.47 | 0.03 | 0.26 | 1.49 | 1.26 | 0.49 | 1.63 | 1.21 |
| **Al2O3** | 10.95 | 2.77 | 23.17 | 2.66 | 12.49 | 5.79 | 3.31 | 2.00 | 14.28 | 1.94 | 3.00 | 19.21 | 18.28 | 12.16 | 19.13 | 18.04 |
| **Fe2O3** | 19.47 | 9.32 | 5.98 | 8.65 | 17.85 | 8.39 | 9.28 | 10.36 | 14.59 | 9.76 | 9.89 | 14.20 | 12.70 | 11.26 | 14.30 | 15.27 |
| **MnO** | 0.23 | 0.11 | 0.10 | 0.13 | 0.15 | 0.13 | 0.11 | 0.11 | 0.20 | 0.11 | 0.14 | 0.15 | 0.15 | 0.17 | 0.16 | 0.17 |
| **MgO** | 7.74 | 40.31 | 8.72 | 41.15 | 16.64 | 27.26 | 37.45 | 42.95 | 7.54 | 44.03 | 40.16 | 6.01 | 5.21 | 12.41 | 5.33 | 6.95 |
| **CaO** | 9.91 | 1.27 | 12.69 | 1.79 | 9.03 | 7.04 | 2.41 | 0.09 | 10.73 | 0.01 | 1.82 | 12.02 | 9.75 | 12.40 | 10.38 | 11.10 |
| **Na2O** | 2.54 | 0.07 | 2.41 | 0.32 | 1.61 | 0.19 | 0.11 | 0.04 | 2.51 | 0.00 | 0.00 | 1.09 | 1.54 | 0.21 | 1.63 | 1.29 |
| **K2O** | 0.33 | 0.01 | 0.12 | 0.01 | 0.21 | 0.01 | 0.00 | 0.00 | 0.36 | 0.00 | 0.00 | 0.83 | 0.71 | 0.76 | 0.86 | 0.97 |
| **P2O5** | 0.051 | 0.010 | 0.004 | 0.003 | 0.039 | 0.058 | 0.002 | 0.003 | 0.163 | 0.000 | 0.010 | 0.501 | 0.492 | 0.062 | 0.527 | 0.403 |
| **BaO** | 0.054 | 0.002 | 0.005 | 0.000 | 0.019 | 0.002 | 0.002 | 0.000 | 0.090 | 0.000 | 0.000 | 0.036 | 0.058 | 0.026 | 0.041 | 0.055 |
| **Cr2O3** | 0.013 | 0.378 | 0.001 | 0.463 | 0.007 | 0.299 | 0.389 | 0.411 | 0.021 | 0.531 | 0.462 | 0.007 | 0.003 | 0.054 | 0.005 | 0.004 |
| **NiO** | 0.012 | 0.278 | 0.025 | 0.267 | 0.023 | 0.163 | 0.270 | 0.349 | 0.007 | 0.367 | 0.339 | 0.003 | 0.003 | 0.008 | 0.002 | 0.003 |
| **Total** | 99.47 | 99.32 | 99.86 | 99.23 | 99.61 | 99.55 | 99.11 | 99.12 | 99.70 | 99.42 | 99.29 | 99.74 | 99.86 | 100.13 | 99.46 | 99.17 |
| **mg#** | 28.45 | 81.22 | 59.32 | 82.63 | 48.25 | 76.47 | 80.14 | 80.57 | 34.07 | 81.86 | 80.24 | 29.74 | 29.09 | 52.43 | 27.15 | 31.28 |
| **LOI** | 0.53 | 10.83 | 0.90 | 11.10 | 2.72 | 5.15 | 9.80 | 11.87 | 0.74 | 12.17 | 11.14 | 1.46 | 1.92 | 1.88 | 1.49 | 1.41 |
| **Rb** | 4.2 | 0.6 | 3.6 | 0.1 | 1.6 | 0.1 | 0.8 | 0.0 | 18.4 | 0.1 | 0.3 | 18.1 | 18.4 | 29.9 | 22.3 | 21.9 |
| **Sr** | 279.2 | 16.6 | 366.7 | 12.3 | 205.1 | 46.8 | 19.4 | 0.6 | 177.1 | 0.7 | 9.7 | 820.6 | 619.7 | 440.1 | 649.8 | 877.7 |
| **Y** | 19.5 | 2.2 | 0.2 | 2.2 | 21.4 | 7.5 | 3.2 | 0.7 | 35.6 | 1.0 | 3.6 | 39.2 | 33.7 | 11.4 | 30.3 | 18.3 |
| **Zr** | 53.9 | 2.9 | -1.7 | 2.4 | 43.4 | 9.6 | 4.8 | 1.9 | 85.8 | 2.0 | 7.0 | 62.7 | 153.2 | 29.8 | 323.1 | 33.4 |
| **Nb** | 38.7 | 0.7 | 0.0 | 0.3 | 8.0 | 1.2 | 0.6 | 0.1 | 3.1 | 0.1 | 0.2 | 8.7 | 9.4 | 1.9 | 10.2 | 4.5 |
| **Zn** | 161.7 | 53.1 | 31.4 | 49.8 | 104.4 | 58.1 | 57.5 | 41.2 | 152.4 | 34.8 | 55.5 | 93.4 | 86.9 | 77.8 | 105.4 | 100.7 |
| **Cu** | 24.2 | 3.6 | 7.7 | 2.9 | 102.7 | 44.4 | 1.2 | 29.6 | 70.5 | 16.4 | 30.8 | 40.7 | 43.3 | 86.0 | 38.4 | 81.2 |
| **Ni** | 119.6 | 1997.1 | 187.2 | 1989.9 | 186.8 | 1245.8 | 1973.4 | 2604.8 | 56.7 | 2707.8 | 2434.3 | 20.8 | 18.2 | 61.2 | 22.4 | 25.0 |
| **Cr** | 91.1 | 3083.0 | 32.5 | 3526.1 | 33.0 | 2339.1 | 3201.2 | 2551.5 | 172.1 | 3192.1 | 3352.0 | 35.4 | 31.8 | 416.6 | 48.2 | 25.4 |
| **V** | 552.0 | 59.8 | 16.9 | 57.0 | 710.4 | 144.0 | 76.2 | 44.1 | 397.0 | 55.0 | 137.7 | 504.9 | 318.7 | 268.5 | 364.4 | 451.8 |
| **Ba** | 164.2 | 9.2 | 42.9 | 5.8 | 73.9 | 9.2 | 5.5 | 3.4 | 30.2 | 2.7 | 3.6 | 274.0 | 510.3 | 203.8 | 263.9 | 452.5 |
| **Sc** | 55.7 | 15.4 | 7.6 | 14.6 | 67.2 | 14.3 | 14.8 | 10.3 | 46.0 | 11.6 | 19.1 | 63.6 | 46.2 | 62.2 | 56.6 | 45.2 |
| **La** | 0.3 | | 2.0 | | 8.4 | | | | 3.7 | | | 32.7 | 30.4 | 10.5 | 28.2 | 29.5 |
| **Ce** | 10.9 | | 1.0 | | 18.3 | | | | 14.0 | | | 87.7 | 69.0 | 26.3 | 67.4 | 66.6 |
| **Nd** | 9.7 | | 1.1 | | 14.1 | | | | 10.1 | | | 61.3 | 41.1 | 14.8 | 42.1 | 35.9 |

| | CLW210 | CLW211 | CLW212 | CLW215 | CLW216 | CLW103 | CLW104 | CLW105 | CLW106 | CLW107 | CLW108 | CLW109 | CLW110 | CLW201 | CLW203 | CLW205 |
|---|---|---|---|---|---|---|---|---|---|---|---|---|---|---|---|---|
| **SiO2** | 51.34 | 49.50 | 45.88 | 49.43 | 48.20 | 44.41 | 53.01 | 49.23 | 48.01 | 48.91 | 55.19 | 44.04 | 44.41 | 51.20 | 51.91 | 45.96 |
| **TiO2** | 1.15 | 0.32 | 0.40 | 0.40 | 0.41 | 0.81 | 0.33 | 0.22 | 0.15 | 0.31 | 0.51 | 1.01 | 1.36 | 0.37 | 0.22 | 0.63 |
| **Al2O3** | 18.20 | 17.34 | 18.22 | 14.82 | 15.08 | 18.50 | 5.91 | 17.47 | 17.37 | 5.16 | 10.15 | 19.48 | 13.14 | 16.92 | 18.98 | 17.40 |
| **Fe2O3** | 12.57 | 8.47 | 9.06 | 8.63 | 8.83 | 14.33 | 10.53 | 7.98 | 11.04 | 11.40 | 10.72 | 14.92 | 18.33 | 9.43 | 8.84 | 15.31 |
| **MnO** | 0.17 | 0.16 | 0.16 | 0.15 | 0.15 | 0.16 | 0.17 | 0.14 | 0.17 | 0.17 | 0.18 | 0.17 | 0.20 | 0.14 | 0.17 | 0.16 |
| **MgO** | 5.29 | 11.11 | 8.47 | 11.92 | 12.29 | 8.12 | 18.07 | 11.32 | 13.15 | 21.67 | 12.20 | 6.40 | 8.80 | 11.68 | 9.73 | 10.52 |
| **CaO** | 9.72 | 12.16 | 13.16 | 12.99 | 13.34 | 12.05 | 10.31 | 12.50 | 9.36 | 10.86 | 9.31 | 12.69 | 12.36 | 7.20 | 5.65 | 7.02 |
| **Na2O** | 0.85 | 0.87 | 0.86 | 0.87 | 0.78 | 0.49 | 0.27 | 0.63 | 0.37 | 0.48 | 1.14 | 0.83 | 0.48 | 1.31 | 2.39 | 1.70 |
| **K2O** | 0.32 | 0.58 | 2.94 | 0.65 | 0.60 | 0.98 | 0.82 | 0.40 | 0.28 | 0.46 | 0.28 | 0.20 | 0.54 | 0.98 | 1.35 | 1.04 |
| **P2O5** | 0.156 | 0.030 | 0.058 | 0.039 | 0.040 | 0.074 | 0.000 | 0.027 | 0.007 | 0.030 | 0.055 | 0.052 | 0.045 | 0.022 | 0.174 | 0.044 |
| **BaO** | 0.027 | 0.018 | 0.118 | 0.024 | 0.027 | 0.027 | 0.022 | 0.016 | 0.013 | 0.022 | 0.012 | 0.023 | 0.039 | 0.054 | 0.049 | 0.061 |
| **Cr2O3** | 0.008 | 0.046 | 0.081 | 0.082 | 0.085 | 0.006 | 0.147 | 0.027 | 0.055 | 0.223 | 0.092 | 0.004 | 0.027 | 0.043 | 0.034 | 0.016 |
| **NiO** | 0.002 | 0.012 | 0.013 | 0.013 | 0.014 | 0.005 | 0.042 | 0.009 | 0.027 | 0.055 | 0.025 | 0.001 | 0.009 | 0.018 | 0.021 | 0.011 |
| **Total** | 99.76 | 100.54 | 99.21 | 99.89 | 99.72 | 99.92 | 99.42 | 99.92 | 99.91 | 99.45 | 99.73 | 99.79 | 99.67 | 99.25 | 99.41 | 99.79 |
| **mg#** | 29.62 | 56.74 | 48.32 | 58.00 | 58.19 | 36.17 | 63.18 | 58.65 | 54.36 | 65.53 | 53.23 | 30.02 | 32.44 | 55.33 | 52.40 | 40.73 |
| **LOI** | 1.00 | 1.24 | 12.58 | 2.00 | 1.87 | 3.06 | 1.54 | 2.06 | 2.15 | 1.44 | 6.08 | 1.11 | 1.06 | 3.85 | 3.66 | 4.10 |
| **Rb** | 16.4 | 21.0 | 104.5 | 22.8 | 20.6 | 27.9 | 33.2 | 11.6 | 8.3 | 14.9 | 9.1 | 5.8 | 18.8 | 25.3 | 40.1 | 28.5 |
| **Sr** | 290.3 | 311.4 | 146.1 | 402.3 | 404.8 | 947.2 | 97.3 | 582.8 | 844.4 | 164.1 | 159.3 | 711.8 | 569.9 | 471.6 | 526.9 | 410.9 |
| **Y** | 8.4 | 6.6 | 9.1 | 9.1 | 9.0 | 6.8 | 9.2 | 5.4 | 1.6 | 8.2 | 24.5 | 8.6 | 16.5 | 9.6 | 12.6 | 7.3 |
| **Zr** | 24.5 | 22.1 | 24.6 | 24.6 | 26.1 | 8.1 | 31.3 | 7.7 | -2.1 | 40.8 | 74.2 | 14.1 | 35.2 | 44.8 | 87.4 | 21.6 |
| **Nb** | 1.9 | 1.1 | 1.6 | 0.9 | 0.9 | 1.6 | 1.4 | 0.5 | 0.0 | 2.0 | 5.1 | 1.9 | 4.1 | 3.1 | 3.1 | 2.5 |
| **Zn** | 54.8 | 57.0 | 76.5 | 58.7 | 58.6 | 79.3 | 58.7 | 46.4 | 69.8 | 61.9 | 104.4 | 86.6 | 106.3 | 64.1 | 84.8 | 108.9 |
| **Cu** | 16.1 | 51.4 | 109.1 | 89.9 | 88.2 | 99.7 | 239.8 | 51.9 | 206.2 | 95.1 | 121.2 | 31.6 | 38.1 | 71.9 | 68.1 | 123.7 |
| **Ni** | 89.7 | 87.0 | 124.4 | 105.6 | 108.3 | 39.2 | 277.2 | 64.0 | 180.6 | 391.4 | 182.0 | 9.6 | 71.8 | 135.1 | 156.1 | 82.1 |
| **Cr** | 407.4 | 364.7 | 711.1 | 677.1 | 683.2 | 42.4 | 1113.3 | 224.1 | 453.0 | 1685.1 | 756.0 | 22.4 | 170.6 | 355.5 | 292.6 | 123.4 |
| **V** | 210.2 | 192.1 | 270.2 | 248.9 | 249.9 | 546.7 | 195.4 | 129.1 | 124.0 | 167.6 | 265.1 | 471.0 | 696.9 | 198.1 | 92.5 | 475.7 |
| **Ba** | 98.6 | 147.0 | 881.8 | 182.1 | 190.6 | 210.9 | 149.5 | 80.6 | 112.3 | 179.5 | 67.5 | 119.3 | 308.3 | 313.2 | 316.4 | 399.9 |
| **Sc** | 52.6 | 49.0 | 63.6 | 62.8 | 62.6 | 43.6 | 56.9 | 42.3 | 37.8 | 50.3 | 57.2 | 43.6 | 62.8 | 35.4 | 29.8 | 33.6 |
| **La** | 4.5 | 6.7 | 10.0 | 6.8 | 4.2 | 5.5 | 7.6 | 7.3 | 3.0 | 9.3 | 13.7 | 8.6 | 9.0 | 13.0 | 21.0 | 9.8 |
| **Ce** | 12.3 | 13.2 | 14.0 | 11.7 | 16.1 | 18.0 | 16.0 | 12.7 | 4.7 | 19.1 | 39.4 | 16.7 | 25.5 | 26.9 | 38.4 | 17.1 |
| **Nd** | 9.3 | 6.9 | 7.6 | 6.9 | 10.2 | 9.7 | 12.0 | 7.1 | 2.9 | 10.9 | 26.4 | 10.1 | 16.4 | 15.7 | 17.2 | 8.4 |

| | CLW206 | CLW207 | DCD101 | DCD104 | DCD105 | DCD106 | DCD109 | DCD110 | DCD116 | DCD118 | Country Rocks: | Ab200 | Ab210 | Ab217 | 6P |
|---|---|---|---|---|---|---|---|---|---|---|---|---|---|---|---|
| **SiO2** | 49.57 | 54.06 | 44.01 | 39.19 | 47.76 | 47.11 | 47.33 | 47.68 | 47.98 | 48.70 | | 62.40 | 53.75 | 55.19 | 51.99 |
| **TiO2** | 0.33 | 0.31 | 0.05 | 0.02 | 0.20 | 0.15 | 0.04 | 0.06 | 1.13 | 0.21 | | 0.98 | 1.30 | 1.25 | 0.73 |
| **Al2O3** | 14.80 | 17.18 | 0.61 | 0.49 | 17.98 | 12.63 | 1.57 | 2.55 | 16.59 | 13.38 | | 17.94 | 23.02 | 22.09 | 19.94 |
| **Fe2O3** | 10.51 | 9.45 | 10.88 | 15.65 | 6.88 | 8.03 | 7.88 | 9.56 | 15.45 | 10.05 | | 8.65 | 11.45 | 10.61 | 6.81 |
| **MnO** | 0.19 | 0.18 | 0.10 | 0.10 | 0.11 | 0.13 | 0.13 | 0.16 | 0.19 | 0.15 | | 0.11 | 0.17 | 0.15 | 0.11 |
| **MgO** | 14.42 | 9.40 | 42.77 | 41.70 | 10.55 | 16.94 | 32.02 | 28.91 | 9.11 | 13.00 | | 2.95 | 3.40 | 3.63 | 7.35 |
| **CaO** | 8.17 | 6.85 | 0.36 | 1.60 | 14.28 | 13.77 | 10.37 | 9.79 | 7.74 | 13.95 | | 1.70 | 2.19 | 1.85 | 10.63 |
| **Na2O** | 0.60 | 1.38 | 0.04 | 0.00 | 0.89 | 0.16 | 0.03 | 0.06 | 0.64 | 0.30 | | 2.45 | 2.29 | 2.26 | 1.97 |
| **K2O** | 1.03 | 1.04 | 0.02 | 0.00 | 1.29 | 0.91 | 0.00 | 0.01 | 0.65 | 0.49 | | 2.61 | 2.43 | 2.96 | 0.57 |
| **P2O5** | 0.062 | 0.024 | 0.006 | 0.000 | 0.005 | 0.000 | 0.004 | 0.003 | 0.114 | 0.002 | | 0.080 | 0.091 | 0.099 | 0.065 |
| **BaO** | 0.043 | 0.041 | 0.001 | 0.004 | 0.007 | 0.007 | 0.000 | 0.006 | 0.031 | 0.008 | | 0.083 | 0.079 | 0.099 | 0.023 |
| **Cr2O3** | 0.054 | 0.034 | 0.820 | 1.088 | 0.055 | 0.147 | 0.604 | 0.653 | 0.041 | 0.060 | | 0.016 | 0.023 | 0.023 | 0.041 |
| **NiO** | 0.023 | 0.009 | 0.310 | 0.324 | 0.021 | 0.047 | 0.120 | 0.950 | 0.018 | 0.014 | | 0.008 | 0.010 | 0.010 | 0.005 |
| **Total** | 99.68 | 99.87 | 98.85 | 98.75 | 99.94 | 99.83 | 99.35 | 98.78 | 99.59 | 100.24 | | 99.87 | 100.08 | 100.09 | 100.17 |
| **mg#** | 57.84 | 49.87 | 79.72 | 72.71 | 60.53 | 67.84 | 80.25 | 75.15 | 37.09 | 56.40 | | 25.43 | 22.90 | 25.49 | 51.91 |
| **LOI** | 2.25 | 1.01 | 10.95 | 12.86 | 3.38 | 1.61 | 6.30 | 3.86 | 1.58 | 1.22 | | 1.12 | 1.43 | 1.32 | 0.97 |
| **Rb** | 31.8 | 33.1 | 1.5 | -0.1 | 32.5 | 19.8 | 0.8 | 1.0 | 18.2 | 17.1 | | 89.2 | 81.9 | 100.2 | 131.3 |
| **Sr** | 468.7 | 550.5 | 5.7 | 1.5 | 176.4 | 120.2 | 4.1 | 3.4 | 303.8 | 163.5 | | 167.6 | 227.8 | 172.7 | 335.0 |
| **Y** | 6.4 | 7.4 | 0.6 | 0.1 | 5.7 | 4.6 | 1.4 | 1.4 | 10.5 | 1.4 | | 21.4 | 39.5 | 31.7 | 18.2 |
| **Zr** | 21.8 | 57.5 | 3.4 | 1.7 | 1.8 | 2.5 | 2.2 | 2.7 | 55.3 | 5.8 | | 197.9 | 213.9 | 248.4 | 280.9 |
| **Nb** | 2.0 | 3.9 | 0.1 | 0.2 | 0.0 | -0.1 | 0.0 | 0.1 | 5.9 | -0.1 | | 16.2 | 20.3 | 20.4 | 27.2 |
| **Zn** | 89.6 | 76.5 | 40.2 | 27.4 | 29.6 | 38.0 | 27.2 | 34.6 | 130.4 | 48.6 | | 104.5 | 113.4 | 177.1 | 133.0 |
| **Cu** | 166.7 | 17.7 | 2.1 | 2.5 | 65.6 | 156.6 | 18.4 | 48.3 | 126.7 | 58.8 | | 37.9 | 36.5 | 47.6 | 59.1 |
| **Ni** | 148.9 | 63.0 | 2230.7 | 2549.5 | 142.7 | 327.7 | 922.6 | 715.6 | 134.2 | 111.0 | | 43.4 | 63.4 | 61.0 | 69.4 |
| **Cr** | 436.9 | 273.6 | 4265.9 | 4017.2 | 439.4 | 1102.3 | 3860.2 | 4599.9 | 319.5 | 457.0 | | 137.0 | 163.2 | 178.0 | 192.1 |
| **V** | 163.2 | 242.4 | 21.2 | 26.0 | 172.3 | 135.5 | 94.5 | 151.0 | 379.6 | 229.4 | | 133.0 | 189.0 | 159.8 | 211.8 |
| **Ba** | 300.9 | 355.5 | 14.9 | 3.0 | 45.1 | 39.7 | 2.1 | 1.8 | 225.6 | 45.4 | | 670.9 | 642.7 | 823.8 | 1007.7 |
| **Sc** | 37.4 | 37.3 | 8.4 | 7.7 | 49.5 | 41.7 | 31.7 | 45.1 | 43.2 | 61.4 | | 24.4 | 31.0 | 27.5 | 40.3 |
| **La** | 8.8 | 11.2 | | | 2.2 | 2.0 | | | 7.3 | 1.8 | | 24.8 | 43.5 | 37.9 | 49.2 |
| **Ce** | 16.7 | 22.2 | | | -0.4 | 3.7 | | | 14.9 | 2.2 | | 50.2 | 87.9 | 82.2 | 97.3 |
| **Nd** | 8.6 | 8.3 | | | 1.0 | 1.2 | | | 7.7 | 1.5 | | 21.9 | 37.3 | 32.7 | 39.3 |

| | 463A | Ab109 | Ab110 | Ab112 | Ab121 | Ab126 | Ab128 | Ab5323 | Ab3828 | Ab20 | HI181 | Ab3913 | Ab740 | MS1516 | 127B | MS1504 |
|---|---|---|---|---|---|---|---|---|---|---|---|---|---|---|---|---|
| **SiO2** | 59.26 | 41.18 | 44.57 | 42.13 | 50.91 | 61.88 | 37.84 | 49.98 | 67.59 | 55.53 | 50.60 | 79.32 | 51.14 | 44.62 | 51.74 | 63.07 |
| **TiO2** | 1.31 | 2.26 | 1.37 | 2.22 | 1.21 | 1.10 | 2.15 | 1.75 | 0.67 | 1.07 | 1.50 | 0.55 | 1.97 | 0.38 | 1.71 | 0.89 |
| **Al2O3** | 20.94 | 20.47 | 13.83 | 19.76 | 25.57 | 18.10 | 22.60 | 23.68 | 16.03 | 23.77 | 23.19 | 7.97 | 23.16 | 18.39 | 22.33 | 16.35 |
| **Fe2O3** | 9.57 | 21.24 | 14.57 | 20.12 | 10.25 | 9.22 | 23.16 | 11.21 | 5.87 | 9.12 | 14.92 | 5.46 | 12.38 | 16.50 | 12.10 | 7.82 |
| **MnO** | 0.13 | 0.32 | 0.18 | 0.34 | 0.13 | 0.12 | 0.42 | 0.16 | 0.07 | 0.13 | 0.07 | 0.07 | 0.19 | 0.23 | 0.15 | 0.13 |
| **MgO** | 2.93 | 7.61 | 13.95 | 7.31 | 3.06 | 2.80 | 7.93 | 3.82 | 1.22 | 2.16 | 2.07 | 2.53 | 3.96 | 6.24 | 3.57 | 4.44 |
| **CaO** | 2.23 | 3.57 | 8.56 | 4.84 | 1.94 | 1.49 | 3.63 | 4.67 | 1.12 | 2.38 | 0.91 | 2.36 | 1.70 | 12.69 | 3.08 | 1.89 |
| **Na2O** | 1.17 | 1.64 | 2.29 | 1.72 | 2.00 | 2.34 | 1.17 | 2.24 | 1.97 | 2.60 | 2.07 | 0.43 | 1.80 | 1.19 | 2.65 | 1.42 |
| **K2O** | 1.93 | 1.61 | 0.17 | 1.15 | 3.72 | 2.63 | 0.69 | 1.92 | 4.61 | 2.50 | 4.00 | 0.99 | 3.21 | 0.09 | 2.42 | 3.66 |
| **P2O5** | 0.426 | 0.020 | 0.060 | 0.065 | 0.661 | 0.117 | 0.022 | 0.110 | 0.059 | 0.105 | 0.356 | 0.191 | 0.075 | 0.001 | 0.109 | 0.193 |
| **BaO** | 0.074 | 0.133 | 0.025 | 0.099 | 0.121 | 0.073 | 0.038 | 0.076 | 0.159 | 0.113 | 0.191 | 0.028 | 0.188 | 0.007 | 0.174 | 0.061 |
| **Cr2O3** | 0.022 | 0.050 | 0.179 | 0.046 | 0.019 | 0.016 | 0.036 | 0.028 | 0.008 | 0.015 | 0.019 | 0.019 | 0.024 | 0.003 | 0.022 | 0.018 |
| **NiO** | 0.007 | 0.024 | 0.064 | 0.018 | 0.010 | 0.008 | 0.016 | 0.007 | 0.004 | 0.006 | 0.009 | 0.008 | 0.003 | 0.000 | 0.007 | 0.009 |
| **Total** | 99.89 | 99.92 | 99.55 | 99.65 | 99.45 | 99.79 | 99.61 | 99.54 | 99.20 | 99.37 | 99.68 | 99.87 | 99.59 | 100.34 | 99.86 | 99.87 |
| **mg#** | 23.44 | 26.38 | 48.91 | 26.65 | 22.99 | 23.29 | 25.51 | 25.42 | 17.21 | 19.15 | 12.18 | 31.66 | 24.24 | 27.44 | 22.78 | 36.22 |
| **LOI** | 1.06 | -0.30 | -0.57 | -0.43 | 0.89 | 0.84 | -0.61 | 1.12 | 0.82 | 1.35 | 3.37 | 1.39 | 0.09 | 0.59 | 0.24 | 2.26 |
| **Rb** | 84.5 | 53.6 | 2.2 | 37.1 | 100.9 | 113.9 | 19.7 | 43.0 | 121.8 | 49.9 | 76.5 | 29.4 | 62.3 | 5.4 | 48.2 | 115.8 |
| **Sr** | 199.1 | 246.7 | 465.4 | 330.7 | 213.5 | 173.4 | 290.9 | 293.4 | 156.4 | 235.9 | 328.3 | 110.6 | 301.4 | 180.7 | 323.0 | 135.3 |
| **Y** | 30.8 | 13.5 | 11.8 | 15.1 | 54.4 | 29.3 | 26.0 | 18.6 | 29.7 | 22.4 | 35.2 | 15.6 | 75.3 | 2.5 | 61.6 | 21.7 |
| **Zr** | 318.8 | 39.9 | 37.3 | 41.0 | 219.7 | 295.9 | 87.2 | 195.6 | 352.1 | 319.0 | 232.3 | 169.3 | 420.7 | 1.0 | 462.9 | 196.4 |
| **Nb** | 21.0 | 15.9 | 0.8 | 14.2 | 28.6 | 22.6 | 17.4 | 19.8 | 18.6 | 16.7 | 16.7 | 7.0 | 33.3 | 0.0 | 31.0 | 15.9 |
| **Zn** | 140.5 | 240.1 | 80.0 | 181.2 | 144.0 | 128.7 | 245.2 | 114.8 | 82.1 | 133.9 | 224.0 | 67.2 | 123.8 | 98.1 | 129.6 | 73.6 |
| **Cu** | 5.1 | 279.2 | 132.7 | 195.4 | 52.8 | 33.0 | 82.8 | 71.2 | 15.9 | 35.9 | 6.6 | 94.8 | 3.6 | 93.5 | 44.8 | 27.8 |
| **Ni** | 53.2 | 181.3 | 426.8 | 160.9 | 59.6 | 44.3 | 143.3 | 55.6 | 27.5 | 39.6 | 72.9 | 38.9 | 28.8 | 13.4 | 51.5 | 67.4 |
| **Cr** | 173.7 | 366.3 | 1182.2 | 339.2 | 149.3 | 129.8 | 271.3 | 186.8 | 71.0 | 118.9 | 127.9 | 135.1 | 164.4 | 12.0 | 147.3 | 132.4 |
| **V** | 156.7 | 519.5 | 255.8 | 504.3 | 159.1 | 137.6 | 432.7 | 230.2 | 59.2 | 112.9 | 124.7 | 157.7 | 174.4 | 640.3 | 184.6 | 219.5 |
| **Ba** | 602.6 | 1169.7 | 152.5 | 889.5 | 911.5 | 571.8 | 257.9 | 545.1 | 1264.5 | 862.3 | 1499.8 | 277.0 | 1509.8 | 26.8 | 1398.8 | 506.0 |
| **Sc** | 25.5 | 58.9 | 29.7 | 57.6 | 33.5 | 29.6 | 55.0 | 32.4 | 23.5 | 17.5 | 30.7 | 18.4 | 35.2 | 61.5 | 28.5 | 24.7 |
| **La** | 43.3 | 17.7 | 3.8 | 16.1 | 71.9 | 36.6 | 20.8 | 32.0 | 31.6 | 62.9 | 40.8 | 13.1 | 32.4 | 1.4 | 63.3 | 22.6 |
| **Ce** | 93.7 | 25.1 | 9.9 | 22.8 | 146.0 | 83.7 | 36.1 | 61.8 | 65.2 | 119.5 | 79.5 | 29.2 | 60.4 | 1.6 | 123.9 | 41.5 |
| **Nd** | 43.9 | 7.7 | 6.2 | 8.2 | 68.1 | 35.3 | 13.6 | 24.7 | 26.0 | 50.2 | 36.9 | 12.6 | 22.6 | -0.2 | 52.3 | 21.0 |

| | MS1508 | Ab3807 | MS1613 | 348Aa | 348Ab | 349A | 353A | 685A | 137A | 140A | 156A | 157A | 163Aa | 163Ab | 171A | 186A |
|---|---|---|---|---|---|---|---|---|---|---|---|---|---|---|---|---|
| **SiO2** | 50.17 | 63.54 | 68.15 | 73.91 | 65.66 | 75.39 | 71.95 | 61.74 | 73.28 | 77.16 | 69.23 | 63.31 | 75.21 | 73.12 | 75.65 | 66.60 |
| **TiO2** | 2.60 | 0.84 | 0.88 | 0.58 | 0.92 | 0.72 | 0.72 | 0.84 | 0.57 | 0.42 | 0.73 | 0.87 | 0.11 | 0.51 | 0.53 | 0.83 |
| **Al2O3** | 14.09 | 18.81 | 15.96 | 14.18 | 17.51 | 12.88 | 14.10 | 20.45 | 10.12 | 10.50 | 14.72 | 17.03 | 14.17 | 9.77 | 11.43 | 15.73 |
| **Fe2O3** | 13.43 | 7.82 | 4.88 | 3.07 | 4.80 | 3.60 | 4.59 | 7.21 | 5.03 | 3.98 | 5.16 | 4.08 | 1.22 | 6.18 | 4.42 | 6.31 |
| **MnO** | 0.15 | 0.08 | 0.09 | 0.04 | 0.07 | 0.04 | 0.09 | 0.02 | 0.05 | 0.06 | 0.04 | 0.05 | 0.02 | 0.07 | 0.12 | 0.10 |
| **MgO** | 5.55 | 2.28 | 1.03 | 1.16 | 1.84 | 1.44 | 1.57 | 3.00 | 5.16 | 2.61 | 3.42 | 1.75 | 1.11 | 5.62 | 2.00 | 3.43 |
| **CaO** | 9.51 | 0.32 | 3.44 | 2.68 | 3.51 | 1.71 | 1.21 | 0.11 | 1.37 | 1.60 | 1.61 | 2.10 | 2.65 | 0.94 | 1.10 | 1.63 |
| **Na2O** | 3.11 | 1.41 | 3.68 | 2.20 | 2.93 | 1.88 | 1.56 | 0.35 | 1.53 | 2.03 | 2.69 | 1.79 | 3.87 | 0.92 | 0.98 | 1.93 |
| **K2O** | 0.47 | 5.61 | 1.66 | 1.72 | 2.34 | 2.12 | 3.96 | 6.21 | 2.42 | 1.68 | 2.44 | 8.38 | 1.13 | 2.51 | 3.13 | 3.75 |
| **P2O5** | 0.556 | 0.097 | 0.192 | 0.049 | 0.057 | 0.031 | 0.054 | 0.068 | 0.089 | 0.131 | 0.031 | 0.559 | 0.098 | 0.150 | 0.149 | 0.167 |
| **BaO** | 0.038 | 0.087 | 0.188 | 0.026 | 0.028 | 0.026 | 0.079 | 0.154 | 0.052 | 0.042 | 0.074 | 0.353 | 0.033 | 0.040 | 0.085 | 0.096 |
| **Cr2O3** | 0.062 | 0.010 | 0.001 | 0.005 | 0.009 | 0.004 | 0.005 | 0.016 | 0.051 | 0.022 | 0.036 | | 0.006 | 0.060 | 0.006 | 0.011 |
| **NiO** | 0.042 | 0.006 | 0.001 | 0.002 | 0.002 | 0.002 | 0.001 | 0.007 | 0.028 | 0.012 | 0.017 | 0.002 | 0.005 | 0.031 | 0.003 | 0.006 |
| **Total** | 99.64 | 100.80 | 99.96 | 99.59 | 99.64 | 99.81 | 99.80 | 100.01 | 99.62 | 100.17 | 100.07 | 99.92 | 99.60 | 99.79 | 99.51 | 100.47 |
| **mg#** | 29.24 | 22.57 | 17.43 | 27.42 | 27.71 | 28.57 | 25.49 | 29.38 | 50.64 | 39.61 | 39.86 | 30.02 | 47.64 | 47.63 | 31.15 | 35.22 |
| **LOI** | 0.45 | 1.58 | 0.52 | 0.65 | 0.62 | 1.02 | 0.87 | 3.06 | 1.28 | 0.84 | 1.04 | 0.52 | 1.23 | 1.84 | 0.98 | 2.17 |
| **Rb** | 11.3 | 124.0 | 50.4 | 54.4 | 81.3 | 69.2 | 93.1 | 153.5 | 1.6 | 51.3 | 82.2 | 150.0 | 34.4 | | 81.5 | 107.6 |
| **Sr** | 509.1 | 135.0 | 236.4 | 114.4 | 130.3 | 75.8 | 104.1 | 56.7 | 208.7 | 128.1 | 155.4 | 176.5 | 186.5 | | 115.0 | 337.8 |
| **Y** | 25.7 | 25.7 | 7.1 | 11.4 | 14.4 | 12.8 | 30.7 | 15.0 | 0.7 | 15.0 | 21.9 | 27.9 | 14.2 | | 17.2 | 23.6 |
| **Zr** | 249.3 | 189.4 | 40.8 | 362.0 | 331.1 | 841.7 | 391.5 | 206.1 | 1.0 | 149.2 | 180.3 | 322.7 | 26.6 | | 286.6 | 206.0 |
| **Nb** | 53.3 | 14.8 | 11.7 | 9.6 | 16.2 | 8.4 | 9.4 | 11.5 | 0.2 | 8.1 | 14.6 | 14.0 | 3.7 | | 11.9 | 17.2 |
| **Zn** | 161.7 | 80.9 | 44.4 | 30.4 | 51.1 | 40.0 | 43.9 | 107.5 | 63.9 | 50.0 | 28.0 | 44.2 | 20.2 | | 60.4 | 103.6 |
| **Cu** | 10.3 | 3.4 | 4.0 | 5.9 | 3.6 | 9.1 | 9.1 | 58.0 | 362.5 | 45.5 | 3.3 | 30.6 | 9.4 | | 31.0 | 4.1 |
| **Ni** | 317.5 | 35.6 | 1.4 | 8.2 | 17.6 | 14.5 | 7.8 | 47.1 | 857.7 | 76.3 | 116.0 | 11.6 | 31.4 | | 14.5 | 39.6 |
| **Cr** | 495.7 | 62.9 | 19.9 | 46.2 | 83.3 | 46.4 | 55.7 | 132.9 | 93.2 | 180.1 | 269.5 | 18.2 | 59.3 | | 53.2 | 93.2 |
| **V** | 242.7 | 64.4 | 65.9 | 81.3 | 140.9 | 65.0 | 57.7 | 103.0 | 10.7 | 73.1 | 93.8 | 50.1 | 7.8 | | 80.5 | 175.3 |
| **Ba** | 233.6 | 663.2 | 1539.8 | 217.9 | 195.0 | 188.1 | 636.7 | 1318.3 | 16.6 | 334.7 | 545.8 | 2721.3 | 269.7 | | 661.1 | 723.2 |
| **Sc** | 27.7 | 23.2 | 15.9 | 13.7 | 15.2 | 14.2 | 20.5 | 24.4 | 9.2 | 16.3 | 21.5 | 19.2 | 10.4 | | 16.3 | 23.5 |
| **La** | 24.0 | 36.4 | 3.3 | 30.3 | 41.9 | 30.8 | 26.7 | 28.1 | | 15.1 | 14.8 | 45.2 | 6.0 | | 18.9 | 30.3 |
| **Ce** | 63.9 | 68.4 | 4.4 | 65.5 | 91.9 | 74.0 | 60.7 | 55.7 | | 32.6 | 32.2 | 83.9 | 12.5 | | 37.6 | 67.7 |
| **Nd** | 30.5 | 30.2 | -0.7 | 29.5 | 40.0 | 31.8 | 25.7 | 22.6 | | 14.2 | 14.0 | 33.3 | 5.4 | | 16.5 | 26.3 |

| | 110Aa | 110Ab | 196A | 240A | 242A | 246A | 248A | 251A | 252A | 254A | 255A | CLW217 | CLW213 | CLW214 | CLW202 | CLW204 |
|---|---|---|---|---|---|---|---|---|---|---|---|---|---|---|---|---|
| **SiO2** | 77.08 | 60.58 | 67.73 | 78.04 | 76.77 | 74.01 | 56.80 | 60.53 | 67.25 | 68.58 | 67.87 | 56.65 | 43.52 | 50.34 | 63.69 | 48.82 |
| **TiO2** | 0.21 | 1.37 | 0.82 | 0.29 | 0.74 | 0.53 | 1.01 | 1.05 | 0.72 | 0.75 | 0.81 | 1.18 | 0.20 | 0.73 | 0.55 | 1.29 |
| **Al2O3** | 13.01 | 17.74 | 14.99 | 11.65 | 11.26 | 13.27 | 16.20 | 18.83 | 14.31 | 13.90 | 14.35 | 15.62 | 29.20 | 11.44 | 12.91 | 13.71 |
| **Fe2O3** | 1.58 | 9.85 | 6.66 | 1.95 | 5.02 | 3.84 | 9.25 | 7.34 | 6.32 | 6.15 | 6.72 | 11.45 | 5.99 | 10.06 | 6.57 | 15.63 |
| **MnO** | 0.02 | 0.10 | 0.10 | 0.02 | 0.04 | 0.04 | 0.10 | 0.15 | 0.11 | 0.14 | 0.13 | 0.16 | 0.08 | 0.15 | 0.09 | 0.26 |
| **MgO** | 0.57 | 3.51 | 2.70 | 0.50 | 1.53 | 1.84 | 8.77 | 3.20 | 3.82 | 3.16 | 3.53 | 3.85 | 3.65 | 13.31 | 1.27 | 9.24 |
| **CaO** | 0.68 | 0.39 | 1.43 | 0.59 | 0.72 | 2.17 | 1.09 | 1.37 | 1.28 | 1.53 | 1.62 | 9.07 | 15.35 | 12.63 | 14.60 | 7.78 |
| **Na2O** | 1.61 | 0.67 | 0.78 | 1.28 | 1.03 | 2.52 | 2.17 | 1.76 | 1.21 | 1.50 | 1.13 | 1.59 | 0.80 | 0.84 | 0.03 | 1.53 |
| **K2O** | 4.92 | 5.37 | 4.61 | 5.46 | 3.10 | 1.93 | 4.31 | 5.70 | 4.38 | 4.54 | 3.71 | 0.29 | 1.70 | 0.65 | 0.00 | 1.29 |
| **P2O5** | 0.170 | 0.141 | 0.165 | 0.159 | 0.103 | 0.076 | 0.064 | 0.187 | 0.153 | 0.184 | 0.185 | 0.225 | 0.028 | 0.096 | 0.038 | 0.080 |
| **BaO** | 0.190 | 0.095 | 0.096 | 0.186 | 0.070 | 0.076 | 0.086 | 0.250 | 0.105 | 0.098 | 0.058 | 0.018 | 0.068 | 0.020 | 0.004 | 0.061 |
| **Cr2O3** | 0.001 | 0.016 | 0.011 | 0.002 | 0.007 | 0.007 | 0.037 | 0.014 | 0.011 | 0.010 | 0.010 | 0.001 | 0.020 | 0.121 | 0.012 | 0.035 |
| **NiO** | 0.001 | 0.006 | 0.005 | 0.002 | 0.003 | 0.040 | 0.032 | 0.006 | 0.006 | 0.004 | 0.006 | 0.001 | 0.027 | 0.020 | 0.003 | 0.011 |
| **Total** | 99.85 | 99.73 | 99.99 | 99.94 | 100.31 | 100.23 | 99.76 | 100.12 | 99.56 | 100.44 | 100.06 | 100.09 | 100.52 | 100.25 | 99.71 | 99.63 |
| **mg#** | 26.51 | 26.27 | 28.85 | 20.41 | 23.36 | 32.39 | 48.67 | 30.36 | 37.67 | 33.94 | 34.44 | 25.16 | 37.86 | 56.95 | 16.20 | 37.15 |
| **LOI** | 1.16 | 2.80 | 3.34 | 0.83 | 1.25 | 0.70 | 2.18 | 1.43 | 1.14 | 1.33 | 1.44 | 0.53 | 3.17 | 1.94 | 1.96 | 1.88 |
| **Rb** | 76.7 | 175.6 | 130.9 | 86.4 | 87.3 | 56.7 | 135.4 | 148.5 | 117.1 | 108.5 | 113.5 | 6.1 | 61.1 | 21.8 | -0.4 | 39.5 |
| **Sr** | 194.3 | 55.8 | 151.7 | 200.5 | 95.3 | 214.4 | 101.6 | 235.5 | 219.7 | 192.3 | 150.7 | 314.1 | 944.7 | 259.3 | 2366.3 | 294.1 |
| **Y** | 14.7 | 27.8 | 25.0 | 12.4 | 20.7 | 8.2 | 18.4 | 29.8 | 22.2 | 21.3 | 22.6 | 26.4 | 0.7 | 15.0 | 3.6 | 26.2 |
| **Zr** | 73.5 | 348.8 | 252.1 | 179.1 | 433.5 | 290.9 | 167.7 | 355.9 | 163.7 | 209.7 | 244.0 | 259.1 | -2.0 | 52.5 | 5.4 | 25.3 |
| **Nb** | 5.5 | 33.2 | 17.8 | 7.5 | 16.3 | 11.4 | 15.1 | 24.1 | 14.6 | 15.8 | 16.7 | 8.4 | 0.2 | 2.7 | 3.7 | 4.6 |
| **Zn** | 23.7 | 142.7 | 97.9 | 45.9 | 67.0 | 49.0 | 111.5 | 107.9 | 102.8 | 93.8 | 108.3 | 80.8 | 62.1 | 76.7 | 14.4 | 120.3 |
| **Cu** | 11.5 | 33.6 | 32.3 | 10.5 | 14.5 | 19.0 | 52.9 | 23.7 | 5.2 | 34.4 | 27.3 | 19.7 | 427.9 | 154.8 | 14.1 | 20.0 |
| **Ni** | 0.8 | 45.0 | 37.5 | 3.0 | 15.2 | 16.7 | 239.2 | 37.8 | 42.6 | 27.9 | 40.1 | 3.9 | 202.0 | 159.8 | 17.0 | 98.4 |
| **Cr** | 20.6 | 134.3 | 90.4 | 29.3 | 68.6 | 62.9 | 308.8 | 118.7 | 89.2 | 85.2 | 95.5 | 14.6 | 176.5 | 1006.0 | 91.1 | 253.5 |
| **V** | 22.3 | 158.0 | 136.8 | 30.5 | 73.2 | 60.1 | 191.5 | 137.1 | 188.5 | 151.7 | 167.3 | 284.2 | 155.2 | 412.2 | 329.8 | 463.2 |
| **Ba** | 1553.3 | 683.2 | 770.2 | 1521.6 | 563.3 | 644.3 | 698.4 | 1899.8 | 814.0 | 768.1 | 472.5 | 87.3 | 659.3 | 103.5 | 11.3 | 428.9 |
| **Sc** | 12.0 | 28.1 | 21.0 | 13.4 | 17.5 | 15.6 | 29.1 | 23.6 | 22.7 | 21.6 | 22.4 | 50.9 | 10.2 | 87.0 | 18.6 | 64.3 |
| **La** | 7.2 | 33.3 | 24.8 | 12.6 | 18.6 | 18.3 | 22.3 | 29.8 | 23.1 | 24.3 | 23.0 | 17.0 | 6.6 | 7.6 | 6.2 | 5.8 |
| **Ce** | 9.9 | 80.4 | 59.4 | 20.3 | 46.7 | 43.1 | 47.8 | 65.0 | 49.5 | 53.1 | 50.8 | 49.4 | 7.3 | 21.7 | 20.8 | 15.1 |
| **Nd** | 3.1 | 34.7 | 24.9 | 7.5 | 19.5 | 16.6 | 20.5 | 27.6 | 19.9 | 21.9 | 20.8 | 30.5 | 2.6 | 16.8 | 6.6 | 10.5 |

| | CLW208 | CLW209 | DCD102 | DCD103 | DCD108 | DCD107 | DCD111 | DCD112 | DCD113 | DCD114 | DCD115 | DCD117 | DCD119 | DCD120 |
|---|---|---|---|---|---|---|---|---|---|---|---|---|---|---|
| SiO2 | 49.84 | 52.86 | 68.42 | 39.46 | 71.42 | 70.96 | 77.01 | 45.19 | 70.81 | 71.95 | 71.65 | 55.73 | 73.00 | 73.43 |
| TiO2 | 0.35 | 0.51 | 0.76 | 0.02 | 0.94 | 1.55 | 0.89 | 2.28 | 0.87 | 1.30 | 1.23 | 0.33 | 1.50 | 1.03 |
| Al2O3 | 15.85 | 18.37 | 9.88 | 0.48 | 13.97 | 13.32 | 10.69 | 15.73 | 14.40 | 10.70 | 12.33 | 5.52 | 9.80 | 12.38 |
| Fe2O3 | 8.70 | 11.85 | 9.04 | 15.65 | 5.98 | 6.92 | 4.66 | 18.86 | 6.46 | 7.86 | 7.28 | 15.75 | 9.31 | 5.85 |
| MnO | 0.16 | 0.17 | 0.15 | 0.10 | 0.07 | 0.07 | 0.04 | 0.24 | 0.11 | 0.10 | 0.07 | 0.21 | 0.09 | 0.06 |
| MgO | 11.14 | 7.32 | 7.62 | 41.52 | 1.58 | 2.37 | 1.29 | 8.12 | 1.82 | 2.66 | 2.03 | 20.58 | 2.76 | 1.56 |
| CaO | 12.09 | 6.68 | 2.49 | 1.60 | 0.64 | 1.15 | 1.34 | 6.92 | 1.19 | 4.16 | 1.62 | 1.62 | 2.31 | 1.33 |
| Na2O | 0.95 | 1.02 | 0.67 | 0.03 | 2.43 | 1.60 | 1.66 | 0.40 | 1.16 | 0.43 | 1.72 | 0.16 | 0.53 | 1.75 |
| K2O | 0.47 | 0.81 | 0.88 | 0.00 | 2.92 | 2.36 | 2.12 | 1.55 | 2.54 | 0.94 | 1.69 | 0.21 | 0.44 | 2.66 |
| P2O5 | 0.048 | 0.145 | 0.225 | 0.003 | 0.124 | 0.090 | 0.055 | 0.197 | 0.062 | 0.007 | 0.073 | 0.018 | 0.015 | 0.055 |
| BaO | 0.016 | 0.037 | 0.042 | 0.001 | 0.086 | 0.117 | 0.111 | 0.054 | 0.108 | 0.027 | 0.096 | 0.016 | 0.029 | 0.107 |
| Cr2O3 | 0.051 | 0.019 | 0.047 | 1.073 | 0.010 | 0.014 | 0.009 | 0.030 | 0.011 | 0.016 | 0.120 | 0.135 | 0.029 | 0.010 |
| NiO | 0.011 | 0.010 | 0.010 | 0.319 | 0.004 | 0.005 | 0.004 | 0.009 | 0.006 | 0.003 | 0.006 | 0.040 | 0.011 | 0.005 |
| Total | 99.60 | 99.73 | 100.14 | 98.83 | 100.07 | 100.39 | 99.76 | 99.49 | 99.43 | 100.11 | 99.70 | 100.13 | 99.75 | 100.10 |
| mg# | 56.15 | 38.18 | 45.74 | 72.63 | 20.90 | 25.51 | 21.68 | 30.10 | 21.98 | 25.29 | 21.80 | 56.65 | 22.87 | 21.05 |
| LOI | 1.81 | 4.56 | 3.46 | 0.84 | 1.91 | 1.70 | 0.99 | 2.32 | 1.51 | 1.20 | 1.88 | 3.54 | 0.63 | 0.78 |
| Rb | 10.0 | 25.8 | 18.4 | 31.4 | 71.4 | 47.3 | 51.5 | 44.4 | 64.1 | 26.2 | 42.7 | 5.8 | 11.5 | 68.5 |
| Sr | 446.1 | 420.8 | 127.7 | 238.8 | 148.2 | 201.5 | 233.5 | 292.2 | 205.2 | 221.1 | 170.9 | 16.4 | 251.9 | 189.2 |
| Y | 8.8 | 18.7 | 14.5 | 9.9 | 22.3 | 21.7 | 7.5 | 5.3 | 21.0 | 2.2 | 18.5 | 3.6 | 3.0 | 13.8 |
| Zr | 56.7 | 99.3 | 120.0 | 270.6 | 280.7 | 276.0 | 244.7 | 186.4 | 270.1 | 646.9 | 262.1 | 25.9 | 94.1 | 243.1 |
| Nb | 5.7 | 5.5 | 8.0 | 9.2 | 19.4 | 16.1 | 8.6 | 8.8 | 12.5 | 4.6 | 13.3 | 2.7 | 6.0 | 12.6 |
| Zn | 81.6 | 135.0 | 97.7 | 55.5 | 77.7 | 60.7 | 59.1 | 172.2 | 63.9 | 70.2 | 81.2 | 127.1 | 96.8 | 67.6 |
| Cu | 71.8 | 134.9 | 89.2 | 28.5 | 19.5 | 4.1 | 5.7 | 72.6 | 25.5 | 17.2 | 6.9 | 131.6 | 35.9 | 27.2 |
| Ni | 18.1 | 82.3 | 75.4 | 18.7 | 26.0 | 37.4 | 22.7 | 84.0 | 35.2 | 19.7 | 37.9 | 304.6 | 60.1 | 27.7 |
| Cr | 31.0 | 151.0 | 359.5 | 69.9 | 76.5 | 108.7 | 74.2 | 215.5 | 114.3 | 115.1 | 93.6 | 1038.0 | 187.2 | 80.4 |
| V | 403.3 | 328.1 | 179.9 | 81.0 | 97.3 | 148.5 | 92.8 | 425.3 | 111.8 | 174.8 | 118.6 | 148.7 | 198.1 | 98.5 |
| Ba | 162.2 | 242.1 | 308.7 | 535.5 | 673.6 | 986.7 | 992.6 | 357.9 | 962.2 | 203.3 | 746.8 | 64.9 | 160.6 | 831.8 |
| Sc | 42.0 | 30.1 | 39.4 | 17.1 | 19.8 | 24.3 | 19.7 | 56.9 | 18.1 | 34.7 | 20.9 | 47.9 | 23.0 | 19.3 |
| La | 11.2 | 10.9 | 16.7 | 17.6 | 27.3 | 21.2 | 18.4 | 3.7 | 18.3 | 2.8 | 16.5 | 6.1 | 6.6 | 16.9 |
| Ce | 22.5 | 26.3 | 34.8 | 39.5 | 61.5 | 47.8 | 36.5 | 9.6 | 39.6 | 11.3 | 30.8 | 7.4 | 13.2 | 36.4 |
| Nd | 11.5 | 10.3 | 18.2 | 15.7 | 26.3 | 20.8 | 13.9 | 3.9 | 16.2 | 2.9 | 10.8 | 3.5 | 5.4 | 14.3 |

# Appendix C.2 - REE data

| Igneous Rocks: | Ab6908 | 1P | 7P | Ab82 | Ab127 | Ab2063 | Ab3826 | Ab1310 | Ab5613 | Ab7801 | MS1595 | Ab243 | Ab661 | WdV(Ol) | WdS | WdHD3 | Wd109 | WdCC2 |
|---|---|---|---|---|---|---|---|---|---|---|---|---|---|---|---|---|---|---|
| **La** | 19.2 | 9.6 | 14.8 | | 2.0 | 1.9 | 21.3 | | 21.3 | | 7.6 | 21.3 | 64.8 | 3.1 | 3.0 | 3.5 | 27.1 | 4.6 |
| **Ce** | 39.4 | 20.2 | 32.7 | | 4.1 | 4.3 | 47.4 | | 42.7 | | 14.8 | 52.7 | 144.7 | 6.8 | 6.4 | 7.6 | 62.9 | 8.3 |
| **Pr*** | 3.9 | 1.9 | 3.3 | | 0.5 | 0.4 | 4.7 | | 4.3 | | 1.4 | 5.2 | 14.2 | 0.8 | 0.7 | 0.7 | 6.0 | 0.8 |
| **Nd** | 19.1 | 9.4 | 16.5 | | 2.4 | 1.5 | 25.6 | | 24.4 | | 8.3 | 35.8 | 67.2 | 5.8 | 4.6 | 3.5 | 36.1 | 3.7 |
| **Sm** | 4.16 | 1.87 | 3.64 | 4.36 | 0.80 | 0.67 | 5.39 | 11.70 | 5.21 | 23.72 | 2.00 | 6.77 | 9.56 | 1.56 | 1.29 | 1.05 | 5.57 | 0.79 |
| **Eu** | 1.48 | 0.93 | 1.09 | 1.05 | 0.43 | 0.29 | 2.09 | 3.68 | 1.72 | 5.40 | 0.61 | 4.23 | 9.37 | 1.13 | 0.87 | 1.70 | 10.32 | 0.82 |
| **Gd** | 4.35 | 2.82 | 3.90 | 3.50 | 1.32 | 1.21 | 5.26 | 9.38 | 4.45 | 13.99 | 1.69 | 6.05 | 6.74 | 2.47 | 2.07 | 1.90 | 3.93 | 1.32 |
| **Dy** | 3.96 | 1.92 | 3.60 | 3.08 | 0.99 | 0.54 | 4.93 | 8.07 | 4.60 | 9.51 | 1.85 | 4.45 | 4.35 | 2.64 | 1.84 | 0.99 | 2.87 | 0.78 |
| **Ho*** | 0.96 | 0.65 | 0.86 | 0.70 | 0.35 | 0.30 | 1.10 | 1.66 | 0.97 | 1.99 | 0.43 | 0.95 | 1.18 | 0.67 | 0.54 | 0.47 | 0.77 | 0.30 |
| **Er** | 2.68 | 1.30 | 2.35 | 1.65 | 1.30 | 1.11 | 4.57 | 4.30 | 2.59 | 5.36 | 1.05 | 2.88 | 3.36 | 2.09 | 1.42 | 2.51 | 2.80 | 1.00 |
| **Yb** | 2.12 | 1.15 | 1.80 | 1.53 | 0.59 | 0.47 | 2.55 | 3.33 | 2.24 | 4.22 | 1.01 | 1.63 | 2.69 | 1.46 | 1.08 | 0.76 | 2.39 | 0.52 |
| **Lu** | 0.33 | 0.17 | 0.27 | 0.27 | 0.07 | 0.06 | 0.41 | 0.53 | 0.38 | 0.78 | 0.17 | 0.27 | 0.53 | 0.22 | 0.16 | 0.10 | 0.54 | 0.07 |

| | WdPY3 | Wd72 | WdR | HI115 | HI47 | HI131 | Ab5661 | MS1537 | Ab94 | MS1601 | 77P | 733C | CLW102 | CLW218 | CLW215 | CLW106 | CLW107 | CLW109 | CLW110 |
|---|---|---|---|---|---|---|---|---|---|---|---|---|---|---|---|---|---|---|---|
| **La** | 3.4 | 29.9 | 3.5 | 62.8 | 75.4 | 38.9 | 1.2 | | | | | | 35.9 | 11.7 | | 3.0 | 9.3 | 8.6 | 9.0 |
| **Ce** | 7.8 | 72.8 | 7.5 | 139.8 | 157.7 | 92.6 | 2.5 | | | | | | 84.5 | 24.7 | | 4.7 | 19.1 | 16.7 | 25.5 |
| **Pr*** | 0.8 | 7.3 | 0.8 | 13.8 | 15.6 | 9.1 | 0.1 | | | | | | 11.1 | 2.5 | | | | | |
| **Nd** | 4.4 | 49.3 | 5.1 | 78.4 | 68.9 | 56.2 | 1.9 | | | | | | 45.9 | 16.4 | | 2.9 | 10.9 | 10.1 | 16.4 |
| **Sm** | 1.19 | 9.08 | 1.34 | 14.37 | 12.55 | 9.01 | 0.79 | 2.84 | 11.03 | 0.17 | 3.08 | 1.02 | 9.71 | 3.44 | 2.17 | 0.98 | 2.76 | 2.82 | 3.87 |
| **Eu** | 0.86 | 5.27 | 1.32 | 3.98 | 2.71 | 8.84 | 0.42 | 1.24 | 2.63 | 0.05 | 2.31 | 0.48 | 2.23 | 0.89 | 0.79 | 0.42 | 0.79 | 1.00 | 0.94 |
| **Gd** | 1.84 | 7.16 | 2.01 | 11.44 | 8.30 | 6.52 | 0.94 | 4.00 | 7.50 | 0.37 | 2.40 | 1.08 | 7.92 | 2.56 | 2.14 | 0.49 | 2.27 | 2.43 | 3.48 |
| **Dy** | 1.54 | 5.46 | 1.98 | 9.35 | 6.04 | 4.81 | 1.15 | 4.95 | 6.45 | 0.13 | 2.06 | 1.13 | 6.54 | 2.30 | 2.03 | 0.58 | 2.00 | 2.14 | 3.25 |
| **Ho*** | 0.46 | 1.18 | 0.54 | 2.04 | 1.18 | 1.18 | 0.32 | 1.19 | 1.40 | 0.07 | 0.48 | 0.28 | 1.19 | 0.53 | 0.47 | 0.17 | 0.44 | 0.54 | 0.75 |
| **Er** | 1.75 | 2.75 | 1.93 | 5.85 | 2.59 | 3.83 | 0.59 | 3.06 | 3.57 | 0.13 | 1.15 | 0.61 | 3.26 | 1.15 | 1.05 | 0.31 | 0.99 | 1.17 | 1.84 |
| **Yb** | 0.84 | 2 | 1.12 | 4.89 | 1.57 | 3.22 | 0.57 | 3.04 | 3.21 | 0.10 | 1.05 | 0.56 | 2.61 | 1.04 | 0.89 | 0.32 | 0.72 | 1.02 | 1.38 |
| **Lu** | 0.12 | 0.34 | 0.17 | 0.81 | 0.25 | 0.67 | 0.10 | 0.49 | 0.56 | 0.01 | 0.19 | 0.09 | 0.37 | 0.17 | 0.14 | 0.07 | 0.12 | 0.17 | 0.22 |

| | DCD106 | DCD116 | Country Rocks: | Ab210 | 6P | 463A | Ab20 | MS1504 | Ab3807 | 685A | 246A | 251A | DCD108 |
|---|---|---|---|---|---|---|---|---|---|---|---|---|---|
| **La** | | | | 78.4 | 82.5 | | | 21.2 | | | | | |
| **Ce** | | | | 162.0 | 172.5 | | | 41.5 | | | | | |
| **Pr*** | | | | 18.3 | 16.9 | | | 5.2 | | | | | |
| **Nd** | | | | 65.0 | 72.9 | | | 19.2 | | | | | |
| **Sm** | 0.63 | 2.20 | | 10.57 | 12.33 | 10.39 | 12.43 | 3.65 | 7.17 | 5.19 | 4.30 | 6.96 | 6.05 |
| **Eu** | 0.29 | 0.73 | | 2.00 | 2.83 | 2.33 | 3.50 | 1.04 | 1.66 | 1.23 | 1.72 | 2.06 | 1.48 |
| **Gd** | 0.81 | 1.97 | | 7.98 | 8.72 | 9.08 | 9.19 | 3.02 | 5.47 | 3.92 | 2.71 | 6.51 | 4.73 |
| **Dy** | 1.06 | 2.12 | | 7.85 | 4.96 | 6.87 | 6.15 | 3.57 | 4.80 | 3.18 | 2.15 | 6.08 | 4.40 |
| **Ho*** | 0.30 | 0.51 | | 1.52 | 1.10 | 1.37 | 1.24 | 0.74 | 1.04 | 0.72 | 0.48 | 1.28 | 0.90 |
| **Er** | 0.56 | 1.29 | | 4.29 | 2.35 | 3.59 | 3.02 | 2.31 | 2.78 | 1.78 | 0.94 | 3.53 | 2.55 |
| **Yb** | 0.49 | 1.27 | | 4.12 | 1.28 | 2.83 | 1.98 | 2.46 | 2.39 | 1.57 | 0.80 | 3.19 | 2.16 |
| **Lu** | 0.09 | 0.22 | | 0.63 | 0.20 | 0.48 | 0.31 | 0.39 | 0.38 | 0.26 | 0.14 | 0.52 | 0.37 |

# Appendix C.3 - Probe Data

**Olivine**

| Sample | Ab127 | Ab127 | Ab127 | Ab127 | Ab127 | Ab127 | Ab127 | Ab135 | Ab135 | Ab135 | Ab135 | Ab135 | Ab135 | Ab135 | Ab135 | Ab135 | Ab140 |
|---|---|---|---|---|---|---|---|---|---|---|---|---|---|---|---|---|---|
| Analysis No. | 1 | 2 | 3 | 4 | 5 | 8 | 9 | 4 | 9 | 12 | 21 | 22 | 24 | 30 | 33 | 34 | 5 |
| Analysis Name. | ol1a | ol2b | ol3 | ol3b | ol4 | ol5 | ol6 | ol1a | ol2a | ol3 | ol4 | ol5 | ol6 | ol7 | ol8 | ol9 | ol1 |
| SiO2 | 39.46 | 39.98 | 39.98 | 39.95 | 39.75 | 39.99 | 39.77 | 40.34 | 40.24 | 40.11 | 39.61 | 39.80 | 40.21 | 39.82 | 40.14 | 39.96 | 40.41 |
| TiO2 | 0.00 | 0.00 | 0.00 | 0.00 | 0.20 | 0.00 | 0.00 | 0.00 | 0.00 | 0.00 | 0.00 | 0.00 | 0.00 | 0.00 | 0.00 | 0.00 | 0.00 |
| Al2O3 | 0.00 | 0.00 | 0.00 | 0.00 | 0.00 | 0.00 | 0.00 | 0.00 | 0.00 | 0.00 | 0.00 | 0.00 | 0.00 | 0.00 | 0.00 | 0.00 | 0.62 |
| Cr2O3 | 0.00 | 0.00 | 0.00 | 0.00 | 0.00 | 0.00 | 0.00 | 0.00 | 0.00 | 0.00 | 0.00 | 0.00 | 0.00 | 0.00 | 0.00 | 0.00 | 0.66 |
| FeO | 20.85 | 20.74 | 21.24 | 20.99 | 22.62 | 21.49 | 21.63 | 13.11 | 13.46 | 13.19 | 13.89 | 13.31 | 13.20 | 13.27 | 13.31 | 13.22 | 12.41 |
| MnO | 0.31 | 0.23 | 0.00 | 0.33 | 0.27 | 0.30 | 0.27 | 0.22 | 0.00 | 0.36 | 0.22 | 0.25 | 0.28 | 0.26 | 0.00 | 0.00 | 0.00 |
| MgO | 41.00 | 40.81 | 40.54 | 40.46 | 39.83 | 40.73 | 40.44 | 45.54 | 45.62 | 45.25 | 45.06 | 44.82 | 44.99 | 45.23 | 45.11 | 44.92 | 46.96 |
| NiO | 0.00 | 0.00 | 0.00 | 0.00 | 0.00 | 0.00 | 0.00 | 0.32 | 0.00 | 0.00 | 0.00 | 0.00 | 0.00 | 0.00 | 0.38 | 0.00 | 0.00 |
| CaO | 0.00 | 0.00 | 0.00 | 0.00 | 0.00 | 0.00 | 0.12 | 0.00 | 0.00 | 0.00 | 0.00 | 0.00 | 0.00 | 0.00 | 0.00 | 0.00 | 0.00 |
| Total | 101.90 | 101.76 | 101.77 | 102.09 | 102.67 | 102.51 | 102.45 | 99.54 | 99.32 | 98.91 | 98.78 | 98.17 | 98.69 | 98.57 | 98.95 | 98.10 | 101.07 |

**Formula (4O)**

| | | | | | | | | | | | | | | | | | |
|---|---|---|---|---|---|---|---|---|---|---|---|---|---|---|---|---|---|
| Si | 1.001 | 1.010 | 1.011 | 1.011 | 1.004 | 1.007 | 1.006 | 1.009 | 1.008 | 1.009 | 1.002 | 1.009 | 1.013 | 1.006 | 1.010 | 1.012 | 0.991 |
| Ti | 0.000 | 0.000 | 0.000 | 0.000 | 0.004 | 0.000 | 0.000 | 0.000 | 0.000 | 0.000 | 0.000 | 0.000 | 0.000 | 0.000 | 0.000 | 0.000 | 0.000 |
| Al | 0.000 | 0.000 | 0.000 | 0.000 | 0.000 | 0.000 | 0.000 | 0.000 | 0.000 | 0.000 | 0.000 | 0.000 | 0.000 | 0.000 | 0.000 | 0.000 | 0.018 |
| Cr | 0.000 | 0.000 | 0.000 | 0.000 | 0.000 | 0.000 | 0.000 | 0.000 | 0.000 | 0.000 | 0.000 | 0.000 | 0.000 | 0.000 | 0.000 | 0.000 | 0.013 |
| Fe(ii) | 0.442 | 0.438 | 0.449 | 0.444 | 0.478 | 0.452 | 0.457 | 0.274 | 0.282 | 0.277 | 0.294 | 0.282 | 0.278 | 0.280 | 0.280 | 0.280 | 0.255 |
| Mn | 0.007 | 0.005 | 0.000 | 0.007 | 0.006 | 0.006 | 0.006 | 0.005 | 0.000 | 0.008 | 0.005 | 0.005 | 0.006 | 0.006 | 0.000 | 0.000 | 0.000 |
| Mg | 1.550 | 1.537 | 1.529 | 1.527 | 1.500 | 1.528 | 1.525 | 1.698 | 1.703 | 1.697 | 1.699 | 1.694 | 1.690 | 1.703 | 1.692 | 1.696 | 1.717 |
| Ni | 0.000 | 0.000 | 0.000 | 0.000 | 0.000 | 0.000 | 0.000 | 0.006 | 0.000 | 0.000 | 0.000 | 0.000 | 0.000 | 0.000 | 0.008 | 0.000 | 0.000 |
| Ca | 0.000 | 0.000 | 0.000 | 0.000 | 0.000 | 0.000 | 0.003 | 0.000 | 0.000 | 0.000 | 0.000 | 0.000 | 0.000 | 0.000 | 0.000 | 0.000 | 0.000 |
| Total | 2.999 | 2.990 | 2.989 | 2.989 | 2.992 | 2.993 | 2.997 | 2.991 | 2.992 | 2.991 | 2.998 | 2.991 | 2.987 | 2.994 | 2.990 | 2.988 | 2.993 |

**Endmembers**

| | | | | | | | | | | | | | | | | | |
|---|---|---|---|---|---|---|---|---|---|---|---|---|---|---|---|---|---|
| Fo | 77.55 | 77.62 | 77.29 | 77.18 | 75.62 | 76.92 | 76.70 | 85.89 | 85.80 | 85.62 | 85.06 | 85.49 | 85.61 | 85.63 | 85.80 | 85.83 | 87.09 |
| Fa | 22.12 | 22.13 | 22.71 | 22.46 | 24.09 | 22.76 | 23.01 | 13.87 | 14.20 | 14.00 | 14.71 | 14.24 | 14.09 | 14.09 | 14.20 | 14.17 | 12.91 |
| Tp | | | | | | | | | | | | | | | | | |

**Olivine**

| Sample | Ab140 | Ab140 | Ab140 | Ab140 | Ab140 | Ab140 | Ab140 | Ab140 | Ab140 | Ab140 | Ab140 | Ab140 | Ab140 | Ab140 | Ab140 | Ab143 | Ab143 |
|---|---|---|---|---|---|---|---|---|---|---|---|---|---|---|---|---|---|
| Analysis No. | 9 | 10 | 11 | 12 | 13 | 14 | 15 | 16 | 17 | 25 | 26 | 37 | 41 | 42 | 44 | 11 | 16 |
| Analysis Name. | ol2a | ol2b | ol3a | ol3b | ol3c | ol4 | ol5 | ol6 | ol7 | ol8a | ol8b | ol9 | ol10a | ol10b | ol10d | ol1 | ol2 |
| SiO2 | 40.72 | 41.50 | 41.11 | 40.83 | 41.06 | 40.92 | 41.34 | 41.49 | 40.99 | 41.05 | 41.16 | 40.61 | 40.64 | 40.70 | 40.67 | 39.99 | 40.05 |
| TiO2 | 0.00 | 0.00 | 0.00 | 0.00 | 0.00 | 0.00 | 0.00 | 0.00 | 0.00 | 0.00 | 0.00 | 0.00 | 0.00 | 0.00 | 0.00 | 0.00 | 0.24 |
| Al2O3 | 0.00 | 0.00 | 0.00 | 0.00 | 0.00 | 0.00 | 0.00 | 0.00 | 0.00 | 0.00 | 0.00 | 0.00 | 0.00 | 0.00 | 0.00 | 0.00 | 0.00 |
| Cr2O3 | 0.18 | 0.00 | 0.00 | 0.00 | 0.00 | 0.00 | 0.00 | 0.00 | 0.00 | 0.00 | 0.00 | 0.00 | 0.00 | 0.00 | 0.00 | 0.00 | 0.00 |
| FeO | 12.19 | 12.08 | 12.43 | 12.39 | 12.29 | 12.60 | 12.46 | 12.05 | 12.35 | 12.40 | 12.47 | 12.13 | 12.16 | 12.36 | 12.32 | 14.33 | 14.61 |
| MnO | 0.22 | 0.00 | 0.24 | 0.00 | 0.00 | 0.00 | 0.19 | 0.19 | 0.00 | 0.00 | 0.19 | 0.28 | 0.00 | 0.31 | 0.00 | 0.21 | 0.33 |
| MgO | 47.61 | 47.47 | 47.70 | 47.36 | 47.47 | 47.67 | 47.65 | 47.65 | 47.75 | 47.41 | 47.67 | 47.27 | 47.10 | 47.10 | 46.86 | 44.06 | 44.50 |
| NiO | 0.00 | 0.00 | 0.00 | 0.00 | 0.00 | 0.00 | 0.00 | 0.00 | 0.00 | 0.00 | 0.00 | 0.26 | 0.00 | 0.00 | 0.00 | 0.00 | 0.00 |
| CaO | 0.00 | 0.00 | 0.00 | 0.00 | 0.00 | 0.00 | 0.00 | 0.00 | 0.00 | 0.00 | 0.00 | 0.11 | 0.00 | 0.00 | 0.00 | 0.00 | 0.00 |
| Total | 100.92 | 101.05 | 101.48 | 100.57 | 100.81 | 101.19 | 101.64 | 101.38 | 101.09 | 100.87 | 101.49 | 100.66 | 99.90 | 100.48 | 99.85 | 98.59 | 100.02 |
| **Formula (4O)** | | | | | | | | | | | | | | | | | |
| Si | 0.999 | 1.013 | 1.003 | 1.004 | 1.007 | 1.001 | 1.006 | 1.010 | 1.003 | 1.006 | 1.004 | 1.001 | 1.006 | 1.004 | 1.007 | 1.014 | 1.006 |
| Ti | 0.000 | 0.000 | 0.000 | 0.000 | 0.000 | 0.000 | 0.000 | 0.000 | 0.000 | 0.000 | 0.000 | 0.000 | 0.000 | 0.000 | 0.000 | 0.000 | 0.005 |
| Al | 0.000 | 0.000 | 0.000 | 0.000 | 0.000 | 0.000 | 0.000 | 0.000 | 0.000 | 0.000 | 0.000 | 0.000 | 0.000 | 0.000 | 0.000 | 0.000 | 0.000 |
| Cr | 0.003 | 0.000 | 0.000 | 0.000 | 0.000 | 0.000 | 0.000 | 0.000 | 0.000 | 0.000 | 0.000 | 0.000 | 0.000 | 0.000 | 0.000 | 0.000 | 0.000 |
| Fe(ii) | 0.250 | 0.247 | 0.254 | 0.255 | 0.252 | 0.258 | 0.254 | 0.245 | 0.253 | 0.254 | 0.254 | 0.250 | 0.252 | 0.255 | 0.255 | 0.304 | 0.307 |
| Mn | 0.005 | 0.000 | 0.005 | 0.000 | 0.000 | 0.000 | 0.004 | 0.004 | 0.000 | 0.000 | 0.004 | 0.006 | 0.000 | 0.006 | 0.000 | 0.005 | 0.007 |
| Mg | 1.742 | 1.727 | 1.735 | 1.737 | 1.735 | 1.739 | 1.729 | 1.730 | 1.742 | 1.733 | 1.734 | 1.737 | 1.737 | 1.731 | 1.730 | 1.665 | 1.666 |
| Ni | 0.000 | 0.000 | 0.000 | 0.000 | 0.000 | 0.000 | 0.000 | 0.000 | 0.000 | 0.000 | 0.000 | 0.005 | 0.000 | 0.000 | 0.000 | 0.000 | 0.000 |
| Ca | 0.000 | 0.000 | 0.000 | 0.000 | 0.000 | 0.000 | 0.000 | 0.000 | 0.000 | 0.000 | 0.000 | 0.003 | 0.000 | 0.000 | 0.000 | 0.000 | 0.000 |
| Total | 2.999 | 2.987 | 2.997 | 2.996 | 2.993 | 2.999 | 2.994 | 2.990 | 2.997 | 2.994 | 2.996 | 3.002 | 2.994 | 2.996 | 2.993 | 2.986 | 2.990 |
| **Endmembers** | | | | | | | | | | | | | | | | | |
| Fo | 87.24 | 87.51 | 87.03 | 87.20 | 87.32 | 87.09 | 87.04 | 87.40 | 87.33 | 87.21 | 87.03 | 87.16 | 87.35 | 86.89 | 87.15 | 84.38 | 84.15 |
| Fa | 12.53 | 12.49 | 12.72 | 12.80 | 12.68 | 12.91 | 12.77 | 12.40 | 12.67 | 12.79 | 12.77 | 12.55 | 12.65 | 12.79 | 12.85 | 15.39 | 15.50 |
| Tp | | | | | | | | | | | | | | | | | |

**Olivine**

| Sample | Ab143 | Ab143 | Ab143 | Ab143 | Ab143 | Ab5612 | Ab5612 | Ab5612 | Ab5612 | Ab5612 | Ab5612 | Ab5612 | Ab5612 | Ab5612 | Ab5612 | Ab7799 | Ab7799 |
|---|---|---|---|---|---|---|---|---|---|---|---|---|---|---|---|---|---|
| Analysis No. | 17 | 18 | 19 | 20 | 21 | 40 | 1 | 2 | 3 | 4 | 7 | 8 | 10 | 11 | 12 | 21 | 22 |
| Analysis Name. | ol3 | ol4a | ol4b | ol5a | ol5b | ol1 | ol2 | ol3 | ol4 | ol5 | ol5 | ol6+1 | ol6 | ol7 | ol8 | ol3a | ol3b |
| SiO2 | 39.73 | 40.02 | 39.88 | 40.40 | 40.44 | 42.05 | 41.82 | 42.09 | 42.09 | 42.36 | 41.87 | 42.12 | 42.35 | 42.32 | 42.11 | 30.31 | 30.20 |
| TiO2 | 0.00 | 0.00 | 0.00 | 0.00 | 0.00 | 0.00 | 0.00 | 0.00 | 0.00 | 0.00 | 0.00 | 0.00 | 0.00 | 0.00 | 0.00 | 0.00 | 0.00 |
| Al2O3 | 0.00 | 0.00 | 0.00 | 0.00 | 0.00 | 0.00 | 0.00 | 0.00 | 0.00 | 0.00 | 0.00 | 0.00 | 0.00 | 0.00 | 0.00 | 0.00 | 0.00 |
| Cr2O3 | 0.00 | 0.00 | 0.00 | 0.00 | 0.00 | 0.00 | 0.00 | 0.00 | 0.00 | 0.00 | 0.00 | 0.00 | 0.00 | 0.00 | 0.00 | 0.00 | 0.00 |
| FeO | 15.35 | 14.74 | 14.71 | 14.52 | 14.05 | 8.46 | 8.39 | 8.04 | 8.37 | 8.61 | 8.45 | 8.23 | 8.43 | 8.37 | 8.47 | 67.01 | 68.39 |
| MnO | 0.33 | 0.00 | 0.00 | 0.00 | 0.41 | 0.00 | 0.00 | 0.27 | 0.00 | 0.00 | 0.00 | 0.44 | 0.00 | 0.00 | 0.00 | 2.30 | 2.54 |
| MgO | 43.66 | 44.81 | 44.52 | 44.99 | 44.96 | 50.67 | 50.63 | 50.48 | 50.08 | 49.98 | 50.24 | 50.11 | 50.50 | 50.67 | 50.54 | 0.40 | 0.58 |
| NiO | 0.00 | 0.30 | 0.00 | 0.00 | 0.00 | 0.00 | 0.43 | 0.29 | 0.00 | 0.00 | 0.30 | 0.00 | 0.39 | 0.00 | 0.00 | 0.00 | 0.00 |
| CaO | 0.00 | 0.00 | 0.00 | 0.00 | 0.00 | 0.00 | 0.00 | 0.00 | 0.00 | 0.00 | 0.00 | 0.00 | 0.00 | 0.00 | 0.00 | 0.00 | 0.00 |
| Total | 99.07 | 99.87 | 99.11 | 99.91 | 99.86 | 101.18 | 101.27 | 101.17 | 100.55 | 100.95 | 100.86 | 100.90 | 101.67 | 101.36 | 101.12 | 100.35 | 101.99 |
| **Formula (4O)** | | | | | | | | | | | | | | | | | |
| Si | 1.008 | 1.004 | 1.007 | 1.010 | 1.011 | 1.009 | 1.005 | 1.010 | 1.015 | 1.018 | 1.009 | 1.014 | 1.012 | 1.013 | 1.011 | 1.017 | 1.002 |
| Ti | 0.000 | 0.000 | 0.000 | 0.000 | 0.000 | 0.000 | 0.000 | 0.000 | 0.000 | 0.000 | 0.000 | 0.000 | 0.000 | 0.000 | 0.000 | 0.000 | 0.000 |
| Al | 0.000 | 0.000 | 0.000 | 0.000 | 0.000 | 0.000 | 0.000 | 0.000 | 0.000 | 0.000 | 0.000 | 0.000 | 0.000 | 0.000 | 0.000 | 0.000 | 0.000 |
| Cr | 0.000 | 0.000 | 0.000 | 0.000 | 0.000 | 0.000 | 0.000 | 0.000 | 0.000 | 0.000 | 0.000 | 0.000 | 0.000 | 0.000 | 0.000 | 0.000 | 0.000 |
| Fe(ii) | 0.326 | 0.309 | 0.311 | 0.304 | 0.294 | 0.170 | 0.169 | 0.161 | 0.169 | 0.173 | 0.170 | 0.166 | 0.168 | 0.167 | 0.170 | 1.880 | 1.897 |
| Mn | 0.007 | 0.000 | 0.000 | 0.000 | 0.009 | 0.000 | 0.000 | 0.005 | 0.000 | 0.000 | 0.000 | 0.009 | 0.000 | 0.000 | 0.000 | 0.065 | 0.071 |
| Mg | 1.651 | 1.676 | 1.676 | 1.677 | 1.676 | 1.812 | 1.814 | 1.807 | 1.801 | 1.791 | 1.805 | 1.798 | 1.800 | 1.807 | 1.809 | 0.020 | 0.029 |
| Ni | 0.000 | 0.006 | 0.000 | 0.000 | 0.000 | 0.000 | 0.008 | 0.006 | 0.000 | 0.000 | 0.006 | 0.000 | 0.007 | 0.000 | 0.000 | 0.000 | 0.000 |
| Ca | 0.000 | 0.000 | 0.000 | 0.000 | 0.000 | 0.000 | 0.000 | 0.000 | 0.000 | 0.000 | 0.000 | 0.000 | 0.000 | 0.000 | 0.000 | 0.000 | 0.000 |
| Total | 2.992 | 2.996 | 2.993 | 2.990 | 2.989 | 2.991 | 2.995 | 2.990 | 2.985 | 2.982 | 2.991 | 2.986 | 2.988 | 2.987 | 2.989 | 2.983 | 2.998 |
| **Endmembers** | | | | | | | | | | | | | | | | | |
| Fo | 83.23 | 84.42 | 84.36 | 84.67 | 84.71 | 91.44 | 91.50 | 91.54 | 91.43 | 91.19 | 91.38 | 91.15 | 91.44 | 91.52 | 91.41 | 1.02 | 1.44 |
| Fa | 16.41 | 15.58 | 15.64 | 15.33 | 14.85 | 8.56 | 8.50 | 8.18 | 8.57 | 8.81 | 8.62 | 8.40 | 8.56 | 8.48 | 8.59 | 95.66 | 94.99 |
| Tp | | | | | | | | | | | | | | | | 3.33 | 3.57 |

**Olivine**

| Sample | Ab7801 | Ab7801 | Ab7801 | Ab7801 | Ab7801 | Ab7801 | MS1595 | MS1595 | MS1595 | MS1595 | MS1595 | MS1595 | MS1595 | Ab93 | Ab93 | Ab93 | Ab93 |
|---|---|---|---|---|---|---|---|---|---|---|---|---|---|---|---|---|---|
| Analysis No. | 8 | 10 | 11 | 22 | 23 | 42 | 3 | 4 | 8 | 10 | 18 | 19 | 30 | 6 | 7 | 25 | 26 |
| Analysis Name. | ol1a | ol1b | ol2 | ol3 | ol4 | ol5 | ol1a | ol1b | ol2 | ol3 | ol4a | ol4b | ol5 | ol1 | ol1b | ol2 | ol3 |
| SiO2 | 33.21 | 32.68 | 32.68 | 32.67 | 32.96 | 33.25 | 39.02 | 38.36 | 38.42 | 38.86 | 38.26 | 38.54 | 38.28 | 35.09 | 35.18 | 34.94 | 35.17 |
| TiO2 | 0.00 | 0.00 | 0.00 | 0.00 | 0.00 | 0.00 | 0.00 | 0.14 | 0.00 | 0.00 | 0.00 | 0.00 | 0.00 | 0.00 | 0.00 | 0.00 | 0.00 |
| Al2O3 | 0.00 | 0.00 | 0.00 | 0.00 | 0.00 | 0.00 | 0.00 | 0.00 | 0.00 | 0.00 | 0.35 | 0.00 | 0.00 | 0.00 | 0.00 | 0.00 | 0.00 |
| Cr2O3 | 0.00 | 0.00 | 0.00 | 0.00 | 0.00 | 0.00 | 0.00 | 0.00 | 0.00 | 0.17 | 0.00 | 0.00 | 0.00 | 0.00 | 0.00 | 0.00 | 0.00 |
| FeO | 58.13 | 57.80 | 58.85 | 58.77 | 58.53 | 58.24 | 19.53 | 20.34 | 20.78 | 19.93 | 20.77 | 20.43 | 20.94 | 40.82 | 40.78 | 41.15 | 41.67 |
| MnO | 1.11 | 1.22 | 1.42 | 1.03 | 1.09 | 1.20 | 0.21 | 0.00 | 0.20 | 0.27 | 0.29 | 0.00 | 0.00 | 0.56 | 0.47 | 0.35 | 0.47 |
| MgO | 9.57 | 10.15 | 9.61 | 9.49 | 9.86 | 10.13 | 38.98 | 39.21 | 38.20 | 38.89 | 38.56 | 38.59 | 38.83 | 22.68 | 22.40 | 22.67 | 22.64 |
| NiO | 0.00 | 0.00 | 0.00 | 0.00 | 0.00 | 0.00 | 0.00 | 0.00 | 0.00 | 0.00 | 0.00 | 0.00 | 0.00 | 0.00 | 0.00 | 0.00 | 0.00 |
| CaO | 0.00 | 0.00 | 0.00 | 0.00 | 0.00 | 0.00 | 0.00 | 0.00 | 0.00 | 0.00 | 0.00 | 0.00 | 0.00 | 0.00 | 0.00 | 0.00 | 0.00 |
| Total | 102.40 | 102.30 | 102.97 | 102.19 | 102.85 | 103.23 | 97.73 | 98.06 | 97.84 | 98.11 | 98.23 | 97.81 | 98.42 | 99.49 | 98.83 | 99.10 | 100.15 |
| **Formula (4O)** | | | | | | | | | | | | | | | | | |
| Si | 1.020 | 1.007 | 1.005 | 1.009 | 1.010 | 1.013 | 1.022 | 1.007 | 1.015 | 1.017 | 1.005 | 1.016 | 1.008 | 1.013 | 1.018 | 1.010 | 1.010 |
| Ti | 0.000 | 0.000 | 0.000 | 0.000 | 0.000 | 0.000 | 0.000 | 0.003 | 0.000 | 0.000 | 0.000 | 0.000 | 0.000 | 0.000 | 0.000 | 0.000 | 0.000 |
| Al | 0.000 | 0.000 | 0.000 | 0.000 | 0.000 | 0.000 | 0.000 | 0.000 | 0.000 | 0.000 | 0.011 | 0.000 | 0.000 | 0.000 | 0.000 | 0.000 | 0.000 |
| Cr | 0.000 | 0.000 | 0.000 | 0.000 | 0.000 | 0.000 | 0.000 | 0.000 | 0.000 | 0.004 | 0.000 | 0.000 | 0.000 | 0.000 | 0.000 | 0.000 | 0.000 |
| Fe(ii) | 1.493 | 1.489 | 1.513 | 1.518 | 1.500 | 1.483 | 0.428 | 0.446 | 0.459 | 0.436 | 0.456 | 0.450 | 0.461 | 0.985 | 0.987 | 0.995 | 1.000 |
| Mn | 0.029 | 0.032 | 0.037 | 0.027 | 0.028 | 0.031 | 0.005 | 0.000 | 0.004 | 0.006 | 0.006 | 0.000 | 0.000 | 0.014 | 0.012 | 0.009 | 0.011 |
| Mg | 0.438 | 0.466 | 0.440 | 0.437 | 0.451 | 0.460 | 1.523 | 1.534 | 1.505 | 1.518 | 1.510 | 1.517 | 1.524 | 0.976 | 0.966 | 0.977 | 0.969 |
| Ni | 0.000 | 0.000 | 0.000 | 0.000 | 0.000 | 0.000 | 0.000 | 0.000 | 0.000 | 0.000 | 0.000 | 0.000 | 0.000 | 0.000 | 0.000 | 0.000 | 0.000 |
| Ca | 0.000 | 0.000 | 0.000 | 0.000 | 0.000 | 0.000 | 0.000 | 0.000 | 0.000 | 0.000 | 0.000 | 0.000 | 0.000 | 0.000 | 0.000 | 0.000 | 0.000 |
| Total | 2.980 | 2.993 | 2.995 | 2.991 | 2.990 | 2.987 | 2.978 | 2.990 | 2.985 | 2.981 | 2.989 | 2.984 | 2.992 | 2.987 | 2.982 | 2.990 | 2.990 |
| **Endmembers** | | | | | | | | | | | | | | | | | |
| Fo | 22.36 | 23.46 | 22.13 | 22.05 | 22.77 | 23.30 | 77.88 | 77.46 | 76.45 | 77.44 | 76.55 | 77.10 | 76.78 | 49.42 | 49.19 | 49.34 | 48.92 |
| Fa | 76.17 | 74.94 | 76.01 | 76.59 | 75.80 | 75.13 | 21.88 | 22.54 | 23.33 | 22.26 | 23.13 | 22.90 | 23.22 | 49.89 | 50.23 | 50.23 | 50.50 |
| Tp | | | | | | | | | | | | | | | | | |

**Olivine**

| Sample | Ab243 | Ab243 | Ab243 | Ab243 | Ab243 | Ab243 | V(Ol) | V(Ol) | V(Ol) | V(Ol) | V(Ol) | DV1 | DV1 | DV1 | DV1 | DV1 | DV1 |
|---|---|---|---|---|---|---|---|---|---|---|---|---|---|---|---|---|---|
| Analysis No. | 3 | 6 | 7 | 27 | 30 | 39 | 3 | 16 | 17 | 23 | 25 | 2 | 3 | 5 | 6 | 9 | 31 |
| Analysis Name. | ol1 | ol2 | ol3 | ol3 | ol4 | ol5 | ol1 | ol2 | ol3 | ol4 | ol5 | ol1 | ol1b | ol2 | ol3 | ol4 | ol5 |
| SiO2 | 33.79 | 33.13 | 33.36 | 33.27 | 32.37 | 32.86 | 37.86 | 37.42 | 37.64 | 37.08 | 37.21 | 35.50 | 35.47 | 35.18 | 35.32 | 35.75 | 37.21 |
| TiO2 | 0.00 | 0.00 | 0.00 | 0.00 | 0.00 | 0.00 | 0.00 | 0.00 | 0.00 | 0.00 | 0.00 | 0.00 | 0.00 | 0.00 | 0.00 | 0.00 | 0.00 |
| Al2O3 | 0.00 | 0.00 | 0.00 | 0.00 | 0.00 | 0.00 | 0.00 | 0.00 | 0.00 | 0.00 | 0.00 | 0.00 | 0.00 | 0.00 | 0.00 | 0.00 | 0.00 |
| Cr2O3 | 0.00 | 0.00 | 0.00 | 0.00 | 0.00 | 0.00 | 0.00 | 0.00 | 0.00 | 0.00 | 0.00 | 0.00 | 0.00 | 0.00 | 0.00 | 0.00 | 0.00 |
| FeO | 53.04 | 52.39 | 53.05 | 51.13 | 53.55 | 52.49 | 32.21 | 32.15 | 31.99 | 31.53 | 31.72 | 30.45 | 30.42 | 31.63 | 31.36 | 30.29 | 32.07 |
| MnO | 1.02 | 1.01 | 0.79 | 1.16 | 0.81 | 0.99 | 0.47 | 0.41 | 0.46 | 0.55 | 0.51 | 0.56 | 0.54 | 0.39 | 0.49 | 0.45 | 0.52 |
| MgO | 14.12 | 14.12 | 14.25 | 13.90 | 11.79 | 13.39 | 31.01 | 30.20 | 30.72 | 30.77 | 30.87 | 29.44 | 29.23 | 28.61 | 29.85 | 29.67 | 30.34 |
| NiO | 0.00 | 0.00 | 0.00 | 0.00 | 0.00 | 0.00 | 0.00 | 0.00 | 0.00 | 0.00 | 0.00 | 0.00 | 0.00 | 0.00 | 0.00 | 0.00 | 0.00 |
| CaO | 0.00 | 0.00 | 0.00 | 0.13 | 0.00 | 0.11 | 0.00 | 0.00 | 0.00 | 0.00 | 0.00 | 0.00 | 0.00 | 0.00 | 0.00 | 0.00 | 0.00 |
| Total | 101.97 | 101.03 | 101.46 | 99.83 | 98.83 | 100.13 | 101.54 | 100.30 | 101.00 | 99.94 | 100.51 | 95.96 | 95.64 | 95.81 | 97.02 | 96.16 | 100.15 |
| **Formula (4O)** | | | | | | | | | | | | | | | | | |
| Si | 1.010 | 1.004 | 1.003 | 1.016 | 1.013 | 1.008 | 1.014 | 1.018 | 1.016 | 1.010 | 1.010 | 1.008 | 1.010 | 1.007 | 0.996 | 1.011 | 1.013 |
| Ti | 0.000 | 0.000 | 0.000 | 0.000 | 0.000 | 0.000 | 0.000 | 0.000 | 0.000 | 0.000 | 0.000 | 0.000 | 0.000 | 0.000 | 0.000 | 0.000 | 0.000 |
| Al | 0.000 | 0.000 | 0.000 | 0.000 | 0.000 | 0.000 | 0.000 | 0.000 | 0.000 | 0.000 | 0.000 | 0.000 | 0.000 | 0.000 | 0.000 | 0.000 | 0.000 |
| Cr | 0.000 | 0.000 | 0.000 | 0.000 | 0.000 | 0.000 | 0.000 | 0.000 | 0.000 | 0.000 | 0.000 | 0.000 | 0.000 | 0.000 | 0.000 | 0.000 | 0.000 |
| Fe(ii) | 1.325 | 1.328 | 1.334 | 1.305 | 1.402 | 1.346 | 0.722 | 0.731 | 0.722 | 0.718 | 0.720 | 0.723 | 0.725 | 0.757 | 0.740 | 0.716 | 0.730 |
| Mn | 0.026 | 0.026 | 0.020 | 0.030 | 0.021 | 0.026 | 0.011 | 0.009 | 0.011 | 0.013 | 0.012 | 0.013 | 0.013 | 0.009 | 0.012 | 0.011 | 0.012 |
| Mg | 0.629 | 0.638 | 0.639 | 0.633 | 0.550 | 0.612 | 1.239 | 1.224 | 1.236 | 1.249 | 1.249 | 1.247 | 1.241 | 1.220 | 1.256 | 1.251 | 1.232 |
| Ni | 0.000 | 0.000 | 0.000 | 0.000 | 0.000 | 0.000 | 0.000 | 0.000 | 0.000 | 0.000 | 0.000 | 0.000 | 0.000 | 0.000 | 0.000 | 0.000 | 0.000 |
| Ca | 0.000 | 0.000 | 0.000 | 0.004 | 0.000 | 0.004 | 0.000 | 0.000 | 0.000 | 0.000 | 0.000 | 0.000 | 0.000 | 0.000 | 0.000 | 0.000 | 0.000 |
| Total | 2.990 | 2.996 | 2.997 | 2.988 | 2.987 | 2.996 | 2.986 | 2.982 | 2.984 | 2.990 | 2.990 | 2.992 | 2.990 | 2.993 | 3.004 | 2.989 | 2.987 |
| **Endmembers** | | | | | | | | | | | | | | | | | |
| Fo | 31.77 | 32.03 | 32.06 | 32.15 | 27.88 | 30.86 | 62.85 | 62.31 | 62.79 | 63.10 | 63.06 | 62.86 | 62.73 | 61.43 | 62.56 | 63.24 | 62.40 |
| Fa | 66.93 | 66.66 | 66.93 | 66.33 | 71.03 | 67.85 | 36.61 | 37.21 | 36.67 | 36.26 | 36.35 | 36.46 | 36.62 | 38.09 | 36.86 | 36.21 | 36.99 |
| Tp | | | | | | | | | | | | | | | | | |

**Olivine**

| Sample | DV1 | Ab3986 | Ab3986 | Ab3986 | Ab3986 | Ab3986 | Ab3986 | Ab3986 | Ab5661 | Ab5661 | Ab5661 | Ab5661 | Ab5661 | Ab5661 | Ab6510 | Ab6510 | Ab6510 |
|---|---|---|---|---|---|---|---|---|---|---|---|---|---|---|---|---|---|
| Analysis No. | 14 | 2 | 4 | 7 | 9 | 11 | 12 | 13 | 2 | 5 | 10 | 11 | 17 | 24 | 2 | 8 | 10 |
| Analysis Name. | ol6 | ol1 | ol2 | ol3 | ol4 | ol5 | ol6 | ol7 | ol1 | ol2 | ol3 | ol4 | ol5 | ol6 | ol1 | ol2 | ol3 |
| SiO2 | 37.53 | 40.00 | 39.74 | 40.18 | 40.37 | 39.87 | 39.93 | 40.15 | 39.78 | 40.35 | 40.56 | 40.36 | 40.39 | 40.02 | 39.72 | 40.09 | 40.21 |
| TiO2 | 0.00 | 0.00 | 0.00 | 0.00 | 0.00 | 0.00 | 0.00 | 0.00 | 0.00 | 0.00 | 0.00 | 0.00 | 0.00 | 0.00 | 0.00 | 0.00 | 0.00 |
| Al2O3 | 0.00 | 0.00 | 0.00 | 0.00 | 0.00 | 0.00 | 0.00 | 0.00 | 0.00 | 0.00 | 0.00 | 0.00 | 0.00 | 0.00 | 0.00 | 0.00 | 0.00 |
| Cr2O3 | 0.00 | 0.00 | 0.00 | 0.00 | 0.00 | 0.00 | 0.00 | 0.00 | 0.00 | 0.00 | 0.00 | 0.00 | 0.00 | 0.00 | 0.00 | 0.00 | 0.00 |
| FeO | 31.77 | 16.25 | 16.77 | 16.58 | 16.72 | 16.75 | 16.10 | 16.51 | 17.44 | 16.97 | 16.85 | 17.23 | 17.02 | 17.29 | 17.75 | 17.55 | 17.54 |
| MnO | 0.50 | 0.45 | 0.00 | 0.21 | 0.24 | 0.23 | 0.34 | 0.40 | 0.30 | 0.00 | 0.24 | 0.24 | 0.00 | 0.00 | 0.21 | 0.00 | 0.31 |
| MgO | 30.95 | 42.97 | 42.77 | 43.70 | 42.94 | 42.73 | 43.08 | 42.94 | 42.61 | 43.33 | 43.53 | 43.55 | 43.32 | 43.18 | 41.74 | 42.57 | 42.16 |
| NiO | 0.00 | 0.00 | 0.00 | 0.00 | 0.34 | 0.00 | 0.00 | 0.00 | 0.00 | 0.00 | 0.00 | 0.00 | 0.00 | 0.00 | 0.00 | 0.00 | 0.00 |
| CaO | 0.00 | 0.00 | 0.00 | 0.00 | 0.00 | 0.00 | 0.00 | 0.00 | 0.00 | 0.00 | 0.00 | 0.00 | 0.00 | 0.00 | 0.00 | 0.00 | 0.00 |
| Total | 100.75 | 99.65 | 99.28 | 100.67 | 100.60 | 99.57 | 99.45 | 99.99 | 100.13 | 100.65 | 101.18 | 101.38 | 100.73 | 100.49 | 99.42 | 100.21 | 100.22 |
| **Formula (4O)** | | | | | | | | | | | | | | | | | |
| Si | 1.013 | 1.012 | 1.011 | 1.007 | 1.014 | 1.012 | 1.012 | 1.014 | 1.008 | 1.012 | 1.012 | 1.007 | 1.012 | 1.008 | 1.014 | 1.013 | 1.017 |
| Ti | 0.000 | 0.000 | 0.000 | 0.000 | 0.000 | 0.000 | 0.000 | 0.000 | 0.000 | 0.000 | 0.000 | 0.000 | 0.000 | 0.000 | 0.000 | 0.000 | 0.000 |
| Al | 0.000 | 0.000 | 0.000 | 0.000 | 0.000 | 0.000 | 0.000 | 0.000 | 0.000 | 0.000 | 0.000 | 0.000 | 0.000 | 0.000 | 0.000 | 0.000 | 0.000 |
| Cr | 0.000 | 0.000 | 0.000 | 0.000 | 0.000 | 0.000 | 0.000 | 0.000 | 0.000 | 0.000 | 0.000 | 0.000 | 0.000 | 0.000 | 0.000 | 0.000 | 0.000 |
| Fe(ii) | 0.717 | 0.344 | 0.357 | 0.348 | 0.351 | 0.355 | 0.341 | 0.348 | 0.369 | 0.356 | 0.352 | 0.360 | 0.357 | 0.364 | 0.379 | 0.371 | 0.371 |
| Mn | 0.011 | 0.010 | 0.000 | 0.004 | 0.005 | 0.005 | 0.007 | 0.009 | 0.006 | 0.000 | 0.005 | 0.005 | 0.000 | 0.000 | 0.005 | 0.000 | 0.007 |
| Mg | 1.245 | 1.621 | 1.622 | 1.633 | 1.608 | 1.616 | 1.628 | 1.616 | 1.609 | 1.620 | 1.619 | 1.621 | 1.619 | 1.621 | 1.589 | 1.603 | 1.589 |
| Ni | 0.000 | 0.000 | 0.000 | 0.000 | 0.007 | 0.000 | 0.000 | 0.000 | 0.000 | 0.000 | 0.000 | 0.000 | 0.000 | 0.000 | 0.000 | 0.000 | 0.000 |
| Ca | 0.000 | 0.000 | 0.000 | 0.000 | 0.000 | 0.000 | 0.000 | 0.000 | 0.000 | 0.000 | 0.000 | 0.000 | 0.000 | 0.000 | 0.000 | 0.000 | 0.000 |
| Total | 2.987 | 2.988 | 2.989 | 2.993 | 2.986 | 2.988 | 2.988 | 2.986 | 2.992 | 2.988 | 2.988 | 2.993 | 2.988 | 2.992 | 2.986 | 2.987 | 2.983 |
| **Endmembers** | | | | | | | | | | | | | | | | | |
| Fo | 63.09 | 82.10 | 81.97 | 82.27 | 81.86 | 81.77 | 82.37 | 81.90 | 81.07 | 81.99 | 81.95 | 81.63 | 81.94 | 81.66 | 80.56 | 81.22 | 80.81 |
| Fa | 36.33 | 17.41 | 18.03 | 17.51 | 17.88 | 17.98 | 17.27 | 17.66 | 18.61 | 18.01 | 17.79 | 18.11 | 18.06 | 18.34 | 19.21 | 18.78 | 18.86 |
| Tp | | | | | | | | | | | | | | | | | |

**Olivine**

| Sample | Ab6510 | Ab6510 | Ab6510 | MS1601 | MS1601 | MS1601 | MS1601 | MS1601 | CLW107 | CLW107 | CLW107 | CLW107 | DCD106 | DCD106 | DCD106 | DCD106 | DCD106 |
|---|---|---|---|---|---|---|---|---|---|---|---|---|---|---|---|---|---|
| Analysis No. | 12 | 15 | 18 | 2 | 3 | 7 | 8 | 11 | 5 | 12 | 19 | 25 | 5 | 6 | 9 | 12 | 13 |
| Analysis Name. | ol4 | ol5 | ol6 | ol1 | ol2 | ol3 | ol4 | ol5 | ol1 | ol2 | ol4 | ol5 | ol1 | ol2 | ol2 | ol3 | ol4 |
| SiO2 | 40.02 | 40.10 | 39.89 | 42.64 | 42.46 | 41.31 | 41.70 | 42.08 | 39.15 | 39.47 | 39.40 | 39.06 | 39.10 | 38.99 | 39.36 | 39.46 | 39.51 |
| TiO2 | 0.00 | 0.00 | 0.00 | 0.00 | 0.00 | 0.00 | 0.00 | 0.00 | 0.00 | 0.00 | 0.00 | 0.00 | 0.00 | 0.00 | 0.00 | 0.00 | 0.20 |
| Al2O3 | 0.00 | 0.00 | 0.00 | 0.00 | 0.00 | 0.00 | 0.00 | 0.00 | 0.00 | 0.00 | 0.00 | 0.00 | 0.00 | 0.00 | 0.00 | 0.00 | 0.00 |
| Cr2O3 | 0.00 | 0.00 | 0.00 | 0.00 | 0.00 | 0.00 | 0.00 | 0.00 | 0.00 | 0.00 | 0.00 | 0.00 | 0.00 | 0.00 | 0.00 | 0.00 | 0.00 |
| FeO | 17.50 | 17.68 | 18.10 | 8.52 | 8.56 | 8.51 | 8.43 | 8.61 | 20.79 | 20.98 | 19.98 | 20.53 | 20.01 | 20.67 | 20.05 | 20.08 | 20.45 |
| MnO | 0.41 | 0.39 | 0.28 | 0.00 | 0.19 | 0.00 | 0.19 | 0.00 | 0.24 | 0.32 | 0.22 | 0.00 | 0.36 | 0.34 | 0.32 | 0.24 | 0.21 |
| MgO | 42.28 | 42.34 | 42.17 | 51.20 | 50.68 | 49.74 | 49.59 | 50.96 | 39.74 | 39.91 | 40.33 | 39.62 | 40.28 | 39.95 | 40.56 | 40.34 | 40.60 |
| NiO | 0.00 | 0.30 | 0.00 | 0.62 | 0.49 | 0.49 | 0.00 | 0.00 | 0.00 | 0.00 | 0.00 | 0.00 | 0.00 | 0.00 | 0.00 | 0.00 | 0.00 |
| CaO | 0.00 | 0.00 | 0.00 | 0.00 | 0.00 | 0.00 | 0.00 | 0.00 | 0.00 | 0.00 | 0.00 | 0.00 | 0.00 | 0.00 | 0.00 | 0.00 | 0.00 |
| Total | 100.21 | 100.81 | 100.44 | 102.99 | 102.38 | 100.05 | 99.91 | 101.65 | 99.93 | 100.67 | 99.93 | 99.21 | 99.75 | 99.94 | 100.29 | 100.11 | 100.98 |
| **Formula (4O)** | | | | | | | | | | | | | | | | | |
| Si | 1.013 | 1.011 | 1.010 | 1.008 | 1.010 | 1.006 | 1.014 | 1.006 | 1.009 | 1.010 | 1.011 | 1.012 | 1.007 | 1.005 | 1.008 | 1.011 | 1.006 |
| Ti | 0.000 | 0.000 | 0.000 | 0.000 | 0.000 | 0.000 | 0.000 | 0.000 | 0.000 | 0.000 | 0.000 | 0.000 | 0.000 | 0.000 | 0.000 | 0.000 | 0.004 |
| Al | 0.000 | 0.000 | 0.000 | 0.000 | 0.000 | 0.000 | 0.000 | 0.000 | 0.000 | 0.000 | 0.000 | 0.000 | 0.000 | 0.000 | 0.000 | 0.000 | 0.000 |
| Cr | 0.000 | 0.000 | 0.000 | 0.000 | 0.000 | 0.000 | 0.000 | 0.000 | 0.000 | 0.000 | 0.000 | 0.000 | 0.000 | 0.000 | 0.000 | 0.000 | 0.000 |
| Fe(ii) | 0.370 | 0.373 | 0.383 | 0.168 | 0.170 | 0.173 | 0.171 | 0.172 | 0.448 | 0.449 | 0.429 | 0.445 | 0.431 | 0.446 | 0.429 | 0.430 | 0.435 |
| Mn | 0.009 | 0.008 | 0.006 | 0.000 | 0.004 | 0.000 | 0.004 | 0.000 | 0.005 | 0.007 | 0.005 | 0.000 | 0.008 | 0.007 | 0.007 | 0.005 | 0.005 |
| Mg | 1.595 | 1.591 | 1.591 | 1.804 | 1.797 | 1.805 | 1.797 | 1.816 | 1.528 | 1.523 | 1.543 | 1.531 | 1.547 | 1.536 | 1.548 | 1.542 | 1.541 |
| Ni | 0.000 | 0.006 | 0.000 | 0.012 | 0.009 | 0.010 | 0.000 | 0.000 | 0.000 | 0.000 | 0.000 | 0.000 | 0.000 | 0.000 | 0.000 | 0.000 | 0.000 |
| Ca | 0.000 | 0.000 | 0.000 | 0.000 | 0.000 | 0.000 | 0.000 | 0.000 | 0.000 | 0.000 | 0.000 | 0.000 | 0.000 | 0.000 | 0.000 | 0.000 | 0.000 |
| Total | 2.987 | 2.989 | 2.990 | 2.992 | 2.990 | 2.994 | 2.986 | 2.994 | 2.991 | 2.990 | 2.989 | 2.988 | 2.993 | 2.995 | 2.992 | 2.989 | 2.990 |
| **Endmembers** | | | | | | | | | | | | | | | | | |
| Fo | 80.80 | 80.68 | 80.35 | 91.46 | 91.17 | 91.24 | 91.11 | 91.34 | 77.11 | 76.96 | 78.07 | 77.48 | 77.90 | 77.22 | 78.02 | 77.97 | 77.79 |
| Fa | 18.76 | 18.90 | 19.34 | 8.54 | 8.64 | 8.76 | 8.69 | 8.66 | 22.63 | 22.69 | 21.69 | 22.52 | 21.71 | 22.41 | 21.63 | 21.77 | 21.98 |
| Tp | | | | | | | | | | | | | | | | | |

**Orthopyroxene**

| Sample | 9P | 9P | 9P | 9P | 9P | 9P | 9P | 9P | Ab82 | Ab82 | Ab82 | Ab82 | Ab82 | Ab82 | Ab82 | Ab82 | Ab82 | Ab82 |
|---|---|---|---|---|---|---|---|---|---|---|---|---|---|---|---|---|---|---|
| Analysis No. | 1 | 2 | 10 | 13 | 18 | 19 | 23 | 25 | 2 | 3 | 8 | 10 | 14 | 15 | 17 | 19 | 20 | 24 |
| Analysis Name. | opx1 | opx2 | opx3 | opx4 | opx2-2 | px3 | px5 | px6 | opx1 | opx2 | opx3 | opx4 | opx5 | opx6 | opx7 | opx8 | px9a | px9e |
| SiO2 | 54.01 | 54.39 | 53.22 | 53.97 | 53.68 | 54.38 | 54.43 | 53.40 | 56.06 | 56.36 | 55.48 | 55.94 | 53.92 | 57.14 | 55.93 | 55.50 | 55.48 | 54.65 |
| TiO2 | 0.00 | 0.30 | 0.00 | 0.18 | 0.25 | 0.00 | 0.00 | 0.28 | 0.22 | 0.00 | 0.31 | 0.22 | 0.36 | 0.23 | 0.23 | 0.19 | 0.00 | 0.16 |
| Al2O3 | 0.77 | 0.95 | 1.18 | 1.19 | 0.89 | 0.81 | 0.82 | 1.30 | 0.64 | 1.94 | 0.56 | 1.39 | 2.20 | 1.29 | 0.63 | 0.71 | 0.90 | 1.94 |
| Cr2O3 | 0.23 | 0.00 | 0.00 | 0.29 | 0.00 | 0.00 | 0.00 | 0.36 | 0.00 | 0.27 | 0.00 | 0.27 | 0.28 | 0.00 | 0.00 | 0.00 | 0.00 | 0.17 |
| FeO | 16.21 | 16.05 | 16.12 | 16.07 | 16.07 | 15.99 | 16.15 | 16.47 | 18.05 | 14.30 | 17.41 | 15.30 | 16.43 | 14.17 | 16.06 | 17.93 | 17.15 | 14.67 |
| MnO | 0.40 | 0.45 | 0.39 | 0.20 | 0.32 | 0.47 | 0.39 | 0.29 | 0.29 | 0.33 | 0.35 | 0.00 | 0.42 | 0.00 | 0.42 | 0.26 | 0.43 | 0.32 |
| MgO | 26.31 | 26.26 | 25.54 | 26.30 | 25.78 | 26.25 | 26.42 | 25.86 | 26.71 | 28.32 | 26.66 | 27.47 | 25.44 | 21.59 | 27.50 | 25.86 | 26.34 | 25.46 |
| CaO | 0.50 | 0.63 | 1.03 | 0.57 | 1.63 | 0.60 | 1.18 | 0.95 | 0.39 | 0.54 | 0.54 | 1.47 | 1.34 | 0.41 | 0.49 | 0.68 | 0.54 | 2.54 |
| Na2O | 0.20 | 0.00 | 0.00 | 0.32 | 0.00 | 0.00 | 0.00 | 0.00 | 0.00 | 0.00 | 0.20 | 0.23 | 0.28 | 0.26 | 0.00 | 0.23 | 0.27 | 0.37 |
| K2O | 0.00 | 0.00 | 0.00 | 0.00 | 0.00 | 0.00 | 0.00 | 0.00 | 0.00 | 0.00 | 0.00 | 0.00 | 0.00 | 0.00 | 0.00 | 0.00 | 0.00 | 0.00 |
| NiO | | | | | | | | | 0.00 | 0.00 | 0.00 | 0.00 | 0.00 | 0.00 | 0.00 | 0.00 | 0.00 | 0.00 |
| Total | 98.63 | 99.02 | 97.48 | 99.09 | 98.62 | 98.50 | 99.39 | 98.90 | 102.37 | 102.05 | 101.51 | 102.29 | 100.66 | 95.08 | 101.27 | 101.36 | 101.11 | 100.29 |
| **Formula (6O)** | | | | | | | | | | | | | | | | | | |
| Si | 1.980 | 1.980 | 1.980 | 1.970 | 1.970 | 1.990 | 1.980 | 1.960 | 1.988 | 1.972 | 1.984 | 1.968 | 1.945 | 2.121 | 1.990 | 1.991 | 1.989 | 1.966 |
| Al | 0.020 | 0.020 | 0.020 | 0.030 | 0.030 | 0.010 | 0.020 | 0.040 | 0.012 | 0.028 | 0.016 | 0.032 | 0.055 | -0.121 | 0.010 | 0.009 | 0.011 | 0.034 |
| Al | 0.020 | 0.020 | 0.030 | 0.020 | 0.010 | 0.030 | 0.020 | 0.020 | 0.015 | 0.052 | 0.008 | 0.026 | 0.039 | 0.178 | 0.016 | 0.021 | 0.027 | 0.049 |
| Fe(iii) | 0.020 | 0.000 | 0.000 | 0.020 | 0.000 | 0.000 | 0.000 | 0.000 | 0.000 | 0.000 | 0.009 | 0.004 | 0.013 | 0.000 | 0.000 | 0.000 | 0.004 | 0.000 |
| Cr | 0.010 | 0.000 | 0.000 | 0.010 | 0.000 | 0.000 | 0.000 | 0.010 | 0.000 | 0.007 | 0.000 | 0.008 | 0.008 | 0.000 | 0.000 | 0.000 | 0.000 | 0.005 |
| Ti | 0.000 | 0.010 | 0.000 | 0.000 | 0.010 | 0.000 | 0.000 | 0.010 | 0.006 | 0.000 | 0.008 | 0.006 | 0.010 | 0.006 | 0.006 | 0.005 | 0.000 | 0.004 |
| Fe(ii) | 0.480 | 0.490 | 0.500 | 0.470 | 0.490 | 0.490 | 0.490 | 0.510 | 0.536 | 0.420 | 0.512 | 0.446 | 0.482 | 0.457 | 0.479 | 0.538 | 0.510 | 0.442 |
| Mn | 0.010 | 0.010 | 0.010 | 0.010 | 0.010 | 0.010 | 0.010 | 0.010 | 0.009 | 0.010 | 0.011 | 0.000 | 0.013 | 0.000 | 0.013 | 0.008 | 0.013 | 0.010 |
| Mg | 1.440 | 1.430 | 1.410 | 1.430 | 1.410 | 1.430 | 1.430 | 1.410 | 1.412 | 1.477 | 1.421 | 1.441 | 1.368 | 1.195 | 1.459 | 1.383 | 1.408 | 1.366 |
| Ca | 0.020 | 0.020 | 0.040 | 0.020 | 0.060 | 0.020 | 0.050 | 0.040 | 0.015 | 0.020 | 0.021 | 0.055 | 0.052 | 0.016 | 0.019 | 0.026 | 0.021 | 0.098 |
| Na | 0.010 | 0.000 | 0.000 | 0.020 | 0.000 | 0.000 | 0.000 | 0.000 | 0.000 | 0.000 | 0.014 | 0.016 | 0.020 | 0.019 | 0.000 | 0.016 | 0.019 | 0.026 |
| K | 0.000 | 0.000 | 0.000 | 0.000 | 0.000 | 0.000 | 0.000 | 0.000 | 0.000 | 0.000 | 0.000 | 0.000 | 0.000 | 0.000 | 0.000 | 0.000 | 0.000 | 0.000 |
| TOTAL | 4.000 | 3.990 | 4.000 | 4.010 | 4.000 | 3.990 | 4.000 | 4.000 | 3.993 | 3.986 | 4.002 | 4.001 | 4.004 | 3.870 | 3.992 | 3.997 | 4.001 | 3.999 |
| **Endmembers** | | | | | | | | | | | | | | | | | | |
| Wo | 0.99 | 1.26 | 2.08 | 1.13 | 3.24 | 1.20 | 2.32 | 1.90 | 0.75 | 1.05 | 1.04 | 2.82 | 2.66 | 0.97 | 0.95 | 1.33 | 1.05 | 5.05 |
| En | 72.61 | 72.95 | 71.84 | 72.58 | 71.32 | 73.04 | 72.29 | 71.94 | 71.61 | 76.65 | 71.54 | 73.44 | 70.25 | 70.85 | 74.08 | 70.16 | 71.31 | 70.37 |
| Fs | 25.69 | 25.79 | 26.07 | 25.14 | 25.44 | 25.76 | 25.39 | 26.16 | 27.64 | 22.30 | 26.72 | 22.94 | 26.08 | 27.07 | 24.97 | 27.71 | 26.69 | 23.25 |
| Ac | 0.72 | 0.00 | 0.00 | 1.15 | 0.00 | 0.00 | 0.00 | 0.00 | 0.00 | 0.00 | 0.70 | 0.80 | 1.01 | 1.11 | 0.00 | 0.81 | 0.95 | 1.33 |

**Orthopyroxene**

| Sample | Ab82 | Ab125 | Ab125 | Ab125 | Ab125 | Ab125 | Ab125 | Ab125 | Ab125 | Ab125 | Ab125 | Ab125 | Ab125 | Ab125 | Ab125 | Ab125 | Ab125 | Ab125 |
|---|---|---|---|---|---|---|---|---|---|---|---|---|---|---|---|---|---|---|
| Analysis No. | 31 | 1 | 3 | 4 | 5 | 6 | 7 | 8 | 9 | 10 | 11 | 13 | 15 | 16 | 17 | 19 | 21 | 25 |
| Analysis Name. | px10a | opx1 | opx3 | opx4 | opx5a | opx5b | opx5c | opx5d | opx5e | opx6 | opx7 | px7a | px7c | px7d | px7e | opx8 | opx9 | opx10 |
| SiO2 | 55.09 | 56.18 | 55.23 | 54.82 | 54.57 | 54.37 | 54.73 | 54.47 | 53.99 | 53.97 | 53.84 | 54.04 | 59.54 | 47.70 | 53.65 | 54.04 | 54.35 | 54.63 |
| TiO2 | 0.18 | 0.36 | 0.00 | 0.00 | 0.18 | 0.23 | 0.16 | 0.25 | 0.24 | 0.40 | 0.00 | 0.28 | 0.15 | 1.71 | 0.37 | 0.32 | 0.23 | 0.24 |
| Al2O3 | 0.56 | 1.73 | 1.63 | 1.74 | 1.95 | 1.92 | 2.20 | 2.14 | 2.05 | 2.54 | 2.12 | 2.09 | 0.97 | 7.74 | 1.89 | 1.96 | 2.06 | 1.58 |
| Cr2O3 | 0.00 | 0.00 | 0.36 | 0.00 | 0.25 | 0.26 | 0.21 | 0.19 | 0.00 | 0.17 | 0.00 | 0.17 | 0.00 | 0.72 | 0.17 | 0.18 | 0.24 | 0.18 |
| FeO | 17.28 | 11.76 | 11.47 | 12.26 | 11.63 | 11.62 | 11.56 | 11.36 | 11.73 | 11.24 | 11.13 | 11.80 | 6.28 | 5.79 | 12.27 | 11.27 | 11.73 | 10.73 |
| MnO | 0.36 | 0.25 | 0.27 | 0.30 | 0.25 | 0.00 | 0.00 | 0.19 | 0.27 | 0.23 | 0.28 | 0.34 | 0.00 | 0.00 | 0.34 | 0.35 | 0.19 | 0.33 |
| MgO | 25.84 | 29.30 | 28.18 | 28.51 | 29.03 | 28.67 | 28.84 | 28.53 | 27.86 | 28.77 | 28.39 | 28.60 | 26.20 | 17.25 | 27.96 | 28.07 | 28.61 | 29.13 |
| CaO | 1.05 | 1.33 | 2.28 | 1.31 | 0.74 | 0.85 | 0.93 | 1.54 | 1.65 | 1.10 | 1.69 | 0.78 | 0.00 | 11.94 | 1.04 | 2.22 | 1.22 | 0.97 |
| Na2O | 0.00 | 0.00 | 0.00 | 0.00 | 0.00 | 0.00 | 0.25 | 0.00 | 0.00 | 0.00 | 0.00 | 0.00 | 0.21 | 1.06 | 0.00 | 0.00 | 0.22 | 0.27 |
| K2O | 0.00 | 0.00 | 0.00 | 0.00 | 0.00 | 0.00 | 0.00 | 0.00 | 0.00 | 0.21 | 0.00 | 0.00 | 0.00 | 0.62 | 0.00 | 0.00 | 0.00 | 0.00 |
| NiO | 0.00 | 0.00 | 0.00 | 0.00 | 0.00 | 0.00 | 0.00 | 0.00 | 0.00 | 0.00 | 0.00 | 0.00 | 0.00 | 0.00 | 0.00 | 0.00 | 0.00 | 0.00 |
| Total | 100.36 | 100.91 | 99.42 | 98.93 | 98.58 | 97.92 | 98.88 | 98.68 | 97.78 | 98.63 | 97.44 | 98.10 | 93.35 | 94.54 | 97.69 | 98.39 | 98.84 | 98.06 |
| **Formula (6O)** | | | | | | | | | | | | | | | | | | |
| Si | 1.993 | 1.970 | 1.972 | 1.968 | 1.959 | 1.963 | 1.958 | 1.955 | 1.960 | 1.939 | 1.957 | 1.953 | 2.158 | 1.820 | 1.954 | 1.951 | 1.951 | 1.967 |
| Al | 0.007 | 0.030 | 0.028 | 0.032 | 0.041 | 0.037 | 0.042 | 0.045 | 0.040 | 0.061 | 0.043 | 0.047 | -0.158 | 0.180 | 0.046 | 0.049 | 0.049 | 0.033 |
| Al | 0.017 | 0.041 | 0.041 | 0.042 | 0.041 | 0.045 | 0.050 | 0.046 | 0.047 | 0.046 | 0.047 | 0.042 | 0.200 | 0.168 | 0.035 | 0.034 | 0.039 | 0.034 |
| Fe(iii) | 0.000 | 0.000 | 0.000 | 0.000 | 0.000 | 0.000 | 0.000 | 0.000 | 0.000 | 0.000 | 0.000 | 0.000 | 0.000 | 0.002 | 0.000 | 0.000 | 0.009 | 0.000 |
| Cr | 0.000 | 0.000 | 0.010 | 0.000 | 0.007 | 0.007 | 0.006 | 0.005 | 0.000 | 0.005 | 0.000 | 0.005 | 0.000 | 0.022 | 0.005 | 0.005 | 0.007 | 0.005 |
| Ti | 0.005 | 0.009 | 0.000 | 0.000 | 0.005 | 0.006 | 0.004 | 0.007 | 0.007 | 0.011 | 0.000 | 0.008 | 0.004 | 0.049 | 0.010 | 0.009 | 0.006 | 0.007 |
| Fe(ii) | 0.524 | 0.346 | 0.343 | 0.368 | 0.350 | 0.352 | 0.346 | 0.342 | 0.357 | 0.338 | 0.338 | 0.357 | 0.199 | 0.183 | 0.374 | 0.341 | 0.343 | 0.323 |
| Mn | 0.011 | 0.007 | 0.008 | 0.009 | 0.008 | 0.000 | 0.000 | 0.006 | 0.008 | 0.007 | 0.009 | 0.010 | 0.000 | 0.000 | 0.010 | 0.011 | 0.006 | 0.010 |
| Mg | 1.394 | 1.532 | 1.500 | 1.526 | 1.553 | 1.543 | 1.538 | 1.527 | 1.508 | 1.541 | 1.538 | 1.541 | 1.416 | 0.981 | 1.518 | 1.511 | 1.531 | 1.564 |
| Ca | 0.041 | 0.050 | 0.087 | 0.050 | 0.028 | 0.033 | 0.036 | 0.059 | 0.064 | 0.042 | 0.066 | 0.030 | 0.000 | 0.488 | 0.041 | 0.086 | 0.047 | 0.037 |
| Na | 0.000 | 0.000 | 0.000 | 0.000 | 0.000 | 0.000 | 0.017 | 0.000 | 0.000 | 0.000 | 0.000 | 0.000 | 0.015 | 0.078 | 0.000 | 0.000 | 0.015 | 0.019 |
| K | 0.000 | 0.000 | 0.000 | 0.000 | 0.000 | 0.000 | 0.000 | 0.000 | 0.000 | 0.010 | 0.000 | 0.000 | 0.000 | 0.030 | 0.000 | 0.000 | 0.000 | 0.000 |
| TOTAL | 3.991 | 3.986 | 3.990 | 3.996 | 3.992 | 3.987 | 3.998 | 3.991 | 3.991 | 3.999 | 3.998 | 3.993 | 3.833 | 4.001 | 3.994 | 3.996 | 4.003 | 4.000 |
| **Endmembers** | | | | | | | | | | | | | | | | | | |
| Wo | 2.07 | 2.58 | 4.50 | 2.58 | 1.47 | 1.71 | 1.84 | 3.06 | 3.31 | 2.20 | 3.37 | 1.56 | 0.00 | 28.17 | 2.09 | 4.41 | 2.40 | 1.92 |
| En | 70.76 | 79.15 | 77.37 | 78.10 | 80.10 | 80.04 | 79.40 | 78.96 | 77.83 | 79.92 | 78.84 | 79.48 | 86.88 | 56.64 | 78.11 | 77.56 | 78.48 | 80.06 |
| Fs | 27.17 | 18.27 | 18.13 | 19.33 | 18.43 | 18.26 | 17.86 | 17.98 | 18.86 | 17.88 | 17.79 | 18.96 | 12.22 | 10.66 | 19.80 | 18.03 | 18.33 | 17.06 |
| Ac | 0.00 | 0.00 | 0.00 | 0.00 | 0.00 | 0.00 | 0.90 | 0.00 | 0.00 | 0.00 | 0.00 | 0.00 | 0.91 | 4.53 | 0.00 | 0.00 | 0.78 | 0.96 |

**Orthopyroxene**

| Sample | Ab140 | Ab143 | Ab143 | Ab143 | Ab143 | Ab143 | Ab143 | Ab143 | Ab143 | Ab143 | Ab143 | Ab143 | Ab143 | Ab143 | Ab143 | Ab143 | Ab143 |
|---|---|---|---|---|---|---|---|---|---|---|---|---|---|---|---|---|---|
| Analysis No. | 24 | 2 | 4 | 5 | 8 | 23 | 25 | 28 | 29 | 30 | 31 | 34 | 37 | 38 | 6 | 7 | 9 |
| Analysis Name. | cor1 | opx1 | opx2? | opx3a | px3d | opx4 | opx5 | opx7a | opx7b | opx7c | opx7d | opx8a | px3f | px3g | px3b | px3c | cpx4 |
| SiO2 | 56.55 | 55.70 | 54.84 | 54.40 | 55.03 | 54.65 | 54.77 | 54.19 | 54.81 | 54.72 | 54.06 | 54.70 | 54.49 | 55.00 | 51.37 | 51.23 | 51.33 |
| TiO2 | 0.00 | 0.20 | 0.30 | 0.00 | 0.00 | 0.00 | 0.00 | 0.00 | 0.21 | 0.00 | 0.21 | 0.00 | 0.23 | 0.21 | 0.59 | 0.51 | 0.49 |
| Al2O3 | 1.49 | 2.91 | 2.80 | 2.73 | 2.44 | 2.70 | 2.46 | 2.78 | 2.86 | 2.63 | 2.98 | 2.90 | 2.45 | 2.61 | 3.82 | 3.88 | 3.68 |
| Cr2O3 | 0.00 | 0.47 | 0.57 | 0.58 | 0.51 | 0.55 | 0.56 | 0.55 | 0.69 | 0.63 | 0.59 | 0.45 | 0.45 | 0.36 | 0.87 | 0.89 | 0.95 |
| FeO | 8.48 | 9.30 | 9.08 | 8.66 | 9.11 | 9.10 | 9.06 | 9.65 | 9.84 | 9.71 | 10.29 | 10.10 | 8.94 | 8.62 | 3.63 | 3.06 | 3.69 |
| MnO | 0.22 | 0.00 | 0.27 | 0.21 | 0.19 | 0.28 | 0.23 | 0.30 | 0.24 | 0.00 | 0.23 | 0.00 | 0.00 | 0.19 | 0.00 | 0.26 | 0.00 |
| MgO | 32.85 | 31.06 | 30.01 | 29.76 | 30.92 | 30.14 | 30.58 | 29.72 | 29.92 | 30.33 | 30.04 | 29.77 | 30.28 | 30.73 | 15.41 | 15.80 | 15.64 |
| CaO | 0.76 | 1.33 | 2.16 | 1.74 | 0.68 | 1.37 | 1.13 | 0.87 | 0.78 | 0.78 | 0.63 | 0.89 | 1.44 | 0.85 | 22.48 | 23.23 | 22.31 |
| Na2O | 0.00 | 0.00 | 0.00 | 0.00 | 0.00 | 0.23 | 0.21 | 0.00 | 0.23 | 0.00 | 0.00 | 0.00 | 0.00 | 0.00 | 0.33 | 0.50 | 0.75 |
| K2O | 0.00 | 0.00 | 0.00 | 0.00 | 0.00 | 0.00 | 0.00 | 0.00 | 0.00 | 0.00 | 0.00 | 0.00 | 0.00 | 0.00 | 0.00 | 0.00 | 0.00 |
| NiO | | 0.00 | 0.00 | 0.00 | 0.00 | 0.32 | 0.00 | 0.28 | 0.00 | 0.00 | 0.00 | 0.00 | 0.00 | 0.00 | 0.00 | 0.00 | 0.00 |
| Total | 100.36 | 100.96 | 100.03 | 98.07 | 98.88 | 99.34 | 99.00 | 98.33 | 99.57 | 98.81 | 99.03 | 98.81 | 98.28 | 98.57 | 98.51 | 99.35 | 98.83 |
| **Formula (6O)** | | | | | | | | | | | | | | | | | |
| Si | 1.960 | 1.933 | 1.928 | 1.943 | 1.947 | 1.938 | 1.941 | 1.941 | 1.936 | 1.943 | 1.923 | 1.944 | 1.942 | 1.947 | 1.905 | 1.888 | 1.900 |
| Al | 0.040 | 0.067 | 0.072 | 0.057 | 0.053 | 0.062 | 0.059 | 0.059 | 0.064 | 0.057 | 0.077 | 0.056 | 0.058 | 0.053 | 0.095 | 0.112 | 0.100 |
| Al | 0.020 | 0.052 | 0.044 | 0.058 | 0.049 | 0.051 | 0.043 | 0.058 | 0.055 | 0.053 | 0.048 | 0.065 | 0.045 | 0.056 | 0.072 | 0.056 | 0.061 |
| Fe(iii) | 0.020 | 0.000 | 0.000 | 0.000 | 0.000 | 0.017 | 0.022 | 0.000 | 0.000 | 0.000 | 0.001 | 0.000 | 0.000 | 0.000 | 0.000 | 0.057 | 0.056 |
| Cr | 0.000 | 0.013 | 0.016 | 0.016 | 0.014 | 0.015 | 0.016 | 0.016 | 0.019 | 0.018 | 0.017 | 0.013 | 0.013 | 0.010 | 0.026 | 0.026 | 0.028 |
| Ti | 0.000 | 0.005 | 0.008 | 0.000 | 0.000 | 0.000 | 0.000 | 0.000 | 0.006 | 0.000 | 0.006 | 0.000 | 0.006 | 0.006 | 0.016 | 0.014 | 0.014 |
| Fe(ii) | 0.230 | 0.270 | 0.267 | 0.259 | 0.270 | 0.252 | 0.246 | 0.290 | 0.291 | 0.289 | 0.305 | 0.301 | 0.267 | 0.256 | 0.113 | 0.037 | 0.058 |
| Mn | 0.010 | 0.000 | 0.008 | 0.006 | 0.006 | 0.008 | 0.007 | 0.009 | 0.007 | 0.000 | 0.007 | 0.000 | 0.000 | 0.006 | 0.000 | 0.008 | 0.000 |
| Mg | 1.700 | 1.607 | 1.573 | 1.585 | 1.631 | 1.593 | 1.615 | 1.587 | 1.575 | 1.605 | 1.593 | 1.577 | 1.609 | 1.622 | 0.852 | 0.868 | 0.863 |
| Ca | 0.030 | 0.049 | 0.081 | 0.067 | 0.026 | 0.052 | 0.043 | 0.033 | 0.030 | 0.030 | 0.024 | 0.034 | 0.055 | 0.032 | 0.893 | 0.917 | 0.885 |
| Na | 0.000 | 0.000 | 0.000 | 0.000 | 0.000 | 0.016 | 0.014 | 0.000 | 0.016 | 0.000 | 0.000 | 0.000 | 0.000 | 0.000 | 0.024 | 0.036 | 0.054 |
| K | 0.000 | 0.000 | 0.000 | 0.000 | 0.000 | 0.000 | 0.000 | 0.000 | 0.000 | 0.000 | 0.000 | 0.000 | 0.000 | 0.000 | 0.000 | 0.000 | 0.000 |
| TOTAL | 4.010 | 3.996 | 3.998 | 3.992 | 3.995 | 4.005 | 4.007 | 3.993 | 3.998 | 3.994 | 4.000 | 3.990 | 3.994 | 3.988 | 3.995 | 4.019 | 4.018 |
| **Endmembers** | | | | | | | | | | | | | | | | | |
| Wo | 1.43 | 2.57 | 4.22 | 3.47 | 1.33 | 2.68 | 2.20 | 1.74 | 1.54 | 1.54 | 1.24 | 1.77 | 2.85 | 1.68 | 47.47 | 47.70 | 46.19 |
| En | 85.84 | 83.41 | 81.52 | 82.67 | 84.41 | 82.17 | 82.94 | 82.70 | 82.11 | 83.45 | 82.54 | 82.49 | 83.33 | 84.66 | 45.28 | 45.14 | 45.06 |
| Fs | 12.74 | 14.02 | 14.26 | 13.85 | 14.26 | 14.33 | 14.11 | 15.56 | 15.53 | 15.01 | 16.22 | 15.74 | 13.82 | 13.66 | 5.99 | 5.30 | 5.94 |
| Ac | 0.00 | 0.00 | 0.00 | 0.00 | 0.00 | 0.82 | 0.74 | 0.00 | 0.82 | 0.00 | 0.00 | 0.00 | 0.00 | 0.00 | 1.26 | 1.86 | 2.81 |

**Orthopyroxene**

| Sample | Ab143 | Ab143 | Ab143 | Ab143 | Ab143 | Ab143 | Ab143 | Ab143 | Ab143 | Ab3826 | Ab3826 | Ab3826 | Ab3826 | Ab3826 | Ab3826 | Ab3826 | Ab3826 | Ab3826 |
|---|---|---|---|---|---|---|---|---|---|---|---|---|---|---|---|---|---|---|
| Analysis No. | 13 | 24 | 26 | 27 | 32 | 33 | 35 | 36 | 3 | 6 | 12 | 14 | 19 | 26 | 27 | 29 | 30 | 32 |
| Analysis Name. | cpx5 | cpx6 | cpx7a | cpx7b | cpx7c | cpx7d | cpx8a | px3e | pig1 | opx1 | opx1b | opx2 | opx3 | opx4 | opx5 | opx6a | opx6b | opx6c |
| SiO2 | 51.12 | 52.08 | 51.98 | 51.41 | 51.82 | 51.92 | 51.42 | 50.51 | 54.05 | 50.07 | 50.15 | 49.62 | 50.03 | 50.33 | 52.36 | 49.84 | 50.18 | 49.96 |
| TiO2 | 0.40 | 0.46 | 0.45 | 0.40 | 0.36 | 0.51 | 0.35 | 0.73 | 0.42 | 0.00 | 0.15 | 0.00 | 0.00 | 0.00 | 0.00 | 0.00 | 0.30 | 0.00 |
| Al2O3 | 3.80 | 3.85 | 3.96 | 3.79 | 3.81 | 3.92 | 3.71 | 4.78 | 2.82 | 0.47 | 0.40 | 0.35 | 0.35 | 0.54 | 0.45 | 0.43 | 0.68 | 0.73 |
| Cr2O3 | 0.90 | 0.89 | 0.99 | 0.98 | 0.95 | 1.09 | 1.00 | 0.85 | 0.51 | 0.00 | 0.00 | 0.00 | 0.00 | 0.00 | 0.00 | 0.00 | 0.00 | 0.00 |
| FeO | 3.49 | 4.65 | 3.62 | 3.90 | 4.20 | 3.30 | 4.27 | 3.41 | 6.76 | 33.35 | 32.94 | 32.90 | 32.71 | 32.63 | 27.20 | 32.70 | 30.80 | 31.75 |
| MnO | 0.23 | 0.00 | 0.00 | 0.00 | 0.00 | 0.26 | 0.00 | 0.20 | 0.00 | 1.25 | 1.01 | 1.07 | 0.96 | 1.00 | 0.69 | 1.05 | 0.87 | 1.02 |
| MgO | 15.39 | 17.40 | 15.81 | 15.56 | 16.79 | 15.64 | 15.99 | 15.24 | 24.83 | 13.26 | 13.38 | 13.29 | 13.07 | 13.48 | 14.27 | 13.56 | 14.23 | 13.84 |
| CaO | 22.05 | 19.82 | 22.27 | 22.50 | 20.84 | 22.42 | 21.63 | 22.58 | 10.64 | 0.94 | 0.85 | 0.89 | 0.86 | 1.33 | 0.82 | 1.05 | 1.96 | 1.75 |
| Na2O | 0.60 | 0.50 | 0.67 | 0.55 | 0.43 | 0.48 | 0.39 | 0.53 | 0.00 | 0.24 | 0.21 | 0.22 | 0.32 | 0.27 | 0.37 | 0.00 | 0.24 | 0.25 |
| K2O | 0.00 | 0.00 | 0.00 | 0.00 | 0.00 | 0.00 | 0.00 | 0.00 | 0.00 | 0.00 | 0.00 | 0.00 | 0.00 | 0.00 | 0.00 | 0.00 | 0.00 | 0.00 |
| NiO | 0.00 | 0.00 | 0.27 | 0.00 | 0.00 | 0.00 | 0.00 | 0.00 | 0.00 | | | | | | | | | |
| Total | 97.98 | 99.65 | 100.02 | 99.09 | 99.67 | 99.53 | 98.76 | 98.84 | 100.03 | 99.58 | 99.09 | 98.35 | 98.30 | 99.58 | 96.15 | 98.62 | 99.27 | 99.29 |
| **Formula (6O)** | | | | | | | | | | | | | | | | | | |
| Si | 1.906 | 1.902 | 1.903 | 1.900 | 1.904 | 1.904 | 1.904 | 1.870 | 1.926 | 1.991 | 1.997 | 1.995 | 2.007 | 1.993 | 2.076 | 1.993 | 1.980 | 1.980 |
| Al | 0.094 | 0.098 | 0.097 | 0.100 | 0.096 | 0.096 | 0.096 | 0.130 | 0.074 | 0.009 | 0.003 | 0.005 | -0.007 | 0.007 | -0.076 | 0.007 | 0.020 | 0.020 |
| Al | 0.073 | 0.068 | 0.074 | 0.065 | 0.069 | 0.073 | 0.065 | 0.079 | 0.044 | 0.013 | 0.016 | 0.011 | 0.024 | 0.018 | 0.097 | 0.014 | 0.012 | 0.014 |
| Fe(iii) | 0.022 | 0.021 | 0.027 | 0.036 | 0.016 | 0.000 | 0.015 | 0.034 | 0.000 | 0.023 | 0.000 | 0.017 | 0.000 | 0.015 | 0.000 | 0.000 | 0.013 | 0.037 |
| Cr | 0.027 | 0.026 | 0.029 | 0.029 | 0.028 | 0.032 | 0.029 | 0.025 | 0.014 | 0.000 | 0.000 | 0.000 | 0.000 | 0.000 | 0.000 | 0.000 | 0.000 | 0.000 |
| Ti | 0.011 | 0.013 | 0.012 | 0.011 | 0.010 | 0.014 | 0.010 | 0.020 | 0.011 | 0.000 | 0.004 | 0.000 | 0.000 | 0.000 | 0.000 | 0.000 | 0.009 | 0.000 |
| Fe(ii) | 0.087 | 0.121 | 0.084 | 0.084 | 0.112 | 0.101 | 0.117 | 0.071 | 0.202 | 1.083 | 1.097 | 1.088 | 1.098 | 1.064 | 0.918 | 1.095 | 1.002 | 1.012 |
| Mn | 0.007 | 0.000 | 0.000 | 0.000 | 0.000 | 0.008 | 0.000 | 0.006 | 0.000 | 0.042 | 0.034 | 0.036 | 0.033 | 0.034 | 0.023 | 0.036 | 0.029 | 0.034 |
| Mg | 0.856 | 0.948 | 0.863 | 0.857 | 0.920 | 0.855 | 0.883 | 0.841 | 1.319 | 0.786 | 0.794 | 0.796 | 0.782 | 0.796 | 0.843 | 0.809 | 0.837 | 0.818 |
| Ca | 0.881 | 0.776 | 0.873 | 0.891 | 0.820 | 0.881 | 0.858 | 0.896 | 0.406 | 0.040 | 0.036 | 0.038 | 0.037 | 0.056 | 0.035 | 0.045 | 0.083 | 0.074 |
| Na | 0.043 | 0.035 | 0.048 | 0.039 | 0.031 | 0.034 | 0.028 | 0.038 | 0.000 | 0.018 | 0.016 | 0.017 | 0.025 | 0.021 | 0.028 | 0.000 | 0.018 | 0.019 |
| K | 0.000 | 0.000 | 0.000 | 0.000 | 0.000 | 0.000 | 0.000 | 0.000 | 0.000 | 0.000 | 0.000 | 0.000 | 0.000 | 0.000 | 0.000 | 0.000 | 0.000 | 0.000 |
| TOTAL | 4.007 | 4.007 | 4.009 | 4.012 | 4.005 | 3.998 | 4.005 | 4.011 | 3.997 | 4.006 | 3.998 | 4.004 | 3.998 | 4.004 | 3.945 | 3.997 | 4.003 | 4.009 |
| **Endmembers** | | | | | | | | | | | | | | | | | | |
| Wo | 46.47 | 40.81 | 46.11 | 46.70 | 43.19 | 46.87 | 45.14 | 47.48 | 21.08 | 2.01 | 1.83 | 1.92 | 1.87 | 2.84 | 1.88 | 2.27 | 4.18 | 3.73 |
| En | 45.13 | 49.86 | 45.55 | 44.94 | 48.42 | 45.50 | 46.44 | 44.59 | 68.46 | 39.43 | 40.15 | 39.97 | 39.59 | 40.08 | 45.64 | 40.76 | 42.22 | 41.00 |
| Fs | 6.11 | 7.46 | 5.84 | 6.30 | 6.78 | 5.82 | 6.95 | 5.91 | 10.46 | 57.63 | 57.20 | 57.25 | 57.27 | 56.04 | 50.94 | 56.97 | 52.67 | 54.31 |
| Ac | 2.29 | 1.86 | 2.51 | 2.07 | 1.61 | 1.82 | 1.47 | 2.02 | 0.00 | 0.93 | 0.82 | 0.86 | 1.26 | 1.04 | 1.54 | 0.00 | 0.93 | 0.96 |

**Orthopyroxene**

| Sample | Ab92 | Ab92 | Ab92 | Ab92 | Ab1310 | Ab1310 | Ab1310 | Ab1310 | Ab1310 | Ab5612 | Ab5612 | Ab5613 | Ab5613 | Ab5613 | Ab5613 | Ab5613 | Ab5613 |
|---|---|---|---|---|---|---|---|---|---|---|---|---|---|---|---|---|---|
| Analysis No. | 4 | 8 | 9 | 15 | 3 | 4 | 5 | 11 | 15 | 5 | 6 | 1 | 2 | 5 | 7 | 20 | 27 |
| Analysis Name. | opx1 | opx2 | opx3 | opx4a | opx1 | opx2 | opx3 | opx4 | opx5 | opx1 | opx2 | opx1 | opx2 | opx3 | opx4 | opx5 | px4e |
| SiO2 | 50.76 | 50.58 | 50.84 | 50.62 | 50.16 | 50.50 | 50.31 | 50.34 | 50.36 | 59.54 | 59.72 | 51.22 | 51.53 | 51.08 | 51.30 | 51.13 | 50.51 |
| TiO2 | 0.00 | 0.00 | 0.00 | 0.00 | 0.23 | 0.22 | 0.00 | 0.21 | 0.21 | 0.00 | 0.00 | 0.00 | 0.00 | 0.18 | 0.00 | 0.28 | 0.00 |
| Al2O3 | 0.23 | 0.64 | 0.69 | 0.34 | 0.39 | 0.63 | 0.57 | 0.54 | 0.68 | 0.00 | 0.00 | 0.49 | 0.62 | 1.01 | 0.59 | 0.80 | 0.64 |
| Cr2O3 | 0.00 | 0.00 | 0.00 | 0.00 | 0.00 | 0.00 | 0.00 | 0.00 | 0.00 | 0.00 | 0.00 | 0.00 | 0.00 | 0.00 | 0.00 | 0.00 | 0.00 |
| FeO | 36.56 | 36.11 | 34.31 | 35.45 | 40.50 | 40.39 | 40.12 | 40.65 | 41.04 | 8.20 | 7.63 | 25.15 | 25.23 | 24.35 | 25.10 | 24.14 | 24.45 |
| MnO | 1.57 | 1.12 | 1.25 | 1.44 | 0.91 | 1.05 | 0.92 | 1.00 | 1.08 | 0.40 | 0.36 | 0.60 | 0.72 | 0.63 | 0.68 | 0.58 | 0.52 |
| MgO | 11.95 | 11.81 | 12.03 | 12.40 | 9.58 | 9.63 | 9.73 | 9.81 | 9.62 | 29.26 | 29.21 | 19.04 | 19.17 | 19.08 | 19.39 | 19.12 | 18.60 |
| CaO | 0.64 | 0.76 | 1.63 | 0.50 | 0.84 | 0.70 | 0.80 | 0.72 | 0.86 | 0.43 | 0.47 | 0.66 | 0.77 | 0.49 | 0.80 | 1.66 | 0.63 |
| Na2O | 0.30 | 0.24 | 0.20 | 0.44 | 0.23 | 0.25 | 0.24 | 0.32 | 0.20 | 0.00 | 0.00 | 0.30 | 0.19 | 0.00 | 0.34 | 0.22 | 0.00 |
| K2O | 0.00 | 0.00 | 0.00 | 0.00 | 0.00 | 0.00 | 0.00 | 0.00 | 0.00 | 0.00 | 0.00 | 0.00 | 0.00 | 0.00 | 0.00 | 0.00 | 0.00 |
| NiO | | | | | | | | | | | | | | | | | |
| Total | 102.00 | 101.27 | 100.95 | 101.20 | 103.16 | 103.36 | 102.68 | 103.59 | 104.06 | 97.83 | 97.38 | 97.45 | 98.23 | 96.83 | 98.21 | 97.92 | 95.34 |
| **Formula (6O)** | | | | | | | | | | | | | | | | | |
| Si | 1.996 | 1.995 | 2.000 | 1.996 | 1.988 | 1.987 | 1.992 | 1.981 | 1.976 | 2.097 | 2.106 | 1.993 | 1.989 | 1.989 | 1.982 | 1.976 | 2.001 |
| Al | 0.004 | 0.005 | 0.000 | 0.004 | 0.012 | 0.013 | 0.008 | 0.019 | 0.024 | -0.097 | -0.106 | 0.007 | 0.011 | 0.011 | 0.018 | 0.024 | -0.001 |
| Al | 0.006 | 0.025 | 0.032 | 0.012 | 0.006 | 0.017 | 0.018 | 0.006 | 0.007 | 0.097 | 0.106 | 0.015 | 0.017 | 0.035 | 0.009 | 0.012 | 0.031 |
| Fe(iii) | 0.032 | 0.000 | 0.000 | 0.038 | 0.015 | 0.003 | 0.012 | 0.038 | 0.029 | 0.000 | 0.000 | 0.022 | 0.012 | 0.000 | 0.052 | 0.018 | 0.000 |
| Cr | 0.000 | 0.000 | 0.000 | 0.000 | 0.000 | 0.000 | 0.000 | 0.000 | 0.000 | 0.000 | 0.000 | 0.000 | 0.000 | 0.000 | 0.000 | 0.000 | 0.000 |
| Ti | 0.000 | 0.000 | 0.000 | 0.000 | 0.007 | 0.007 | 0.000 | 0.006 | 0.006 | 0.000 | 0.000 | 0.000 | 0.000 | 0.005 | 0.000 | 0.008 | 0.000 |
| Fe(ii) | 1.167 | 1.192 | 1.131 | 1.127 | 1.326 | 1.326 | 1.315 | 1.295 | 1.314 | 0.247 | 0.231 | 0.794 | 0.801 | 0.796 | 0.756 | 0.761 | 0.813 |
| Mn | 0.052 | 0.037 | 0.042 | 0.048 | 0.031 | 0.035 | 0.031 | 0.033 | 0.036 | 0.012 | 0.011 | 0.020 | 0.024 | 0.021 | 0.022 | 0.019 | 0.017 |
| Mg | 0.700 | 0.695 | 0.706 | 0.729 | 0.566 | 0.565 | 0.574 | 0.575 | 0.563 | 1.536 | 1.535 | 1.104 | 1.103 | 1.108 | 1.117 | 1.101 | 1.099 |
| Ca | 0.027 | 0.032 | 0.069 | 0.021 | 0.036 | 0.030 | 0.034 | 0.030 | 0.036 | 0.016 | 0.018 | 0.028 | 0.032 | 0.020 | 0.033 | 0.069 | 0.027 |
| Na | 0.023 | 0.018 | 0.015 | 0.034 | 0.018 | 0.019 | 0.018 | 0.024 | 0.015 | 0.000 | 0.000 | 0.023 | 0.014 | 0.000 | 0.025 | 0.016 | 0.000 |
| K | 0.000 | 0.000 | 0.000 | 0.000 | 0.000 | 0.000 | 0.000 | 0.000 | 0.000 | 0.000 | 0.000 | 0.000 | 0.000 | 0.000 | 0.000 | 0.000 | 0.000 |
| TOTAL | 4.007 | 3.999 | 3.994 | 4.009 | 4.003 | 4.001 | 4.003 | 4.009 | 4.007 | 3.909 | 3.901 | 4.006 | 4.003 | 3.986 | 4.014 | 4.005 | 3.987 |
| **Endmembers** | | | | | | | | | | | | | | | | | |
| Wo | 1.35 | 1.63 | 3.50 | 1.06 | 1.79 | 1.49 | 1.71 | 1.52 | 1.81 | 0.90 | 0.99 | 1.38 | 1.60 | 1.05 | 1.65 | 3.46 | 1.37 |
| En | 35.00 | 35.19 | 35.96 | 36.50 | 28.44 | 28.57 | 28.94 | 28.82 | 28.23 | 84.79 | 85.54 | 55.47 | 55.54 | 56.94 | 55.70 | 55.50 | 56.16 |
| Fs | 62.51 | 62.26 | 59.76 | 60.76 | 68.88 | 68.97 | 68.42 | 68.44 | 69.19 | 14.32 | 13.47 | 42.01 | 42.14 | 42.01 | 41.38 | 40.20 | 42.47 |
| Ac | 1.14 | 0.93 | 0.78 | 1.68 | 0.89 | 0.96 | 0.93 | 1.22 | 0.76 | 0.00 | 0.00 | 1.14 | 0.72 | 0.00 | 1.27 | 0.83 | 0.00 |

**Orthopyroxene**

| Sample | Ab5613 | Ab5613 | Ab5613 | Ab5613 | Ab5613 | Ab5613 | Ab5613 | Ab5613 | Ab5613 | Ab7801 | Ab7801 | Ab7801 | Ab7801 | Ab7801 | Ab7801 | Ab7801 | Ab7802 |
|---|---|---|---|---|---|---|---|---|---|---|---|---|---|---|---|---|---|
| Analysis No. | 28 | 30 | 31 | 32 | 33 | 34 | 35 | 36 | 39 | 18 | 19 | 25 | 26 | 27 | 30 | 41 | 4 |
| Analysis Name. | px4f | px4h | px4i | px5a | px5b | px4j | px4k | px4l | opx6 | opx1 | opx1b | opx2a | opx2b | opx3 | opx4a | opx4 | opx1 |
| SiO2 | 51.15 | 51.07 | 49.01 | 51.19 | 50.95 | 50.82 | 50.79 | 51.00 | 51.05 | 51.76 | 51.62 | 51.10 | 52.00 | 51.40 | 51.71 | 51.75 | 51.92 |
| TiO2 | 0.00 | 0.21 | 0.98 | 0.30 | 0.00 | 0.00 | 0.18 | 0.23 | 0.18 | 0.24 | 0.23 | 0.00 | 0.00 | 0.22 | 0.34 | 0.22 | 0.15 |
| Al2O3 | 0.74 | 1.12 | 3.61 | 0.74 | 0.58 | 0.69 | 0.67 | 0.65 | 0.49 | 0.54 | 0.56 | 0.93 | 0.69 | 0.56 | 0.60 | 0.62 | 0.57 |
| Cr2O3 | 0.00 | 0.00 | 0.45 | 0.00 | 0.00 | 0.00 | 0.00 | 0.00 | 0.00 | 0.00 | 0.00 | 0.00 | 0.00 | 0.00 | 0.00 | 0.00 | 0.00 |
| FeO | 23.33 | 24.53 | 17.96 | 24.39 | 24.66 | 24.36 | 24.59 | 24.88 | 24.97 | 35.11 | 34.63 | 34.04 | 32.96 | 34.65 | 35.33 | 35.34 | 29.10 |
| MnO | 0.50 | 0.54 | 0.40 | 0.68 | 0.54 | 0.58 | 0.55 | 0.42 | 0.65 | 0.96 | 0.79 | 0.86 | 0.91 | 0.91 | 1.00 | 1.10 | 0.72 |
| MgO | 18.61 | 19.11 | 16.58 | 19.51 | 18.92 | 18.85 | 19.19 | 19.17 | 18.61 | 13.12 | 12.97 | 13.21 | 13.62 | 13.48 | 13.08 | 12.72 | 16.67 |
| CaO | 2.51 | 0.56 | 5.80 | 0.86 | 0.81 | 1.36 | 0.75 | 0.98 | 0.88 | 1.29 | 1.96 | 2.11 | 2.56 | 1.38 | 1.19 | 1.43 | 1.73 |
| Na2O | 0.21 | 0.24 | 0.78 | 0.33 | 0.00 | 0.20 | 0.25 | 0.00 | 0.20 | 0.00 | 0.24 | 0.24 | 0.33 | 0.32 | 0.31 | 0.30 | 0.26 |
| K2O | 0.00 | 0.30 | 0.26 | 0.00 | 0.00 | 0.00 | 0.00 | 0.00 | 0.00 | 0.00 | 0.00 | 0.00 | 0.09 | 0.00 | 0.00 | 0.00 | 0.00 |
| NiO | | | | | | | | | | | | | | | | | 0.00 |
| Total | 97.05 | 97.67 | 95.83 | 98.00 | 96.47 | 96.86 | 96.97 | 97.33 | 97.03 | 103.03 | 102.99 | 102.50 | 103.16 | 102.92 | 103.55 | 103.48 | 101.13 |
| Formula (6O) | | | | | | | | | | | | | | | | | |
| Si | 1.991 | 1.978 | 1.914 | 1.976 | 1.997 | 1.987 | 1.982 | 1.983 | 1.995 | 1.991 | 1.987 | 1.975 | 1.988 | 1.980 | 1.983 | 1.988 | 1.985 |
| Al | 0.009 | 0.022 | 0.086 | 0.024 | 0.003 | 0.013 | 0.018 | 0.017 | 0.005 | 0.009 | 0.013 | 0.025 | 0.012 | 0.020 | 0.017 | 0.012 | 0.015 |
| Al | 0.025 | 0.029 | 0.080 | 0.010 | 0.024 | 0.019 | 0.013 | 0.013 | 0.017 | 0.016 | 0.012 | 0.018 | 0.019 | 0.006 | 0.010 | 0.016 | 0.010 |
| Fe(iii) | 0.001 | 0.020 | 0.009 | 0.032 | 0.000 | 0.015 | 0.019 | 0.000 | 0.000 | 0.000 | 0.008 | 0.038 | 0.034 | 0.038 | 0.015 | 0.009 | 0.024 |
| Cr | 0.000 | 0.000 | 0.014 | 0.000 | 0.000 | 0.000 | 0.000 | 0.000 | 0.000 | 0.000 | 0.000 | 0.000 | 0.000 | 0.000 | 0.000 | 0.000 | 0.000 |
| Ti | 0.000 | 0.006 | 0.029 | 0.009 | 0.000 | 0.000 | 0.005 | 0.007 | 0.005 | 0.007 | 0.007 | 0.000 | 0.000 | 0.006 | 0.010 | 0.006 | 0.004 |
| Fe(ii) | 0.758 | 0.773 | 0.577 | 0.753 | 0.810 | 0.781 | 0.782 | 0.810 | 0.817 | 1.133 | 1.106 | 1.059 | 1.017 | 1.074 | 1.116 | 1.126 | 0.904 |
| Mn | 0.016 | 0.018 | 0.013 | 0.022 | 0.018 | 0.019 | 0.018 | 0.014 | 0.022 | 0.031 | 0.026 | 0.028 | 0.029 | 0.030 | 0.032 | 0.036 | 0.023 |
| Mg | 1.080 | 1.103 | 0.965 | 1.123 | 1.106 | 1.099 | 1.117 | 1.111 | 1.084 | 0.753 | 0.744 | 0.761 | 0.776 | 0.774 | 0.748 | 0.728 | 0.950 |
| Ca | 0.105 | 0.023 | 0.243 | 0.036 | 0.034 | 0.057 | 0.031 | 0.041 | 0.037 | 0.053 | 0.081 | 0.087 | 0.105 | 0.057 | 0.049 | 0.059 | 0.071 |
| Na | 0.016 | 0.018 | 0.059 | 0.025 | 0.000 | 0.015 | 0.019 | 0.000 | 0.015 | 0.000 | 0.018 | 0.018 | 0.024 | 0.024 | 0.023 | 0.022 | 0.019 |
| K | 0.000 | 0.015 | 0.013 | 0.000 | 0.000 | 0.000 | 0.000 | 0.000 | 0.000 | 0.000 | 0.000 | 0.000 | 0.004 | 0.000 | 0.000 | 0.000 | 0.000 |
| TOTAL | 4.000 | 4.005 | 4.003 | 4.009 | 3.992 | 4.004 | 4.005 | 3.996 | 3.997 | 3.992 | 4.002 | 4.009 | 4.008 | 4.009 | 4.004 | 4.002 | 4.006 |
| Endmembers | | | | | | | | | | | | | | | | | |
| Wo | 5.30 | 1.19 | 13.00 | 1.79 | 1.73 | 2.87 | 1.58 | 2.07 | 1.87 | 2.70 | 4.08 | 4.39 | 5.28 | 2.85 | 2.46 | 2.97 | 3.56 |
| En | 54.65 | 56.43 | 51.72 | 56.41 | 56.18 | 55.34 | 56.21 | 56.24 | 54.91 | 38.21 | 37.54 | 38.22 | 39.09 | 38.76 | 37.70 | 36.79 | 47.70 |
| Fs | 39.26 | 41.46 | 32.11 | 40.56 | 42.09 | 41.03 | 41.25 | 41.69 | 42.45 | 59.09 | 57.48 | 56.49 | 54.40 | 57.19 | 58.68 | 59.10 | 47.78 |
| Ac | 0.80 | 0.92 | 3.16 | 1.24 | 0.00 | 0.76 | 0.95 | 0.00 | 0.77 | 0.00 | 0.90 | 0.90 | 1.23 | 1.20 | 1.16 | 1.13 | 0.97 |

**Orthopyroxene**

| Sample | Ab7802 | Ab7802 | Ab7802 | Ab7802 | Ab7802 | MS1595 | MS1595 | MS1595 | MS1595 | MS1595 | MS1595 | Ab93 | Ab93 | Ab93 | Ab93 | Ab93 | Ab93 |
|---|---|---|---|---|---|---|---|---|---|---|---|---|---|---|---|---|---|
| Analysis No. | 12 | 16 | 18 | 20 | 23 | 1 | 2 | 12 | 13 | 14 | 31 | 9 | 10 | 16 | 17 | 19 | 27 |
| Analysis Name. | opx4b | opx2 | cpx6 | opx3 | opx4 | opx1a | opx1b | opx2a | opx2b | opx2c | opx4 | opx1 | opx2 | opx3 | opx4 | opx5 | opx6 |
| SiO2 | 51.64 | 51.95 | 51.79 | 52.32 | 51.68 | 54.83 | 54.45 | 53.98 | 54.41 | 53.34 | 55.23 | 51.77 | 52.35 | 51.84 | 52.04 | 51.84 | 52.52 |
| TiO2 | 0.20 | 0.34 | 0.28 | 0.21 | 0.20 | 0.41 | 0.33 | 0.32 | 0.30 | 0.20 | 0.23 | 0.35 | 0.36 | | 0.38 | 0.43 | |
| Al2O3 | 0.50 | 0.68 | 0.61 | 0.89 | 0.83 | 1.29 | 1.33 | 1.71 | 1.31 | 1.78 | 0.71 | 0.89 | 1.13 | 1.21 | 1.00 | 1.09 | 1.18 |
| Cr2O3 | 0.00 | 0.00 | 0.00 | 0.00 | 0.00 | 0.30 | 0.00 | 0.47 | 0.29 | 0.33 | 0.00 | | | | | | |
| FeO | 29.81 | 29.36 | 29.01 | 28.56 | 29.13 | 11.52 | 11.82 | 10.24 | 11.03 | 10.75 | 11.84 | 23.00 | 23.29 | 23.96 | 22.82 | 23.84 | 24.82 |
| MnO | 0.76 | 0.81 | 0.54 | 0.54 | 0.45 | 0.24 | 0.25 | 0.26 | 0.00 | 0.22 | 0.23 | 0.51 | 0.40 | 0.63 | 0.57 | 0.44 | 0.45 |
| MgO | 16.41 | 17.34 | 16.70 | 17.02 | 16.84 | 28.39 | 27.97 | 29.18 | 28.65 | 28.35 | 28.87 | 20.00 | 20.23 | 19.93 | 19.98 | 19.44 | 19.71 |
| CaO | 0.97 | 0.82 | 1.32 | 1.67 | 1.18 | 1.64 | 1.77 | 1.70 | 2.15 | 1.79 | 1.12 | 1.92 | 1.89 | 1.12 | 1.83 | 1.62 | 1.11 |
| Na2O | 0.00 | 0.30 | 0.21 | 0.19 | 0.30 | 0.00 | 0.00 | 0.00 | 0.00 | 0.00 | 0.00 | | | | | | |
| K2O | 0.00 | 0.00 | 0.00 | 0.00 | 0.00 | 0.00 | 0.00 | 0.00 | 0.00 | 0.00 | 0.00 | | | | | | |
| NiO | 0.00 | 0.00 | 0.00 | 0.00 | 0.00 | 0.00 | 0.00 | 0.00 | 0.00 | 0.00 | 0.00 | | | | | | |
| Total | 100.29 | 101.62 | 100.47 | 101.41 | 100.61 | 98.62 | 97.94 | 97.85 | 98.14 | 96.76 | 98.24 | 98.44 | 99.83 | 98.68 | 98.62 | 98.70 | 99.80 |
| **Formula (6O)** | | | | | | | | | | | | | | | | | |
| Si | 1.992 | 1.974 | 1.988 | 1.984 | 1.981 | 1.972 | 1.975 | 1.950 | 1.965 | 1.953 | 1.992 | 1.976 | 1.973 | 1.977 | 1.980 | 1.978 | 1.984 |
| Al | 0.008 | 0.026 | 0.012 | 0.016 | 0.019 | 0.028 | 0.025 | 0.050 | 0.035 | 0.047 | 0.008 | 0.024 | 0.027 | 0.023 | 0.020 | 0.022 | 0.016 |
| Al | 0.015 | 0.005 | 0.016 | 0.024 | 0.018 | 0.027 | 0.032 | 0.022 | 0.020 | 0.030 | 0.022 | 0.016 | 0.023 | 0.032 | 0.024 | 0.027 | 0.036 |
| Fe(iii) | 0.000 | 0.035 | 0.000 | 0.000 | 0.017 | 0.000 | 0.000 | 0.000 | 0.000 | 0.000 | 0.000 | 0.000 | 0.000 | 0.000 | 0.000 | 0.000 | 0.000 |
| Cr | 0.000 | 0.000 | 0.000 | 0.000 | 0.000 | 0.009 | 0.000 | 0.013 | 0.008 | 0.010 | 0.000 | 0.000 | 0.000 | 0.000 | 0.000 | 0.000 | 0.000 |
| Ti | 0.006 | 0.010 | 0.008 | 0.006 | 0.006 | 0.011 | 0.009 | 0.009 | 0.008 | 0.006 | 0.006 | 0.010 | 0.010 | 0.000 | 0.011 | 0.012 | 0.000 |
| Fe(ii) | 0.964 | 0.895 | 0.932 | 0.906 | 0.915 | 0.348 | 0.360 | 0.309 | 0.333 | 0.329 | 0.358 | 0.735 | 0.735 | 0.765 | 0.728 | 0.763 | 0.786 |
| Mn | 0.025 | 0.026 | 0.018 | 0.017 | 0.015 | 0.007 | 0.008 | 0.008 | 0.000 | 0.007 | 0.007 | 0.016 | 0.013 | 0.020 | 0.018 | 0.014 | 0.014 |
| Mg | 0.944 | 0.982 | 0.956 | 0.962 | 0.962 | 1.522 | 1.512 | 1.571 | 1.542 | 1.547 | 1.552 | 1.138 | 1.136 | 1.133 | 1.133 | 1.106 | 1.110 |
| Ca | 0.040 | 0.033 | 0.054 | 0.068 | 0.048 | 0.063 | 0.069 | 0.066 | 0.083 | 0.070 | 0.043 | 0.079 | 0.076 | 0.046 | 0.075 | 0.066 | 0.045 |
| Na | 0.000 | 0.022 | 0.016 | 0.014 | 0.022 | 0.000 | 0.000 | 0.000 | 0.000 | 0.000 | 0.000 | 0.000 | 0.000 | 0.000 | 0.000 | 0.000 | 0.000 |
| K | 0.000 | 0.000 | 0.000 | 0.000 | 0.000 | 0.000 | 0.000 | 0.000 | 0.000 | 0.000 | 0.000 | 0.000 | 0.000 | 0.000 | 0.000 | 0.000 | 0.000 |
| TOTAL | 3.993 | 4.009 | 3.998 | 3.998 | 4.004 | 3.987 | 3.989 | 3.999 | 3.996 | 3.999 | 3.988 | 3.995 | 3.994 | 3.996 | 3.989 | 3.988 | 3.992 |
| **Endmembers** | | | | | | | | | | | | | | | | | |
| Wo | 2.03 | 1.67 | 2.75 | 3.45 | 2.45 | 3.26 | 3.53 | 3.37 | 4.25 | 3.59 | 2.21 | 3.99 | 3.89 | 2.33 | 3.82 | 3.40 | 2.30 |
| En | 47.85 | 49.26 | 48.39 | 48.90 | 48.60 | 78.45 | 77.62 | 80.40 | 78.73 | 79.20 | 79.17 | 57.82 | 57.96 | 57.69 | 57.98 | 56.72 | 56.77 |
| Fs | 50.12 | 47.96 | 48.07 | 46.94 | 47.83 | 18.30 | 18.85 | 16.24 | 17.02 | 17.20 | 18.63 | 38.19 | 38.15 | 39.98 | 38.20 | 39.88 | 40.93 |
| Ac | 0.00 | 1.11 | 0.79 | 0.71 | 1.13 | 0.00 | 0.00 | 0.00 | 0.00 | 0.00 | 0.00 | | | | | | |

**Orthopyroxene**

| Sample | Ab243 | Ab243 | Ab243 | Ab243 | Ab661 | Ab661 | Ab661 | V(Ol) | V(Ol) | V(Ol) | V(Ol) | DV1 | DV1 | Ab3986 | Ab3986 | Ab5661 |
|---|---|---|---|---|---|---|---|---|---|---|---|---|---|---|---|---|
| Analysis No. | 33 | 34 | 37 | 38 | 24 | 27 | 28 | 1 | 12 | 22 | 24 | 23 | 37 | 30 | 14 | 23 |
| Analysis Name. | opx1 | opx1b | opx1c | opx2 | opx1 | opx2 | opx3 | opx1 | opx2 | opx3 | opx4 | opx1 | opx4 | opx1 | cor1 | cor1 |
| SiO2 | 51.05 | 50.91 | 50.90 | 50.67 | 49.68 | 48.73 | 49.61 | 54.12 | 53.89 | 54.41 | 51.31 | 54.43 | 53.82 | 54.46 | 55.79 | 56.06 |
| TiO2 | 0.28 | | 0.28 | 0.35 | | | | 0.39 | 0.26 | 0.32 | 1.67 | 0.25 | 0.35 | 0.27 | | |
| Al2O3 | 0.61 | 0.55 | 0.77 | 0.74 | 0.31 | 0.50 | 0.50 | 1.32 | 1.21 | 1.42 | 3.85 | 1.35 | 1.54 | 1.92 | 2.01 | 1.00 |
| Cr2O3 | | | | | | | | | | | | | | | | 0.17 |
| FeO | 31.11 | 30.95 | 31.05 | 30.36 | 43.00 | 41.72 | 42.30 | 19.24 | 19.05 | 19.21 | 16.29 | 19.72 | 18.92 | 11.22 | 11.05 | 11.00 |
| MnO | 0.81 | 0.92 | 0.84 | 0.94 | 2.30 | 3.12 | 2.56 | 0.59 | 0.33 | 0.50 | | 0.42 | 0.56 | 0.36 | 0.37 | 0.32 |
| MgO | 14.88 | 14.92 | 15.01 | 14.77 | 2.48 | 1.94 | 2.55 | 24.04 | 23.99 | 24.36 | 21.29 | 24.01 | 23.80 | 28.96 | 30.54 | 30.22 |
| CaO | 1.93 | 1.49 | 1.13 | 1.34 | 0.68 | 0.90 | 0.76 | 1.04 | 1.22 | 1.01 | 3.91 | 0.97 | 0.75 | 0.91 | 0.16 | 0.60 |
| Na2O | | | | 0.28 | 0.40 | 0.36 | 0.26 | | | | 0.77 | | | | | |
| K2O | | | | | | | | | | | 0.19 | | | | | |
| NiO | | | | | | | | | | | | | | | | |
| Total | 100.68 | 99.76 | 99.96 | 99.45 | 98.83 | 97.26 | 98.54 | 100.73 | 100.10 | 101.21 | 99.30 | 101.14 | 99.74 | 98.11 | 99.91 | 99.38 |
| **Formula (6O)** | | | | | | | | | | | | | | | | |
| Si | 1.982 | 1.993 | 1.985 | 1.986 | 2.090 | 2.087 | 2.089 | 1.972 | 1.977 | 1.970 | 1.896 | 1.976 | 1.975 | 1.962 | 1.965 | 1.987 |
| Al | 0.018 | 0.007 | 0.015 | 0.014 | -0.090 | -0.087 | -0.089 | 0.028 | 0.023 | 0.030 | 0.104 | 0.024 | 0.025 | 0.038 | 0.035 | 0.013 |
| Al | 0.010 | 0.018 | 0.021 | 0.020 | 0.105 | 0.113 | 0.113 | 0.028 | 0.029 | 0.031 | 0.064 | 0.033 | 0.042 | 0.043 | 0.048 | 0.029 |
| Fe(iii) | 0.000 | 0.000 | 0.000 | 0.000 | 0.000 | 0.000 | 0.000 | 0.000 | 0.000 | 0.000 | 0.017 | 0.000 | 0.000 | 0.000 | 0.000 | 0.000 |
| Cr | 0.000 | 0.000 | 0.000 | 0.000 | 0.000 | 0.000 | 0.000 | 0.000 | 0.000 | 0.000 | 0.000 | 0.000 | 0.000 | 0.000 | 0.000 | 0.005 |
| Ti | 0.008 | 0.000 | 0.008 | 0.010 | 0.000 | 0.000 | 0.000 | 0.011 | 0.007 | 0.009 | 0.046 | 0.007 | 0.010 | 0.007 | 0.000 | 0.000 |
| Fe(ii) | 1.011 | 1.014 | 1.015 | 0.996 | 1.544 | 1.527 | 1.524 | 0.588 | 0.586 | 0.583 | 0.486 | 0.600 | 0.583 | 0.339 | 0.326 | 0.327 |
| Mn | 0.027 | 0.030 | 0.028 | 0.031 | 0.082 | 0.113 | 0.091 | 0.018 | 0.010 | 0.015 | 0.000 | 0.013 | 0.017 | 0.011 | 0.011 | 0.010 |
| Mg | 0.861 | 0.871 | 0.873 | 0.863 | 0.156 | 0.124 | 0.160 | 1.306 | 1.312 | 1.315 | 1.173 | 1.299 | 1.302 | 1.555 | 1.603 | 1.597 |
| Ca | 0.080 | 0.062 | 0.047 | 0.056 | 0.031 | 0.041 | 0.034 | 0.041 | 0.048 | 0.039 | 0.155 | 0.038 | 0.029 | 0.035 | 0.006 | 0.023 |
| Na | 0.000 | 0.000 | 0.000 | 0.021 | 0.033 | 0.030 | 0.021 | 0.000 | 0.000 | 0.000 | 0.055 | 0.000 | 0.000 | 0.000 | 0.000 | 0.000 |
| K | 0.000 | 0.000 | 0.000 | 0.000 | 0.000 | 0.000 | 0.000 | 0.000 | 0.000 | 0.000 | 0.009 | 0.000 | 0.000 | 0.000 | 0.000 | 0.000 |
| TOTAL | 3.997 | 3.996 | 3.992 | 3.998 | 3.950 | 3.947 | 3.944 | 3.991 | 3.992 | 3.992 | 4.005 | 3.990 | 3.984 | 3.991 | 3.994 | 3.990 |
| **Endmembers** | | | | | | | | | | | | | | | | |
| Wo | 4.06 | 3.16 | 2.41 | 2.86 | 1.66 | 2.25 | 1.87 | 2.08 | 2.45 | 2.01 | 8.21 | 1.93 | 1.53 | 1.81 | 0.31 | 1.16 |
| En | 43.52 | 44.02 | 44.46 | 43.87 | 8.43 | 6.75 | 8.74 | 66.88 | 67.08 | 67.35 | 62.21 | 66.62 | 67.39 | 80.16 | 82.38 | 81.63 |
| Fs | 52.43 | 52.82 | 53.14 | 52.19 | 88.14 | 89.37 | 88.22 | 31.04 | 30.47 | 30.64 | 26.66 | 31.44 | 31.09 | 18.03 | 17.31 | 17.20 |
| Ac | 0.00 | 0.00 | 0.00 | 1.08 | 1.77 | 1.63 | 1.16 | 0.00 | 0.00 | 0.00 | 2.93 | 0.00 | 0.00 | 0.00 | 0.00 | 0.00 |

**Orthopyroxene**

| Sample | Ab5661 | 773C | 773C | 773C | MS1601 | MS1601 | MS1601 | MS1601 | 77P | 77P | 77P | 77P | 77P | 77P | 77P | CLW106 | CLW106 |
|---|---|---|---|---|---|---|---|---|---|---|---|---|---|---|---|---|---|
| Analysis No. | 26 | 8 | 11 | 12 | 1 | 6 | 9 | 10 | 4 | 5 | 6 | 8 | 9 | 16 | 21 | 2 | 3 |
| Analysis Name. | cor2 | opx1 | opx2 | opx3 | opx1 | opx2 | opx3 | opx4 | opx1 | opx2 | opx3 | opx4 | opx5 | opx6 | opx7 | opx1 | opx2 |
| SiO2 | 57.01 | 55.09 | 54.29 | 55.06 | 57.66 | 56.92 | 57.18 | 57.35 | 52.02 | 52.10 | 51.50 | 51.84 | 52.76 | 52.26 | 52.82 | 54.84 | 54.56 |
| TiO2 | | 0.50 | 0.39 | 0.55 | | | | | | 0.34 | | 0.25 | 0.26 | | 0.27 | | |
| Al2O3 | 0.44 | 2.01 | 2.28 | 2.15 | 1.57 | 1.91 | 1.54 | 1.61 | 0.97 | 1.04 | 1.11 | 1.03 | 1.07 | 1.00 | 0.93 | 1.92 | 1.84 |
| Cr2O3 | | 0.30 | 0.31 | 0.33 | 0.50 | 0.51 | 0.82 | 0.54 | | | | | | | | | |
| FeO | 10.79 | 12.51 | 12.94 | 11.96 | 5.64 | 5.61 | 5.69 | 5.62 | 26.61 | 26.06 | 25.40 | 26.26 | 26.05 | 25.88 | 26.94 | 17.20 | 17.29 |
| MnO | | 0.38 | 0.26 | | | | 0.23 | | 0.55 | 0.58 | 0.67 | 0.55 | 0.55 | 0.69 | 0.51 | 0.34 | 0.48 |
| MgO | 31.20 | 28.97 | 28.36 | 28.12 | 34.60 | 34.13 | 34.34 | 33.90 | 19.00 | 18.68 | 18.97 | 18.89 | 19.27 | 18.71 | 19.08 | 26.16 | 26.38 |
| CaO | 0.15 | 1.20 | 1.56 | 1.68 | 0.79 | 0.59 | 0.48 | 0.97 | 1.16 | 1.25 | 1.47 | 0.99 | 1.39 | 1.50 | 1.15 | 0.28 | 0.22 |
| Na2O | | | | | | | | | | | | | | | | | |
| K2O | | | | | | | | | | | | | | | | | |
| NiO | | | | | | | | | | | | | | | | | |
| Total | 99.59 | 100.96 | 100.39 | 99.85 | 100.76 | 99.67 | 100.29 | 100.00 | 100.32 | 100.06 | 99.12 | 99.82 | 101.34 | 100.35 | 101.69 | 101.01 | 100.77 |
| **Formula (6O)** | | | | | | | | | | | | | | | | | |
| Si | 2.006 | 1.943 | 1.933 | 1.956 | 1.968 | 1.962 | 1.964 | 1.972 | 1.975 | 1.978 | 1.973 | 1.975 | 1.975 | 1.984 | 1.977 | 1.970 | 1.963 |
| Al | -0.006 | 0.057 | 0.067 | 0.044 | 0.032 | 0.038 | 0.036 | 0.028 | 0.025 | 0.022 | 0.027 | 0.025 | 0.025 | 0.016 | 0.023 | 0.030 | 0.037 |
| Al | 0.025 | 0.027 | 0.028 | 0.046 | 0.031 | 0.040 | 0.026 | 0.038 | 0.018 | 0.025 | 0.023 | 0.021 | 0.022 | 0.029 | 0.018 | 0.051 | 0.041 |
| Fe(iii) | 0.000 | 0.000 | 0.015 | 0.000 | 0.000 | 0.000 | 0.000 | 0.000 | 0.010 | 0.000 | 0.006 | 0.000 | 0.000 | 0.000 | 0.000 | 0.000 | 0.000 |
| Cr | 0.000 | 0.008 | 0.009 | 0.009 | 0.013 | 0.014 | 0.022 | 0.015 | 0.000 | 0.000 | 0.000 | 0.000 | 0.000 | 0.000 | 0.000 | 0.000 | 0.000 |
| Ti | 0.000 | 0.013 | 0.010 | 0.015 | 0.000 | 0.000 | 0.000 | 0.000 | 0.000 | 0.010 | 0.000 | 0.007 | 0.007 | 0.000 | 0.008 | 0.000 | 0.000 |
| Fe(ii) | 0.319 | 0.369 | 0.370 | 0.357 | 0.161 | 0.162 | 0.164 | 0.162 | 0.834 | 0.830 | 0.807 | 0.837 | 0.817 | 0.823 | 0.844 | 0.518 | 0.520 |
| Mn | 0.000 | 0.011 | 0.008 | 0.000 | 0.000 | 0.000 | 0.007 | 0.000 | 0.018 | 0.019 | 0.022 | 0.018 | 0.017 | 0.022 | 0.016 | 0.010 | 0.015 |
| Mg | 1.637 | 1.523 | 1.505 | 1.490 | 1.760 | 1.754 | 1.758 | 1.738 | 1.075 | 1.057 | 1.083 | 1.073 | 1.075 | 1.059 | 1.065 | 1.401 | 1.415 |
| Ca | 0.006 | 0.045 | 0.059 | 0.064 | 0.029 | 0.022 | 0.018 | 0.036 | 0.047 | 0.051 | 0.060 | 0.040 | 0.056 | 0.061 | 0.046 | 0.011 | 0.008 |
| Na | 0.000 | 0.000 | 0.000 | 0.000 | 0.000 | 0.000 | 0.000 | 0.000 | 0.000 | 0.000 | 0.000 | 0.000 | 0.000 | 0.000 | 0.000 | 0.000 | 0.000 |
| K | 0.000 | 0.000 | 0.000 | 0.000 | 0.000 | 0.000 | 0.000 | 0.000 | 0.000 | 0.000 | 0.000 | 0.000 | 0.000 | 0.000 | 0.000 | 0.000 | 0.000 |
| TOTAL | 3.986 | 3.998 | 4.004 | 3.981 | 3.994 | 3.992 | 3.994 | 3.988 | 4.003 | 3.991 | 4.002 | 3.996 | 3.995 | 3.995 | 3.996 | 3.991 | 3.999 |
| **Endmembers** | | | | | | | | | | | | | | | | | |
| Wo | 0.29 | 2.33 | 3.04 | 3.35 | 1.48 | 1.12 | 0.91 | 1.85 | 2.38 | 2.60 | 3.05 | 2.05 | 2.84 | 3.10 | 2.34 | 0.56 | 0.43 |
| En | 83.46 | 78.15 | 76.90 | 77.96 | 90.26 | 90.51 | 90.34 | 89.78 | 54.19 | 54.04 | 54.75 | 54.50 | 54.72 | 53.89 | 54.01 | 72.21 | 72.25 |
| Fs | 16.25 | 19.52 | 20.06 | 18.69 | 8.26 | 8.36 | 8.75 | 8.37 | 43.43 | 43.36 | 42.20 | 43.45 | 42.44 | 43.01 | 43.65 | 27.23 | 27.32 |
| Ac | 0.00 | 0.00 | 0.00 | 0.00 | 0.00 | 0.00 | 0.00 | 0.00 | 0.00 | 0.00 | 0.00 | 0.00 | 0.00 | 0.00 | 0.00 | | |

**Orthopyroxene**

| Sample | CLW106 | CLW106 | CLW106 | CLW106 | CLW106 | CLW106 | CLW106 | CLW107 | CLW107 | CLW107 | CLW107 | CLW107 | CLW107 | DCD106 | DCD106 | DCD106 | DCD106 |
|---|---|---|---|---|---|---|---|---|---|---|---|---|---|---|---|---|---|
| Analysis No. | 7 | 9 | 12 | 14 | 26 | 28 | 30 | 1 | 3 | 7 | 13 | 17 | 21 | 4 | 7 | 8 | 14 |
| Analysis Name. | opx3 | opx4 | opx5 | opx6 | opx8 | opx9 | opx10 | opx1 | opx2 | opx3 | opx4 | opx5 | opx6 | opx1 | opx2 | opx3 | opx4 |
| SiO2 | 54.28 | 54.02 | 53.96 | 53.79 | 53.76 | 53.96 | 53.79 | 54.66 | 55.14 | 55.00 | 54.59 | 55.00 | 55.10 | 54.39 | 54.28 | 54.84 | 54.91 |
| TiO2 | | | | | | | | | | | 0.23 | | | | | | |
| Al2O3 | 1.79 | 1.61 | 1.81 | 1.89 | 2.15 | 1.67 | 1.68 | 2.23 | 1.92 | 2.35 | 2.44 | 1.97 | 1.92 | 2.81 | 3.44 | 2.74 | 2.94 |
| Cr2O3 | 0.19 | | | | 0.24 | | | | | | 0.23 | 0.18 | | 0.22 | 0.25 | | 0.20 |
| FeO | 16.94 | 16.83 | 17.42 | 17.41 | 16.11 | 16.28 | 17.58 | 12.70 | 12.66 | 12.33 | 12.77 | 13.17 | 11.76 | 12.65 | 12.59 | 12.60 | 12.57 |
| MnO | 0.43 | 0.27 | 0.38 | 0.47 | 0.33 | 0.41 | 0.26 | 0.24 | 0.26 | 0.20 | 0.24 | 0.35 | 0.29 | 0.29 | 0.27 | 0.33 | 0.21 |
| MgO | 26.32 | 25.83 | 25.70 | 26.00 | 25.51 | 25.45 | 25.80 | 28.58 | 29.29 | 28.33 | 28.34 | 28.09 | 28.82 | 28.51 | 28.20 | 28.28 | 28.74 |
| CaO | 0.36 | 0.36 | 0.37 | 0.33 | 1.02 | 0.74 | 0.31 | 1.14 | 0.37 | 1.37 | 1.10 | 0.92 | 1.47 | 0.49 | 0.57 | 0.55 | 0.67 |
| Na2O | | | | | | | | | | | | | | | | | |
| K2O | | | | | | | | | | | | | | | | | |
| NiO | | | | | | | | | | | | | | | | | |
| Total | 100.31 | 98.92 | 99.64 | 99.87 | 99.11 | 98.51 | 99.43 | 99.54 | 99.64 | 99.57 | 100.08 | 99.67 | 99.36 | 99.38 | 99.59 | 99.35 | 100.24 |
| **Formula (6O)** | | | | | | | | | | | | | | | | | |
| Si | 1.961 | 1.975 | 1.966 | 1.956 | 1.961 | 1.979 | 1.965 | 1.953 | 1.963 | 1.960 | 1.945 | 1.966 | 1.965 | 1.944 | 1.935 | 1.958 | 1.944 |
| Al | 0.039 | 0.025 | 0.034 | 0.044 | 0.039 | 0.021 | 0.035 | 0.047 | 0.037 | 0.040 | 0.055 | 0.034 | 0.035 | 0.056 | 0.065 | 0.042 | 0.056 |
| Al | 0.037 | 0.045 | 0.043 | 0.037 | 0.054 | 0.052 | 0.037 | 0.047 | 0.043 | 0.059 | 0.047 | 0.049 | 0.046 | 0.062 | 0.079 | 0.073 | 0.066 |
| Fe(iii) | 0.000 | 0.000 | 0.000 | 0.010 | 0.000 | 0.000 | 0.000 | 0.000 | 0.000 | 0.000 | 0.000 | 0.000 | 0.000 | 0.000 | 0.000 | 0.000 | 0.000 |
| Cr | 0.005 | 0.000 | 0.000 | 0.000 | 0.007 | 0.000 | 0.000 | 0.000 | 0.000 | 0.000 | 0.006 | 0.005 | 0.000 | 0.006 | 0.007 | 0.000 | 0.006 |
| Ti | 0.000 | 0.000 | 0.000 | 0.000 | 0.000 | 0.000 | 0.000 | 0.000 | 0.000 | 0.000 | 0.006 | 0.000 | 0.000 | 0.000 | 0.000 | 0.000 | 0.000 |
| Fe(ii) | 0.512 | 0.516 | 0.531 | 0.519 | 0.493 | 0.501 | 0.537 | 0.379 | 0.377 | 0.368 | 0.381 | 0.395 | 0.351 | 0.379 | 0.376 | 0.378 | 0.373 |
| Mn | 0.013 | 0.008 | 0.012 | 0.014 | 0.010 | 0.013 | 0.008 | 0.007 | 0.008 | 0.006 | 0.007 | 0.011 | 0.009 | 0.009 | 0.008 | 0.010 | 0.006 |
| Mg | 1.417 | 1.408 | 1.396 | 1.410 | 1.387 | 1.392 | 1.405 | 1.522 | 1.554 | 1.505 | 1.505 | 1.497 | 1.533 | 1.519 | 1.498 | 1.505 | 1.517 |
| Ca | 0.014 | 0.014 | 0.014 | 0.013 | 0.040 | 0.029 | 0.012 | 0.044 | 0.014 | 0.052 | 0.042 | 0.035 | 0.056 | 0.019 | 0.022 | 0.021 | 0.025 |
| Na | 0.000 | 0.000 | 0.000 | 0.000 | 0.000 | 0.000 | 0.000 | 0.000 | 0.000 | 0.000 | 0.000 | 0.000 | 0.000 | 0.000 | 0.000 | 0.000 | 0.000 |
| K | 0.000 | 0.000 | 0.000 | 0.000 | 0.000 | 0.000 | 0.000 | 0.000 | 0.000 | 0.000 | 0.000 | 0.000 | 0.000 | 0.000 | 0.000 | 0.000 | 0.000 |
| TOTAL | 3.999 | 3.991 | 3.996 | 4.003 | 3.991 | 3.986 | 3.999 | 4.000 | 3.997 | 3.991 | 3.995 | 3.991 | 3.995 | 3.994 | 3.991 | 3.986 | 3.993 |
| **Endmembers** | | | | | | | | | | | | | | | | | |
| Wo | 0.71 | 0.72 | 0.74 | 0.65 | 2.07 | 1.50 | 0.62 | 2.23 | 0.72 | 2.71 | 2.17 | 1.82 | 2.88 | 0.97 | 1.14 | 1.10 | 1.32 |
| En | 72.45 | 72.34 | 71.46 | 71.70 | 71.88 | 71.93 | 71.60 | 77.96 | 79.57 | 77.91 | 77.77 | 77.27 | 78.64 | 78.90 | 78.68 | 78.65 | 78.95 |
| Fs | 26.84 | 26.93 | 27.80 | 27.64 | 26.06 | 26.57 | 27.78 | 19.80 | 19.71 | 19.38 | 20.06 | 20.92 | 18.47 | 20.12 | 20.18 | 20.25 | 19.73 |
| Ac | | | | | | | | 0.00 | 0.00 | 0.00 | 0.00 | 0.00 | 0.00 | 0.00 | 0.00 | 0.00 | 0.00 |

**Orthopyroxene**

| Sample | DCD118 | DCD118 | DCD118 | DCD118 | DCD118 | DCD118 |
|---|---|---|---|---|---|---|
| Analysis No. | 3 | 5 | 7 | 16 | 19 | 22 |
| Analysis Name. | opx1 | opx2 | opx3 | opx3 | opx4 | opx5 |
| SiO2 | 53.33 | 53.55 | 53.86 | 53.49 | 54.16 | 53.34 |
| TiO2 | | | | | | |
| Al2O3 | 2.60 | 2.50 | 2.34 | 2.31 | 2.42 | 2.70 |
| Cr2O3 | 0.18 | | | 0.18 | | 0.19 |
| FeO | 17.28 | 18.17 | 18.14 | 17.53 | 18.12 | 18.34 |
| MnO | 0.35 | 0.23 | 0.44 | 0.43 | 0.40 | 0.32 |
| MgO | 24.54 | 24.89 | 25.34 | 24.53 | 24.92 | 24.70 |
| CaO | 1.60 | 1.12 | 0.45 | 1.43 | 0.43 | 1.04 |
| Na2O | | | | | | |
| K2O | | | | | | |
| NiO | | | | | | |
| Total | 99.87 | 100.46 | 100.55 | 99.88 | 100.46 | 100.63 |
| Formula (6O) | | | | | | |
| Si | 1.945 | 1.945 | 1.951 | 1.952 | 1.961 | 1.937 |
| Al | 0.055 | 0.055 | 0.049 | 0.048 | 0.039 | 0.063 |
| Al | 0.057 | 0.052 | 0.051 | 0.052 | 0.064 | 0.053 |
| Fe(iii) | 0.000 | 0.005 | 0.000 | 0.000 | 0.000 | 0.007 |
| Cr | 0.005 | 0.000 | 0.000 | 0.005 | 0.000 | 0.005 |
| Ti | 0.000 | 0.000 | 0.000 | 0.000 | 0.000 | 0.000 |
| Fe(ii) | 0.527 | 0.546 | 0.549 | 0.536 | 0.550 | 0.549 |
| Mn | 0.011 | 0.007 | 0.013 | 0.013 | 0.012 | 0.010 |
| Mg | 1.334 | 1.348 | 1.368 | 1.335 | 1.345 | 1.337 |
| Ca | 0.063 | 0.044 | 0.017 | 0.056 | 0.017 | 0.040 |
| Na | 0.000 | 0.000 | 0.000 | 0.000 | 0.000 | 0.000 |
| K | 0.000 | 0.000 | 0.000 | 0.000 | 0.000 | 0.000 |
| TOTAL | 3.997 | 4.002 | 3.999 | 3.996 | 3.989 | 4.002 |
| Endmembers | | | | | | |
| Wo | 3.23 | 2.23 | 0.90 | 2.88 | 0.87 | 2.08 |
| En | 68.95 | 69.12 | 70.21 | 68.82 | 69.90 | 68.78 |
| Fs | 27.82 | 28.65 | 28.89 | 28.30 | 29.24 | 29.13 |
| Ac | 0.00 | 0.00 | 0.00 | 0.00 | 0.00 | 0.00 |

**Clinopyroxene**

| Sample | Ab82 | Ab82 | Ab82 | Ab82 | Ab82 | Ab82 | Ab82 | Ab82 | Ab82 | Ab127 | Ab127 | Ab127 | Ab127 | Ab127 | Ab127 | Ab127 | Ab135 |
|---|---|---|---|---|---|---|---|---|---|---|---|---|---|---|---|---|---|
| Analysis No. | 9 | 5 | 18 | 21 | 22 | 23 | 25 | 26 | 32 | 14 | 16 | 20 | 22 | 23 | 24 | 27 | 26 |
| Analysis Name. | cpx2 | cpx1 | cpx3 | px9b | px9c | px9d | px9f | px9g | px10b | cpx1? | cpx3? | cpx3b | cpx4a? | cpx4b? | cpx5 | cpx6 | cpx1 |
| SiO2 | 53.16 | 53.24 | 52.46 | 50.16 | 48.24 | 46.67 | 45.14 | 48.66 | 48.31 | 53.31 | 51.38 | 54.10 | 52.92 | 52.86 | 52.75 | 52.61 | 51.69 |
| TiO2 | 0.55 | 1.07 | 1.11 | 1.43 | 1.78 | 2.22 | 2.90 | 1.55 | 1.55 | 0.69 | 0.51 | 0.68 | 0.34 | 0.58 | 0.41 | 0.54 | 0.56 |
| Al2O3 | 2.42 | 4.27 | 5.17 | 7.48 | 8.71 | 10.05 | 11.13 | 9.13 | 8.33 | 3.28 | 3.39 | 2.83 | 3.68 | 4.03 | 3.95 | 3.87 | 4.19 |
| Cr2O3 | 0.32 | 0.23 | 0.00 | 0.47 | 0.52 | 0.63 | 0.44 | 0.30 | 0.51 | 0.26 | 0.68 | 0.41 | 0.92 | 0.77 | 1.19 | 1.11 | 1.21 |
| FeO | 6.56 | 7.80 | 8.00 | 8.07 | 7.86 | 8.27 | 8.46 | 7.70 | 8.43 | 6.19 | 7.24 | 5.97 | 6.32 | 5.49 | 5.87 | 5.55 | 3.67 |
| MnO | 0.34 | 0.00 | 0.00 | 0.00 | 0.00 | 0.00 | 0.00 | 0.00 | 0.00 | 0.36 | 0.27 | 0.00 | 0.31 | 0.00 | 0.00 | 0.00 | 0.00 |
| MgO | 15.87 | 18.92 | 18.30 | 17.44 | 16.45 | 15.59 | 14.92 | 16.89 | 16.28 | 16.59 | 16.68 | 15.56 | 16.18 | 15.75 | 16.30 | 16.28 | 15.80 |
| CaO | 20.59 | 11.77 | 11.84 | 11.45 | 11.77 | 11.60 | 11.78 | 11.42 | 11.46 | 20.82 | 17.92 | 21.56 | 20.13 | 21.32 | 20.51 | 21.75 | 22.04 |
| Na2O | 0.64 | 0.85 | 0.97 | 1.60 | 1.54 | 1.94 | 1.93 | 1.73 | 1.36 | 0.43 | 0.56 | 0.27 | 0.37 | 0.40 | 0.49 | 0.34 | 0.64 |
| K2O | 0.15 | 0.33 | 0.23 | 0.23 | 0.53 | 0.74 | 0.69 | 0.35 | 0.48 | 0.00 | 0.00 | 0.00 | 0.00 | 0.00 | 0.00 | 0.00 | 0.00 |
| NiO | 0.00 | 0.00 | 0.00 | 0.00 | 0.00 | 0.00 | 0.00 | 0.00 | 0.00 | | | | | | | | 0.00 |
| Total | 100.61 | 98.49 | 98.07 | 98.31 | 97.40 | 97.72 | 97.40 | 97.73 | 96.70 | 101.94 | 98.62 | 101.37 | 101.17 | 101.20 | 101.47 | 102.04 | 99.79 |
| **Formula (6O)** | | | | | | | | | | | | | | | | | |
| Si | 1.945 | 1.944 | 1.925 | 1.847 | 1.801 | 1.749 | 1.702 | 1.803 | 1.817 | 1.919 | 1.912 | 1.952 | 1.918 | 1.911 | 1.905 | 1.893 | 1.892 |
| Al | 0.055 | 0.056 | 0.075 | 0.153 | 0.199 | 0.251 | 0.298 | 0.197 | 0.183 | 0.081 | 0.088 | 0.048 | 0.082 | 0.089 | 0.095 | 0.107 | 0.108 |
| Al | 0.049 | 0.128 | 0.149 | 0.171 | 0.184 | 0.192 | 0.197 | 0.202 | 0.187 | 0.058 | 0.061 | 0.073 | 0.075 | 0.083 | 0.073 | 0.057 | 0.073 |
| Fe(iii) | 0.029 | 0.000 | 0.000 | 0.021 | 0.054 | 0.135 | 0.144 | 0.060 | 0.023 | 0.013 | 0.028 | 0.000 | 0.000 | 0.000 | 0.001 | 0.018 | 0.022 |
| Cr | 0.009 | 0.007 | 0.000 | 0.014 | 0.015 | 0.019 | 0.013 | 0.009 | 0.015 | 0.007 | 0.020 | 0.012 | 0.026 | 0.022 | 0.034 | 0.032 | 0.035 |
| Ti | 0.015 | 0.029 | 0.031 | 0.040 | 0.050 | 0.063 | 0.082 | 0.043 | 0.044 | 0.019 | 0.014 | 0.018 | 0.009 | 0.016 | 0.011 | 0.015 | 0.015 |
| Fe(ii) | 0.172 | 0.240 | 0.247 | 0.227 | 0.190 | 0.121 | 0.120 | 0.177 | 0.241 | 0.173 | 0.197 | 0.181 | 0.192 | 0.166 | 0.176 | 0.148 | 0.090 |
| Mn | 0.011 | 0.000 | 0.000 | 0.000 | 0.000 | 0.000 | 0.000 | 0.000 | 0.000 | 0.011 | 0.009 | 0.000 | 0.010 | 0.000 | 0.000 | 0.000 | 0.000 |
| Mg | 0.866 | 1.030 | 1.001 | 0.957 | 0.916 | 0.871 | 0.839 | 0.933 | 0.913 | 0.890 | 0.925 | 0.837 | 0.874 | 0.849 | 0.877 | 0.873 | 0.862 |
| Ca | 0.807 | 0.461 | 0.466 | 0.452 | 0.471 | 0.466 | 0.476 | 0.453 | 0.462 | 0.803 | 0.714 | 0.834 | 0.782 | 0.826 | 0.793 | 0.839 | 0.864 |
| Na | 0.045 | 0.060 | 0.069 | 0.114 | 0.111 | 0.141 | 0.141 | 0.124 | 0.099 | 0.030 | 0.040 | 0.019 | 0.026 | 0.028 | 0.034 | 0.024 | 0.045 |
| K | 0.007 | 0.015 | 0.011 | 0.011 | 0.025 | 0.035 | 0.033 | 0.017 | 0.023 | 0.000 | 0.000 | 0.000 | 0.000 | 0.000 | 0.000 | 0.000 | 0.000 |
| TOTAL | 4.009 | 3.971 | 3.974 | 4.007 | 4.017 | 4.043 | 4.045 | 4.019 | 4.007 | 4.004 | 4.009 | 3.974 | 3.994 | 3.990 | 4.000 | 4.006 | 4.007 |
| **Endmembers** | | | | | | | | | | | | | | | | | |
| Wo | 41.84 | 25.71 | 26.11 | 25.50 | 27.02 | 26.86 | 27.68 | 25.93 | 26.56 | 41.81 | 37.34 | 44.55 | 41.50 | 44.18 | 42.15 | 44.08 | 45.87 |
| En | 44.88 | 57.52 | 56.15 | 54.05 | 52.56 | 50.23 | 48.78 | 53.38 | 52.51 | 46.36 | 48.36 | 44.74 | 46.42 | 45.42 | 46.61 | 45.91 | 45.76 |
| Fs | 10.93 | 13.41 | 13.87 | 14.00 | 14.02 | 14.78 | 15.33 | 13.58 | 15.22 | 10.26 | 12.19 | 9.70 | 10.69 | 8.90 | 9.41 | 8.77 | 5.95 |
| Ac | 2.35 | 3.36 | 3.87 | 6.45 | 6.40 | 8.13 | 8.21 | 7.11 | 5.70 | 1.56 | 2.11 | 1.01 | 1.38 | 1.50 | 1.82 | 1.25 | 2.41 |

**Clinopyroxene**

| Sample | Ab135 | Ab135 | Ab135 | Ab135 | Ab135 | Ab135 | Ab135 | Ab135 | Ab135 | Ab135 | Ab135 | Ab135 | Ab135 | Ab135 | Ab135 | Ab135 | Ab135 | Ab135 |
|---|---|---|---|---|---|---|---|---|---|---|---|---|---|---|---|---|---|---|
| Analysis No. | 1 | 2 | 3 | 8 | 13 | 14 | 15 | 16 | 17 | 18 | 20 | 25 | 26 | 27 | 28 | 29 | 31 | 32 |
| Analysis Name. | cpx2 | cpx3 | cpx3+1 | cpx4 | cpx5a | cpx5b | cpx5c | cpx5d | cpx5e | cpx5f | cpx6 | cpx7 | px8a | px8b | px9a | px9b | px10a | px10b |
| SiO2 | 51.04 | 53.43 | 52.05 | 52.16 | 51.29 | 50.77 | 51.31 | 51.08 | 50.75 | 51.08 | 50.74 | 50.95 | 51.01 | 50.75 | 50.99 | 50.86 | 51.07 | 50.89 |
| TiO2 | 0.64 | 0.44 | 0.52 | 0.48 | 0.58 | 0.64 | 0.58 | 0.63 | 0.69 | 0.61 | 0.65 | 0.48 | 0.65 | 0.49 | 0.45 | 0.52 | 0.50 | 0.38 |
| Al2O3 | 3.89 | 2.88 | 3.84 | 3.56 | 4.04 | 3.79 | 4.02 | 4.21 | 3.98 | 3.83 | 3.91 | 4.02 | 4.08 | 4.17 | 4.14 | 4.26 | 3.76 | 4.15 |
| Cr2O3 | 0.96 | 0.72 | 0.97 | 1.14 | 1.10 | 0.95 | 1.16 | 1.18 | 0.96 | 0.87 | 1.01 | 0.96 | 0.99 | 0.93 | 1.03 | 1.03 | 1.00 | 1.12 |
| FeO | 3.90 | 6.68 | 5.06 | 5.43 | 3.78 | 4.11 | 3.80 | 3.84 | 4.01 | 3.71 | 4.08 | 3.93 | 3.67 | 3.83 | 3.71 | 2.93 | 4.55 | 3.75 |
| MnO | 0.23 | 0.00 | 0.22 | 0.00 | 0.19 | 0.00 | 0.00 | 0.00 | 0.00 | 0.20 | 0.00 | 0.00 | 0.00 | 0.00 | 0.21 | 0.00 | 0.23 | 0.00 |
| MgO | 16.08 | 26.09 | 18.52 | 18.99 | 15.86 | 16.09 | 16.06 | 16.10 | 15.88 | 15.70 | 16.10 | 15.81 | 15.62 | 16.04 | 15.46 | 14.96 | 17.32 | 15.33 |
| CaO | 22.11 | 8.09 | 17.41 | 16.37 | 21.73 | 20.78 | 21.35 | 20.81 | 21.44 | 21.80 | 21.05 | 21.55 | 21.11 | 20.99 | 22.12 | 22.40 | 18.67 | 21.79 |
| Na2O | 0.73 | 0.34 | 0.45 | 0.39 | 0.52 | 0.52 | 0.60 | 0.47 | 0.57 | 0.49 | 0.54 | 0.55 | 0.59 | 0.46 | 0.57 | 0.57 | 0.31 | 0.53 |
| K2O | 0.00 | 0.00 | 0.00 | 0.00 | 0.00 | 0.00 | 0.00 | 0.00 | 0.00 | 0.00 | 0.00 | 0.00 | 0.00 | 0.00 | 0.00 | 0.00 | 0.00 | 0.00 |
| NiO | 0.00 | 0.00 | 0.00 | 0.00 | 0.00 | 0.00 | 0.00 | 0.00 | 0.00 | 0.00 | 0.00 | 0.00 | 0.00 | 0.00 | 0.00 | 0.00 | 0.00 | 0.00 |
| Total | 99.58 | 98.65 | 99.04 | 98.53 | 99.10 | 97.65 | 98.88 | 98.32 | 98.27 | 98.28 | 98.07 | 98.25 | 97.72 | 97.64 | 98.68 | 97.53 | 97.41 | 97.96 |
| **Formula (6O)** | | | | | | | | | | | | | | | | | | |
| Si | 1.880 | 1.920 | 1.905 | 1.915 | 1.892 | 1.898 | 1.894 | 1.893 | 1.888 | 1.899 | 1.890 | 1.895 | 1.902 | 1.894 | 1.891 | 1.901 | 1.905 | 1.898 |
| Al | 0.120 | 0.080 | 0.095 | 0.085 | 0.108 | 0.102 | 0.106 | 0.107 | 0.112 | 0.101 | 0.110 | 0.105 | 0.098 | 0.106 | 0.109 | 0.099 | 0.095 | 0.102 |
| Al | 0.049 | 0.042 | 0.071 | 0.069 | 0.068 | 0.065 | 0.069 | 0.077 | 0.063 | 0.067 | 0.062 | 0.071 | 0.081 | 0.078 | 0.072 | 0.088 | 0.070 | 0.081 |
| Fe(iii) | 0.089 | 0.025 | 0.000 | 0.000 | 0.020 | 0.017 | 0.021 | 0.000 | 0.035 | 0.015 | 0.031 | 0.028 | 0.000 | 0.010 | 0.034 | 0.000 | 0.000 | 0.008 |
| Cr | 0.028 | 0.020 | 0.028 | 0.033 | 0.032 | 0.028 | 0.034 | 0.035 | 0.028 | 0.026 | 0.030 | 0.028 | 0.029 | 0.027 | 0.030 | 0.030 | 0.029 | 0.033 |
| Ti | 0.018 | 0.012 | 0.014 | 0.013 | 0.016 | 0.018 | 0.016 | 0.018 | 0.019 | 0.017 | 0.018 | 0.013 | 0.018 | 0.014 | 0.013 | 0.015 | 0.014 | 0.011 |
| Fe(ii) | 0.031 | 0.175 | 0.155 | 0.167 | 0.097 | 0.111 | 0.096 | 0.119 | 0.090 | 0.101 | 0.096 | 0.094 | 0.115 | 0.109 | 0.081 | 0.092 | 0.142 | 0.109 |
| Mn | 0.007 | 0.000 | 0.007 | 0.000 | 0.006 | 0.000 | 0.000 | 0.000 | 0.000 | 0.006 | 0.000 | 0.000 | 0.000 | 0.000 | 0.007 | 0.000 | 0.007 | 0.000 |
| Mg | 0.883 | 1.398 | 1.011 | 1.039 | 0.872 | 0.897 | 0.884 | 0.889 | 0.881 | 0.870 | 0.894 | 0.877 | 0.868 | 0.892 | 0.855 | 0.833 | 0.963 | 0.852 |
| Ca | 0.873 | 0.311 | 0.683 | 0.644 | 0.859 | 0.832 | 0.844 | 0.826 | 0.855 | 0.868 | 0.840 | 0.859 | 0.843 | 0.839 | 0.879 | 0.897 | 0.746 | 0.871 |
| Na | 0.052 | 0.024 | 0.032 | 0.028 | 0.037 | 0.038 | 0.043 | 0.034 | 0.041 | 0.035 | 0.039 | 0.040 | 0.043 | 0.033 | 0.041 | 0.041 | 0.022 | 0.038 |
| K | 0.000 | 0.000 | 0.000 | 0.000 | 0.000 | 0.000 | 0.000 | 0.000 | 0.000 | 0.000 | 0.000 | 0.000 | 0.000 | 0.000 | 0.000 | 0.000 | 0.000 | 0.000 |
| TOTAL | 4.029 | 4.008 | 4.000 | 3.993 | 4.006 | 4.005 | 4.007 | 3.997 | 4.011 | 4.005 | 4.010 | 4.009 | 3.997 | 4.003 | 4.011 | 3.996 | 3.995 | 4.003 |
| **Endmembers** | | | | | | | | | | | | | | | | | | |
| Wo | 45.11 | 16.11 | 36.18 | 34.28 | 45.43 | 43.92 | 44.72 | 44.22 | 44.96 | 45.81 | 44.22 | 45.27 | 45.13 | 44.54 | 46.36 | 48.13 | 39.66 | 46.36 |
| En | 45.66 | 72.30 | 53.56 | 55.34 | 46.14 | 47.32 | 46.81 | 47.60 | 46.34 | 45.91 | 47.06 | 46.21 | 46.46 | 47.36 | 45.08 | 44.73 | 51.20 | 45.38 |
| Fs | 6.54 | 10.36 | 8.57 | 8.89 | 6.47 | 6.77 | 6.20 | 6.37 | 6.54 | 6.41 | 6.67 | 6.43 | 6.13 | 6.34 | 6.40 | 4.92 | 7.94 | 6.22 |
| Ac | 2.70 | 1.23 | 1.69 | 1.48 | 1.97 | 1.99 | 2.27 | 1.81 | 2.16 | 1.86 | 2.05 | 2.09 | 2.28 | 1.77 | 2.16 | 2.22 | 1.19 | 2.04 |

**Clinopyroxene**

| Sample | 85P | 85P | 85P | 85P | 85P | Ab3826 | Ab3826 | Ab3826 | Ab3826 | Ab3826 | Ab3826 | Ab3826 | Ab92 | Ab92 | Ab92 | Ab5613 | Ab5613 |
|---|---|---|---|---|---|---|---|---|---|---|---|---|---|---|---|---|---|
| Analysis No. | 5 | 9 | 10 | 12 | 13 | 8 | 10 | 15 | 21 | 25 | 28 | 37 | 3 | 11 | 17 | 3 | 6 |
| Analysis Name. | cpx1 | cpx2a | cpx2b | cpx3 | cpx3b | cpx1 | cpx2 | cpx2 | cpx3 | cpx4 | cpx5 | cpx6 | cpx1 | cpx2 | cpx3 | cpx1 | cpx2 |
| SiO2 | 52.84 | 52.77 | 53.37 | 52.88 | 53.48 | 50.77 | 51.38 | 51.14 | 51.11 | 51.00 | 51.24 | 51.33 | 52.55 | 51.35 | 52.37 | 51.40 | 51.16 |
| TiO2 | 0.00 | 0.26 | 0.28 | 0.00 | 0.00 | 0.00 | 0.00 | 0.00 | 0.00 | 0.20 | 0.19 | 0.00 | 0.33 | 0.28 | 0.27 | 0.25 | 0.19 |
| Al2O3 | 0.70 | 0.70 | 0.73 | 0.49 | 0.66 | 0.87 | 0.75 | 0.61 | 0.39 | 0.76 | 0.96 | 0.68 | 0.97 | 0.98 | 0.89 | 1.05 | 0.94 |
| Cr2O3 | 0.19 | 0.18 | 0.00 | 0.00 | 0.23 | 0.00 | 0.00 | 0.00 | 0.00 | 0.00 | 0.00 | 0.26 | 0.25 | 0.00 | 0.00 | 0.29 | 0.00 |
| FeO | 14.40 | 14.13 | 14.19 | 15.08 | 14.85 | 15.44 | 14.88 | 14.23 | 19.14 | 14.76 | 14.42 | 14.56 | 16.04 | 17.69 | 15.97 | 11.17 | 9.97 |
| MnO | 0.55 | 0.68 | 0.79 | 0.63 | 0.42 | 0.67 | 0.40 | 0.36 | 0.49 | 0.58 | 0.45 | 0.54 | 0.30 | 0.49 | 0.43 | 0.22 | 0.33 |
| MgO | 9.64 | 9.57 | 9.87 | 10.02 | 10.10 | 10.34 | 10.60 | 10.48 | 11.03 | 10.42 | 10.59 | 10.55 | 9.64 | 10.35 | 9.76 | 13.52 | 13.08 |
| CaO | 23.49 | 23.23 | 23.82 | 22.59 | 22.86 | 20.00 | 20.84 | 21.27 | 16.57 | 20.81 | 21.63 | 21.18 | 22.35 | 18.73 | 21.82 | 20.18 | 21.50 |
| Na2O | 0.48 | 0.52 | 0.52 | 0.40 | 0.49 | 0.30 | 0.45 | 0.37 | 0.36 | 0.26 | 0.26 | 0.30 | 0.35 | 0.52 | 0.36 | 0.34 | 0.30 |
| K2O | 0.00 | 0.00 | 0.00 | 0.00 | 0.00 | 0.00 | 0.00 | 0.00 | 0.00 | 0.00 | 0.00 | 0.00 | 0.00 | 0.00 | 0.00 | 0.00 | 0.00 |
| NiO | | | | | | | | | | | | | | | | | |
| Total | 102.28 | 102.03 | 103.57 | 102.08 | 103.08 | 98.39 | 99.30 | 98.46 | 99.10 | 98.79 | 99.75 | 99.40 | 102.78 | 100.39 | 101.87 | 98.42 | 97.47 |
| Formula (6O) | | | | | | | | | | | | | | | | | |
| Si | 1.986 | 1.986 | 1.980 | 1.992 | 1.991 | 1.982 | 1.983 | 1.988 | 1.993 | 1.980 | 1.969 | 1.980 | 1.971 | 1.974 | 1.980 | 1.964 | 1.971 |
| Al | 0.014 | 0.014 | 0.020 | 0.008 | 0.009 | 0.018 | 0.017 | 0.012 | 0.007 | 0.020 | 0.031 | 0.020 | 0.029 | 0.026 | 0.020 | 0.036 | 0.029 |
| Al | 0.017 | 0.017 | 0.012 | 0.014 | 0.020 | 0.022 | 0.017 | 0.016 | 0.011 | 0.015 | 0.013 | 0.011 | 0.014 | 0.019 | 0.019 | 0.012 | 0.014 |
| Fe(iii) | 0.040 | 0.021 | 0.044 | 0.035 | 0.027 | 0.028 | 0.049 | 0.035 | 0.035 | 0.020 | 0.039 | 0.034 | 0.020 | 0.044 | 0.018 | 0.039 | 0.039 |
| Cr | 0.006 | 0.005 | 0.000 | 0.000 | 0.007 | 0.000 | 0.000 | 0.000 | 0.000 | 0.000 | 0.000 | 0.008 | 0.007 | 0.000 | 0.000 | 0.009 | 0.000 |
| Ti | 0.000 | 0.007 | 0.008 | 0.000 | 0.000 | 0.000 | 0.000 | 0.000 | 0.000 | 0.006 | 0.005 | 0.000 | 0.009 | 0.008 | 0.008 | 0.007 | 0.006 |
| Fe(ii) | 0.411 | 0.423 | 0.395 | 0.438 | 0.434 | 0.475 | 0.429 | 0.426 | 0.587 | 0.458 | 0.423 | 0.434 | 0.482 | 0.522 | 0.486 | 0.316 | 0.281 |
| Mn | 0.018 | 0.022 | 0.025 | 0.020 | 0.013 | 0.022 | 0.013 | 0.012 | 0.016 | 0.019 | 0.015 | 0.018 | 0.010 | 0.016 | 0.014 | 0.007 | 0.011 |
| Mg | 0.540 | 0.537 | 0.546 | 0.562 | 0.560 | 0.602 | 0.610 | 0.607 | 0.641 | 0.603 | 0.607 | 0.607 | 0.539 | 0.593 | 0.550 | 0.770 | 0.751 |
| Ca | 0.946 | 0.936 | 0.947 | 0.912 | 0.912 | 0.836 | 0.862 | 0.886 | 0.692 | 0.865 | 0.891 | 0.875 | 0.898 | 0.771 | 0.884 | 0.826 | 0.888 |
| Na | 0.035 | 0.038 | 0.037 | 0.029 | 0.036 | 0.023 | 0.034 | 0.028 | 0.027 | 0.020 | 0.019 | 0.022 | 0.025 | 0.039 | 0.026 | 0.025 | 0.022 |
| K | 0.000 | 0.000 | 0.000 | 0.000 | 0.000 | 0.000 | 0.000 | 0.000 | 0.000 | 0.000 | 0.000 | 0.000 | 0.000 | 0.000 | 0.000 | 0.000 | 0.000 |
| TOTAL | 4.012 | 4.006 | 4.013 | 4.010 | 4.008 | 4.008 | 4.014 | 4.010 | 4.010 | 4.006 | 4.012 | 4.010 | 4.006 | 4.013 | 4.005 | 4.012 | 4.012 |
| Endmembers | | | | | | | | | | | | | | | | | |
| Wo | 47.54 | 47.38 | 47.50 | 45.65 | 46.00 | 42.12 | 43.16 | 44.42 | 34.63 | 43.59 | 44.68 | 43.98 | 45.49 | 38.84 | 44.68 | 41.63 | 44.55 |
| En | 27.14 | 27.17 | 27.38 | 28.17 | 28.27 | 30.30 | 30.55 | 30.46 | 32.08 | 30.37 | 30.44 | 30.48 | 27.30 | 29.87 | 27.81 | 38.81 | 37.71 |
| Fs | 23.55 | 23.54 | 23.26 | 24.73 | 23.94 | 26.44 | 24.61 | 23.72 | 31.94 | 25.05 | 23.91 | 24.42 | 25.92 | 29.33 | 26.18 | 18.29 | 16.61 |
| Ac | 1.77 | 1.90 | 1.86 | 1.45 | 1.79 | 1.14 | 1.69 | 1.40 | 1.36 | 0.99 | 0.97 | 1.13 | 1.29 | 1.95 | 1.33 | 1.27 | 1.12 |

**Clinopyroxene**

| Sample | Ab5613 | Ab5613 | Ab5613 | Ab5613 | Ab5613 | Ab5613 | Ab5613 | Ab7799 | Ab7799 | Ab7799 | Ab7799 | Ab7799 | Ab7799 | Ab7799 | Ab7799 | Ab7801 | Ab7801 |
|---|---|---|---|---|---|---|---|---|---|---|---|---|---|---|---|---|---|
| Analysis No. | 22 | 23 | 24 | 25 | 26 | 29 | 40 | 3 | 4 | 6 | 12 | 13 | 14 | 15 | 18 | 2 | 6 |
| Analysis Name. | cpx3 | cpx4a | cpx4b | cpx4c | cpx4d | px4g | cpx4 | cpx2 | cpx3 | cpx4 | cpx5 | cpx6 | cpx7 | cpx8 | cpx9 | cpx1 | cpx2 |
| SiO2 | 51.40 | 51.42 | 51.11 | 51.40 | 51.32 | 51.39 | 51.51 | 48.24 | 49.24 | 48.02 | 48.72 | 48.67 | 48.91 | 48.43 | 49.71 | 52.65 | 52.15 |
| TiO2 | 0.35 | 0.00 | 0.00 | 0.38 | 0.27 | 0.18 | 0.00 | 0.43 | 0.00 | 0.79 | 0.35 | 0.59 | 0.00 | 0.61 | 0.00 | 0.25 | 0.22 |
| Al2O3 | 1.16 | 0.93 | 1.17 | 1.23 | 1.39 | 0.98 | 0.76 | 1.08 | 0.64 | 1.22 | 1.06 | 1.06 | 0.94 | 1.26 | 0.63 | 1.19 | 1.10 |
| Cr2O3 | 0.24 | 0.00 | 0.37 | 0.00 | 0.00 | 0.00 | 0.00 | 0.00 | 0.00 | 0.00 | 0.00 | 0.28 | 0.00 | 0.00 | 0.00 | 0.00 | 0.00 |
| FeO | 11.06 | 9.48 | 9.63 | 10.10 | 10.30 | 10.08 | 10.35 | 29.86 | 29.43 | 29.44 | 29.81 | 30.04 | 30.21 | 29.52 | 28.63 | 17.54 | 17.28 |
| MnO | 0.38 | 0.35 | 0.00 | 0.29 | 0.00 | 0.25 | 0.00 | 0.87 | 1.16 | 0.60 | 0.84 | 0.95 | 0.90 | 1.03 | 0.93 | 0.53 | 0.52 |
| MgO | 13.40 | 13.04 | 12.99 | 12.71 | 12.94 | 12.83 | 13.14 | 0.55 | 0.52 | 0.61 | 0.63 | 0.54 | 0.61 | 0.69 | 1.67 | 9.51 | 10.13 |
| CaO | 19.55 | 21.45 | 21.50 | 21.24 | 21.00 | 21.28 | 20.75 | 20.19 | 20.62 | 19.76 | 20.30 | 19.91 | 20.58 | 19.87 | 20.40 | 21.18 | 20.33 |
| Na2O | 0.35 | 0.28 | 0.32 | 0.42 | 0.55 | 0.33 | 0.34 | 0.44 | 0.42 | 0.45 | 0.60 | 0.29 | 0.43 | 0.53 | 0.42 | 0.59 | 0.37 |
| K2O | 0.00 | 0.00 | 0.00 | 0.00 | 0.00 | 0.00 | 0.00 | 0.00 | 0.00 | 0.00 | 0.00 | 0.00 | 0.00 | 0.00 | 0.00 | 0.00 | 0.00 |
| NiO | | | | | | | | | | | | | | | | | |
| Total | 97.90 | 96.94 | 97.11 | 97.76 | 97.76 | 97.32 | 96.84 | 101.98 | 102.02 | 100.88 | 102.31 | 102.32 | 102.58 | 101.94 | 102.39 | 103.62 | 102.10 |
| **Formula (6O)** | | | | | | | | | | | | | | | | | |
| Si | 1.971 | 1.985 | 1.972 | 1.973 | 1.968 | 1.981 | 1.992 | 1.961 | 1.990 | 1.960 | 1.965 | 1.963 | 1.971 | 1.958 | 1.988 | 1.970 | 1.972 |
| Al | 0.029 | 0.015 | 0.028 | 0.027 | 0.032 | 0.019 | 0.008 | 0.039 | 0.010 | 0.040 | 0.035 | 0.037 | 0.029 | 0.042 | 0.012 | 0.030 | 0.028 |
| Al | 0.023 | 0.028 | 0.025 | 0.028 | 0.031 | 0.025 | 0.026 | 0.012 | 0.020 | 0.018 | 0.016 | 0.013 | 0.016 | 0.018 | 0.018 | 0.023 | 0.021 |
| Fe(iii) | 0.007 | 0.012 | 0.022 | 0.013 | 0.039 | 0.012 | 0.011 | 0.053 | 0.034 | 0.014 | 0.067 | 0.003 | 0.070 | 0.042 | 0.040 | 0.053 | 0.034 |
| Cr | 0.007 | 0.000 | 0.011 | 0.000 | 0.000 | 0.000 | 0.000 | 0.000 | 0.000 | 0.000 | 0.000 | 0.009 | 0.000 | 0.000 | 0.000 | 0.000 | 0.000 |
| Ti | 0.010 | 0.000 | 0.000 | 0.011 | 0.008 | 0.005 | 0.000 | 0.013 | 0.000 | 0.024 | 0.011 | 0.018 | 0.000 | 0.019 | 0.000 | 0.007 | 0.006 |
| Fe(ii) | 0.347 | 0.294 | 0.288 | 0.311 | 0.291 | 0.312 | 0.323 | 0.958 | 0.958 | 0.990 | 0.933 | 1.010 | 0.943 | 0.953 | 0.915 | 0.493 | 0.511 |
| Mn | 0.012 | 0.011 | 0.000 | 0.009 | 0.000 | 0.008 | 0.000 | 0.030 | 0.040 | 0.021 | 0.029 | 0.032 | 0.031 | 0.035 | 0.032 | 0.017 | 0.017 |
| Mg | 0.766 | 0.751 | 0.747 | 0.727 | 0.740 | 0.737 | 0.757 | 0.033 | 0.031 | 0.037 | 0.038 | 0.032 | 0.037 | 0.042 | 0.100 | 0.531 | 0.571 |
| Ca | 0.803 | 0.887 | 0.889 | 0.873 | 0.863 | 0.879 | 0.860 | 0.879 | 0.893 | 0.864 | 0.877 | 0.860 | 0.889 | 0.861 | 0.874 | 0.849 | 0.823 |
| Na | 0.026 | 0.021 | 0.024 | 0.031 | 0.041 | 0.025 | 0.025 | 0.035 | 0.033 | 0.036 | 0.047 | 0.023 | 0.034 | 0.042 | 0.033 | 0.043 | 0.027 |
| K | 0.000 | 0.000 | 0.000 | 0.000 | 0.000 | 0.000 | 0.000 | 0.000 | 0.000 | 0.000 | 0.000 | 0.000 | 0.000 | 0.000 | 0.000 | 0.000 | 0.000 |
| TOTAL | 4.002 | 4.004 | 4.007 | 4.004 | 4.012 | 4.004 | 4.003 | 4.013 | 4.009 | 4.003 | 4.017 | 4.001 | 4.017 | 4.011 | 4.010 | 4.015 | 4.010 |
| **Endmembers** | | | | | | | | | | | | | | | | | |
| Wo | 40.94 | 44.90 | 45.11 | 44.44 | 43.74 | 44.53 | 43.48 | 44.23 | 44.90 | 44.06 | 44.07 | 43.88 | 44.39 | 43.61 | 43.88 | 42.76 | 41.53 |
| En | 39.04 | 37.99 | 37.93 | 37.01 | 37.50 | 37.36 | 38.32 | 1.68 | 1.58 | 1.89 | 1.90 | 1.66 | 1.83 | 2.11 | 5.00 | 26.72 | 28.79 |
| Fs | 18.69 | 16.05 | 15.74 | 16.96 | 16.69 | 16.86 | 16.91 | 52.34 | 51.87 | 52.23 | 51.67 | 53.31 | 52.10 | 52.18 | 49.49 | 28.36 | 28.31 |
| Ac | 1.33 | 1.06 | 1.22 | 1.59 | 2.07 | 1.25 | 1.29 | 1.74 | 1.65 | 1.82 | 2.36 | 1.16 | 1.68 | 2.10 | 1.63 | 2.16 | 1.37 |

**Clinopyroxene**

| Sample | Ab7801 | Ab7801 | Ab7801 | Ab7801 | Ab7801 | Ab7801 | Ab7801 | Ab7801 | Ab7802 | Ab7802 | Ab7802 | Ab7802 | Ab7802 | Ab7802 | Ab7802 | Ab7802 | MS1595 |
|---|---|---|---|---|---|---|---|---|---|---|---|---|---|---|---|---|---|
| Analysis No. | 12 | 13 | 14 | 15 | 16 | 20 | 31 | 32 | 3 | 5 | 6 | 11 | 17 | 26 | 27 | 19 | 25 |
| Analysis Name. | cpx3 | cpx4 | cpx5 | cpx6a | cpx6b | cpx7 | cpx8a | cpx8b | cpx1 | cpx2 | cpx3 | cpx4a | cpx5 | px8a | px8b | cpx7 | cpx3a |
| SiO2 | 52.71 | 52.33 | 52.93 | 52.45 | 52.60 | 52.17 | 53.14 | 53.08 | 52.54 | 52.29 | 51.94 | 52.55 | 52.98 | 52.34 | 52.55 | 52.04 | 51.70 |
| TiO2 | 0.00 | 0.27 | 0.33 | 0.28 | 0.34 | 0.00 | 0.00 | 0.23 | 0.22 | 0.37 | 0.44 | 0.25 | 0.31 | 0.49 | 0.27 | 0.30 | 0.56 |
| Al2O3 | 1.11 | 1.16 | 1.28 | 1.17 | 1.41 | 1.26 | 1.25 | 1.26 | 1.19 | 1.20 | 1.50 | 1.36 | 1.37 | 1.66 | 1.26 | 0.79 | 2.12 |
| Cr2O3 | 0.00 | 0.28 | 0.34 | 0.00 | 0.00 | 0.00 | 0.24 | 0.00 | 0.00 | 0.00 | 0.00 | 0.19 | 0.20 | 0.00 | 0.00 | 0.27 | 0.37 |
| FeO | 16.92 | 20.82 | 16.63 | 17.61 | 17.41 | 20.92 | 16.36 | 16.58 | 11.89 | 12.19 | 14.17 | 12.35 | 14.44 | 12.05 | 11.46 | 22.13 | 4.26 |
| MnO | 0.40 | 0.53 | 0.44 | 0.49 | 0.42 | 0.44 | 0.44 | 0.43 | 0.44 | 0.00 | 0.29 | 0.22 | 0.33 | 0.36 | 0.00 | 0.56 | 0.24 |
| MgO | 9.99 | 10.68 | 10.20 | 10.09 | 10.11 | 10.33 | 10.44 | 10.31 | 12.18 | 12.16 | 12.09 | 12.15 | 12.20 | 12.09 | 12.17 | 13.94 | 16.16 |
| CaO | 21.40 | 16.91 | 21.38 | 20.04 | 20.96 | 16.99 | 21.52 | 21.59 | 22.28 | 21.53 | 20.09 | 22.18 | 19.23 | 21.46 | 22.32 | 11.19 | 22.02 |
| Na2O | 0.34 | 0.32 | 0.38 | 0.38 | 0.43 | 0.22 | 0.59 | 0.64 | 0.43 | 0.54 | 0.26 | 0.24 | 0.32 | 0.49 | 0.54 | 0.26 | 0.50 |
| K2O | 0.00 | 0.00 | 0.00 | 0.00 | 0.00 | 0.00 | 0.00 | 0.00 | 0.00 | 0.00 | 0.00 | 0.00 | 0.00 | 0.00 | 0.00 | 0.00 | 0.00 |
| NiO | | | | | | | | | 0.00 | 0.00 | 0.00 | 0.00 | 0.00 | 0.00 | 0.00 | 0.00 | 0.00 |
| Total | 102.87 | 103.30 | 103.91 | 102.52 | 103.68 | 102.33 | 103.98 | 104.10 | 101.18 | 100.28 | 100.79 | 101.49 | 101.38 | 100.94 | 100.59 | 101.49 | 97.93 |
| **Formula (6O)** | | | | | | | | | | | | | | | | | |
| Si | 1.976 | 1.967 | 1.963 | 1.974 | 1.959 | 1.978 | 1.968 | 1.965 | 1.967 | 1.971 | 1.959 | 1.962 | 1.980 | 1.960 | 1.972 | 1.973 | 1.934 |
| Al | 0.024 | 0.033 | 0.037 | 0.026 | 0.041 | 0.022 | 0.032 | 0.035 | 0.033 | 0.029 | 0.041 | 0.038 | 0.020 | 0.040 | 0.028 | 0.027 | 0.066 |
| Al | 0.025 | 0.018 | 0.019 | 0.026 | 0.021 | 0.034 | 0.022 | 0.020 | 0.019 | 0.024 | 0.026 | 0.022 | 0.040 | 0.033 | 0.028 | 0.008 | 0.028 |
| Fe(iii) | 0.034 | 0.023 | 0.025 | 0.017 | 0.046 | 0.006 | 0.067 | 0.072 | 0.049 | 0.034 | 0.014 | 0.022 | 0.000 | 0.022 | 0.037 | 0.019 | 0.047 |
| Cr | 0.000 | 0.008 | 0.010 | 0.000 | 0.000 | 0.000 | 0.007 | 0.000 | 0.000 | 0.000 | 0.000 | 0.006 | 0.006 | 0.000 | 0.000 | 0.008 | 0.011 |
| Ti | 0.000 | 0.008 | 0.009 | 0.008 | 0.010 | 0.000 | 0.000 | 0.006 | 0.006 | 0.010 | 0.012 | 0.007 | 0.009 | 0.014 | 0.008 | 0.009 | 0.016 |
| Fe(ii) | 0.495 | 0.630 | 0.489 | 0.536 | 0.494 | 0.657 | 0.437 | 0.438 | 0.322 | 0.349 | 0.432 | 0.363 | 0.452 | 0.355 | 0.322 | 0.682 | 0.086 |
| Mn | 0.013 | 0.017 | 0.014 | 0.016 | 0.013 | 0.014 | 0.014 | 0.013 | 0.014 | 0.000 | 0.009 | 0.007 | 0.010 | 0.011 | 0.000 | 0.018 | 0.008 |
| Mg | 0.558 | 0.598 | 0.564 | 0.566 | 0.561 | 0.584 | 0.576 | 0.569 | 0.680 | 0.683 | 0.680 | 0.676 | 0.680 | 0.675 | 0.681 | 0.788 | 0.901 |
| Ca | 0.860 | 0.681 | 0.849 | 0.808 | 0.837 | 0.690 | 0.854 | 0.856 | 0.894 | 0.869 | 0.812 | 0.887 | 0.770 | 0.861 | 0.897 | 0.455 | 0.883 |
| Na | 0.025 | 0.023 | 0.027 | 0.028 | 0.031 | 0.016 | 0.042 | 0.046 | 0.031 | 0.039 | 0.019 | 0.017 | 0.023 | 0.036 | 0.039 | 0.019 | 0.036 |
| K | 0.000 | 0.000 | 0.000 | 0.000 | 0.000 | 0.000 | 0.000 | 0.000 | 0.000 | 0.000 | 0.000 | 0.000 | 0.000 | 0.000 | 0.000 | 0.000 | 0.000 |
| TOTAL | 4.010 | 4.006 | 4.007 | 4.005 | 4.013 | 4.002 | 4.020 | 4.021 | 4.015 | 4.010 | 4.004 | 4.007 | 3.991 | 4.007 | 4.011 | 4.005 | 4.015 |
| **Endmembers** | | | | | | | | | | | | | | | | | |
| Wo | 43.32 | 34.52 | 43.14 | 41.00 | 42.19 | 35.08 | 42.90 | 42.92 | 44.92 | 44.01 | 41.29 | 44.97 | 39.78 | 43.94 | 45.41 | 22.95 | 45.02 |
| En | 28.14 | 30.34 | 28.64 | 28.72 | 28.32 | 29.68 | 28.96 | 28.52 | 34.17 | 34.59 | 34.57 | 34.28 | 35.12 | 34.44 | 34.46 | 39.79 | 45.97 |
| Fs | 27.30 | 33.96 | 26.84 | 28.87 | 27.92 | 34.42 | 26.01 | 26.25 | 19.34 | 19.40 | 23.17 | 19.86 | 23.91 | 19.80 | 18.14 | 36.29 | 7.16 |
| Ac | 1.25 | 1.18 | 1.39 | 1.41 | 1.57 | 0.82 | 2.13 | 2.30 | 1.57 | 2.00 | 0.97 | 0.88 | 1.20 | 1.82 | 1.99 | 0.97 | 1.85 |

**Clinopyroxene**

| Sample | MS1595 | MS1595 | MS1595 | Ab93 | Ab93 | Ab93 | Ab93 | Ab93 | Ab93 | Ab93 | Ab243 | Ab243 | Ab243 | Ab243 | Ab243 | Ab243 | Ab243 |
|---|---|---|---|---|---|---|---|---|---|---|---|---|---|---|---|---|---|
| Analysis No. | 26 | 27 | 28 | 1 | 24 | 28 | 29 | 32 | 33 | 35 | 5 | 9 | 10 | 12 | 13 | 14 | 15 |
| Analysis Name. | cpx3b | cpx3c | cpx3d | cpx1 | cpx2 | cpx2 | cpx2b | cpx3 | cpx3b | cpx4 | cpx1 | cpx2 | cpx3 | cpx4 | cpx4a | cpx4b | cpx5 |
| SiO2 | 51.69 | 52.20 | 52.19 | 50.38 | 51.76 | 51.59 | 52.27 | 51.52 | 51.45 | 51.85 | 51.13 | 51.89 | 51.38 | 51.38 | 51.32 | 51.24 | 48.09 |
| TiO2 | 0.63 | 0.72 | 0.65 | 0.50 | 0.64 | 0.72 | 0.50 | 0.61 | 0.67 | 0.81 | 0.42 | 0.55 | 0.33 | 0.51 | 0.42 | 0.49 | 0.45 |
| Al2O3 | 2.34 | 2.63 | 2.55 | 2.01 | 2.28 | 2.22 | 1.81 | 2.20 | 2.25 | 1.98 | 1.60 | 1.54 | 1.09 | 1.93 | 1.57 | 1.07 | 1.45 |
| Cr2O3 | 0.55 | 0.45 | 0.41 | 0.26 | 0.00 | 0.21 | 0.00 | 0.22 | 0.00 | 0.00 | 0.00 | 0.19 | 0.00 | 0.00 | 0.00 | 0.00 | 0.00 |
| FeO | 6.83 | 4.84 | 4.53 | 11.23 | 10.73 | 10.91 | 11.57 | 11.77 | 11.60 | 11.12 | 21.49 | 14.69 | 16.14 | 14.75 | 19.19 | 23.84 | 13.52 |
| MnO | 0.00 | 0.00 | 0.00 | 0.25 | 0.25 | 0.24 | 0.27 | 0.29 | 0.26 | 0.33 | 0.74 | 0.42 | 0.37 | 0.41 | 0.38 | 0.77 | 0.34 |
| MgO | 17.90 | 16.43 | 15.65 | 12.90 | 13.11 | 13.00 | 13.43 | 13.12 | 13.09 | 13.03 | 12.21 | 10.99 | 10.78 | 10.81 | 11.59 | 12.53 | 10.25 |
| CaO | 18.11 | 20.92 | 21.45 | 20.09 | 21.40 | 21.08 | 20.10 | 20.23 | 20.84 | 20.33 | 13.49 | 20.94 | 19.84 | 20.68 | 15.72 | 10.29 | 22.50 |
| Na2O | 0.49 | 0.42 | 0.42 | 0.00 | 0.35 | 0.29 | 0.00 | 0.00 | 0.00 | 0.00 | 0.25 | 0.23 | 0.25 | 0.00 | 0.00 | 0.00 | 0.24 |
| K2O | 0.00 | 0.00 | 0.00 | 0.00 | 0.00 | 0.00 | 0.00 | 0.00 | 0.00 | 0.00 | 0.00 | 0.00 | 0.00 | 0.00 | 0.00 | 0.00 | 0.00 |
| NiO | 0.00 | 0.00 | 0.00 | | | | | | | | | | | | | | |
| Total | 98.53 | 98.59 | 97.85 | 97.61 | 100.51 | 100.25 | 99.97 | 99.97 | 100.55 | 99.44 | 101.51 | 101.44 | 100.16 | 100.48 | 100.18 | 100.25 | 96.83 |
| **Formula (6O)** | | | | | | | | | | | | | | | | | |
| Si | 1.922 | 1.933 | 1.947 | 1.941 | 1.935 | 1.935 | 1.961 | 1.939 | 1.934 | 1.954 | 1.951 | 1.955 | 1.969 | 1.952 | 1.967 | 1.978 | 1.916 |
| Al | 0.078 | 0.067 | 0.053 | 0.059 | 0.065 | 0.065 | 0.039 | 0.061 | 0.066 | 0.046 | 0.049 | 0.045 | 0.031 | 0.048 | 0.033 | 0.022 | 0.068 |
| Al | 0.024 | 0.048 | 0.059 | 0.032 | 0.035 | 0.033 | 0.041 | 0.037 | 0.033 | 0.042 | 0.023 | 0.024 | 0.018 | 0.039 | 0.038 | 0.027 | 0.000 |
| Fe(iii) | 0.057 | 0.000 | 0.000 | 0.000 | 0.029 | 0.011 | 0.000 | 0.000 | 0.000 | 0.000 | 0.030 | 0.002 | 0.018 | 0.000 | 0.000 | 0.000 | 0.137 |
| Cr | 0.016 | 0.013 | 0.012 | 0.008 | 0.000 | 0.006 | 0.000 | 0.007 | 0.000 | 0.000 | 0.000 | 0.006 | 0.000 | 0.000 | 0.000 | 0.000 | 0.000 |
| Ti | 0.018 | 0.020 | 0.018 | 0.014 | 0.018 | 0.020 | 0.014 | 0.017 | 0.019 | 0.023 | 0.012 | 0.016 | 0.010 | 0.015 | 0.012 | 0.014 | 0.013 |
| Fe(ii) | 0.155 | 0.150 | 0.142 | 0.362 | 0.306 | 0.331 | 0.364 | 0.371 | 0.365 | 0.352 | 0.655 | 0.461 | 0.498 | 0.470 | 0.617 | 0.773 | 0.308 |
| Mn | 0.000 | 0.000 | 0.000 | 0.008 | 0.008 | 0.008 | 0.009 | 0.009 | 0.008 | 0.011 | 0.024 | 0.013 | 0.012 | 0.013 | 0.012 | 0.025 | 0.011 |
| Mg | 0.992 | 0.907 | 0.870 | 0.741 | 0.731 | 0.727 | 0.751 | 0.736 | 0.733 | 0.732 | 0.695 | 0.617 | 0.616 | 0.612 | 0.662 | 0.721 | 0.609 |
| Ca | 0.721 | 0.830 | 0.857 | 0.829 | 0.857 | 0.847 | 0.808 | 0.816 | 0.839 | 0.821 | 0.552 | 0.845 | 0.815 | 0.842 | 0.646 | 0.426 | 0.960 |
| Na | 0.035 | 0.030 | 0.030 | 0.000 | 0.025 | 0.021 | 0.000 | 0.000 | 0.000 | 0.000 | 0.018 | 0.017 | 0.019 | 0.000 | 0.000 | 0.000 | 0.019 |
| K | 0.000 | 0.000 | 0.000 | 0.000 | 0.000 | 0.000 | 0.000 | 0.000 | 0.000 | 0.000 | 0.000 | 0.000 | 0.000 | 0.000 | 0.000 | 0.000 | 0.000 |
| TOTAL | 4.018 | 3.998 | 3.989 | 3.995 | 4.009 | 4.003 | 3.987 | 3.993 | 3.998 | 3.981 | 4.008 | 4.001 | 4.005 | 3.991 | 3.988 | 3.986 | 4.041 |
| **Endmembers** | | | | | | | | | | | | | | | | | |
| Wo | 36.80 | 43.29 | 45.13 | 42.73 | 43.83 | 43.56 | 41.82 | 42.21 | 43.13 | 42.85 | 27.96 | 43.22 | 41.19 | 43.46 | 33.32 | 21.88 | 46.97 |
| En | 50.62 | 47.31 | 45.82 | 38.18 | 37.36 | 37.38 | 38.88 | 38.10 | 37.70 | 38.21 | 35.21 | 31.57 | 31.15 | 31.61 | 34.18 | 37.08 | 29.78 |
| Fs | 10.78 | 7.82 | 7.46 | 19.09 | 17.52 | 17.97 | 19.30 | 19.69 | 19.17 | 18.94 | 35.89 | 24.35 | 26.72 | 24.94 | 32.50 | 41.04 | 22.34 |
| Ac | 1.80 | 1.57 | 1.60 | 0.00 | 1.30 | 1.08 | 0.00 | 0.00 | 0.00 | 0.00 | 0.94 | 0.86 | 0.94 | 0.00 | 0.00 | 0.00 | 0.91 |

**Clinopyroxene**

| Sample | Ab243 | Ab243 | Ab243 | Ab243 | Ab243 | V(Ol) | V(Ol) | V(Ol) | V(Ol) | V(Ol) | DV1 | DV1 | DV1 | DV1 | DV1 | DV1 | DV1 |
|---|---|---|---|---|---|---|---|---|---|---|---|---|---|---|---|---|---|
| Analysis No. | 23 | 24 | 25 | 26 | 35 | 2 | 13 | 14 | 27 | 31 | 7 | 8 | 10 | 15 | 17 | 18 | 19 |
| Analysis Name. | cpx6 | cpx6b | cpx6c | cpx6c | cpx7 | cpx1 | cpx2 | cpx2b | cpx3 | cpx4 | cpx1 | cpx2 | cpx3 | cpx5 | cpx6 | cpx6b | cpx6c |
| SiO2 | 51.01 | 50.60 | 50.99 | 51.33 | 51.60 | 52.53 | 52.41 | 49.05 | 52.09 | 52.43 | 49.13 | 50.48 | 52.45 | 52.11 | 51.96 | 52.31 | 52.27 |
| TiO2 | 0.43 | 0.34 | 0.33 | 0.43 | 0.27 | 0.79 | 0.82 | 0.77 | 0.65 | 0.69 | 0.85 | 0.51 | 0.72 | 0.78 | 0.71 | 0.91 | 1.02 |
| Al2O3 | 1.57 | 1.54 | 1.59 | 1.80 | 1.48 | 2.60 | 2.52 | 5.18 | 2.42 | 2.52 | 2.77 | 2.53 | 2.94 | 2.61 | 2.62 | 2.88 | 3.14 |
| Cr2O3 | 0.00 | 0.00 | 0.00 | 0.00 | 0.00 | 0.27 | 0.00 | 0.00 | 0.00 | 0.28 | 0.27 | 0.00 | 0.41 | 0.00 | 0.30 | 0.00 | 0.00 |
| FeO | 15.27 | 20.09 | 17.93 | 14.36 | 14.54 | 8.83 | 9.19 | 11.36 | 9.14 | 8.91 | 7.63 | 7.30 | 8.40 | 8.28 | 8.09 | 9.26 | 8.62 |
| MnO | 0.40 | 0.43 | 0.47 | 0.32 | 0.44 | 0.28 | 0.24 | 0.22 | 0.00 | 0.00 | 0.21 | 0.00 | 0.22 | 0.30 | 0.25 | 0.00 | 0.23 |
| MgO | 11.24 | 11.73 | 11.35 | 11.02 | 10.88 | 14.44 | 14.78 | 16.43 | 14.95 | 14.58 | 13.49 | 14.01 | 14.67 | 14.57 | 14.24 | 14.87 | 14.57 |
| CaO | 19.86 | 14.20 | 16.83 | 20.83 | 21.04 | 20.60 | 20.24 | 14.59 | 20.11 | 21.04 | 21.12 | 21.33 | 21.34 | 21.29 | 22.43 | 19.41 | 20.43 |
| Na2O | 0.24 | 0.00 | 0.00 | 0.00 | 0.29 | 0.43 | 0.25 | 0.33 | 0.55 | 0.39 | 0.27 | 0.32 | 0.50 | 0.44 | 0.23 | 0.00 | 0.49 |
| K2O | 0.00 | 0.00 | 0.00 | 0.00 | 0.00 | 0.00 | 0.00 | 0.00 | 0.00 | 0.00 | 0.00 | 0.00 | 0.00 | 0.00 | 0.00 | 0.00 | 0.00 |
| NiO | | | | | | | | | | | | | | | | | |
| Total | 100.01 | 98.94 | 99.49 | 100.07 | 100.52 | 100.76 | 100.44 | 97.93 | 99.92 | 100.84 | 95.74 | 96.49 | 101.66 | 100.39 | 100.82 | 99.62 | 100.77 |
| **Formula (6O)** | | | | | | | | | | | | | | | | | |
| Si | 1.952 | 1.968 | 1.966 | 1.955 | 1.962 | 1.936 | 1.937 | 1.856 | 1.936 | 1.932 | 1.910 | 1.937 | 1.918 | 1.928 | 1.919 | 1.940 | 1.923 |
| Al | 0.048 | 0.032 | 0.034 | 0.045 | 0.038 | 0.064 | 0.063 | 0.144 | 0.064 | 0.068 | 0.090 | 0.063 | 0.082 | 0.072 | 0.081 | 0.060 | 0.077 |
| Al | 0.023 | 0.038 | 0.038 | 0.036 | 0.028 | 0.049 | 0.047 | 0.087 | 0.042 | 0.042 | 0.037 | 0.052 | 0.044 | 0.042 | 0.033 | 0.066 | 0.059 |
| Fe(iii) | 0.028 | 0.000 | 0.000 | 0.000 | 0.023 | 0.000 | 0.000 | 0.055 | 0.038 | 0.011 | 0.022 | 0.008 | 0.032 | 0.026 | 0.023 | 0.000 | 0.000 |
| Cr | 0.000 | 0.000 | 0.000 | 0.000 | 0.000 | 0.008 | 0.000 | 0.000 | 0.000 | 0.008 | 0.008 | 0.000 | 0.012 | 0.000 | 0.009 | 0.000 | 0.000 |
| Ti | 0.012 | 0.010 | 0.010 | 0.012 | 0.008 | 0.022 | 0.023 | 0.022 | 0.018 | 0.019 | 0.025 | 0.015 | 0.020 | 0.022 | 0.020 | 0.025 | 0.028 |
| Fe(ii) | 0.459 | 0.655 | 0.580 | 0.458 | 0.438 | 0.272 | 0.284 | 0.303 | 0.245 | 0.264 | 0.225 | 0.226 | 0.224 | 0.229 | 0.226 | 0.289 | 0.265 |
| Mn | 0.013 | 0.014 | 0.015 | 0.010 | 0.014 | 0.009 | 0.008 | 0.007 | 0.000 | 0.000 | 0.007 | 0.000 | 0.007 | 0.009 | 0.008 | 0.000 | 0.007 |
| Mg | 0.641 | 0.680 | 0.652 | 0.626 | 0.617 | 0.793 | 0.814 | 0.927 | 0.828 | 0.801 | 0.782 | 0.802 | 0.800 | 0.804 | 0.784 | 0.822 | 0.799 |
| Ca | 0.814 | 0.592 | 0.695 | 0.850 | 0.857 | 0.813 | 0.801 | 0.592 | 0.801 | 0.831 | 0.880 | 0.877 | 0.836 | 0.844 | 0.888 | 0.771 | 0.805 |
| Na | 0.018 | 0.000 | 0.000 | 0.000 | 0.021 | 0.031 | 0.018 | 0.024 | 0.040 | 0.028 | 0.020 | 0.024 | 0.035 | 0.032 | 0.016 | 0.000 | 0.035 |
| K | 0.000 | 0.000 | 0.000 | 0.000 | 0.000 | 0.000 | 0.000 | 0.000 | 0.000 | 0.000 | 0.000 | 0.000 | 0.000 | 0.000 | 0.000 | 0.000 | 0.000 |
| TOTAL | 4.008 | 3.989 | 3.990 | 3.993 | 4.007 | 3.997 | 3.995 | 4.017 | 4.012 | 4.003 | 4.007 | 4.003 | 4.010 | 4.008 | 4.007 | 3.974 | 3.999 |
| **Endmembers** | | | | | | | | | | | | | | | | | |
| Wo | 41.25 | 30.48 | 35.79 | 43.72 | 43.49 | 42.39 | 41.62 | 31.01 | 41.02 | 42.95 | 45.43 | 45.29 | 43.22 | 43.41 | 45.62 | 40.97 | 42.12 |
| En | 32.49 | 35.03 | 33.58 | 32.18 | 31.29 | 41.35 | 42.29 | 48.59 | 42.44 | 41.42 | 40.38 | 41.39 | 41.35 | 41.34 | 40.31 | 43.67 | 41.80 |
| Fs | 25.36 | 34.49 | 30.63 | 24.10 | 24.13 | 14.65 | 15.16 | 19.13 | 14.51 | 14.18 | 13.14 | 12.09 | 13.60 | 13.63 | 13.22 | 15.36 | 14.25 |
| Ac | 0.90 | 0.00 | 0.00 | 0.00 | 1.08 | 1.60 | 0.93 | 1.27 | 2.03 | 1.44 | 1.05 | 1.23 | 1.83 | 1.62 | 0.85 | 0.00 | 1.83 |

**Clinopyroxene**

| Sample | DV1 | DV1 | DV1 | DV1 | Ab3986 | Ab3986 | Ab3986 | Ab3986 | Ab3986 | Ab3986 | Ab3986 | Ab5661 | Ab5661 | Ab5661 | Ab5661 | Ab5661 | Ab5661 |
|---|---|---|---|---|---|---|---|---|---|---|---|---|---|---|---|---|---|
| Analysis No. | 26 | 27 | 38 | 33 | 15 | 16 | 17 | 26 | 27 | 28 | 29 | 1 | 4 | 13 | 14 | 15 | 18 |
| Analysis Name. | cpx7 | cpx7b | cpx8 | opx3 | cpx1 | cpx2 | cpx2b | cpx3 | cpx3b | cpx3c | cpx4 | cpx1 | cpx2 | cpx3 | cpx4 | cpx5 | cpx6 |
| SiO2 | 52.20 | 51.86 | 52.21 | 51.91 | 52.63 | 51.60 | 51.98 | 51.08 | 51.16 | 51.13 | 51.50 | 52.70 | 52.29 | 52.56 | 52.55 | 52.67 | 52.40 |
| TiO2 | 0.63 | 1.01 | 0.87 | 0.90 | 0.61 | 1.01 | 0.68 | 1.22 | 0.53 | 0.75 | 0.65 | 0.62 | 0.53 | 0.73 | 0.65 | 0.93 | 0.60 |
| Al2O3 | 2.67 | 2.98 | 3.01 | 2.85 | 2.71 | 3.38 | 3.73 | 3.97 | 4.37 | 3.91 | 3.60 | 3.55 | 3.77 | 3.88 | 3.58 | 3.79 | 3.83 |
| Cr2O3 | 0.31 | 0.25 | 0.00 | 0.00 | 0.56 | 0.68 | 0.91 | 0.96 | 1.43 | 0.93 | 0.91 | 0.84 | 0.84 | 0.64 | 0.76 | 0.62 | 0.76 |
| FeO | 9.76 | 8.15 | 8.30 | 8.72 | 4.38 | 4.78 | 5.28 | 4.60 | 4.61 | 4.76 | 5.33 | 4.95 | 4.85 | 4.58 | 5.02 | 5.06 | 5.13 |
| MnO | 0.00 | 0.27 | 0.00 | 0.00 | 0.00 | 0.00 | 0.23 | 0.00 | 0.00 | 0.00 | 0.00 | 0.00 | 0.00 | 0.00 | 0.00 | 0.21 | 0.00 |
| MgO | 14.80 | 14.07 | 14.24 | 14.93 | 16.21 | 16.01 | 16.59 | 15.15 | 15.92 | 15.20 | 16.64 | 16.22 | 16.46 | 16.13 | 16.76 | 16.32 | 16.47 |
| CaO | 19.66 | 21.87 | 21.63 | 20.45 | 22.24 | 21.27 | 20.25 | 22.30 | 21.59 | 22.39 | 20.12 | 20.88 | 21.13 | 21.44 | 20.24 | 20.79 | 20.66 |
| Na2O | 0.24 | 0.39 | 0.37 | 0.35 | 0.29 | 0.38 | 0.00 | 0.35 | 0.40 | 0.33 | 0.00 | 0.00 | 0.45 | 0.37 | 0.35 | 0.39 | 0.00 |
| K2O | 0.00 | 0.00 | 0.00 | 0.00 | 0.00 | 0.00 | 0.00 | 0.00 | 0.00 | 0.00 | 0.00 | 0.00 | 0.00 | 0.00 | 0.00 | 0.00 | 0.00 |
| NiO | | | | | | | | | | | | | | | | | |
| Total | 100.28 | 100.84 | 100.82 | 100.12 | 99.62 | 99.10 | 99.96 | 99.61 | 100.01 | 99.87 | 98.73 | 99.76 | 100.60 | 100.35 | 99.93 | 101.15 | 99.87 |
| **Formula (6O)** | | | | | | | | | | | | | | | | | |
| Si | 1.934 | 1.913 | 1.925 | 1.922 | 1.931 | 1.905 | 1.905 | 1.882 | 1.876 | 1.890 | 1.905 | 1.925 | 1.905 | 1.911 | 1.917 | 1.909 | 1.913 |
| Al | 0.066 | 0.087 | 0.075 | 0.078 | 0.069 | 0.095 | 0.095 | 0.118 | 0.124 | 0.110 | 0.095 | 0.075 | 0.095 | 0.089 | 0.083 | 0.091 | 0.087 |
| Al | 0.050 | 0.043 | 0.056 | 0.047 | 0.048 | 0.052 | 0.066 | 0.055 | 0.065 | 0.060 | 0.061 | 0.077 | 0.067 | 0.077 | 0.070 | 0.071 | 0.078 |
| Fe(iii) | 0.000 | 0.013 | 0.000 | 0.008 | 0.000 | 0.000 | 0.000 | 0.000 | 0.026 | 0.008 | 0.000 | 0.000 | 0.010 | 0.000 | 0.000 | 0.000 | 0.000 |
| Cr | 0.009 | 0.007 | 0.000 | 0.000 | 0.016 | 0.020 | 0.026 | 0.028 | 0.041 | 0.027 | 0.027 | 0.024 | 0.024 | 0.018 | 0.022 | 0.018 | 0.022 |
| Ti | 0.018 | 0.028 | 0.024 | 0.025 | 0.017 | 0.028 | 0.019 | 0.034 | 0.015 | 0.021 | 0.018 | 0.017 | 0.015 | 0.020 | 0.018 | 0.025 | 0.016 |
| Fe(ii) | 0.303 | 0.239 | 0.256 | 0.261 | 0.134 | 0.148 | 0.163 | 0.142 | 0.115 | 0.139 | 0.165 | 0.152 | 0.137 | 0.140 | 0.153 | 0.154 | 0.158 |
| Mn | 0.000 | 0.008 | 0.000 | 0.000 | 0.000 | 0.000 | 0.007 | 0.000 | 0.000 | 0.000 | 0.000 | 0.000 | 0.000 | 0.000 | 0.000 | 0.006 | 0.000 |
| Mg | 0.817 | 0.774 | 0.783 | 0.824 | 0.886 | 0.881 | 0.907 | 0.832 | 0.870 | 0.837 | 0.917 | 0.883 | 0.894 | 0.874 | 0.911 | 0.882 | 0.896 |
| Ca | 0.780 | 0.864 | 0.854 | 0.811 | 0.874 | 0.841 | 0.795 | 0.880 | 0.848 | 0.886 | 0.797 | 0.817 | 0.825 | 0.835 | 0.791 | 0.807 | 0.808 |
| Na | 0.017 | 0.028 | 0.026 | 0.025 | 0.021 | 0.027 | 0.000 | 0.025 | 0.028 | 0.024 | 0.000 | 0.000 | 0.032 | 0.026 | 0.025 | 0.027 | 0.000 |
| K | 0.000 | 0.000 | 0.000 | 0.000 | 0.000 | 0.000 | 0.000 | 0.000 | 0.000 | 0.000 | 0.000 | 0.000 | 0.000 | 0.000 | 0.000 | 0.000 | 0.000 |
| TOTAL | 3.995 | 4.004 | 3.999 | 4.003 | 3.996 | 3.997 | 3.983 | 3.996 | 4.008 | 4.003 | 3.986 | 3.971 | 4.003 | 3.990 | 3.990 | 3.990 | 3.978 |
| **Endmembers** | | | | | | | | | | | | | | | | | |
| Wo | 40.69 | 44.89 | 44.51 | 42.03 | 45.63 | 44.34 | 42.49 | 46.84 | 44.92 | 46.79 | 42.40 | 44.10 | 43.45 | 44.54 | 42.06 | 43.02 | 43.40 |
| En | 42.62 | 40.18 | 40.78 | 42.70 | 46.28 | 46.44 | 48.44 | 44.28 | 46.10 | 44.20 | 48.80 | 47.67 | 47.10 | 46.63 | 48.46 | 46.99 | 48.14 |
| Fs | 15.79 | 13.48 | 13.33 | 13.98 | 7.02 | 7.78 | 9.07 | 7.55 | 7.47 | 7.76 | 8.80 | 8.22 | 7.78 | 7.44 | 8.16 | 8.54 | 8.46 |
| Ac | 0.90 | 1.45 | 1.38 | 1.30 | 1.08 | 1.43 | 0.00 | 1.33 | 1.51 | 1.25 | 0.00 | 0.00 | 1.67 | 1.39 | 1.32 | 1.46 | 0.00 |

**Clinopyroxene**

| Sample | Ab5661 | Ab5661 | Ab5661 | Ab5661 | Ab6510 | Ab6510 | Ab6510 | Ab6510 | Ab6510 | Ab6510 | 773C | 773C | 773C | 773C | 773C | 773C | 773C |
|---|---|---|---|---|---|---|---|---|---|---|---|---|---|---|---|---|---|
| Analysis No. | 19 | 25 | 28 | 29 | 1 | 3 | 4 | 6 | 7 | 20 | 1 | 2 | 9 | 13 | 15 | 16 | 17 |
| Analysis Name. | px6 | cpx7 | cpx8 | px8a | cpx1 | cpx2 | cpx3 | cpx4 | cpx4b | cpx5 | cpx1 | cpx2 | cpx3 | cpx4 | cpx5 | cpx6 | px6b |
| SiO2 | 52.20 | 52.03 | 51.94 | 49.52 | 52.25 | 52.59 | 52.06 | 52.53 | 51.79 | 52.19 | 52.68 | 51.86 | 52.03 | 51.86 | 51.63 | 51.70 | 51.43 |
| TiO2 | 0.50 | 0.44 | 0.72 | 0.56 | 0.65 | 0.49 | 0.57 | 0.52 | 0.92 | 0.56 | 0.43 | 0.44 | 0.53 | 0.54 | 0.64 | 0.54 | 0.60 |
| Al2O3 | 3.50 | 3.72 | 3.80 | 4.52 | 3.47 | 3.31 | 3.85 | 3.32 | 3.57 | 3.56 | 3.17 | 4.13 | 3.83 | 3.91 | 3.72 | 3.92 | 4.00 |
| Cr2O3 | 0.77 | 0.93 | 0.78 | 0.94 | 0.68 | 0.46 | 0.42 | 0.69 | 0.53 | 0.60 | 1.02 | 1.20 | 1.19 | 0.98 | 1.07 | 1.12 | 1.34 |
| FeO | 4.60 | 4.68 | 5.24 | 5.54 | 5.56 | 5.09 | 5.45 | 4.86 | 4.84 | 4.96 | 6.20 | 5.40 | 4.87 | 4.24 | 5.68 | 6.05 | 5.37 |
| MnO | 0.20 | 0.19 | 0.00 | 0.00 | 0.00 | 0.00 | 0.00 | 0.23 | 0.00 | 0.00 | 0.00 | 0.00 | 0.20 | 0.00 | 0.00 | 0.00 | 0.00 |
| MgO | 15.78 | 16.56 | 16.44 | 17.14 | 16.44 | 17.33 | 16.70 | 17.22 | 16.25 | 15.96 | 17.78 | 16.04 | 16.01 | 15.14 | 16.47 | 16.20 | 16.03 |
| CaO | 21.98 | 20.89 | 20.51 | 17.45 | 20.89 | 20.48 | 20.70 | 20.92 | 21.30 | 21.72 | 18.97 | 21.33 | 21.91 | 22.36 | 19.61 | 20.12 | 20.88 |
| Na2O | 0.36 | 0.36 | 0.49 | 0.00 | 0.36 | 0.22 | 0.40 | 0.24 | 0.34 | 0.47 | 0.49 | 0.38 | 0.35 | 0.41 | 0.43 | 0.43 | 0.32 |
| K2O | 0.00 | 0.00 | 0.00 | 0.00 | 0.00 | 0.00 | 0.00 | 0.00 | 0.00 | 0.00 | 0.00 | 0.00 | 0.00 | 0.00 | 0.00 | 0.00 | 0.00 |
| NiO | | | | | | | | | | | | | | | | | |
| Total | 99.89 | 99.80 | 99.91 | 95.68 | 100.30 | 99.97 | 100.15 | 100.53 | 99.54 | 100.02 | 100.72 | 100.74 | 100.92 | 99.44 | 99.26 | 100.07 | 99.96 |
| Formula (6O) | | | | | | | | | | | | | | | | | |
| Si | 1.913 | 1.905 | 1.901 | 1.882 | 1.908 | 1.917 | 1.901 | 1.909 | 1.903 | 1.911 | 1.912 | 1.889 | 1.892 | 1.908 | 1.903 | 1.895 | 1.887 |
| Al | 0.087 | 0.095 | 0.099 | 0.118 | 0.092 | 0.083 | 0.099 | 0.091 | 0.097 | 0.089 | 0.088 | 0.111 | 0.108 | 0.092 | 0.097 | 0.105 | 0.113 |
| Al | 0.065 | 0.065 | 0.065 | 0.085 | 0.057 | 0.060 | 0.067 | 0.051 | 0.057 | 0.064 | 0.048 | 0.066 | 0.057 | 0.078 | 0.064 | 0.065 | 0.060 |
| Fe(iii) | 0.000 | 0.006 | 0.010 | 0.000 | 0.007 | 0.000 | 0.025 | 0.013 | 0.000 | 0.015 | 0.033 | 0.020 | 0.019 | 0.000 | 0.000 | 0.012 | 0.004 |
| Cr | 0.022 | 0.027 | 0.023 | 0.028 | 0.020 | 0.013 | 0.012 | 0.020 | 0.015 | 0.017 | 0.029 | 0.035 | 0.034 | 0.029 | 0.031 | 0.032 | 0.039 |
| Ti | 0.014 | 0.012 | 0.020 | 0.016 | 0.018 | 0.013 | 0.016 | 0.014 | 0.025 | 0.015 | 0.012 | 0.012 | 0.014 | 0.015 | 0.018 | 0.015 | 0.017 |
| Fe(ii) | 0.141 | 0.137 | 0.150 | 0.177 | 0.163 | 0.155 | 0.141 | 0.135 | 0.149 | 0.136 | 0.155 | 0.144 | 0.129 | 0.131 | 0.175 | 0.173 | 0.160 |
| Mn | 0.006 | 0.006 | 0.000 | 0.000 | 0.000 | 0.000 | 0.000 | 0.007 | 0.000 | 0.000 | 0.000 | 0.000 | 0.006 | 0.000 | 0.000 | 0.000 | 0.000 |
| Mg | 0.862 | 0.904 | 0.897 | 0.971 | 0.895 | 0.942 | 0.909 | 0.933 | 0.890 | 0.871 | 0.962 | 0.871 | 0.868 | 0.830 | 0.905 | 0.885 | 0.877 |
| Ca | 0.863 | 0.819 | 0.804 | 0.711 | 0.817 | 0.800 | 0.810 | 0.814 | 0.838 | 0.852 | 0.738 | 0.832 | 0.854 | 0.881 | 0.774 | 0.790 | 0.821 |
| Na | 0.026 | 0.026 | 0.035 | 0.000 | 0.025 | 0.016 | 0.028 | 0.017 | 0.024 | 0.033 | 0.034 | 0.027 | 0.025 | 0.029 | 0.031 | 0.031 | 0.023 |
| K | 0.000 | 0.000 | 0.000 | 0.000 | 0.000 | 0.000 | 0.000 | 0.000 | 0.000 | 0.000 | 0.000 | 0.000 | 0.000 | 0.000 | 0.000 | 0.000 | 0.000 |
| TOTAL | 3.999 | 4.002 | 4.003 | 3.987 | 4.002 | 3.999 | 4.008 | 4.004 | 3.999 | 4.005 | 4.011 | 4.007 | 4.006 | 3.993 | 3.998 | 4.004 | 4.001 |
| Endmembers | | | | | | | | | | | | | | | | | |
| Wo | 45.47 | 43.17 | 42.41 | 38.23 | 42.85 | 41.82 | 42.32 | 42.44 | 44.09 | 44.65 | 38.38 | 43.94 | 44.92 | 47.09 | 41.07 | 41.78 | 43.54 |
| En | 45.43 | 47.63 | 47.31 | 52.26 | 46.92 | 49.25 | 47.52 | 48.62 | 46.81 | 45.65 | 50.06 | 45.98 | 45.68 | 44.37 | 48.01 | 46.81 | 46.52 |
| Fs | 7.76 | 7.86 | 8.45 | 9.51 | 8.90 | 8.11 | 8.68 | 8.06 | 7.82 | 7.95 | 9.76 | 8.67 | 8.11 | 6.98 | 9.29 | 9.80 | 8.74 |
| Ac | 1.35 | 1.35 | 1.83 | 0.00 | 1.34 | 0.81 | 1.48 | 0.88 | 1.27 | 1.75 | 1.79 | 1.42 | 1.30 | 1.56 | 1.63 | 1.62 | 1.21 |

**Clinopyroxene**

| Sample | MS1526c | MS1526c | MS1526c | MS1526c | MS1526c | MS1526c | MS1526c | 110P | 110P | 110P | 110P | 110P | 110P | 110P | Ab94 | Ab94 | Ab94 |
|---|---|---|---|---|---|---|---|---|---|---|---|---|---|---|---|---|---|
| Analysis No. | 1 | 2 | 3 | 5 | 6 | 7 | 11 | 1 | 4 | 6 | 8 | 10 | 13 | 15 | 11 | 13 | 18 |
| Analysis Name. | cpx1 | cpx2 | cpx3 | cpx4 | cpx5 | cpx6 | cpx7 | cpx1 | cpx2 | cpx3 | cpx4 | cpx5 | cpx6 | cpx7 | cpx1 | cpx2 | cpx3 |
| SiO2 | 55.88 | 55.45 | 54.82 | 54.73 | 55.00 | 55.38 | 54.71 | 48.03 | 52.59 | 50.97 | 52.20 | 52.38 | 52.08 | 50.58 | 53.43 | 52.84 | 53.04 |
| TiO2 | 0.00 | 0.00 | 0.00 | 0.00 | 0.00 | 0.00 | 0.00 | 0.67 | 0.96 | 0.82 | 0.80 | 0.80 | 0.55 | 0.56 | 0.22 | 0.40 | 0.22 |
| Al2O3 | 0.47 | 0.53 | 1.16 | 0.91 | 0.84 | 0.33 | 0.68 | 2.60 | 1.91 | 2.47 | 2.03 | 2.07 | 1.58 | 3.06 | 0.96 | 1.74 | 1.43 |
| Cr2O3 | 0.00 | 0.00 | 0.27 | 0.33 | 0.20 | 0.00 | 0.00 | 0.20 | 0.29 | 0.43 | 0.25 | 0.54 | 0.48 | 0.50 | 0.00 | 0.00 | 0.26 |
| FeO | 1.60 | 1.45 | 2.02 | 1.64 | 1.75 | 1.45 | 1.57 | 5.39 | 6.20 | 5.99 | 5.67 | 5.86 | 4.90 | 4.98 | 11.91 | 12.93 | 13.74 |
| MnO | 0.00 | 0.00 | 0.00 | 0.00 | 0.00 | 0.00 | 0.00 | 0.21 | 0.00 | 0.00 | 0.00 | 0.00 | 0.00 | 0.00 | 0.32 | 0.43 | 0.29 |
| MgO | 17.72 | 17.87 | 17.69 | 17.49 | 17.67 | 17.61 | 17.53 | 15.50 | 15.37 | 15.86 | 15.19 | 15.29 | 14.89 | 16.40 | 12.76 | 12.89 | 12.90 |
| CaO | 26.01 | 26.39 | 26.05 | 25.98 | 26.10 | 25.64 | 26.02 | 18.42 | 21.73 | 20.64 | 22.21 | 21.92 | 22.60 | 20.49 | 22.00 | 20.60 | 20.20 |
| Na2O | 0.00 | 0.00 | 0.00 | 0.00 | 0.00 | 0.00 | 0.00 | 0.27 | 0.00 | 0.00 | 0.34 | 0.32 | 0.81 | 0.35 | 0.24 | 0.46 | 0.35 |
| K2O | 0.00 | 0.00 | 0.00 | 0.00 | 0.00 | 0.00 | 0.00 | 0.00 | 0.00 | 0.00 | 0.00 | 0.00 | 0.12 | 0.00 | 0.00 | 0.00 | 0.00 |
| NiO | | | | | | | | | | | | | | | | | |
| Total | 101.68 | 101.69 | 102.01 | 101.08 | 101.56 | 100.41 | 100.51 | 91.27 | 99.05 | 97.34 | 98.70 | 99.18 | 98.22 | 96.93 | 101.85 | 102.30 | 102.43 |
| Formula (6O) | | | | | | | | | | | | | | | | | |
| Si | 1.993 | 1.981 | 1.958 | 1.969 | 1.970 | 1.998 | 1.978 | 1.925 | 1.951 | 1.926 | 1.945 | 1.943 | 1.956 | 1.910 | 1.980 | 1.954 | 1.962 |
| Al | 0.007 | 0.019 | 0.042 | 0.031 | 0.030 | 0.002 | 0.022 | 0.075 | 0.049 | 0.074 | 0.055 | 0.057 | 0.044 | 0.090 | 0.020 | 0.046 | 0.038 |
| Al | 0.013 | 0.003 | 0.007 | 0.008 | 0.006 | 0.012 | 0.007 | 0.048 | 0.035 | 0.036 | 0.035 | 0.033 | 0.026 | 0.046 | 0.022 | 0.030 | 0.024 |
| Fe(iii) | 0.000 | 0.024 | 0.041 | 0.020 | 0.027 | 0.000 | 0.022 | 0.002 | 0.000 | 0.000 | 0.000 | 0.000 | 0.055 | 0.035 | 0.006 | 0.041 | 0.028 |
| Cr | 0.000 | 0.000 | 0.008 | 0.009 | 0.006 | 0.000 | 0.000 | 0.006 | 0.009 | 0.013 | 0.007 | 0.016 | 0.014 | 0.015 | 0.000 | 0.000 | 0.008 |
| Ti | 0.000 | 0.000 | 0.000 | 0.000 | 0.000 | 0.000 | 0.000 | 0.020 | 0.027 | 0.023 | 0.022 | 0.022 | 0.016 | 0.016 | 0.006 | 0.011 | 0.006 |
| Fe(ii) | 0.048 | 0.019 | 0.019 | 0.030 | 0.025 | 0.044 | 0.025 | 0.179 | 0.193 | 0.190 | 0.177 | 0.182 | 0.099 | 0.122 | 0.363 | 0.358 | 0.396 |
| Mn | 0.000 | 0.000 | 0.000 | 0.000 | 0.000 | 0.000 | 0.000 | 0.007 | 0.000 | 0.000 | 0.000 | 0.000 | 0.000 | 0.000 | 0.010 | 0.013 | 0.009 |
| Mg | 0.942 | 0.952 | 0.942 | 0.938 | 0.944 | 0.947 | 0.945 | 0.926 | 0.850 | 0.893 | 0.844 | 0.846 | 0.834 | 0.923 | 0.705 | 0.711 | 0.711 |
| Ca | 0.994 | 1.010 | 0.997 | 1.002 | 1.002 | 0.991 | 1.008 | 0.791 | 0.864 | 0.835 | 0.887 | 0.871 | 0.910 | 0.829 | 0.873 | 0.816 | 0.801 |
| Na | 0.000 | 0.000 | 0.000 | 0.000 | 0.000 | 0.000 | 0.000 | 0.021 | 0.000 | 0.000 | 0.025 | 0.023 | 0.059 | 0.026 | 0.017 | 0.033 | 0.025 |
| K | 0.000 | 0.000 | 0.000 | 0.000 | 0.000 | 0.000 | 0.000 | 0.000 | 0.000 | 0.000 | 0.000 | 0.000 | 0.006 | 0.000 | 0.000 | 0.000 | 0.000 |
| TOTAL | 3.997 | 4.008 | 4.013 | 4.007 | 4.009 | 3.995 | 4.007 | 4.001 | 3.977 | 3.990 | 3.996 | 3.993 | 4.018 | 4.011 | 4.002 | 4.012 | 4.008 |
| Endmembers | | | | | | | | | | | | | | | | | |
| Wo | 50.10 | 50.38 | 49.87 | 50.35 | 50.14 | 50.00 | 50.39 | 41.07 | 45.28 | 43.55 | 45.90 | 45.33 | 46.51 | 42.85 | 44.23 | 41.39 | 40.63 |
| En | 47.49 | 47.47 | 47.12 | 47.17 | 47.24 | 47.79 | 47.24 | 48.09 | 44.57 | 46.56 | 43.68 | 44.00 | 42.64 | 47.72 | 35.70 | 36.04 | 36.11 |
| Fs | 2.41 | 2.16 | 3.01 | 2.48 | 2.62 | 2.21 | 2.37 | 9.75 | 10.15 | 9.89 | 9.15 | 9.47 | 7.83 | 8.10 | 19.19 | 20.89 | 21.98 |
| Ac | 0.00 | 0.00 | 0.00 | 0.00 | 0.00 | 0.00 | 0.00 | 1.09 | 0.00 | 0.00 | 1.27 | 1.20 | 3.02 | 1.32 | 0.87 | 1.67 | 1.27 |

**Clinopyroxene**

| Sample | Ab94 | Ab94 | Ab94 | 77P | 77P | 77P | 77P | 77P | CLW107 | CLW107 | CLW107 | CLW107 | CLW110 | CLW110 | CLW110 | CLW110 | CLW110 |
|---|---|---|---|---|---|---|---|---|---|---|---|---|---|---|---|---|---|
| Analysis No. | 24 | 27 | 28 | 2 | 10 | 17 | 18 | 22 | 6 | 14 | 15 | 23 | 5 | 10 | 12 | 13 | 23 |
| Analysis Name. | cpx4 | cpx5 | cpx6a | cpx1 | cpx2 | cpx3 | cpx4 | cpx5 | cpx1 | cpx1 | cpx2 | cpx3 | cpx1 | cpx2 | cpx3 | cpx4 | cpx5 |
| SiO2 | 53.39 | 53.82 | 53.29 | 52.09 | 51.53 | 51.78 | 52.16 | 52.46 | 52.09 | 53.63 | 53.43 | 52.29 | 51.64 | 52.51 | 51.67 | 52.37 | 51.56 |
| TiO2 | 0.00 | 0.29 | 0.00 | 0.47 | 0.31 | 0.52 | 0.49 | 0.30 | 0.25 | 0.00 | 0.31 | 0.00 | 0.52 | 0.00 | 0.32 | 0.26 | 0.00 |
| Al2O3 | 0.81 | 1.14 | 1.11 | 1.97 | 2.27 | 2.35 | 2.33 | 1.91 | 2.43 | 1.53 | 2.28 | 2.75 | 3.12 | 1.59 | 1.91 | 1.88 | 2.44 |
| Cr2O3 | 0.00 | 0.00 | 0.00 | 0.00 | 0.00 | 0.00 | 0.00 | 0.00 | 0.76 | 0.27 | 0.44 | 0.54 | 0.00 | 0.00 | 0.00 | 0.17 | 0.00 |
| FeO | 11.84 | 11.12 | 11.71 | 11.09 | 12.48 | 10.80 | 11.72 | 13.25 | 8.36 | 4.55 | 5.33 | 4.87 | 8.93 | 8.08 | 9.10 | 8.55 | 8.96 |
| MnO | 0.00 | 0.23 | 0.47 | 0.22 | 0.23 | 0.28 | 0.30 | 0.36 | 0.23 | 0.00 | 0.00 | 0.00 | 0.00 | 0.34 | 0.00 | 0.00 | 0.21 |
| MgO | 13.04 | 13.03 | 12.97 | 12.74 | 12.79 | 12.38 | 12.40 | 14.00 | 18.83 | 15.82 | 16.69 | 15.51 | 13.97 | 14.12 | 13.59 | 13.72 | 13.88 |
| CaO | 22.15 | 22.56 | 21.82 | 22.01 | 19.95 | 21.53 | 21.11 | 18.59 | 16.81 | 24.04 | 21.59 | 23.42 | 20.18 | 22.78 | 21.81 | 22.26 | 21.64 |
| Na2O | 0.45 | 0.34 | 0.30 | 0.33 | 0.00 | 0.42 | 0.34 | 0.38 | 0.00 | 0.00 | 0.21 | 0.00 | 0.49 | 0.30 | 0.34 | 0.26 | 0.39 |
| K2O | 0.00 | 0.10 | 0.00 | 0.00 | 0.00 | 0.00 | 0.00 | 0.00 | 0.00 | 0.00 | 0.00 | 0.00 | 0.22 | 0.00 | 0.00 | 0.00 | 0.00 |
| NiO | | | | | | | | | | | | | | | | | |
| Total | 101.68 | 102.63 | 101.68 | 100.91 | 99.54 | 100.06 | 100.82 | 101.43 | 99.76 | 99.84 | 100.28 | 99.60 | 99.09 | 99.71 | 98.73 | 99.48 | 99.08 |
| Formula (6O) | | | | | | | | | | | | | | | | | |
| Si | 1.981 | 1.974 | 1.977 | 1.945 | 1.949 | 1.945 | 1.948 | 1.952 | 1.917 | 1.969 | 1.948 | 1.932 | 1.935 | 1.962 | 1.953 | 1.959 | 1.941 |
| Al | 0.019 | 0.026 | 0.023 | 0.055 | 0.051 | 0.055 | 0.052 | 0.048 | 0.083 | 0.031 | 0.052 | 0.068 | 0.065 | 0.038 | 0.047 | 0.041 | 0.059 |
| Al | 0.016 | 0.023 | 0.025 | 0.031 | 0.051 | 0.050 | 0.050 | 0.035 | 0.023 | 0.035 | 0.046 | 0.052 | 0.073 | 0.032 | 0.038 | 0.042 | 0.050 |
| Fe(iii) | 0.053 | 0.023 | 0.029 | 0.032 | 0.000 | 0.009 | 0.000 | 0.036 | 0.036 | 0.000 | 0.000 | 0.000 | 0.013 | 0.043 | 0.024 | 0.000 | 0.056 |
| Cr | 0.000 | 0.000 | 0.000 | 0.000 | 0.000 | 0.000 | 0.000 | 0.000 | 0.022 | 0.008 | 0.013 | 0.016 | 0.000 | 0.000 | 0.000 | 0.005 | 0.000 |
| Ti | 0.000 | 0.008 | 0.000 | 0.013 | 0.009 | 0.015 | 0.014 | 0.008 | 0.007 | 0.000 | 0.009 | 0.000 | 0.015 | 0.000 | 0.009 | 0.007 | 0.000 |
| Fe(ii) | 0.313 | 0.318 | 0.334 | 0.313 | 0.396 | 0.330 | 0.366 | 0.375 | 0.220 | 0.140 | 0.163 | 0.150 | 0.267 | 0.209 | 0.263 | 0.268 | 0.225 |
| Mn | 0.000 | 0.007 | 0.015 | 0.007 | 0.007 | 0.009 | 0.009 | 0.011 | 0.007 | 0.000 | 0.000 | 0.000 | 0.000 | 0.011 | 0.000 | 0.000 | 0.007 |
| Mg | 0.721 | 0.713 | 0.717 | 0.709 | 0.721 | 0.693 | 0.690 | 0.776 | 1.033 | 0.866 | 0.907 | 0.854 | 0.780 | 0.786 | 0.766 | 0.765 | 0.779 |
| Ca | 0.880 | 0.887 | 0.867 | 0.880 | 0.809 | 0.867 | 0.845 | 0.741 | 0.663 | 0.946 | 0.843 | 0.927 | 0.810 | 0.912 | 0.883 | 0.892 | 0.873 |
| Na | 0.032 | 0.024 | 0.022 | 0.024 | 0.000 | 0.031 | 0.025 | 0.027 | 0.000 | 0.000 | 0.015 | 0.000 | 0.036 | 0.022 | 0.025 | 0.019 | 0.028 |
| K | 0.000 | 0.005 | 0.000 | 0.000 | 0.000 | 0.000 | 0.000 | 0.000 | 0.000 | 0.000 | 0.000 | 0.000 | 0.011 | 0.000 | 0.000 | 0.000 | 0.000 |
| TOTAL | 4.016 | 4.007 | 4.009 | 4.010 | 3.992 | 4.003 | 3.999 | 4.011 | 4.011 | 3.994 | 3.996 | 4.000 | 4.004 | 4.013 | 4.008 | 3.999 | 4.017 |
| Endmembers | | | | | | | | | | | | | | | | | |
| Wo | 44.03 | 44.98 | 43.73 | 44.79 | 41.83 | 44.70 | 43.65 | 37.67 | 33.82 | 48.46 | 43.74 | 47.99 | 42.51 | 46.00 | 45.04 | 45.90 | 44.36 |
| En | 36.07 | 36.15 | 36.17 | 36.08 | 37.32 | 35.77 | 35.68 | 39.47 | 52.72 | 44.37 | 47.05 | 44.22 | 40.95 | 39.68 | 39.05 | 39.37 | 39.59 |
| Fs | 18.29 | 17.64 | 19.02 | 17.92 | 20.85 | 17.95 | 19.41 | 21.47 | 13.46 | 7.17 | 8.44 | 7.79 | 14.67 | 13.23 | 14.64 | 13.76 | 14.61 |
| Ac | 1.62 | 1.23 | 1.09 | 1.22 | 0.00 | 1.58 | 1.27 | 1.39 | 0.00 | 0.00 | 0.77 | 0.00 | 1.87 | 1.10 | 1.27 | 0.97 | 1.45 |

**Clinopyroxene**

| Sample | DCD106 | DCD106 | DCD106 | DCD106 | DCD106 | DCD106 | DCD106 | DCD118 | DCD118 | DCD118 | DCD118 | DCD118 |
|---|---|---|---|---|---|---|---|---|---|---|---|---|
| Analysis No. | 1 | 2 | 3 | 10 | 11 | 16 | 17 | 4 | 8 | 10 | 15 | 17 |
| Analysis Name. | cpx1 | cpx2 | px2a | cpx3 | cpx4 | cpx5 | px5b | cpx1 | cpx2 | cpx3 | cpx4 | cpx5 |
| SiO2 | 51.82 | 51.25 | 51.14 | 52.14 | 51.03 | 51.92 | 52.59 | 52.34 | 51.42 | 49.24 | 51.56 | 51.75 |
| TiO2 | 0.46 | 0.38 | 0.62 | 0.40 | 0.23 | 0.25 | 0.36 | 0.49 | 0.42 | 0.64 | 0.63 | 0.46 |
| Al2O3 | 3.78 | 4.57 | 4.58 | 3.96 | 5.40 | 3.77 | 3.17 | 3.26 | 4.06 | 8.63 | 3.69 | 3.50 |
| Cr2O3 | 0.38 | 0.37 | 0.36 | 0.21 | 0.32 | 0.34 | 0.38 | 0.19 | 0.00 | 0.22 | 0.24 | 0.00 |
| FeO | 5.27 | 5.04 | 5.15 | 4.57 | 5.82 | 4.96 | 4.99 | 6.41 | 6.66 | 9.16 | 6.77 | 6.64 |
| MnO | 0.28 | 0.20 | 0.00 | 0.00 | 0.30 | 0.00 | 0.00 | 0.29 | 0.22 | 0.00 | 0.00 | 0.00 |
| MgO | 14.93 | 14.46 | 14.60 | 14.97 | 14.75 | 15.40 | 15.45 | 14.99 | 13.99 | 16.08 | 14.37 | 14.38 |
| CaO | 23.09 | 23.11 | 22.75 | 23.43 | 22.39 | 22.96 | 23.53 | 23.76 | 23.88 | 12.82 | 23.56 | 24.18 |
| Na2O | 0.21 | 0.23 | 0.34 | 0.00 | 0.34 | 0.37 | 0.26 | 0.00 | 0.00 | 0.71 | 0.28 | 0.00 |
| K2O | 0.00 | 0.00 | 0.00 | 0.00 | 0.00 | 0.00 | 0.00 | 0.00 | 0.00 | 0.00 | 0.00 | 0.00 |
| NiO | | | | | | | | | | | | |
| Total | 100.22 | 99.60 | 99.55 | 99.69 | 100.57 | 99.96 | 100.72 | 101.72 | 100.64 | 97.50 | 101.12 | 100.89 |
| Formula (6O) | | | | | | | | | | | | |
| Si | 1.904 | 1.892 | 1.888 | 1.915 | 1.870 | 1.907 | 1.919 | 1.905 | 1.895 | 1.835 | 1.892 | 1.902 |
| Al | 0.096 | 0.108 | 0.112 | 0.085 | 0.130 | 0.093 | 0.081 | 0.095 | 0.105 | 0.165 | 0.108 | 0.098 |
| Al | 0.068 | 0.091 | 0.087 | 0.086 | 0.103 | 0.070 | 0.055 | 0.045 | 0.071 | 0.214 | 0.052 | 0.053 |
| Fe(iii) | 0.011 | 0.002 | 0.006 | 0.000 | 0.044 | 0.038 | 0.020 | 0.025 | 0.017 | 0.000 | 0.050 | 0.029 |
| Cr | 0.011 | 0.011 | 0.011 | 0.006 | 0.009 | 0.010 | 0.011 | 0.005 | 0.000 | 0.006 | 0.007 | 0.000 |
| Ti | 0.013 | 0.011 | 0.017 | 0.011 | 0.006 | 0.007 | 0.010 | 0.013 | 0.012 | 0.018 | 0.017 | 0.013 |
| Fe(ii) | 0.151 | 0.154 | 0.153 | 0.141 | 0.133 | 0.114 | 0.132 | 0.169 | 0.188 | 0.287 | 0.157 | 0.174 |
| Mn | 0.009 | 0.006 | 0.000 | 0.000 | 0.009 | 0.000 | 0.000 | 0.009 | 0.007 | 0.000 | 0.000 | 0.000 |
| Mg | 0.818 | 0.796 | 0.804 | 0.820 | 0.806 | 0.843 | 0.840 | 0.814 | 0.768 | 0.893 | 0.786 | 0.788 |
| Ca | 0.909 | 0.914 | 0.900 | 0.922 | 0.879 | 0.904 | 0.920 | 0.927 | 0.943 | 0.512 | 0.926 | 0.952 |
| Na | 0.015 | 0.016 | 0.024 | 0.000 | 0.024 | 0.026 | 0.018 | 0.000 | 0.000 | 0.051 | 0.020 | 0.000 |
| K | 0.000 | 0.000 | 0.000 | 0.000 | 0.000 | 0.000 | 0.000 | 0.000 | 0.000 | 0.000 | 0.000 | 0.000 |
| TOTAL | 4.003 | 4.001 | 4.002 | 3.986 | 4.014 | 4.012 | 4.007 | 4.008 | 4.005 | 3.982 | 4.016 | 4.009 |
| Endmembers | | | | | | | | | | | | |
| Wo | 47.53 | 48.41 | 47.69 | 48.97 | 46.36 | 46.93 | 47.64 | 47.67 | 49.02 | 29.36 | 47.76 | 48.99 |
| En | 42.77 | 42.15 | 42.59 | 43.54 | 42.50 | 43.81 | 43.53 | 41.85 | 39.96 | 51.24 | 40.54 | 40.54 |
| Fs | 8.92 | 8.57 | 8.42 | 7.48 | 9.86 | 7.89 | 7.87 | 10.48 | 11.01 | 16.45 | 10.67 | 10.47 |
| Ac | 0.78 | 0.87 | 1.29 | 0.00 | 1.27 | 1.37 | 0.95 | 0.00 | 0.00 | 2.94 | 1.03 | 0.00 |

**Plagioclase feldspar**

| Sample | 9P | 9P | 9P | 9P | Ab82 | Ab82 | Ab82 | Ab82 | Ab82 | Ab82 | Ab125 | Ab125 | Ab125 | Ab125 | Ab125 | Ab125 | Ab127 |
|---|---|---|---|---|---|---|---|---|---|---|---|---|---|---|---|---|---|
| Analysis No. | 11 | 16 | 21 | 22 | 1 | 7 | 11 | 13 | 28 | 29 | 18 | 20 | 22 | 23 | 24 | 26 | 12 |
| Analysis Name. | plag1 | plag2 | plag3 | plag4 | plag1 | plag2 | plag3 | plag4 | plag5 | plag6 | plag1 | plag2 | plag3 | plag4 | plag5 | plag6 | plag1 |
| SiO2 | 49.11 | 49.64 | 50.07 | 49.08 | 55.02 | 56.68 | 62.11 | 63.93 | 62.62 | 62.69 | 48.98 | 48.82 | 49.04 | 48.94 | 48.47 | 49.03 | 51.06 |
| Al2O3 | 30.62 | 30.18 | 29.74 | 30.65 | 29.09 | 27.00 | 23.30 | 23.04 | 23.13 | 22.86 | 29.73 | 30.27 | 30.06 | 30.18 | 30.56 | 30.16 | 30.92 |
| FeO | 0.00 | 0.00 | 0.00 | 0.00 | 0.00 | 0.00 | 0.58 | 0.26 | 0.00 | 0.00 | 0.28 | 0.00 | 0.00 | 0.24 | 0.31 | 0.00 | 0.00 |
| CaO | 15.44 | 14.88 | 14.07 | 15.45 | 12.71 | 10.38 | 5.85 | 4.95 | 5.31 | 5.35 | 14.83 | 14.89 | 14.91 | 14.81 | 15.04 | 14.94 | 14.80 |
| Na2O | 2.55 | 2.99 | 3.08 | 2.63 | 4.59 | 6.03 | 8.14 | 8.73 | 8.43 | 8.35 | 2.81 | 2.77 | 2.83 | 2.82 | 2.76 | 2.57 | 3.14 |
| K2O | 0.11 | 0.10 | 0.13 | 0.00 | 0.00 | 0.11 | 0.00 | 0.00 | 0.14 | 0.11 | 0.00 | 0.00 | 0.00 | 0.11 | 0.00 | 0.00 | 0.00 |
| BaO | 0.00 | 0.00 | 0.00 | 0.00 | 0.00 | 0.00 | 0.00 | 0.00 | 0.00 | 0.00 | 0.00 | 0.00 | 0.00 | 0.00 | 0.00 | 0.00 | 0.00 |
| Total | 97.83 | 97.78 | 97.10 | 97.81 | 101.41 | 100.20 | 100.17 | 100.92 | 99.63 | 99.35 | 96.64 | 96.75 | 96.85 | 97.28 | 97.14 | 96.71 | 99.92 |
| **Formula (32O)** | | | | | | | | | | | | | | | | | |
| Si | 9.167 | 9.260 | 9.378 | 9.161 | 9.807 | 10.183 | 11.039 | 11.205 | 11.128 | 11.164 | 9.255 | 9.201 | 9.235 | 9.207 | 9.123 | 9.236 | 9.301 |
| Al | 6.736 | 6.635 | 6.564 | 6.742 | 6.111 | 5.716 | 4.880 | 4.759 | 4.844 | 4.798 | 6.620 | 6.723 | 6.671 | 6.691 | 6.779 | 6.696 | 6.637 |
| Fe(ii) | 0.000 | 0.000 | 0.000 | 0.000 | 0.000 | 0.000 | 0.086 | 0.038 | 0.000 | 0.000 | 0.044 | 0.000 | 0.000 | 0.038 | 0.049 | 0.000 | 0.000 |
| Ca | 3.088 | 2.974 | 2.823 | 3.089 | 2.427 | 1.998 | 1.114 | 0.929 | 1.011 | 1.021 | 3.002 | 3.007 | 3.008 | 2.985 | 3.033 | 3.015 | 2.888 |
| Na | 0.923 | 1.081 | 1.118 | 0.952 | 1.586 | 2.100 | 2.805 | 2.966 | 2.904 | 2.883 | 1.029 | 1.012 | 1.033 | 1.028 | 1.007 | 0.939 | 1.109 |
| K | 0.026 | 0.024 | 0.031 | 0.000 | 0.000 | 0.025 | 0.000 | 0.000 | 0.032 | 0.025 | 0.000 | 0.000 | 0.000 | 0.026 | 0.000 | 0.000 | 0.000 |
| Ba | | | | | 0.000 | 0.000 | 0.000 | 0.000 | 0.000 | 0.000 | 0.000 | 0.000 | 0.000 | 0.000 | 0.000 | 0.000 | 0.000 |
| TOTAL | 19.940 | 19.975 | 19.915 | 19.944 | 19.931 | 20.022 | 19.924 | 19.898 | 19.918 | 19.891 | 19.950 | 19.943 | 19.947 | 19.975 | 19.991 | 19.885 | 19.935 |
| **Endmembers** | | | | | | | | | | | | | | | | | |
| An | 76.49 | 72.91 | 71.07 | 76.45 | 60.48 | 48.45 | 28.43 | 23.86 | 25.61 | 25.98 | 74.47 | 74.81 | 74.43 | 73.89 | 75.07 | 76.26 | 72.26 |
| Ab | 22.86 | 26.51 | 28.15 | 23.55 | 39.52 | 50.94 | 71.57 | 76.14 | 73.58 | 73.38 | 25.53 | 25.19 | 25.57 | 25.46 | 24.93 | 23.74 | 27.74 |
| Or | 0.65 | 0.58 | 0.78 | 0.00 | 0.00 | 0.61 | 0.00 | 0.00 | 0.80 | 0.64 | 0.00 | 0.00 | 0.00 | 0.65 | 0.00 | 0.00 | 0.00 |
| Cn | | | | | | | | | | | | | | | | | |

**Plagioclase feldspar**

| Sample | Ab127 | Ab127 | Ab127 | Ab127 | Ab127 | Ab140 | Ab140 | Ab140 | Ab140 | Ab140 | Ab140 | Ab140 | Ab140 | Ab140 | Ab140 | Ab140 | Ab140 | Ab140 |
|---|---|---|---|---|---|---|---|---|---|---|---|---|---|---|---|---|---|---|
| Analysis No. | 13 | 17 | 18 | 19 | 25 | 7 | 8 | 18 | 19 | 20 | 21 | 22 | 23 | 38 | 39 | 40 | 47 | 49 |
| Analysis Name. | plag2 | plag3a | plag3b | plag3c | plag4 | plag1b | plag2 | plag3 | plag4a | plag4b | plag5 | plag6 | plag7 | plag8a | plag8b | plag8c | plag9a | plag9b |
| SiO2 | 50.49 | 50.09 | 52.21 | 50.57 | 52.19 | 47.41 | 48.02 | 47.95 | 48.25 | 48.77 | 48.32 | 47.98 | 47.76 | 47.40 | 47.50 | 47.53 | 47.58 | 47.31 |
| Al2O3 | 31.76 | 32.06 | 30.51 | 32.29 | 30.84 | 31.78 | 32.06 | 32.13 | 32.18 | 32.12 | 31.97 | 32.41 | 32.13 | 32.23 | 31.68 | 32.10 | 32.09 | 32.57 |
| FeO | 0.00 | 0.00 | 0.00 | 0.00 | 0.00 | 0.00 | 0.00 | 0.00 | 0.24 | 0.00 | 0.00 | 0.20 | 0.22 | 0.34 | 0.21 | 0.00 | 0.33 | 0.00 |
| CaO | 15.77 | 15.96 | 14.15 | 15.89 | 14.60 | 16.94 | 16.65 | 16.97 | 17.06 | 16.36 | 16.34 | 17.08 | 16.97 | 16.91 | 16.50 | 16.39 | 16.57 | 16.96 |
| Na2O | 2.69 | 2.71 | 3.60 | 2.77 | 3.50 | 1.96 | 1.98 | 1.84 | 2.02 | 2.11 | 2.09 | 1.94 | 1.75 | 2.01 | 2.11 | 1.96 | 1.99 | 2.08 |
| K2O | 0.00 | 0.00 | 0.00 | 0.00 | 0.00 | 0.00 | 0.00 | 0.00 | 0.00 | 0.00 | 0.00 | 0.00 | 0.00 | 0.00 | 0.00 | 0.00 | 0.00 | 0.00 |
| BaO | 0.00 | 0.00 | 0.00 | 0.00 | 0.00 | 0.00 | 0.00 | 0.00 | 0.00 | 0.00 | 0.00 | 0.00 | 0.00 | 0.00 | 0.00 | 0.00 | 0.00 | 0.00 |
| Total | 100.71 | 100.81 | 100.46 | 101.52 | 101.13 | 98.09 | 98.71 | 99.15 | 99.75 | 99.36 | 98.73 | 99.60 | 98.82 | 98.89 | 98.00 | 98.15 | 98.55 | 98.91 |
| **Formula (32O)** | | | | | | | | | | | | | | | | | | |
| Si | 9.147 | 9.077 | 9.439 | 9.095 | 9.386 | 8.870 | 8.910 | 8.887 | 8.883 | 8.975 | 8.954 | 8.844 | 8.866 | 8.812 | 8.894 | 8.881 | 8.860 | 8.782 |
| Al | 6.781 | 6.847 | 6.500 | 6.844 | 6.536 | 7.007 | 7.010 | 7.018 | 6.982 | 6.966 | 6.982 | 7.041 | 7.029 | 7.062 | 6.991 | 7.068 | 7.042 | 7.125 |
| Fe(ii) | 0.000 | 0.000 | 0.000 | 0.000 | 0.000 | 0.000 | 0.000 | 0.000 | 0.037 | 0.000 | 0.000 | 0.031 | 0.034 | 0.053 | 0.033 | 0.000 | 0.051 | 0.000 |
| Ca | 3.061 | 3.099 | 2.741 | 3.062 | 2.813 | 3.395 | 3.310 | 3.369 | 3.365 | 3.225 | 3.244 | 3.373 | 3.375 | 3.368 | 3.310 | 3.281 | 3.306 | 3.373 |
| Na | 0.945 | 0.952 | 1.262 | 0.966 | 1.220 | 0.711 | 0.712 | 0.661 | 0.721 | 0.753 | 0.751 | 0.693 | 0.630 | 0.724 | 0.766 | 0.710 | 0.718 | 0.749 |
| K | 0.000 | 0.000 | 0.000 | 0.000 | 0.000 | 0.000 | 0.000 | 0.000 | 0.000 | 0.000 | 0.000 | 0.000 | 0.000 | 0.000 | 0.000 | 0.000 | 0.000 | 0.000 |
| Ba | 0.000 | 0.000 | 0.000 | 0.000 | 0.000 | 0.000 | 0.000 | 0.000 | 0.000 | 0.000 | 0.000 | 0.000 | 0.000 | 0.000 | 0.000 | 0.000 | 0.000 | 0.000 |
| TOTAL | 19.934 | 19.975 | 19.942 | 19.966 | 19.956 | 19.982 | 19.941 | 19.935 | 19.987 | 19.919 | 19.931 | 19.982 | 19.934 | 20.019 | 19.994 | 19.940 | 19.978 | 20.029 |
| **Endmembers** | | | | | | | | | | | | | | | | | | |
| An | 76.41 | 76.50 | 68.47 | 76.02 | 69.74 | 82.69 | 82.29 | 83.60 | 82.35 | 81.08 | 81.20 | 82.95 | 84.27 | 82.30 | 81.21 | 82.21 | 82.15 | 81.84 |
| Ab | 23.59 | 23.50 | 31.53 | 23.98 | 30.26 | 17.31 | 17.71 | 16.40 | 17.65 | 18.92 | 18.80 | 17.05 | 15.73 | 17.70 | 18.79 | 17.79 | 17.85 | 18.16 |
| Or | 0.00 | 0.00 | 0.00 | 0.00 | 0.00 | 0.00 | 0.00 | 0.00 | 0.00 | 0.00 | 0.00 | 0.00 | 0.00 | 0.00 | 0.00 | 0.00 | 0.00 | 0.00 |
| Cn | | | | | | | | | | | | | | | | | | |

**Plagioclase feldspar**

| Sample | Ab143 | Ab143 | Ab143 | Ab143 | 85P | 85P | 85P | Ab3826 | Ab3826 | Ab3826 | Ab3826 | Ab92 | Ab92 | Ab92 | Ab1310 | Ab1310 |
|---|---|---|---|---|---|---|---|---|---|---|---|---|---|---|---|---|
| Analysis No. | 10 | 14 | 15 | 22 | 4 | 8 | 14 | 2 | 18 | 24 | 31 | 2 | 10 | 14 | 7 | 9 |
| Analysis Name. | plag1 | plag2 | plag3 | plag4 | plag1 | plag2 | plag3 | plag1 | plag2 | plag4 | plag5 | plag1 | plag2 | plag3 | plag1 | plag2 |
| SiO2 | 47.70 | 48.56 | 47.57 | 47.78 | 61.90 | 59.90 | 61.83 | 56.52 | 53.87 | 54.05 | 51.81 | 54.59 | 57.68 | 55.00 | 60.33 | 56.02 |
| Al2O3 | 30.98 | 30.01 | 30.96 | 30.78 | 25.28 | 25.13 | 25.25 | 25.19 | 27.48 | 27.05 | 29.39 | 29.19 | 27.09 | 28.63 | 26.21 | 28.82 |
| FeO | 0.00 | 0.00 | 0.20 | 0.00 | 0.00 | 0.00 | 0.00 | 0.00 | 0.27 | 0.00 | 0.00 | 0.00 | 0.20 | 0.20 | 0.22 | 0.20 |
| CaO | 15.57 | 15.15 | 15.68 | 16.02 | 7.12 | 7.93 | 7.44 | 8.89 | 11.35 | 11.30 | 13.39 | 12.89 | 9.94 | 11.84 | 8.67 | 12.06 |
| Na2O | 2.40 | 2.83 | 2.29 | 2.20 | 7.68 | 7.01 | 7.48 | 6.02 | 4.82 | 4.84 | 3.83 | 4.59 | 5.88 | 4.92 | 6.69 | 4.90 |
| K2O | 0.00 | 0.00 | 0.00 | 0.00 | 0.19 | 0.23 | 0.27 | 0.26 | 0.15 | 0.20 | 0.13 | 0.10 | 0.20 | 0.12 | 0.19 | 0.14 |
| BaO | 0.00 | 0.00 | 0.00 | 0.00 | 0.00 | 0.00 | 0.00 | 0.00 | 0.00 | 0.00 | 0.00 | 0.00 | 0.00 | 0.00 | 0.00 | 0.00 |
| Total | 96.66 | 96.55 | 96.70 | 96.95 | 102.15 | 100.20 | 102.49 | 96.89 | 97.95 | 97.45 | 98.54 | 101.36 | 100.99 | 100.71 | 102.31 | 102.14 |
| **Formula (32O)** | | | | | | | | | | | | | | | | |
| Si | 9.023 | 9.187 | 9.004 | 9.033 | 10.785 | 10.669 | 10.771 | 10.449 | 9.937 | 10.007 | 9.544 | 9.753 | 10.260 | 9.871 | 10.545 | 9.909 |
| Al | 6.906 | 6.691 | 6.906 | 6.858 | 5.190 | 5.275 | 5.184 | 5.488 | 5.974 | 5.902 | 6.380 | 6.146 | 5.679 | 6.055 | 5.399 | 6.008 |
| Fe(ii) | 0.000 | 0.000 | 0.032 | 0.000 | 0.000 | 0.000 | 0.000 | 0.000 | 0.042 | 0.000 | 0.000 | 0.000 | 0.030 | 0.030 | 0.032 | 0.030 |
| Ca | 3.155 | 3.071 | 3.180 | 3.245 | 1.328 | 1.513 | 1.388 | 1.761 | 2.243 | 2.241 | 2.643 | 2.467 | 1.894 | 2.276 | 1.624 | 2.285 |
| Na | 0.880 | 1.038 | 0.840 | 0.806 | 2.593 | 2.421 | 2.526 | 2.158 | 1.724 | 1.737 | 1.368 | 1.590 | 2.028 | 1.712 | 2.267 | 1.680 |
| K | 0.000 | 0.000 | 0.000 | 0.000 | 0.041 | 0.053 | 0.060 | 0.061 | 0.035 | 0.047 | 0.031 | 0.023 | 0.045 | 0.027 | 0.042 | 0.032 |
| Ba | 0.000 | 0.000 | 0.000 | 0.000 | 0.000 | 0.000 | 0.000 | 0.000 | 0.000 | 0.000 | 0.000 | 0.000 | 0.000 | 0.000 | 0.000 | 0.000 |
| TOTAL | 19.964 | 19.987 | 19.963 | 19.941 | 19.937 | 19.931 | 19.930 | 19.917 | 19.955 | 19.934 | 19.965 | 19.980 | 19.937 | 19.971 | 19.910 | 19.943 |
| **Endmembers** | | | | | | | | | | | | | | | | |
| An | 78.19 | 74.74 | 79.10 | 80.10 | 33.52 | 37.96 | 34.93 | 44.24 | 56.05 | 55.67 | 65.39 | 60.47 | 47.75 | 56.69 | 41.28 | 57.17 |
| Ab | 21.81 | 25.26 | 20.90 | 19.90 | 65.44 | 60.72 | 63.55 | 54.22 | 43.07 | 43.15 | 33.85 | 38.97 | 51.11 | 42.63 | 57.64 | 42.04 |
| Or | 0.00 | 0.00 | 0.00 | 0.00 | 1.04 | 1.32 | 1.52 | 1.54 | 0.88 | 1.17 | 0.76 | 0.56 | 1.14 | 0.68 | 1.08 | 0.79 |
| Cn | | | | | | | | | | | | | | | | |

**Plagioclase feldspar**

| Sample | Ab1310 | Ab7799 | Ab7799 | Ab7799 | Ab7801 | Ab7801 | Ab7801 | Ab7801 | Ab7801 | Ab7801 | Ab7801 | Ab7801 | Ab7801 | Ab7801 | Ab7801 | Ab7801 | Ab7801 |
|---|---|---|---|---|---|---|---|---|---|---|---|---|---|---|---|---|---|
| Analysis No. | 10 | 1 | 11 | 23 | 3 | 9 | 24 | 28 | 33 | 34 | 35 | 36 | 37 | 38 | 39 | 40 | 43 |
| Analysis Name. | plag3 | plag1 | plag2 | plag3 | plag1 | plag2 | plag3 | plag3+1 | plag4a | plag4b | plag4c | plag4d | plag4e | plag4f | plag4g | plag4h | plag5 |
| SiO2 | 57.88 | 61.33 | 62.30 | 61.86 | 59.41 | 58.15 | 59.50 | 59.19 | 59.23 | 59.63 | 60.72 | 60.51 | 60.28 | 59.87 | 59.83 | 59.23 | 59.73 |
| Al2O3 | 27.55 | 24.63 | 24.12 | 24.26 | 26.25 | 27.28 | 26.35 | 26.72 | 26.58 | 26.23 | 25.73 | 25.67 | 26.22 | 26.01 | 26.27 | 26.49 | 26.33 |
| FeO | 0.44 | 0.00 | 0.00 | 0.41 | 0.00 | 0.49 | 0.25 | 0.00 | 0.54 | 0.31 | 0.22 | 0.00 | 0.00 | 0.30 | 0.49 | 0.54 | 0.00 |
| CaO | 10.59 | 7.16 | 6.65 | 6.68 | 8.97 | 9.92 | 8.96 | 9.37 | 9.23 | 8.78 | 8.60 | 8.22 | 8.80 | 8.85 | 8.86 | 9.20 | 8.99 |
| Na2O | 5.79 | 7.74 | 7.89 | 7.85 | 6.40 | 5.78 | 6.35 | 6.21 | 6.25 | 6.51 | 6.64 | 6.66 | 6.78 | 6.30 | 6.45 | 6.33 | 6.38 |
| K2O | 0.00 | 0.13 | 0.22 | 0.29 | 0.42 | 0.48 | 0.49 | 0.52 | 0.45 | 0.49 | 0.53 | 0.53 | 0.40 | 0.63 | 0.50 | 0.48 | 0.57 |
| BaO | 0.00 | 0.00 | 0.00 | 0.00 | 0.00 | 0.32 | 0.00 | 0.00 | 0.00 | 0.00 | 0.00 | 0.00 | 0.00 | 0.00 | 0.00 | 0.00 | 0.00 |
| Total | 102.25 | 100.99 | 101.18 | 101.35 | 101.44 | 102.40 | 101.89 | 102.00 | 102.27 | 101.94 | 102.73 | 101.60 | 102.49 | 101.95 | 102.41 | 102.52 | 102.00 |
| **Formula (32O)** | | | | | | | | | | | | | | | | | |
| Si | 10.189 | 10.816 | 10.945 | 10.883 | 10.486 | 10.247 | 10.470 | 10.407 | 10.407 | 10.489 | 10.612 | 10.639 | 10.531 | 10.529 | 10.487 | 10.412 | 10.491 |
| Al | 5.715 | 5.119 | 4.994 | 5.030 | 5.460 | 5.665 | 5.464 | 5.537 | 5.504 | 5.438 | 5.300 | 5.319 | 5.398 | 5.391 | 5.426 | 5.488 | 5.450 |
| Fe(ii) | 0.065 | 0.000 | 0.000 | 0.060 | 0.000 | 0.072 | 0.037 | 0.000 | 0.079 | 0.046 | 0.032 | 0.000 | 0.000 | 0.044 | 0.072 | 0.079 | 0.000 |
| Ca | 1.997 | 1.353 | 1.252 | 1.259 | 1.696 | 1.873 | 1.689 | 1.765 | 1.737 | 1.655 | 1.610 | 1.548 | 1.647 | 1.667 | 1.664 | 1.733 | 1.692 |
| Na | 1.976 | 2.646 | 2.687 | 2.677 | 2.190 | 1.975 | 2.166 | 2.117 | 2.129 | 2.220 | 2.250 | 2.270 | 2.296 | 2.148 | 2.192 | 2.157 | 2.173 |
| K | 0.000 | 0.029 | 0.049 | 0.065 | 0.095 | 0.108 | 0.110 | 0.117 | 0.101 | 0.110 | 0.118 | 0.119 | 0.089 | 0.141 | 0.112 | 0.108 | 0.128 |
| Ba | 0.000 | 0.000 | 0.000 | 0.000 | 0.000 | 0.022 | 0.000 | 0.000 | 0.000 | 0.000 | 0.000 | 0.000 | 0.000 | 0.000 | 0.000 | 0.000 | 0.000 |
| TOTAL | 19.942 | 19.963 | 19.927 | 19.974 | 19.926 | 19.962 | 19.936 | 19.942 | 19.957 | 19.957 | 19.922 | 19.896 | 19.962 | 19.920 | 19.952 | 19.977 | 19.934 |
| *Endmembers* | | | | | | | | | | | | | | | | | |
| An | 50.27 | 33.58 | 31.38 | 31.46 | 42.61 | 47.09 | 42.60 | 44.14 | 43.79 | 41.52 | 40.48 | 39.32 | 40.84 | 42.14 | 41.94 | 43.34 | 42.38 |
| Ab | 49.73 | 65.69 | 67.38 | 66.91 | 55.01 | 49.65 | 54.63 | 52.94 | 53.66 | 55.72 | 56.55 | 57.66 | 56.95 | 54.29 | 55.25 | 53.97 | 54.42 |
| Or | 0.00 | 0.73 | 1.24 | 1.63 | 2.38 | 2.71 | 2.77 | 2.92 | 2.54 | 2.76 | 2.97 | 3.02 | 2.21 | 3.57 | 2.82 | 2.69 | 3.20 |
| Cn | | | | | | 0.56 | | | | | | | | | | | |

**Plagioclase feldspar**

| Sample | Ab7802 | Ab7802 | Ab7802 | Ab7802 | MS1595 | MS1595 | MS1595 | MS1595 | MS1595 | MS1595 | MS1595 | Ab93 | Ab93 | Ab93 | Ab93 | Ab93 | Ab93 |
|---|---|---|---|---|---|---|---|---|---|---|---|---|---|---|---|---|---|
| Analysis No. | 14 | 21 | 22 | 25 | 11 | 15 | 20 | 21 | 22 | 23 | 24 | 11 | 12 | 13 | 14 | 15 | 20 |
| Analysis Name. | plag1 | plag2 | plag3 | plag4 | plag1 | plag2a | plag3a | plag3b | plag3c | plag3d | plag3e | plag1a | plag1b | plag1c | plag1d | plag1e | plag2 |
| SiO2 | 56.45 | 53.49 | 54.72 | 52.15 | 52.95 | 48.39 | 47.07 | 48.04 | 47.85 | 47.63 | 47.55 | 53.23 | 53.64 | 53.27 | 53.22 | 53.50 | 53.51 |
| Al2O3 | 27.59 | 29.46 | 28.03 | 29.66 | 27.64 | 30.80 | 30.73 | 30.62 | 30.62 | 30.72 | 31.05 | 28.05 | 27.81 | 28.05 | 28.25 | 28.40 | 27.72 |
| FeO | 0.00 | 0.00 | 0.19 | 0.22 | 0.00 | 0.00 | 0.00 | 0.00 | 0.00 | 0.00 | 0.00 | 0.29 | 0.00 | 0.00 | 0.00 | 0.00 | 0.42 |
| CaO | 10.82 | 12.79 | 11.69 | 13.47 | 11.45 | 15.14 | 16.04 | 15.68 | 15.61 | 15.69 | 15.75 | 12.13 | 12.02 | 11.99 | 11.95 | 12.18 | 11.90 |
| Na2O | 5.65 | 4.32 | 4.64 | 3.72 | 4.65 | 2.66 | 2.27 | 2.47 | 2.48 | 2.32 | 2.17 | 4.03 | 4.44 | 4.40 | 4.21 | 4.40 | 4.26 |
| K2O | 0.16 | 0.12 | 0.15 | 0.19 | 0.00 | 0.00 | 0.00 | 0.00 | 0.00 | 0.00 | 0.00 | 0.26 | 0.26 | 0.26 | 0.17 | 0.19 | 0.00 |
| BaO | 0.00 | 0.00 | 0.00 | 0.00 | 0.00 | 0.00 | 0.00 | 0.00 | 0.00 | 0.00 | 0.00 | 0.00 | 0.00 | 0.00 | 0.00 | 0.00 | 0.00 |
| Total | 100.67 | 100.18 | 99.42 | 99.41 | 96.68 | 96.99 | 96.10 | 97.12 | 96.75 | 96.36 | 96.52 | 98.24 | 98.16 | 97.95 | 97.78 | 98.65 | 97.80 |
| **Formula (32O)** | | | | | | | | | | | | | | | | | |
| Si | 10.100 | 9.669 | 9.934 | 9.532 | 9.878 | 9.107 | 8.974 | 9.075 | 9.063 | 9.039 | 9.005 | 9.826 | 9.877 | 9.831 | 9.823 | 9.803 | 9.883 |
| Al | 5.818 | 6.276 | 5.997 | 6.389 | 6.077 | 6.832 | 6.904 | 6.817 | 6.835 | 6.870 | 6.930 | 6.102 | 6.035 | 6.100 | 6.145 | 6.133 | 6.034 |
| Fe(ii) | 0.000 | 0.000 | 0.029 | 0.034 | 0.000 | 0.000 | 0.000 | 0.000 | 0.000 | 0.000 | 0.000 | 0.045 | 0.000 | 0.000 | 0.000 | 0.000 | 0.065 |
| Ca | 2.074 | 2.477 | 2.274 | 2.638 | 2.288 | 3.053 | 3.276 | 3.173 | 3.167 | 3.190 | 3.196 | 2.399 | 2.371 | 2.370 | 2.363 | 2.391 | 2.355 |
| Na | 1.960 | 1.514 | 1.633 | 1.318 | 1.682 | 0.971 | 0.839 | 0.905 | 0.911 | 0.854 | 0.797 | 1.442 | 1.585 | 1.574 | 1.506 | 1.563 | 1.525 |
| K | 0.037 | 0.028 | 0.035 | 0.044 | 0.000 | 0.000 | 0.000 | 0.000 | 0.000 | 0.000 | 0.000 | 0.061 | 0.061 | 0.061 | 0.040 | 0.044 | 0.000 |
| Ba | 0.000 | 0.000 | 0.000 | 0.000 | 0.000 | 0.000 | 0.000 | 0.000 | 0.000 | 0.000 | 0.000 | 0.000 | 0.000 | 0.000 | 0.000 | 0.000 | 0.000 |
| TOTAL | 19.989 | 19.964 | 19.901 | 19.955 | 19.925 | 19.962 | 19.993 | 19.969 | 19.975 | 19.953 | 19.928 | 19.875 | 19.929 | 19.937 | 19.878 | 19.934 | 19.862 |
| **Endmembers** | | | | | | | | | | | | | | | | | |
| An | 50.95 | 61.64 | 57.69 | 65.94 | 57.64 | 75.88 | 79.61 | 77.82 | 77.67 | 78.89 | 80.04 | 61.47 | 59.02 | 59.18 | 60.44 | 59.80 | 60.69 |
| Ab | 48.15 | 37.67 | 41.43 | 32.95 | 42.36 | 24.12 | 20.39 | 22.18 | 22.33 | 21.11 | 19.96 | 36.96 | 39.45 | 39.30 | 38.53 | 39.09 | 39.31 |
| Or | 0.90 | 0.69 | 0.88 | 1.11 | 0.00 | 0.00 | 0.00 | 0.00 | 0.00 | 0.00 | 0.00 | 1.57 | 1.52 | 1.53 | 1.02 | 1.11 | 0.00 |
| Cn | | | | | | | | | | | | | | | | | |

**Plagioclase feldspar**

| Sample | Ab93 | Ab93 | Ab93 | Ab243 | Ab243 | Ab243 | Ab243 | Ab243 | Ab243 | Ab243 | Ab243 | Ab243 | Ab243 | Ab243 | Ab661 | Ab661 | Ab661 |
|---|---|---|---|---|---|---|---|---|---|---|---|---|---|---|---|---|---|
| Analysis No. | 21 | 31 | 34 | 2 | 11 | 16 | 18 | 19 | 20 | 21 | 22 | 28 | 29 | 36 | 6 | 9 | 25 |
| Analysis Name. | plag3 | plag4 | plag5 | plag1 | plag2 | plag3 | plag4a | plag4b | plag4c | plag4d | plag4e | plag5 | plag6 | plag7 | per-kfel3b | fspr1 | plag3 |
| SiO2 | 52.81 | 54.51 | 53.62 | 55.87 | 56.38 | 55.49 | 55.76 | 55.45 | 52.86 | 54.91 | 55.24 | 54.90 | 56.42 | 55.82 | 62.73 | 59.69 | 63.17 |
| Al2O3 | 27.71 | 27.89 | 28.20 | 27.58 | 27.08 | 27.59 | 27.32 | 27.01 | 26.22 | 27.26 | 27.27 | 27.33 | 26.96 | 27.66 | 22.92 | 25.00 | 22.99 |
| FeO | 0.00 | 0.22 | 0.00 | 0.00 | 0.25 | 0.27 | 0.00 | 0.00 | 1.63 | 0.00 | 0.30 | 0.00 | 0.00 | 0.23 | 0.00 | 0.00 | 0.00 |
| CaO | 11.97 | 11.74 | 12.32 | 11.08 | 10.49 | 11.14 | 10.79 | 10.62 | 10.30 | 11.46 | 11.21 | 11.14 | 10.22 | 10.79 | 5.32 | 7.94 | 5.13 |
| Na2O | 4.22 | 4.56 | 4.37 | 5.21 | 5.44 | 4.99 | 5.03 | 5.02 | 4.68 | 4.83 | 5.01 | 5.01 | 5.56 | 4.99 | 8.06 | 7.11 | 8.57 |
| K2O | 0.19 | 0.28 | 0.22 | 0.33 | 0.26 | 0.17 | 0.22 | 0.16 | 0.22 | 0.18 | 0.17 | 0.20 | 0.27 | 0.28 | 0.48 | 0.00 | 0.15 |
| BaO | 0.00 | 0.00 | 0.00 | 0.00 | 0.00 | 0.00 | 0.00 | 0.00 | 0.00 | 0.00 | 0.00 | 0.00 | 0.00 | 0.00 | 0.00 | 0.00 | 0.00 |
| Total | 96.91 | 99.21 | 98.94 | 100.07 | 100.13 | 99.80 | 99.11 | 98.26 | 96.91 | 98.64 | 99.20 | 98.58 | 99.59 | 99.76 | 99.50 | 99.74 | 100.01 |
| **Formula (32O)** | | | | | | | | | | | | | | | | | |
| Si | 9.846 | 9.929 | 9.824 | 10.065 | 10.163 | 10.040 | 10.116 | 10.140 | 10.000 | 10.036 | 10.049 | 10.037 | 10.200 | 10.074 | 11.165 | 10.672 | 11.176 |
| Al | 6.088 | 5.987 | 6.089 | 5.856 | 5.753 | 5.883 | 5.841 | 5.821 | 5.846 | 5.872 | 5.846 | 5.888 | 5.744 | 5.883 | 4.807 | 5.268 | 4.793 |
| Fe(ii) | 0.000 | 0.034 | 0.000 | 0.000 | 0.038 | 0.041 | 0.000 | 0.000 | 0.258 | 0.000 | 0.046 | 0.000 | 0.000 | 0.035 | 0.000 | 0.000 | 0.000 |
| Ca | 2.391 | 2.291 | 2.418 | 2.138 | 2.026 | 2.159 | 2.097 | 2.081 | 2.088 | 2.244 | 2.185 | 2.182 | 1.979 | 2.086 | 1.014 | 1.521 | 0.972 |
| Na | 1.525 | 1.610 | 1.552 | 1.820 | 1.901 | 1.750 | 1.769 | 1.780 | 1.717 | 1.711 | 1.767 | 1.776 | 1.949 | 1.746 | 2.781 | 2.465 | 2.939 |
| K | 0.045 | 0.065 | 0.051 | 0.076 | 0.060 | 0.039 | 0.051 | 0.037 | 0.053 | 0.042 | 0.039 | 0.047 | 0.062 | 0.064 | 0.109 | 0.000 | 0.034 |
| Ba | 0.000 | 0.000 | 0.000 | 0.000 | 0.000 | 0.000 | 0.000 | 0.000 | 0.000 | 0.000 | 0.000 | 0.000 | 0.000 | 0.000 | 0.000 | 0.000 | 0.000 |
| TOTAL | 19.895 | 19.915 | 19.934 | 19.955 | 19.941 | 19.913 | 19.874 | 19.858 | 19.961 | 19.905 | 19.931 | 19.930 | 19.934 | 19.889 | 19.877 | 19.926 | 19.914 |
| **Endmembers** | | | | | | | | | | | | | | | | | |
| An | 60.35 | 57.76 | 60.13 | 53.01 | 50.81 | 54.68 | 53.54 | 53.38 | 54.12 | 56.14 | 54.74 | 54.49 | 49.60 | 53.54 | 25.98 | 38.16 | 24.64 |
| Ab | 38.50 | 40.60 | 38.59 | 45.11 | 47.69 | 44.32 | 45.16 | 45.66 | 44.50 | 42.81 | 44.27 | 44.35 | 48.84 | 44.81 | 71.23 | 61.84 | 74.50 |
| Or | 1.14 | 1.64 | 1.28 | 1.88 | 1.50 | 0.99 | 1.30 | 0.96 | 1.38 | 1.05 | 0.99 | 1.16 | 1.56 | 1.65 | 2.79 | 0.00 | 0.86 |
| Cn | | | | | | | | | | | | | | | | | |

**Plagioclase feldspar**

| Sample | Ab661 | V(Ol) | V(Ol) | V(Ol) | V(Ol) | V(Ol) | V(Ol) | V(Ol) | V(Ol) | V(Ol) | DV1 | DV1 | DV1 | DV1 | DV1 | DV1 | DV1 |
|---|---|---|---|---|---|---|---|---|---|---|---|---|---|---|---|---|---|
| Analysis No. | 26 | 4 | 8 | 9 | 10 | 18 | 19 | 20 | 21 | 26 | 13 | 28 | 29 | 34 | 35 | 36 | 40 |
| Analysis Name. | plag3b | plag1 | plag2 | plag2b | plag2c | plag3a | plag3b | plag3c | plag3d | plag4 | plag2 | plagp1 | plagp2 | plagp3 | plag1 | plag2 | plagp4 |
| SiO2 | 62.32 | 50.88 | 53.09 | 52.30 | 52.92 | 52.24 | 52.45 | 52.78 | 52.38 | 52.15 | 52.43 | 49.01 | 48.47 | 48.55 | 52.27 | 49.52 | 50.46 |
| Al2O3 | 23.02 | 30.80 | 29.58 | 29.56 | 29.67 | 30.02 | 29.45 | 29.97 | 29.56 | 29.84 | 30.05 | 32.28 | 32.47 | 31.62 | 29.84 | 31.30 | 30.47 |
| FeO | 0.00 | 0.00 | 0.00 | 0.00 | 0.23 | 0.52 | 0.31 | 0.34 | 0.74 | 0.00 | 0.36 | 0.27 | 0.27 | 0.00 | 0.00 | 0.26 | 0.31 |
| CaO | 5.16 | 15.03 | 13.75 | 13.99 | 13.96 | 13.78 | 13.50 | 13.69 | 13.47 | 13.63 | 13.69 | 16.66 | 17.23 | 16.36 | 13.78 | 15.73 | 15.26 |
| Na2O | 8.45 | 3.18 | 3.83 | 3.51 | 3.68 | 3.57 | 3.81 | 4.01 | 3.61 | 3.82 | 3.78 | 1.92 | 1.83 | 2.30 | 3.57 | 2.55 | 2.99 |
| K2O | 0.00 | 0.00 | 0.21 | 0.00 | 0.00 | 0.00 | 0.11 | 0.20 | 0.13 | 0.14 | 0.00 | 0.00 | 0.00 | 0.00 | 0.00 | 0.00 | 0.11 |
| BaO | 0.00 | 0.00 | 0.00 | 0.00 | 0.00 | 0.00 | 0.00 | 0.00 | 0.00 | 0.00 | 0.00 | 0.00 | 0.00 | 0.00 | 0.00 | 0.00 | 0.00 |
| Total | 98.95 | 99.88 | 100.47 | 99.37 | 100.46 | 100.14 | 99.63 | 100.98 | 100.17 | 99.57 | 100.32 | 100.41 | 100.27 | 98.84 | 99.64 | 99.37 | 99.60 |
| **Formula (32O)** | | | | | | | | | | | | | | | | | |
| Si | 11.138 | 9.283 | 9.596 | 9.550 | 9.567 | 9.487 | 9.566 | 9.515 | 9.543 | 9.512 | 9.500 | 8.961 | 8.873 | 8.993 | 9.530 | 9.112 | 9.261 |
| Al | 4.848 | 6.623 | 6.301 | 6.361 | 6.321 | 6.425 | 6.330 | 6.367 | 6.347 | 6.414 | 6.417 | 6.956 | 7.005 | 6.903 | 6.412 | 6.787 | 6.590 |
| Fe(ii) | 0.000 | 0.000 | 0.000 | 0.000 | 0.035 | 0.079 | 0.047 | 0.051 | 0.113 | 0.000 | 0.055 | 0.041 | 0.041 | 0.000 | 0.000 | 0.040 | 0.048 |
| Ca | 0.988 | 2.938 | 2.662 | 2.737 | 2.704 | 2.681 | 2.638 | 2.644 | 2.629 | 2.663 | 2.657 | 3.263 | 3.379 | 3.247 | 2.692 | 3.101 | 3.000 |
| Na | 2.928 | 1.125 | 1.342 | 1.243 | 1.290 | 1.257 | 1.347 | 1.401 | 1.275 | 1.351 | 1.328 | 0.681 | 0.649 | 0.826 | 1.262 | 0.910 | 1.064 |
| K | 0.000 | 0.000 | 0.048 | 0.000 | 0.000 | 0.000 | 0.026 | 0.046 | 0.030 | 0.033 | 0.000 | 0.000 | 0.000 | 0.000 | 0.000 | 0.000 | 0.026 |
| Ba | 0.000 | 0.000 | 0.000 | 0.000 | 0.000 | 0.000 | 0.000 | 0.000 | 0.000 | 0.000 | 0.000 | 0.000 | 0.000 | 0.000 | 0.000 | 0.000 | 0.000 |
| TOTAL | 19.902 | 19.968 | 19.949 | 19.891 | 19.917 | 19.929 | 19.955 | 20.025 | 19.937 | 19.973 | 19.956 | 19.902 | 19.949 | 19.968 | 19.895 | 19.949 | 19.989 |
| **Endmembers** | | | | | | | | | | | | | | | | | |
| An | 25.23 | 72.31 | 65.69 | 68.77 | 67.70 | 68.08 | 65.77 | 64.62 | 66.82 | 65.82 | 66.68 | 82.74 | 83.88 | 79.72 | 68.08 | 77.32 | 73.36 |
| Ab | 74.77 | 27.69 | 33.11 | 31.23 | 32.30 | 31.92 | 33.59 | 34.25 | 32.41 | 33.38 | 33.32 | 17.26 | 16.12 | 20.28 | 31.92 | 22.68 | 26.01 |
| Or | 0.00 | 0.00 | 1.19 | 0.00 | 0.00 | 0.00 | 0.64 | 1.12 | 0.77 | 0.80 | 0.00 | 0.00 | 0.00 | 0.00 | 0.00 | 0.00 | 0.63 |
| Cn | | | | | | | | | | | | | | | | | |

**Plagioclase feldspar**

| Sample | Ab3986 | Ab3986 | Ab3986 | Ab3986 | Ab3986 | Ab3986 | Ab3986 | Ab3986 | Ab3986 | Ab3986 | Ab3986 | Ab3986 | Ab5661 | Ab5661 | Ab5661 | Ab5661 | Ab5661 | Ab5661 |
|---|---|---|---|---|---|---|---|---|---|---|---|---|---|---|---|---|---|---|
| Analysis No. | 3 | 5 | 6 | 10 | 18 | 19 | 20 | 21 | 22 | 23 | 24 | 25 | 3 | 6 | 7 | 8 | 12 | 16 |
| Analysis Name. | plag1 | plag2 | plag3 | plag4 | plag5 | plag6 | plag6 | plag7 | plag8a | plag8b | plag8c | plag8d | plag1 | plag2 | plag3 | plag4 | plag5 | plag6 |
| SiO2 | 49.68 | 49.24 | 49.83 | 49.70 | 50.75 | 48.68 | 49.35 | 49.68 | 49.13 | 48.86 | 49.11 | 49.28 | 50.95 | 51.00 | 50.83 | 51.18 | 50.56 | 50.55 |
| Al2O3 | 30.73 | 30.78 | 29.99 | 30.74 | 30.30 | 30.89 | 30.54 | 30.42 | 30.91 | 31.29 | 30.78 | 30.77 | 30.37 | 30.64 | 30.21 | 30.38 | 29.79 | 30.35 |
| FeO | 0.00 | 0.00 | 0.20 | 0.00 | 0.00 | 0.00 | 0.00 | 0.00 | 0.00 | 0.00 | 0.00 | 0.00 | 0.00 | 0.00 | 0.00 | 0.00 | 0.25 | 0.00 |
| CaO | 15.05 | 15.68 | 14.82 | 15.35 | 14.69 | 15.57 | 14.91 | 15.06 | 15.59 | 15.91 | 15.67 | 15.17 | 14.46 | 14.71 | 14.93 | 14.45 | 13.98 | 14.76 |
| Na2O | 2.88 | 2.47 | 3.09 | 2.88 | 3.02 | 2.69 | 2.81 | 2.90 | 2.62 | 2.37 | 2.61 | 2.83 | 3.07 | 3.11 | 3.07 | 3.13 | 3.34 | 3.23 |
| K2O | 0.00 | 0.00 | 0.00 | 0.00 | 0.00 | 0.00 | 0.00 | 0.00 | 0.00 | 0.00 | 0.00 | 0.00 | 0.00 | 0.00 | 0.00 | 0.10 | 0.00 | 0.00 |
| BaO | 0.00 | 0.00 | 0.00 | 0.00 | 0.00 | 0.00 | 0.00 | 0.00 | 0.00 | 0.00 | 0.00 | 0.00 | 0.38 | 0.00 | 0.00 | 0.00 | 0.00 | 0.00 |
| Total | 98.34 | 98.17 | 97.92 | 98.68 | 98.76 | 97.83 | 97.81 | 98.06 | 98.43 | 98.43 | 98.18 | 98.05 | 99.23 | 99.47 | 99.05 | 99.40 | 98.30 | 98.88 |
| Formula (32O) | | | | | | | | | | | | | | | | | | |
| Si | 9.211 | 9.156 | 9.286 | 9.194 | 9.348 | 9.096 | 9.214 | 9.238 | 9.133 | 9.070 | 9.139 | 9.171 | 9.359 | 9.329 | 9.346 | 9.378 | 9.395 | 9.313 |
| Al | 6.714 | 6.745 | 6.586 | 6.702 | 6.577 | 6.802 | 6.720 | 6.667 | 6.772 | 6.846 | 6.751 | 6.749 | 6.575 | 6.605 | 6.546 | 6.560 | 6.524 | 6.589 |
| Fe(ii) | 0.000 | 0.000 | 0.031 | 0.000 | 0.000 | 0.000 | 0.000 | 0.000 | 0.000 | 0.000 | 0.000 | 0.000 | 0.000 | 0.000 | 0.000 | 0.000 | 0.039 | 0.000 |
| Ca | 2.989 | 3.124 | 2.959 | 3.042 | 2.899 | 3.117 | 2.982 | 3.000 | 3.105 | 3.164 | 3.124 | 3.025 | 2.846 | 2.883 | 2.941 | 2.837 | 2.783 | 2.913 |
| Na | 1.035 | 0.890 | 1.116 | 1.033 | 1.078 | 0.974 | 1.017 | 1.046 | 0.944 | 0.853 | 0.942 | 1.021 | 1.093 | 1.103 | 1.094 | 1.112 | 1.203 | 1.154 |
| K | 0.000 | 0.000 | 0.000 | 0.000 | 0.000 | 0.000 | 0.000 | 0.000 | 0.000 | 0.000 | 0.000 | 0.000 | 0.000 | 0.000 | 0.000 | 0.023 | 0.000 | 0.000 |
| Ba | 0.000 | 0.000 | 0.000 | 0.000 | 0.000 | 0.000 | 0.000 | 0.000 | 0.000 | 0.000 | 0.000 | 0.000 | 0.027 | 0.000 | 0.000 | 0.000 | 0.000 | 0.000 |
| TOTAL | 19.950 | 19.916 | 19.979 | 19.971 | 19.903 | 19.990 | 19.934 | 19.951 | 19.953 | 19.933 | 19.956 | 19.965 | 19.900 | 19.920 | 19.928 | 19.910 | 19.944 | 19.969 |
| Endmembers | | | | | | | | | | | | | | | | | | |
| An | 74.28 | 77.82 | 72.61 | 74.65 | 72.88 | 76.18 | 74.57 | 74.16 | 76.68 | 78.77 | 76.84 | 74.76 | 71.75 | 72.33 | 72.88 | 71.42 | 69.82 | 71.63 |
| Ab | 25.72 | 22.18 | 27.39 | 25.35 | 27.12 | 23.82 | 25.43 | 25.84 | 23.32 | 21.23 | 23.16 | 25.24 | 27.56 | 27.67 | 27.12 | 27.99 | 30.18 | 28.37 |
| Or | 0.00 | 0.00 | 0.00 | 0.00 | 0.00 | 0.00 | 0.00 | 0.00 | 0.00 | 0.00 | 0.00 | 0.00 | 0.00 | 0.00 | 0.00 | 0.59 | 0.00 | 0.00 |
| Cn | | | | | | | | | | | | | 0.69 | | | | | |

**Plagioclase feldspar**

| Sample | Ab5661 | Ab5661 | Ab5661 | Ab6510 | Ab6510 | Ab6510 | Ab6510 | Ab6510 | Ab6510 | Ab6510 | Ab6510 | 773C | 773C | 773C | 773C | 773C | 773C |
|---|---|---|---|---|---|---|---|---|---|---|---|---|---|---|---|---|---|
| Analysis No. | 20 | 21 | 22 | 5 | 9 | 11 | 13 | 14 | 17 | 21 | 22 | 3 | 4 | 5 | 19 | 20 | 23 |
| Analysis Name. | plag7 | plag8 | plag8b | plag1 | plag2 | plag3 | plag4 | plag4a | plag5 | plag6 | plag7 | plag1 | plag2 | plag3 | plag6 | plag7a | plag7d |
| SiO2 | 50.48 | 50.61 | 50.82 | 50.30 | 49.92 | 45.81 | 49.80 | 49.38 | 48.95 | 51.06 | 49.71 | 50.31 | 50.71 | 50.74 | 50.79 | 50.87 | 50.31 |
| Al2O3 | 30.39 | 30.01 | 30.52 | 30.56 | 29.92 | 28.70 | 30.94 | 29.66 | 30.75 | 29.84 | 31.29 | 29.28 | 29.47 | 30.05 | 30.28 | 30.85 | 30.60 |
| FeO | 0.00 | 0.00 | 0.00 | 0.00 | 0.00 | 0.20 | 0.27 | 0.95 | 0.25 | 0.00 | 0.00 | 0.37 | 0.00 | 0.00 | 0.00 | 0.00 | 0.00 |
| CaO | 15.13 | 14.75 | 14.79 | 14.89 | 15.24 | 14.12 | 15.29 | 14.02 | 15.48 | 14.32 | 15.67 | 13.91 | 14.03 | 14.39 | 14.22 | 14.62 | 15.02 |
| Na2O | 3.00 | 3.26 | 3.11 | 3.04 | 3.11 | 3.58 | 2.74 | 2.95 | 2.70 | 3.29 | 2.48 | 3.12 | 3.29 | 3.37 | 3.39 | 3.23 | 3.03 |
| K2O | 0.00 | 0.00 | 0.00 | 0.00 | 0.00 | 0.00 | 0.11 | 0.11 | 0.00 | 0.00 | 0.00 | 0.10 | 0.10 | 0.00 | 0.00 | 0.00 | 0.00 |
| BaO | 0.00 | 0.00 | 0.00 | 0.00 | 0.00 | 0.00 | 0.00 | 0.00 | 0.00 | 0.00 | 0.00 | 0.00 | 0.00 | 0.00 | 0.00 | 0.00 | 0.00 |
| Total | 98.98 | 98.62 | 99.24 | 98.79 | 98.19 | 92.41 | 99.15 | 97.56 | 98.13 | 98.51 | 99.15 | 97.41 | 97.59 | 98.54 | 98.69 | 99.82 | 98.96 |
| **Formula (32O)** | | | | | | | | | | | | | | | | | |
| Si | 9.294 | 9.349 | 9.322 | 9.276 | 9.284 | 9.098 | 9.178 | 9.299 | 9.125 | 9.423 | 9.146 | 9.432 | 9.445 | 9.370 | 9.361 | 9.298 | 9.266 |
| Al | 6.594 | 6.533 | 6.598 | 6.642 | 6.557 | 6.718 | 6.720 | 6.582 | 6.755 | 6.490 | 6.785 | 6.469 | 6.469 | 6.540 | 6.577 | 6.645 | 6.642 |
| Fe(ii) | 0.000 | 0.000 | 0.000 | 0.000 | 0.000 | 0.033 | 0.042 | 0.150 | 0.039 | 0.000 | 0.000 | 0.058 | 0.000 | 0.000 | 0.000 | 0.000 | 0.000 |
| Ca | 2.984 | 2.919 | 2.906 | 2.942 | 3.036 | 3.004 | 3.019 | 2.828 | 3.091 | 2.831 | 3.089 | 2.794 | 2.800 | 2.847 | 2.808 | 2.863 | 2.964 |
| Na | 1.071 | 1.167 | 1.106 | 1.087 | 1.121 | 1.378 | 0.979 | 1.077 | 0.976 | 1.177 | 0.885 | 1.134 | 1.188 | 1.207 | 1.211 | 1.145 | 1.082 |
| K | 0.000 | 0.000 | 0.000 | 0.000 | 0.000 | 0.000 | 0.026 | 0.026 | 0.000 | 0.000 | 0.000 | 0.024 | 0.024 | 0.000 | 0.000 | 0.000 | 0.000 |
| Ba | 0.000 | 0.000 | 0.000 | 0.000 | 0.000 | 0.000 | 0.000 | 0.000 | 0.000 | 0.000 | 0.000 | 0.000 | 0.000 | 0.000 | 0.000 | 0.000 | 0.000 |
| TOTAL | 19.944 | 19.968 | 19.932 | 19.946 | 19.998 | 20.232 | 19.964 | 19.962 | 19.986 | 19.921 | 19.904 | 19.912 | 19.926 | 19.963 | 19.957 | 19.951 | 19.954 |
| **Endmembers** | | | | | | | | | | | | | | | | | |
| An | 73.59 | 71.43 | 72.44 | 73.02 | 73.03 | 68.55 | 75.03 | 71.94 | 76.01 | 70.63 | 77.74 | 70.70 | 69.79 | 70.23 | 69.86 | 71.44 | 73.26 |
| Ab | 26.41 | 28.57 | 27.56 | 26.98 | 26.97 | 31.45 | 24.33 | 27.39 | 23.99 | 29.37 | 22.26 | 28.70 | 29.62 | 29.77 | 30.14 | 28.56 | 26.74 |
| Or | 0.00 | 0.00 | 0.00 | 0.00 | 0.00 | 0.00 | 0.64 | 0.67 | 0.00 | 0.00 | 0.00 | 0.61 | 0.59 | 0.00 | 0.00 | 0.00 | 0.00 |
| Cn | | | | | | | | | | | | | | | | | |

**Plagioclase feldspar**

| Sample | 773C | 773C | 110P | 110P | 110P | 110P | 110P | 110P | 110P | 110P | Ab94 | Ab94 | Ab94 | Ab94 | Ab94 | 77P | 77P |
|---|---|---|---|---|---|---|---|---|---|---|---|---|---|---|---|---|---|
| Analysis No. | 24 | 25 | 2 | 3 | 5 | 7 | 9 | 11 | 12 | 14 | 12 | 21 | 30 | 31 | 34 | 1 | 11 |
| Analysis Name. | plag7e | plag7f | plag1 | plag2 | plag3 | plag4 | plag5 | plag6 | plag7 | plag8 | plag1 | plag2 | plag3 | plag4 | plag5 | plag1 | plag2 |
| SiO2 | 49.57 | 50.24 | 50.30 | 50.74 | 50.00 | 51.84 | 49.73 | 50.93 | 50.91 | 50.41 | 56.87 | 58.30 | 58.04 | 55.16 | 57.76 | 54.40 | 53.98 |
| Al2O3 | 30.88 | 30.86 | 29.52 | 29.62 | 29.51 | 28.99 | 29.49 | 29.68 | 28.99 | 29.80 | 27.64 | 26.90 | 26.11 | 28.54 | 26.50 | 27.78 | 28.16 |
| FeO | 0.21 | 0.00 | 0.00 | 0.00 | 0.00 | 0.00 | 0.21 | 0.00 | 0.00 | 0.00 | 0.00 | 0.00 | 0.00 | 0.32 | 0.00 | 0.00 | 0.00 |
| CaO | 15.46 | 15.32 | 14.02 | 14.38 | 14.16 | 13.36 | 14.06 | 13.89 | 13.57 | 14.83 | 11.04 | 9.78 | 9.56 | 11.92 | 9.65 | 11.49 | 12.06 |
| Na2O | 2.82 | 2.84 | 3.41 | 3.33 | 3.27 | 3.96 | 3.15 | 3.31 | 3.47 | 3.19 | 5.32 | 6.48 | 6.27 | 4.70 | 6.15 | 4.90 | 4.54 |
| K2O | 0.00 | 0.00 | 0.00 | 0.15 | 0.00 | 0.10 | 0.15 | 0.00 | 0.00 | 0.00 | 0.16 | 0.11 | 0.00 | 0.22 | 0.10 | 0.24 | 0.26 |
| BaO | 0.00 | 0.00 | 0.00 | 0.00 | 0.00 | 0.00 | 0.00 | 0.00 | 0.00 | 0.00 | 0.00 | 0.00 | 0.00 | 0.00 | 0.00 | 0.00 | 0.00 |
| Total | 98.96 | 99.26 | 97.25 | 98.22 | 96.92 | 98.24 | 97.08 | 97.99 | 96.93 | 98.23 | 101.02 | 101.59 | 99.98 | 100.87 | 100.17 | 99.28 | 99.00 |
| **Formula (32O)** | | | | | | | | | | | | | | | | | |
| Si | 9.158 | 9.229 | 9.407 | 9.409 | 9.384 | 9.581 | 9.362 | 9.452 | 9.529 | 9.353 | 10.128 | 10.308 | 10.402 | 9.888 | 10.341 | 9.941 | 9.858 |
| Al | 6.724 | 6.681 | 6.506 | 6.473 | 6.527 | 6.314 | 6.543 | 6.492 | 6.395 | 6.516 | 5.801 | 5.605 | 5.515 | 6.030 | 5.592 | 5.982 | 6.061 |
| Fe(ii) | 0.032 | 0.000 | 0.000 | 0.000 | 0.000 | 0.000 | 0.033 | 0.000 | 0.000 | 0.000 | 0.000 | 0.000 | 0.000 | 0.048 | 0.000 | 0.000 | 0.000 |
| Ca | 3.060 | 3.015 | 2.809 | 2.857 | 2.847 | 2.645 | 2.836 | 2.762 | 2.721 | 2.948 | 2.106 | 1.853 | 1.836 | 2.289 | 1.851 | 2.249 | 2.359 |
| Na | 1.010 | 1.011 | 1.236 | 1.197 | 1.190 | 1.419 | 1.150 | 1.191 | 1.259 | 1.147 | 1.837 | 2.221 | 2.178 | 1.633 | 2.135 | 1.736 | 1.607 |
| K | 0.000 | 0.000 | 0.000 | 0.035 | 0.000 | 0.024 | 0.036 | 0.000 | 0.000 | 0.000 | 0.036 | 0.025 | 0.000 | 0.050 | 0.023 | 0.056 | 0.061 |
| Ba | 0.000 | 0.000 | 0.000 | 0.000 | 0.000 | 0.000 | 0.000 | 0.000 | 0.000 | 0.000 | 0.000 | 0.000 | 0.000 | 0.000 | 0.000 | 0.000 | 0.000 |
| TOTAL | 19.985 | 19.936 | 19.958 | 19.971 | 19.948 | 19.983 | 19.959 | 19.897 | 19.904 | 19.963 | 19.908 | 20.012 | 19.930 | 19.939 | 19.942 | 19.964 | 19.946 |
| **Endmembers** | | | | | | | | | | | | | | | | | |
| An | 75.18 | 74.88 | 69.44 | 69.86 | 70.53 | 64.71 | 70.52 | 69.87 | 68.36 | 71.98 | 52.93 | 45.20 | 45.73 | 57.62 | 46.18 | 55.66 | 58.59 |
| Ab | 24.82 | 25.12 | 30.56 | 29.27 | 29.47 | 34.71 | 28.59 | 30.13 | 31.64 | 28.02 | 46.16 | 54.19 | 54.27 | 41.11 | 53.25 | 42.95 | 39.91 |
| Or | 0.00 | 0.00 | 0.00 | 0.87 | 0.00 | 0.58 | 0.90 | 0.00 | 0.00 | 0.00 | 0.91 | 0.61 | 0.00 | 1.27 | 0.57 | 1.38 | 1.50 |
| Cn | | | | | | | | | | | | | | | | | |

**Plagioclase feldspar**

| Sample | 77P | 77P | 77P | 77P | 77P | 77P | 77P | 77P | 77P | 77P | CLW218 | CLW218 | CLW218 | CLW218 | CLW215 | CLW215 | CLW215 |
|---|---|---|---|---|---|---|---|---|---|---|---|---|---|---|---|---|---|
| Analysis No. | 12 | 15 | 20 | 23 | 24 | 25 | 26 | 27 | 28 | 29 | 2 | 4 | 16 | 17 | 1 | 2 | 10 |
| Analysis Name. | plag3 | plag4 | plag4b | plag5 | plag5a | plag5b | plag5c | plag5d | plag5e | plag5f | plag1 | plag2 | plag3a | plag3b | plag1 | plag2 | plag3 |
| SiO2 | 54.65 | 55.18 | 55.53 | 56.15 | 56.55 | 54.89 | 54.63 | 54.47 | 54.73 | 56.70 | 54.18 | 47.98 | 47.06 | 47.44 | 46.19 | 47.59 | 64.54 |
| Al2O3 | 28.21 | 27.98 | 28.25 | 27.77 | 27.78 | 28.14 | 28.56 | 28.44 | 28.35 | 27.36 | 28.37 | 32.09 | 32.20 | 32.78 | 34.00 | 32.67 | 23.96 |
| FeO | 0.00 | 0.00 | 0.00 | 0.25 | 0.00 | 0.00 | 0.00 | 0.37 | 0.44 | 0.00 | 0.21 | 0.35 | 0.21 | 0.25 | 0.24 | 0.00 | 0.00 |
| CaO | 11.95 | 11.49 | 11.97 | 11.31 | 11.30 | 11.84 | 12.18 | 12.11 | 12.06 | 10.86 | 12.09 | 17.02 | 17.45 | 17.62 | 18.87 | 17.75 | 13.00 |
| Na2O | 4.67 | 5.10 | 4.73 | 4.91 | 5.44 | 4.59 | 4.71 | 4.50 | 4.72 | 5.47 | 4.54 | 1.73 | 1.60 | 1.49 | 0.93 | 1.53 | 0.78 |
| K2O | 0.10 | 0.25 | 0.26 | 0.25 | 0.18 | 0.21 | 0.18 | 0.20 | 0.15 | 0.29 | 0.17 | 0.00 | 0.00 | 0.00 | 0.00 | 0.00 | 0.00 |
| BaO | 0.00 | 0.00 | 0.00 | 0.00 | 0.00 | 0.00 | 0.00 | 0.00 | 0.00 | 0.00 | 0.31 | 0.00 | 0.00 | 0.00 | 0.00 | 0.00 | 0.00 |
| Total | 99.57 | 99.98 | 100.73 | 100.64 | 101.24 | 99.66 | 100.43 | 100.09 | 100.44 | 100.69 | 99.87 | 99.16 | 98.53 | 99.57 | 100.22 | 99.54 | 102.47 |
| **Formula (32O)** | | | | | | | | | | | | | | | | | |
| Si | 9.905 | 9.963 | 9.951 | 10.058 | 10.070 | 9.935 | 9.850 | 9.848 | 9.865 | 10.143 | 9.836 | 8.881 | 8.783 | 8.757 | 8.504 | 8.781 | 11.097 |
| Al | 6.025 | 5.954 | 5.966 | 5.863 | 5.830 | 6.003 | 6.069 | 6.060 | 6.022 | 5.768 | 6.070 | 7.000 | 7.082 | 7.131 | 7.377 | 7.104 | 4.855 |
| Fe(ii) | 0.000 | 0.000 | 0.000 | 0.037 | 0.000 | 0.000 | 0.000 | 0.056 | 0.066 | 0.000 | 0.032 | 0.054 | 0.033 | 0.039 | 0.037 | 0.000 | 0.000 |
| Ca | 2.320 | 2.223 | 2.298 | 2.171 | 2.156 | 2.296 | 2.353 | 2.346 | 2.329 | 2.081 | 2.351 | 3.375 | 3.489 | 3.484 | 3.722 | 3.509 | 2.395 |
| Na | 1.641 | 1.785 | 1.643 | 1.705 | 1.878 | 1.611 | 1.646 | 1.577 | 1.649 | 1.897 | 1.598 | 0.621 | 0.579 | 0.533 | 0.332 | 0.547 | 0.260 |
| K | 0.023 | 0.058 | 0.059 | 0.057 | 0.041 | 0.048 | 0.041 | 0.046 | 0.034 | 0.066 | 0.039 | 0.000 | 0.000 | 0.000 | 0.000 | 0.000 | 0.000 |
| Ba | 0.000 | 0.000 | 0.000 | 0.000 | 0.000 | 0.000 | 0.000 | 0.000 | 0.000 | 0.000 | 0.022 | 0.000 | 0.000 | 0.000 | 0.000 | 0.000 | 0.000 |
| TOTAL | 19.915 | 19.982 | 19.917 | 19.891 | 19.975 | 19.893 | 19.959 | 19.933 | 19.966 | 19.955 | 19.948 | 19.930 | 19.966 | 19.944 | 19.973 | 19.941 | 18.606 |
| **Endmembers** | | | | | | | | | | | | | | | | | |
| An | 58.24 | 54.67 | 57.44 | 55.19 | 52.91 | 58.05 | 58.23 | 59.10 | 58.04 | 51.46 | 58.63 | 84.46 | 85.77 | 86.73 | 91.81 | 86.51 | 90.21 |
| Ab | 41.18 | 43.91 | 41.07 | 43.36 | 46.09 | 40.72 | 40.75 | 39.74 | 41.10 | 46.90 | 39.84 | 15.54 | 14.23 | 13.27 | 8.19 | 13.49 | 9.79 |
| Or | 0.58 | 1.42 | 1.49 | 1.45 | 1.00 | 1.23 | 1.02 | 1.16 | 0.86 | 1.64 | 0.98 | 0.00 | 0.00 | 0.00 | 0.00 | 0.00 | 0.00 |
| Cn | | | | | | | | | | | 0.55 | | | | | | |

**Plagioclase feldspar**

| Sample | CLW106 | CLW106 | CLW106 | CLW106 | CLW106 | CLW106 | CLW106 | CLW106 | CLW106 | CLW106 | CLW106 | CLW106 | CLW106 | CLW106 | CLW106 | CLW106 | CLW110 | CLW110 |
|---|---|---|---|---|---|---|---|---|---|---|---|---|---|---|---|---|---|---|
| Analysis No. | 4 | 6 | 10 | 15 | 16 | 17 | 18 | 19 | 20 | 21 | 24 | 31 | 33 | 34 | 35 | 36 | 1 | 6 |
| Analysis Name. | plag1 | plag2 | plag3 | plag4a | plag4b | plag4c | plag4d | plag4e | plag4f | plag4g | plag5 | plag6 | plag7a | plag7b | plag7c | plag7d | plag1 | plag2 |
| SiO2 | 46.68 | 47.06 | 46.96 | 45.70 | 45.35 | 45.94 | 45.42 | 45.34 | 45.32 | 45.35 | 45.51 | 45.59 | 46.24 | 45.65 | 38.57 | 45.87 | 45.77 | 46.85 |
| Al2O3 | 32.85 | 32.99 | 31.80 | 33.68 | 33.43 | 32.35 | 33.20 | 33.68 | 33.13 | 33.22 | 32.99 | 32.76 | 32.41 | 32.74 | 28.74 | 32.76 | 32.63 | 32.50 |
| FeO | 0.00 | 0.23 | 0.00 | 0.00 | 0.26 | 0.22 | 0.35 | 0.41 | 0.00 | 0.23 | 0.49 | 0.00 | 0.29 | 0.00 | 9.19 | 0.00 | 0.31 | 0.29 |
| CaO | 17.72 | 18.15 | 17.00 | 18.49 | 18.46 | 18.10 | 18.38 | 18.83 | 18.43 | 18.43 | 17.95 | 17.84 | 17.71 | 17.82 | 13.67 | 17.72 | 17.96 | 17.07 |
| Na2O | 1.53 | 1.64 | 1.85 | 1.04 | 0.98 | 1.29 | 1.13 | 0.67 | 1.10 | 1.02 | 1.05 | 1.18 | 1.36 | 1.11 | 1.93 | 1.21 | 1.23 | 1.68 |
| K2O | 0.00 | 0.00 | 0.00 | 0.00 | 0.00 | 0.00 | 0.00 | 0.00 | 0.00 | 0.00 | 0.00 | 0.00 | 0.00 | 0.00 | 0.00 | 0.00 | 0.00 | 0.11 |
| BaO | 0.00 | 0.00 | 0.00 | 0.00 | 0.00 | 0.00 | 0.00 | 0.00 | 0.00 | 0.36 | 0.00 | 0.00 | 0.00 | 0.00 | 0.00 | 0.00 | 0.00 | 0.00 |
| Total | 98.78 | 100.08 | 97.60 | 98.91 | 98.49 | 97.90 | 98.49 | 98.92 | 97.98 | 98.61 | 97.98 | 97.37 | 98.01 | 97.32 | 92.62 | 97.55 | 97.90 | 98.49 |
| **Formula (32O)** | | | | | | | | | | | | | | | | | | |
| Si | 8.690 | 8.671 | 8.832 | 8.514 | 8.499 | 8.653 | 8.519 | 8.466 | 8.530 | 8.512 | 8.567 | 8.615 | 8.688 | 8.626 | 8.112 | 8.644 | 8.620 | 8.748 |
| Al | 7.207 | 7.164 | 7.049 | 7.395 | 7.384 | 7.181 | 7.339 | 7.411 | 7.349 | 7.348 | 7.319 | 7.295 | 7.177 | 7.291 | 7.124 | 7.276 | 7.242 | 7.152 |
| Fe(ii) | 0.000 | 0.035 | 0.000 | 0.000 | 0.041 | 0.035 | 0.055 | 0.064 | 0.000 | 0.036 | 0.077 | 0.000 | 0.046 | 0.000 | 1.616 | 0.000 | 0.049 | 0.045 |
| Ca | 3.534 | 3.583 | 3.425 | 3.691 | 3.707 | 3.652 | 3.693 | 3.767 | 3.716 | 3.706 | 3.620 | 3.611 | 3.565 | 3.608 | 3.080 | 3.577 | 3.624 | 3.415 |
| Na | 0.552 | 0.586 | 0.675 | 0.376 | 0.356 | 0.471 | 0.411 | 0.243 | 0.401 | 0.371 | 0.383 | 0.432 | 0.495 | 0.407 | 0.787 | 0.442 | 0.449 | 0.608 |
| K | 0.000 | 0.000 | 0.000 | 0.000 | 0.000 | 0.000 | 0.000 | 0.000 | 0.000 | 0.000 | 0.000 | 0.000 | 0.000 | 0.000 | 0.000 | 0.000 | 0.000 | 0.026 |
| Ba | 0.000 | 0.000 | 0.000 | 0.000 | 0.000 | 0.000 | 0.000 | 0.000 | 0.000 | 0.026 | 0.000 | 0.000 | 0.000 | 0.000 | 0.000 | 0.000 | 0.000 | 0.000 |
| TOTAL | 19.983 | 20.040 | 19.981 | 19.976 | 19.987 | 19.992 | 20.017 | 19.950 | 19.996 | 20.000 | 19.966 | 19.954 | 19.971 | 19.932 | 20.719 | 19.939 | 19.984 | 19.994 |
| **Endmembers** | | | | | | | | | | | | | | | | | | |
| An | 86.49 | 85.95 | 83.55 | 90.76 | 91.24 | 88.58 | 89.99 | 93.95 | 90.25 | 90.31 | 90.43 | 89.31 | 87.80 | 89.87 | 79.65 | 89.00 | 88.97 | 84.33 |
| Ab | 13.51 | 14.05 | 16.45 | 9.24 | 8.76 | 11.42 | 10.01 | 6.05 | 9.75 | 9.04 | 9.57 | 10.69 | 12.20 | 10.13 | 20.35 | 11.00 | 11.03 | 15.02 |
| Or | 0.00 | 0.00 | 0.00 | 0.00 | 0.00 | 0.00 | 0.00 | 0.00 | 0.00 | 0.00 | 0.00 | 0.00 | 0.00 | 0.00 | 0.00 | 0.00 | 0.00 | 0.65 |
| Cn | | | | | | | | | | 0.65 | | | | | | | | |

**Plagioclase feldspar**

| Sample | CLW110 | CLW110 | CLW110 | CLW110 | CLW110 | CLW110 | DCD118 | DCD118 | DCD118 | DCD118 | DCD118 |
|---|---|---|---|---|---|---|---|---|---|---|---|
| Analysis No. | 11 | 18 | 19 | 20 | 21 | 22 | 6 | 13 | 21 | 25 | 14 |
| Analysis Name. | plag3 | plag4 | plag5 | plag5b | plag6a | plag6b | plag1 | plag2 | plag3 | plag4 | odd2 |
| SiO2 | 45.50 | 46.41 | 46.05 | 45.92 | 45.79 | 46.91 | 44.41 | 45.09 | 43.15 | 44.00 | 45.11 |
| Al2O3 | 32.28 | 32.40 | 32.53 | 32.80 | 32.84 | 32.09 | 34.90 | 34.60 | 34.11 | 33.94 | 34.35 |
| FeO | 0.22 | 0.37 | 0.00 | 0.36 | 0.30 | 0.44 | 0.00 | 0.22 | 0.00 | 0.00 | 0.00 |
| CaO | 17.84 | 17.50 | 18.08 | 18.07 | 17.99 | 17.29 | 20.04 | 19.48 | 20.01 | 19.80 | 19.74 |
| Na2O | 1.32 | 1.39 | 1.27 | 1.36 | 1.21 | 1.56 | 0.35 | 0.29 | 0.33 | 0.50 | 0.47 |
| K2O | 0.00 | 0.00 | 0.00 | 0.00 | 0.00 | 0.00 | 0.00 | 0.00 | 0.00 | 0.00 | 0.00 |
| BaO | 0.00 | 0.00 | 0.00 | 0.00 | 0.00 | 0.00 | 0.00 | 0.00 | -0.00 | 0.00 | 0.00 |
| Total | 97.14 | 98.32 | 97.92 | 98.50 | 98.14 | 98.28 | 99.69 | 99.68 | 97.59 | 98.24 | 99.67 |
| **Formula (32O)** | | | | | | | | | | | |
| Si | 8.634 | 8.710 | 8.658 | 8.603 | 8.603 | 8.781 | 8.247 | 8.356 | 8.202 | 8.297 | 8.366 |
| Al | 7.219 | 7.166 | 7.208 | 7.242 | 7.271 | 7.079 | 7.638 | 7.556 | 7.641 | 7.543 | 7.508 |
| Fe(ii) | 0.035 | 0.058 | 0.000 | 0.056 | 0.047 | 0.069 | 0.000 | 0.034 | 0.000 | 0.000 | 0.000 |
| Ca | 3.627 | 3.519 | 3.642 | 3.627 | 3.621 | 3.467 | 3.987 | 3.867 | 4.075 | 4.000 | 3.922 |
| Na | 0.486 | 0.506 | 0.463 | 0.494 | 0.441 | 0.566 | 0.126 | 0.104 | 0.122 | 0.183 | 0.169 |
| K | 0.000 | 0.000 | 0.000 | 0.000 | 0.000 | 0.000 | 0.000 | 0.000 | 0.000 | 0.000 | 0.000 |
| Ba | 0.000 | 0.000 | 0.000 | 0.000 | 0.000 | 0.000 | 0.000 | 0.000 | 0.000 | 0.000 | 0.000 |
| TOTAL | 20.000 | 19.959 | 19.970 | 20.023 | 19.982 | 19.962 | 19.997 | 19.918 | 20.039 | 20.023 | 19.965 |
| **Endmembers** | | | | | | | | | | | |
| An | 88.19 | 87.43 | 88.72 | 88.01 | 89.15 | 85.96 | 96.94 | 97.38 | 97.10 | 95.63 | 95.87 |
| Ab | 11.81 | 12.57 | 11.28 | 11.99 | 10.85 | 14.04 | 3.06 | 2.62 | 2.90 | 4.37 | 4.13 |
| Or | 0.00 | 0.00 | 0.00 | 0.00 | 0.00 | 0.00 | 0.00 | 0.00 | 0.00 | 0.00 | 0.00 |
| Cn | | | | | | | | | | | |

**Alkali Feldspar**

| Sample | Ab7799 | Ab7799 | Ab7799 | Ab7801 | Ab7801 | Ab661 | Ab661 | Ab661 | Ab661 |
|---|---|---|---|---|---|---|---|---|---|
| Analysis No. | 4 | 5 | 1 | 44 | 45 | 3 | 4 | 29 | 5 |
| Analysis Name. | kfel1 | kfel2 | kfel3 | kfel1a | kfel1b | kfel1 | kfel2 | kfel | per-kfel3 |
| SiO2 | 66.45 | 66.59 | 66.63 | 65.54 | 65.51 | 64.07 | 64.30 | 64.48 | 64.10 |
| Al2O3 | 18.31 | 19.63 | 18.03 | 18.97 | 18.86 | 18.25 | 18.39 | 18.09 | 18.56 |
| FeO | 0.00 | 0.00 | 0.00 | 0.00 | 0.00 | 0.00 | 0.00 | 0.00 | 0.00 |
| CaO | 0.00 | 1.35 | 0.00 | 0.17 | 0.00 | 0.00 | 0.00 | 0.00 | 0.25 |
| Na2O | 1.11 | 5.79 | 1.15 | 1.48 | 1.13 | 1.07 | 1.60 | 1.27 | 1.36 |
| K2O | 15.71 | 7.72 | 15.28 | 14.51 | 14.86 | 14.29 | 13.88 | 14.35 | 13.88 |
| BaO | 0.47 | 0.33 | 0.33 | 1.94 | 2.27 | 1.93 | 2.18 | 1.72 | 2.60 |
| Total | 102.05 | 101.42 | 101.42 | 102.61 | 102.62 | 99.62 | 100.36 | 99.90 | 100.72 |
| **Formula (32O)** | | | | | | | | | |
| Si | 12.044 | 11.839 | 12.106 | 11.900 | 11.923 | 11.968 | 11.937 | 11.997 | 11.893 |
| Al | 3.911 | 4.113 | 3.861 | 4.059 | 4.045 | 4.018 | 4.024 | 3.966 | 4.058 |
| Fe(ii) | 0.000 | 0.000 | 0.000 | 0.000 | 0.000 | 0.000 | 0.000 | 0.000 | 0.000 |
| Ca | 0.000 | 0.257 | 0.000 | 0.033 | 0.000 | 0.000 | 0.000 | 0.000 | 0.050 |
| Na | 0.390 | 1.996 | 0.405 | 0.521 | 0.399 | 0.387 | 0.576 | 0.458 | 0.489 |
| K | 3.632 | 1.751 | 3.541 | 3.361 | 3.450 | 3.405 | 3.287 | 3.406 | 3.285 |
| Ba | 0.033 | 0.023 | 0.023 | 0.138 | 0.162 | 0.141 | 0.159 | 0.125 | 0.189 |
| TOTAL | 20.011 | 19.978 | 19.937 | 20.011 | 19.979 | 19.919 | 19.982 | 19.952 | 19.965 |
| **Endmembers** | | | | | | | | | |
| An | 0.00 | 6.39 | 0.00 | 0.82 | 0.00 | 0.00 | 0.00 | 0.00 | 1.24 |
| Ab | 9.62 | 49.56 | 10.20 | 12.85 | 9.94 | 9.85 | 14.32 | 11.48 | 12.19 |
| Or | 89.56 | 43.48 | 89.20 | 82.92 | 86.02 | 86.56 | 81.74 | 85.37 | 81.86 |
| Cn | 0.82 | 0.57 | 0.59 | 3.41 | 4.04 | 3.59 | 3.94 | 3.14 | 4.71 |

**Biotite**

| Sample | 9P | 9P | 9P | 9P | 9P | 9P | Ab82 | Ab82 | Ab82 | Ab82 | Ab82 | Ab135 | 85P | 85P | 85P | Ab3826 | Ab3826 |
|---|---|---|---|---|---|---|---|---|---|---|---|---|---|---|---|---|---|
| Analysis No. | 3 | 5 | 6 | 7 | 14 | 24 | 4 | 6 | 12 | 27 | 30 | 19 | 1 | 7 | 11 | 1 | 5 |
| Analysis Name. | bio1 | bio2 | bio3 | bio4 | bio5 | bio6 | bio1 | bio2 | biot3 | bio4 | bio5 | bio1 | bio1 | bio2 | bio3 | bio1 | bio2 |
| SiO2 | 37.64 | 37.83 | 37.64 | 37.48 | 37.58 | 37.74 | 38.24 | 39.99 | 39.09 | 38.92 | 40.13 | 37.77 | 36.57 | 36.07 | 36.42 | 34.93 | 35.59 |
| TiO2 | 4.54 | 5.38 | 4.64 | 5.09 | 5.41 | 5.00 | 4.52 | 4.53 | 4.53 | 4.71 | 4.53 | 2.76 | 4.13 | 4.88 | 4.31 | 4.77 | 5.33 |
| Al2O3 | 13.45 | 13.51 | 13.81 | 13.23 | 13.67 | 13.31 | 13.57 | 13.72 | 13.55 | 13.59 | 14.35 | 14.92 | 14.01 | 13.82 | 13.92 | 13.42 | 13.38 |
| Cr2O3 | 0.37 | 0.43 | 0.31 | 0.47 | 0.45 | 0.39 | 0.34 | 0.32 | 0.23 | 0.32 | 0.28 | 1.26 | 0.00 | 0.00 | 0.00 | 0.00 | 0.00 |
| FeO | 10.57 | 10.84 | 10.27 | 10.30 | 10.79 | 10.25 | 9.65 | 9.78 | 9.61 | 10.17 | 9.90 | 5.23 | 23.60 | 23.95 | 24.24 | 22.42 | 22.39 |
| MnO | 0.00 | 0.00 | 0.00 | 0.00 | 0.00 | 0.00 | 0.00 | 0.00 | 0.00 | 0.00 | 0.00 | 0.00 | 0.22 | 0.00 | 0.00 | 0.20 | 0.00 |
| MgO | 17.22 | 16.57 | 16.85 | 16.41 | 16.34 | 16.63 | 17.42 | 17.97 | 17.87 | 17.56 | 18.14 | 20.43 | 7.97 | 7.79 | 7.81 | 8.46 | 8.58 |
| CaO | 0.00 | 0.00 | 0.00 | 0.00 | 0.00 | 0.00 | 0.00 | 0.00 | 0.00 | 0.00 | 0.00 | 0.00 | 0.18 | 0.31 | 0.14 | 0.14 | 0.23 |
| Na2O | 0.00 | 0.00 | 0.00 | 0.00 | 0.00 | 0.00 | 0.48 | 0.41 | 0.34 | 0.46 | 0.35 | 0.66 | 0.32 | 0.42 | 0.30 | 0.00 | 0.20 |
| K2O | 9.68 | 9.24 | 9.53 | 9.71 | 9.57 | 9.37 | 8.98 | 9.17 | 9.23 | 9.05 | 9.51 | 9.08 | 9.79 | 9.17 | 9.52 | 9.11 | 8.97 |
| BaO | 0.00 | 0.00 | 0.00 | 0.00 | 0.00 | 0.00 | 0.00 | 0.00 | 0.00 | 0.00 | 0.00 | 0.00 | 0.00 | 0.00 | 0.00 | 0.00 | 0.00 |
| NiO | | | | | | | | | | | | | | | | | |
| Total | 93.47 | 93.79 | 93.05 | 92.70 | 93.80 | 92.69 | 93.47 | 96.20 | 94.46 | 94.80 | 97.18 | 92.12 | 96.79 | 96.42 | 96.66 | 93.46 | 94.66 |
| **Formula (22O)** | | | | | | | | | | | | | | | | | |
| Si | 5.633 | 5.631 | 5.640 | 5.654 | 5.606 | 5.674 | 5.688 | 5.764 | 5.729 | 5.700 | 5.714 | 5.583 | 5.640 | 5.583 | 5.629 | 5.559 | 5.572 |
| Al | 2.367 | 2.369 | 2.360 | 2.346 | 2.394 | 2.326 | 2.312 | 2.236 | 2.271 | 2.300 | 2.286 | 2.417 | 2.360 | 2.417 | 2.371 | 2.441 | 2.428 |
| Al | 0.005 | 0.001 | 0.078 | 0.006 | 0.009 | 0.032 | 0.067 | 0.094 | 0.069 | 0.045 | 0.122 | 0.183 | 0.185 | 0.104 | 0.164 | 0.075 | 0.040 |
| Cr | 0.044 | 0.051 | 0.037 | 0.056 | 0.053 | 0.046 | 0.040 | 0.036 | 0.027 | 0.037 | 0.032 | 0.147 | 0.000 | 0.000 | 0.000 | 0.000 | 0.000 |
| Ti | 0.511 | 0.602 | 0.523 | 0.578 | 0.607 | 0.565 | 0.506 | 0.491 | 0.499 | 0.519 | 0.485 | 0.307 | 0.479 | 0.568 | 0.501 | 0.571 | 0.628 |
| Fe(ii) | 1.323 | 1.349 | 1.287 | 1.299 | 1.346 | 1.289 | 1.200 | 1.179 | 1.178 | 1.245 | 1.179 | 0.646 | 3.043 | 3.100 | 3.133 | 2.983 | 2.931 |
| Mn | 0.000 | 0.000 | 0.000 | 0.000 | 0.000 | 0.000 | 0.000 | 0.000 | 0.000 | 0.000 | 0.000 | 0.000 | 0.029 | 0.000 | 0.000 | 0.027 | 0.000 |
| Mg | 3.842 | 3.677 | 3.764 | 3.691 | 3.634 | 3.727 | 3.863 | 3.861 | 3.904 | 3.834 | 3.851 | 4.502 | 1.832 | 1.796 | 1.800 | 2.007 | 2.003 |
| Ca | 0.000 | 0.000 | 0.000 | 0.000 | 0.000 | 0.000 | 0.000 | 0.000 | 0.000 | 0.000 | 0.000 | 0.000 | 0.030 | 0.051 | 0.023 | 0.024 | 0.039 |
| Na | 0.000 | 0.000 | 0.000 | 0.000 | 0.000 | 0.000 | 0.138 | 0.115 | 0.097 | 0.131 | 0.097 | 0.189 | 0.095 | 0.125 | 0.090 | 0.000 | 0.061 |
| K | 1.848 | 1.754 | 1.821 | 1.869 | 1.821 | 1.797 | 1.704 | 1.686 | 1.725 | 1.691 | 1.727 | 1.712 | 1.926 | 1.811 | 1.877 | 1.849 | 1.791 |
| Ba | 0.000 | 0.000 | 0.000 | 0.000 | 0.000 | 0.000 | 0.000 | 0.000 | 0.000 | 0.000 | 0.000 | 0.000 | 0.000 | 0.000 | 0.000 | 0.000 | 0.000 |
| Ni | | | | | | | | | | | | | | | | | |
| TOTAL | 15.572 | 15.434 | 15.510 | 15.498 | 15.470 | 15.457 | 15.518 | 15.462 | 15.499 | 15.501 | 15.493 | 15.687 | 15.619 | 15.556 | 15.586 | 15.537 | 15.492 |

**Biotite**

| Sample | Ab3826 | Ab92 | Ab92 | Ab1310 | Ab1310 | Ab5613 | Ab5613 | Ab5613 | Ab7799 | Ab7799 | Ab7801 | Ab7801 | Ab7801 | Ab7801 | Ab7801 | Ab7802 |
|---|---|---|---|---|---|---|---|---|---|---|---|---|---|---|---|---|
| Analysis No. | 17 | 6 | 7 | 1 | 13 | 4 | 9 | 41 | 8 | 20 | 1 | 7 | 17 | 21 | 29 | 1 |
| Analysis Name. | bio3 | bio1 | bio2 | bio1 | bio2 | bio1 | bio2 | bio3 | bio2 | bio3 | bio1 | bio2 | bio3 | bio4 | bio5 | bio1 |
| SiO2 | 35.22 | 36.33 | 36.07 | 36.05 | 36.02 | 36.01 | 35.77 | 35.33 | 33.78 | 32.70 | 35.59 | 36.72 | 36.38 | 35.98 | 36.49 | 36.62 |
| TiO2 | 5.12 | 4.56 | 4.44 | 4.20 | 4.57 | 5.53 | 5.24 | 5.07 | 4.04 | 0.96 | 6.56 | 5.71 | 5.71 | 6.45 | 5.97 | 6.06 |
| Al2O3 | 13.23 | 14.29 | 14.17 | 14.34 | 14.38 | 13.02 | 13.23 | 12.82 | 13.26 | 13.77 | 13.46 | 14.14 | 14.12 | 14.03 | 14.20 | 13.63 |
| Cr2O3 | 0.00 | 0.00 | 0.00 | 0.00 | 0.00 | 0.00 | 0.00 | 0.00 | 0.00 | 0.00 | 0.00 | 0.00 | 0.00 | 0.00 | 0.00 | 0.00 |
| FeO | 22.20 | 25.43 | 24.62 | 26.82 | 26.96 | 16.94 | 15.73 | 16.42 | 36.56 | 38.35 | 24.52 | 22.42 | 23.03 | 23.18 | 24.15 | 19.22 |
| MnO | 0.00 | 0.00 | 0.00 | 0.00 | 0.00 | 0.00 | 0.00 | 0.00 | 0.29 | 0.33 | 0.00 | 0.00 | 0.00 | 0.00 | 0.00 | 0.00 |
| MgO | 8.85 | 7.71 | 7.60 | 6.83 | 6.76 | 11.99 | 12.37 | 11.98 | 0.45 | 0.39 | 7.26 | 9.56 | 9.15 | 8.00 | 8.05 | 10.72 |
| CaO | 0.31 | 0.00 | 0.00 | 0.20 | 0.00 | 0.00 | 0.16 | 0.00 | 0.17 | 0.20 | 0.00 | 0.00 | 0.00 | 0.00 | 0.00 | 0.00 |
| Na2O | 0.38 | 0.35 | 0.22 | 0.42 | 0.26 | 0.20 | 0.23 | 0.00 | 0.00 | 0.22 | 0.00 | 0.23 | 0.39 | 0.23 | 0.00 | 0.00 |
| K2O | 8.70 | 9.44 | 9.34 | 8.94 | 9.44 | 9.17 | 8.79 | 9.12 | 8.02 | 7.36 | 9.14 | 9.52 | 9.87 | 9.64 | 9.87 | 9.34 |
| BaO | 0.00 | 0.00 | 0.00 | 0.00 | 0.00 | 0.00 | 0.00 | 0.00 | 0.00 | 0.00 | 0.00 | 0.00 | 0.00 | 0.00 | 0.00 | 0.00 |
| NiO | | | | | | | | | | | | | | | | |
| Total | 94.01 | 98.09 | 96.45 | 97.79 | 98.39 | 92.86 | 91.76 | 90.99 | 96.57 | 94.29 | 97.26 | 98.30 | 98.64 | 97.51 | 99.27 | 95.59 |
| **Formula (22O)** | | | | | | | | | | | | | | | | |
| Si | 5.553 | 5.554 | 5.590 | 5.558 | 5.533 | 5.601 | 5.605 | 5.618 | 5.552 | 5.567 | 5.514 | 5.521 | 5.486 | 5.491 | 5.515 | 5.577 |
| Al | 2.447 | 2.446 | 2.410 | 2.442 | 2.467 | 2.387 | 2.395 | 2.382 | 2.448 | 2.433 | 2.458 | 2.479 | 2.510 | 2.509 | 2.485 | 2.423 |
| Al | 0.011 | 0.129 | 0.178 | 0.163 | 0.136 | 0.000 | 0.048 | 0.020 | 0.120 | 0.329 | 0.000 | 0.027 | 0.000 | 0.015 | 0.045 | 0.023 |
| Cr | 0.000 | 0.000 | 0.000 | 0.000 | 0.000 | 0.000 | 0.000 | 0.000 | 0.000 | 0.000 | 0.000 | 0.000 | 0.000 | 0.000 | 0.000 | 0.000 |
| Ti | 0.607 | 0.524 | 0.518 | 0.487 | 0.528 | 0.647 | 0.618 | 0.606 | 0.499 | 0.123 | 0.764 | 0.646 | 0.648 | 0.740 | 0.679 | 0.694 |
| Fe(ii) | 2.927 | 3.251 | 3.191 | 3.457 | 3.463 | 2.203 | 2.061 | 2.183 | 5.024 | 5.459 | 3.177 | 2.819 | 2.904 | 2.958 | 3.052 | 2.448 |
| Mn | 0.000 | 0.000 | 0.000 | 0.000 | 0.000 | 0.000 | 0.000 | 0.000 | 0.040 | 0.048 | 0.000 | 0.000 | 0.000 | 0.000 | 0.000 | 0.000 |
| Mg | 2.080 | 1.757 | 1.756 | 1.570 | 1.548 | 2.780 | 2.890 | 2.840 | 0.110 | 0.099 | 1.677 | 2.143 | 2.057 | 1.820 | 1.814 | 2.434 |
| Ca | 0.052 | 0.000 | 0.000 | 0.033 | 0.000 | 0.000 | 0.027 | 0.000 | 0.030 | 0.036 | 0.000 | 0.000 | 0.000 | 0.000 | 0.000 | 0.000 |
| Na | 0.116 | 0.104 | 0.066 | 0.126 | 0.077 | 0.060 | 0.070 | 0.000 | 0.000 | 0.073 | 0.000 | 0.067 | 0.114 | 0.068 | 0.000 | 0.000 |
| K | 1.750 | 1.841 | 1.846 | 1.758 | 1.850 | 1.819 | 1.757 | 1.850 | 1.681 | 1.598 | 1.806 | 1.826 | 1.899 | 1.877 | 1.903 | 1.814 |
| Ba | 0.000 | 0.000 | 0.000 | 0.000 | 0.000 | 0.000 | 0.000 | 0.000 | 0.000 | 0.000 | 0.000 | 0.000 | 0.000 | 0.000 | 0.000 | 0.000 |
| Ni | | | | | | | | | | | | | | | | |
| TOTAL | 15.544 | 15.606 | 15.555 | 15.594 | 15.601 | 15.498 | 15.470 | 15.500 | 15.505 | 15.765 | 15.396 | 15.527 | 15.618 | 15.479 | 15.493 | 15.413 |

**Biotite**

| Sample | Ab7802 | Ab7802 | MS1595 | MS1595 | MS1595 | Ab93 | Ab93 | Ab93 | Ab243 | Ab243 | Ab243 | Ab661 | Ab661 | Ab661 | V(Ol) | V(Ol) |
|---|---|---|---|---|---|---|---|---|---|---|---|---|---|---|---|---|
| Analysis No. | 13 | 24 | 5 | 9 | 29 | 4 | 18 | 22 | 8 | 17 | 31 | 1 | 12 | 14 | 7 | 29 |
| Analysis Name. | bio2 | bio3 | bio1 | bio2 | bio3 | bio1 | bio2 | bio4 | bio1 | bio2 | bio3 | bio1 | bio2 | bio3 | bio1 | bio2 |
| SiO2 | 37.06 | 36.49 | 37.91 | 37.12 | 37.96 | 35.96 | 36.71 | 35.60 | 34.88 | 34.60 | 35.17 | 32.15 | 33.61 | 32.27 | 36.75 | 36.99 |
| TiO2 | 5.81 | 5.44 | 3.00 | 3.18 | 3.18 | 4.84 | 3.72 | 2.42 | 6.04 | 5.79 | 5.25 | 3.19 | 3.97 | 3.67 | 4.44 | 5.02 |
| Al2O3 | 13.82 | 13.80 | 15.15 | 15.63 | 15.48 | 15.01 | 15.14 | 16.01 | 14.27 | 13.75 | 13.89 | 14.12 | 13.60 | 14.20 | 14.87 | 14.88 |
| Cr2O3 | 0.00 | 0.00 | 0.00 | 0.00 | 0.00 | 0.00 | 0.00 | 0.00 | 0.00 | 0.00 | 0.00 | 0.00 | 0.00 | 0.00 | 0.00 | 0.00 |
| FeO | 19.65 | 19.28 | 6.51 | 7.00 | 6.30 | 13.20 | 13.57 | 12.96 | 20.83 | 19.60 | 20.78 | 33.42 | 33.33 | 33.62 | 12.98 | 13.02 |
| MnO | 0.00 | 0.00 | 0.00 | 0.00 | 0.00 | 0.00 | 0.00 | 0.00 | 0.00 | 0.00 | 0.00 | 0.27 | 0.39 | 0.00 | 0.00 | 0.00 |
| MgO | 11.06 | 10.87 | 20.25 | 19.98 | 20.09 | 14.18 | 14.99 | 16.87 | 9.69 | 10.08 | 9.83 | 2.48 | 2.32 | 2.40 | 14.55 | 15.58 |
| CaO | 0.00 | 0.00 | 0.23 | 0.26 | 0.12 | 0.00 | 0.00 | 0.18 | 0.00 | 0.00 | 0.00 | 0.33 | 0.41 | 0.23 | 0.00 | 0.00 |
| Na2O | 0.28 | 0.22 | 1.36 | 1.11 | 1.50 | 0.00 | 0.00 | 0.00 | 0.30 | 0.36 | 0.00 | 0.00 | 0.00 | 0.23 | 0.00 | 0.00 |
| K2O | 9.57 | 9.44 | 6.89 | 6.59 | 7.58 | 9.58 | 9.69 | 8.29 | 8.59 | 8.69 | 8.74 | 6.57 | 7.62 | 6.88 | 9.80 | 9.90 |
| BaO | 0.00 | 0.00 | 0.00 | 0.00 | 0.00 | 0.00 | 0.00 | 0.00 | 2.32 | 1.50 | 1.38 | 0.00 | 0.00 | 0.00 | 0.00 | 0.75 |
| NiO | | | | | | | | | | | | | | | | |
| Total | 97.26 | 95.55 | 91.30 | 90.86 | 92.19 | 92.76 | 93.82 | 92.32 | 97.09 | 94.37 | 95.04 | 92.53 | 95.25 | 93.50 | 93.59 | 96.14 |
| **Formula (22O)** | | | | | | | | | | | | | | | | |
| Si | 5.562 | 5.570 | 5.609 | 5.523 | 5.578 | 5.493 | 5.545 | 5.416 | 5.381 | 5.433 | 5.490 | 5.421 | 5.510 | 5.390 | 5.566 | 5.478 |
| Al | 2.438 | 2.430 | 2.391 | 2.477 | 2.422 | 2.507 | 2.455 | 2.584 | 2.594 | 2.544 | 2.510 | 2.579 | 2.490 | 2.610 | 2.434 | 2.522 |
| Al | 0.007 | 0.053 | 0.250 | 0.264 | 0.259 | 0.195 | 0.240 | 0.286 | 0.000 | 0.000 | 0.045 | 0.227 | 0.138 | 0.185 | 0.220 | 0.075 |
| Cr | 0.000 | 0.000 | 0.000 | 0.000 | 0.000 | | | | 0.000 | 0.000 | 0.000 | | | | 0.000 | 0.000 |
| Ti | 0.656 | 0.625 | 0.334 | 0.356 | 0.351 | 0.556 | 0.423 | 0.277 | 0.701 | 0.684 | 0.616 | 0.405 | 0.490 | 0.461 | 0.506 | 0.559 |
| Fe(ii) | 2.466 | 2.461 | 0.805 | 0.871 | 0.774 | 1.686 | 1.714 | 1.649 | 2.687 | 2.573 | 2.712 | 4.712 | 4.569 | 4.696 | 1.644 | 1.612 |
| Mn | 0.000 | 0.000 | 0.000 | 0.000 | 0.000 | 0.000 | 0.000 | 0.000 | 0.000 | 0.000 | 0.000 | 0.039 | 0.054 | 0.000 | 0.000 | 0.000 |
| Mg | 2.475 | 2.474 | 4.466 | 4.432 | 4.401 | 3.229 | 3.375 | 3.826 | 2.228 | 2.360 | 2.288 | 0.623 | 0.567 | 0.598 | 3.285 | 3.440 |
| Ca | 0.000 | 0.000 | 0.036 | 0.041 | 0.019 | 0.000 | 0.000 | 0.029 | 0.000 | 0.000 | 0.000 | 0.060 | 0.072 | 0.041 | 0.000 | 0.000 |
| Na | 0.081 | 0.065 | 0.390 | 0.320 | 0.427 | 0.000 | 0.000 | 0.000 | 0.090 | 0.110 | 0.000 | 0.000 | 0.000 | 0.074 | 0.000 | 0.000 |
| K | 1.832 | 1.838 | 1.300 | 1.251 | 1.421 | 1.867 | 1.867 | 1.609 | 1.690 | 1.741 | 1.740 | 1.413 | 1.594 | 1.466 | 1.893 | 1.870 |
| Ba | 0.000 | 0.000 | 0.000 | 0.000 | 0.000 | 0.000 | 0.000 | 0.000 | 0.140 | 0.092 | 0.084 | 0.000 | 0.000 | 0.000 | 0.000 | 0.044 |
| Ni | | | | | | | | | | | | | | | | |
| TOTAL | 15.517 | 15.515 | 15.582 | 15.536 | 15.654 | 15.533 | 15.619 | 15.676 | 15.511 | 15.536 | 15.486 | 15.478 | 15.483 | 15.521 | 15.548 | 15.600 |

**Biotite**

| Sample | V(Ol) | 773C | Ab94 | Ab94 | Ab94 | Ab94 | Ab94 | 77P | 77P | 77P | 77P | CLW218 | CLW218 | CLW218 | CLW106 | CLW106 |
|---|---|---|---|---|---|---|---|---|---|---|---|---|---|---|---|---|
| Analysis No. | 30 | 18 | 10 | 14 | 17 | 23 | 26 | 7 | 13 | 14 | 19 | 5 | 9 | 11 | 5 | 13 |
| Analysis Name. | bio3 | bio2 | bio1 | bio2 | bio3 | bio4 | bio5 | bio1 | bio2 | bio3 | bio4 | bio1 | bio2 | bio3 | bio1 | bio2 |
| SiO2 | 36.40 | 38.46 | 37.78 | 38.03 | 37.02 | 37.79 | 37.30 | 35.71 | 35.83 | 35.29 | 36.65 | 36.13 | 35.80 | 36.49 | 37.69 | 37.99 |
| TiO2 | 6.07 | 0.97 | 5.32 | 5.18 | 4.93 | 5.58 | 4.81 | 4.43 | 5.00 | 5.61 | 4.93 | 4.71 | 4.60 | 4.95 | 3.88 | 2.69 |
| Al2O3 | 14.05 | 14.97 | 13.64 | 13.95 | 13.66 | 13.78 | 13.88 | 14.63 | 14.65 | 14.10 | 14.76 | 13.33 | 14.07 | 13.84 | 15.04 | 15.49 |
| Cr2O3 | 0.00 | 0.24 | 0.00 | 0.00 | 0.00 | 0.00 | 0.00 | 0.00 | 0.00 | 0.00 | 0.00 | 0.00 | 0.00 | 0.20 | 0.75 | 0.00 |
| FeO | 10.75 | 9.90 | 18.72 | 18.96 | 19.77 | 19.23 | 18.50 | 17.39 | 17.80 | 18.36 | 16.53 | 17.73 | 18.28 | 15.89 | 8.89 | 8.99 |
| MnO | 0.00 | 0.00 | 0.00 | 0.00 | 0.00 | 0.00 | 0.00 | 0.00 | 0.00 | 0.00 | 0.00 | 0.00 | 0.36 | 0.00 | 0.00 | 0.00 |
| MgO | 15.21 | 17.49 | 11.70 | 11.60 | 11.32 | 11.35 | 11.67 | 11.94 | 11.73 | 11.08 | 13.08 | 12.26 | 12.04 | 12.92 | 18.18 | 18.67 |
| CaO | 1.59 | 1.34 | 0.00 | 0.00 | 0.00 | 0.00 | 0.00 | 0.00 | 0.00 | 0.00 | 0.00 | 0.18 | 0.00 | 0.00 | 0.00 | 0.00 |
| Na2O | 0.00 | 0.00 | 0.29 | 0.24 | 0.29 | 0.34 | 0.31 | 0.23 | 0.00 | 0.22 | 0.00 | 0.00 | 0.26 | 0.00 | 0.59 | 0.51 |
| K2O | 9.50 | 7.28 | 9.57 | 9.74 | 9.33 | 9.44 | 8.96 | 9.41 | 9.36 | 9.26 | 9.32 | 8.52 | 8.56 | 9.02 | 8.09 | 8.21 |
| BaO | 0.51 | 0.00 | 0.58 | 0.46 | 0.96 | 0.48 | 1.12 | 0.80 | 1.10 | 1.61 | 0.00 | 0.95 | 1.02 | 0.50 | 0.61 | 0.62 |
| NiO | | | | | | | | | | | | | | | | |
| Total | 94.11 | 90.64 | 97.60 | 98.14 | 97.27 | 98.00 | 96.85 | 94.55 | 95.47 | 95.54 | 95.50 | 93.80 | 94.98 | 93.80 | 93.88 | 93.19 |
| **Formula (22O)** | | | | | | | | | | | | | | | | |
| Si | 5.470 | 5.813 | 5.639 | 5.642 | 5.593 | 5.622 | 5.632 | 5.501 | 5.480 | 5.446 | 5.520 | 5.597 | 5.506 | 5.589 | 5.557 | 5.619 |
| Al | 2.488 | 2.187 | 2.361 | 2.358 | 2.407 | 2.378 | 2.368 | 2.499 | 2.520 | 2.554 | 2.480 | 2.403 | 2.494 | 2.411 | 2.443 | 2.381 |
| Al | 0.000 | 0.479 | 0.039 | 0.081 | 0.025 | 0.038 | 0.102 | 0.156 | 0.120 | 0.010 | 0.140 | 0.031 | 0.056 | 0.088 | 0.171 | 0.320 |
| Cr | 0.000 | 0.029 | 0.000 | 0.000 | 0.000 | 0.000 | 0.000 | 0.000 | 0.000 | 0.000 | 0.000 | 0.000 | 0.000 | 0.024 | 0.087 | 0.000 |
| Ti | 0.686 | 0.110 | 0.597 | 0.578 | 0.560 | 0.624 | 0.546 | 0.513 | 0.575 | 0.651 | 0.558 | 0.549 | 0.532 | 0.570 | 0.430 | 0.299 |
| Fe(ii) | 1.351 | 1.251 | 2.337 | 2.352 | 2.498 | 2.392 | 2.336 | 2.240 | 2.276 | 2.369 | 2.082 | 2.297 | 2.351 | 2.035 | 1.096 | 1.112 |
| Mn | 0.000 | 0.000 | 0.000 | 0.000 | 0.000 | 0.000 | 0.000 | 0.000 | 0.000 | 0.000 | 0.000 | 0.000 | 0.047 | 0.000 | 0.000 | 0.000 |
| Mg | 3.408 | 3.941 | 2.604 | 2.566 | 2.550 | 2.517 | 2.627 | 2.742 | 2.674 | 2.549 | 2.937 | 2.831 | 2.761 | 2.950 | 3.996 | 4.117 |
| Ca | 0.256 | 0.217 | 0.000 | 0.000 | 0.000 | 0.000 | 0.000 | 0.000 | 0.000 | 0.000 | 0.000 | 0.030 | 0.000 | 0.000 | 0.000 | 0.000 |
| Na | 0.000 | 0.000 | 0.084 | 0.069 | 0.085 | 0.098 | 0.091 | 0.069 | 0.000 | 0.066 | 0.000 | 0.000 | 0.078 | 0.000 | 0.169 | 0.146 |
| K | 1.821 | 1.404 | 1.822 | 1.843 | 1.798 | 1.791 | 1.726 | 1.849 | 1.826 | 1.823 | 1.790 | 1.684 | 1.679 | 1.762 | 1.522 | 1.549 |
| Ba | 0.030 | 0.000 | 0.034 | 0.027 | 0.057 | 0.028 | 0.066 | 0.048 | 0.066 | 0.097 | 0.000 | 0.058 | 0.061 | 0.030 | 0.035 | 0.036 |
| Ni | | | | | | | | | | | | | | | | |
| TOTAL | 15.510 | 15.431 | 15.517 | 15.516 | 15.572 | 15.490 | 15.495 | 15.617 | 15.538 | 15.565 | 15.507 | 15.479 | 15.565 | 15.460 | 15.507 | 15.579 |

**Biotite**

| Sample | CLW106 | CLW106 | CLW106 | CLW107 | CLW107 | CLW107 | CLW107 | CLW110 | CLW110 | CLW110 |
|---|---|---|---|---|---|---|---|---|---|---|
| Analysis No. | 22 | 23 | 29 | 2 | 8 | 20 | 22 | 15 | 16 | 17 |
| Analysis Name. | bio3 | bio4 | bio5 | bio1 | bio2 | bio3 | bio4 | bio1 | bio2 | bio3 |
| SiO2 | 38.01 | 37.47 | 37.71 | 37.91 | 37.06 | 37.86 | 37.52 | 35.49 | 36.67 | 36.81 |
| TiO2 | 3.16 | 3.32 | 2.48 | 2.08 | 2.38 | 1.14 | 1.71 | 4.59 | 4.57 | 4.13 |
| Al2O3 | 15.44 | 14.77 | 15.30 | 15.62 | 15.53 | 16.10 | 15.51 | 13.92 | 13.65 | 14.32 |
| Cr2O3 | 0.32 | 0.00 | 0.00 | 0.39 | 0.19 | 0.26 | 0.34 | 0.00 | 0.00 | 0.00 |
| FeO | 8.75 | 10.48 | 8.23 | 7.50 | 8.51 | 6.65 | 7.99 | 16.42 | 15.80 | 15.42 |
| MnO | 0.00 | 0.00 | 0.00 | 0.00 | 0.00 | 0.00 | 0.00 | 0.24 | 0.00 | 0.00 |
| MgO | 18.27 | 16.90 | 18.99 | 20.21 | 19.89 | 20.78 | 19.72 | 13.13 | 13.46 | 13.67 |
| CaO | 0.00 | 0.00 | 0.00 | 0.00 | 0.00 | 0.00 | 0.00 | 0.16 | 0.00 | 0.13 |
| Na2O | 0.73 | 0.47 | 0.50 | 0.37 | 0.30 | 0.51 | 0.53 | 0.21 | 0.00 | 0.35 |
| K2O | 8.18 | 8.36 | 8.15 | 9.51 | 8.67 | 9.24 | 9.10 | 7.45 | 8.90 | 8.63 |
| BaO | 0.77 | 0.85 | 0.44 | 0.00 | 0.49 | 0.00 | 0.00 | 0.00 | 0.71 | 0.00 |
| NiO | | | | 0.00 | 0.00 | 0.28 | 0.00 | | | |
| Total | 93.61 | 92.62 | 91.78 | 93.56 | 93.00 | 92.81 | 92.42 | 91.61 | 93.97 | 93.69 |
| **Formula (22O)** | | | | | | | | | | |
| Si | 5.604 | 5.641 | 5.634 | 5.566 | 5.503 | 5.577 | 5.584 | 5.533 | 5.619 | 5.608 |
| Al | 2.396 | 2.359 | 2.366 | 2.434 | 2.497 | 2.423 | 2.416 | 2.467 | 2.381 | 2.392 |
| Al | 0.286 | 0.262 | 0.328 | 0.268 | 0.221 | 0.372 | 0.304 | 0.090 | 0.084 | 0.179 |
| Cr | 0.037 | 0.000 | 0.000 | 0.045 | 0.022 | 0.030 | 0.040 | 0.000 | 0.000 | 0.000 |
| Ti | 0.350 | 0.376 | 0.279 | 0.230 | 0.266 | 0.126 | 0.191 | 0.538 | 0.527 | 0.473 |
| Fe(ii) | 1.079 | 1.319 | 1.028 | 0.921 | 1.057 | 0.819 | 0.994 | 2.140 | 2.024 | 1.964 |
| Mn | 0.000 | 0.000 | 0.000 | 0.000 | 0.000 | 0.000 | 0.000 | 0.032 | 0.000 | 0.000 |
| Mg | 4.015 | 3.793 | 4.230 | 4.423 | 4.403 | 4.563 | 4.375 | 3.051 | 3.075 | 3.105 |
| Ca | 0.000 | 0.000 | 0.000 | 0.000 | 0.000 | 0.000 | 0.000 | 0.027 | 0.000 | 0.021 |
| Na | 0.209 | 0.137 | 0.145 | 0.105 | 0.086 | 0.146 | 0.153 | 0.063 | 0.000 | 0.103 |
| K | 1.538 | 1.606 | 1.553 | 1.781 | 1.642 | 1.736 | 1.727 | 1.481 | 1.740 | 1.677 |
| Ba | 0.044 | 0.050 | 0.026 | 0.000 | 0.029 | 0.000 | 0.000 | 0.000 | 0.043 | 0.000 |
| Ni | | | | 0.000 | 0.000 | 0.033 | 0.000 | | | |
| TOTAL | 15.559 | 15.544 | 15.589 | 15.774 | 15.725 | 15.825 | 15.785 | 15.423 | 15.492 | 15.523 |

**Amphibole**

| Sample | 9P | 9P | 9P | Ab140 | 85P | Ab3826 | Ab3826 | Ab3826 | Ab3826 | Ab3826 | Ab3826 | Ab92 | Ab92 | Ab92 | Ab1310 | Ab1310 |
|---|---|---|---|---|---|---|---|---|---|---|---|---|---|---|---|---|
| Analysis No. | 12 | 15 | 17 | 54 | 6 | 3 | 7 | 11 | 20 | 22 | 38 | 1 | 13 | 16 | 6 | 14 |
| Analysis Name. | hbl1 | hbl2 | hbl3 | cor4 | amph1 | amph1 | amph2 | amph3 | amph4a | amph4b | amph7 | amph1 | amph2 | amph4b | amph1 | amph2 |
| SiO2 | 50.32 | 49.24 | 49.62 | 43.51 | 44.61 | 44.59 | 44.69 | 45.16 | 44.45 | 45.30 | 45.26 | 44.64 | 44.09 | 44.52 | 44.16 | 44.68 |
| TiO2 | 1.09 | 1.47 | 1.34 | 1.34 | 1.88 | 1.33 | 1.56 | 1.54 | 1.38 | 1.43 | 1.68 | 1.60 | 2.06 | 1.72 | 1.59 | 1.74 |
| Al2O3 | 5.52 | 6.07 | 6.00 | 14.14 | 8.58 | 8.13 | 7.73 | 8.00 | 8.18 | 7.61 | 8.19 | 9.11 | 9.39 | 9.55 | 9.73 | 9.32 |
| Cr2O3 | 0.25 | 0.41 | 0.21 | 0.47 | 0.00 | 0.00 | 0.00 | 0.00 | 0.00 | 0.00 | 0.00 | 0.25 | 0.00 | 0.00 | 0.00 | 0.00 |
| FeO | 7.97 | 8.56 | 8.73 | 4.35 | 20.85 | 19.74 | 20.55 | 19.40 | 19.40 | 19.90 | 19.29 | 22.53 | 22.79 | 21.43 | 25.70 | 26.27 |
| MnO | 0.00 | 0.00 | 0.00 | 0.00 | 0.32 | 0.00 | 0.28 | 0.00 | 0.38 | 0.30 | 0.24 | 0.00 | 0.43 | 0.00 | 0.29 | 0.00 |
| MgO | 17.70 | 16.90 | 16.95 | 16.94 | 7.54 | 9.47 | 8.98 | 9.35 | 9.28 | 9.43 | 9.28 | 7.72 | 7.33 | 8.00 | 6.42 | 6.78 |
| CaO | 11.64 | 11.84 | 11.71 | 12.61 | 11.89 | 10.80 | 10.74 | 11.20 | 11.16 | 11.02 | 10.87 | 11.03 | 11.00 | 11.18 | 10.68 | 10.16 |
| Na2O | 0.65 | 0.80 | 0.57 | 2.02 | 1.18 | 1.31 | 1.19 | 1.22 | 1.21 | 1.21 | 1.10 | 1.37 | 1.39 | 1.43 | 1.53 | 1.20 |
| K2O | 0.32 | 0.53 | 0.43 | 0.67 | 1.11 | 0.72 | 0.75 | 0.71 | 0.71 | 0.76 | 0.78 | 1.11 | 1.11 | 0.97 | 0.66 | 0.73 |
| Total | 95.45 | 95.81 | 95.56 | 96.04 | 97.96 | 96.08 | 96.47 | 96.57 | 96.15 | 96.97 | 96.67 | 99.37 | 99.60 | 98.80 | 100.75 | 100.88 |
| **Formula (23O)** | | | | | | | | | | | | | | | | |
| Si | 7.293 | 7.165 | 7.221 | 6.279 | 6.810 | 6.861 | 6.883 | 6.898 | 6.843 | 6.917 | 6.898 | 6.742 | 6.669 | 6.722 | 6.657 | 6.715 |
| Al | 0.707 | 0.835 | 0.779 | 1.721 | 1.190 | 1.139 | 1.117 | 1.102 | 1.157 | 1.083 | 1.102 | 1.258 | 1.331 | 1.278 | 1.343 | 1.285 |
| Al | 0.236 | 0.206 | 0.250 | 0.684 | 0.350 | 0.335 | 0.286 | 0.338 | 0.327 | 0.287 | 0.369 | 0.363 | 0.342 | 0.421 | 0.386 | 0.366 |
| Fe(iii) | 0.607 | 0.428 | 0.560 | 0.185 | 0.000 | 0.702 | 0.736 | 0.429 | 0.573 | 0.620 | 0.560 | 0.554 | 0.583 | 0.429 | 0.990 | 1.315 |
| Cr | 0.029 | 0.047 | 0.024 | 0.054 | 0.000 | 0.000 | 0.000 | 0.000 | 0.000 | 0.000 | 0.000 | 0.030 | 0.000 | 0.000 | 0.000 | 0.000 |
| Ti | 0.119 | 0.161 | 0.147 | 0.145 | 0.220 | 0.154 | 0.181 | 0.177 | 0.160 | 0.164 | 0.193 | 0.182 | 0.234 | 0.195 | 0.180 | 0.197 |
| Fe(ii) | 0.408 | 0.662 | 0.557 | 0.350 | 2.660 | 1.917 | 1.998 | 2.137 | 2.004 | 2.005 | 1.992 | 2.372 | 2.379 | 2.357 | 2.336 | 2.091 |
| Mn | 0.000 | 0.000 | 0.000 | 0.000 | 0.040 | 0.000 | 0.037 | 0.000 | 0.050 | 0.039 | 0.031 | 0.000 | 0.055 | 0.000 | 0.037 | 0.000 |
| Mg | 3.825 | 3.666 | 3.677 | 3.645 | 1.720 | 2.172 | 2.062 | 2.129 | 2.130 | 2.147 | 2.109 | 1.738 | 1.653 | 1.801 | 1.443 | 1.519 |
| Ca | 1.807 | 1.846 | 1.826 | 1.950 | 1.940 | 1.780 | 1.772 | 1.833 | 1.841 | 1.803 | 1.775 | 1.785 | 1.782 | 1.808 | 1.725 | 1.636 |
| Na | 0.183 | 0.226 | 0.161 | 0.565 | 0.350 | 0.391 | 0.355 | 0.361 | 0.361 | 0.358 | 0.325 | 0.401 | 0.408 | 0.419 | 0.447 | 0.350 |
| K | 0.059 | 0.098 | 0.080 | 0.123 | 0.220 | 0.141 | 0.147 | 0.138 | 0.139 | 0.148 | 0.152 | 0.214 | 0.214 | 0.187 | 0.127 | 0.140 |
| TOTAL | 15.272 | 15.340 | 15.280 | 15.701 | 15.490 | 15.593 | 15.574 | 15.542 | 15.585 | 15.571 | 15.506 | 15.639 | 15.650 | 15.617 | 15.671 | 15.613 |

**Amphibole**

| Sample | Ab7799 | Ab7799 | Ab93 | Ab661 | Ab661 | Ab661 | Ab661 | Ab661 | Ab661 | Ab661 | V(Ol) | V(Ol) | DV1 | DV1 | DV1 | DV1 | DV1 |
|---|---|---|---|---|---|---|---|---|---|---|---|---|---|---|---|---|---|
| Analysis No. | 5 | 19 | 3 | 2 | 7 | 11 | 21 | 16 | 17 | 22 | 11 | 28 | 12 | 16 | 20 | 21 | 22 |
| Analysis Name. | amph1 | amph3 | amphcor1 | hbl1 | hbl2 | hbl3 | hbl4 | amph1 | amph2 | amph3 | amph1 | amph2 | odd1 | odd2 | odd3 | odd4 | odd5 |
| SiO2 | 40.60 | 40.22 | 41.01 | 40.83 | 41.38 | 41.50 | 41.23 | 40.82 | 42.37 | 38.35 | 42.20 | 42.95 | 42.60 | 42.40 | 42.87 | 42.15 | 42.16 |
| TiO2 | 2.05 | 0.00 | 3.65 | 2.13 | 2.04 | 2.26 | 1.12 | 0.00 | 0.27 | 0.00 | 3.95 | 2.99 | 2.67 | 3.57 | 2.77 | 3.33 | 3.82 |
| Al2O3 | 9.34 | 10.37 | 11.43 | 9.13 | 9.18 | 9.14 | 10.40 | 10.66 | 8.83 | 13.35 | 12.00 | 11.53 | 12.24 | 12.28 | 12.43 | 12.50 | 12.18 |
| Cr2O3 | 0.00 | 0.00 | 0.00 | 0.00 | 0.00 | 0.00 | 0.20 | 0.00 | 0.00 | 0.00 | 0.00 | 0.00 | 0.36 | 0.00 | 0.00 | 0.00 | 0.00 |
| FeO | 32.38 | 32.96 | 14.50 | 28.18 | 28.87 | 28.99 | 29.34 | 31.43 | 32.85 | 30.50 | 12.31 | 12.46 | 11.50 | 11.94 | 11.57 | 13.18 | 12.14 |
| MnO | 0.63 | 0.43 | 0.00 | 0.57 | 0.49 | 0.50 | 0.80 | 0.82 | 1.04 | 0.74 | 0.25 | 0.00 | 0.00 | 0.00 | 0.00 | 0.00 | 0.00 |
| MgO | 0.45 | 0.32 | 10.22 | 2.59 | 2.65 | 2.45 | 1.72 | 1.26 | 0.94 | 0.51 | 12.24 | 12.33 | 13.14 | 12.45 | 12.90 | 12.31 | 12.15 |
| CaO | 10.64 | 10.61 | 11.36 | 10.65 | 10.90 | 10.86 | 10.69 | 9.97 | 10.28 | 10.85 | 11.61 | 11.65 | 11.70 | 11.83 | 11.74 | 11.41 | 11.64 |
| Na2O | 1.77 | 1.66 | 1.89 | 1.56 | 1.49 | 1.58 | 1.49 | 1.03 | 1.34 | 1.44 | 2.29 | 2.15 | 2.17 | 2.40 | 2.06 | 2.47 | 2.07 |
| K2O | 1.33 | 1.22 | 1.37 | 1.41 | 1.26 | 1.30 | 1.07 | 0.82 | 0.91 | 1.35 | 1.09 | 1.13 | 1.09 | 0.96 | 1.14 | 0.94 | 0.95 |
| Total | 99.19 | 97.80 | 95.41 | 97.05 | 98.26 | 98.56 | 98.07 | 96.82 | 98.82 | 97.07 | 97.92 | 97.19 | 97.47 | 98.07 | 97.49 | 98.29 | 97.11 |
| **Formula (23O)** | | | | | | | | | | | | | | | | | |
| Si | 6.528 | 6.564 | 6.290 | 6.579 | 6.587 | 6.589 | 6.580 | 6.633 | 6.796 | 6.253 | 6.235 | 6.379 | 6.288 | 6.250 | 6.317 | 6.215 | 6.258 |
| Al | 1.472 | 1.436 | 1.710 | 1.421 | 1.413 | 1.411 | 1.420 | 1.367 | 1.204 | 1.747 | 1.765 | 1.621 | 1.712 | 1.750 | 1.683 | 1.785 | 1.742 |
| Al | 0.298 | 0.559 | 0.356 | 0.313 | 0.309 | 0.299 | 0.536 | 0.675 | 0.465 | 0.818 | 0.325 | 0.397 | 0.417 | 0.383 | 0.476 | 0.387 | 0.389 |
| Fe(iii) | 0.329 | 0.676 | 0.000 | 0.241 | 0.320 | 0.227 | 0.449 | 1.251 | 0.933 | 0.703 | 0.044 | 0.029 | 0.235 | 0.000 | 0.148 | 0.304 | 0.039 |
| Cr | 0.000 | 0.000 | 0.000 | 0.000 | 0.000 | 0.000 | 0.025 | 0.000 | 0.000 | 0.000 | 0.000 | 0.000 | 0.042 | 0.000 | 0.000 | 0.000 | 0.000 |
| Ti | 0.248 | 0.000 | 0.421 | 0.258 | 0.244 | 0.270 | 0.134 | 0.000 | 0.033 | 0.000 | 0.439 | 0.334 | 0.296 | 0.396 | 0.307 | 0.369 | 0.426 |
| Fe(ii) | 4.094 | 3.871 | 1.860 | 3.633 | 3.605 | 3.705 | 3.558 | 3.131 | 3.574 | 3.499 | 1.505 | 1.549 | 1.208 | 1.472 | 1.305 | 1.344 | 1.503 |
| Mn | 0.086 | 0.059 | 0.000 | 0.078 | 0.066 | 0.067 | 0.108 | 0.113 | 0.141 | 0.102 | 0.031 | 0.000 | 0.000 | 0.000 | 0.000 | 0.000 | 0.000 |
| Mg | 0.108 | 0.078 | 2.337 | 0.622 | 0.629 | 0.580 | 0.409 | 0.305 | 0.225 | 0.124 | 2.696 | 2.730 | 2.892 | 2.736 | 2.834 | 2.706 | 2.689 |
| Ca | 1.833 | 1.855 | 1.867 | 1.839 | 1.859 | 1.847 | 1.828 | 1.736 | 1.766 | 1.895 | 1.838 | 1.854 | 1.850 | 1.868 | 1.853 | 1.802 | 1.851 |
| Na | 0.552 | 0.525 | 0.562 | 0.487 | 0.460 | 0.486 | 0.461 | 0.324 | 0.417 | 0.455 | 0.656 | 0.619 | 0.621 | 0.686 | 0.588 | 0.706 | 0.596 |
| K | 0.273 | 0.254 | 0.268 | 0.290 | 0.256 | 0.263 | 0.218 | 0.170 | 0.186 | 0.281 | 0.205 | 0.214 | 0.205 | 0.181 | 0.214 | 0.177 | 0.180 |
| TOTAL | 15.820 | 15.877 | 15.671 | 15.761 | 15.748 | 15.744 | 15.726 | 15.705 | 15.740 | 15.877 | 15.740 | 15.725 | 15.766 | 15.721 | 15.725 | 15.795 | 15.673 |

**Amphibole**

| Sample | DV1 | DV1 | DV1 | Ab6510 | Ab6510 | Ab94 | Ab94 | Ab94 | Ab94 | CLW218 | CLW218 | CLW218 | CLW218 | CLW218 | CLW218 | CLW218 | CLW218 |
|---|---|---|---|---|---|---|---|---|---|---|---|---|---|---|---|---|---|
| Analysis No. | 30 | 32 | 25 | 16 | 19 | 19 | 20 | 32 | 33 | 1 | 8 | 12 | 13 | 14 | 15 | 19 | 20 |
| Analysis Name. | odd6 | odd7 | amph-cor1 | cor1 | cor2 | amph1 | amph2 | amph3 | amph4 | hbl1 | hbl2 | hbl3 | hbl3b | hbl3c | hbl3d | hbl4 | hbl4b |
| SiO2 | 42.65 | 42.63 | 41.99 | 51.22 | 51.22 | 54.98 | 55.79 | 51.65 | 49.06 | 44.70 | 45.24 | 43.87 | 44.22 | 45.17 | 47.06 | 44.53 | 45.56 |
| TiO2 | 3.53 | 4.03 | 3.08 | 1.42 | 1.26 | 0.23 | 0.00 | 0.30 | 1.09 | 2.12 | 2.08 | 2.81 | 2.19 | 2.42 | 1.55 | 2.42 | 1.89 |
| Al2O3 | 11.80 | 11.53 | 13.05 | 3.77 | 3.55 | 1.60 | 1.86 | 4.46 | 6.60 | 9.56 | 9.49 | 10.42 | 10.22 | 9.28 | 8.55 | 9.91 | 9.86 |
| Cr2O3 | 0.00 | 0.00 | 0.00 | 0.35 | 0.30 | 0.00 | 0.00 | 0.00 | 0.00 | 0.00 | 0.21 | 0.00 | 0.39 | 0.19 | 0.25 | 0.21 | 0.23 |
| FeO | 11.34 | 11.85 | 11.61 | 5.43 | 4.98 | 14.31 | 15.06 | 15.01 | 15.65 | 12.95 | 12.64 | 13.44 | 12.79 | 12.32 | 11.98 | 13.09 | 12.17 |
| MnO | 0.00 | 0.00 | 0.23 | 0.00 | 0.00 | 0.00 | 0.50 | 0.46 | 0.19 | 0.00 | 0.20 | 0.00 | 0.00 | 0.00 | 0.00 | 0.00 | 0.00 |
| MgO | 12.90 | 12.43 | 12.45 | 15.81 | 15.36 | 14.69 | 15.73 | 13.49 | 12.93 | 13.29 | 13.27 | 12.36 | 12.59 | 13.30 | 14.53 | 12.61 | 13.37 |
| CaO | 11.61 | 11.57 | 12.04 | 21.17 | 22.40 | 12.80 | 10.74 | 11.93 | 11.59 | 11.67 | 11.75 | 12.16 | 11.89 | 11.75 | 11.77 | 11.99 | 12.16 |
| Na2O | 2.47 | 2.37 | 2.11 | 0.44 | 0.43 | 0.21 | 0.45 | 0.60 | 1.01 | 1.08 | 1.06 | 1.16 | 1.39 | 1.14 | 1.03 | 1.10 | 1.06 |
| K2O | 0.91 | 0.90 | 1.14 | 0.00 | 0.00 | 0.00 | 0.00 | 0.24 | 0.61 | 1.03 | 1.09 | 1.36 | 1.34 | 1.13 | 0.83 | 1.24 | 0.93 |
| Total | 97.39 | 97.33 | 97.69 | 99.61 | 99.50 | 98.82 | 100.14 | 98.15 | 98.74 | 96.42 | 97.04 | 97.77 | 97.22 | 96.67 | 97.56 | 97.09 | 97.23 |
| **Formula (23O)** | | | | | | | | | | | | | | | | | |
| Si | 6.304 | 6.309 | 6.198 | 7.233 | 7.252 | 7.858 | 7.859 | 7.509 | 7.154 | 6.661 | 6.693 | 6.507 | 6.576 | 6.696 | 6.864 | 6.611 | 6.699 |
| Al | 1.696 | 1.691 | 1.802 | 0.767 | 0.748 | 0.142 | 0.141 | 0.491 | 0.846 | 1.339 | 1.307 | 1.493 | 1.424 | 1.304 | 1.136 | 1.389 | 1.301 |
| Al | 0.360 | 0.320 | 0.468 | -0.140 | -0.156 | 0.128 | 0.168 | 0.273 | 0.288 | 0.340 | 0.347 | 0.328 | 0.367 | 0.317 | 0.334 | 0.345 | 0.408 |
| Fe(iii) | 0.000 | 0.000 | 0.041 | 0.000 | 0.000 | 0.000 | 1.053 | 0.390 | 0.524 | 0.505 | 0.417 | 0.146 | 0.138 | 0.266 | 0.539 | 0.198 | 0.248 |
| Cr | 0.000 | 0.000 | 0.000 | 0.039 | 0.034 | 0.000 | 0.000 | 0.000 | 0.000 | 0.000 | 0.025 | 0.000 | 0.046 | 0.022 | 0.029 | 0.025 | 0.027 |
| Ti | 0.392 | 0.449 | 0.342 | 0.151 | 0.134 | 0.025 | 0.000 | 0.033 | 0.120 | 0.238 | 0.231 | 0.313 | 0.245 | 0.270 | 0.170 | 0.270 | 0.209 |
| Fe(ii) | 1.402 | 1.466 | 1.416 | 0.641 | 0.590 | 1.710 | 0.833 | 1.533 | 1.464 | 1.159 | 1.198 | 1.567 | 1.494 | 1.312 | 0.976 | 1.477 | 1.300 |
| Mn | 0.000 | 0.000 | 0.029 | 0.000 | 0.000 | 0.000 | 0.060 | 0.057 | 0.023 | 0.000 | 0.025 | 0.000 | 0.000 | 0.000 | 0.000 | 0.000 | 0.000 |
| Mg | 2.843 | 2.742 | 2.740 | 3.328 | 3.242 | 3.130 | 3.303 | 2.924 | 2.811 | 2.953 | 2.927 | 2.733 | 2.791 | 2.939 | 3.160 | 2.791 | 2.931 |
| Ca | 1.839 | 1.834 | 1.904 | 3.203 | 3.398 | 1.960 | 1.621 | 1.858 | 1.811 | 1.863 | 1.862 | 1.932 | 1.894 | 1.866 | 1.839 | 1.907 | 1.916 |
| Na | 0.708 | 0.680 | 0.604 | 0.120 | 0.118 | 0.058 | 0.123 | 0.169 | 0.286 | 0.312 | 0.304 | 0.334 | 0.401 | 0.328 | 0.291 | 0.317 | 0.302 |
| K | 0.172 | 0.170 | 0.215 | 0.000 | 0.000 | 0.000 | 0.000 | 0.045 | 0.113 | 0.196 | 0.206 | 0.257 | 0.254 | 0.214 | 0.154 | 0.235 | 0.174 |
| TOTAL | 15.715 | 15.662 | 15.758 | 15.343 | 15.360 | 15.011 | 15.160 | 15.281 | 15.439 | 15.566 | 15.542 | 15.611 | 15.630 | 15.534 | 15.492 | 15.566 | 15.515 |

**Amphibole**

| Sample | CLW218 | CLW218 | CLW215 | CLW215 | CLW215 | CLW215 | CLW215 | CLW215 | CLW106 | CLW106 | CLW106 | CLW107 | CLW107 | CLW107 | CLW107 | CLW107 | CLW110 |
|---|---|---|---|---|---|---|---|---|---|---|---|---|---|---|---|---|---|
| Analysis No. | 22 | 23 | 3 | 5 | 6 | 7 | 8 | 9 | 8 | 11 | 27 | 4 | 9 | 10 | 11 | 24 | 4 |
| Analysis Name. | hbl5a | hbl5b | hbl1 | hbl2 | hbl4 | hbl4 | hbl5 | hbl6 | amph1 | amph2 | amph4 | hbl1 | hbl2 | hbl3 | hbl3b | hbl4 | hbl2 |
| SiO2 | 44.83 | 45.65 | 47.56 | 58.21 | 54.82 | 53.44 | 48.29 | 57.00 | 48.66 | 46.11 | 46.35 | 43.50 | 43.30 | 43.04 | 43.07 | 42.95 | 46.76 |
| TiO2 | 2.46 | 1.94 | 1.82 | 0.00 | 0.23 | 0.00 | 1.87 | 0.00 | 1.09 | 1.07 | 1.61 | 0.64 | 0.66 | 0.73 | 0.67 | 1.00 | 1.37 |
| Al2O3 | 9.67 | 9.07 | 8.83 | 0.90 | 4.11 | 4.41 | 8.91 | 1.98 | 7.96 | 7.81 | 9.62 | 12.97 | 12.97 | 12.92 | 13.14 | 12.57 | 8.30 |
| Cr2O3 | 0.00 | 0.20 | 0.45 | 0.00 | 0.00 | 0.00 | 0.26 | 0.00 | 0.35 | 0.00 | 0.21 | 0.47 | 0.40 | 0.26 | 0.39 | 0.50 | 0.00 |
| FeO | 12.92 | 12.28 | 11.17 | 7.13 | 9.36 | 11.45 | 11.35 | 8.00 | 8.75 | 8.49 | 9.80 | 9.17 | 9.16 | 9.42 | 8.95 | 8.37 | 12.60 |
| MnO | 0.00 | 0.00 | 0.00 | 0.28 | 0.22 | 0.00 | 0.00 | 0.39 | 0.00 | 0.00 | 0.00 | 0.00 | 0.00 | 0.19 | 0.00 | 0.00 | 0.22 |
| MgO | 13.12 | 13.45 | 14.65 | 20.86 | 18.24 | 15.95 | 14.91 | 19.54 | 16.30 | 15.34 | 15.37 | 15.18 | 14.71 | 15.11 | 14.89 | 15.28 | 13.75 |
| CaO | 11.98 | 11.94 | 12.10 | 12.70 | 12.38 | 12.38 | 12.61 | 12.30 | 11.88 | 11.20 | 11.78 | 12.29 | 12.37 | 12.17 | 12.33 | 12.14 | 12.11 |
| Na2O | 1.14 | 0.93 | 0.68 | 0.00 | 0.42 | 0.30 | 0.69 | 0.00 | 0.65 | 0.51 | 0.94 | 1.59 | 1.65 | 1.61 | 1.65 | 1.65 | 0.98 |
| K2O | 1.22 | 1.03 | 1.01 | 0.00 | 0.10 | 0.00 | 0.97 | 0.00 | 0.41 | 0.41 | 0.68 | 1.26 | 1.01 | 1.20 | 1.13 | 1.20 | 0.77 |
| Total | 97.33 | 96.67 | 98.28 | 100.07 | 99.89 | 97.94 | 99.86 | 99.20 | 96.06 | 90.95 | 96.36 | 97.21 | 96.25 | 96.64 | 96.22 | 95.64 | 96.86 |
| **Formula (23O)** | | | | | | | | | | | | | | | | | |
| Si | 6.629 | 6.767 | 6.860 | 7.926 | 7.587 | 7.607 | 6.857 | 7.858 | 7.053 | 7.053 | 6.771 | 6.362 | 6.381 | 6.335 | 6.348 | 6.358 | 6.899 |
| Al | 1.371 | 1.233 | 1.140 | 0.074 | 0.413 | 0.393 | 1.143 | 0.142 | 0.947 | 0.947 | 1.229 | 1.638 | 1.619 | 1.665 | 1.652 | 1.642 | 1.101 |
| Al | 0.315 | 0.351 | 0.361 | 0.071 | 0.257 | 0.347 | 0.348 | 0.180 | 0.413 | 0.461 | 0.427 | 0.598 | 0.633 | 0.577 | 0.630 | 0.551 | 0.342 |
| Fe(iii) | 0.275 | 0.301 | 0.379 | 0.522 | 0.536 | 0.330 | 0.287 | 0.573 | 0.540 | 0.589 | 0.601 | 0.538 | 0.397 | 0.651 | 0.438 | 0.453 | 0.353 |
| Cr | 0.000 | 0.023 | 0.051 | 0.000 | 0.000 | 0.000 | 0.029 | 0.000 | 0.040 | 0.000 | 0.024 | 0.054 | 0.047 | 0.030 | 0.045 | 0.059 | 0.000 |
| Ti | 0.274 | 0.216 | 0.197 | 0.000 | 0.024 | 0.000 | 0.200 | 0.000 | 0.119 | 0.123 | 0.177 | 0.070 | 0.073 | 0.081 | 0.074 | 0.111 | 0.152 |
| Fe(ii) | 1.371 | 1.276 | 1.025 | 0.344 | 0.610 | 1.117 | 1.117 | 0.412 | 0.573 | 0.552 | 0.642 | 0.600 | 0.751 | 0.524 | 0.682 | 0.599 | 1.258 |
| Mn | 0.000 | 0.000 | 0.000 | 0.032 | 0.026 | 0.000 | 0.000 | 0.046 | 0.000 | 0.000 | 0.000 | 0.000 | 0.000 | 0.024 | 0.000 | 0.000 | 0.027 |
| Mg | 2.892 | 2.972 | 3.150 | 4.234 | 3.763 | 3.385 | 3.156 | 4.016 | 3.522 | 3.498 | 3.347 | 3.310 | 3.232 | 3.316 | 3.272 | 3.372 | 3.024 |
| Ca | 1.898 | 1.896 | 1.870 | 1.853 | 1.836 | 1.888 | 1.918 | 1.817 | 1.845 | 1.835 | 1.844 | 1.926 | 1.953 | 1.919 | 1.947 | 1.925 | 1.914 |
| Na | 0.327 | 0.267 | 0.190 | 0.000 | 0.113 | 0.083 | 0.190 | 0.000 | 0.183 | 0.151 | 0.266 | 0.451 | 0.471 | 0.459 | 0.471 | 0.474 | 0.280 |
| K | 0.230 | 0.195 | 0.186 | 0.000 | 0.018 | 0.000 | 0.176 | 0.000 | 0.076 | 0.080 | 0.127 | 0.235 | 0.190 | 0.225 | 0.212 | 0.227 | 0.145 |
| TOTAL | 15.581 | 15.499 | 15.411 | 15.056 | 15.182 | 15.149 | 15.421 | 15.043 | 15.309 | 15.290 | 15.455 | 15.782 | 15.747 | 15.806 | 15.773 | 15.771 | 15.495 |

**Amphibole**

| Sample | CLW110 | CLW110 | CLW110 | CLW110 | CLW110 |
|---|---|---|---|---|---|
| Analysis No. | 7 | 8 | 9 | 24 | 25 |
| Analysis Name. | hbl3 | hbl3b | hbl3c | hbl4 | hbl5 |
| SiO2 | 44.40 | 45.55 | 45.28 | 45.94 | 45.06 |
| TiO2 | 1.52 | 1.58 | 1.58 | 1.40 | 1.74 |
| Al2O3 | 9.10 | 8.83 | 8.62 | 9.15 | 8.96 |
| Cr2O3 | 0.00 | 0.00 | 0.00 | 0.00 | 0.00 |
| FeO | 14.20 | 13.35 | 13.26 | 13.37 | 13.38 |
| MnO | 0.24 | 0.00 | 0.21 | 0.00 | 0.00 |
| MgO | 12.65 | 13.20 | 13.11 | 13.01 | 13.08 |
| CaO | 11.04 | 11.71 | 11.42 | 11.95 | 11.50 |
| Na2O | 0.87 | 1.01 | 1.12 | 1.02 | 1.03 |
| K2O | 0.93 | 1.03 | 0.87 | 0.89 | 1.02 |
| Total | 94.95 | 96.29 | 95.46 | 96.73 | 95.94 |
| **Formula (23O)** | | | | | |
| Si | 6.746 | 6.798 | 6.813 | 6.813 | 6.763 |
| Al | 1.254 | 1.202 | 1.187 | 1.187 | 1.237 |
| Al | 0.376 | 0.351 | 0.342 | 0.412 | 0.348 |
| Fe(iii) | 0.868 | 0.461 | 0.546 | 0.359 | 0.528 |
| Cr | 0.000 | 0.000 | 0.000 | 0.000 | 0.000 |
| Ti | 0.174 | 0.177 | 0.179 | 0.156 | 0.196 |
| Fe(ii) | 0.997 | 1.260 | 1.177 | 1.357 | 1.206 |
| Mn | 0.031 | 0.000 | 0.027 | 0.000 | 0.000 |
| Mg | 2.865 | 2.937 | 2.941 | 2.876 | 2.927 |
| Ca | 1.797 | 1.872 | 1.841 | 1.899 | 1.849 |
| Na | 0.256 | 0.292 | 0.327 | 0.293 | 0.300 |
| K | 0.180 | 0.196 | 0.167 | 0.168 | 0.195 |
| TOTAL | 15.544 | 15.546 | 15.547 | 15.520 | 15.549 |